Development of Picolinic Acid-derived Anti-Parasitics and Methods for the Synthesis of Ring-Fused Quinazolin- and Quinolin-ones

By
Muhammad M. Khalifa

A dissertation submitted in partial fulfillment of
the requirements for the degree of

Doctor of Philosophy
(Pharmaceutical Sciences)

at the
UNIVERSITY OF WISCONSIN-MADISON
2020

Date of final oral examination: 06/12/2020

The dissertation is approved by the following members of the Final Oral Committee:

Jennifer E. Golden, Assistant Professor, School of Pharmacy and Department of Chemistry

Weiping Tang, Professor, School of Pharmacy and Department of Chemistry

Charles Lauhon, Associate Professor, School of Pharmacy

Arash Bashirullah, Associate Professor, School of Pharmacy and Department of Genetics

Bill Sugden, Associate Professor, McArdle Laboratory for Cancer Research and Department of Oncology

Dedication

To Faridah Haron, Amr Khalifa, and Ibrahim Khalifa, who made this journey possible.

And to Kimberly Buchanan, who made it enjoyable.

Acknowledgements

"He who does not thank the people is not thankful to Allah" – The Prophet (ﷺ)

To attempt to thank the many individuals who have contributed along the way to the person I am and the successes I have enjoyed would be to undertake writing a document far longer than this one, but I will here attempt to articulate a small measure of the gratitude I owe.

To my advisor, Prof. Jennifer Golden, I will be ever indebted for her patience, trust, and caring mentorship up the (occasionally) Sisyphean slope that is a PhD. Your guidance, understanding, and unwavering support has always been more than I could ever ask, and it continues to be a privilege to be counted among the founding members of your research group. Thank you so much for the singular opportunity.

In so many ways (least of all procedurally), this would not be possible without the support of my thesis committee: Prof. Weiping Tang, Prof. Charles Lauhon, Prof. Arash Bashirullah, and Prof. Bill Sugden. Our conversations over the past five years were pivotal in my development as a student, a scientist, and as an individual. Your enthusiasm in mentorship is something to which I continue to aspire.

The men and women of the Golden lab over the past half-decade deserve more thanks than there is space here to express: To Dr. Xufeng Cao, Dr. Alok Nerurkar, Dr. Satish Philkhana, Dr. Gang Yan, Dr. Victor Jaffett, Dr. Xiaoyu Li, Dr. Michael Ryan, Dr. Jongwoo Son, Bereket Zekarias, Jhewelle Fitz-Henley, Soren Rozema, Matt Lish, and Tyler Ogorek - it has been a joy to work with you, to learn from you, to share the same (occasionally solvent-tainted) air with you, and to call you colleagues, collaborators, and friends. I consider the many wonderful meals, small victories,

medium-sized failures, and 7th-floor views we have shared among the most treasured memories of my graduate career.

Research is a team sport, and I am fortunate to count all the many colleagues and collaborators at the University of Wisconsin-Madison as part of my team. This work benefitted tremendously from the expertise (and endless patience) of the staff and faculty of the Medicinal Chemistry Center (Dr. John Feltenberger, Dr. Zhi-Xiong Ma, and Dr. Zhen-Qing Ye), the Analytical Instrumentation Center (Dr. Thomas Stringfellow, Dr. Cameron Scarlett, Molly Pellitteri-Hahn, Gary Girdaukas, and all of the associated project assistants and staff), and the Zeeh Pharmaceutical Experiment Station (Dr. Ed Elder) at the School of Pharmacy during my time as a graduate student. Ken Niemeyer deserves unique recognition as the only person to top both my list of compelling reasons to *join* the PharmSci graduate program in Madison, and later, of compelling reasons to *leave* it - his friendship has been invaluable these past years.

This work is made possible by the generous support of many funding sources, past and present, and my securing of such support owes much to the efforts of Joan Palmer. In particular, the Daniel H. Rich Distinguished Scholarship program, the John & Jane Roudebush Distinguished Graduate Research Fellowship program, the National Science Foundation Graduate Research Fellowship program (Grant No. DGE-1256259), the American Foundation for Pharmaceutical Education Pre-Doctoral Fellowship program, and the Graduate School Student Research Grant Competition programs have contributed to my ability to conduct and communicate this research over the past five years.

And to my family of friends – thank you for your support through all the many hurdles we call graduate school. I would not have made it through without you.

Abstract

As part of a research program at the interface of synthetic organic chemistry and drug discovery, the Golden lab is interested in new methodology development for heterocycle synthesis, implementation of such methods to generate diverse libraries of small molecules in drug-like chemical space, and the medicinal chemistry of these drug-like scaffolds from screening to lead optimization. Three distinct projects will be discussed that highlight the importance of heterocycle synthesis to the drug discovery process. First, we developed a strategy to construct > 80 diverse ring-fused, *N*-substituted quinolin-4-ones, a privileged structural class associated with a variety of reported bioactivity. The method also enabled the shortest and highest yielding synthesis to date of penicinotam, an insecticidal natural product derivative. Second, we recently discovered that members of an underexplored scaffold family, tetrahydropyrrolopyrazino[2,1-*b*]quinazolin-11-ones, result from a novel domino quinazolinone rearrangement and intramolecular ring closure of *ortho*-amido-*NH*-benzamidines. We developed a method for diastereoselective, multicomponent quinazolinone assembly followed by this domino process. Third, a series of benzoic acid derivatives were structurally refined to adjust physiochemical properties and resulted in inhibitors of multiple parasites for which effective treatments remain an unmet medical need. As part of ongoing medicinal chemistry efforts, progress has been made *in vitro* and *in vivo* with second generation picolinic acid derivatives. Advantages of these series will be described in terms of synthetic approach, *in vitro* profile and *in vivo* efficacy.

Table of Contents

Chapter 1 – Introduction and Research Summary

As part of a research program at the interface of synthetic organic chemistry and drug discovery, the Golden lab is interested in new methodology development for heterocycle synthesis, implementation of such methods to generate diverse libraries of small molecules in drug-like chemical space, and the medicinal chemistry of these drug-like scaffolds from screening to lead optimization. This dissertation focused on the development of new synthetic methodologies for drug-like heterocyclic small molecules and the medicinal chemistry of a series of benzoic acid derivatives with broad spectrum anti-parasitic activity.

Section 1-1: Synthetic methodology development of drug-like heterocycles

Heterocyclic small molecules are important molecular motifs, being essential components of myriad biologically important natural products, drugs for animal and human health, and compounds that are vital to food security for a growing, global human population. Some heterocyclic motifs appear more commonly in compounds with applications to human health, and continued study towards the synthesis, diversification, and development of such privileged scaffolds is important to drug discovery. Here, new methodology for the synthesis of two such privileged heterocyclic cores is discussed (**Chapter 2** and **Chapter 3**).

In Chapter 2, a new method to construct a diverse collection of ring-fused, *N*-substituted quinolin-4-ones is described. Our studies enabled base-promoted annulation between isatoic anhydrides **1-1.1** and enolates **1-1.2** of a broad (> 15 unit) pK_aH range that reliably afforded > 80 examples of quinolin-4-ones **1-1.3** in yields up to 94% (**Scheme 1-1.1**).[1]

Scheme 1-1.1 Method for the synthesis of ring-fused quinolin-4-ones by pK_a-guided annulation of enolates with isatoic anhydrides

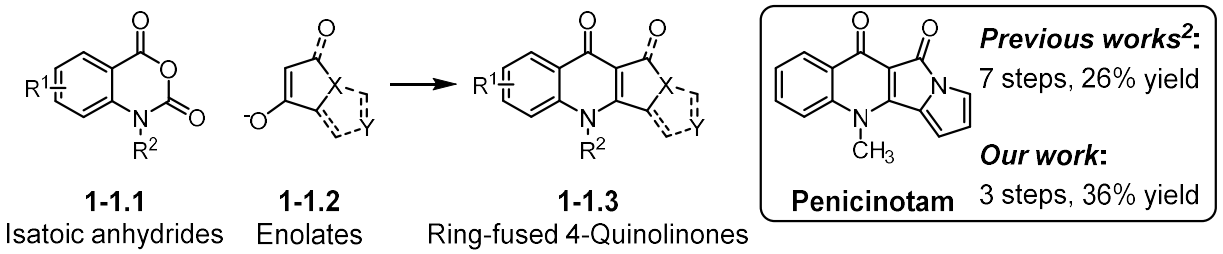

Development of three complementary procedures, the selection of which could be guided by predicted pK_aH of the enolizable starting material and desired product, facilitated the unique breadth of scope for our reaction compared to preceding methods. The new method also enabled the shortest and highest yielding synthesis to date of penicinotam, an insecticidal natural product derivative, in 3 steps and 36% overall yield. Previous syntheses of this target compound required at least twice the number of steps and featured a lower overall yield.[2]

In Chapter 3, we developed a diastereoselective, multicomponent method for the synthesis of tetrahydropyrrolopyrazino[2,1-*b*]quinazolin-11-ones **1-1.4**, an underexplored heterocyclic scaffold family that shares core similarities with a number of natural products and patented bioactive molecules (**Scheme 1-1.2**).

Scheme 1-1.2 Telescoped, diastereoselective, multicomponent method for the synthesis of tetrahydropyrrolopyrazino[2,1-*b*]quinaozlin-11-ones

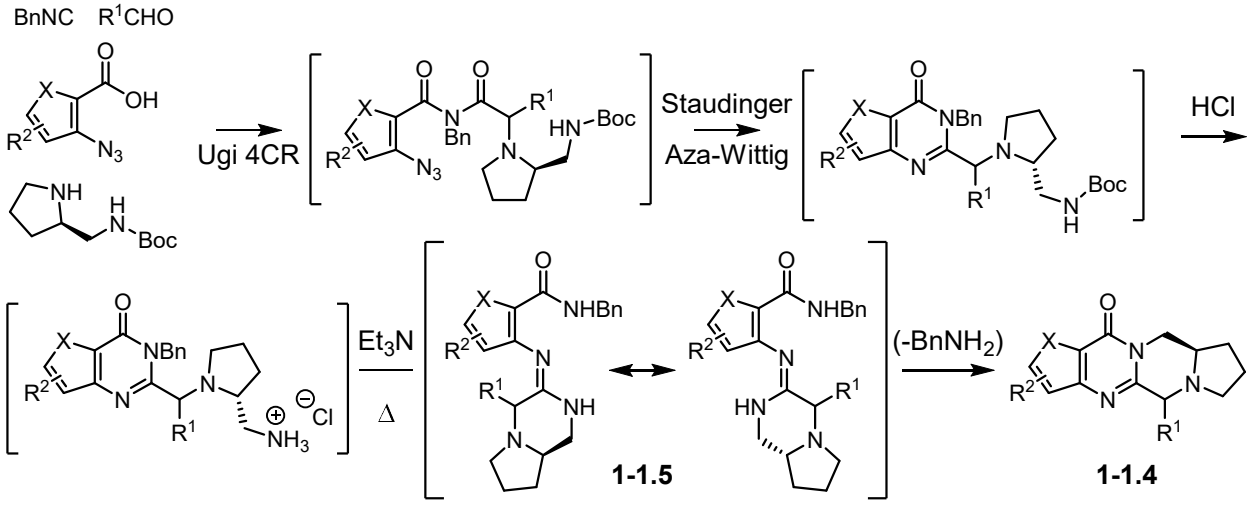

The method leverages our recent discovery of a novel, domino quinazolinone rearrangement/ring-closure process that enables access to a variety of diverse structures from transient *ortho*-amido-*NH*-benzamidines **1-1.5**.[3] This provided a telescoped procedure involving 7 chemical transformations that required only a single, terminal purification, and afforded 20 examples in up to 86% isolated yield over 4 steps and with a maximum of 8:1 d.r. of separable diastereomers (40 total analogs). Studies probing the generality of the ring-closure in the context of total syntheses of a family of natural products will be discussed, as well as preliminary results regarding the intersection of this ring-closure chemistry with extant technology in the realm of complex heterocycle synthesis.

Section 1-2: Medicinal chemistry of heterocyclic benzoic acid-derived anti-parasitics

Discovery and development of new drugs for infectious diseases caused by parasites remain important areas of investigation due to continued unmet medical need. This dissertation

discusses the medicinal chemistry optimization of a series of benzoic acid derivatives against several important threats to human health, including *Naegleria fowleri*, *Toxoplasma gondii*, *Trypanosoma brucei*, and *Leishmania donovani*. In Chapter 4, the divergent structure-activity and structure-property relationships of this series against each of the pathogens will be discussed, as well as synthetic challenges and improvements in the compound series.

Section 4-1 introduces the parasite hopping strategy for drug discovery, while Section 4-2 introduces a benzamidobenzoic acid scaffold developed in our group with hexokinase-mediated inhibitory activity against kinetoplastids and physicochemical properties that limited further development for drug discovery. Section 4-3 details scaffold modifications to arrive at a benzamidopicolinic acid template with improved solubility and microsomal stability. From this new series, a potent growth inhibitor of *T. gondii* was identified, and Section 4-4 describes the development of a *T. gondii* inhibitor **1-2.2** with activity against both tachyzoites and bradyzoites and > 2X potency, > 10X solubility, and > 30% better microsomal stability compared to the parent benzamidobenzoic acid **1-2.1** (**Scheme 1-2.1**). Efforts to increase route efficiency led to an improved synthesis that enabled access to this inhibitor at 100X scale with > 95% reduction in cost of materials, eliminated the use of a highly toxic reagent, and could be performed in the same number of steps.

Scheme 1-2.1 Optimization of a dual-stage *T. gondii* growth inhibitor with improved physicochemical properties

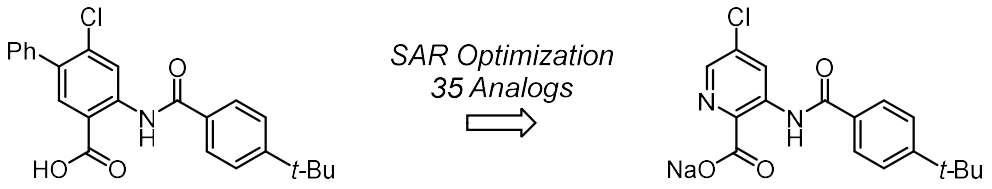

1-2.1 **1-2.2**

T. gondii tachyzoite	EC_{50} = 0.57 μM	*T. gondii* tachyzoite	EC_{50} = 0.27 μM
T. gondii bradyzoite	EC_{50} = 0.79 μM	*T. gondii* bradyzoite	EC_{50} = 0.04 μM
Human foreskin fibroblasts	CC_{50} > 50 μM	Human foreskin fibroblasts	CC_{50} = 2.1 μM
[a]cLogD (pH 5.0-7.4)	6.75 - 5.42	[a]cLogD (pH 5.0-7.4)	ND
[b]Solubility (PBS 1X, pH 7.4)	9.6 μM	[b]Solubility (PBS 1X, pH 7.4)	164 μM
[c]Microsomal stability	69.2%	[c]Microsomal stability	100%
[d]Permeability (PAMPA)	Moderate	[d]Permeability (PAMPA)	ND

EC_{50}: concentration at which growth inhibition is half-maximal; CC_{50}: concentration at which toxicity is half-maximal; [a]cLogD: calculated partition coefficient between octanol and water at given pH; [b]Kinetic aqueous solubility at pH 7.4; PBS: phosphate-buffered saline; [c]Microsomal stability: percent parent compound remaining after 1 h exposure to mouse microsomes; [d]PAMPA: parallel artificial membrane permeability assay.

Discovery of hexokinase-independent inhibitors of bloodstream *T. brucei* based on the benzamidopicolinic acid template is described in Section 4-5. In this project, divergent structure activity requirements in the benzamidopicolinic acids led to discover of a benzylamino picolinic acid with attractive anti-parasitic activity but potential metabolic liabilities. Developing the series further required improvements in strategy for analog synthesis. Ultimately, we found compounds with greatly improved metabolic stability (anti-parasitic screening is ongoing). Deployment of the series in *L. donovani* is discussed in Section 4-6. Based on these efforts we have also identified a new class of small molecule inhibitors for *N. fowleri* glucokinase and results of this work are discussed in Section 4-7.[4]

References

(1) Khalifa, M. M.; Philkhana, S. C.; Golden, J. E. Synthesis of Ring-Fused, N-Substituted 4-Quinolinones Using PKa-Guided, Base-Promoted Annulations with Isatoic Anhydrides: Total Synthesis of Penicinotam. *J. Org. Chem.* **2020**, *85* (2), 464–481. https://doi.org/10.1021/acs.joc.9b02541.

(2) Saito, K.; Yoshida, M.; Uekusa, H.; Doi, T. Facile Synthesis of Pyrrolyl 4-Quinolinone Alkaloid Quinolactacide by 9-AJ-Catalyzed Tandem Acyl Transfer–Cyclization of *o* -Alkynoylaniline Derivatives. *ACS Omega* **2017**, *2* (8), 4370–4381. https://doi.org/10.1021/acsomega.7b00793.

(3) Jaffett, V. A.; Nerurkar, A.; Cao, X.; Guzei, I. A.; Golden, J. E. Telescoped Synthesis of C3-Functionalized (*E*)-Arylamidines Using Ugi–Mumm and Regiospecific Quinazolinone Rearrangements. *Org. Biomol. Chem.* **2019**, *17* (12), 3118–3128. https://doi.org/10.1039/C9OB00073A.

(4) Milanes, J. E.; Suryadi, J.; Abendroth, J.; Voorhis, W. C. V.; Barrett, K. F.; Dranow, D. M.; Phan, I. Q.; Patrick, S. L.; Rozema, S. D.; Khalifa, M. M.; Golden, J. E.; Morris, J. C. Enzymatic and Structural Characterization of the Naegleria Fowleri Glucokinase. *Antimicrob. Agents Chemother.* **2019**, *63* (5). https://doi.org/10.1128/AAC.02410-18.

Chapter 2 – Methods for the Synthesis of Ring-Fused 4-Quinonlinones via Enolate Addition to Isatoic Anhydrides: Total Synthesis of Penicinotam

This chapter is adapted in part from published work.[1] *The project was completed in collaboration with Dr. Satish Chandra Philkhana, a former postdoctoral researcher in the Golden group. Dr. Phikhana's contributions included assistance in the development of DBU-mediated conditions, synthesis of the N-benzyl lactam-fused derivatives, development of the LiHMDS-mediated protocol for ketone use and assessment of its substrate scope, and optimization of the oxidation reaction that enabled completion of the penicinotam synthesis.*

Section 2-1: Introduction

Discovery and development of new drugs often requires the identification of new chemical matter with bioactivity that can affect a disease state of interest. One of the ways to identify such starting points for drug development involves the broad screening of compounds to identify "hit" molecules that can be subsequently investigated and optimized for pharmacological activity. The design of new drug-like molecules to populate compound collections (or " screening libraries, as well as the development of appropriate methods by which to synthesize them, continues to be a research interest of the Golden lab. As part of a research program aimed at the efficient generation of a differentiated library of pharmacologically-biased molecular templates that could be screened broadly for activity, we sought to develop new methods for the synthesis of a collection of compounds with embedded, privileged scaffolds.

The term "privileged scaffold" was coined over 50 years ago, and refers to molecular templates for which a variety of distinct bioactivities can be optimized based on a common core motif.[2,3] This was a way to articulate the observation that certain molecular motifs appear in drugs

and bioactive natural products more often than others. Importantly, individual compounds that share a centrally embedded "privileged scaffold" may not share the same bioactivity; indeed it is the ability to arrive at orthogonal bioactivities via different modifications to the central motif that makes privileged scaffolds so useful for medicinal chemistry. For example, the 4-quinolinone motif appears within a variety of ring-fused small molecules in the natural product and patent literature with diverse reported bioactivity, the abundance and breadth of which qualify it as a privileged scaffold for drug discovery efforts (**Figure 2-1.1**, blue highlight).[4–16] For example, quinolactacins **2-1.1** are a family of natural products that share a lactam-fused quinolinone core; members of this family were reported to inhibit TNF and acetylcholinesterase. Alternatively, carbocycle-fused quinolinones have been studied as antimalarial agents (e.g., floxacrine **2-1.2** and tetrahydroacridinones **2-1.8**).

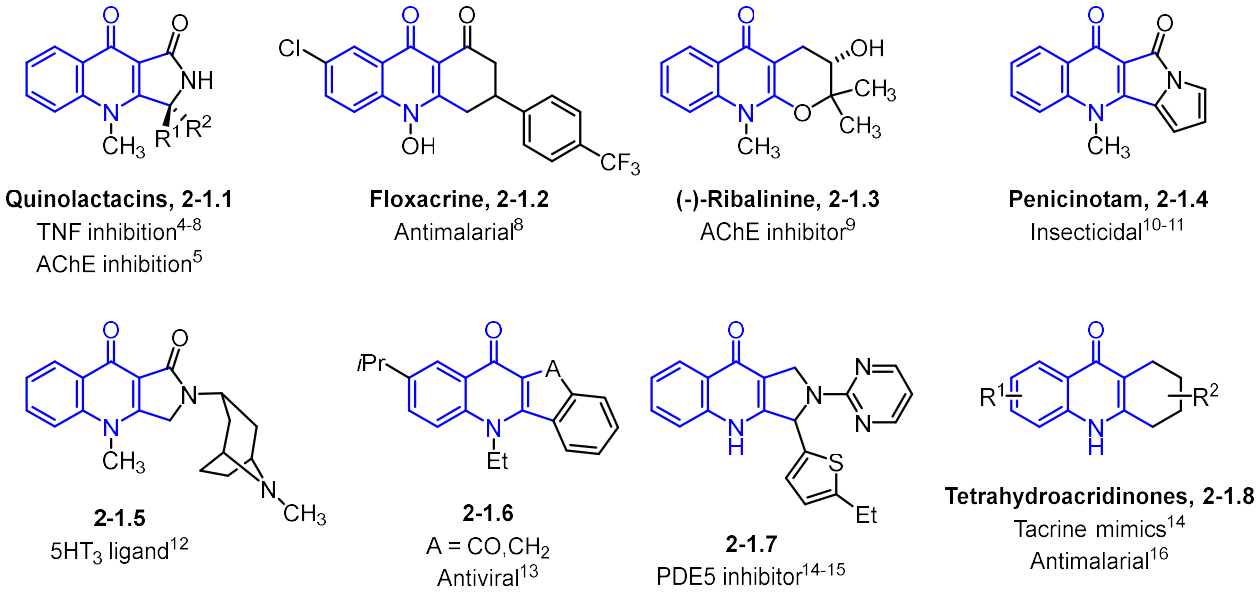

Figure 2-1.1 Selected examples of bioactive, ring-fused *N*-substituted 4-quinolinones with 4-quinolinone motif highlighted in blue. TNF: tumor necrosis factor; AChE: acetylcholinesterase; $5HT_3$: 5-hydroxytryptamine receptor type 3; PDE5: phosphodiesterase type 5.

We sought a strategy to access a structurally diverse library of *N*-substituted 4-quinolinones in a highly modular format from readily accessible starting materials. Upon review of existing methods to access this motif, several limitations were revealed.[6,17–27] Many of the syntheses were devised originally to address challenges unique to a specific natural product's stereochemical features and consisted of long, linear routes to a single example. While they are elegant examples in the context of total synthesis efforts towards a natural product, such routes are not amenable to efficient library synthesis and subsequent analog generation in parallel. Efforts by Lee, Zhang, and Tatsuta are illustrative of the limitations of these precedents in total synthesis for library-oriented methods (**Scheme 2-1.1**).[6,17,18]

In Lee's case, the *N*-substituted quinolinone motif is constructed by annulation of the enolate of β-ketoester **2-1.9** with *N*-methyl isatoic anhydride **2-1.10**. The yield for this reaction was maximally 42% with substantial degradation of **2-1.10** to *N*-methyl anthranilic acid, though the cause(s) were not investigated and the experimental details provided scant (see **Figure 2-1.3** for more details regarding reaction pathways and mechanism).[6] A subsequent step was required to finish formation of the lactam-fused 4-quinolinone motif that makes up the core architecture of the quinolactacin family of natural products. Despite the limitations, this route was the most direct for synthesis of lactam-fused 4-quinolinones. Zhang and Tatsuta also reported total syntheses of quinolactacins, but accessing the intermediates needed for entry into the ring-fused 4-quinolinone systems required at least twice the number of steps from commercial material.[17,18] Other strategies for constructing lactam-fused 4-quinolinones appear in the total syntheses of penicinotam, but are no less step-intensive (see **Section 2-3**). Tatsuta's work is notable for reporting four analogs based on the quinolactacin template, but is also the lengthiest of the routes, requiring 9 linear steps to construct the ring-fused, *N*-substituted quinolinone core.[17]

Scheme 2-1.1 Selected examples of precedents in *N*-substituted 4-quinolinone formation in total synthesis

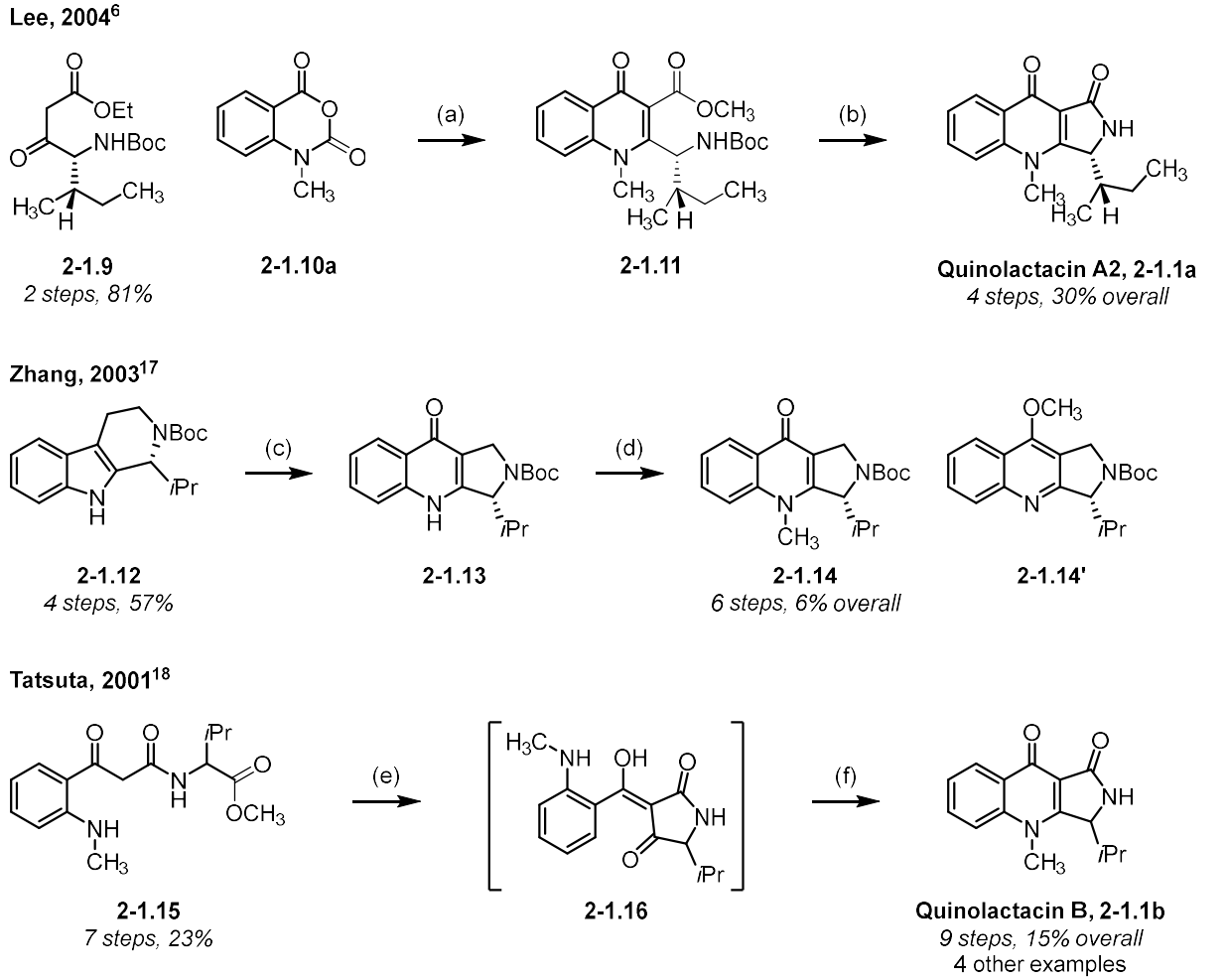

Reagents and conditions: (a) *N*-methyl isatoic anhydride, 3Å molecular sieves, DBU, CH_2Cl_2, 20 h, 42% (b) Et_2O/H_2O/TFA, 2 h, 87% (c) KO_2, 18-crown-6, DMF, then chiral HPLC-MS separation, 75% (d) K_2CO_3, CH_3I, 1:6 mixture of regioisomers, 88% (e) $NaOCH_3$, CH_3OH, rt, 12 h (f) Silica gel, 65% over 2 steps.

Methodology reports featured few examples of our core scaffold of interest. Only three examples of furan-fused 4-quinolinones were previously reported and both featured low yields of the final products (**Scheme 2-1.2**).[20,21] The work of Husson was further limited by a lengthy route to the requisite intermediate **2-1.20** with little information given regarding the efficiency with which it could be synthesized.[21]

Scheme 2-1.2 Precedents in synthesis of furan-fused *N*-substituted 4-quinolinones

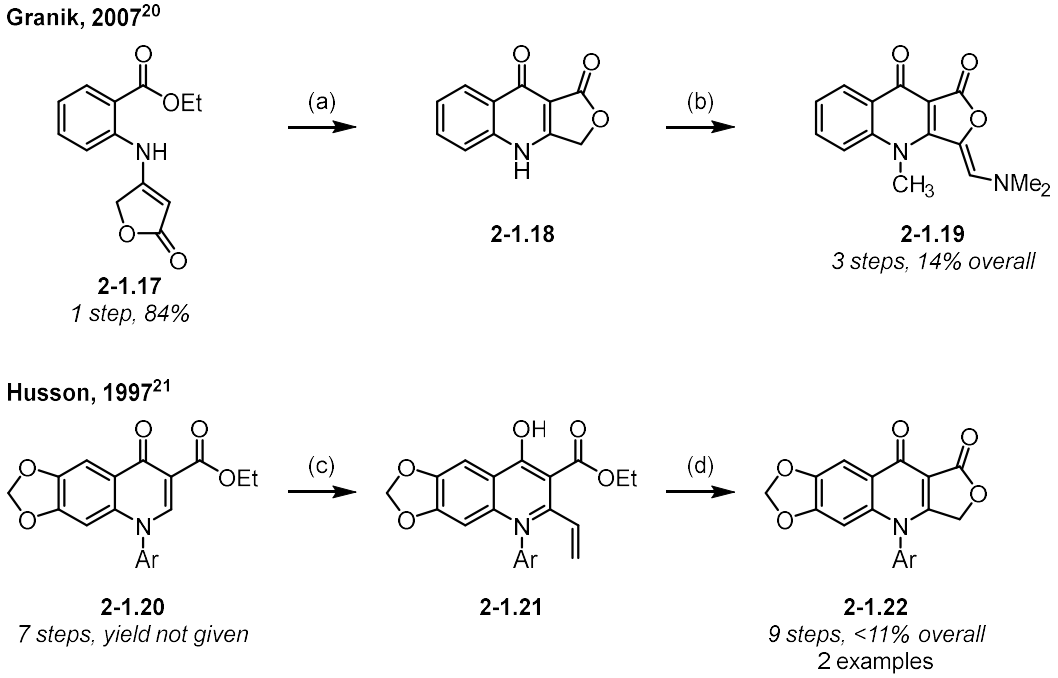

Reagents and conditions: (a) EtONa, EtOH, 40°C to 45°C, 6 h, 68% (b) DMF, DMF acetal, reflux, 3 h, 25% (c) $CH_2CHMgBr$, CuI, THF, -70°C to -40°C, 5 h, 62% (d) $KMnO_4$, H_2O/acetone, 0°C to 20°C, 36 h, 20%.

Literature regarding construction of carbocycle-fused derivatives were slightly more numerous, but typically consisted of only 1-2 examples of the desired ring-fused quinolinone system (**Scheme 2-1.3**).[24–27] Since our aim was synthesis of diversely substituted quinolinone derivatives, the limited scope of compatible substrates for these methods (Reed, Coppola, Deng) and their use of strong bases (Werbel, Coppola) or extremely high temperatures (Reed) were important challenges to their implementation.[23-25]

Of the precedents, we noted that the most direct routes appeared to be ones using base-promoted ring-opening of isatoic anhydrides (**2-1.10a-e**) by an enolate species generated from a suitable starting material (**2-1.9**, **2-1.24a-b**, **2-1.27**), followed by intramolecular annulation to form

the quinolinone motif. This strategy had been used by Lee, Werbel, and Coppola and taken together represented the most substantiated approach, with examples of lactam and carbocycle fused compounds.[6,24,25] However, the factors determining reaction efficiency were not well established.

Scheme 2-1.3 Precedents in synthesis of carbocycle-fused *N*-substituted 4-quinolinones

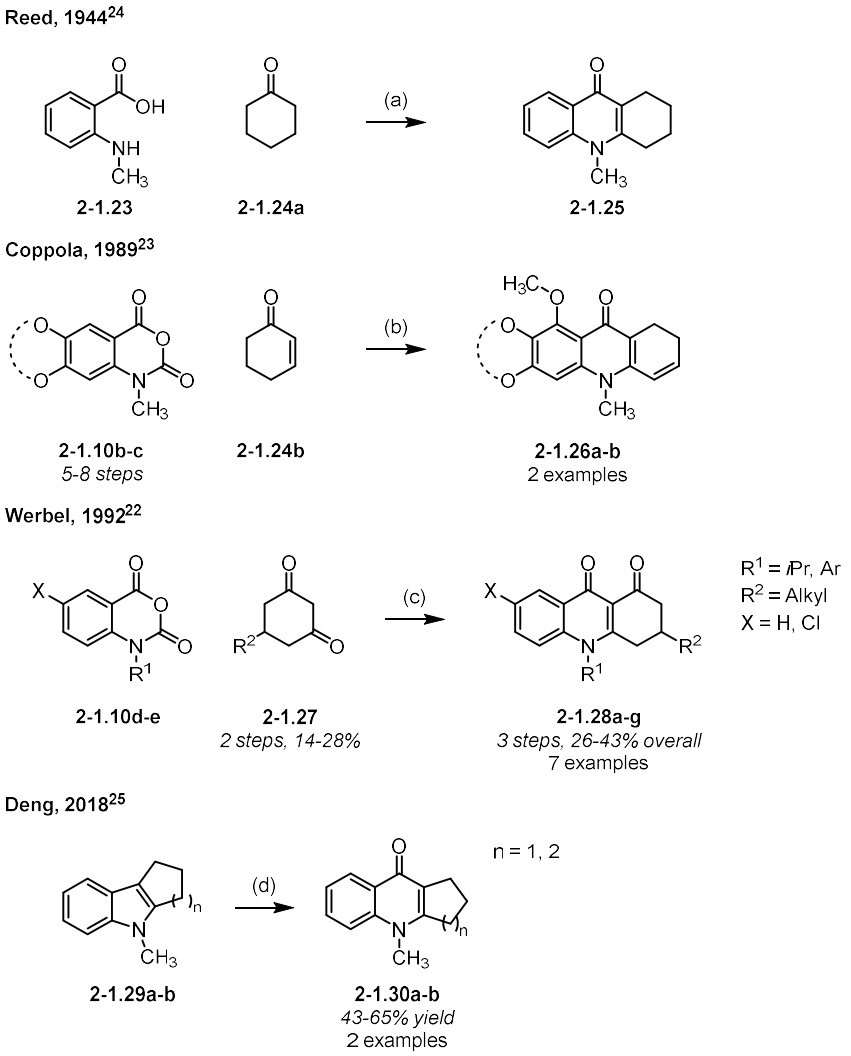

Reagents and conditions: (a) 240°C, 2 h, 60% (b) LDA, THF, -50°C, 6 h, 40-49% (c) NaH, DMF, -10°C to 90°C, 4 h, 26-43% (d) $Ru(bpy)_3*6H_2O$, KOH, O_2, CH_3CN, rt, blue LED, 43-65%.

To prepare a diversified library of ring-fused quinolinones, a comprehensive methodological platform was needed from which to synthesize the scaffold of interest. We expected that synthesis by the addition of an enolate, derived from enolizable substrates of type **2-1.31** and an appropriate base, to an isatoic anhydride (**2-1.10**) would be advantageous (**Figure 2-1.2**). Isatoic anhydrides and enolates are readily available and the approach would form the desired core motif in a single step, accommodate diversification at a variety of positions along the quinolinone scaffold, and could be implemented in a modular way for subsequent medicinal chemistry optimization of hits generated from screening.

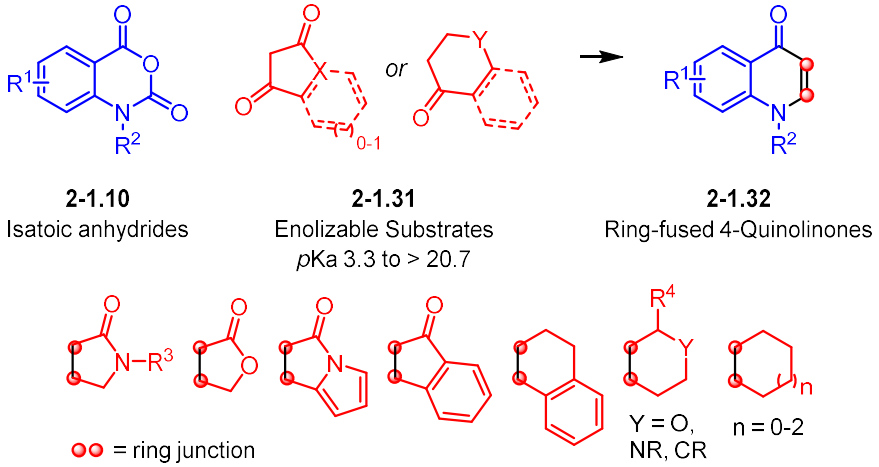

Figure 2-1.2 Proposed approach to a comprehensive synthetic platform for the synthesis of diverse ring-fused *N*-substituted 4-quinolinones.

It was unclear from the precedent literature how to accommodate such a wide range of enolizable substrates; the range of acidities (pK_a) for our desired building blocks spanned a range of more than 17 log units. Questions regarding necessary requisite base strength, reactivity of the generated enolates, and functional group compatibility loomed large. Furthermore, reports of unexplained anhydride (**2-1.10**) degradation to anthranilic acid (**2-1.34**) in Lee's total synthesis, along with a reaction mechanism for which the efficiency-determining steps had not been well

elucidated, called for a better understanding of the prevailing reaction pathways to improve overall reaction outcomes in the context of methodology development (**Figure 2-1.3**).[6]

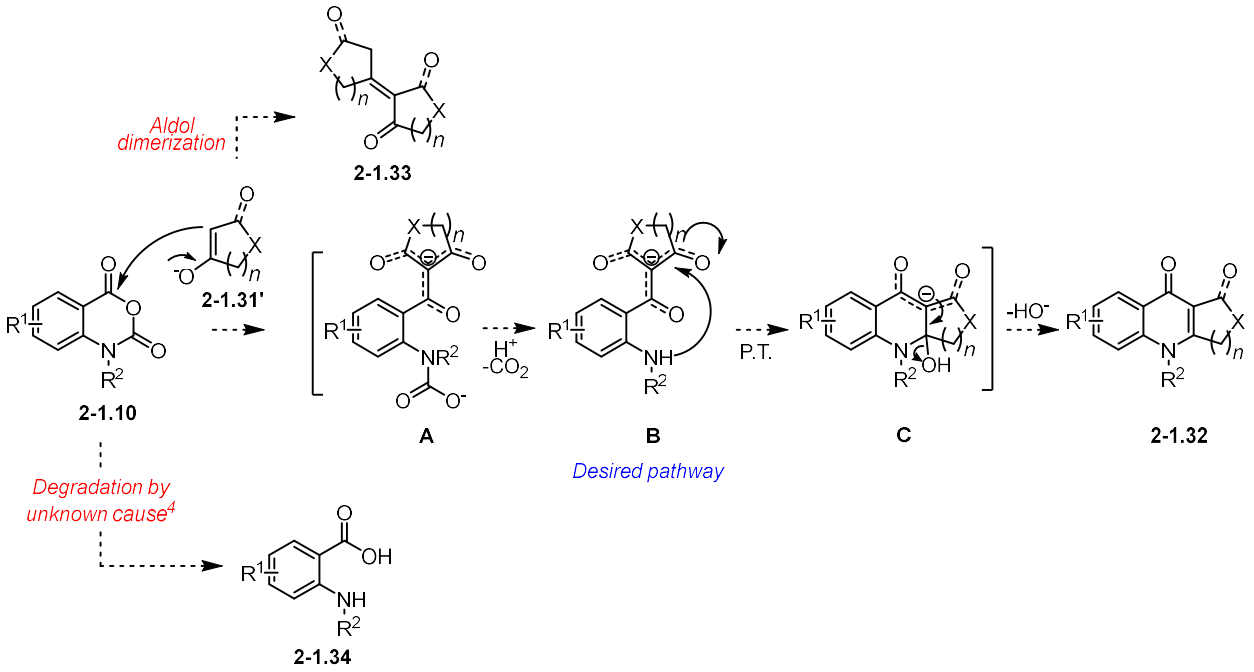

Figure 2-1.3 Mechanism for proposed annulation process between enolates and isatoic anhydrides

The desired reaction to give ring-fused quinolinones **2-1.32** was expected to proceed through a cascade of steps beginning with conversion of the enolizable substrate **2-1.31** to the enolate **2-1.31'** and addition to the anhydride **2-1.10**. Efficient and quantitative formation of the enolate **2-1.31'** was therefore an expected prerequisite and would depend heavily on the choice of base and temperature(s) at which the reaction was carried out. Once formed, however, the enolate must react with the anhydride productively. Addition to another equivalent of **2-1.31** would give the undesired product of aldol dimerization (**2-1.33**) and curtail the desired transformation by unproductive consumption of starting material. Degradation of the anhydride **2-1.10** to **2-1.34** by an unknown cause had already been reported, and we anticipated a need to determine the source of this unproductive process and find ways to circumvent or overcome the problem.[6] Even

successful entry into the desired reaction pathway would not guarantee successful formation of product. Arrest at any of the intermediate steps, for example slow decarboxylation following ring opening of the anhydride by the enolate (**A**), failure to cyclize intramolecularly (**B**), or unsuccessful E1cB elimination of hydroxide (**C**) would have a detrimental impact on our ability to generate quinolinones **2-1.32** efficiently.

Furthermore, given the broad scope of enolate sources and isatoic anhydrides we hoped to use with this method, it was possible that different steps would be problematic in particular cases or substrates but not others. Virtually no reports investigating these challenges to a comprehensive synthetic platform were available prior to this work. We therefore sought to identify the factors influencing successful annulation across the substrate set and to establish a comprehensive synthetic platform for generating ring-fused, *N*-substituted quinolinones that could accommodate a broad range of enolizable starting materials and isatoic anhydrides. This would enable us to reliably synthesize a diverse collection of novel small molecules based on a privileged scaffold template for broad screening and opportunistic development.

Section 2-2: Development of a comprehensive platform for the synthesis of derivatives based on the ring-fused, *N*-substituted 4-quinolinone privileged scaffold

Studies were initiated using commercially available *N*-methyl isatoic anhydride **2-2.1a** and *N*-Boc tetramic acid **2-2.2a**, which could be prepared at multi-gram scale according to a literature procedure (**Scheme 2-2.1A**).[6,28] Lee *et al*'s total synthesis of quinolactacin A2 (**Scheme 2-2.1B**) presented an opportunity to study, optimize, and expand a basic protocol towards a robust, predictable and adaptable transformation. In addition to their use of the same electrophile *N*-methyl isatoic anhydride **2-2.1a**, the enolizable β-ketoester **2-2.4** used by the Lee group represented a close acyclic analog of our chosen prototype starting material *N*-Boc tetramic acid **2-2.2a**. The acidity

of **2-2.4** (calculated pK_a = 10.1 at 25°C, MarvinSketch v18.25) was the lowest of the starting materials studied in literature reports, and the tetramic acid **2-2.2a** is 4-5 orders of magnitude more acidic (calculated pK_a = 3.1 at 25°C, MarvinSketch v18.25). We therefore expected that enolate formation with our tetramic acid of interest would be facile under the reaction conditions reported by Lee *et al*., providing us a convenient starting point for optimization.

Scheme 2-2.1 Quinolinone annulation in the Lee total synthesis of quinolactacin A2 and proposed pilot system for our reaction development

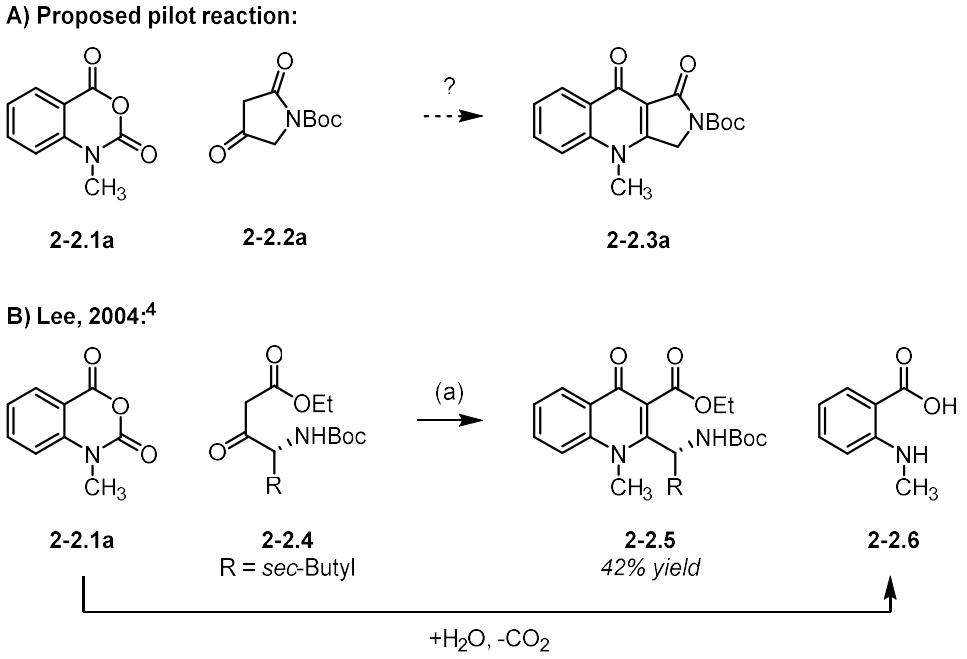

Reagents and conditions: (a) 1,8-diazabicyclo(5.4.0)undec-7-ene (DBU), CH_2Cl_2, 3Å molecular sieves, 20 h.

Our attempts to adapt the previously reported conditions were limited by the scant experimental detail available, but good-faith efforts led to limited quantities of desired product, even at the boiling point of the solvent (CH_2Cl_2, 45°C) (**Table 2-2.1**). Consistent with the preceding work, we observed substantial quantities of *N*-methyl anthranilic acid **2-2.6**, which can result from addition of water to the anhydride starting material **2-2.1a** followed by CO_2 elimination.

Table 2-2.1 Initial attempts to adapt precedent literature conditions

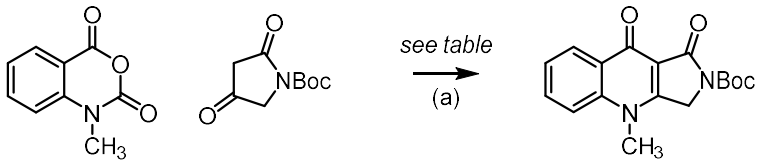

2-2.1a **2-2.2a** **2-2.3a**

Entry	DBU (equiv.)	2-2.1a (equiv.)	2-2.2a (equiv.)	Temperature	2-2.3a Yield
1	1.0	1.3	1.0	23°C	13%
2	1.1	1.3	1.0	45°C	< 25%
3	1.6	1.0	1.5	45°C	10%

Reagents and conditions: (a) DBU, 3Å molecular sieves, CH_2Cl_2, 20 h.

The cause of this unproductive ring-opening of the anhydride had not been previously investigated, so a set of control experiments testing the stability of **2-2.1a** was carried out (**Table 2-2.2**). We evaluated reaction turnover and whether unreacted **2-2.1a** remained when the reaction was carried out in the presence of a variety of bases, with and without the tetramic acid reaction partner **2-2.2a**. Given the acidity of tetramic acid **2-2.2a** compared to the β-ketoester **2-2.4**, we anticipated that a weaker base than DBU might be sufficient for our pilot transformation, enabling us to develop milder conditions for the annulation reaction. Reactions were assessed qualitatively by thin-layer chromatography (TLC) and low-resolution mass spectrometry (MS). The bases were chosen as representative examples within the basicity range required for enolate formation from **2-2.2a**: Because the tetramic acid has a calculated pK_a of 3.1 at 25°C (MarvinSketch v18.25), quantitative enolate formation would be expected using a base with a conjugate acid that has a pK_a of at least 6.1. This is based on a rule of thumb derived from the Henderson-Hasselbalch equation. A difference of 3 units between a given base's conjugate acid pK_a (i.e., pK_aH of the base) and an

acid to be deprotonated (with the lower pK_a) corresponds to an equilibrium ratio of 99.9% to 0.1% in favor of deprotonating the stronger acid (with the lower pK_a).[29]

Table 2-2.2 Control experiments to assess isatoic anhydride compatibility with base

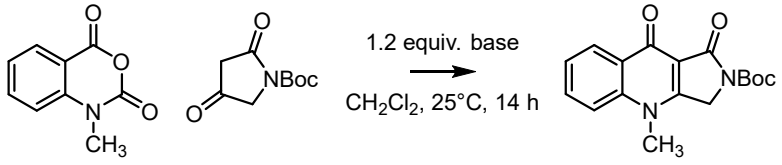

2-2.1a (1.1 equiv.) **2-2.2a** (1.0 equiv.) **2-2.3a**

Entry	Base	Base pK_aH	**2-2.2a** present		**2-2.2a** not present	
			Turnover?	**2-2.1a** remains?	Turnover?	**2-2.1a** remains?
1	NaOEt	15.5	Yes	No	Yes	No
2	DBU	13.5	Yes	No	Yes	No
3	DMAP	9.6	Yes	Yes	No	Yes
4	K_2CO_3	10.3	Yes	Yes	No	Yes
5	Et_3N	10.8	Yes	Yes	No	Yes
6	iPr$_2$NEt	10.8	Yes	Yes	No	Yes

NaOEt: sodium ethoxide, DBU: 1,8-diazabicyclo(5.4.0)undec-7-ene, DMAP: 4-dimethylaminopyridine, K_2CO_3: potassium carbonate, Et_3N: triethylamine, iPr$_2$NEt: diisopropylethylamine

These experiments revealed that anhydride **2-2.1a** was consumed entirely in the presence of DBU (**Table 2-2.2,** entry **2**), with or without the enolizable starting material, tetramic acid **2-2.2a**. This contrasted with almost all of the other bases tested, wherein reaction turnover only occurred when the enolizable starting material was present. The DBU reaction outcomes were similar to those with the negative control, sodium ethoxide, which was expected to degrade the anhydride starting material exclusively with no formation of the desired product (**Table 2-2.2,** entry **1**). Alkoxide bases like sodium ethoxide are known to act readily as nucleophiles and have been used to form anthranilic esters by nucleophilic addition to isatoic anhydrides.[30]

Amidine and guanidine bases, of which DBU is an often-used example, have a rich history of use as nucleophilic acyl transfer catalysts.[31] In some reports, intramolecular trapping of an intermediate cationic DBU-carbonyl adduct can occur if a suitable nucleophilic group is present.[31] We hypothesized that DBU may act as a nucleophile, thereby generating an activated *N*-acyl intermediate **2-2.7**. The fate of this intermediate could well determine the tractability and efficiency of our desired annulation, since it could be hydrolyzed unproductively in the presence of water to give the degradation product *N*-methyl anthranilic acid **2-2.6**, intercepted by an enolate to give the desired product **2-2.3a**, or trapped intramolecularly to form an undesired covalent adduct **2-2.8** (**Figure 2-2.1**).

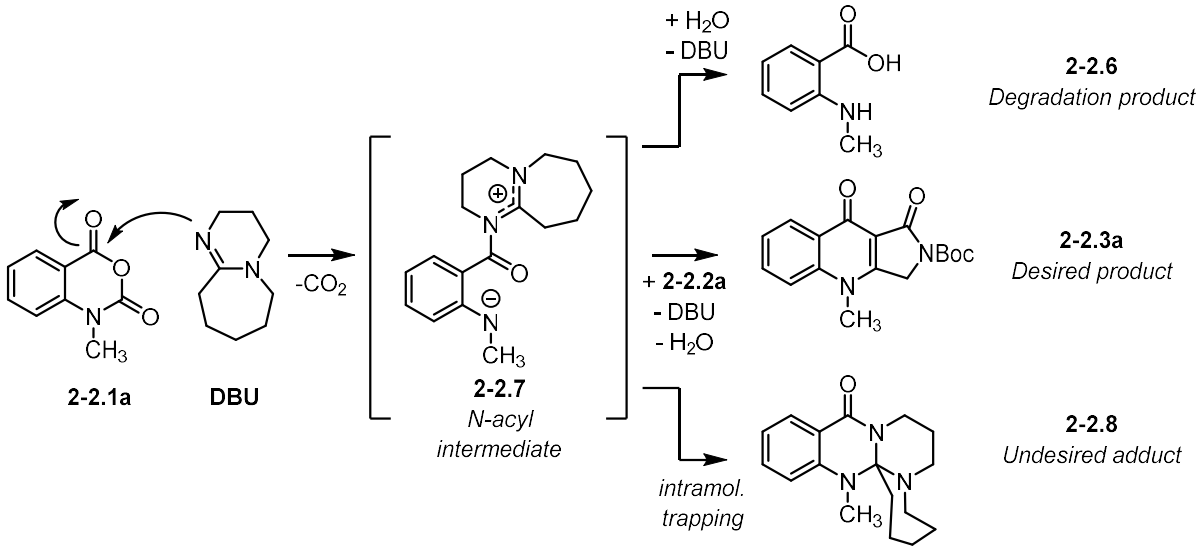

Figure 2-2.1 Reaction outcomes based on fate of a putative *N*-acyl intermediate formed by nucleophilic addition of an amidine base (DBU) to *N*-methyl isatoic anhydride. DBU: 1,8-diazabicyclo(5.4.0)undec-7-ene.

Suspecting that the degradation of the anhydride **2-2.1a** might operate through a mechanism of nucleophilic attack by the base, and realizing that our system possessed a suitable intramolecular trap in the form of an *N*-methyl aniline residue upon decarboxylation of the

anhydride, we sought experimental evidence for formation of a DBU adduct. LC-MS analysis of the reaction mixture revealed a species with a mass-ion pair corresponding to that of the putative DBU adduct **2-2.7** (expected for $[M+H]^+$ = 286.4, observed m/z = 286.1); however, attempts to isolate and characterize the species definitively were unsuccessful. By contrast, substitution of tetramethyl guanidine (TMG), which is of similar nucleophilicity and basicity to DBU, enabled the isolation and characterization of TMG adduct **2-2.9** by nuclear magnetic resonance (NMR) spectroscopy (**Scheme 2-2.3**).[31]

Scheme 2-2.3 Intramolecular trapping of a covalent guanidine base (TMG) adduct

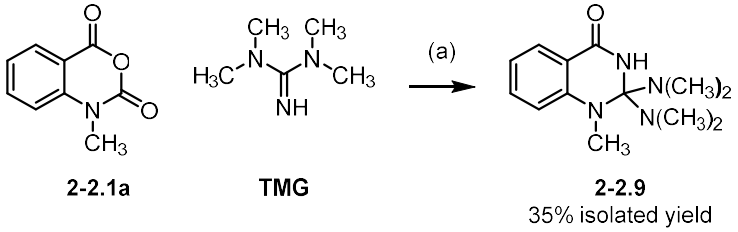

Reagents and conditions: (a) CH_3CN, rt, 15 min, 35%; TMG: tetramethyl guanidine.

It is worth noting that nucleophilic addition of an amidine or guanidine base to the isatoic anhydride was not necessarily a detrimental or unproductive pathway for our transformation, as a species such as **2-2.5** could be an intermediate to our desired product if intercepted by the enolate. We anticipated that such an acyl-transfer catalysis process could be advantageous, and may have prompted the use of DBU in literature reports.[6] However, the reactivity of **2-2.5** might be a double edged sword, in that it can also be easily intercepted by another nucleophile (e.g., water or a tethered amine) to lead to degradation products. With evidence for the suspected degradation mechanism in hand, we attempted the reaction under alternative acyl-transfer catalysis conditions. No evidence of desired product was obtained in the presence of a combination of 4-dimethylaminopyridine (DMAP) and triethylamine (Et_3N) at 45°C. In retrospect, lack of turnover

to the desired product may be due in part to insufficient reaction temperatures, as the subsequent work in this chapter shows that higher temperatures were required for optimal reaction efficiency. However, at the time of reaction screening and optimization, the acyl-transfer catalysis conditions of DMAP and Et_3N remained inferior to other conditions that supported only a base promoted, enolate-driven annulation mechanism. Therefore, acyl-transfer catalysis type conditions were not investigated further. While contributions of an acyl-transfer catalysis mechanism to the desired transformation could not be ruled out, we knew that similar reactions had been reported without an acyl-transfer catalyst.[25] We therefore sought to find conditions under which starting material degradation might be significantly curtailed.

Evidence of the suspected degradation mechanism prompted a search for a less nucleophilic base for this transformation. A multiplex screen using DBU, K_2CO_3, and Et_3N in a variety of solvents revealed evidence of the desired product by low resolution mass spectrometry in the presence of triethylamine and polar aprotic solvents such as DMF and DMSO (**Table 2-2.3**).

Table 2-2.3 Qualitative assessment of product formation in a multiplex solvent & base screen

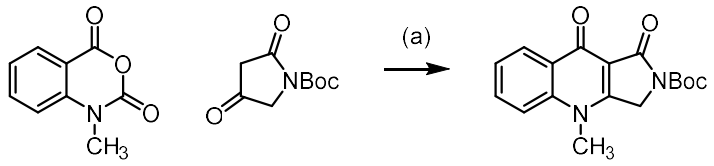

Entry	Solvent	Assessment of product formation by mass spectrometry		
		DBU	K_2CO_3	Et_3N
1	CH_2Cl_2	Not detected	Not detected	Not detected
2	THF	Not detected	Not detected	Not detected
3	Et_2O	Not detected	Not detected	Not detected
4	CH_3CN	Not detected	Not detected	Not detected
5	DMSO	Not detected	Not detected	**Found**
6	DMF	Not detected	Not detected	**Found**
7	$PhCH_3$	Not detected	Not detected	Not detected

Reagents and conditions: (a) 1.1 equiv. **2-2.2a**, 1.2 equiv. base, 0.1 M in dry solvent, 25°C, 15 h.

Having detected putative product in the presence of triethylamine and DMSO, we sought to observe reaction progression more closely using ^{1}H nuclear magnetic resonance spectrometry (NMR). Reaction monitoring using ^{1}H NMR in DMSO-d_6, coupled with increases in reaction concentration to 0.5M and higher equivalency of tetramic acid **2-2.2a** and base (3 equiv. and 4 equiv., respectively) relative to the isatoic anhydride **2-2.1a**, revealed slow conversion at room temperature. This enabled isolation of the desired quinolinone **2-2.3a** in 43% yield and provided a handle for subsequent reaction optimization (**Table 2-2.4**, entry **1**). The increased reaction concentrations and equivalencies motivated a repeated assessment of solvents for this transformation and revealed that these modifications provided a general improvement in isolated yields for all solvents tested. In fact, shorter reaction times at room temperature in a number of solvents (**Table 2-2.4**, entries **2-6**) were possible with comparable yield to the initial DMSO benchmark (**Table 2-2.4**, entry **1**).

Although acetonitrile and dioxane both provided similar yields on initial evaluation (**Table 2-2.4**, entries **5-6**), we observed that starting material solubility was poor in dioxane and therefore explored further modifications of reaction parameters using only acetonitrile. To further reduce the required reaction time, elevated reaction temperatures were assessed. We found that the equivalency of tetramic acid **2-2.2a** relative to the anhydride could be reduced slightly to 2.5 equivalence, and that yields trended generally upwards with increased reaction temperature (**Table 2-2.4**, entries **7-9**). Optimal results were achieved using 4 equivalents of triethylamine and 2.5 equivalents of tetramic acid **2-2.2a** in acetonitrile at 85°C, giving a 95% yield of the desired product **2-2.3a**. For reasons that will become clear further on in the discussion of this work, this procedure was referred to as "Protocol A". Conducting the reaction without molecular sieves had a detrimental effect on yield (**Table 2-2.4**, entry **11**), as did lowering the equivalence of base (**Table 2-2.4**, entries **12-13**) or tetramic acid (**Table 2-2.4**, entries **14-15**).

Table 2-2.4 Selected reaction optimization for the synthesis of **2-2.3a**.

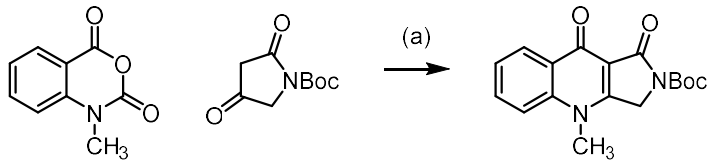

2-2.1a **2-2.2a** **2-2.3a**

Entry	Solvent	Equiv. Et_3N	Equiv. 2-2.2a	Temperature	Time	Yield
1	DMSO	4	3	25°C	240 h	43%
2	CH_2Cl_2	4	3	25°C	96 h	50%
3	EtOAc	4	3	25°C	96 h	34%
4	DMF	4	3	25°C	96 h	51%
5	1,4-Dioxane	4	3	25°C	96 h	62%
6	CH_3CN	4	3	25°C	96 h	61%
7	CH_3CN	4	2.5	35°C	20 h	54%
8	CH_3CN	4	2.6	45°C	18 h	55%
9	CH_3CN	4	2.5	50°C	28 h	68%
10	CH_3CN	4	2.5	85°C	13 h	95%
11	CH_3CN	4	3	85°C	17 h	35%[a]
12	CH_3CN	4	1	85°C	17 h	33%
13	CH_3CN	4	0.5	85°C	17 h	32%
14	CH_3CN	2.2	3	85°C	17 h	34%
15	CH_3CN	0.7	3	85°C	17 h	50%

Reagents and conditions: (a) Et_3N, 3Å molecular sieves, 0.5M in dry solvent, N_2 (g) atmosphere. [a]Reaction conducted without molecular sieves. Reaction completion was assessed by thin-layer chromatography (TLC) for consumption of the anhydride starting material **2-2.1a**.

During the reaction optimization process, various methods for reaction quenching, workup, and product isolation/purification were also surveyed. These experiments revealed that after the conclusion of the reaction and quenching with a strong acid, only two non-aqueous-soluble components were isolated in appreciable quantities: the desired product **2.2-3a**, and an impurity **2-2.10** resulting from dimerization of excess tetramic acid by aldol condensation (**Figure 2-2.2**). The latter is expected to be readily ionizable under basic conditions (lowest calculated pK_a = 6.4 at 25°C) due to extensive delocalization of the resulting negative charge. We reasoned that the

ionized species **2-2.10'** might be water soluble. This insight enabled development of a neutral or weakly basic aqueous reaction quenching procedure, by which **2-2.3a** could be precipitated cleanly and isolated by filtration to afford the desired product without need for column chromatography or other purification methods. To assess the reaction's scalability, it was carried out at 10X the original scale (2.5 mmol) to give **2-2.3a** in 56% isolated yield.

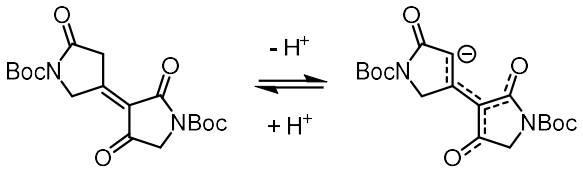

2-2.10 *Non-aqueous-soluble* **2-2.10'** *Aqueous-soluble*

Figure 2-2.2 Aldol condensation dimer **2-2.10** is ionizable, and thus potentially water soluble, under basic conditions

A variety of isatoic anhydrides **2-2.1b-u** were then used to generate a series of *N*-Boc γ-lactam-fused 4-quinolinones **2-2.3b-u** using protocol A (**Scheme 2-2.4**). The reaction afforded 21 examples of quinolinones with a variety of substitutions, although the reaction was less tolerant of electron-rich anhydrides, such as those with methyl or methoxy substituents on the aryl ring. As expected, the electronic effects of substituents on reactivity were most pronounced for substitution corresponding to the 6- and 8-positions of the resulting quinolinone, as these positions contribute most strongly to electrophilicity of the anhydride at its carbonyl group. For example, while the 6-OCH_3 analog **2-2.3o** could only be generated in 18% yield, the 7- OCH_3 substituted analog **2-2.3i** and 5-OCH_3 substituted analog **2-2.3t** were isolated with yields of 54% and 72%, respectively. The 8-CH_3 substituted compound **2-2.3g** was detected only in trace quantities while the corresponding 7-CH_3 substituted analog **2-2.3j** was isolated in 72% yield.

Scheme 2-2.4 Substrate scope of isatoic anhydrides with *N*-Boc tetramic acid using protocol A

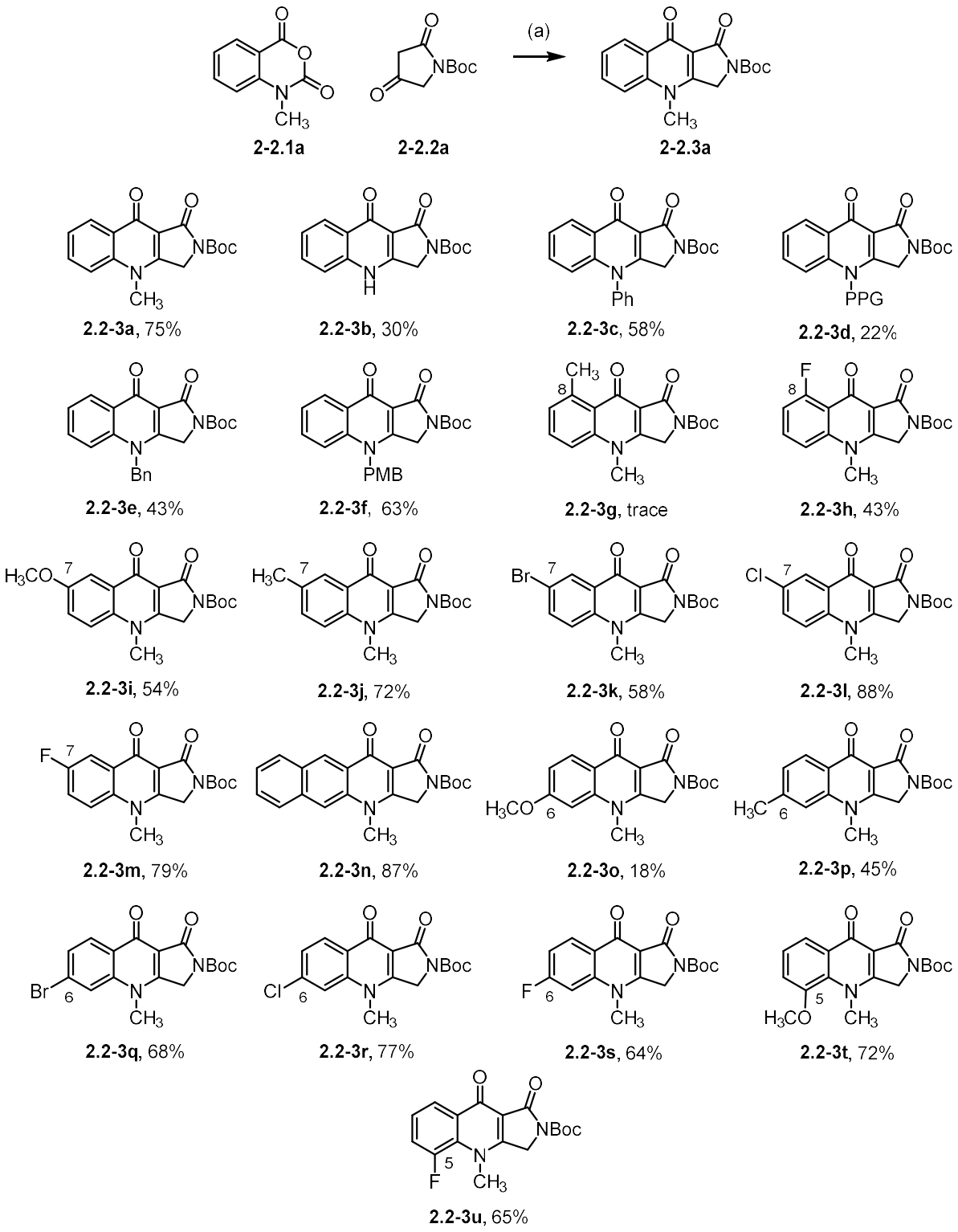

Reagents and conditions: (a) Et_3N, 3Å molecular sieves, CH_3CN, 85°C, 13 h; PPG: propargyl; PMB: *p*-methoxybenzyl.

Substitution of the anhydride nitrogen in the form of aryl or alkyl groups was generally tolerated, although the *N*-propargyl example **2.2-3d** was isolated in only 22% yield. To our surprise, the *N*-H example **2.2-3b** generated from isatoic anhydride could be obtained in 30% yield despite the starting material's pronounced acidity. Notably, *N*-H isatoic anhydrides can be deprotonated at nitrogen and alkylated readily at room temperature in the presence of $i\text{Pr}_2\text{EtN}$, which is a weaker base than the triethylamine used for enolate generation in this procedure ($p\text{K}_a$ of conjugate acids in DMSO = 8.5 and 9.0, respectively).[1,32]

The *N*-Boc quinolinones **2-2.3a-u** were readily deprotected with trifluoroacetic acid, affording the corresponding *N*-H quinolinones **2-2.11a-u** (**Scheme 2-2.5**). The *N*-H quinolinones **2-2.11** could also be isolated without column chromatography or other purification. Concentration of the organic solvent system, followed by trituration with water, enabled isolation of the desired products by vacuum filtration. This effort afforded 19 examples of the ring-fused quinolinone core of interest, with yields of at least 63%, except for compounds **2-2.11b** and **2-2.11d**, which were obtained in 32% and 17% respectively.

Scheme 2-2.5 Generation of *N*-H quinolinones by deprotection of *N*-Boc quinolinones

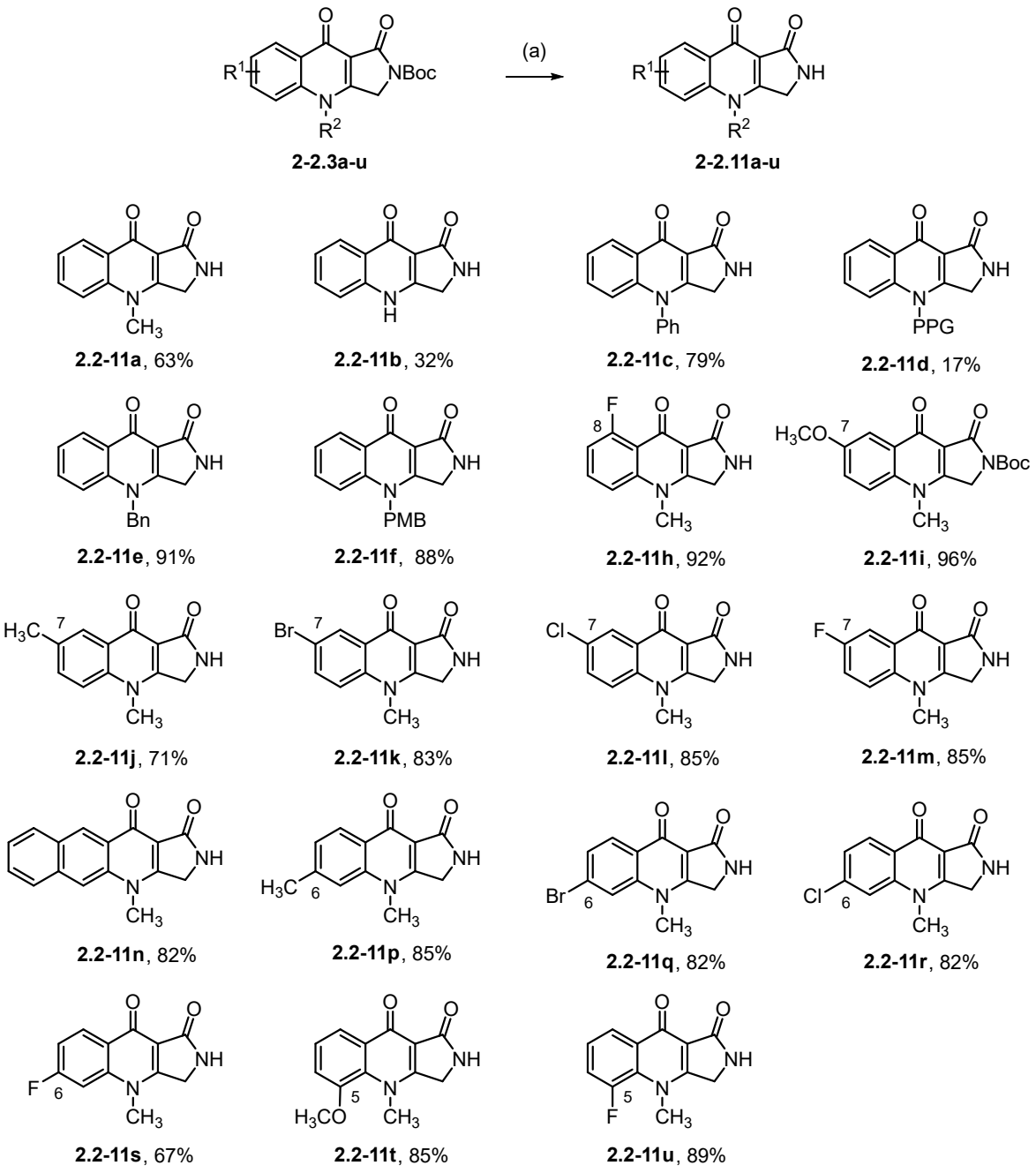

Reagents and conditions: (a) 1:15 TFA/CH_2Cl_2, 0°C to rt, 20 min; PPG: propargyl; PMB: *p*-methoxybenzyl.

Next, we sought to explore the use of other enolizable building blocks under the optimized reaction conditions. We anticipated that reduced starting material acidity might have a negative impact on reaction efficiency. Several substrates with calculated pK_a values higher than that of *N*-Boc tetramic acid **2-2.2a** were selected to test the hypothesis (**Table 2-2.5**). We found that yields of the resulting products were poor using protocol A for these less acidic substrates ($pK_a \geq 6.6$), such as *N*-phenyl tetramic acid **2-2.2b** to give **2.2-11** or *N*-benzyl tetramic acid **2-2.2c** to give **2.2-12a**.

We hypothesized that the drop in reaction efficiency could be attributed to a temperature effect on base strength in our reaction system. A general rule of thumb based on the Henderson-Hasselbalch equation holds that for efficient enolate generation, the pK_aH of the base employed must be ≥ 3 units higher than the pK_a of the enolizable starting material.[29] Indeed, the calculated pK_aH value of each of the starting materials was within the requisite range for enolate formation at room temperature in the presence of triethylamine (**Table 2-2.5**). However, the calculated pK_aH of triethylamine is reduced by 1.5 units at the reaction temperature of 85°C. This reduction in pK_a with increased temperature is a general one, but the effect is less pronounced in the enolizable starting materials (i.e., most compounds experience an increase in acidity or attenuation of basicity at elevated temperature, but the starting materials are predicted to be less strongly affected). We reasoned this renders triethylamine too weak to form the corresponding enolates leading to products **2-2.15** – **2.2-19** under the reaction conditions (85°C).

Table 2-2.5 Calculated pK_a for starting materials and conjugate acids of bases used for enolization at varying temperature

Entry	Starting Material	pK_a (25°C)[a]	pK_a (85°C)[a]	Product	Protocol A Yield[b]
1	Et_3NH^+	10.2	8.7	-	-
2	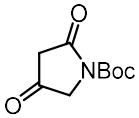 **2-2.2a**	3.1	3.3	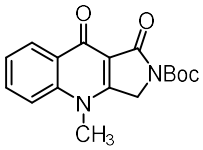 **2-2.3a**	95%
3	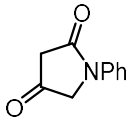 **2-2.2b**	7.1	6.7	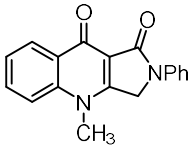 **2-2.15**	< 28%
4	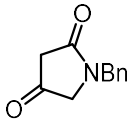 **2-2.2c**	7.3	6.8	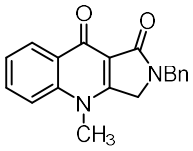 **2-2.16a**	trace
5	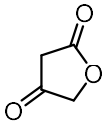 **2-2.12**	7.0	6.6	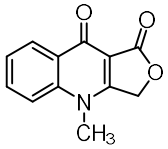 **2-2.17**	47%
6	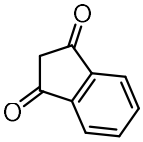 **2-2.13**	7.2	6.7	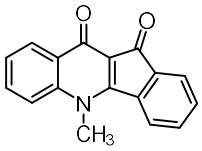 **2-2.18**	42%
7	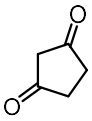 **2-2.14a**	8.3	7.6	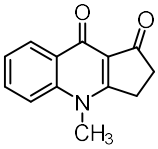 **2-2.19**	24%
8	$DBUH^+$	11.3	9.6	-	-

[a]Calculated pK_a values determined using MarvinSketch v18.25. [b]Isolated yields.

We expected that switching from triethylamine to a stronger base might enable the desired transformation for substrates with a predicted $pK_a > 5.7$ at 85°C. Using *N*-benzyl tetramic acid **2.2-2c** as a test case, we found that a switch to DBU ($pK_aH = 9.6$ at 85°C) was sufficient to provide **2.2-16a** in 31% yield (**Table 2-2.6**, entry **2**). This enabled subsequent optimization to a second set of reaction conditions that accommodated starting materials with $pK_a > 5.7$ at 85°C.

From our prior study on the optimization of reaction conditions for synthesis of **2.2-3a**, we realized that using DBU would necessitate balancing **2-2.1a** degradation by DBU with the desired enolate formation. We were encouraged by the possibility that the stronger enolate used here for synthesis of **2.2-16a** might compete more effectively for any reactive *N*-acyl intermediate that formed. Our experiments showed that using the anhydride **2-2.1a** in excess and the tetramic acid **2-2.2c** as the limiting reagent provided a substantial improvement in yield for the desired product **2-2.16a** (**Table 2-2.6**, entry **5**). This is at least in part due to enabling a smaller quantity of base to be used, which we know can degrade the anhydride material. Furthermore, the stronger enolate appears to react faster and at lower temperature, enabling a lower temperature and greatly reduced reaction duration. Thus using the tetramic acid as the limiting reagent, with DBU as the base in CH_3CN at 50°C for 2 hours (protocol B) enabled isolation of the *N*-benzyl lactam-fused quinolinone **2.2-16a** in 77% yield after routine column chromatography.

Table 2-2.6 Selected reaction optimization for the synthesis of **2-2.16a**

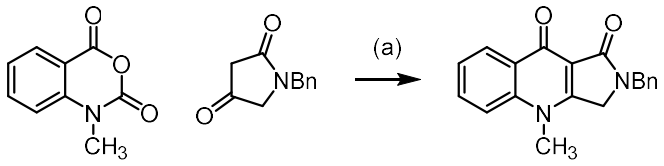

2-2.1a **2-2.2c** **2-2.16a**

Entry	Base	Equiv. base	Equiv. 2-2.2c	Temperature	Time	Yield[a]
1	Et_3N	2.5	2.5	85°C	13 h	Trace
2	DBU	4	3	85°C	13 h	31%
3	DBU	4	1.2	85°C	13 h	39%
4	DBU	2	2.5	85°C	13 h	47%
5	DBU	2	0.5	50°C	2 h	77%

Reagents and conditions: (a) Base, 3Å molecular sieves, 0.5M in dry CH_3CN; [a]Isolated yield; DBU: 1,8-diazabicyclo(5.4.0)undec-7-ene.

With protocol B in hand, we attempted to revisit the synthesis of **2.2-3a** and were surprised to find that it could only be obtained in 29% yield when using the new procedure that relied on DBU as the base. We suspected that acidity of **2.2-3a** at C3 could mediate product degradation in the presence of a sufficiently strong base, such as DBU. Indeed, the calculated pK_a at C3 of **2.2-3a**, but not **2.2-16a**, at 50°C was sufficiently low compared to that of DBU for deprotonation to occur (**Table 2-2.7**). Additionally, the calculated pK_a at C3 of **2-2.3a** was sufficiently high (8.7) that deprotonation by Et_3N at 85°C would not be expected to occur readily.

Table 2-2.7 Table of calculated pK_a values for substrates and comparative yields of synthesis by different protocols

Entry	Compound	pK_a (50°C)[a]	pK_a (85°C)[a]	Protocol A Isolated Yield[b]	Protocol B Isolated Yield[c]
1	$DBUH^+$	10.5	-	-	-
2	Et_3NH^+	-	8.7	-	-
3	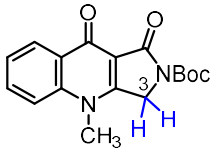 **2-2.3a**	9.2	8.7	95%	29%
4	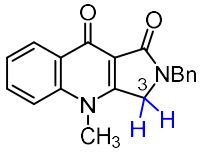 **2-2.16a**	11.8	6.8	Trace	77%

[a]Calculated pK_a values determined using MarvinSketch v18.25. [b]Protocol A conditions: Et_3N, 3Å molecular sieves, CH_3CN, 85°C, 13 h; [c]Protocol B conditions: DBU, 3Å molecular sieves, CH_3CN, 50°C, 2 h.

To test our hypothesis that DBU was degrading **2-2.3a** by deprotonation at C3 and leading to inferior yields of product under protocol B despite the base being strong enough to form the enolate of *N*-Boc tetramic acid **2-2.2a** (pK_a = 3.2 at the protocol B reaction temperature of 50°C), a pure sample of **2.2-3a** was subjected to the reaction conditions and monitored by ^1H NMR (**Figure 2-2.3**). These experiments revealed signal broadening and disappearance of the C3 methylene ^1H resonance, followed by compound degradation, in the presence of DBU but not Et_3N. Furthermore, only 20% of **2-2.3a** could be recovered from the DBU experiment, further supporting our hypothesis that the more acidic starting material **2-2.2a** leads to quinolinones of type **2-2.3** that are more acidic at C3 and therefore incompatible with the stronger base conditions (DBU) of protocol B due to subsequent product degradation. This is in contrast to less acidic enolizable starting materials like *N*-benzyl tetramic acid **2-2.2c** (pK_a > 5.7 at 85°C), which require a stronger

base to drive the desired reaction, giving products of type **2-2.16**, which are less prone to degradation due to the C3 carbon being less susceptible to deprotonation and are therefore compatible with using DBU as a base.

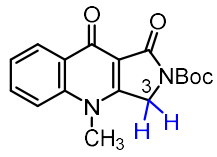

2-2.3a

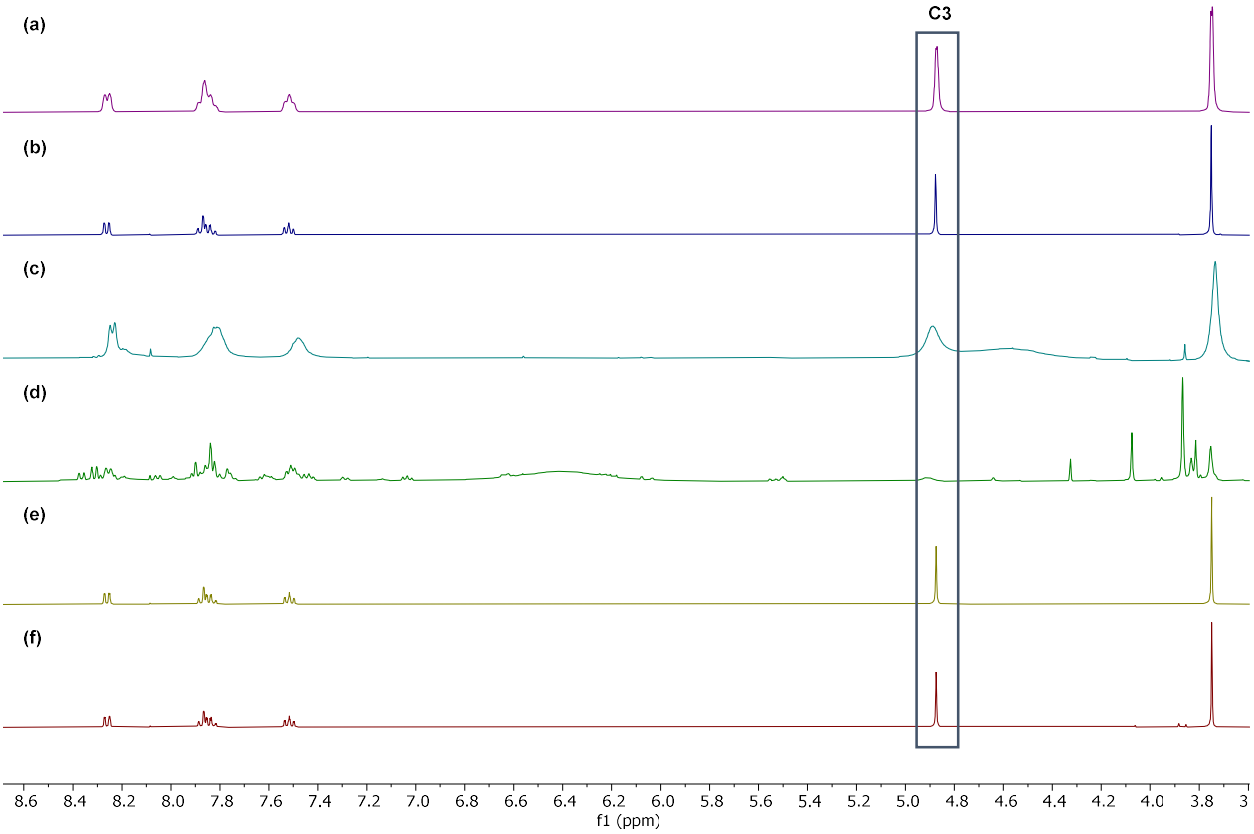

Figure 2-2.3 ^{1}H NMR spectra of **2-2.3a** in DMSO-d_6: (a) No base, 25°C, 16 h (b) No base, 85°C, 16 h (c) DBU, 25°C, 15 min (d) DBU, 85°C, 16 h (e) Et_3N, 25°C, 15 min (f) Et_3N, 85°C, 16 h

With these protocols in hand, and an understanding of the limitations for each procedure with respect to the enolizable starting material being used, we examined the scope of the DBU-promoted protocol B using *N*-benzyl tetramic acid **2-2.2c** with a variety of isatoic anhydrides to

give **2-2.16a-u** (**Scheme 2-2.6**). The desired products were obtained in good yield and with broad tolerance for anhydride substitution. A notable difference between the anhydride compatibility for protocol A (using Et_3N and *N*-Boc tetramic acid **2-2.2a** to synthesize the first set of compounds, **2-2.3a-u**) and protocol B (using DBU and *N*-benzyl tetramic acid **2-2.2c** to form **2-2.16a-u**) was observed in that the latter showed a greater tolerance for electron rich anhydrides, presumably due to the presence of a stronger and more reactive enolate when using DBU to drive reactivity of compounds with a $pK_a > 5.7$ at 85°C. For example, while the *N*-Boc, 6-OCH_3 quinolinone **2-2.3o** was only obtained in trace quantities using the Et_3N conditions (protocol A), the corresponding *N*-Bn, 6-OCH_3 **2-2.16o** was isolated in 70% yield using the DBU-mediated conditions (protocol B).

Scheme 2-2.6 Substrate scope of isatoic anhydrides with *N*-benzyl tetramic acid using DBU-mediated conditions

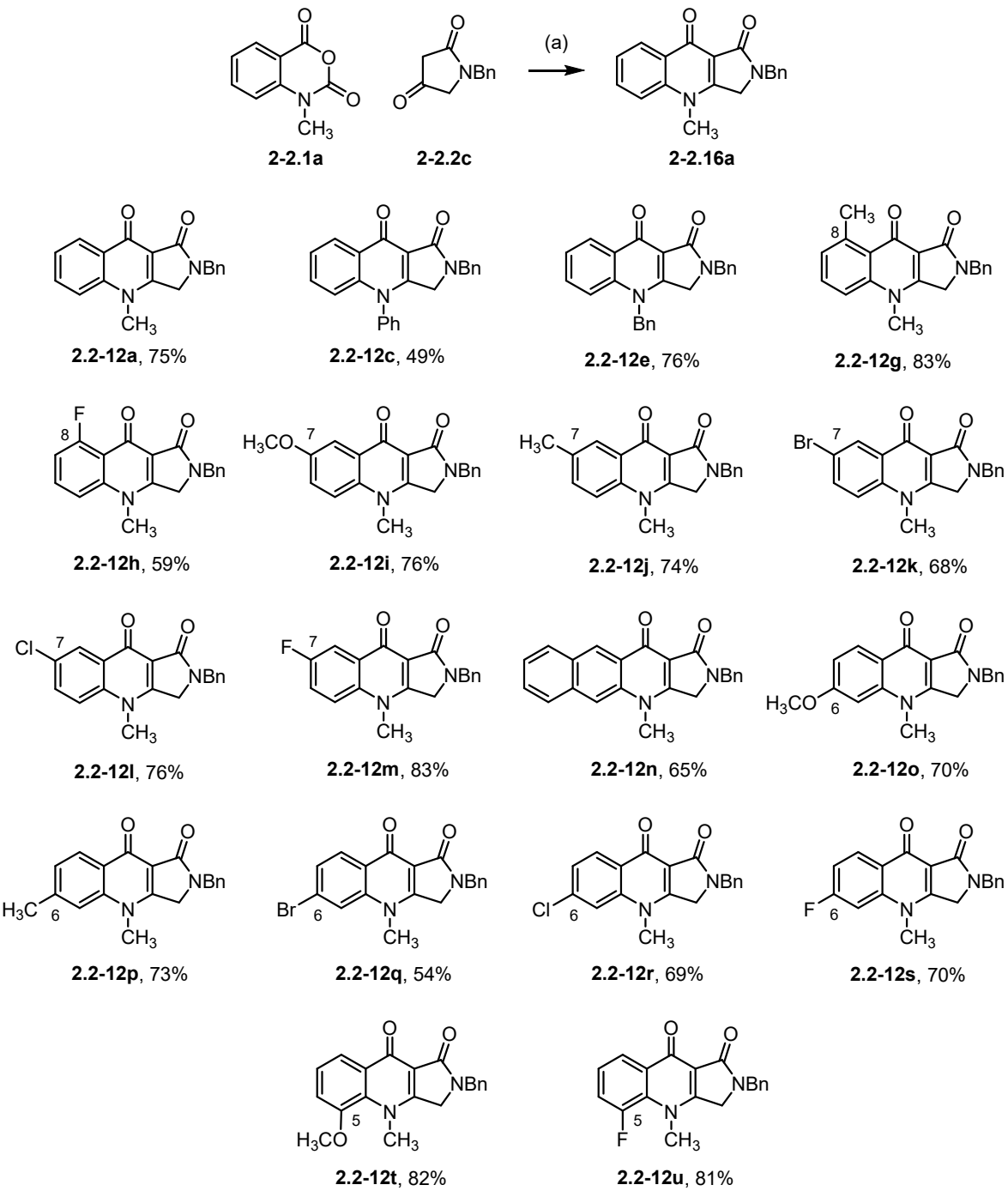

Reagents and conditions: (a) DBU, 3Å molecular sieves, CH_3CN, 50°C, 2 h.

In addition to the 18 examples thus obtained, the DBU-mediated conditions (protocol B) were used to access compounds **2.2-15**, **2.2-18**, and **2.2-20** – **2.2-22** in good yield (**Scheme 2-2.7**). Thus for less acidic building blocks (pK_a > 5.7 at 85°C) the second method using DBU as a base provides a substantial improvement in reaction efficiency, since enolate formation is more favorable with the stronger base, as long as the resulting products are stable (C3 pK_a > 10.5 at 50°C). For example, yields of **2-2.15** and **2.2-18** improved from <28% and 42%, respectively, when synthesized via protocol A (Et_3N-mediated) to 71% and 67%, respectively, when synthesized via protocol B (DBU-mediated). The expansion of compatible substrates represented an important feature for our synthetic platform, as it made accessible an even more diverse set of possible molecular templates based on the ring-fused quinolinone scaffold.

Scheme 2-2.7 Use of DBU-mediated reaction conditions gives improved yields of quinolinones from less enolizable starting materials

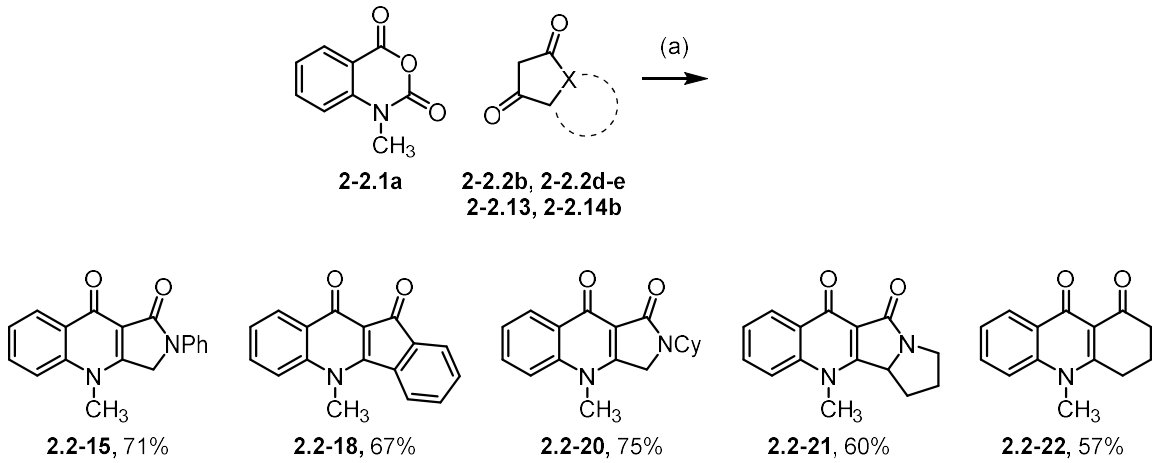

Reagents and conditions: (a) DBU, 3Å molecular sieves, CH_3CN, 50°C, 2 h.

We sought to further expand the scope of enolizable substrates usable in our methodology by developing a protocol that could accommodate ketones. Such building blocks are commercially ubiquitous but are many orders of magnitude less acidic than the starting materials thus far

described (calculated pK_as = 16.6 to 20.7). Literature precedents for similar transformations are reported using very strong, pyrophoric bases such as lithium diisopropylamide (LDA), or a combination of *n*-butyllithium (*n*BuLi) and tetramethylethylenediamine (TMEDA).[13,25] In an attempt to develop slightly milder conditions, and with the importance of base nucleophilicity to starting material integrity in mind, as well as concern for the stability of our desired products to excessive base strength, we explored the use of lithium bis(trimethylsilyl)amide (LiHMDS), a weaker and less nucleophilic base than those used in previous reports. Using ketone **2-2.23a** as the prototypical enolizable partner, we screened conditions using toluene as a solvent due to the incompatibility of CH_3CN with bases possessing a $pK_aH > 19$. Rewardingly, the desired product **2-2.24a** was obtained in 51% yield under the initial conditions and further optimization to 84% was possible using elevated temperature and a small change in reactant equivalencies (**Table 2-2.8**). In this case, resuming use of isatoic anhydride **2-2.1a** as the limiting reagent was preferable, likely due to reduced base-mediated degradation. With the LiHMDS-mediated set of reaction conditions (protocol C), a diverse set of carbocycle-fused derivatives could then be obtained (**Scheme 2-2.8**).

Table 2-2.8 Reaction optimization for a ketone-compatible protocol

2-2.1a **2-2.23a** **2-2.24a**

Entry	Equiv. base	Equiv. 2-2.23	Temperature	Time	Yield
1	1.3	1.4	25°C	4 h	51%
2	1.3	1.4	110°C	4 h	56%
3	2.5	2.7	25°C	2 h	75%
4	2.1	2.3	80°C	2 h	84%

Reagents and conditions: (a) LiHMDS, 3Å molecular sieves, 0.5M in dry $PhCH_3$.

Scheme 2-2.8 Representative examples for scope of derivatives using LiHMDS conditions[a]

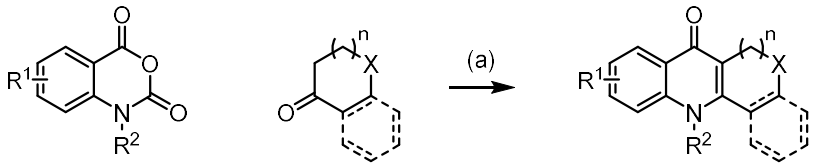

2-2.1a, e-f, h-i, l-m, s, u-x **2-2.23a-j** **2-2.24a-n, 2-2.25 - 2-2.31**

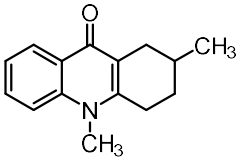

2-2.24a, 84%

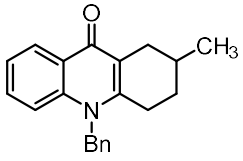

2-2.24b, 73%

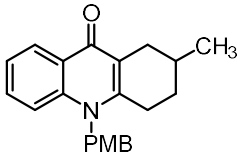

2-2.24c, 74%

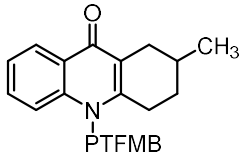

2-2.24d, 70%

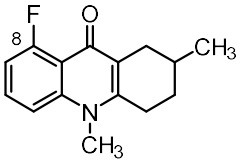

2-2.24e, 63%

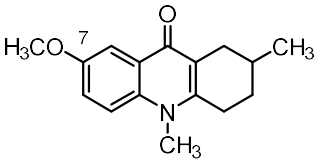

2-2.24f, 90%

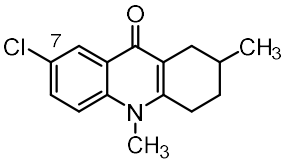

2-2.24g, 65%

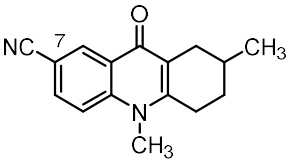

2-2.24h, 72%

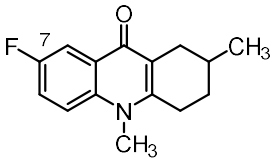

2-2.24i, 72%

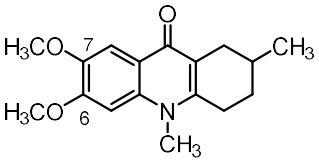

2-2.24j, 32%

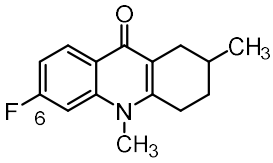

2-2.24k, 56%

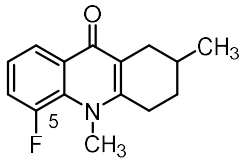

2-2.24l, 69%

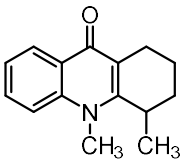

2-2.24m, 78%

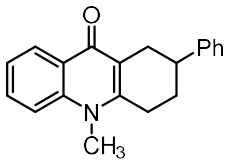

2-2.24n, 80%

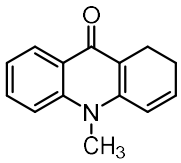

2-2.25, 65%

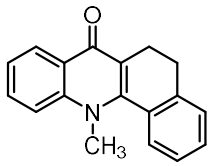

2-2.26, 65%

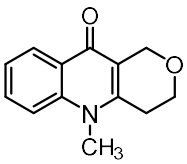

2-2.27, 90%

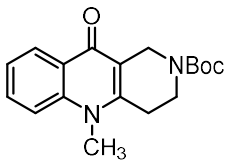

2-2.28, 78%

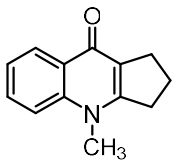

2-2.29, 45%

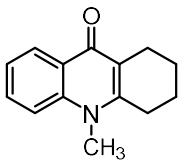

2-2.30, 74%

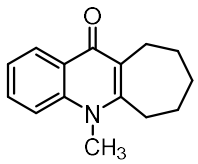

2-2.31, 39%

Reagents and conditions: (a) LiHMDS, $PhCH_3$, 0°C - 80°C, 2 h; PMB: *p*-methoxybenzyl; PTFMB: *p*-trifluoromethylbenzyl. [a]This work was performed by Dr. Satish Chandra Philkhana

Once again, we observed that increased enolate strength led to a greater tolerance for electron rich anhydrides. For example, the di-OCH_3 derivative **2-2.24j** was obtained in 32% yield. Although this is a relatively low yield compared to the overall set, the corresponding *N*-Boc or *N*-benzyl lactam-fused derivatives are unobtainable via protocols A (with Et_3N) or B (with DBU), respectively, presumably because the anhydride is insufficiently reactive and the enolates involved are too weak to compensate. However, with a sufficiently strong enolate partner, as when LiHMDS is used to form the enolate of a ketone, the transformation proceeded to the desired product. A total of 25 examples were synthesized using protocol C.

These combined efforts provided a general approach to the synthesis of *N*-substituted ring-fused quinolinones by base-promoted annulation of enolates with isatoic anhydrides. Choosing an appropriate protocol that relied on a particular base for the transformation depended on the acidity of both the enolizable starting material and the resulting product. The protocol selected needed to use a base that was strong enough to efficiently form enolate, but not so strong that it would degrade the starting material or the resulting desired product. Though we understood the underlying basis for the complementarity of our methods, we sought to develop a framework that enabled efficient protocol selection *a priori* given a new enolate of interest. This was necessary to increase the utility of our methodology, because some enolizable building blocks are more costly or limited in quantity than others and empirical determination of the optimal protocol in parallel might not always be practical. We found that an enolizable starting material's calculated pK_a correlated well with the calculated pK_a of the labile proton in the corresponding product for those with a susceptible acidic proton and can therefore be used as an indicator for both its ability to react in the presence of a given base and the stability of the resulting product (**Table 2-2.9**).

Table 2-2.9 Calculated pK_a of enolizable starting materials and corresponding products under reaction conditions for different protocols

Entry	Starting Material	Calculated pK_a under reaction conditions[a] for protocol:			Product	Calculated pK_a under reaction conditions[a] for protocol:		
		(A)	**(B)**	**(C)**		**(A)**	**(B)**	**(C)**
1	Et_3NH^+	8.7	-	-	-	8.7	-	-
2	$DBUH^+$	-	10.5	-	-	-	10.5	-
3	HMDS	-	-	25	-	-	-	25
4	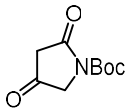 **2-2.2a**	3.3	3.2	3.3	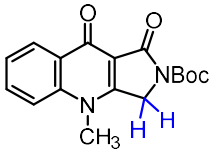 **2-2.3a**	8.7	9.2	8.9
5	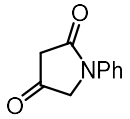 **2-2.2b**	6.7	6.9	6.7	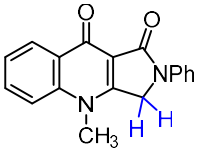 **2-2.15**	10.3	11.0	10.4
6	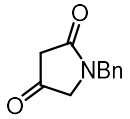 **2-2.2c**	6.8	7.0	6.8	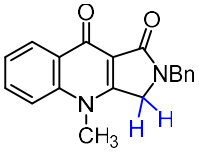 **2-2.16a**	11.1	11.8	11.2
7	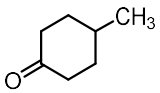 **2-2.23a**	17.5	18.9	17.7	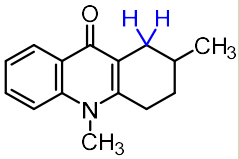 **2-2.24a**	25.5	27.8	25.8

[a]Reagent and conditions: (A) *N*-methyl isatoic anhydride, Et_3N, 3Å molecular sieves, CH_3CN, 85°C, 13 h (B) *N*-methyl isatoic anhydride, DBU, 3Å molecular sieves, CH_3CN, 50°C, 2 h (C) *N*-methyl isatoic anhydride, LiHMDS, $PhCH_3$, 0°C - 80°C, 2 h. Green highlight: compatible, orange highlight: incompatible.

From this analysis, we determined that starting materials with a calculated pK_a of 3.3-6.3 at 85°C were compatible with conditions using Et_3N (protocol A), while materials with a calculated pK_a in the range 6.3-7.9 at 50°C were compatible with conditions using DBU (protocol B), and

materials with pK_a 16.6-20.7 were compatible with the LiHMDS-mediated conditions (protocol C). Given the closeness of the ranges for protocols A and B, we verified our conclusions by subjecting several enolizable starting materials with different pK_a values to both protocols and compared the yields of desired product (Table **2.2-10**).

Table 2.2-10 Results using Et_3N- or DBU-mediated conditions and comparison to predicted best

Entry	Starting Material	Predicted Best Protocol[a]	Product	Protocol A Yield	Protocol B Yield
1	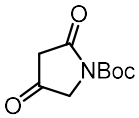 **2-2.2a**	(A)	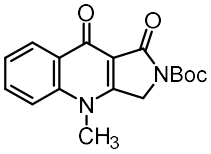 **2-2.3a**	95%	29%
2	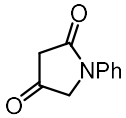 **2-2.2b**	(B)	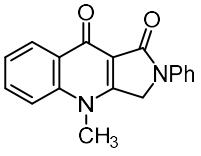 **2-2.11**	<28%	71%
3	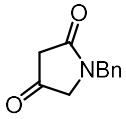 **2-2.2c**	(B)	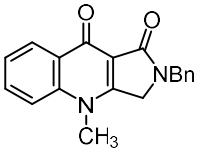 **2-2.16a**	Trace	77%
4	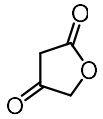 **2-2.12**	(B)	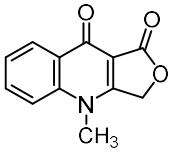 **2-2.16**	47%	10%
5	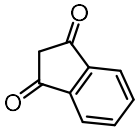 **2-2.13**	(B)	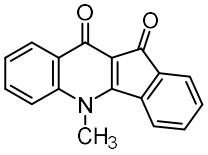 **2-2.17**	45%	67%

Reagents and conditions: (A) *N*-methyl isatoic anhydride, Et_3N, 3Å molecular sieves, CH_3CN, 85°C, 13 h (B) *N*-methyl isatoic anhydride, DBU, 3Å molecular sieves, CH_3CN, 50°C, 2 h.

With the exception of tetronic acid **2-2.13**, all the starting materials gave the best yields when subjected to the reaction conditions predicted by our pK_a range guidance. The apparent inconsistency with formation of **2-2.16** can be explained by precipitation of the product from solution in protocol A, which is expected to drive the reaction forward despite a less acidic starting material being used with triethylamine. By contrast, though enolization occurs readily in protocol B, the resulting product appears unstable to the stronger base, as exemplified by only 34% recovery of when pure **2-2.16** is subjected to the reaction conditions. With this pK_a-based protocol selection system in hand, we expected that future syntheses could be effectively guided to the optimal conditions with minimal resource expenditure.

Section 2-3: Total Synthesis of Penicinotam

To further demonstrate the utility of our methodology we pursued a total synthesis of penicinotam, an insecticidal natural product derivative with a synthetically challenging and structurally interesting fused tetracyclic core.[10,11,22] Retrosynthetic analysis of penicinotam in light of our recent work led to the simple disconnection of penicinotam to the starting materials **2-3.2** (commercially available) and **2-3.3** (previously reported), potentially furnishing the desired product in a single step (**Scheme 2-3.1**).

Scheme 2-3.1 Structure and initial retrosynthetic analysis of penicinotam by base-promoted annulation

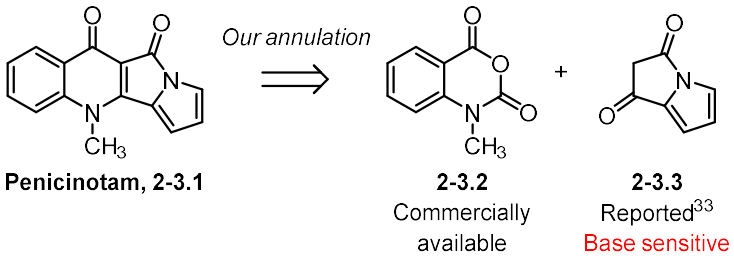

Though this was attractive in theory, it hinged on access to **2-3.3** for use as the enolizable building block in our annulation. The extant literature regarding **2-3.3** consists of a single report of its synthesis in 3 steps, which required flash-vacuum pyrolysis, and documented its extensive reactivity, including a marked instability in the presence of even minute quantities of mild base.[33] This was a nonstarter for our use in our methodology, which is predicated on a base-promoted annulation to access the central core. Instead, we envisioned assembling the tetracyclic skeleton from the alicyclic lactam **2-3.6**, which can be obtained commercially (albeit expensively) or synthesized from proline, and does not suffer from the same sensitivity to base (**Scheme 2-3.2**).[11]

Scheme 2-3.2 Updated retrosynthesis of penicinotam with more base-stable starting materials

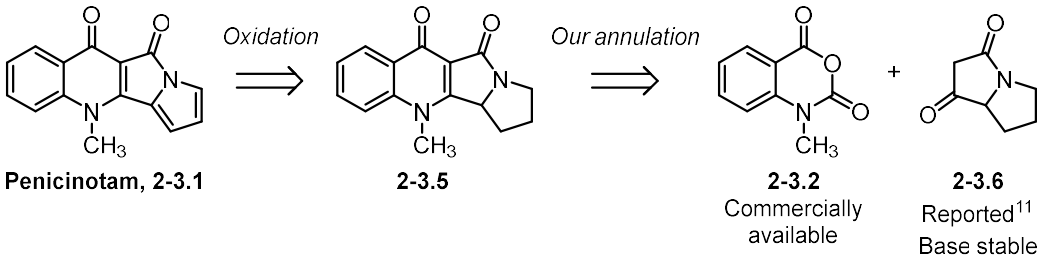

Interestingly, our key proposed intermediate **2-3.5** had previously been synthesized in 10 steps in a 2001 report by Tatsuta et al. as an analog in their biomimetic synthesis of quinolactacin B. Annulation to form the quinolinone was achieved in the two final steps of the synthesis after a lengthy, linear route to the intermediate **2-3.7** (**Fig. 2-3.3**).[17] This predated the report in which Shao et al. discovered penicinotam via dehydration of penicinoline isolated from a *Penicillium* species in 2010, as well as the discovery of the *N*-unsubstituted natural product quinolactacide **2-3.11** by Abe and coworkers in 2005.[10,34] Subsequent work by Abe et al. detailed a seven step synthesis of quinolactacide relying on formation of the contiguous tetracyclic core in two steps from **2-3.8**, followed by oxidation with MnO_2 in 21% yield to aromatize the lactam moiety and arrive at their

target.[11] Despite a relatively low yield for the final oxidation, we anticipated the transformation of **2-3.10** to quinolactacide **2-3.11** might provide a basis for optimization in the development of the endgame of our synthesis (i.e., oxidation of **2-3.5** to penicinotam **2-3.1**).

Scheme 2-3.3 Precedents in the synthesis of penicinotam-related structural motifs

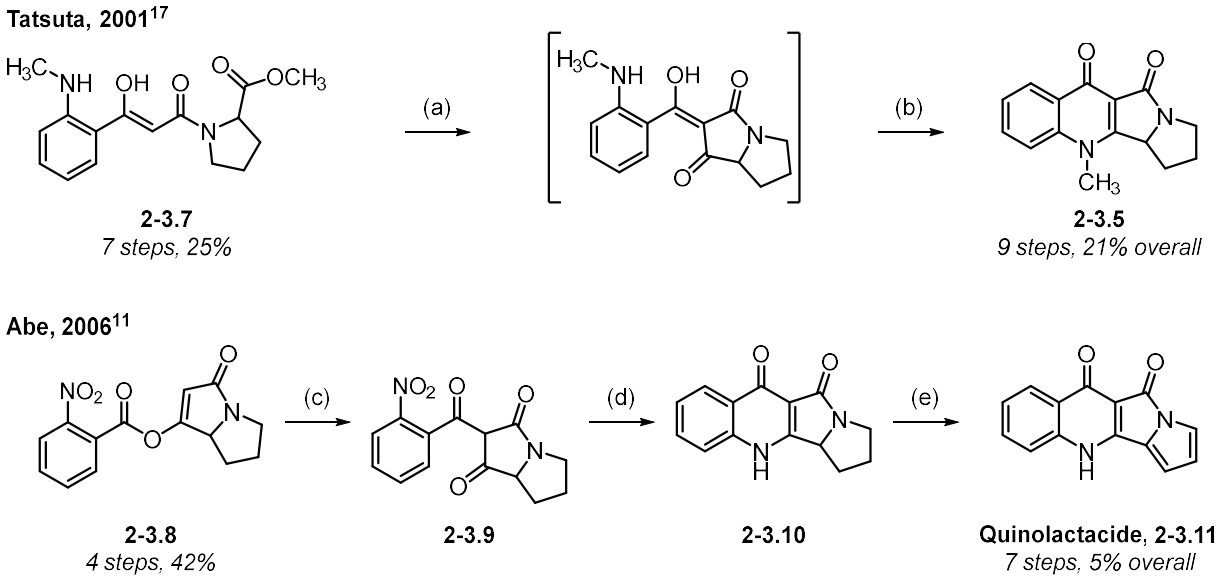

Reagents and conditions: (a) $NaOCH_3$, MeOH, rt, 12 h (b) AcOH, rt, 30 min, 84% over 2 steps (c) Acetone cyanohydrin, Et_3N, CH_3CN, quant. (d) H_2, Pd-C, MeOH, 52% (e) MnO_2, 3:1 $CHCl_3$/DMF, reflux, 21%.

Our route using **2-3.6** as the enolizable starting material would comprise a three step synthesis of penicinotam, which was attractive when compared to prior total syntheses of penicinotam from commercial materials, both in terms of starting material and step count economy, with the potential to reduce the synthetic steps by at least half (**Fig. 2-3.4**).[22,23] Only two routes to penicinotam itself have been previously reported, both are relatively recent having been published while our initial methodology development on quinolinones was underway. The Shao *et al.* synthesis (8 total steps, 7% yield overall) mimicked conditions from their original serendipitous discovery of penicinotam nearly a decade earlier, relying on conversion of penicinoline ethyl ester

2-3.15, which must be synthesized in 7 steps.[23] Meanwhile the Doi *et al.* report (7 steps, 26% yield overall) used an organo-catalyzed cyclization developed by their group as the keystone for their synthesis, converting the alkyne-linked compound **2-3.12** obtained in 5 steps to penicinoline methyl ester **2-3.13**.[22] We expected that our approach would offer a substantial improvement in strategy for the synthesis of this target.

Scheme 2-3.4 Discovery and precedents in the synthesis of penicinotam

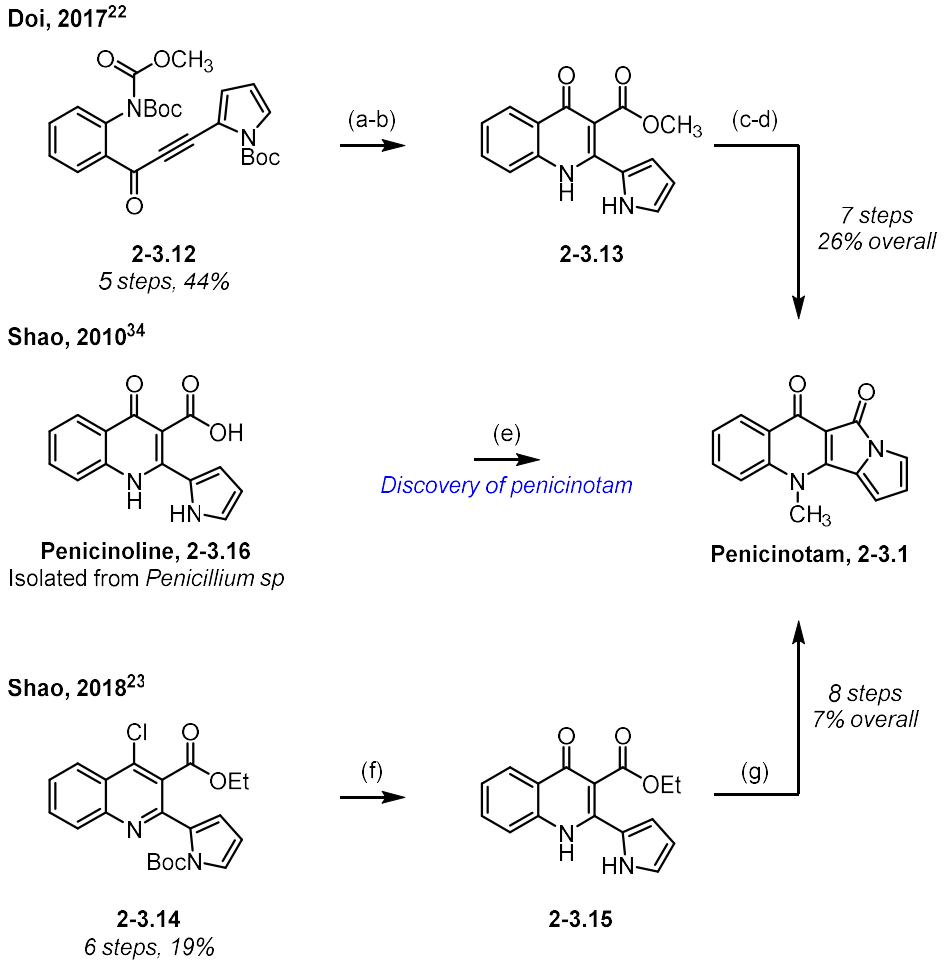

Reagents and conditions: (a) 30 mol% 9-azajulolidine, DMF, 80°C, 36 h (b) TFA, CH_2Cl_2, rt, 9 h, 54% over 2 steps (c) DBU, THF, reflux, 9 h, 91% (d) CH_3I, K_2CO_3, acetone, rt, 14 h, 95% (e) CH_3I or $(CH_3)_2SO_4$, K_2CO_3, acetone, rt, 12 h, yield not given (f) AcOH, EtOH, H_2O, 80°C, 18 h, 54% (g) CH_3I, K_2CO_3, CH_3CN, 60°C, 12 h, 68%.

Our forward synthesis comprised 3 steps from commercially available materials (**Scheme 2-3.5**). The requisite lactam **2-3.6** was synthesized by known procedures from purchased *N*-acetyl proline methyl ester **2-3.17** in 83% yield.[11] Analysis of the starting material's calculated pK_a value at various temperatures suggested the annulation would be most efficient using the DBU-mediated conditions in protocol B (**Table 2-3.1**). Indeed, the corresponding annulation product **2-3.5** was obtained in 60% yield using protocol B, which represents a substantial advancement over previous strategies (e.g., the 10-step route utilized by Tatsuta et al.). Encouragingly, our control experiment using protocol A failed to give any of the desired tetracycle, further supporting the pK_a-guided protocol selection system that we developed.

Scheme 2-3.5 Synthesis of penicinotam by base-mediated annulation of an enolate with *N*-methyl isatoic anhydride

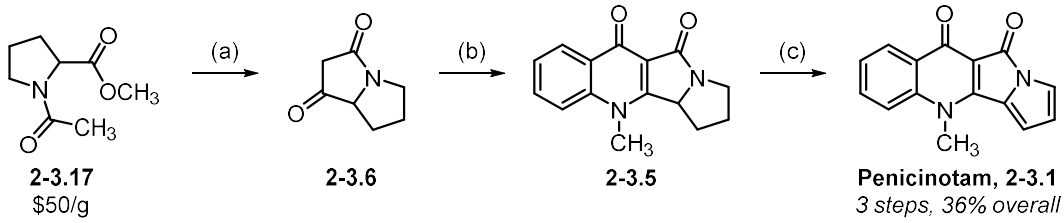

2-3.17 \$50/g — **2-3.6** — **2-3.5** — **Penicinotam, 2-3.1** *3 steps, 36% overall*

Reagents and conditions: (a) tBuOK, THF, reflux, 18 h, 83% (b) *N*-methyl isatoic anhydride, DBU, 3Å molecular sieves, CH_3CN, 50°C, 2 h, 60% (c) Chloranil, $PhCH_3$, 125°C, 72% .

Table 2-3.1 Calculated pK_a-guided reaction selection for annulation of alicyclic lactam **2-3.6**

Starting Material	**pK_a**			**Product**	**pK_a**		
	85°C	**50°C**	**80°C**		**85°C**	**50°C**	**80°C**
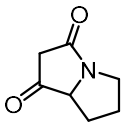 **2-3.6**	6.3	6.7	6.4	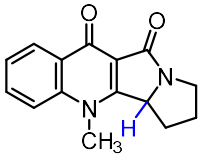 **2-3.5**	11.3	12.7	11.4

Orange highlight: incompatible, green highlight: compatible.

Oxidation of **2-3.5** to the final target proved to be more challenging. In our hands the main product of oxidation of **2-3.5** by MnO_2 in the manner described Abe et al. resulted in cleavage of the C3a-C3b bond to form **2-3.18** with minimal desired product (**Table 2-3.2**). More effective conditions were sought through screening alternative oxidants under various conditions, and ultimately, the use of chloranil at elevated temperature in toluene furnished penicinotam in 72% yield.

Table 2-3.2 Screening of oxidation conditions for the conversion of **2-3.5** to penicinotam

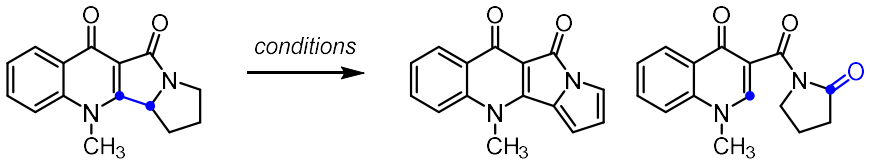

Entry	Solvent	Oxidant	Temperature	Time	Yield
1	CH_2Cl_2	MnO_2	45°C	12 h	< 5%
2	CH_2Cl_2	DDQ	45°C	12 h	0%
3	$PhCH_3$	DDQ	80°C	12 h	0%
4	$PhCH_3$	DDQ	90°C	12 h	6%
5	$PhCH_3$	DDQ	110°C	14 h	7%
6	$PhCH_3$	Chloranil	110°C	10 h	22%
7	$PhCH_3$	Chloranil	110°C	14 h	19%
8	$PhCH_3$	Chloranil	125°C[a]	2 h	< 10%
9	$PhCH_3$	Chloranil	125°C	16 h	72%

[a]Heated by microwave irradiation. Blue highlight: bond prone to oxidative cleavage and resulting product.

To our knowledge, this synthesis represents the shortest and highest yielding to date, providing the desired compound in three steps from commercially available starting materials and 36% overall yield. The route highlights the broader synthetic utility of our methods for the generation of a diverse library of ring-fused quinolinones, including our ability to reliably select an optimal set of reaction conditions for a given substrate based on a comparison of predicted pK_a

for the conjugate acid of the base employed, the starting material of interest, and the resulting product.

Section 2-4: Conclusion

To generate a diverse library of privileged heterocyclic small molecules, we developed a methodology to access ring-fused quinolinone structures via base-promoted annulation cascade of enolizable starting materials and isatoic anhydrides. The method consists of three complementary reaction conditions that are optimized for starting materials with defined pK_a range to balance the strength of the mediating base with starting material enolizability and product stability. Appropriate protocol selection for a given starting material is possible *a priori* via simple calculation using the freely available software MarvinSketch v18.25 and enabled the generation of over 80 examples of quinolinones with lactam, lactone, and carbocyclic ring fusions. The method was further applied to the total synthesis of penicinotam, an insecticidal natural product derivative, to provide the shortest and highest yielding route to the compound to date. Penicinotam was synthesized in three steps and 36% overall yield.

Section 2-5: Perspective and Future Directions

The synthetic methodology platform described here accommodates a wide range of starting materials in terms of both isatoic anhydrides and enolizable building blocks, however, it is not without some limitations. Future work to address these limitations via modifications of our new method would further broaden the accessibility of this important heterocyclic scaffold family. One such modification would be a base-free iteration of the reaction developed here. This might be realized through protected silyl enol ether equivalents of the enolizable starting materials, of the type **2-5.1**, which could be revealed to their reactive form in the presence of a fluoride ion source (**Figure 2-5.1**). The absence of an appreciable Brønsted-Lowry base during the annulation process

may enable use of *N*-unsubstituted isatoic anhydrides (**2-5.2**, R^2 = H), which are acidic enough to be deprotonated by even the weakest base used in this work (Et_3N, triethylamine) and are therefore largely incompatible in our new method. Inefficient access to the resulting *N*-unsubstituted 4-quinolinones (**2-5.3**, R^2 = H) is thus a limitation that may be overcome under a base-free adaptation of this work.

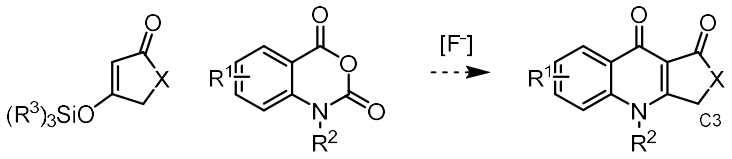

2-5.1 **2-5.2** **2-5.3**

Figure 2-5.1 Potential reaction manifold for access to 4-quinolinones under base-free conditions

Furthermore, we observed that using anhydrides with strong electron-withdrawing groups (**2-5.2**, R^1 = NO_2, I, CF_3) did not provide appreciable ring-fused quinolinone product **2-5.3** under any of the optimized procedures despite evidence of starting material consumption and reaction turnover by TLC. We hypothesized that the desired products might be acutely sensitive to base due to pronounced acidity at C3 resulting from electron withdrawal by such substituents. Unfortunately, the computational tools used in this work were unable to delineate the effects of such remote substitution patterns on acidity for the protons of interest, and additional work is required to test this hypothesis. Nevertheless, base-free reaction conditions may enable subsequent access to the resulting quinolinones. Expansion of the compatible set of substrates for this transformation in the future will be important to overcome synthetic limitations in the context of a medicinal chemistry campaign or to further expand the compound library for opportunistic screening.

Despite generating over 80 examples using a variety of isatoic anhydrides and enolizable building blocks, several related classes of compounds that might serve as effective substrates for

such an annulation were not explored in this work. Expansion of the substrate set to include amino acid-derived *N*-carboxy anhydrides (NCAs) **2-5.4**, benzo[*c*][1,2,5]oxathiazin-3(4*H*)-one 1,1-dioxides **2-5.5**, or heterocyclic analogs of isatoic anhydride such as **2-5.6** could provide access to entirely novel scaffolds **2-5.7**, **2-5.8**, and **2-5.9** (**Figure 2-5.2**).

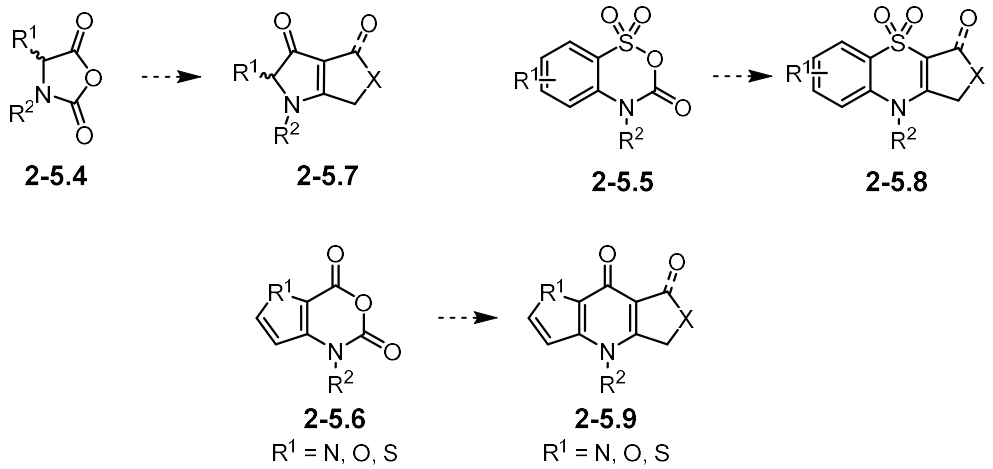

Figure 2-5.2 Substrate scope expansion would enable access to novel heterocyclic scaffolds related to the privileged ring-fused 4-quinolinone template

Additionally, preliminary experiments during the course of this study revealed that the use of Meldrum's acid as the enolizable component may enable rapid access to highly functionalized and substituted quinoline-2,4-diones **2-5.10**, a valuable class of building blocks for which few reported syntheses are available (**Fig. 2-5.3**).[35]

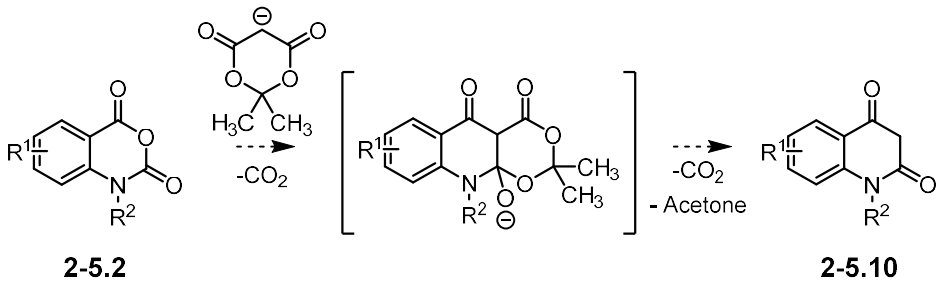

Figure 2-5.3 Potential access to highly substituted quinoline-2,4-diones using Meldrum's acid

Taken together, continued work in this area of synthetic methodology development may enable access to new members of the ring-fused, 4-quinolinone family, underexplored building blocks for synthesis, and unprecedented heterocyclic small molecule scaffolds.

Section 2-6: Experimental

The experimental data for this work is published and has been reproduced here with minimal modification.[1]

General Information. Commercial reagents and solvents were used as received. All thin layer chromatography was performed using precoated silica gel 60 F_{254} plates (EMD Millipore). Flash chromatography separations were carried out using a Teledyne Isco CombiFlash Rf 200 purification system (MPLC) with silica gel columns. Purity of all final compounds was confirmed by HPLC/MS analysis and determined to be ≥ 95% AUC at 254nm. Melting points were measured on OptiMelt MPA100 Automated Melting Point System. ^{1}H, ^{19}F, and ^{13}C nuclear magnetic resonance (NMR) spectra were recorded on a Varian Unity-Inova 400 MHz NMR Spectrometer (operating at 400, 376, and 101 MHz, respectively) or a Varian Unity-Inova 500 MHz NMR Spectrometer (operating at 500, 470, and 126 MHz, respectively) or Bruker Ascend 400 MHz Spectrometer (operating at 400, 376, and 101 MHz, respectively) in $CDCl_3$ or DMSO-d_6. The chemical shifts (δ) reported are given in parts per million (ppm). The Signal splitting patterns were described as s = singlet, d = doublet, t = triplet, q = quartet, p = pentuplet, dd = doublet of doublet, dt = doublet of triplet, td = triplet of doublet, tt = triplet of triplet, ddd = doublet of doublet of doublet, br = broad and m = multiplet, with coupling constants (J) in hertz (Hz). The LC-MS analysis was performed on an Agilent 1290 Infinity II HPLC system with 1290 Infinity II Diode Array Detector and an Agilent 6120 Quadrupole LC-MS system. The analytical chromatography method utilized the following parameters: Poroshell 120 EC-C18, 1.9 μm column, UV detection wavelength = 254 nm, Flow rate = 1.0 mL/min, Gradient = 5-100% LC-MS grade Methanol over 4 min; The organic mobile phase and aqueous mobile phase contained 0.1% LC-MS grade formic acid. The mass spectrometer utilized the following parameters: an Agilent multimode source that

simultaneously acquires ESI+/APCI+. High resolution mass spectra (HRMS) were performed by the Analytical Instrument Center at the School of Pharmacy on a Bruker MaXis 4G mass spectrometer. Chemical nomenclature was generated using ChemBioDraw Ultra version 14.0. Calculated *p*Ka values were obtained using MarvinSketch version 18.25, ChemAxon: Budapest, Hungary, 2018.

Synthesis of the isatoic anhydrides **2-2.1a-x** has been previously reported.[1]

General Procedure A. *Synthesis of tert-Butyl 4-substituted-1,9-dioxo-1,3,4,9-tetrahydro-2H-pyrrolo[3,4-b]quinolone-2-carboxylates* (**2-2.3a-u**).

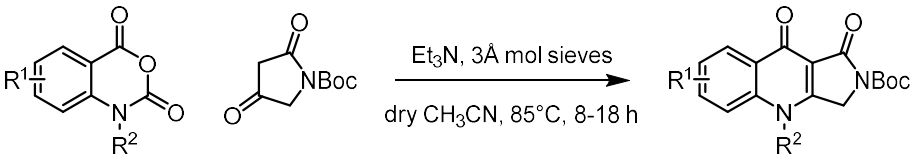

2-2.1a-u **2-2.2a** **2-2.3a-u**

To an oven dry screw cap vial with heat-activated, inert-atmosphere-cooled 3Å molecular sieves (3 beads, 4-8 mesh) was added the corresponding isatoic anhydride **2-2.1** (0.25 mmol, 1.0 equiv.) and *N*-Boc tetramic acid **2-2.2a** (0.63 mmol, 2.5 equiv.). The vial was evacuated and backfilled with N_2 before adding dry CH_3CN (0.5 mL) followed by Et_3N (0.15 mL, 1.08 mmol, 4.3 equiv.). The reaction tube was transferred to a preheated sand bath at 85°C and stirred 8-18 h (monitored by TLC for consumption of the anhydride). A gentle reflux was observed in the screw-capped vial which were tall enough to permit air-cooled condensation at roughly the half-way point in the vial. Upon completion of the reaction, or at the conclusion 18 h, the reaction was cooled to rt and then poured into ice water (7 mL) and stirred 30 min. Unless otherwise indicated, the precipitate was then collected by filtration to give the desired product **2-2.3**.

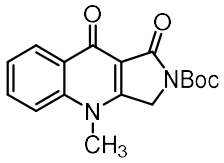

2-2.3a

*tert-Butyl 4-methyl-1,9-dioxo-1,3,4,9-tetrahydro-2H-pyrrolo[3,4-b]quinoline-2-carboxylate (**2-2.3a**)*. **2-2.1a** (44.3 mg, 0.25 mmol) was subjected to procedure A to give **2-2.1a** (74.3 mg, 95% yield) as an amorphous off-white solid. ^{1}H NMR (400 MHz, DMSO-d_6) δ 8.27 (dd, J = 8.0, 1.5 Hz, 1H), 7.92 – 7.80 (m, 2H), 7.52 (ddd, J = 8.0, 6.6, 1.4 Hz, 1H), 4.88 (s, 2H), 3.75 (s, 3H), 1.52

(s, 9H). $^{13}C\{^{1}H\}$ NMR (101 MHz, DMSO-d_6) δ 171.5, 163.0, 160.7, 149.4, 140.7, 133.0, 127.8, 126.1, 124.9, 116.9, 108.1, 81.7, 46.6, 34.9, 27.8. HRMS (ESI-QTOF) m/z: $[M + H]^+$ Calcd for $C_{17}H_{19}N_2O_4^+$ 315.1339; Found: 315.1327.

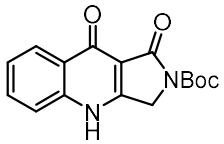

2-2.3b

*tert-Butyl 1,9-dioxo-1,3,4,9-tetrahydro-2H-pyrrolo[3,4-b]quinoline-2-carboxylate (**2-2.3b**)*. **2-2.1b** (40 mg, 0.25 mmol) was subjected to procedure A to give **2-2.3b** (27 mg, 36% yield) as an amorphous white solid. ^{1}H NMR (400 MHz, DMSO-d_6) δ 12.77 (s, 1H), 8.17 (d, J = 8.1 Hz, 1H), 7.75 (t, J = 7.5 Hz, 1H), 7.58 (d, J = 8.2 Hz, 1H), 7.43 (t, J = 7.6 Hz, 1H), 4.74 (s, 2H), 1.51 (s, 9H). $^{13}C\{^{1}H\}$ NMR (101 MHz, DMSO-d_6) δ 172.1, 163.1, 158.8, 149.5, 139.5, 132.8, 126.8, 125.7, 124.5, 118.8, 107.6, 81.5, 46.0, 27.8.

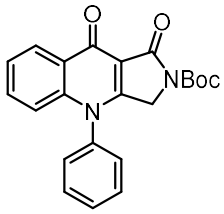

2-2.3c

*tert-Butyl 1,9-dioxo-4-phenyl-1,3,4,9-tetrahydro-2H-pyrrolo[3,4-b]quinoline-2-carboxylate (**2-2.3c**)*. **2-2.1c** (57.0 mg, 0.24 mmol) was subjected to procedure A to give **2-2.3c** (42.9 mg, 48% yield) as an amorphous off-white solid. ^{1}H NMR (400 MHz, DMSO-d_6) δ 8.31 (d, J = 7.1 Hz, 1H), 7.79 – 7.61 (m, 6H), 7.52 (d, J = 8.9 Hz, 1H), 6.85 (d, J = 7.2 Hz, 1H), 4.28 (s, 2H), 1.43 (s, 9H). $^{13}C\{^{1}H\}$ NMR (101 MHz, DMSO-d_6) δ 171.7, 162.7, 160.5, 149.4, 141.6, 135.8, 133.1, 130.8,

130.7, 128.3, 127.4, 126.0, 125.0, 117.6, 108.4, 81.8, 46.5, 27.7. HRMS (ESI-QTOF) m/z: $[M + H]^+$ Calcd for $C_{22}H_{21}N_2O_4^+$ 377.1496; Found: 377.1482.

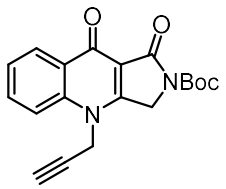

2-2.3d

*tert-Butyl 1,9-dioxo-4-(prop-2-yn-1-yl)-1,3,4,9-tetrahydro-2H-pyrrolo[3,4-b]quinoline-2-carboxylate (**2-2.3d**)*. **2-2.1d** (48 mg, 0.24 mmol) was subjected to procedure A to give **2-2.3d** (18 mg, 22% yield) as an amorphous pale yellow solid. ^{1}H NMR (400 MHz, DMSO-d_6) δ 8.28 (dd, J = 7.9, 1.5 Hz, 1H), 7.97 – 7.82 (m, 2H), 7.55 (t, J = 7.5 Hz, 1H), 5.21 (d, J = 2.5 Hz, 2H), 4.90 (s, 2H), 3.60 (t, J = 2.4 Hz, 1H), 1.52 (s, 9H). ^{13}C{^{1}H} NMR (101 MHz, DMSO-d_6) δ 171.5, 162.7, 160.0, 149.3, 139.3, 133.1, 127.9, 126.3, 125.2, 117.2, 108.9, 81.8, 77.4, 76.8, 46.4, 37.0, 27.8.

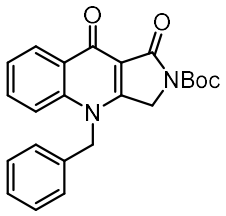

2-2.3e

*tert-Butyl 4-benzyl-1,9-dioxo-1,3,4,9-tetrahydro-2H-pyrrolo[3,4-b]quinoline-2-carboxylate (**2-2.3e**)*. **2-2.1e** (61.6 mg, 0.24 mmol) was subjected to procedure A to give **2-2.3e** (40.7 mg, 43% yield) as an amorphous off-white solid. ^{1}H NMR (400 MHz, DMSO-d_6) δ 8.28 (dd, J = 8.0, 1.5 Hz, 1H), 7.70 – 7.66 (m, 2H), 7.46 (t, J = 7.4 Hz, 1H), 7.35 – 7.26 (m, 5H), 5.58 (s, 2H), 4.85 (s, 2H), 1.49 (s, 9H). ^{13}C{^{1}H} NMR (101 MHz, DMSO-d_6) δ 171.6, 162.9, 160.8, 149.3, 139.9, 134.9, 133.0, 129.0, 128.2, 127.7, 126.2, 126.1, 124.9, 117.6, 108.7, 81.7, 50.3, 46.8, 27.8. HRMS (ESI-QTOF) m/z: $[M + H]^+$ Calcd for $C_{23}H_{23}N_2O_4^+$ 391.1652; Found: 391.1633.

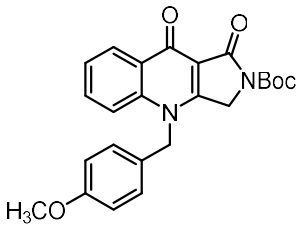

2-2.3f

*tert-Butyl 4-(4-methoxybenzyl)-1,9-dioxo-1,3,4,9-tetrahydro-2H-pyrrolo[3,4-b]quinoline-2-carboxylate (**2-2.3f**)*. **2-2.1f** (44 mg, 0.16 mmol) was subjected to procedure A to give **2-2.3f** (36 mg, 56 yield) as an orange solid. ^{1}H NMR (400 MHz, DMSO-d_6) δ ^{1}H NMR (500 MHz, DMSO) δ 8.27 (dd, J = 7.9, 1.5 Hz, 1H), 7.73 – 7.65 (m, 2H), 7.46 (ddd, J = 8.0, 6.4, 1.6 Hz, 1H), 7.22 (d, J = 8.7 Hz, 2H), 6.89 (d, J = 8.8 Hz, 2H), 5.49 (s, 2H), 4.86 (s, 2H), 3.71 (s, 3H), 1.50 (s, 9H). ^{13}C{^{1}H} NMR (126 MHz, DMSO-d_6) δ 171.57, 162.94, 160.62, 158.76, 149.34, 139.90, 132.91, 128.20, 127.57, 126.56, 126.18, 124.86, 117.65, 114.35, 108.68, 81.69, 55.08, 49.87, 46.76, 27.81.

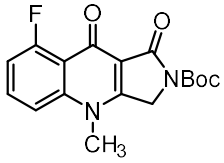

2-2.3h

*tert-Butyl 8-fluoro-9-hydroxy-4-methyl-1-oxo-1,4-dihydro-2H-pyrrolo[3,4-b]quinoline-2-carboxylate (**2-2.3h**).* **2-2.1h** (47.8 mg, 0.25 mmol) was subjected to procedure A to give **2-2.3h** (37.2 mg, 46% yield) as an amorphous off-white solid. This compound is observed exclusively as the enol tautomer by ^{1}H NMR (400 MHz, DMSO-d_6) δ 14.40 (s, 1H), 7.70 (t, J = 8.3 Hz, 1H), 7.24 (d, J = 8.5 Hz, 1H), 6.83 (d, J = 8.1 Hz, 1H), 4.91 (s, 2H), 3.73 (s, 3H), 1.53 (s, 9H). ^{13}C{^{1}H} NMR (101 MHz, DMSO-d_6) δ 178.2, 163.1, 162.5, 161.6, 149.7, 142.1, 135.6, 113.9, 111.8, 107.4, 106.4, 82.4, 47.3, 36.2, 28.3. ^{19}F{^{1}H} NMR (376 MHz, DMSO-d_6) δ -107.81, -112.37. HRMS (ESI-QTOF) m/z: $[M + H]^+$ Calcd for $C_{17}H_{18}FN_2O_4^+$ 333.1245; Found: 333.1244.

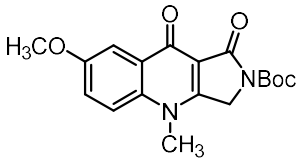

2-2.3i

*tert-Butyl 7-methoxy-4-methyl-1,9-dioxo-1,3,4,9-tetrahydro-2H-pyrrolo[3,4-b]quinoline-2-carboxylate (**2-2.3i**)*. **2-2.3i** (42.7 mg, 0.21 mmol) was subjected to procedure A to give **2-2.3i** (39.5 mg, 56% yield) as an off-white amorphous solid. ^{1}H NMR (400 MHz, DMSO-d_6) δ 7.84 (d, J = 9.3 Hz, 1H), 7.68 (d, J = 3.1 Hz, 1H), 7.44 (dd, J = 9.2, 3.1 Hz, 1H), 4.86 (s, 2H), 3.88 (s, 3H), 3.74 (s, 3H), 1.52 (s, 9H). ^{13}C{^{1}H} NMR (101 MHz, DMSO-d_6) δ 170.9, 163.1, 159.2, 156.6, 149.5, 135.0, 129.1, 121.9, 118.7, 107.2, 106.6, 81.7, 55.6, 46.4, 35.0, 27.8. HRMS (ESI-QTOF) m/z: [M + H]$^+$ Calcd for $C_{18}H_{21}N_2O_5^+$ 345.1445; Found: 345.1430.

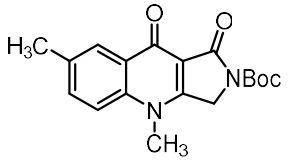

2-2.3j

*tert-Butyl 4,7-dimethyl-1,9-dioxo-1,3,4,9-tetrahydro-2H-pyrrolo[3,4-b]quinoline-2-carboxylate (**2-2.3j**)*. **2-2.1j** (47.5 mg, 0.25 mmol) was subjected to procedure A to give **2-2.3j** (62.4 mg, 77% yield) as an off-white amorphous solid. ^{1}H NMR (400 MHz, DMSO-d_6) δ 8.05 (d, J = 2.0 Hz, 1H), 7.77 (d, J = 8.7 Hz, 1H), 7.66 (dd, J = 8.7, 2.1 Hz, 1H), 4.85 (s, 2H), 3.73 (s, 3H), 2.45 (s, 3H), 1.52 (s, 9H). ^{13}C{^{1}H} NMR (101 MHz, DMSO-d_6) δ 171.4, 163.1, 160.1, 149.4, 138.7, 134.4, 134.1, 127.7, 125.6, 116.9, 107.8, 81.7, 46.5, 34.9, 27.8, 20.4. HRMS (ESI-QTOF) m/z: [M + H]$^+$ Calcd for $C_{18}H_{21}N_2O_4^+$ 329.1496; Found: 329.1491.

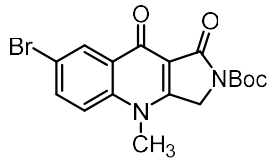

2-2.3k

*tert-Butyl 7-bromo-4-methyl-1,9-dioxo-1,3,4,9-tetrahydro-2H-pyrrolo[3,4-b]quinoline-2-carboxylate (**2-2.3k**)*. **2-2.1k** (64.2 mg, 0.25 mmol) was subjected to procedure A to give **2-2.3k** (51.8 mg, 53% yield) as an amorphous off-white solid. ^{1}H NMR (400 MHz, DMSO-d_6) δ 8.27 (d, J = 2.5 Hz, 1H), 7.97 (dd, J = 9.0, 2.5 Hz, 1H), 7.85 (d, J = 9.1 Hz, 1H), 4.85 (s, 2H), 3.74 (s, 3H), 1.52 (s, 9H). ^{13}C{^{1}H} NMR (101 MHz, DMSO-d_6) δ 170.1, 162.70, 161.0, 149.3, 139.8, 135.5, 129.3, 128.1, 119.8, 118.0, 108.5, 81.8, 46.7, 35.1, 27.8. HRMS (ESI-QTOF) m/z: $[M + H]^+$ Calcd for $C_{17}H_{18}BrN_2O_4^+$ 393.0445; Found: 393.0442.

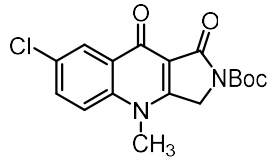

2-2.3l

*tert-Butyl 7-chloro-4-methyl-1,9-dioxo-1,3,4,9-tetrahydro-2H-pyrrolo[3,4-b]quinoline-2-carboxylate (**2-2.3l**)*. **2-2.1l** (53.0 mg, 0.25 mmol) was subjected to procedure A to give **2-2.3l** (68.7 mg, 79% yield) as an off-white amorphous solid. ^{1}H NMR (400 MHz, DMSO-d_6) δ 8.17 (d, J = 2.5 Hz, 1H), 8.01 – 7.81 (m, 2H), 4.88 (s, 2H), 3.76 (s, 3H), 1.52 (s, 9H). ^{13}C{^{1}H} NMR (101 MHz, DMSO-d_6) δ 170.2, 162.7, 161.0, 149.3, 139.4, 132.8, 129.9, 129.0, 125.0, 119.6, 108.4, 81.8, 46.7, 35.2, 27.8. HRMS (ESI-QTOF) m/z: $[M + H]^+$ Calcd for $C_{17}H_{18}ClN_2O_4^+$ 349.0950; Found: 349.0950.

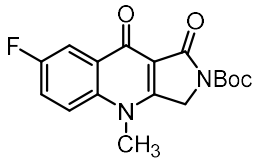

2-2.3m

*tert-Butyl 7-fluoro-4-methyl-1,9-dioxo-1,3,4,9-tetrahydro-2H-pyrrolo[3,4-b]quinoline-2-carboxylate (**2-2.3m**)*. **2-2.1m** (51.2 mg, 0.26 mmol) was subjected to procedure A to give **2-2.3m** (67.7 mg, 78% yield) as an amorphous off-white solid. ^{1}H NMR (400 MHz, DMSO-d_6) δ 7.97 (dd, J = 9.4, 4.3 Hz, 1H), 7.90 (dd, J = 8.9, 3.1 Hz, 1H), 7.74 (dd, J = 8.0, 3.1 Hz, 1H), 4.86 (s, 2H), 3.76 (s, 3H), 1.52 (s, 9H). ^{13}C{^{1}H} NMR (101 MHz, DMSO-d_6) δ 171.0, 163.3, 161.0, 159.7 (d, J = 244.9 Hz), 149.8, 137.8, 130.0 (d, J = 6.5 Hz), 121.5 (d, J = 24.3 Hz), 120.5 (d, J = 8.3 Hz), 111.1 (d, J = 22.9 Hz), 108.1, 82.3, 47.1, 35.8, 28.3. ^{19}F{^{1}H} NMR (376 MHz, DMSO-d_6) δ -116.57. HRMS (ESI-QTOF) m/z: $[M + H]^+$ Calcd for $C_{17}H_{18}FN_2O_4^+$ 333.1245; Found: 333.1238.

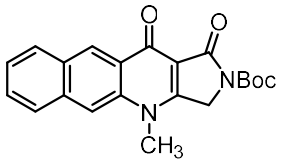

2-2.3n

*tert-Butyl 4-methyl-1,11-dioxo-1,3,4,11-tetrahydro-2H-benzo[g]pyrrolo[3,4-b]quinoline-2-carboxylate (**2-2.3n**)*. **2-2.1n** (56.4 mg, 0.25 mmol) was subjected to procedure A to give **2-2.3n** (78.7 mg, 87% yield) as an off-white amorphous solid. ^{1}H NMR (400 MHz, DMSO-d_6) δ 8.90 (s, 1H), 8.40 (s, 1H), 8.23 (d, J = 8.4 Hz, 1H), 8.12 (d, J = 8.4 Hz, 1H), 7.70 (t, J = 7.1 Hz, 1H), 7.60 (t, J = 7.9 Hz, 1H), 4.91 (s, 2H), 3.84 (s, 3H), 1.53 (s, 9H). ^{13}C{^{1}H} NMR (101 MHz, DMSO-d_6) δ 172.3, 163.0, 162.1, 149.4, 137.6, 134.7, 129.3, 129.2, 128.8, 127.7, 127.1, 126.4, 114.3, 106.1, 81.7, 46.8, 35.1, 27.9. HRMS (ESI-QTOF) m/z: $[M + H]^+$ Calcd for $C_{21}H_{21}N_2O_4^+$ 365.1496; Found: 365.1496.

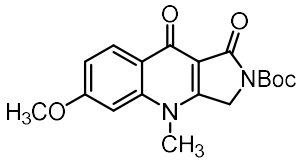

2-2.3o

*tert-Butyl 6-methoxy-4-methyl-1,9-dioxo-1,3,4,9-tetrahydro-2H-pyrrolo[3,4-b]quinoline-2-carboxylate (**2-2.3o**)*. **2-2.1o** (49.3 mg, 0.24 mmol) was subjected to procedure A to give **2-2.3o** (14.6 mg, 18% yield) as an off-white amorphous solid. ^{1}H NMR (400 MHz, DMSO-d_6) δ 8.17 (d, J = 8.8 Hz, 1H), 7.20 (d, J = 2.2 Hz, 1H), 7.11 (dd, J = 8.8, 2.2 Hz, 1H), 4.85 (s, 2H), 3.96 (s, 3H), 3.72 (s, 3H), 1.53 (s, 9H). ^{13}C{^{1}H} NMR (101 MHz, DMSO-d_6) δ 163.0, 160.8, 149.4, 142.6, 140.5, 127.9, 121.7, 121.2, 113.2, 108.0, 100.0, 81.6, 56.0, 46.6, 35.0, 27.8. HRMS (ESI-QTOF) m/z: [M + H]$^{+}$ Calcd for $C_{18}H_{21}N_2O_5^{+}$ 345.1445; Found: 345.1445.

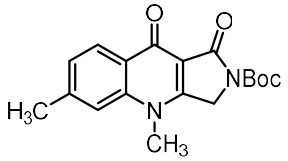

2-2.3p

*tert-Butyl 4,6-dimethyl-1,9-dioxo-1,3,4,9-tetrahydro-2H-pyrrolo[3,4-b]quinoline-2-carboxylate (**2-2.3p**)*. **2-2.1p** (47.0 mg, 0.25 mmol) was subjected to procedure A to give **2-2.3p** (35.6 mg, 44% yield) as an off-white amorphous solid. ^{1}H NMR (400 MHz, DMSO-d_6) δ 8.14 (d, J = 8.1 Hz, 1H), 7.69 (s, 1H), 7.34 (d, J = 8.2 Hz, 1H), 4.86 (s, 2H), 3.73 (s, 3H), 2.51 (s, 3H), 1.52 (s, 9H). ^{13}C{^{1}H} NMR (101 MHz, DMSO-d_6) δ 171.4, 163.0, 160.5, 149.4, 143.6, 140.8, 126.2, 126.0, 125.7, 116.7, 107.9, 81.7, 46.6, 34.8, 27.8, 21.5. HRMS (ESI-QTOF) m/z: [M + H]$^{+}$ Calcd for $C_{18}H_{21}N_2O_4^{+}$ 329.1496; Found: 329.1479.

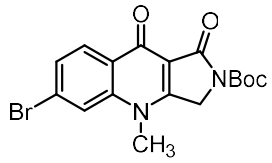

2-2.3q

*tert-Butyl 6-bromo-4-methyl-1,9-dioxo-1,3,4,9-tetrahydro-2H-pyrrolo[3,4-b]quinoline-2-carboxylate (**2-2.3q**)*. **2-2.1q** (61.9 mg, 0.24 mmol) was subjected to procedure A to give **2-2.3q** (64.2 mg, 68% yield) as an amorphous off-white solid. ^{1}H NMR (400 MHz, DMSO-d_6) δ 8.16 – 8.13 (m, 2H), 7.68 (dd, J = 8.5, 1.6 Hz, 1H), 4.87 (s, 2H), 3.75 (s, 3H), 1.52 (s, 9H). ^{13}C{^{1}H} NMR (101 MHz, DMSO-d_6) δ 170.9, 161.3, 149.3, 141.7, 128.1, 128.0, 127.0, 126.8, 119.8, 108.6, 81.8, 46.7, 35.2, 27.8. HRMS (ESI-QTOF) m/z: $[M + H]^+$ Calcd for $C_{17}H_{18}BrN_2O_4^+$ 393.0445; Found: 393.0446.

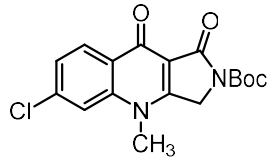

2-2.3r

*tert-Butyl 6-chloro-4-methyl-1,9-dioxo-1,3,4,9-tetrahydro-2H-pyrrolo[3,4-b]quinoline-2-carboxylate (**2-2.3r**)*. **2-2.1r** (39.2 mg, 0.19 mmol) was subjected to procedure A to give **2-2.3r** (53.0 mg, 82% yield) as an off-white amorphous solid. ^{1}H NMR (400 MHz, DMSO-d_6) δ 8.23 (dd, J = 8.6, 2.4 Hz, 1H), 7.99 (d, J = 1.8 Hz, 1H), 7.54 (d, J = 8.3Hz, 1H), 4.86 (s, 2H), 3.74 (s, 3H), 1.52 (s, 9H). ^{13}C{^{1}H} NMR (101 MHz, DMSO-d_6) δ 170.8, 162.7, 161.3, 149.3, 141.6, 138.0, 128.0, 126.5, 125.1, 116.9, 108.6, 81.8, 46.7, 35.2, 27.8. HRMS (ESI-QTOF) m/z: $[M + H]^+$ Calcd for $C_{17}H_{18}ClN_2O_4^+$ 349.0950; Found: 349.0934.

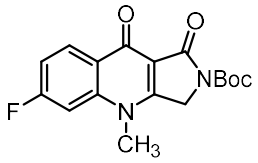

2-2.3s

*tert-Butyl 6-fluoro-4-methyl-1,9-dioxo-1,3,4,9-tetrahydro-2H-pyrrolo[3,4-b]quinoline-2-carboxylate (**2-2.3s**)*. **2-2.1s** (42.1 mg, 0.22 mmol) was subjected to procedure A to give **2-2.3s** (41.9 mg, 58% yield) as an amorphous off-white solid. ^{1}H NMR (400 MHz, DMSO-d_6) δ 8.29 (ddd, J = 9.0, 6.7, 2.5 Hz, 1H), 7.77 (dd, J = 11.4, 2.4 Hz, 1H), 7.37 (td, J = 8.6, 7.3, 4.1 Hz, 1H), 4.86 (s, 2H), 3.72 (s, 3H), 1.51 (s, 9H). ^{13}C{^{1}H} NMR (101 MHz, DMSO-d_6) δ 170.7, 164.70 (d, J = 249.3 Hz), 162.8, 161.4, 149.3, 142.5 (d, J = 11.9 Hz), 129.2 (d, J = 11.0 Hz), 124.7, 113.0 (d, J = 23.1 Hz), 108.4, 103.8 (d, J = 27.2 Hz), 81.8, 46.6, 35.2, 27.8. ^{19}F{^{1}H} NMR (376 MHz, DMSO-d_6) δ -104.88. HRMS (ESI-QTOF) m/z: [M + H]$^+$ Calcd for $C_{17}H_{18}FN_2O_4^+$ 333.1245; Found: 333.1244.

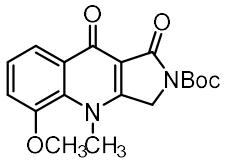

2-2.3t

*tert-Butyl 5-methoxy-4-methyl-1,9-dioxo-1,3,4,9-tetrahydro-2H-pyrrolo[3,4-b]quinoline-2-carboxylate (**2-2.3t**)*. **2-2.1t** (51.0 mg, 0.25 mmol) was subjected to procedure A to give **2-2.3t** (66.4 mg, 78% yield) as an off-white amorphous solid. ^{1}H NMR (400 MHz, DMSO-d_6) δ 7.86 (dd, J = 7.4, 2.0 Hz, 1H), 7.47 – 7.40 (m, 2H), 4.84 (s, 2H), 3.95 (s, 3H), 3.94 (s, 3H), 1.52 (s, 9H). ^{13}C{^{1}H} NMR (101 MHz, DMSO-d_6) δ 170.9, 162.8, 161.7, 150.8, 149.4, 131.5, 130.4, 125.5, 118.0, 116.3, 108.0, 81.7, 56.1, 47.0, 27.8. HRMS (ESI-QTOF) m/z: [M + H]$^+$ Calcd for $C_{18}H_{21}N_2O_5^+$ 345.1445; Found: 345.1449.

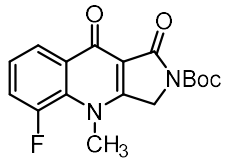

2-2.3u

*tert-Butyl 5-fluoro-4-methyl-1,9-dioxo-1,3,4,9-tetrahydro-2H-pyrrolo[3,4-b]quinoline-2-carboxylate (**2-2.3u**)*. **2-2.1u** (43.8 mg, 0.22 mmol) was subjected to procedure A to give **2-2.3u** (43.1 mg, 58% yield) as an amorphous off-white solid. ^{1}H NMR (400 MHz, DMSO-d_6) δ 8.10 (dd, J = 8.1, 1.5 Hz, 1H), 7.71 (ddd, J = 15.0, 7.9, 1.6 Hz, 1H), 7.48 (td, J = 8.0, 4.1 Hz, 1H), 4.87 (s, 2H), 3.89 (d, J = 7.5 Hz, 3H), 1.52 (s, 9H). ^{13}C{^{1}H} NMR (101 MHz, DMSO-d_6) δ 189.4, 170.2 (d, J = 2.5 Hz), 162.6, 161.9, 152.3 (d, J = 248.8 Hz), 149.2, 130.7, 129.9, 125.5 (d, J = 8.4 Hz), 122.2 (d, J = 3.3 Hz), 120.5 (d, J = 23.5 Hz), 108.3, 81.9, 46.9, 27.8. ^{19}F{^{1}H} NMR (376 MHz, DMSO-d_6) δ -119.85. HRMS (ESI-QTOF) m/z: $[M + H]^+$ Calcd for $C_{17}H_{18}FN_2O_4^+$ 333.1245; Found: 333.1247.

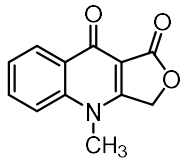

2-2.17

*4-Methylfuro[3,4-b]quinoline-1,9(3H,4H)-dione (**2-2.17**)*. **2-2.1a** (42.0 mg, 0.237 mmol) was treated analogously as in procedure A but using tetronic acid **2-2.12** (77.2 mg, 0.77 mmol) to give **2-2.17** (25.6 mg, 50% yield) as an amorphous white solid. ^{1}H NMR (400 MHz, DMSO-d_6) δ 8.28 (d, J = 7.9 Hz, 1H), 7.88 (d, J = 3.9 Hz, 2H), 7.55 (dt, J = 8.1, 4.1 Hz, 1H), 5.39 (s, 2H), 3.72 (s, 3H). ^{13}C{^{1}H} NMR (101 MHz, DMSO-d_6) δ 171.5, 167.6, 166.4, 140.9, 133.3, 127.8, 126.1, 125.2, 117.0, 102.3, 65.1, 35.2. HRMS (ESI-QTOF) m/z: $[M + H]^+$ Calcd for $C_{12}H_{10}NO_3^+$ 216.0655; Found: 216.0657.

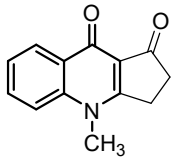

2-2.19

*4-Methyl-2,3-dihydro-1H-cyclopenta[b]quinoline-1,9(4H)-dione (**2-2.19**)*. **2-2.1a** (35 mg, 0.20 mmol) was treated analogously as in procedure A but using 1,3-cyclopentanedione (76 mg, 0.77 mmol) to give **2-2.19** as an amorphous white solid (10 mg, 24%). ^{1}H NMR (400 MHz, DMSO-d_6) δ 8.24 (dd, J = 7.9, 1.6 Hz, 1H), 7.88 – 7.77 (m, 2H), 7.49 (ddd, J = 8.0, 6.5, 1.5 Hz, 1H), 3.80 (s, 3H), 3.21 – 3.13 (m, 2H), 2.49 (d, J = 2.3 Hz, 2H). ^{13}C NMR (101 MHz, DMSO) δ 199.2, 173.4, 171.8, 140.9, 133.0, 128.0, 126.3, 124.7, 117.1, 116.5, 34.7, 33.9, 25.3.

General Procedure B. *Synthesis of 4-substituted-2,3-Dihydro-1H-pyrrolo[3,4-b]quinolone-1,9(4H)-diones* **(2-2.11a-u).**

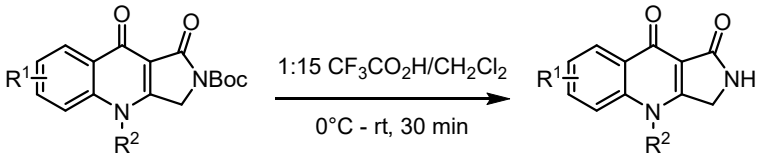

2-2.3a-u **2-2.11a-u**

To a screw cap vial was added **2-2.3** (0.10 mmol, 1.0 equiv.) and CH_2Cl_2 (0.5 mL). The solution was cooled to 0°C in an ice bath before adding trifluoroacetic acid (0.10 mL, 1.30 mmol, 13 equiv.). The reaction mixture was then shaken at r.t. (550 rpm) with a mini plate shaker for 30 min. The reaction mixture was concentrated, triturated with H_2O (1 mL) and sonicated 30 sec. The resulting precipitate was collected by filtration to give the desired product **2-2.11**.

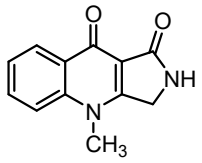

2-2.11a

*4-Methyl-2,3-dihydro-1H-pyrrolo[3,4-b]quinoline-1,9(4H)-dione (**2-2.11a**).* **2-2.3a** (31.9 mg, 0.10 mmol) was subjected to procedure B to give **2-2.11a** (13.4 mg, 62% yield) as an amorphous off-white solid. ^{1}H NMR (400 MHz, DMSO-d_6) δ 8.27 (d, J = 8.0 Hz, 1H), 7.93 (s, 1H), 7.87 – 7.76 (m, 2H), 7.48 (t, J = 7.5 Hz, 1H), 4.49 (s, 2H), 3.72 (s, 3H). ^{13}C{^{1}H} NMR (101 MHz, DMSO-d_6) δ 172.0, 169.4, 163.4, 141.2, 132.9, 128.5, 126.5, 124.6, 117.1, 109.9, 43.7, 35.0. HRMS (ESI-QTOF) m/z: $[M + H]^+$ Calcd for $C_{12}H_{11}N_2O_2^+$ 215.0815; Found: 215.0814.

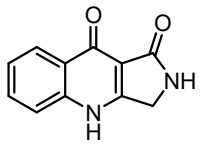

2-2.11b

*2,3-Dihydro-1H-pyrrolo[3,4-b]quinoline-1,9(4H)-dione (**2-2.11b**).* **2-2.3b** (3.3 mg, 0.01 mmol) was subjected to procedure B to give **2-2.11b** (0.7 mg, 32% yield) as an amorphous off-white solid. ^{1}H NMR (400 MHz, DMSO-d_6) δ 12.56 (s, 1H), 8.17 (dd, J = 8.1, 1.4 Hz, 1H), 7.77 (s, 1H), 7.70 (ddd, J = 8.4, 7.0, 1.5 Hz, 1H), 7.56 (d, J = 8.2 Hz, 1H), 7.38 (t, J = 7.5 Hz, 1H), 4.35 (s, 2H). Quantity available precluded ^{13}C NMR and HRMS.

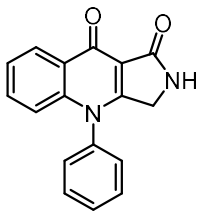

2-2.11c

*4-Phenyl-2,3-dihydro-1H-pyrrolo[3,4-b]quinoline-1,9(4H)-dione (**2-2.11c**)*. **2-2.3c** (39.9 mg, 0.11 mmol) was subjected to procedure B to give **2-2.11c** (23.2 mg, 79% yield) as an amorphous off-white solid. ^{1}H NMR (400 MHz, DMSO-d_6) δ 8.31 (dd, J = 8.0, 1.6 Hz, 1H), 7.87 (s, 1H), 7.76 – 7.53 (m, 6H), 7.46 (t, J = 7.5 Hz, 1H), 6.84 (d, J = 8.5 Hz, 1H), 3.91 (s, 2H). ^{13}C{^{1}H} NMR (101 MHz, DMSO-d_6) δ 172.0, 168.8, 162.7, 141.8, 136.4, 132.6, 130.8, 130.5, 128.4, 127.6, 126.1, 124.4, 117.3, 109.7, 43.4. HRMS (ESI-QTOF) m/z: $[M + H]^+$ Calcd for $C_{17}H_{13}N_2O_2^+$ 277.0972; Found: 277.0961.

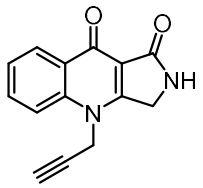

2-2.11d

*4-(Prop-2-yn-1-yl)-2,3-dihydro-1H-pyrrolo[3,4-b]quinoline-1,9(4H)-dione (**2-2.11d**)*. **2-2.3d** (7.7 mg, 0.02 mmol) was subjected to procedure B to give **2-2.11d** (0.9 mg, 17% yield) as an amorphous off-white solid. ^{1}H NMR (400 MHz, DMSO-d_6) δ 8.28 (dd, J = 8.0, 1.6 Hz, 1H), 8.03 (s, 1H), 7.90 (d, J = 8.5 Hz, 1H), 7.85 (ddd, J = 8.6, 6.8, 1.7 Hz, 1H), 7.50 (ddd, J = 8.0, 6.8, 1.1 Hz, 1H), 5.13 (d, J = 2.5 Hz, 2H), 4.51 (s, 2H), 3.54 (t, J = 2.3 Hz, 1H). Quantity available precluded ^{13}C NMR and HRMS.

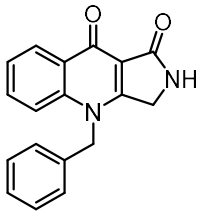

2-2.11e

*4-Benzyl-2,3-dihydro-1H-pyrrolo[3,4-b]quinoline-1,9(4H)-dione (**2-2.11e**)*. **2-2.3e** (18.2 mg, 0.05 mmol) was subjected to procedure B to give **2-2.11e** (12.0 mg, 88% yield) as an amorphous off-

white solid. ^{1}H NMR (400 MHz, DMSO-d_6) δ 8.29 (dd, J = 8.0, 1.4 Hz, 1H), 7.98 (s, 1H), 7.70 – 7.60 (m, 2H), 7.43 (ddd, J = 7.9, 6.3, 1.5 Hz, 1H), 7.37 – 7.25 (m, 3H), 7.18 (d, J = 7.0 Hz, 2H), 5.53 (s, 2H), 4.46 (s, 2H). ^{13}C{^{1}H} NMR (101 MHz, DMSO) δ 171.7, 168.8, 163.0, 140.1, 135.2, 132.5, 129.0, 127.7, 126.3, 126.0, 124.3, 117.2, 109.9, 99.5, 50.0, 43.4. HRMS (ESI-QTOF) m/z: $[M + H]^+$ Calcd for $C_{18}H_{15}N_2O_2^+$ 291.1128; Found: 291.1122.

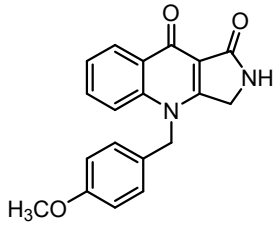

2-2.11f

*4-(4-methoxybenzyl)-2,3-dihydro-1H-pyrrolo[3,4-b]quinoline-1,9(4H)-dione (**2-2.11f**)*. **2-2.3f** (34 mg, 0.08 mmol) was subjected to procedure A to give **2-2.11f** (24 mg, 91% yield) as an amorphous off-white solid. ^{1}H NMR (400 MHz, DMSO-d_6) δ 8.28 (d, J = 8.0 Hz, 1H), 7.99 (s, 1H), 7.68 (d, J = 3.7 Hz, 2H), 7.43 (dt, J = 8.0, 4.0 Hz, 1H), 7.13 (d, J = 8.7 Hz, 2H), 6.89 (d, J = 8.7 Hz, 2H), 5.45 (s, 2H), 4.47 (s, 2H), 3.70 (s, 3H). ^{13}C{^{1}H} NMR (101 MHz, DMSO-d_6) δ 171.7, 168.8, 162.9, 158.7, 140.0, 132.5, 128.4, 127.4, 126.9, 126.2, 124.2, 117.4, 114.4, 109.8, 55.1, 49.5, 43.4.

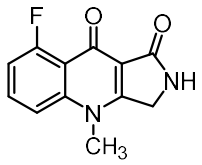

2-2.11h

*8-Fluoro-9-hydroxy-4-methyl-2,4-dihydro-1H-pyrrolo[3,4-b]quinoline-1,9(4H)-dione (**2-2.11h**)*. **2-2.3h** (26.7 mg, 0.08 mmol) was subjected to procedure B to give **2-2.11h** (17.0 mg, 92% yield) as an amorphous off-white solid. This compound is observed exclusively as the enol tautomer by ^{1}H NMR (400 MHz, DMSO-d_6) δ 14.78 (s, 1H), 8.09 (s, 1H), 7.65 (t, J = 8.3 Hz, 1H), 7.18 (d, J

= 8.5 Hz, 1H), 6.76 (d, *J* = 8.1 Hz, 1H), 4.52 (s, 2H), 3.68 (s, 3H). Solubility precluded ^{13}C NMR. ^{19}F{^{1}H} NMR (376 MHz, DMSO-d_6) δ -73.48, -112.64. HRMS (ESI-QTOF) m/z: $[M + H]^+$ Calcd for $C_{12}H_{10}FN_2O_2^+$ 233.0721; Found: 233.0720.

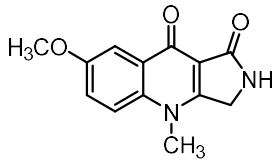

2-2.11i

*7-Methoxy-4-methyl-2,3-dihydro-1H-pyrrolo[3,4-b]quinoline-1,9(4H)-dione (**2-2.11i**)*. **2-2.3i** (33.8 mg, 0.10 mmol) was subjected to procedure B to give **2-2.11i** (22.9 mg, 96% yield) as an amorphous off-white solid. ^{1}H NMR (400 MHz, DMSO-d_6) δ 7.90 (s, 1H), 7.80 (d, *J* = 9.3 Hz, 1H), 7.69 (d, *J* = 3.1 Hz, 1H), 7.42 (dd, *J* = 9.2, 3.1 Hz, 1H), 4.46 (s, 2H), 3.88 (s, 3H), 3.71 (s, 3H). ^{13}C{^{1}H} NMR (101 MHz, DMSO-d_6) δ 171.0, 169.1, 161.6, 156.1, 135.2, 129.3, 121.5, 118.4, 108.5, 106.4, 55.5, 43.1, 34.7. HRMS (ESI-QTOF) m/z: $[M + H]^+$ Calcd for $C_{13}H_{13}N_2O_3^+$ 245.0921; Found: 245.0929.

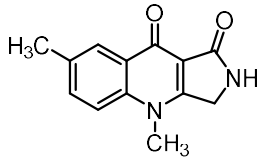

2-2.11j

*4,7-Dimethyl-2,3-dihydro-1H-pyrrolo[3,4-b]quinoline-1,9(4H)-dione (**2-2.11j**)*. **2-2.3j** (36.9 mg, 0.10 mmol) was subjected to procedure B to give **2-2.11j** (16.1 mg, 71% yield) as an amorphous off-white solid. ^{1}H NMR (400 MHz, DMSO-d_6) δ 8.05 (d, *J* = 1.6 Hz, 1H), 7.89 (s, 1H), 7.72 (d, *J* = 8.7 Hz, 1H), 7.62 (dd, *J* = 8.7, 2.2 Hz, 1H), 4.46 (s, 2H), 3.69 (s, 3H), 2.44 (s, 3H). ^{13}C{^{1}H} NMR (101 MHz, DMSO-d_6) δ 171.6, 169.2, 162.5, 138.9, 133.68, 133.67, 127.9, 125.6, 116.6,

109.2, 43.2, 34.6, 20.5. HRMS (ESI-QTOF) m/z: $[M + H]^+$ Calcd for $C_{13}H_{13}N_2O_2^+$ 229.0972; Found: 229.0977.

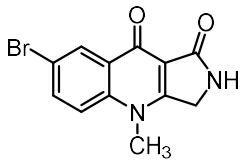

2-2.11k

*7-Bromo-4-methyl-2,3-dihydro-1H-pyrrolo[3,4-b]quinoline-1,9(4H)-dione (**2-2.11k**)*. **2-2.3k** (38.8 mg, 0.10 mmol) was subjected to procedure B to give **2-2.11k** (24.1 mg, 83% yield) as an amorphous off-white solid. ^{1}H NMR (400 MHz, DMSO-d_6) δ 8.31 (d, J = 2.3 Hz, 1H), 8.01 (s, 1H), 7.95 (dd, J = 9.0, 2.4 Hz, 1H), 7.82 (dd, J = 9.1, 1.9 Hz, 1H), 4.48 (s, 2H), 3.70 (s, 3H). ^{13}C{^{1}H} NMR (101 MHz, DMSO-d_6) δ 170.4, 168.8, 163.5, 134.0, 135.4, 135.2, 128.2, 119.6, 117.4, 109.9, 43.5, 35.0. HRMS (ESI-QTOF) m/z: $[M + H]^+$ Calcd for $C_{12}H_{10}BrN_2O_2^+$ 292.9920; Found: 292.9916.

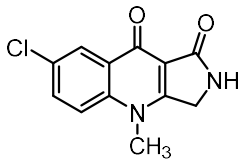

2-2.11l

*7-Chloro-4-methyl-2,3-dihydro-1H-pyrrolo[3,4-b]quinoline-1,9(4H)-dione (**2-2.11l**)*. **2-2.3l** (34.2 mg, 0.10 mmol) was subjected to procedure B above to give **2-2.11l** (20.7 mg, 85% yield) as an amorphous off-white solid. ^{1}H NMR (400 MHz, DMSO-d_6) δ 8.15 (d, J = 2.5 Hz, 1H), 8.00 (s, 1H), 7.88 (d, J = 9.1 Hz, 1H), 7.83 (dd, J = 9.1, 2.5 Hz, 1H), 4.48 (s, 2H), 3.71 (s, 3H). ^{13}C{^{1}H} NMR (101 MHz, DMSO-d_6) δ 170.3, 168.6, 163.3, 139.5, 132.3, 129.2, 129.1, 125.0, 119.3, 109.8, 43.3, 34.8. HRMS (ESI-QTOF) m/z: $[M + H]^+$ Calcd for $C_{12}H_{10}ClN_2O_2^+$ 249.0425; Found: 249.0429.

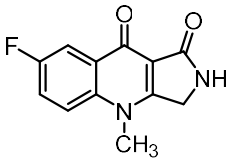

2-2.11m

*7-Fluoro-4-methyl-2,3-dihydro-1H-pyrrolo[3,4-b]quinoline-1,9(4H)-dione (**2-2.11m**)*. **2-2.3m** (32.8 mg, 0.10 mmol) was subjected to procedure B to give **2-2.11m** (19.5 mg, 85% yield) as an amorphous off-white solid. ^{1}H NMR (400 MHz, DMSO-d_6) δ 7.98 (s, 1H), 7.96 – 7.85 (m, 2H), 7.71 (ddd, J = 9.5, 7.8, 3.2 Hz, 1H), 4.48 (s, 2H), 3.72 (s, 3H). ^{13}C{^{1}H} NMR (101 MHz, DMSO-d_6) δ 170.6, 168.7, 162.9, 158.9 (d, J = 243.7 Hz), 137.5, 129.6 (d, J = 6.2 Hz), 120.5 (d, J = 24.6 Hz), 119.6 (d, J = 8.1 Hz), 110.5 (d, J = 22.8 Hz), 109.0, 43.3, 34.9. ^{19}F{^{1}H} NMR (376 MHz, DMSO-d_6) δ -117.65. HRMS (ESI-QTOF) m/z: $[M + H]^+$ Calcd for $C_{12}H_{10}FN_2O_2^+$ 233.0721; Found: 233.0722.

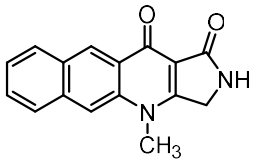

2-2.11n

*4-Methyl-2,3-dihydro-1H-benzo[g]pyrrolo[3,4-b]quinoline-1,11(4H)-dione (**2-2.11n**)*. **2-2.3n** (35.8 mg, 0.10 mmol) was subjected to procedure B to give **2-2.11n** (21.4 mg, 82% yield) as an amorphous off-white solid. ^{1}H NMR (400 MHz, DMSO-d_6) δ 8.90 (s, 1H), 8.34 (s, 1H), 8.21 (d, J = 8.3 Hz, 1H), 8.11 (d, J = 8.4 Hz, 1H), 7.90 (s, 1H), 7.68 (t, J = 7.5 Hz, 1H), 7.57 (t, J = 7.5 Hz, 1H), 4.53 (s, 2H), 3.80 (s, 3H). Solubility precluded ^{13}C NMR. HRMS (ESI-QTOF) m/z: $[M + H]^+$ Calcd for $C_{16}H_{13}N_2O_2^+$ 265.0972; Found: 265.0968.

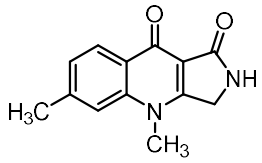

2-2.11p

*4,6-Dimethyl-2,3-dihydro-1H-pyrrolo[3,4-b]quinoline-1,9(4H)-dione (**2-2.11p**)*. **2-2.3p** (29.3 mg, 0.09 mmol) was subjected to procedure B to give **2-2.11p** (17.3 mg, 85% yield) as an amorphous off-white solid. ^{1}H NMR (400 MHz, DMSO-d_6) δ 8.14 (d, J = 8.1 Hz, 1H), 7.89 (s, 1H), 7.63 (s, 1H), 7.29 (dd, J = 8.3, 1.4 Hz, 1H), 4.46 (s, 2H), 3.69 (s, 3H). ^{13}C{^{1}H} NMR (101 MHz, DMSO-d_6) δ 171.5, 169.1, 162.8, 142.9, 140.9, 126.0, 125.9, 125.5, 116.3, 109.3, 43.2, 34.5, 21.5. HRMS (ESI-QTOF) m/z: $[M + H]^+$ Calcd for $C_{13}H_{13}N_2O_2^+$ 229.0972; Found: 229.0967.

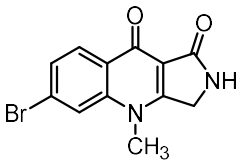

2-2.11q

*6-Bromo-4-methyl-2,3-dihydro-1H-pyrrolo[3,4-b]quinoline-1,9(4H)-dione (**2-2.11q**)*. **2-2.3q** (21.1 mg, 0.05 mmol) was subjected to procedure B to give **2-2.11q** (12.9 mg, 82% yield) as an amorphous off-white solid. ^{1}H NMR (400 MHz, DMSO-d_6) δ 8.15 (d, J = 8.5 Hz, 1H), 8.07 (d, J = 1.7 Hz, 1H), 7.99 (s, 1H), 7.63 (dd, J = 8.5, 1.7 Hz, 1H), 4.47 (s, 2H), 3.70 (s, 3H). ^{13}C{^{1}H} NMR (101 MHz, DMSO-d_6) δ 171.0, 168.6, 163.5, 141.8, 128.1, 127.2, 127.0, 126.4, 119.4, 110.0, 43.4, 34.8. HRMS (ESI-QTOF) m/z: $[M + H]^+$ Calcd for $C_{12}H_{10}BrN_2O_2^+$ 292.9920; Found: 292.9914.

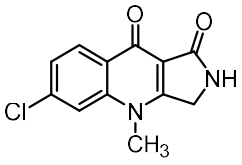

2-2.11r

*6-Chloro-4-methyl-2,3-dihydro-1H-pyrrolo[3,4-b]quinoline-1,9(4H)-dione (**2-2.11r**)*. **2-2.3r** (35.3 mg, 0.10 mmol) was subjected to procedure B to give **2-2.11r** (20.6 mg, 82% yield) as an amorphous off-white solid. ^{1}H NMR (400 MHz, DMSO-d_6) δ 8.23 (d, J = 8.6 Hz, 1H), 7.99 (s, 1H), 7.94 (d, J = 1.9 Hz, 1H), 7.49 (dd, J = 8.6, 1.9 Hz, 1H), 4.47 (s, 2H), 3.70 (s, 3H). ^{13}C{^{1}H} NMR (101 MHz, DMSO-d_6) δ 170.9, 168.6, 163.6, 141.7, 137.4, 128.1, 126.7, 124.4, 116.5, 110.0, 43.4, 34.8. HRMS (ESI-QTOF) m/z: [M + H]$^+$ Calcd for $C_{12}H_{10}ClN_2O_2^+$ 249.0425; Found: 249.0414.

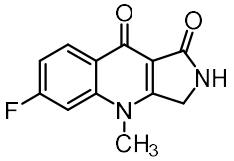

2-2.11s

*6-Fluoro-4-methyl-2,3-dihydro-1H-pyrrolo[3,4-b]quinoline-1,9(4H)-dione (**2-2.11s**)*. **2-2.3s** (36.4 mg, 0.11 mmol) was subjected to procedure B to give **2-2.11s** (17.0 mg, 67% yield) as an amorphous off-white solid. ^{1}H NMR (400 MHz, DMSO-d_6) δ 8.31 (ddd, J = 8.8, 6.6, 2.0 Hz, 1H), 7.98 (s, 1H), 7.72 (dt, J = 11.4, 2.2 Hz, 1H), 7.33 (tt, J = 8.6, 2.0 Hz, 1H), 4.48 (s, 2H), 3.69 (d, J = 2.0 Hz, 3H). ^{13}C{^{1}H} NMR (101 MHz, DMSO-d_6) δ 171.0, 168.8, 164.5 (d, J = 248.3 Hz), 163.8, 142.7, 129.2 (d, J = 10.6 Hz), 124.9, 112.4 (d, J = 23.2 Hz), 109.9, 103.4 (d, J = 26.9 Hz), 43.3, 35.0. ^{19}F{^{1}H} NMR (376 MHz, DMSO-d_6) δ -105.91. HRMS (ESI-QTOF) m/z: [M + H]$^+$ Calcd for $C_{12}H_{10}FN_2O_2^+$ 233.0721; Found: 233.0717.

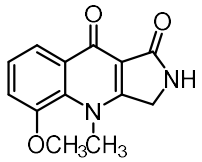

2-2.11t

*5-Methoxy-4-methyl-2,3-dihydro-1H-pyrrolo[3,4-b]quinoline-1,9(4H)-dione (**2-2.11t**)*. **2-2.3t** (34.1 mg, 0.10 mmol) was subjected to procedure B to give **2-2.11t** (20.6 mg, 85% yield) as an

amorphous off-white solid. ^{1}H NMR (400 MHz, DMSO-d_6) δ 7.95 (s, 1H), 7.88 (dd, J = 7.5, 1.9 Hz, 1H), 7.49 – 7.26 (m, 2H), 4.45 (s, 2H), 3.94 (s, 3H), 3.93 (s, 3H). Solubility precluded ^{13}C NMR. HRMS (ESI-QTOF) m/z: $[M + H]^+$ Calcd for $C_{13}H_{13}N_2O_3^+$ 245.0921; Found: 245.0914.

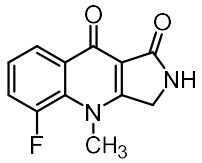

2-2.11u

*5-Fluoro-4-methyl-2,3-dihydro-1H-pyrrolo[3,4-b]quinoline-1,9(4H)-dione (**2-2.11u**).* **2-2.3u** (33.5 mg, 0.10 mmol) was subjected to procedure B to give **2-2.11u** (20.9 mg, 89% yield) as an amorphous off-white solid. ^{1}H NMR (400 MHz, DMSO-d_6) δ 8.10 (dd, J = 8.0, 1.5 Hz, 1H), 8.03 (s, 1H), 7.67 (ddd, J = 15.1, 7.9, 1.6 Hz, 1H), 7.43 (td, J = 8.0, 4.2 Hz, 1H), 4.48 (s, 2H), 3.86 (d, J = 7.5 Hz, 3H). Solubility precluded ^{13}C NMR. ^{19}F{^{1}H} NMR (376 MHz, DMSO-d_6) δ -120.62. HRMS (ESI-QTOF) m/z: $[M + H]^+$ Calcd for $C_{12}H_{10}FN_2O_2^+$ 233.0721; Found: 233.0714.

General Procedure C. *Synthesis of 2-benzyl 4-substituted-2,3-dihydro-1H-pyrrolo[3,4-b]quinolone-1,9(4H)-diones* (**2-2.16a-u**).

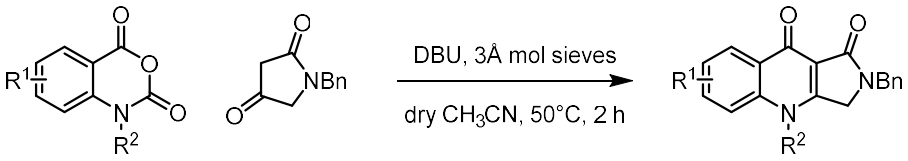

2-2.1a-u **2-2.2c** **2-2.16a-u**

To a 4 mL screw cap vial was added the corresponding isatoic anhydride **2-2.1** (2.0 equiv.) and *N*-benzyl tetramic acid **2-2.2c** before the addition of anhydrous acetonitrile (0.5 M) under Argon(g). The vial was then charged with 3Å molecular sieves followed by addition of DBU (2.0 equiv.). The vial was then stirred at 50°C for 2 h. Reaction progress was monitored through thin layer

chromatography. The reaction mixture was then cooled to room temperature and was added with 1:1 saturated aqueous NH_4Cl solution and water. The contents were transferred to a separating funnel and extracted with CH_2Cl_2 (3 x 5 mL). The combined organic layers were washed with saturated brine (5 mL), dried over anhydrous Na_2SO_4 and concentrated to give the crude material, which was purified by column chromatography (MPLC, Solvents: MeOH/CH_2Cl_2 or EtOAc/CH_2Cl_2; 4 g silica column; Flow rate:12 mL/min) to obtain the desired product **2-2.16**.

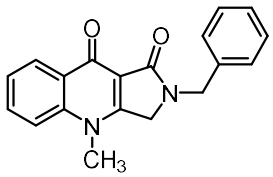

2-2.16a

*2-Benzyl-4-methyl-2,3-dihydro-1H-pyrrolo[3,4-b]quinoline-1,9(4H)-dione (**2-2.16a**)*. Following procedure C, **2-2.2c** (35 mg, 0.18 mmol) was treated with **2-2.1a** (65 mg, 0.37 mmol) to obtain **2-2.16a** after column chromatography (3.6% MeOH/CH_2Cl_2) as an amorphous off-white solid (43 mg, 77% yield). ^{1}H NMR (400 MHz, DMSO-d_6) δ 8.35 – 8.32 (m, 1H), 7.88 – 7.82 (m, 2H), 7.55 – 7.51 (m, 1H), 7.44 – 7.40 (m, 2H), 7.37 – 7.32 (m, 3H), 4.68 (s, 2H), 4.56 (s, 2H), 3.73 (s, 3H). ^{13}C{^{1}H} NMR (101 MHz, DMSO-d_6) δ 171.7, 166.7, 161.4, 141.1, 138.2, 133.0, 129.1 (2C), 128.5, 128.1 (2C), 127.7, 126.5, 124.7, 117.1, 109.5, 47.9, 44.9, 35.3. HRMS (ESI-QTOF) m/z: $[M + H]^+$ Calcd for $C_{19}H_{17}N_2O_2^+$ 305.1285; Found 305.1289.

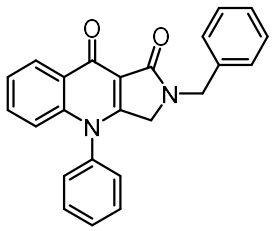

2-2.16c

*2-Benzyl-4-phenyl-2,3-dihydro-1H-pyrrolo[3,4-b]quinoline-1,9(4H)-dione (**2-2.16c**)*. Following procedure C, **2-2.2c** (35 mg, 0.18 mmol) was treated with **2-2.1c** (88 mg, 0.37 mmol) to obtain **2-**

2.16c after column chromatography (2.5-4% MeOH/CH_2Cl_2) as an amorphous yellow solid (33 mg, 49%). ^{1}H NMR (400 MHz, DMSO-d_6) δ 8.33 (dd, J = 8.0, 1.5 Hz, 1H), 7.72 – 7.62 (m, 6H), 7.47 (t, J = 7.5 Hz, 1H), 7.33 – 7.22 (m, 5H), 6.82 (d, J = 8.5 Hz, 1H), 4.54 (s, 2H), 3.94 (s, 2H). ^{13}C{^{1}H} NMR (101 MHz, DMSO-d_6) δ 172.0, 166.5, 161.1, 142.1, 138.1, 136.8, 133.0, 131.2 (2C), 130.9, 129.0 (2C), 128.8 (2C), 128.1 (2C), 127.7 (2C), 126.4, 124.9, 117.8, 109.8, 47.9, 44.8. HRMS (ESI-QTOF) m/z: $[M + H]^+$ Calcd for $C_{24}H_{19}N_2O_2^+$ 367.1441; Found 367.1437.

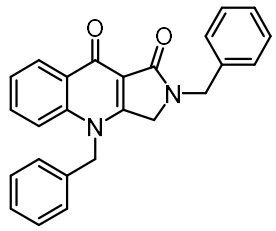

2-2.16e

2,4-Dibenzyl-2,3-dihydro-1H-pyrrolo[3,4-b]quinoline-1,9(4H)-dione ***(2-2.16e)****.* Following procedure C, **2-2.2c** (35 mg, 0.18 mmol) was treated with **2-2.1e** (94 mg, 0.37 mmol) to obtain **2-2.16e** after column chromatography (1-3% MeOH/CH_2Cl_2) as an amorphous pale-yellow solid (53 mg, 76%). ^{1}H NMR (400 MHz, DMSO-d_6) δ 8.32 (dd, J = 8.1, 1.5 Hz, 1H), 7.71 – 7.62 (m, 2H), 7.45 (t, J = 7.4 Hz, 1H), 7.37 – 7.25 (m, 8H), 7.18 – 7.14 (m, 2H), 5.52 (s, 2H), 4.62 (s, 2H), 4.50 (s, 2H). ^{13}C{^{1}H} NMR (101 MHz, DMSO-d_6) δ 171.8, 166.6, 161.5, 140.4, 138.1, 135.5, 133.1, 129.4 (2C), 129.1 (2C), 128.9, 128.8, 128.1 (2C), 127.7, 126.7, 126.3 (2C), 124.9, 117.7, 109.9, 50.7, 48.1, 44.9. HRMS (ESI-QTOF) m/z: $[M + H]^+$ Calcd for $C_{25}H_{21}N_2O_2^+$ 381.1598; Found 381.1597.

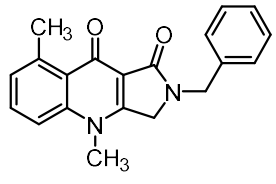

2-2.16g

2-Benzyl-4,8-dimethyl-2,3-dihydro-1H-pyrrolo[3,4-b]quinoline-1,9(4H)-dione ***(2-2.16g)***. Following procedure C, **2-2.2c** (35 mg, 0.18 mmol) was treated with **2-2.1g** (71 mg, 0.37 mmol) to obtain **2-2.16g** after column chromatography (5-6% MeOH/CH_2Cl_2) as an amorphous light brown solid (49 mg, 83% yield). ^{1}H NMR (400 MHz, DMSO-d_6) δ 7.62 – 7.61 (m, 2H), 7.38 – 7.35 (m, 2H), 7.30 – 7.27 (m, 3H), 7.20 – 7.18 (m, 1H), 4.62 (s, 2H), 4.46 (s, 2H), 3.62 (s, 3H), 2.86 (s, 3H). ^{13}C{^{1}H} NMR (101 MHz, DMSO-d_6) δ 174.6, 166.9, 160.3, 142.8, 141.3, 138.3, 131.9, 129.1 (2C), 128.0 (2C), 127.9, 127.7, 126.7, 115.2, 110.4, 47.6, 44.9, 35.9, 24.2. HRMS (ESI-QTOF) m/z: $[M + H]^+$ Calcd for $C_{20}H_{19}N_2O_2^+$ 319.1441; Found 319.1440.

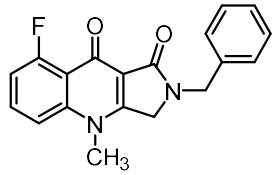

2-2.16h

2-Benzyl-8-fluoro-4-methyl-2,3-dihydro-1H-pyrrolo[3,4-b]quinoline-1,9(4H)-dione ***(2-2.16h)***. Following procedure C, **2-2.2c** (35 mg, 0.18 mmol) was treated with **2-2.1h** (72 mg, 0.37 mmol) to obtain **2-2.16h** after column chromatography (2.5-3.2% MeOH/CH_2Cl_2) as an amorphous yellow solid (35 mg, 59% yield). ^{1}H NMR (400 MHz, DMSO-d_6) δ 7.78 – 7.73 (m, 1H), 7.60 (d, J = 8.7 Hz, 1H), 7.39 – 7.35 (m, 2H), 7.31 – 7.26 (m, 3H), 7.22 – 7.16 (m, 1H), 4.62 (s, 2H), 4.48 (s, 2H), 3.64 (s, 3H). ^{13}C{^{1}H} NMR (101 MHz, DMSO-d_6) δ 170.7, 166.4, 162.1 (d, J = 260.5 Hz), 161.1, 143.2 (d, J = 3.7 Hz), 138.1, 134.0 (d, J = 11.3 Hz), 129.1 (2C), 128.1 (2C), 127.7, 118.0 (d, J = 7.4 Hz), 113.2 (d, J = 4.0 Hz), 111.7 (d, J = 21.0 Hz), 110.6, 47.8, 44.9, 36.2. ^{19}F{^{1}H} NMR (376 MHz, DMSO-d_6) δ -112.56. HRMS (ESI-QTOF) m/z: $[M + H]^+$ Calcd for $C_{19}H_{16}FN_2O_2^+$ 323.1190; Found 323.1188.

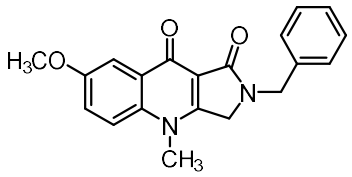

2-2.16i

2-Benzyl-7-methoxy-4-methyl-2,3-dihydro-1H-pyrrolo[3,4-b]quinoline-1,9(4H)-dione ***(2-2.16i)***. Following procedure C, **2-2.2c** (35 mg, 0.18 mmol) was treated with **2-2.1i** (76 mg, 0.37 mmol) to obtain **2-2.16i** after column chromatography (3.8-4% MeOH/CH_2Cl_2) as an amorphous off-white solid (47 mg, 76% yield). ^{1}H NMR (400 MHz, DMSO-d_6) δ 7.80 (d, J = 9.3 Hz, 1H), 7.71 (d, J = 3.1 Hz, 1H), 7.44 – 7.34 (m, 3H), 7.31 – 7.27 (m, 3H), 4.63 (s, 2H), 4.49 (s, 2H), 3.89 (s, 3H), 3.69 (s, 3H). ^{13}C{^{1}H} NMR (101 MHz, DMSO-d_6) δ 171.1, 166.8, 160.0, 156.7, 138.2, 135.5, 129.8, 129.1 (2C), 128.1 (2C), 127.7, 122.0, 118.9, 108.6, 106.9, 56.0, 47.8, 44.9, 35.5. HRMS (ESI-QTOF) m/z: $[M + H]^+$ Calcd for $C_{20}H_{19}N_2O_3^+$ 335.1390; Found 335.1389.

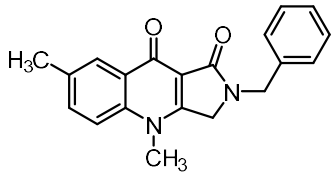

2-2.16j

2-Benzyl-4,7-dimethyl-2,3-dihydro-1H-pyrrolo[3,4-b]quinoline-1,9(4H)-dione ***(2-2.16j)***. Following procedure C, **2-2.2c** (35 mg, 0.18 mmol) was treated with **2-2.1j** (71 mg, 0.37 mmol) to obtain **2-2.16j** after column chromatography (5-6% MeOH/CH_2Cl_2) as an amorphous off-white solid (44 mg, 74% yield). ^{1}H NMR (400 MHz, DMSO-d_6) δ 8.08 (d, J = 2.3 Hz, 1H), 7.72 (d, J = 8.6 Hz, 1H), 7.62 (dd, J = 8.7, 2.2 Hz, 1H), 7.39 – 7.36 (m, 2H), 7.31 – 7.27 (m, 3H), 4.62 (s, 2H), 4.49 (s, 2H), 3.66 (s, 3H), 2.46 (s, 3H). ^{13}C{^{1}H} NMR (101 MHz, DMSO-d_6) δ 171.5, 166.8, 160.8, 139.1, 138.2, 134.2, 134.1, 129.1 (2C), 128.4, 128.1 (2C), 127.7, 126.0, 117.0, 109.2, 47.9, 44.9, 35.3, 20.9. HRMS (ESI-QTOF) m/z: $[M + H]^+$ Calcd for $C_{20}H_{19}N_2O_2^+$ 319.1441; Found 319.1438.

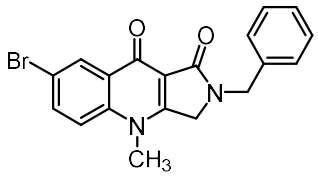

2-2.16k

2-Benzyl-7-bromo-4-methyl-2,3-dihydro-1H-pyrrolo[3,4-b]quinoline-1,9(4H)-dione ***(2-2.16k)***. Following procedure C, **2-2.2c** (35 mg, 0.18 mmol) was treated with **2-2.1k** (95 mg, 0.37 mmol) to obtain **2-2.16k** after column chromatography (1-2% MeOH/CH_2Cl_2) as an amorphous yellow solid (48 mg, 68% yield). ^{1}H NMR (400 MHz, DMSO-d_6) δ 8.32 (d, J = 2.5 Hz, 1H), 7.96 (dd, J = 9.0, 2.5 Hz, 1H), 7.82 (d, J = 9.1 Hz, 1H), 7.42 – 7.27 (m, 5H), 4.63 (s, 2H), 4.51 (s, 2H), 3.68 (s, 3H). ^{13}C{^{1}H} NMR (101 MHz, DMSO-d_6) δ 170.3, 166.3, 161.8, 140.2, 138.0, 135.5, 130.0, 129.1 (2C), 128.6, 128.1 (2C), 127.7, 119.9, 117.8, 109.9, 48.1, 44.9, 35.6. HRMS (ESI-QTOF) m/z: $[M + H]^+$ Calcd for $C_{19}H_{16}BrN_2O_2^+$ 383.0390; Found 383.0386.

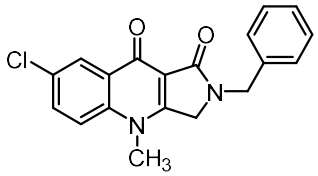

2-2.16l

2-Benzyl-7-chloro-4-methyl-2,3-dihydro-1H-pyrrolo[3,4-b]quinoline-1,9(4H)-dione ***(2-2.16l)***. Following procedure C, **2-2.2c** (35 mg, 0.18 mmol) was treated with **2-2.1l** (79 mg, 0.37 mmol) to obtain **2-2.16l** after column chromatography (4-5% MeOH/CH_2Cl_2) as an amorphous pale-yellow solid (53 mg, 76% yield). ^{1}H NMR (400 MHz, DMSO-d_6) δ 8.19 (d, J = 2.4 Hz, 1H), 7.91 – 7.82 (m, 2H), 7.39 – 7.28 (m, 5H), 4.63 (s, 2H), 4.52 (s, 2H), 3.69 (s, 3H). ^{13}C{^{1}H} NMR (101 MHz, DMSO-d_6) δ 170.4, 166.4, 161.8, 139.8, 138.1, 132.8, 129.8, 129.1 (2C), 128.9, 128.1 (2C), 127.7, 125.4, 119.8, 109.8, 48.1, 44.9, 35.6. HRMS (ESI-QTOF) m/z: $[M + H]^+$ Calcd for $C_{19}H_{16}ClN_2O_2^+$ 339.0895; Found 339.0892.

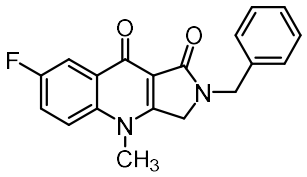

2-2.16m

2-Benzyl-7-fluoro-4-methyl-2,3-dihydro-1H-pyrrolo[3,4-b]quinoline-1,9(4H)-dione ***(2-2.16m)***. Following procedure C, **2-2.2c** (35 mg, 0.18 mmol) was treated with **2-2.1m** (72 mg, 0.37 mmol) to obtain **2-2.16m** after column chromatography (2.8-3% MeOH/CH_2Cl_2) as an amorphous light brown solid (50 mg, 83% yield). ^{1}H NMR (400 MHz, DMSO-d_6) δ 7.94 – 7.91 (m, 2H), 7.74 – 7.69 (m, 1H), 7.39 – 7.35 (m, 2H), 7.31 – 7.27 (m, 3H), 4.63 (s, 2H), 4.51 (s, 2H), 3.70 (s, 3H). ^{13}C{^{1}H} NMR (101 MHz, DMSO-d_6) δ 170.7 (d, J = 2.4 Hz), 166.5, 161.4, 159.5 (d, J = 244.0 Hz), 138.1, 137.8, 130.2 (d, J = 6.6 Hz), 129.1 (2C), 128.1 (2C), 127.7, 121.1 (d, J = 24.3 Hz), 120.2 (d, J = 8.1 Hz), 111.0 (d, J = 22.6 Hz), 109.0, 48.0, 44.9, 35.8. ^{19}F{^{1}H} NMR (376 MHz, DMSO-d_6) δ -117.39. HRMS (ESI-QTOF) m/z: $[M + H]^+$ Calcd for $C_{19}H_{16}FN_2O_2^+$ 323.1190; Found 323.1187.

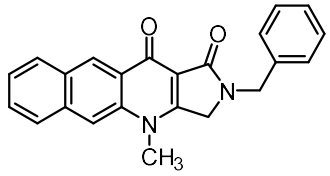

2-2.16n

2-Benzyl-4-methyl-2,3-dihydro-1H-benzo[g]pyrrolo[3,4-b]quinoline-1,11(4H)-dione ***(2-2.16n)***. Following general procedure C, **2-2.2c** (35 mg, 0.18 mmol) was treated with **2-2.1b** (84 mg, 0.37 mmol) to obtain **2-2.16b** after column chromatography (2-5% MeOH/CH_2Cl_2) as an amorphous yellow solid (42 mg, 65% yield). ^{1}H NMR (400 MHz, DMSO-d_6) δ 8.91 (s, 1H), 8.31 (s, 1H), 8.22 (d, J = 8.3 Hz, 1H), 8.08 (d, J = 8.3 Hz, 1H), 7.68 – 7.63 (m, 1H), 7.58 – 7.43 (m, 1H), 7.40 – 7.28 (m, 5H), 4.64 (s, 2H), 4.54 (s, 2H), 3.76 (s, 3H). ^{13}C{^{1}H} NMR (101 MHz, DMSO-d_6) δ 172.4, 166.8, 162.9, 138.3, 138.2, 135.0, 129.6, 129.5, 129.1 (2C), 128.9, 128.1 (2C), 128.0, 127.7, 127.4,

127.2, 126.5, 114.3, 107.4, 48.2, 44.9, 35.5. HRMS (ESI-QTOF) m/z: $[M + H]^+$ Calcd for $C_{23}H_{19}N_2O_2^+$ 355.1441; Found 355.1438.

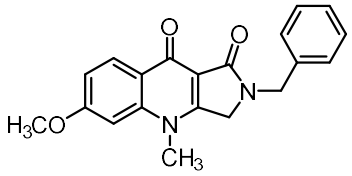

2-2.16o

2-Benzyl-6-methoxy-4-methyl-2,3-dihydro-1H-pyrrolo[3,4-b]quinoline-1,9(4H)-dione ***(2-2.16o)***

Following procedure C, **2-2.2c** (35 mg, 0.18 mmol) was treated with **2-2.16o** (76 mg, 0.37 mmol) to obtain **2-2.16o** after column chromatography (2.5-3% MeOH/CH_2Cl_2) as an amorphous pale-yellow solid (43 mg, 70% yield). ^{1}H NMR (400 MHz, DMSO-d_6) δ 8.19 (d, J = 8.9 Hz, 1H), 7.39 – 7.27 (m, 5H), 7.13 – 7.06 (m, 2H), 4.62 (s, 2H), 4.48 (s, 2H), 3.94 (s, 3H), 3.65 (s, 3H). ^{13}C{^{1}H} NMR (101 MHz, DMSO-d_6) δ 171.3, 166.8, 163.1, 161.4, 142.9, 138.2, 129.1 (2C), 128.3, 128.1 (2C), 127.7, 122.4, 113.2, 109.3, 100.0, 56.3, 47.9, 44.9, 35.4. HRMS (ESI-QTOF) m/z: $[M + H]^+$ Calcd for $C_{20}H_{19}N_2O_3^+$ 335.1390; Found 335.1390.

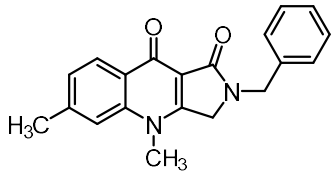

2-2.16p

2-Benzyl-4,6-dimethyl-2,3-dihydro-1H-pyrrolo[3,4-b]quinoline-1,9(4H)-dione ***(2-2.16p)***.

Following general procedure C, **2-2.2c** (35 mg, 0.18 mmol) was treated with **2-2.1p** (71 mg, 0.37 mmol) to obtain **2-2.16p** after column chromatography (2.5-2.6% MeOH/CH_2Cl_2) as an amorphous off-white solid (43 mg, 73% yield). ^{1}H NMR (400 MHz, DMSO-d_6) δ 8.16 (d, J = 8.1 Hz, 1H), 7.63 (s, 1H), 7.39 – 7.27 (m, 6H), 4.62 (s, 2H), 4.49 (s, 2H), 3.66 (s, 3H), 2.50 (s overlapped, 3H). ^{13}C{^{1}H} NMR (101 MHz, DMSO-d_6) δ 171.6, 166.8, 161.2, 143.5, 141.2, 138.2,

129.1 (2C), 128.1 (2C), 127.7, 126.4, 126.4, 126.1, 116.8, 109.3, 47.9, 44.9, 35.3, 22.0. HRMS (ESI-QTOF) m/z: $[M + H]^+$ Calcd for $C_{20}H_{19}N_2O_2^+$ 319.1441; Found 319.1440.

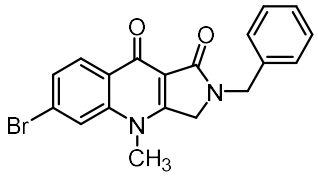

2-2.16q

2-Benzyl-6-bromo-4-methyl-2,3-dihydro-1H-pyrrolo[3,4-b]quinoline-1,9(4H)-dione ***(2-2.16q)***. Following procedure C, **2-2.2c** (35 mg, 0.18 mmol) was treated with **2-2.1q** (95 mg, 0.37 mmol) to obtain **2-2.16q** after column chromatography (3-5% MeOH/CH_2Cl_2) as an amorphous yellow solid (38 mg, 54% yield). ^{1}H NMR (400 MHz, DMSO-d_6) δ 8.18 (d, J = 8.5 Hz, 1H), 8.07 (d, J = 1.6 Hz, 1H), 7.65 (dd, J = 8.5, 1.6 Hz, 1H), 7.39 – 7.28 (m, 5H), 4.63 (s, 2H), 4.52 (s, 2H), 3.68 (s, 3H). ^{13}C{^{1}H} NMR (101 MHz, DMSO-d_6) δ 170.6, 165.9, 161.5, 141.6, 137.6, 128.6, 128.1, 127.6, 127.4, 127.3, 127.0, 126.4, 119.5, 109.6, 47.6, 44.4, 35.1. HRMS (ESI-QTOF) m/z: $[M + H]^+$ Calcd for $C_{19}H_{16}BrN_2O_2^+$ 383.0390; Found 383.0386.

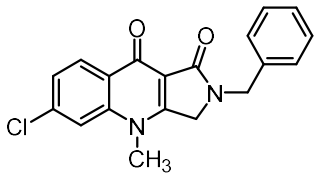

2-2.16r

2-Benzyl-6-chloro-4-methyl-2,3-dihydro-1H-pyrrolo[3,4-b]quinoline-1,9(4H)-dione ***(2-2.16r)***. Following procedure C, **2-2.2c** (35 mg, 0.18 mmol) was treated with **2-2.1r** (79 mg, 0.37 mmol) to obtain **2-2.16r** after column chromatography (1-1.2% MeOH/CH_2Cl_2) as an amorphous pale-yellow solid (43 mg, 69% yield). ^{1}H NMR (400 MHz, DMSO-d_6) δ 8.26 (d, J = 8.6 Hz, 1H), 7.94 (d, J = 1.8 Hz, 1H), 7.52 (dd, J = 8.6, 1.8 Hz, 1H), 7.37 – 7.29 (m, 5H), 4.63 (s, 2H), 4.51 (s, 2H), 3.68 (s, 3H). ^{13}C{^{1}H} NMR (101 MHz, DMSO-d_6) δ 171.0, 166.4, 162.1, 142.0, 138.1, 137.9,

129.1 (2C), 128.5, 128.1 (2C), 127.7, 127.2, 125.0, 117.1, 110.0, 48.1, 44.9, 35.6. HRMS (ESI-QTOF) m/z: $[M + H]^+$ Calcd for $C_{19}H_{16}ClN_2O_2^+$ 339.0895; Found 339.0891.

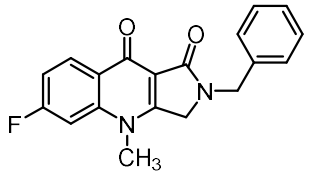

2-2.16s

2-Benzyl-6-fluoro-4-methyl-2,3-dihydro-1H-pyrrolo[3,4-b]quinoline-1,9(4H)-dione ***(2-2.16s)***. Following procedure C, **2-2.2c** (35 mg, 0.18 mmol) was treated with **2-2.1s** (72 mg, 0.37 mmol) to obtain **2-2.16s** after column chromatography (45-50% EtOAc/CH_2Cl_2) as an amorphous light brown solid (19 mg, 70%). ^{1}H NMR (400 MHz, DMSO-d_6) δ 8.32 (dd, J = 8.9, 6.6 Hz, 1H), 7.72 (dd, J = 11.4, 2.3 Hz, 1H), 7.39 – 7.27 (m, 6H), 4.63 (s, 2H), 4.51 (s, 2H), 3.66 (s, 3H). ^{13}C{^{1}H} NMR (101 MHz, DMSO-d_6) δ 171.0, 166.5, 164.9 (d, J = 248.2 Hz), 162.2, 142.9 (d, J = 12.0 Hz), 138.1, 129.6 (d, J = 11.0 Hz), 129.1, 128.9, 128.1, 127.7, 125.4 (d, J = 1.5 Hz), 113.0 (d, J = 23.1 Hz), 109.9, 103.8 (d, J = 27.2 Hz), 48.0, 44.9, 35.7. ^{19}F{^{1}H} NMR (376 MHz, DMSO-d_6) δ -105.79. HRMS (ESI-QTOF) m/z: $[M + H]^+$ Calcd for $C_{19}H_{16}FN_2O_2^+$ 323.1190; Found 323.1183.

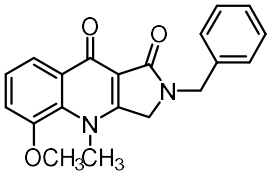

2-2.16t

2-Benzyl-5-methoxy-4-methyl-2,3-dihydro-1H-pyrrolo[3,4-b]quinoline-1,9(4H)-dione ***(2-2.16t)***. Following procedure C, **2-2.2c** (35 mg, 0.18 mmol) was treated with **2-2.1t** (76 mg, 0.37 mmol) to obtain **2-2.16t** after column chromatography (3-3.1% MeOH/CH_2Cl_2) as an amorphous off-white solid (51 mg, 82% yield). ^{1}H NMR (400 MHz, DMSO-d_6) δ 7.90 (dd, J = 6.9, 2.6 Hz, 1H), 7.42 – 7.27 (m, 7H), 4.62 (s, 2H), 4.47 (s, 2H), 3.93 (s, 3H), 3.89 (s, 3H). ^{13}C{^{1}H} NMR (101 MHz,

DMSO-d_6) δ 171.0, 166.5, 162.5, 151.1, 138.1, 132.1, 131.1, 129.1 (2C), 128.1 (2C), 127.7, 125.3, 118.5, 116.2, 109.4, 57.3, 48.5, 44.9, 40.6. HRMS (ESI-QTOF) m/z: $[M + H]^+$ Calcd for $C_{20}H_{19}N_2O_3^+$ 335.1390; found 335.1390.

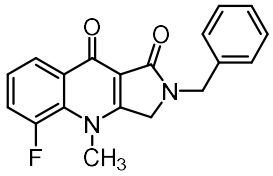

2-2.16u

2-Benzyl-5-fluoro-4-methyl-2,3-dihydro-1H-pyrrolo[3,4-b]quinoline-1,9(4H)-dione ***(2-2.16u)*****.** Following procedure C, **2-2.2c** (35 mg, 0.18 mmol) was treated with **2-2.1u** (72 mg, 0.37 mmol) to obtain **2-2.16u** after column chromatography (3.5-3.7% MeOH/CH_2Cl_2) as an amorphous off-white solid (48 mg, 81%). ^{1}H NMR (400 MHz, DMSO-d_6) δ 8.12 (dd, J = 8.0, 1.5 Hz, 1H), 7.66 (ddd, J = 15.0, 7.9, 1.6 Hz, 1H), 7.47 – 7.42 (m, 1H), 7.41 – 7.35 (m, 2H), 7.31 – 7.27 (m, 3H), 4.63 (s, 2H), 4.50 (s, 2H), 3.83 (d, J = 7.6 Hz, 3H). ^{13}C{^{1}H} NMR (101 MHz, DMSO-d_6) δ 170.4 (d, J = 2.4 Hz), 166.3, 162.7, 152.7 (d, J = 248.5 Hz), 138.0, 131.5, 130.4 (d, J = 6.5 Hz), 129.1 (2C), 128.1 (2C), 127.8, 125.3 (d, J = 8.3 Hz), 122.7 (d, J = 3.5 Hz), 120.3 (d, J = 23.1 Hz), 109.7, 48.3, 44.9. ^{19}F{^{1}H} NMR (376 MHz, DMSO-d_6) δ -120.48. HRMS (ESI-QTOF) m/z: $[M + H]^+$ Calcd for $C_{19}H_{16}FN_2O_2^+$ 323.1190; Found 323.1188.

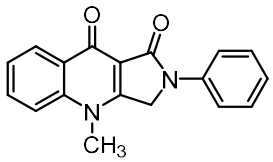

2-2.15

4-Methyl-2-phenyl-2,3-dihydro-1H-pyrrolo[3,4-b]quinoline-1,9(4H)-dione ***(2-2.15)***. Following procedure C, **2-2.2b** (35 mg, 0.20 mmol) was treated with **2-2.1a** (70 mg, 0.41 mmol) to obtain **2-2.15** after column chromatography (3-5% MeOH/CH_2Cl_2) as an amorphous yellow solid (41 mg, 71%). ^{1}H NMR (400 MHz, DMSO-d_6) δ 8.31 (dd, J = 7.9, 1.5 Hz, 1H), 7.90 – 7.82 (m, 4H), 7.54

– 7.50 (m, 1H), 7.46 – 7.40 (m, 2H), 7.15 – 7.11 (m, 1H), 5.11 (s, 2H), 3.84 (s, 3H). $^{13}C\{^{1}H\}$ NMR (101 MHz, DMSO-d_6) δ 171.7, 165.6, 160.8, 141.1, 139.9, 133.2, 129.4 (2C), 128.5, 126.5, 124.9, 123.6, 118.9 (2C), 117.3, 109.9, 48.7, 35.4. HRMS (ESI-QTOF) m/z: $[M + H]^+$ Calcd for $C_{18}H_{15}N_2O_2^+$ 291.1128; Found 291.1129.

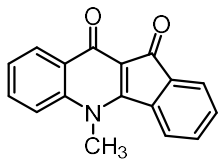

2-2.18

*5-Methyl-5H-indeno[1,2-b]quinoline-10,11-dione (**2-2.18**).* Following procedure C, **2-2.13** (35 mg, 0.24 mmol) was treated with **2-2.1a** (85 mg, 0.48 mmol) to obtain **2-2.18** (40 mg, 67%) as an amorphous indigo purple solid. ^{1}H NMR (400 MHz, DMSO-d_6) δ 8.27 (dd, J = 7.9, 1.6 Hz, 1H), 8.20 (d, J = 7.4 Hz, 1H), 8.05 (d, J = 8.6 Hz, 1H), 7.83 (ddd, J = 8.7, 7.0, 1.7 Hz, 1H), 7.74 – 7.61 (m, 3H), 7.54 (t, J = 7.5 Hz, 1H), 4.30 (s, 3H). $^{13}C\{^{1}H\}$ NMR (101 MHz, DMSO-d_6) δ 187.6, 170.7, 163.2, 141.7, 135.3, 135.2, 133.5, 132.9, 132.7, 129.9, 126.5, 126.1, 125.8, 122.6, 118.5, 110.6, 37.7. HRMS (ESI-QTOF) m/z: $[M + H]^+$ Calcd for $C_{17}H_{12}NO_2^+$ 262.0863; Found: 262.0851.

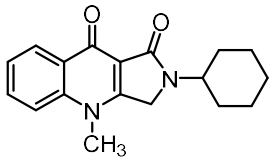

2-2.20

*2-Cyclohexyl-4-methyl-2,3-dihydro-1H-pyrrolo[3,4-b]quinoline-1,9(4H)-dione (**2-2.20**).* Following procedure C, *N*-cyclohexyl tetramic acid (35 mg, 0.19 mmol) was treated with **2-2.1a** (69 mg, 0.41 mmol) to obtain **2-2.20** after column chromatography (3-4% MeOH/CH_2Cl_2) as an amorphous pale-yellow solid (43 mg, 75%). ^{1}H NMR (400 MHz, DMSO-d_6) δ 8.27 (dd, J = 8.0, 1.4 Hz, 1H), 7.86 – 7.77 (m, 2H), 7.50 – 7.46 (m, 1H), 4.57 (s, 2H), 3.98 – 3.90 (m, 1H), 3.75 (s,

3H), 1.84 – 1.79 (m, 2H), 1.73 – 1.65 (m, 3H), 1.57 – 1.47 (m, 2H), 1.43 – 1.32 (m, 2H), 1.19 – 1.08 (m, 1H). $^{13}C\{^{1}H\}$ NMR (101 MHz, DMSO-d_6) δ 171.6, 165.9, 161.5, 141.1, 132.9, 128.5, 126.5, 124.6, 117.0, 110.2, 49.6, 44.8, 35.2, 31.1 (2C), 25.7 (2C), 25.6. HRMS (ESI-QTOF) m/z: $[M + H]^+$ Calcd for $C_{18}H_{21}N_2O_2^+$ 297.1598; Found 297.1596.

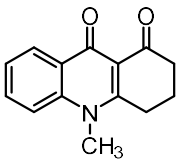

2-2.22

*10-Methyl-3,4-dihydroacridine-1,9(2H,10H)-dione (**2-2.22**).* Following procedure C, 1,3-cyclohexanedione (35 mg, 0.31 mmol) was treated with **2-2.1a** (110 mg, 0.62 mmol) to obtain **2-2.22** after column chromatography (0.8-5% MeOH/CH_2Cl_2) as an amorphous pale-yellow solid (40 mg, 57%). ^{1}H NMR (400 MHz, DMSO-d_6) δ 8.20 (dd, J = 7.9, 1.7 Hz, 1H), 7.84 (d, J = 8.5 Hz, 1H), 7.77 –7.73 (m, 1H), 7.45 – 7.41 (m, 1H), 3.80 (s, 3H), 3.13 (t, J = 6.2 Hz, 2H), 2.39 – 2.36 (m, 2H), 2.01 (p, J = 6.3 Hz, 2H). $^{13}C\{^{1}H\}$ NMR (101 MHz, DMSO-d_6) δ 193.7, 173.6, 163.1, 141.0, 133.1, 128.2, 126.5, 124.8, 117.6, 115.6, 38.5, 35.7, 29.2, 20.9. HRMS (ESI-QTOF) m/z: $[M + H]^+$ Calcd for $C_{14}H_{14}NO_2^+$ 228.1019; Found 228.1021.

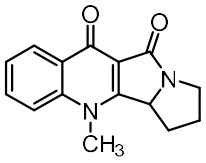

2-3.5

*4-Methyl-1,2,3,3a-tetrahydro-9H-pyrrolizino[1,2-b]quinoline-9,10(4H)-dione (**2-3.5**)*. Following procedure C, **2-3.6** (123 mg, 0.88 mmol) was treated with **2-2.1a** (313 mg, 1.77 mmol) to obtain **2-3.5** after column chromatography (4.8-5% MeOH/CH_2Cl_2) as an amorphous off-white solid (134 mg, 60%). ^{1}H NMR (400 MHz, DMSO-d_6) δ 8.28 – 8.25 (m, 1H), 7.87 – 7.76 (m, 2H), 7.51 – 7.47 (m, 1H), 4.89 (dd, J = 9.8, 6.5 Hz, 1H), 3.82 (s, 3H), 3.54 – 3.47 (m, 1H), 3.18 – 3.12 (m, 1H),

2.49 – 2.44 (m, 1H), 2.23 – 2.15 (m, 2H), 1.54 – 1.44 (m, 1H). $^{13}C\{^{1}H\}$ NMR (101 MHz, DMSO-d_6) δ 172.1, 171.3, 165.3, 141.2, 133.1, 128.7, 126.5, 124.9, 117.4, 109.4, 62.0, 43.0, 36.1, 28.7, 28.6. HRMS (ESI-QTOF) m/z: $[M + H]^+$ Calcd for $C_{15}H_{15}N_2O_2^+$ 255.1128; Found 255.1127.

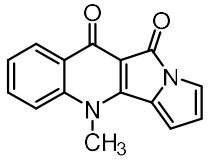

2-3.1

*4-Methyl-9H-pyrrolizino[1,2-b]quinoline-9,10(4H)-dione (**2-3.1**)*. A 4 mL vial was charged with **2-3.5** (20 mg, 0.08 mmol) and commercially available 2,3,5,6-tetrachlorocyclohexa-2,5-diene-1,4-dione (Chloranil) (78 mg, 0.31 mmol). It was then flushed with Argon(g) followed by addition of anhydrous toluene (2 mL). The vial was sealed and heated to 125 °C for 16 h. The reaction mixture was then cooled to room temperature and toluene was removed under reduced pressure to obtain a crude mixture which was directly purified by column chromatography (MPLC) to obtain penicinotam, **2-3.1** after column chromatography (0.9-1.1% MeOH/CH_2Cl_2) as an amorphous bright yellow solid (14 mg, 72%). ^{1}H NMR (400 MHz, DMSO-d_6) δ 8.20 (d, J = 7.9 Hz, 1H), 7.91 (d, J = 8.5 Hz, 1H), 7.79 (t, J = 7.8 Hz, 1H), 7.51 – 7.48 (m, 2H), 7.11 (d, J = 3.3 Hz, 1H), 6.44 (d, J = 3.2 Hz, 1H), 3.99 (s, 3H). $^{13}C\{^{1}H\}$ NMR (101 MHz, DMSO-d_6) δ 169.9, 159.5, 153.7, 140.4, 132.7, 128.7, 125.9, 125.6, 125.5, 120.2, 117.8, 116.6, 116.6, 104.2, 36.7 HRMS (ESI-QTOF) m/z: $[M + H]^+$ Calcd for $C_{15}H_{11}N_2O_2^+$ 251.0815; Found 251.0815.

General Procedure D. *Annulation using monoketones with LiHMDS*

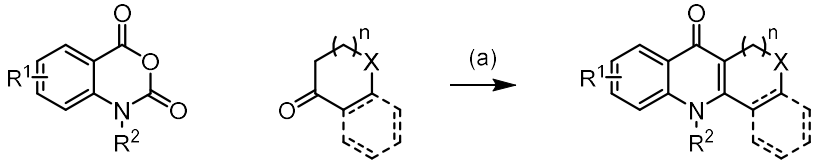

2-2.1a, e-f, h-i, l-m, s, u-x **2-2.23a-j** **2-2.24a-n, 2-2.25 - 2-2.31**

A two-neck round bottom flask equipped with a reflux condenser was charged with the corresponding isatoic anhydride **2-2.1** (1.0 equiv.) and ketone **2-2.23** (2.1 equiv.). The contents were dissolved in anhydrous toluene under Argon(g) and cooled to 0°C before addition of LiHMDS (2.3 equiv., 1M in toluene) dropwise. The resulting mixture was heated to 80°C and stirred for 2 h. The progress of the reaction was monitored by thin layer chromatography. The reaction mixture was then cooled to room temperature and was added with saturated aqueous NH_4Cl solution followed by extraction with ethyl acetate (3 x 5 mL). The combined organic layers were washed with brine solution (1 x 5 mL) and concentrated *in vacuo* to obtain a crude mixture which was purified by column chromatography (MPLC, Solvents: MeOH/CH_2Cl_2 or EtOAc/CH_2Cl_2; 4 g silica column; Flow rate:12 mL/min) to obtain the desired product.

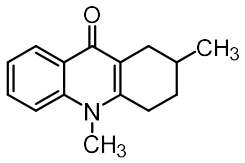

2-2.24a

*2,10-Dimethyl-1,3,4,10-tetrahydroacridin-9(2H)-one (**2-2.24a**)*. Following procedure D, **2-2.1a** (100 mg, 0.56 mmol) was treated with **2-2.23a** (132 mg, 1.19 mmol) to obtain **2-2.24a** after column chromatography (24-30% EtOAc/CH_2Cl_2) as an amorphous light yellow solid (108 mg, 84% yield). ^{1}H NMR (400 MHz, $CDCl_3$) δ 8.47 (dd, J = 8.0, 1.7 Hz, 1H), 7.62 – 7.58 (m, 1H), 7.44 (d, J = 8.6 Hz, 1H), 7.31 (t, J = 7.5 Hz, 1H), 3.69 (s, 3H), 3.04 – 2.97 (m, 1H), 2.90 – 2.71 (m, 2H), 2.18 – 2.07 (m, 1H), 2.03 – 1.94 (m, 1H), 1.79 – 1.67 (m, 1H), 1.49 – 1.36 (m, 1H), 1.11 (d, J = 6.5 Hz, 3H). ^{13}C{^{1}H} NMR (101 MHz, $CDCl_3$) δ 176.8, 147.9, 141.1, 131.5, 126.8, 124.6, 122.5, 118.8, 114.8, 33.5, 31.1, 30.8, 28.6, 27.5, 21.3. HRMS (ESI-QTOF) m/z: $[M + H]^+$ Calcd for $C_{15}H_{18}NO^+$ 228.1383; Found 228.1375.

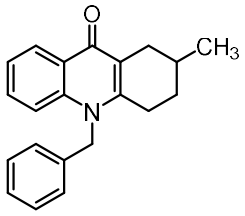

2-2.24b

*10-Benzyl-2-methyl-1,3,4,10-tetrahydroacridin-9(2H)-one (**2-2.24b**)*. Following procedure D, **2-2.1e** (50 mg, 0.19 mmol) was treated with **2-2.23a** (46 mg, 0.41 mmol) to obtain title compound **2-2.24b** after column chromatography (17-19% EtOAc/CH_2Cl_2) as an amorphous off white solid (44 mg, 73% yield). ^{1}H NMR (400 MHz, $CDCl_3$) δ 8.51 (dd, J = 8.0, 1.7 Hz, 1H), 7.50 – 7.45 (m, 1H), 7.37 – 7.28 (m, 5H), 7.03 (d, J = 7.2 Hz, 2H), 5.43 (s, 2H), 3.17 – 3.00 (m, 1H), 2.79 (br. s, 2H), 2.20 (dd, J = 17.0, 10.2 Hz, 1H), 1.96 J = 6.7 Hz 1.87 (m, 1H), 1.83 – 1.71 (m, 1H), 1.49 – 1.37 (m, 1H), 1.11 (d, J = 6.5 Hz, 3H). ^{13}C{^{1}H} NMR (126 MHz, $CDCl_3$) δ 177.1, 148.1, 140.9, 135.9, 131.8, 129.3(2C), 127.8, 126.8, 125.3(2C), 124.9, 122.8, 118.9, 115.7, 49.4, 31.2, 30.8, 27.9 27.7, 21.4. HRMS (ESI-QTOF) m/z: $[M + H]^+$ Calcd for $C_{21}H_{22}NO^+$ 304.1696; Found 304.1685.

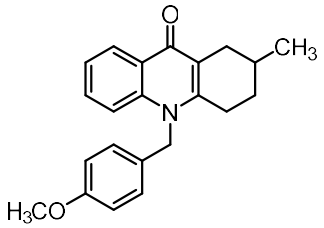

2-2.24c

*10-(4-Methoxybenzyl)-2-methyl-1,3,4,10-tetrahydroacridin-9(2H)-one (**2-2.24c**)*. Following procedure D, **2-2.1f** (50 mg, 0.18 mmol) was treated with **2-2.23a** (42 mg, 0.37 mmol) to obtain **2-2.24c** after column chromatography (50-60% EtOAc/Hexanes) as an amorphous off white solid (43 mg, 74% yield). ^{1}H NMR (400 MHz, $CDCl_3$) δ 8.50 (dd, J = 8.2, 1.7 Hz, 1H), 7.48 (ddd, J = 8.8, 6.9, 1.8 Hz, 1H), 7.33 – 7.28 (m, 2H), 6.95 – 6.91 (m, 2H), 6.88 – 6.84 (m, 2H), 5.36 (s, 2H), 3.77 (s, 3H), 3.09 – 3.04 (m, 1H), 2.80 – 2.77 (m, 2H), 2.25 – 2.11 (m, 1H), 1.97 – 1.87 (m, 1H),

1.82 – 1.73 (m, 1H), 1.48 – 1.36 (m, 1H), 1.11 (d, J = 6.6 Hz, 3H). $^{13}C\{^{1}H\}$ NMR (101 MHz, $CDCl_3$) δ 177.0, 159.1, 148.0, 140.9, 131.7, 127.6, 126.8, 126.4 (2C), 124.8, 122.7, 118.9, 115.66, 114.6 (2C), 55.3, 48.8, 31.1, 30.7, 27.8, 27.7, 21.3. HRMS (ESI-QTOF) m/z: $[M + H]^+$ Calcd for $C_{22}H_{24}NO_2^+$ 334.1802; Found 334.1801.

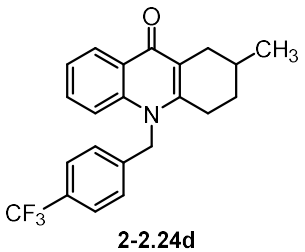

2-2.24d

2-Methyl-10-(4-(trifluoromethyl)benzyl)-1,3,4,10-tetrahydroacridin-9(2H)-one ***(2-2.24d)***. Following procedure D, **2-2.1v** (50 mg, 0.15 mmol) was treated with **2-2.23a** (37 mg, 0.33 mmol) to obtain **2-2.24d** after column chromatography (25-29% EtOAc/CH_2Cl_2) as an amorphous yellow solid (40 mg, 70% yield). ^{1}H NMR (400 MHz, $CDCl_3$) δ 8.51 (dd, J = 8.1, 1.7 Hz, 1H), 7.60 (d, J = 8.1 Hz, 2H), 7.52 – 7.46 (m, 1H), 7.31 (t, J = 7.5 Hz, 1H), 7.19 – 7.15 (m, 3H), 5.47 (s, 2H), 3.18 – 2.97 (m, 1H), 2.74 (br. s, 2H), 2.19 (dd, J = 17.2, 10.2 Hz, 1H), 1.97 – 1.88 (m, 1H), 1.83 – 1.76 (m overlapped, 1H), 1.48 – 1.35 (m, 1H), 1.11 (d, J = 6.5 Hz, 3H). $^{13}C\{^{1}H\}$ NMR (101 MHz, $CDCl_3$) δ 177.1, 147.6, 140.7, 140.1, 132.0, 130.3 (q, J = 32.7 Hz), 127.1, 126.3 (q, J = 3.8 Hz), 125.7, 124.8, 123.2 (q, J = 271.7 Hz), 123.0, 119.3, 115.2, 49.0, 31.0, 30.7, 27.9, 27.6, 21.3. $^{19}F\{^{1}H\}$ NMR (376 MHz, $CDCl_3$) δ -62.65. HRMS (ESI-QTOF) m/z: $[M + H]^+$ Calcd for $C_{22}H_{21}F_3NO^+$ 372.1570; Found 372.1556.

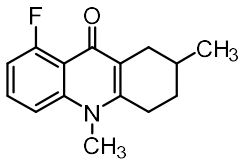

2-2.24e

*8-Fluoro-2,10-dimethyl-1,3,4,10-tetrahydroacridin-9(2H)-one (**2-2.24e**)*. Following procedure D, **2-2.1h** (50 mg, 0.25 mmol) was treated with **2-2.23a** (60 mg, 0.54 mmol) to obtain **2-2.24e** after column chromatography (35-45% EtOAc/CH_2Cl_2) as an amorphous off white solid (40 mg, 63% yield). ^{1}H NMR (400 MHz, $CDCl_3$) δ 7.52 – 7.46 (m, 1H), 7.21 (d, J = 8.8 Hz, 1H), 6.94 – 6.89 (m, 1H), 3.67 (s, 3H), 2.96 (dd, J = 17.3, 5.1 Hz, 1H), 2.89 – 2.67 (m, 2H), 2.10 – 1.90 (m, 2H), 1.77 – 1.68 (m, 1H), 1.47 – 1.35 (m, 1H), 1.10 (d, J = 6.6 Hz, 3H). ^{13}C{^{1}H} NMR (101 MHz, $CDCl_3$) δ 175.8 (d, J = 1.4 Hz), 162.2 (d, J = 262.7 Hz), 147.0, 143.3 (d, J = 4.0 Hz), 131.4 (d, J = 11.3 Hz), 120.6, 114.8 (d, J = 7.5 Hz), 110.5 (d, J = 4.6 Hz), 109.0 (d, J = 21.7 Hz), 34.3, 30.74, 30.71, 28.6, 27.5, 21.3. ^{19}F{^{1}H} NMR (376 MHz, $CDCl_3$) δ -111.71. HRMS (ESI-QTOF) m/z: [M + H]$^+$ Calcd for $C_{15}H_{17}FNO^+$ 246.1290; Found 246.1280.

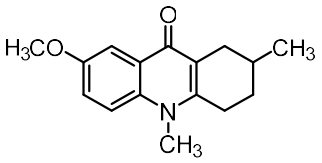

2-2.24f

*7-Methoxy-2,10-dimethyl-1,3,4,10-tetrahydroacridin-9(2H)-one (**2-2.24f**)*. Following procedure D, **2-2.1i** (50 mg, 0.24 mmol) was treated with **2-2.23a** (57 mg, 0.51 mmol) to obtain **2-2.24f** after column chromatography (3.5-3.8% MeOH/CH_2Cl_2) as an amorphous white solid (56 mg, 90% yield). ^{1}H NMR (500 MHz, $CDCl_3$) δ 7.88 (s, 1H), 7.40 (d, J = 9.3 Hz, 1H), 7.23 (d, J = 9.4 Hz, 1H), 3.92 (s, 3H), 3.70 (s, 3H), 3.02 (dd, J = 17.0, 5.0 Hz, 1H), 2.92 – 2.71 (m, 2H), 2.16 – 2.10 (m, 1H), 2.03 – 1.97 (m, 1H), 1.76 (br. s, 1H), 1.47 – 1.39 (m, 1H), 1.11 (d, J = 6.3 Hz, 3H). ^{13}C{^{1}H} NMR (126 MHz, $CDCl_3$) δ 176.0, 155.4, 147.1, 135.9, 125.6, 122.2, 117.8, 116.6, 105.5, 55.8, 33.6, 31.3, 30.8, 28.5, 27.6, 21.4. HRMS (ESI-QTOF) m/z: [M + H]$^+$ Calcd for $C_{16}H_{20}NO_2^+$ 258.1489; Found 258.1479.

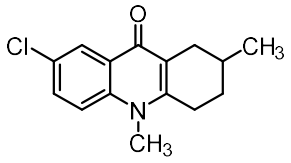

2-2.24g

*7-Chloro-2,10-dimethyl-1,3,4,10-tetrahydroacridin-9(2H)-one (**2-2.24g**)*. Following procedure D, **2-2.1l** (50 mg, 0.24 mmol) was treated with **2-2.23a** (56 mg, 0.50 mmol) to obtain **2-2.24g** after column chromatography (16-20% EtOAc/CH_2Cl_2) as an amorphous off white solid (40 mg, 65% yield). ^{1}H NMR (400 MHz, $CDCl_3$) δ 8.40 (d, J = 2.6 Hz, 1H), 7.50 (dd, J = 9.1, 2.6 Hz, 1H), 7.37 (d, J = 9.1 Hz, 1H), 3.69 (s, 3H), 3.03 – 2.70 (m, 3H), 2.15 – 1.96 (m, 2H), 1.72 (br s, overlapped, 1H), 1.50 – 1.35 (m, 1H), 1.11 (d, J = 6.6 Hz, 3H). ^{13}C{^{1}H} NMR (101 MHz, $CDCl_3$) δ 175.6, 148.2, 139.4, 131.6, 128.6, 125.9, 125.5, 119.2, 116.7, 33.7, 31.1, 30.7, 28.6, 27.4, 21.3. HRMS (ESI-QTOF) m/z: $[M + H]^+$ Calcd for $C_{15}H_{17}ClNO^+$ 262.0993; Found 262.0985.

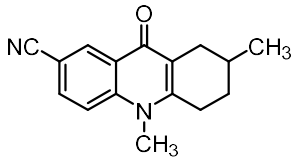

2-2.24h

*7,10-Dimethyl-9-oxo-5,6,7,8,9,10-hexahydroacridine-2-carbonitrile (**2-2.24h**)*. Following procedure D, **2-2.1w** (50 mg, 0.24 mmol) was treated with **2-2.23a** (59 mg, 0.52 mmol) to obtain **2-2.24i** after column chromatography (EtOAc/CH_2Cl_2) as an amorphous white solid (45 mg, 72% yield). ^{1}H NMR (500 MHz, $CDCl_3$) δ 8.75 (s, 1H), 7.75 (d, J = 8.5 Hz, 1H), 7.52 (d, J = 8.9 Hz, 1H), 3.75 (s, 3H), 3.04 – 2.72 (m, 3H), 2.14 – 2.00 (m, 2H), 1.72 (s overlapped, 1H), 1.49-1.41 (m, 1H), 1.12 (d, J = 6.5 Hz, 3H). ^{13}C{^{1}H} NMR (126 MHz, $CDCl_3$) δ 175.5, 149.1, 142.9, 133.2, 132.4, 124.2, 120.9, 118.7, 116.3, 105.7, 33.9, 31.0, 30.6, 28.8, 27.3, 21.3. HRMS (ESI-QTOF) m/z: $[M + H]^+$ Calcd for $C_{16}H_{17}N_2O^+$ 253.1335; Found 253.1326.

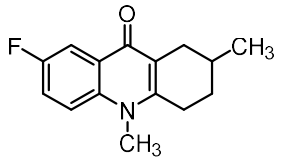

2-2.24i

*7-Fluoro-2,10-dimethyl-1,3,4,10-tetrahydroacridin-9(2H)-one (**2-2.24i**)*. Following procedure D, **2-2.1m** (50 mg, 0.25 mmol) was treated with **2-2.23a** (60 mg, 0.54 mmol) to obtain **2-2.24i** after column chromatography (15-22% EtOAc/CH_2Cl_2) as an amorphous yellow solid (45 mg, 72% yield). ^{1}H NMR (400 MHz, $CDCl_3$) δ 8.10 (dd, J = 9.0, 3.1 Hz, 1H), 7.45 (dd, J = 9.4, 4.1 Hz, 1H), 7.35 – 7.30 (m, 1H), 3.72 (s, 3H), 3.02 – 2.73 (m, 3H), 2.15 – 1.97 (m, 2H), 1.73 (br s, overlapped, 1H), 1.49 – 1.38 (m, 1H), 1.11 (d, J = 6.6 Hz, 3H). ^{13}C{^{1}H} NMR (101 MHz, $CDCl_3$) δ 176.0 (d, J = 2.7 Hz), 158.5 (d, J = 243.9 Hz), 148.0, 137.7 (d, J = 1.0 Hz), 125.9 (d, J = 6.8 Hz), 120.0 (d, J = 25.0 Hz), 118.3, 117.0 (d, J = 7.6 Hz), 111.0 (d, J = 22.2 Hz), 33.8, 31.1, 30.7, 28.6, 27.5, 21.3. ^{19}F{^{1}H} NMR (376 MHz, $CDCl_3$) δ -119.63. HRMS (ESI-QTOF) m/z: $[M + H]^+$ Calcd for $C_{15}H_{17}FNO^+$ 246.12889; Found 246.1280.

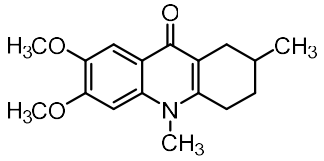

2-2.24j

*6,7-Dimethoxy-2,10-dimethyl-1,3,4,10-tetrahydroacridin-9(2H)-one (**2-2.24j**)*. Following procedure D, **2-2.1x** (50 mg, 0.21 mmol) was treated with **2-2.23a** (50 mg, 0.44 mmol) to obtain **2-2.24j** after column chromatography (4-5% MeOH/CH_2Cl_2) as an amorphous off white solid (19 mg, 32% yield). ^{1}H NMR (400 MHz, $CDCl_3$) δ 7.86 (s, 1H), 6.78 (s, 1H), 4.01 (s, 3H), 4.00 (s, 3H), 3.70 (s, 3H), 3.05 – 2.98 (m, 1H), 2.95 – 2.68 (m, 2H), 2.19 – 2.08 (m, 1H), 2.05 – 1.94 (m, 1H), 1.72 (br s, overlapped, 1H), 1.50 – 1.38 (m, 1H), 1.12 (d, J = 6.6 Hz, 3H). ^{13}C{^{1}H} NMR (101 MHz, $CDCl_3$) δ 175.6, 152.9, 146.5, 146.2, 136.8, 118.9, 118.1, 106.1, 96.5, 56.2, 56.1, 33.7,

31.2, 30.9, 28.6, 27.6, 21.4. HRMS (ESI-QTOF) m/z: $[M + H]^+$ Calcd for $C_{17}H_{22}NO_3^+$ 288.1594; Found 288.1584.

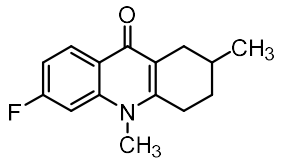

2-2.24k

*6-Fluoro-2,10-dimethyl-1,3,4,10-tetrahydroacridin-9(2H)-one (**2-2.24k**)*. Following procedure D, **2-2.1s** (40 mg, 0.20 mmol) was treated with **2-2.23a** (48 mg, 0.43 mmol) to obtain **2-2.24k** after column chromatography (45-50% EtOAc/CH_2Cl_2) as an amorphous off white solid (28 mg, 56% yield). ^{1}H NMR (400 MHz, $CDCl_3$) δ 8.46 (dd, J = 8.9, 6.8 Hz, 1H), 7.11 – 7.00 (m, 2H), 3.64 (s, 3H), 3.02 – 2.93 (m, 1H), 2.92 – 2.71 (m, 2H), 2.14 – 2.06 (m, 1H), 2.02 – 1.96 (m, 1H), 1.79 – 1.65 (m, 1H), 1.49 – 1.38 (m, 1H), 1.11 (d, J = 6.6 Hz, 3H). ^{13}C{^{1}H} NMR (101 MHz, $CDCl_3$) δ 176.2, 164.8 (d, J = 249.5 Hz), 148.2 (d, J = 1.5 Hz), 142.5 (d, J = 11.2 Hz), 129.7 (d, J = 10.6 Hz), 121.4 (d, J = 1.5 Hz), 119.1, 111.2 (d, J = 23.0 Hz), 100.9 (d, J = 26.7 Hz), 33.7, 30.9, 30.7, 28.6, 27.5, 21.3. ^{19}F{^{1}H} NMR (376 MHz, $CDCl_3$) δ -106.38. HRMS (ESI-QTOF) m/z: $[M + H]^+$ Calcd for $C_{15}H_{17}FNO^+$ 246.12890; Found 246.1279.

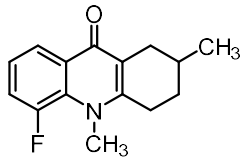

2-2.24l

*5-Fluoro-2,10-dimethyl-1,3,4,10-tetrahydroacridin-9(2H)-one (**2-2.24l**)*. Following procedure D, **2-2.1u** (50 mg, 0.25 mmol) was treated with **2-2.23a** (60 mg, 0.54 mmol) to obtain **2-2.24l** after column chromatography (35-45% EtOAc/CH_2Cl_2) as an amorphous off white solid (43 mg, 69% yield). ^{1}H NMR (400 MHz, $CDCl_3$) δ 8.26 – 8.21 (m, 1H), 7.33 – 7.29 (m, 1H), 7.18 – 7.23 (m, 1H), 3.86 (d, J = 6.7 Hz, 3H), 3.07 – 2.95 (m, 1H), 2.89 – 2.67 (m, 2H), 2.13 – 1.95 (m, 2H), 1.82

– 1.70 (m, 1H), 1.48 – 1.36 (m, 1H), 1.11 (d, J = 6.5 Hz, 3H). $^{13}C\{^{1}H\}$ NMR (101 MHz, $CDCl_3$) δ 175.9 (d, J = 2.4 Hz), 152.0 (d, J = 247.5 Hz), 149.9, 131.6 (d, J = 5.7 Hz), 127.6, 122.6 (d, J = 8.2 Hz), 122.4 (d, J = 3.6 Hz), 119.2, 118.2 (d, J = 23.4 Hz), 37.8 (d, J = 17.7 Hz), 30.9, 30.7, 28.5, 27.5, 21.4. $^{19}F\{^{1}H\}$ NMR (376 MHz, $CDCl_3$) δ -119.02. HRMS (ESI-QTOF) m/z: $[M + H]^+$ Calcd for $C_{15}H_{17}FNO^+$ 246.12890; Found 246.1283.

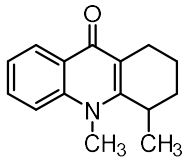

2-2.24m

*4,10-Dimethyl-1,3,4,10-tetrahydroacridin-9(2H)-one (**2-2.24m**)*. Following procedure D, **2-2.1a** (100 mg, 0.56 mmol) was treated with **2-2.23b** (133 mg, 1.19 mmol) to obtain **2-2.24m** after column chromatography (5-7% MeOH/CH_2Cl_2) as an amorphous white solid (99 mg, 78% yield). ^{1}H NMR (500 MHz, $CDCl_3$) δ 8.48 (dd, J = 8.0, 1.7 Hz, 1H), 7.63 (ddd, J = 8.7, 6.9, 1.7 Hz, 1H), 7.50 (d, J = 8.6 Hz, 1H), 7.33 (ddd, J = 7.9, 6.8, 0.9 Hz, 1H), 3.78 (s, 3H), 3.22 – 3.16 (m, 1H), 2.97 – 2.92 (m, 1H), 2.56 – 2.49 (m, 1H), 1.92 – 1.83 (m, 3H), 1.81 – 1.71 (m, 1H), 1.33 (d, J = 7.0 Hz, 3H). $^{13}C\{^{1}H\}$ NMR (126 MHz, $CDCl_3$) δ 177.3, 152.3, 141.5, 131.6, 126.6, 124.5, 122.6, 118.0, 115.2, 33.6, 30.1, 30.1, 22.9, 20.4, 16.4. HRMS (ESI-QTOF) m/z: $[M + H]^+$ Calcd for $C_{15}H_{18}NO^+$ 228.1383; Found 228.1378.

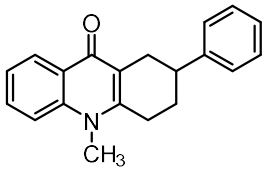

2-2.24n

*10-Methyl-2-phenyl-1,3,4,10-tetrahydroacridin-9(2H)-one (**2-2.24n**)*. Following general procedure D, **2-2.1a** (50 mg, 0.28 mmol) was treated with **2-2.23c** (103 mg, 0.59 mmol) to obtain **2-2.24n** after column chromatography (21-25% EtOAc/CH_2Cl_2) as an amorphous white solid (66

mg, 80% yield). ^{1}H NMR (500 MHz, $CDCl_3$) δ 8.50 (dd, J = 8.0, 1.7 Hz, 1H), 7.64 (ddd, J = 8.7, 7.0, 1.7 Hz, 1H), 7.48 (d, J = 8.6 Hz, 1H), 7.37 – 7.28 (m, 5H), 7.25 – 7.21 (m, 1H), 3.74 (s, 3H), 3.29 – 3.20 (m, 1H), 2.99 – 2.87 (m, 3H), 2.7. – 2.65 (m, 1H), 2.32 – 2.22 (m, 1H), 2.03 – 1.95 (m, 1H). ^{13}C{^{1}H} NMR (126 MHz, $CDCl_3$) δ 176.7, 147.8, 145.4, 141.2, 131.7, 128.5(2C), 126.9(2C), 126.8, 126.4, 124.7, 122.7, 118.7, 114.9, 38.5, 33.6, 30.3, 29.7, 28.9. HRMS (ESI-QTOF) m/z: [M + H]$^{+}$ Calcd for $C_{20}H_{20}NO^{+}$ 290.1539; Found 290.1530.

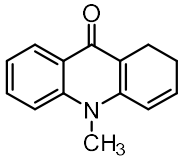

2-2.25

*10-Methyl-1,10-dihydroacridin-9(2H)-one (**2-2.25**)*. Following general procedure D, **2-2.1a** (100 mg, 0.56 mmol) was treated with **2-2.23d** (114 mg, 1.19 mmol) to obtain **2-2.25** after column chromatography (1.5-2% MeOH/CH_2Cl_2) as an amorphous yellow solid (77 mg, 65% yield). ^{1}H NMR (400 MHz, $CDCl_3$) δ 8.48 (dd, J = 7.9, 1.6 Hz, 1H), 7.63 – 7.58 (m, 1H), 7.47 (d, J = 8.7 Hz, 1H), 7.35 – 7.31 (m, 1H), 6.66 – 6.60 (m, 2H), 3.77 (s, 3H), 2.91 – 2.86 (m, 2H), 2.34 – 2.29 (m, 2H). ^{13}C{^{1}H} NMR (101 MHz, $CDCl_3$) δ 175.8, 144.4, 140.7, 139.8, 131.5, 126.8, 125.9, 122.9, 120.4, 116.1, 115.2, 34.5, 22.3, 19.3. HRMS (ESI-QTOF) m/z: [M + H]$^{+}$ Calcd for $C_{14}H_{14}NO^{+}$ 212.1070; Found 212.1069.

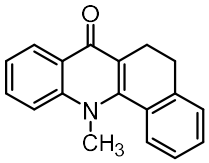

2-2.26

*12-Methyl-6,12-dihydrobenzo[c]acridin-7(5H)-one (**2-2.26**)*. Following procedure D, **2-2.1a** (50 mg, 0.28 mmol) was treated with **2-2.23e** (86 mg, 0.59 mmol) to obtain **2-2.26** after column chromatography (20-24% EtOAc/CH_2Cl_2) as an amorphous yellow solid (52 mg, 70% yield). ^{1}H

NMR (500 MHz, $CDCl_3$) 8.50 (dd, J = 8.0, 1.6 Hz, 1H), 7.68 (ddd, J = 8.5, 6.8, 1.7 Hz, 1H), 7.57 (d, J = 8.6 Hz, 1H), 7.52 – 7.45 (m, 1H), 7.40 – 7.32 (m, 4H), 3.95 (s, 3H), 2.89 – 2.86 (m, 2H), 2.82 – 2.78 (m, 2H). $^{13}C\{^1H\}$ NMR (126 MHz, $CDCl_3$) δ 176.3, 148.2, 143.3, 141.9, 131.9, 130.0, 129.6, 128.5, 128.2, 126.7, 126.1, 125.5, 123.1, 122.5, 116.4, 40.9, 29.0, 21.3. HRMS (ESI-QTOF) m/z: $[M + H]^+$ Calcd for $C_{18}H_{16}NO^+$ 262.1226; Found 262.1225.

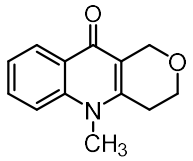

2-2.27

*5-Methyl-1,3,4,5-tetrahydro-10H-pyrano[4,3-b]quinolin-10-one (**2-2.27**)*. Following general procedure D, **2-2.1a** (80 mg, 0.45 mmol) was treated with **2-2.23f** (95 mg, 0.95 mmol) to obtain **2-2.27** after column chromatography (10% MeOH/CH_2Cl_2) as an amorphous off white solid (88 mg, 90% yield). ^1H NMR (400 MHz, $CDCl_3$) δ 8.43 (d, J = 8.0 Hz, 1H), 7.64 (t, J = 7.9 Hz, 1H), 7.46 (d, J = 8.7 Hz, 1H), 7.35 (t, J = 7.5 Hz, 1H), 4.75 (s, 2H), 4.01 – 3.98 (m, 2H), 3.69 (s, 3H), 2.83 – 2.80 (m, 2H). $^{13}C\{^1H\}$ NMR (101 MHz, $CDCl_3$) δ 174.9, 145.4, 141.0, 131.9, 126.4, 124.9, 123.1, 116.8, 115.0, 64.4, 63.8, 33.1, 27.4. HRMS (ESI-QTOF) m/z: $[M + H]^+$ Calcd for $C_{13}H_{14}NO_2^+$ 216.1019; Found 216.1019.

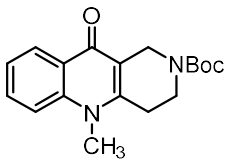

2-2.28

*tert-Butyl-5-methyl-10-oxo-3,4,5,10-tetrahydrobenzo[b][1,6]naphthyridine-2(1H)-carboxylate (**2-2.28**)*. Following general procedure D, **2-2.1a** (100 mg, 0.56 mmol) was treated with **2-2.23g** (236 mg, 1.19 mmol) to obtain title compound **2-2.28** after column chromatography (35-40% EtOAc/CH_2Cl_2) as an amorphous off white solid (137 mg, 78% yield). ^1H NMR (500 MHz,

$CDCl_3$) δ 8.47 (d, J = 8.0 Hz, 1H), 7.68 – 7.65 (m, 1H), 7.49 (d, J = 8.7 Hz, 1H), 7.38 – 7.35 (m, 1H), 4.52 (s, 2H), 3.74 (s, 3H), 3.75 –3.73 (m, overlapped 2H), 2.90 – 2.87 (m, 2H), 1.50 (s, 9H). $^{13}C\{^1H\}$ NMR (126 MHz, $CDCl_3$) δ 175.4, 154.9, 146.5, 141.2, 132.1, 126.4, 124.8, 123.1, 116.0, 115.1, 80.3, 41.7, 39.5, 33.6, 28.5(3C), 27.9. HRMS (ESI-QTOF) m/z: $[M + H]^+$ Calcd for $C_{18}H_{23}N_2O_3^+$ 315.1703; Found 315.1702.

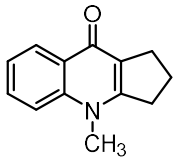

2-2.29

*4-Methyl-1,2,3,4-tetrahydro-9H-cyclopenta[b]quinolin-9-one (**2-2.29**)*. Following procedure D, **2-2.1a** (100 mg, 0.56 mmol) was treated with **2-2.23h** (100 mg, 1.19 mmol) to obtain title compound **2-2.29** after column chromatography (1-1.5% MeOH/CH_2Cl_2) as an amorphous off white solid (50 mg, 45% yield). ^1H NMR (400 MHz, $CDCl_3$) δ 8.49 (dd, J = 8.0, 1.7 Hz, 1H), 7.64 – 7.59 (m, 1H), 7.43 (d, J = 8.5 Hz, 1H), 7.37 – 7.33 (m, 1H), 3.72 (s, 3H), 3.11 – 3.07 (m, 2H), 2.99 – 2.95 (m, 2H), 2.16 – 2.08 (m, 2H). $^{13}C\{^1H\}$ NMR (101 MHz, $CDCl_3$) δ 175.1, 155.4, 141.3, 131.2, 126.8, 126.7, 122.9, 121.8, 114.7, 35.6, 33.8, 28.4, 21.2. HRMS (ESI-QTOF) m/z: $[M + H]^+$ Calcd for $C_{13}H_{14}NO^+$ 200.1070; Found 200.1075.

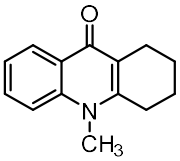

2-2.30

*10-Methyl-1,3,4,10-tetrahydroacridin-9(2H)-one (**2-2.30**)*. Following procedure D, **2-2.1a** (100 mg, 0.56 mmol) was treated with **2-2.23i** (116 mg, 1.19 mmol) to obtain **2-2.30** after column chromatography (40-43% EtOAc/CH_2Cl_2) as an amorphous yellow solid (88 mg, 74% yield). ^1H NMR (500 MHz, $CDCl_3$) δ 8.45 (d, J = 8.0 Hz, 1H), 7.58 (t, J = 7.8 Hz, 1H), 7.41 (d, J = 8.7 Hz,

1H), 7.29 (t, J = 7.5 Hz, 1H), 3.65 (s, 3H), 2.70 (dt, J = 27.8, 6.5 Hz, 4H), 1.86 (p, J = 5.9 Hz, 2H), 1.71 (p, J = 6.1 Hz, 2H). $^{13}C\{^1H\}$ NMR (126 MHz, $CDCl_3$) δ 176.8, 148.3, 141.1, 131.5, 126.7, 124.6, 122.5, 119.2, 114.9, 33.4, 28.6, 22.9, 22.9, 21.4. HRMS (ESI-QTOF) m/z: $[M + H]^+$ Calcd for $C_{14}H_{16}NO^+$ 214.1226; Found 214.1225.

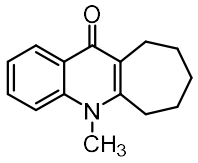

2-2.31

5-Methyl-5,6,7,8,9,10-hexahydro-11H-cyclohepta[b]quinolin-11-one ***(2-2.31)***. Following procedure D, **2-2.1a** (100 mg, 0.56 mmol) was treated with **2-2.23j** (133 mg, 1.19 mmol) to obtain **2-2.31** after column chromatography (42-60% EtOAc/CH_2Cl_2) as an amorphous white solid (50 mg, 39% yield). ^1H NMR (500 MHz, $CDCl_3$) δ 8.49 (dd, J = 8.0, 1.7 Hz, 1H), 7.60 (ddd, J = 8.7, 6.9, 1.7 Hz, 1H), 7.47 (d, J = 8.6 Hz, 1H), 7.32 (ddd, J = 8.0, 6.9, 1.0 Hz, 1H), 3.79 (s, 3H), 3.04 – 2.99 (m, 4H), 1.90 – 1.85 (m, 2H), 1.75 – 1.72 (m, 2H), 1.67 – 1.58 (m, 2H). $^{13}C\{^1H\}$ NMR (126 MHz, $CDCl_3$) δ 175.5, 155.1, 141.1, 131.3, 127.0, 125.4, 124.1, 122.7, 115.6, 35.4, 31.7, 30.9, 26.9, 24.7, 23.9. HRMS (ESI-QTOF) m/z: $[M + H]^+$ Calcd for $C_{15}H_{18}NO^+$ 228.1383; Found 228.1382.

References

(1) Khalifa, M. M.; Philkhana, S. C.; Golden, J. E. Synthesis of Ring-Fused, N-Substituted 4-Quinolinones Using PKa-Guided, Base-Promoted Annulations with Isatoic Anhydrides: Total Synthesis of Penicinotam. *J. Org. Chem.* **2020**, *85* (2), 464–481. https://doi.org/10.1021/acs.joc.9b02541.

(2) Welsch, M. E.; Snyder, S. A.; Stockwell, B. R. Privileged Scaffolds for Library Design and Drug Discovery. *Curr. Opin. Chem. Biol.* **2010**, *14* (3), 347–361. https://doi.org/10.1016/j.cbpa.2010.02.018.

(3) Zhao, H.; Dietrich, J. Privileged Scaffolds in Lead Generation. *Expert Opin. Drug Discov.* **2015**, *10* (7), 781–790. https://doi.org/10.1517/17460441.2015.1041496.

(4) Kirikae, F.; Kirikae, T.; Nakagawa, A. Quinolactacins A, B and C: Novel Quinolone Compounds from Penicillium Sp. EPF-6 I. Taxonomy, Production, Isolation and Biological Properties. *J. Antibiot. (Tokyo)* **2000**, *53* (11), 1247–1251.

(5) Kim, W.-G.; Song, N.-K. Quinolactacins Al and A2, New Acetylcholinesterase Inhibitors from Penicillium Citrinum. *J. Antibiot. (Tokyo)* **2001**, *84* (10), 831–835.

(6) Park, S.-J.; Cho, K.-N.; Kim, W.-G.; Lee, K.-I. An Expedient Synthesis of (+)-Quinolactacin A2. *Tetrahedron Lett.* **2004**, *45* (48), 8793–8795. https://doi.org/10.1016/j.tetlet.2004.10.001.

(7) Clark, B.; Capon, R. J.; Lacey, E.; Tennant, S.; Gill, J. H. Quinolactacins Revisited: From Lactams to Imide and Beyond. *Org. Biomol. Chem.* **2006**, *4* (8), 1512. https://doi.org/10.1039/b600959j.

(8) Schmidt, L. H. Antimalarial Properties of Floxacrine, a Dihydroacridinedione Derivative. *Antimicrob. Agents Chemother.* **1979**, *16* (4), 475–485. https://doi.org/10.1128/AAC.16.4.475.

(9) -Rahman, A.; Khalid, A.; Sultana, N.; Nabeel Ghayur, M.; Ahmed Mesaik, M.; Riaz Khan, M.; Gilani, A. H.; Iqbal Choudhary, M. New Natural Cholinesterase Inhibiting and Calcium Channel Blocking Quinoline Alkaloids. *J. Enzyme Inhib. Med. Chem.* **2006**, *21* (6), 703–710. https://doi.org/10.1080/14756360600889708.

(10) Abe, M.; Imai, T.; Ishii, N.; Usui, M.; Okuda, T.; Oki, T. Quinolactacide, a New Quinolone Insecticide from *Penicillium Citrinum* Thom F 1539. *Biosci. Biotechnol. Biochem.* **2005**, *69* (6), 1202–1205. https://doi.org/10.1271/bbb.69.1202.

(11) Abe, M.; Imai, T.; Ishii, N.; Usui, M. Synthesis of Quinolactacide *via* an Acyl Migration Reaction and Dehydrogenation with Manganese Dioxide, and Its Insecticidal Activities. *Biosci. Biotechnol. Biochem.* **2006**, *70* (1), 303–306. https://doi.org/10.1271/bbb.70.303.

(12) Cappelli, A.; Anzini, M.; Vomero, S.; Mennuni, L.; Makovec, F.; Doucet, E.; Hamon, M.; Menziani, M. C.; De Benedetti, P. G.; Giorgi, G.; Ghelardini, C.; Collina, S. Novel Potent 5-HT3 Receptor Ligands Based on the Pyrrolidone Structure: Synthesis, Biological Evaluation, and Computational Rationalization of the Ligand–Receptor Interaction Modalities. *Bioorg. Med. Chem.* **2002**, *10* (3), 779–801. https://doi.org/10.1016/S0968-0896(01)00332-7.

(13) Tamura, T.; Kuriyama, H.; Agoh, M.; Agoh, Y.; Mori, T. 1,2-Disubstituted 1,4-Dihydro-4-Oxoquinoline Compounds. US007109338B2.

(14) Lanter, J. C.; Sui, Z.; Macielag, M. J.; Fiordeliso, J. J.; Jiang, W.; Qiu, Y.; Bhattacharjee, S.; Kraft, P.; John, T. M.; Haynes-Johnson, D.; Craig, E.; Clancy, J. Structure−Activity Relationships of *N* -Acyl Pyrroloquinolone PDE-5 Inhibitors. *J. Med. Chem.* **2004**, *47* (3), 656–662. https://doi.org/10.1021/jm020521s.

(15) Zheng, H.; Li, L.; Sun, B.; Gao, Y.; Song, W.; Zhao, X.; Gao, Y.; Xie, Z.; Zhang, N.; Ji, J.; Yuan, H.; Lou, H. Design and Synthesis of Furyl/Thienyl Pyrroloquinolones Based on

Natural Alkaloid Perlolyrine, Lead to the Discovery of Potent and Selective PDE5 Inhibitors. *Eur. J. Med. Chem.* **2018**, *150*, 30–38. https://doi.org/10.1016/j.ejmech.2018.02.039.

(16) Ojha, P.; Roy, K. First Report on Exploring Structural Requirements of 1,2,3,4-Tetrahydroacridin-9(10H)-One Analogs as Antimalarials Using Multiple QSAR Approaches: Descriptor-Based QSAR, CoMFA-CoMSIA 3DQSAR, HQSAR and G-QSAR Approaches. *Comb. Chem. High Throughput Screen.* **2013**, *16* (1), 7–21. https://doi.org/10.2174/1386207311316010003.

(17) Tatsuta, K.; Misawa, H.; Chikauchi, K. Biomimetic Total Synthesis of Quinolactacin B, TNF Production Inhibitor, and Its Analogs. *J. Antibiot. (Tokyo)* **2001**, *54* (1), 109–112. https://doi.org/10.7164/antibiotics.54.109.

(18) Zhang, X.; Jiang, W.; Sui, Z. Concise Enantioselective Syntheses of Quinolactacins A and B through Alternative Winterfeldt Oxidation. *J. Org. Chem.* **2003**, *68* (11), 4523–4526. https://doi.org/10.1021/jo020746a.

(19) Shankaraiah, N.; da Silva, W. A.; Andrade, C. K. Z.; Santos, L. S. Enantioselective Total Synthesis of (S)-(−)-Quinolactacin B. *Tetrahedron Lett.* **2008**, *49* (27), 4289–4291. https://doi.org/10.1016/j.tetlet.2008.04.130.

(20) Savina, S. A.; Lyubchanskaya, V. M.; Alekseeva, L. M.; Shashkov, A. S.; Granik, V. G. Synthesis of Novel Furoquinolines and Furobenzodiazepines from Tetronic Acid. *Russ. Chem. Bull.* **2007**, *56* (11), 2298–2304. https://doi.org/10.1007/s11172-007-0363-y.

(21) Guillou, C. C.-L.; Giorgi-Renault, S.; Quirion, J.-C.; Husson, H.-P. Synthesis of γ-and δ-Lactones Derived from 4-Quinolone-3-Carboxylic Acid. *Tetrahedron Lett.* **1997**, *38* (6), 1037–1040. https://doi.org/10.1016/S0040-4039(96)02496-3.

(22) Saito, K.; Yoshida, M.; Uekusa, H.; Doi, T. Facile Synthesis of Pyrrolyl 4-Quinolinone Alkaloid Quinolactacide by 9-AJ-Catalyzed Tandem Acyl Transfer–Cyclization of *o* -Alkynoylaniline Derivatives. *ACS Omega* **2017**, *2* (8), 4370–4381. https://doi.org/10.1021/acsomega.7b00793.

(23) Shao, C.; Li, D.; Jiao, Y. Method for Preparing Penicinotam Compound. CN108623581 (A).

(24) Kesten, S. J.; Degnan, M. J.; Hung, J.; McNamara, D. J.; Ortwine, D. F.; Uhlendorf, S. E.; Werbel, L. M. Antimalarial Drugs. 64. Synthesis and Antimalarial Properties of 1-Imino Derivatives of 7-Chloro-3-Substituted-3,4-Dihydro-1,9(2H,10H)-Acridinediones and Related Structures. *J. Med. Chem.* **1992**, *35* (19), 3429–3447. https://doi.org/10.1021/jm00097a001.

(25) Coppola, G. M.; Schuster, H. F. The Chemistry of 2H-3,1-Benzoxazine-2,4(1H)-Dione (Isatoic Anhydride). 21. A Mild Process for the Preparation of 10-Alkyl-9-Acridanones and Its Application to the Synthesis of Acridone Alkaloids. *J. Heterocycl. Chem.* **1989**, *26* (4), 957–964. https://doi.org/10.1002/jhet.5570260414.

(26) Reed, R. A. 47. Hydroacridones: Synthesis and Dehydrogenation. Part II. *J. Chem. Soc. Resumed* **1945**, 186. https://doi.org/10.1039/jr9450000186.

(27) Ji, X.; Li, D.; Wang, Z.; Tan, M.; Huang, H.; Deng, G.-J. Visible Light-Induced Aerobic Oxidation of Indoles: One-Pot Formation of 4-Quinolones at Room Temperature. *Asian J. Org. Chem.* **2018**, *7* (4), 711–714. https://doi.org/10.1002/ajoc.201800036.

(28) Myrtle, J. D.; Beekman, A. M.; Barrow, R. A. Ravynic Acid, an Antibiotic Polyeneyne Tetramic Acid from Penicillium Sp. Elucidated through Synthesis. *Org. Biomol. Chem.* **2016**, *14* (35), 8253–8260. https://doi.org/10.1039/C6OB00938G.

(29) Grossman, R. B. *The Art of Writing Reasonable Organic Reaction Mechanisms*, 2. ed.; Springer: New York, NY, 2010.

(30) Adepu, R.; Sunke, R.; Meda, C. L. T.; Rambabu, D.; Krishna, G. R.; Reddy, C. M.; Deora, G. S.; Parsa, K. V. L.; Pal, M. Facile Assembly of Two 6-Membered Fused N-Heterocyclic Rings: A Rapid Access to Novel Small Molecules via Cu-Mediated Reaction. *Chem. Commun.* **2012**, *49* (2), 190–192. https://doi.org/10.1039/C2CC37070K.

(31) Taylor, J. E.; Bull, S. D.; Williams, J. M. J. Amidines, Isothioureas, and Guanidines as Nucleophilic Catalysts. *Chem. Soc. Rev.* **2012**, *41* (6), 2109. https://doi.org/10.1039/c2cs15288f.

(32) Lepore, S. D.; Khoram, A.; Bromfield, D. C.; Cohn, P.; Jairaj, V.; Silvestri, M. A. Studies on the Manganese-Mediated Isomerization of Alkynyl Carbonyls to Allenyl Carbonyls. *J. Org. Chem.* **2005**, *70* (18), 7443–7446. https://doi.org/10.1021/jo051040u.

(33) McNab, H.; Montgomery, J.; Parsons, S.; Tredgett, D. G. Pyrrolizine-1,3-Dione. *Org. Biomol. Chem.* **2010**, *8* (19), 4383. https://doi.org/10.1039/c0ob00116c.

(34) Shao, C.-L.; Wang, C.-Y.; Gu, Y.-C.; Wei, M.-Y.; Pan, J.-H.; Deng, D.-S.; She, Z.-G.; Lin, Y.-C. Penicinoline, a New Pyrrolyl 4-Quinolinone Alkaloid with an Unprecedented Ring System from an Endophytic Fungus Penicillium Sp. *Bioorg. Med. Chem. Lett.* **2010**, *20* (11), 3284–3286. https://doi.org/10.1016/j.bmcl.2010.04.043.

(35) Choudhary, C. D.; Das, R. R. Study of Condensation Reaction of 4-Hydroxy Carbostyril/ Substituted 4-Hydroxy Carbostyril With Aromatic Aldehyde/Substituted Aromatic Aldehyde. *Orient. J. Chem.* **2007**, *23* (1).

Chapter 3 – Diastereoselective, Telescoped Multicomponent Reaction for the Synthesis of Tetrahydropyrrolopyrazino[2,1-*b*]quinazolinones and Progress Towards Total Syntheses of Quinazolinone-containing Natural Products

This chapter is adapted in part from work prepared for publication.[1] *The project was completed in collaboration with Lt. Col. Victor Jaffett, PhD, and Jhewelle Fitz-Henley. Reaction development and optimization was completed by Dr. Jaffett. Substrate scope was investigated in collaboration with Dr. Jaffett and Jhewelle Fitz-Henley.*

Section 3-1: Introduction

As discussed in Chapter 2, the discovery and development of new drugs often requires the identification of new chemical matter with bioactivity via broad screening of compound libraries. The design and synthesis of novel molecules for screening libraries, including the development of efficient methods by which to synthesize them, continues to be a research interest of the Golden lab. To generate a differentiated library of pharmacologically biased small molecules, we sought to develop new methods for the synthesis of collections of compounds with embedded, privileged scaffolds.

The term "privileged scaffold" refers to molecular templates for which a variety of distinct bioactivities can be optimized based on a common core motif, and articulates that certain molecular motifs appear in drugs and bioactive natural products more often than others.[2,3] Importantly, individual compounds that share a centrally embedded "privileged scaffold" may not share the same bioactivity; indeed it is the ability to arrive at orthogonal bioactivities via different modifications to the central motif that makes privileged scaffolds so useful for medicinal chemistry.

Quinazolinones are a well-established privileged scaffold in medicinal chemistry.[2] They appear embedded in a plethora of reported compounds, including discovered natural products, patented synthetic molecules, and approved drugs. The ring-fused subset of related structures exemplifies this while showcasing the rich diversity of pharmacologically-relevant activity available from modification of the shared core (**Figure 3-1.1**, blue highlight).[4–11]

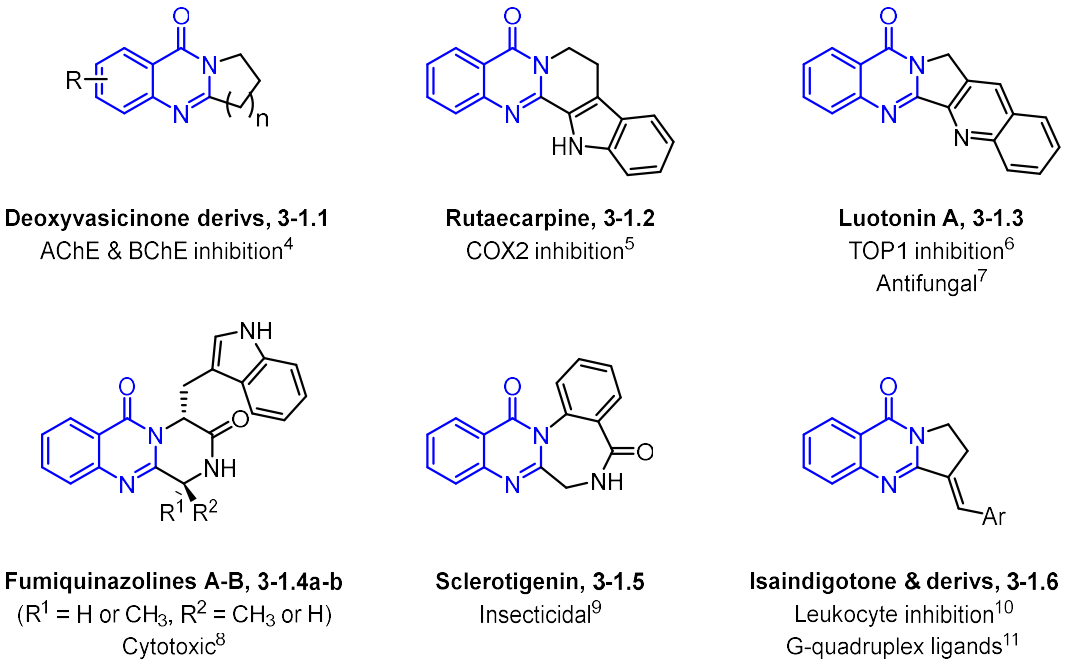

Figure 3-1.1 Selected examples of bioactive compounds featuring a ring-fused quinazolinone motif (highlighted in blue). AChE: acetylcholinesterase; BChE: butyrylcholinesterase; COX2: cyclooxygenase 2; TOP1: DNA topoisomerase 1.

Within the ring-fused subgrouping of the expansive privileged scaffold class of quinazolinones, the tetrahydropyrrolopyrazino-fused framework featured in the series of compounds **3-1.9a-e** is underexplored. They appear in a single report by Hardy *et al.* in 2011 in which they are explored as allosteric metabotropic glutamate receptor 5 modulators.[12] The scaffold core is constructed in four steps from commercial material to arrive at **3-1.8**, with no information given regarding reaction efficiency (**Scheme 3-1.2**).[12] Importantly, the five examples synthesized relied on

elaboration of the key intermediate **3-1.8**, in which the tetrahydropyrrolopyrazino-fused is already constructed, via coupling at the bromide substituent attached to C8. This significantly narrowed the accessible chemical space in terms of analog generation, as altering substitution in positions other than at C8 would require restarting the synthesis at least two steps before the ring-fused system's formation. This makes the modifications that accompany a medicinal chemistry optimization effort on a hit molecule more time and resource intensive to perform. Notably, the work by Hardy *et al*. work did not explore substitution at C5 of the tetrahydropyrrolopyrazino-fused quinazolinone system, likely due to its limited accessibility via their synthetic strategy.

Scheme 3-1.1 Precedent in the synthesis of tetrahydropyrrolopyrazino-fused quinazolinones

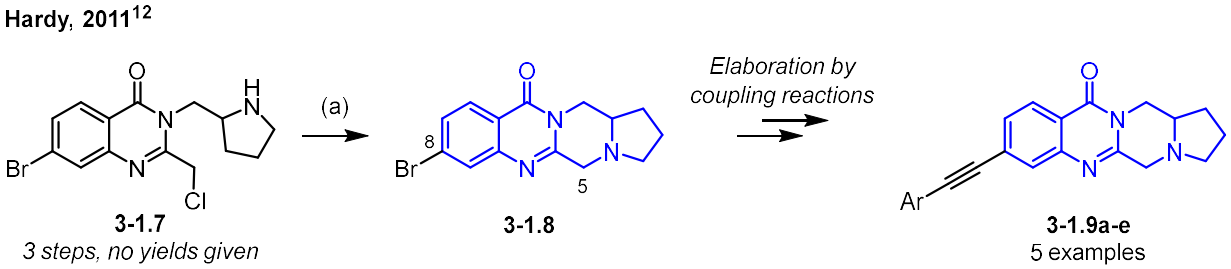

Reagents and conditions: (a) K_2CO_3, CH_3CN, reflux, 1.5 h, yield not given

As part of a research program aimed at the efficient generation of a differentiated library of pharmacologically-biased templates that could be screened broadly for activity, we were interested in developing a method that enabled greater access to compounds featuring this tetrahydropyrrolopyrazino-fused framework. Our group's experience in the synthesis of other quinazolinone-containing small molecules provided an excellent opportunity to explore a new approach to construction of this scaffold. We expected that doing so might expand the tractable synthetic landscape for tetrahydropyrrolopyrazino-fused quinazolinones and provide opportunities

for potential drug discovery using an underrepresented heterocyclic motif within a well-established privileged scaffold class.

We recently disclosed a synthetic method that enabled access to the related motif **3-1.13** via deaminative ring-closure of a transient, unsubstituted *ortho*-amido cyclic arylguanidine species **3-1.12** (**Fig. 3-2.3**).[13] In an effort to further elaborate on the power of this transformation to access novel heterocyclic compounds relevant to drug discovery, we sought to expand the application of such a strategy to the use of *ortho*-amidobenzamidines.

Scheme 3-1.2 Precedents in related annulation reactions of aryl amidines and guanidines and proposed approach to synthesis of tetrahydropyrrolopyrazino-fused quinazolinones

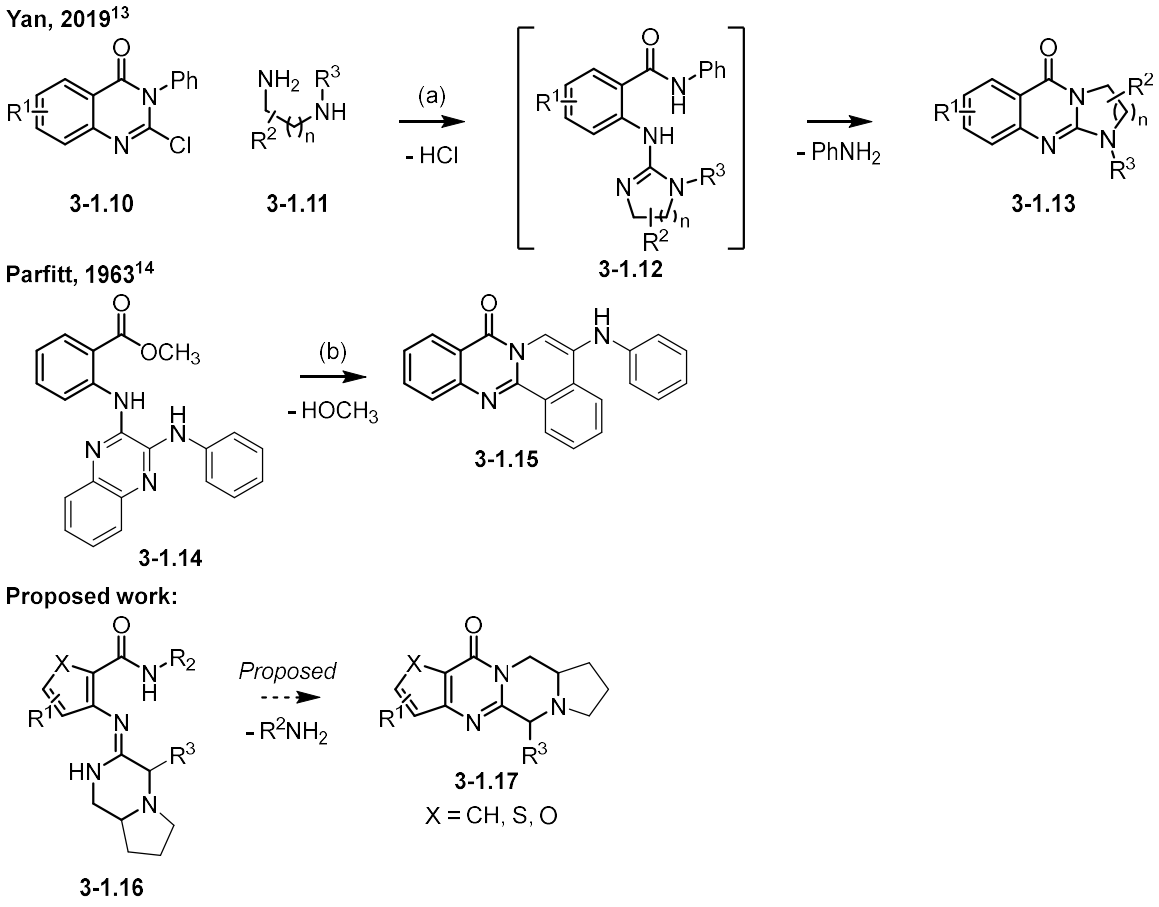

Reagents and conditions: (a) Et_3N, CH_3CN, 150°C, 2 h, microwave irradiation, 53-90% (b) Neat, 210°C, 1 h, 88%.

Given the similarity in basicity and nucleophilicity of the guanidine and amidine functional groups, as well as precedent by Parfitt of an intramolecular annulation using *ortho*-amidine benzoic acid esters (see **Scheme 3-3.2**), we hypothesized that a similar annulation reaction might be possible using analogous *ortho*-amidobenzamidines.[14,15] Although we were encouraged by the precedent in related reactions, it was unclear if the less electron-rich amidine moiety (compared to the precedented guanidine) would serve as an adequately strong nucleophile. Additionally, amides are more electron-rich than esters, which renders them less electrophilic. Given the high temperature (210°C) required in the annulation reactions of relatively electron rich *ortho*-amidine benzoic acid ester **3-1.14**, and the singular example given, we expected this could be a significant challenge as our proposed substrates for accessing the ring-fused quinazolinone system were thus simultaneously less reactive in terms of both the nucleophile and the electrophile. Nonetheless, we sought to investigate if it were possible to form tetrahydropyrrolopyrazino-fused quinazolinones **3-1.17** from the deaminative ring-closure reaction of *ortho*-amidobenzamidines **3-1.16**.

Section 3-2: Development of a diastereoselective, multicomponent method for the synthesis of tetrahydropyrrolopyrazino[2,1-*b*]quinazolin-11-ones

A prerequisite for this investigation was being able to synthesize the appropriate unsubstituted *ortho*-amidobenzamidines reliably. Fortunately, our group had recently reported an efficient multicomponent reaction yielding highly functionalized *ortho*-amidobenzamidines **3-2.7** (**Scheme 3-2.1**).[16] The method used a sequence of four operations (six reactions, seven chemical transformations), with the crude material from one being used directly in the next step without intermediate purification, a practice known as “telescoping”. In the first step, a Ugi multicomponent reaction between an isocyanide (**3-2.1**), aldehyde (**3-2.2**), carboxylic acid (**3-2.3**), and mono-Boc diamine (**3-2.4**) formed a highly substituted imide (**3-2.5**). In this case, the

carboxylic acid was an *ortho*-azido aryl acid, which enabled the imide to be converted by a Staudinger/Aza-Wittig combination of reactions to a quinazolinone, tethered to a Boc-protected diamine (**3-2.6**) in a single step. These quinazolinones with a tethered Boc-protected diamine **3-2.6** could then be deprotected under acidic conditions (step c) to quinazolinones with a tethered amine hydrochloride **3-2.7**, which undergo a rearrangement to amidines (**3-2.8**) under basic conditions (step d).[17]

Scheme 3-2.1 Precedent in synthesis of highly functionalized *ortho*-amidobenzamidines

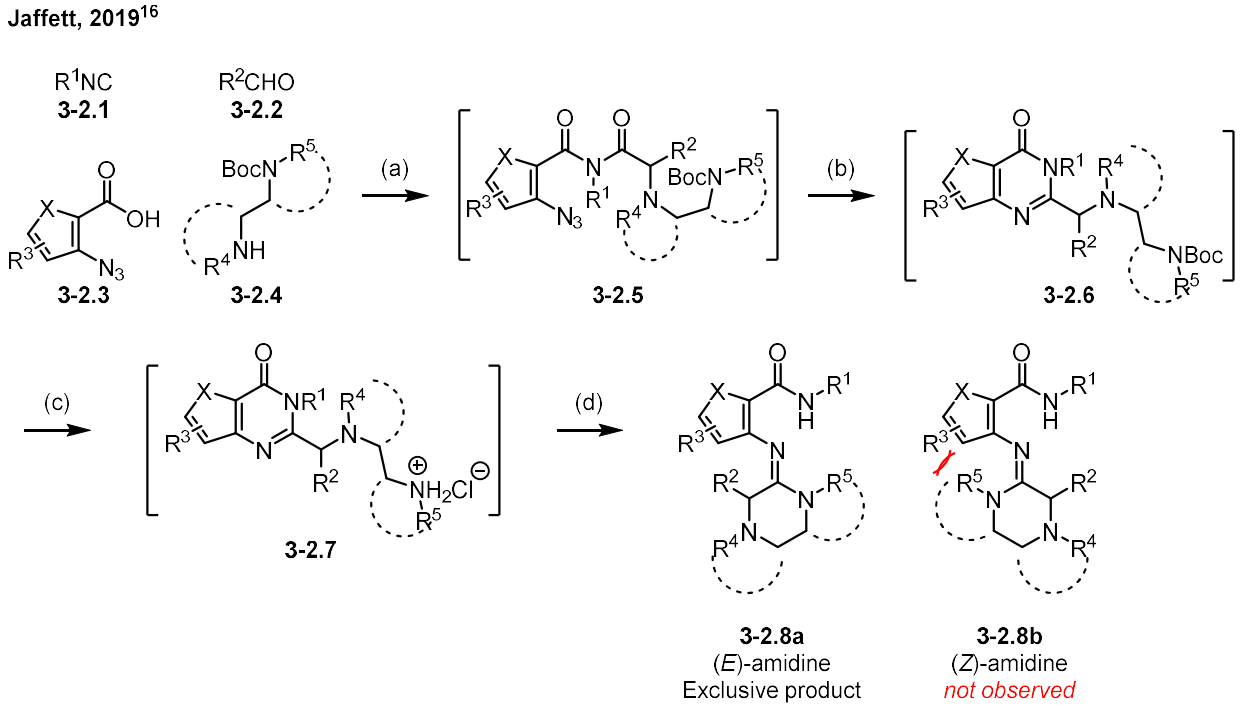

Reagents and conditions: (a) 4Å molecular sieves, 3:1 CH_2Cl_2/CH_3OH, rt, 12 h (b) PS-PPh_3, $PhCH_3$, rt, 1 h then 110°C, 12 h (c) 4N HCl, dioxane, 0°C – rt, 12 h (d) Et_3N, CH_3OH, 100°C, 1 h, microwave irradiation, 21-88% over 4 steps. Red highlight indicates putative steric interactions disfavoring the unobserved (*Z*)-amidine.

Notably, the amidines were isolated exclusive as © isomers **3-2.8a**, presumably due to steric clash that would occur in the (*Z*) isomers **3-2.8b** between bulky R^5-substituents on the substituted amidine nitrogen and the aryl system of the benzamidine (red highlight). In this earlier

work with a multicomponent, telescoped strategy for amidine synthesis, annulation to the ring-fused quinazolinones was not possible since the diamines (**3-2.4**) being used led to fully substituted amidines **3-2.8** ($R^5 \neq H$). We therefore set out to build upon the established chemistry of these amidines to develop a method for generation of our ring-fused quinazolinone core of interest.

To generate the desired tetrahydropyrrolopyrazino-fused quinazolinones **3-2.10**, we needed access to the precursor *N*-unsubstituted (*Z*)-amidines **3-2.9b**, and in particular the tautomeric form that would be able to undergo deaminative ring closure **3-2.9b'** (**Scheme 3-2.2**). We reasoned that the multicomponent method to fully substituted amidines **3-2.8** could be repurposed to generate the necessary unsubstituted amidines **3-2.9** if the appropriate diamine, a Boc-protected pyrrolidine-2-methanamine **3-2.4a**, was employed. The first three steps would proceed analogously as in the original methodology that was used to generate fully substituted amidines. In the final stage, **3-2.7a** could rearrange to either (or both) the ©- or (*Z*)-amidine(s) (**3-2.9a** and **3-2.9b**, respectively), since the steric bulk from nitrogen substitution on the amidine would no longer be present. Further, since the resulting amidine **3-2.9** was unsubstituted at nitrogen, it could tautomerize to a cyclic imine form that can freely rotate between a pseudo-© or pseudo-(*Z*) configuration (**3-2.9a'** and **3-2.9b'**, respectively). We expected that these species would be free to interconvert, and that an equilibrium across all four species might be operative; however, since the pseudo-(*Z*) tautomer **3-2.9b'** is the only species competent to undergo an irreversible, deaminative ring-closure to the tetrahydropyrrolopyrazino-fused quinazolinone **3-2.10**, the process should ultimately shuttle to the desired compound by Le Chatelier's principle.

Scheme 3-2.2 Proposed route to tetrahydropyrrolopyrazino-fused quinazolinones via *N*-unsubstituted *ortho*-benzamidines

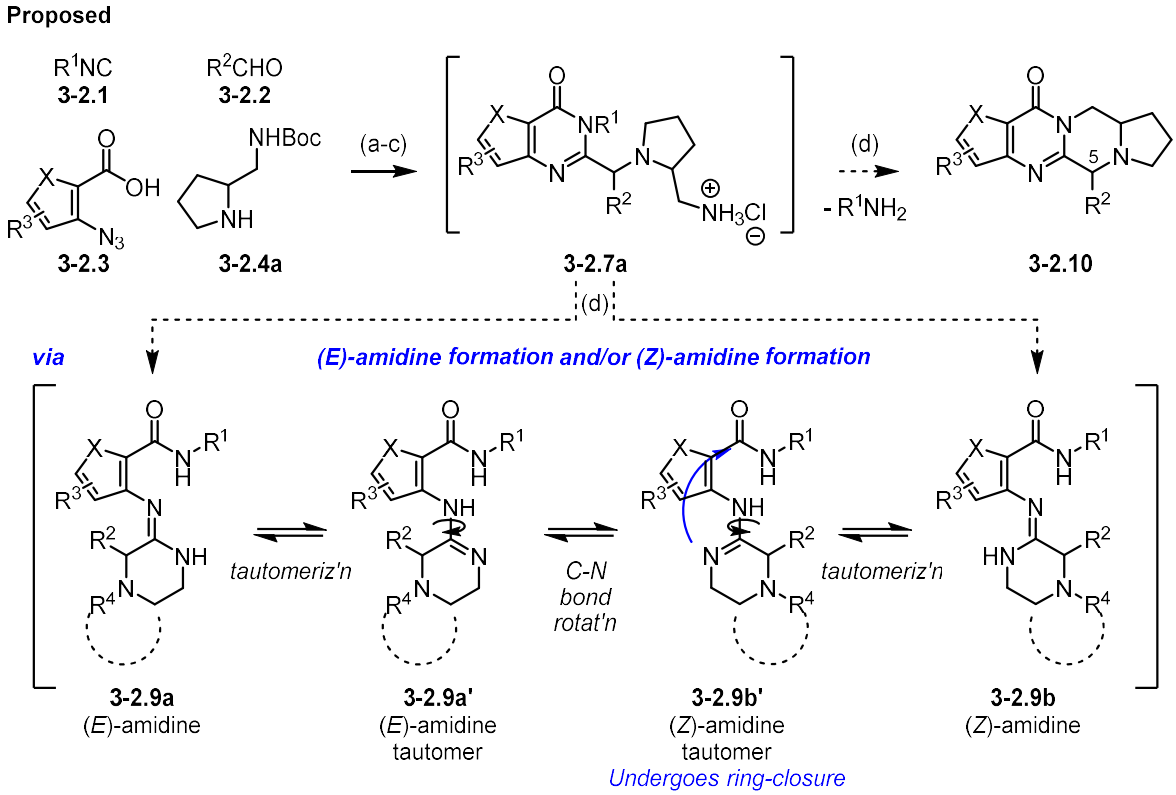

Reagents and conditions: (a) 4Å molecular sieves, 3:1 CH_2Cl_2/CH_3OH, rt, 12 h (b) PS-PPh_3, $PhCH_3$, rt, 1 h then 110°C, 12 h (c) 4N HCl, dioxane, 0°C – rt, 12 h (d) Et_3N, CH_3OH, 100°C, 1 h, microwave irradiation.

This approach offered several attractive features for our purposes. Firstly, the original method giving *N*-substituted amidines (**3-2.8**, $R^5 \neq H$) enabled diverse substitution at what would eventually become the C5 position of the resulting tetrahydropyrrolopyrazino-fused quinazolinone (R^2) if the unsubstituted analogs (**3-2.9**) cyclized as we hoped. The substitution would be introduced at the start of the synthesis via commercially ubiquitous aldehyde starting materials (**3-2.2**), making the strategy highly attractive for diversification and medicinal chemistry purposes.

Secondly, we envisioned that use of chiral starting materials would enable control of the stereochemistry at the C5 position via the mechanism of the initial reaction in the sequence (**Scheme 3-2.2**). In the Ugi multicomponent reaction, isocyanide (**3-2.1**) attack on the imine (**3-**

2.11) determines the configuration at the resulting stereocenter. The state of the art in asymmetric Ugi reactions rely on steric bulk proximal to the electrophilic carbon to direct attack of the isocyanide to the opposite face of the imine.[18–20] In our system, we envisioned that this could be induced by the stereocenter at C2 of the pyrrolidine-2-methanamine **3-2.4a**, with the preferred (and therefore major) product **3-2.12** being that of isocyanide addition to the opposite face of the imine intermediate **3-2.11** relative to the methanamine substituent on the pyrrolidine. This configuration would then be preserved throughout the remainder of the synthesis, provided that the intervening steps did not cause epimerization at either stereocenter. Using racemic **3-2.4a** would be expected to give a racemic mixture of diastereomers **3-2.12** and **3-2.12'**, while using an enantiopure source of **3-2.4a** would have the potential to produce only the major and minor diastereomeric forms of a compound with the same configuration at C2 of the pyrrolidine. Beyond the synthetic utility of such substrate-mediated stereocontrol, the prospect of compound library generation using such a method was attractive because it would enable simultaneous access to at least two, and up to four, individual isomers of a single analog after separation. Since the 3D configuration of a molecule can be critical to its bioactivity, from a library generation perspective such a synthesis of tetrahydropyrrolopyrazino-fused quinolinones represents a "two (or four) for the price of one" opportunity. While separation of enantiomers is often a resource-intensive task, the ability to synthesize only two diastereomers, which are typically much easier to separate from one another because they do not require chiral column chromatography, by using enantiopure **3-2.4a** provided access to the best of both worlds in terms of multi-analog synthesis and simplicity in isolation.

Scheme 3-2.2 Mechanism of Ugi 4-component reaction and stereoinduction of resulting imide

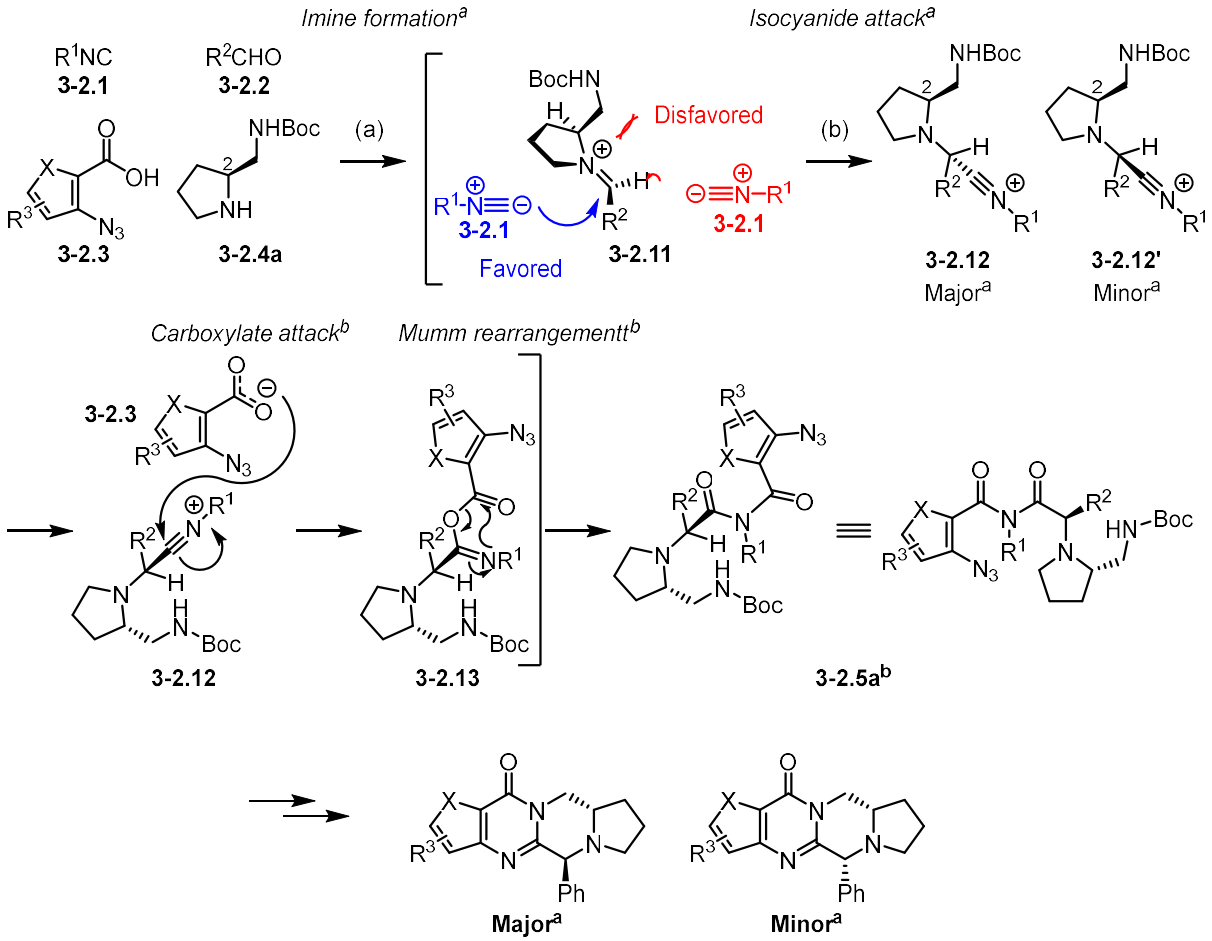

Reagents and conditions: (a) 4Å molecular sieves, aldehyde **3-2.2**, carboxylic acid **3-2.3**, mono-Boc protected diamine **3-2.4**, 3:1 CH_2Cl_2/CH_3OH, rt, 10 min (b) isocyanide **3-2.1**, CH_2Cl_2, rt, 12 h. [a]Single enantiomer shown; [b]Single enantiomer of major diastereomer shown.

Reaction development based on the previously published method to fully substituted amidines was performed by Dr. Victor Jaffett. Ultimately, the same conditions that proved optimal in the preceding work gave the best results for this transformation as well, and these were used to synthesize a diverse array of tetrahydropyrrolopyrazino-fused quinazolinone derivatives (**Scheme 3-2.3**). Attempts to improve the atom economy and diastereoselectivity of the reaction beyond those observed in the pilot reactions met with inferior results. Since the isocyanide substituent is

ultimately eliminated in the deaminative ring closure for this reaction, smaller isocyanides were explored to make the process more atom economical. Lower molecular weight isocyanides (isopropyl isocyanide, cyclohexyl isocyanide) for the reaction led to reductions in overall yield and/or deterioration in diastereoselectivity. Attempts to reduce the equivalencies of excess starting materials in the Ugi four-component reaction were also unsuccessful. An inherent diastereoselectivity of up to 89:11 was observed for the reaction, and attempts to improve this diastereoselectivity by using sterically demanding aldehydes led to either reduced overall reaction efficiency (24% yield with pivaldehyde, **3-2.10n**) or no selectivity between diastereomers (55:45 d.r. with 2,6-dimethylbenzaldehyde, **3-2.10o**), presumably because the bulky aldehyde disfavors attack on either face of the imine altogether during the stereo-determining step. A crystal structure of the minor diastereomer of iodo-substituted analog **3-2.10e** confirmed the reaction outcomes were consistent with our stereochemical rationale (**Figure 3-2.1**).

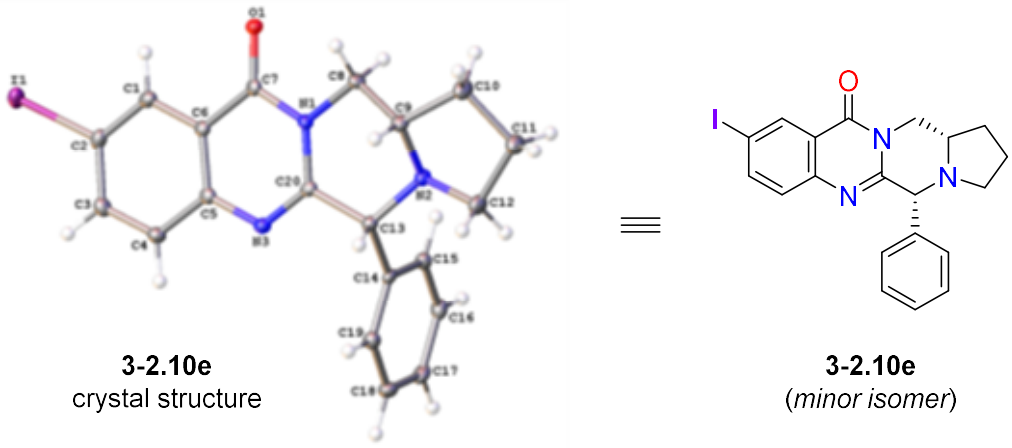

Figure 3-2.1 Comparison of crystal structure of minor isolated isomer and predicted minor isomer based on stereochemical rationale.

Scheme 3-2.3 Substrate scope of telescoped, diastereoselective method to tetrahydropyrrolopyrazino-fused quinazolinones

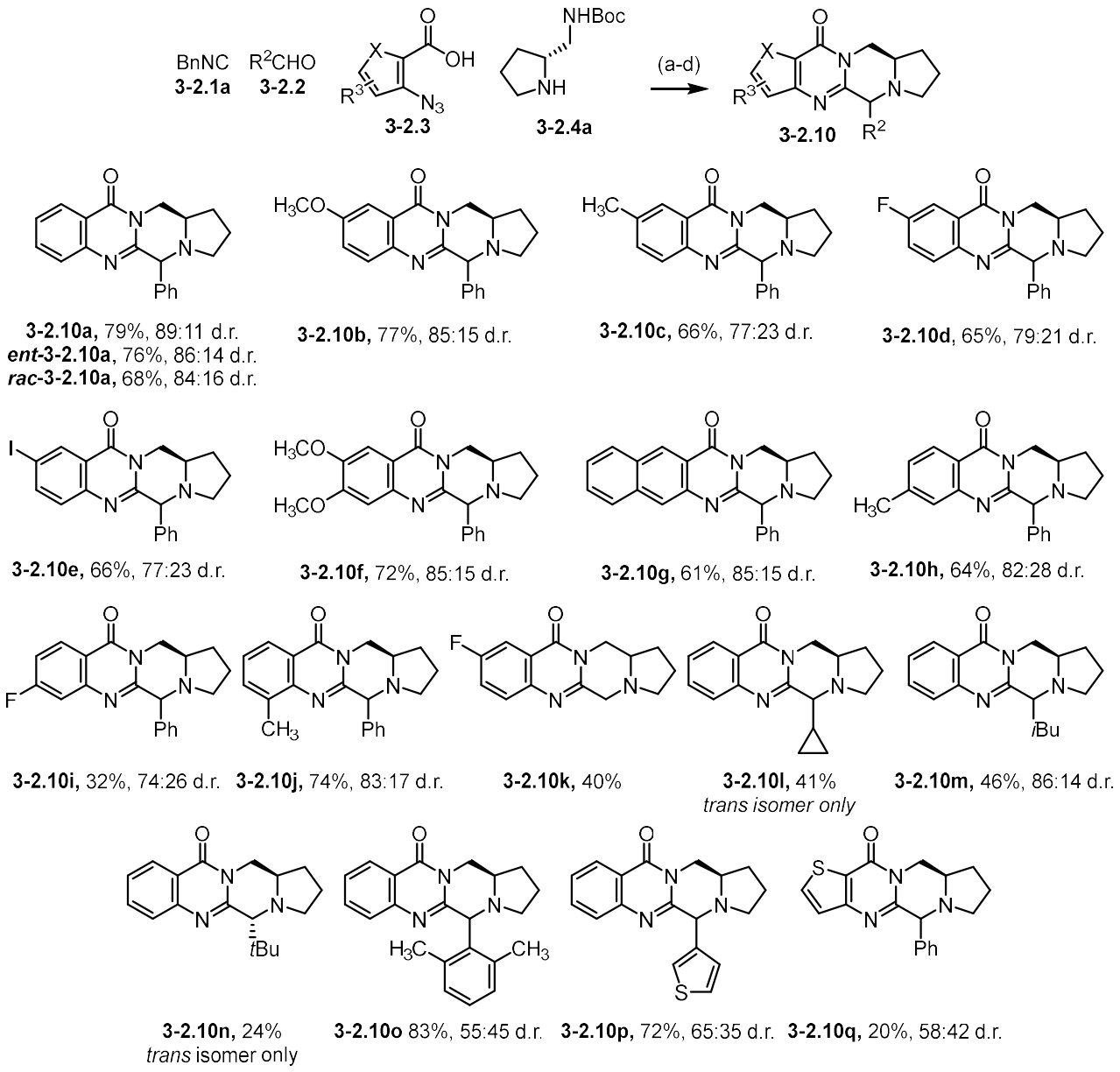

Reagents and conditions: (a) 4 equiv. aldehyde **3-2.2**, 2 equiv. amine **3-2.4a**, 1 equiv. carboxylic acid **3-2.3**, 4 equiv. benzyl isocyanide **3-2.1a**, 4Å molecular sieves, 3:1 CH_2Cl_2/CH_3OH, rt, 12 h (b) PS-PPh_3, $PhCH_3$, rt, 1 h then 110°C, 12 h (c) 4N HCl, dioxane, 0°C – rt, 12 h (d) Et_3N, CH_3OH, 100°C, 1 h, microwave irradiation. Yields are an average of at least 2 independent experiments.

The scope of tolerated substrates for this reaction was quite broad. Formalin, primary, secondary, tertiary, and aryl aldehydes were permitted. Substitution on the aryl ring of the 2-azido-

benzoic acid was broadly tolerated, though a slight reduction in yield for the 8-F analog **3-2.10i** was observed, presumably due to decreased nucleophilicity of the carboxylate during the Ugi reaction. Heterocycles could be incorporated through the aldehyde (**3-2.10p**) or the carboxylic acid substrate (**3-2.10q**), giving rise to an even more diverse array of derivatives based on the tetrahydropyrrolopyrazino-fused quinazolinone scaffold. Even the low yield (20%) over four steps for the thiophene analog **3-2.10q** corresponds to an average per-step yield of about 67%. We then became interested in testing the limits of this ring closure process, as well as investigating potential applications of transient amidine intermediates in the context of natural product total synthesis.

Section 3-3: Progress towards total syntheses of natural products containing the ring-fused quinazolinone motif

We wondered if the deaminative ring closure of amidines might provide a new entry into the quinazolinone-containing natural product family exemplified by glyantrypine **3-3.1**. Retrosynthetic analysis of the glyantrypine scaffold revealed that the quinazolinone **3-2.5** derived from a simple tetrapeptide **3-3.6** could serve as a precursor for the amidine ring-closure to serve as the keystone of our synthesis. Employing a ring-opening-polymerization (ROP) strategy to the tetrapeptide would be expected to generate it in a single step via sequential building block addition, and finding conditions to cyclize the peptide intermediate to the quinazolinone in situ and under basic conditions might then enable a completely telescoped, one-pot synthesis of the natural product scaffold (**Scheme 3-3.1**).[21] Since the ROP strategy is amenable to changing each individual building block in the form of an amino-acid *N*-carboxy anhydride ("AA NCAs", **3-3.8**), the synthesis would also be highly modular and might enable access to related natural products fumiquinazoline F (**3-3.2**) and fiscalin B (**3-3.3**) with minimal adjustment to reaction conditions. The requisite AA NCAs are well characterized, being important building blocks in peptide

synthesis. Many are commercially available, and ample literature precedent existed reporting their syntheses.[22–24]

Scheme 3-3.1 Retrosynthetic analysis of glyantrypine-type natural products in the context of deaminative ring-closure of amidines and proposed one-pot total synthesis by ROP/ring-closure

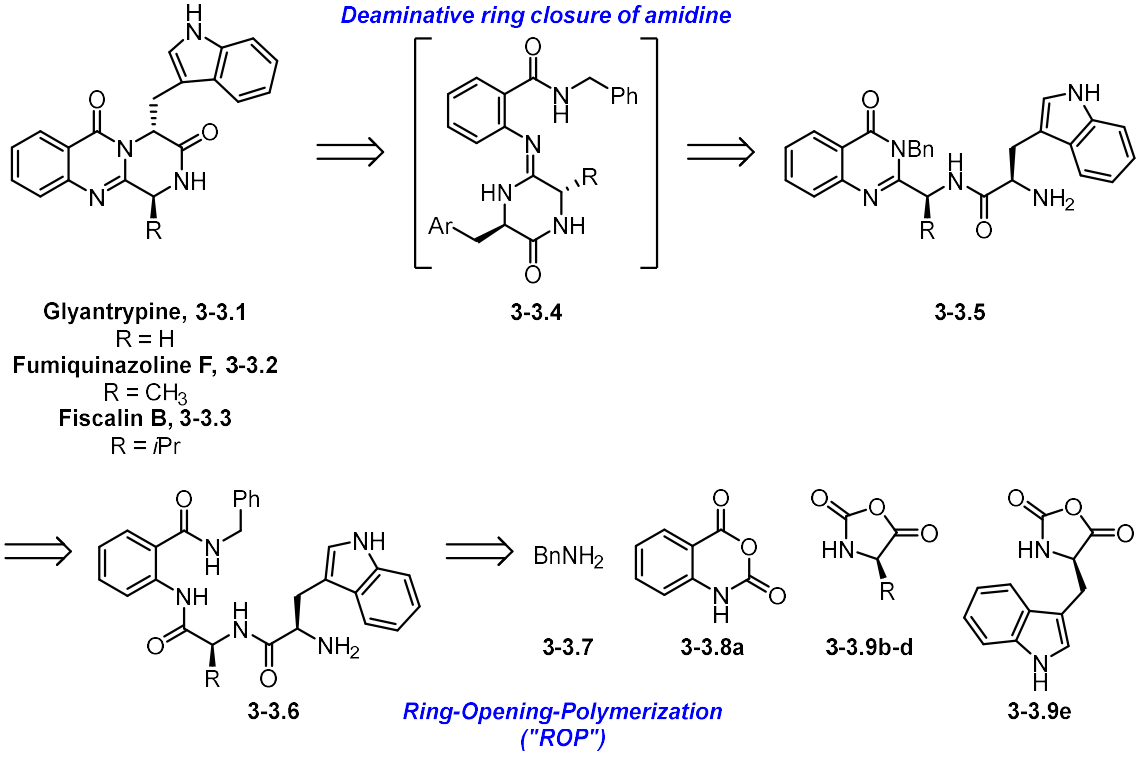

Previous syntheses of such natural products required high temperatures or long linear procedures. They also featured epimerization of the stereocenters, which we hoped our approach might ameliorate. Syntheses by Ganesan and Liu are representative of the best in class for syntheses of this family of natural products (**Scheme 3-3.2**). Ganesan's work in 2000 detailed a 4-5 step synthesis for these compounds with overall yields in the range of 40-50% and epimerization rates of < 5% in the finished products.[25] Follow-on work adapted their solution-phase chemistry to solid-phase, enabling a small library of natural products to be synthesized with 5-10% epimerization and similar yields.[26] Liu's synthesis 5 years later generated glyantrypine,

fumiquinazoline F, and fiscalin B in a one-pot, two-step procedure but relied on very high temperatures to drive in-situ building block deprotection and cyclization (210-230°C), leading to low yields (20-55%) and substantial epimerization of the products.[27]

Scheme 3-3.2 Precedents in the total synthesis of glyantrypine-type natural products

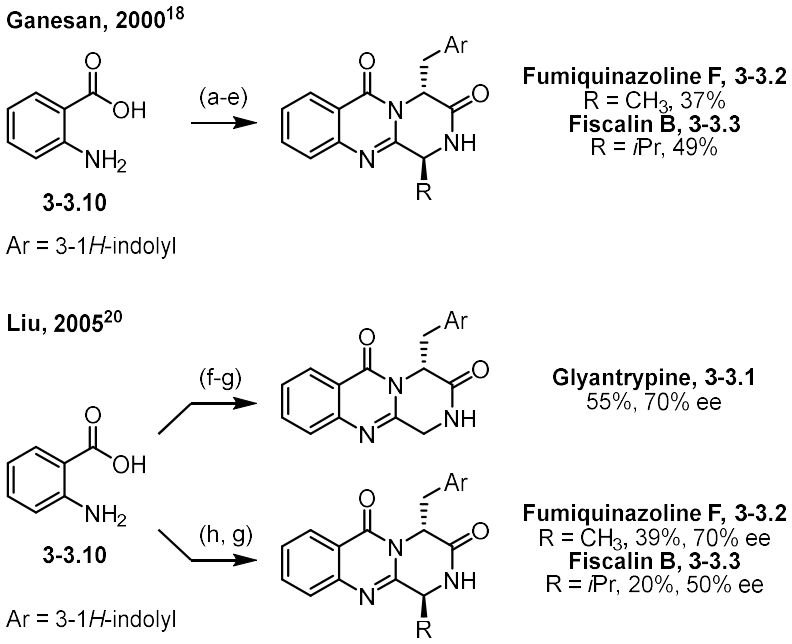

Reagents and conditions: (a) D-tryptophan methyl ester, EDC, CH_3CN, rt, 3 h, 93% (b) Fmoc-NH(C)CHCOCl, CH_2Cl_2/Na_2CO_3 (aq), rt, 2 h, 67-90% (c) Ph_3P, I_2, *i*$PrEt_2N$, rt, 8 h, 71-82% (d) 20% piperidine/CH_2Cl_2, rt, 12 min © DMAP, CH_3CN, reflux, 19 h, 72-83% over 2 steps (f) Boc-Gly, $P(OPh)_3$, pyridine, 150°C, 10 min, microwave irradiation (g) D-tryptophan HCl, 220°C, 1.5 min, microwave irradiation (h) Boc-Ala or Boc-Val, $P(OPh)_3$, pyridine, 55°C, 16 h.

Thus, our approach was attractive in that the ring-opening-polymerization (ROP) strategy might enable a modular, one-pot synthesis of the natural product scaffold under relatively mild conditions. The ROP phase of synthesis and conversion of the resulting tetrapeptide **3-3.6** to the quinazolinone precursor **3-3.5** could be conducted at room temperature. The amidine ring-closure to ring-fused quinazolinones required heating, but not to temperatures as high as used in the Liu syntheses. However, use of amide tethers, as in quinazolinones of type **3-3.5**, and their undergoing

rearrangement to amidines such as **3-3.4** had not previously been investigated. The successful rearrangement of such a compound would also have implications for synthesis of antiviral amidines for medicinal chemistry, as these represented novel examples of a known antiviral template.[16,17,28,29]

To test whether amide-linker quinazolinones of type **3-3.5** could participate in the amidine rearrangement chemistry prior to attempting a ROP-based strategy for tetrapeptide synthesis, the quinazolinone precursor to glyantrypine **3-3.11** was synthesized by a routine step-wise peptide coupling sequence with intermediate protection/deprotection steps. Unfortunately, it did not undergo rearrangement despite prolonged heating under basic conditions (**Scheme 3-3.3**). To determine whether the amide linker was a problem for the reaction or whether the steric bulk from the methyl-3-indolyl group proximal to the reactive amine was the issue, the quinazolinone **3-3.12** was similarly synthesized and subjected to heating. If cyclization to **3-3.13** was successful, it would indicate the steric bulk was responsible for failure of **3-3.11** to convert to glyantrypine **3-3.1**. Sadly, the simplified substrate **3-3.12** also failed to turn over to the desired amidine or ring-fused quinazolinone natural product as assessed by thin-layer chromatography (TLC) and LC-MS. In both cases, the quinazolinone starting intermediates were stable, exhibiting no degradation or off-target reactivity. Concurrent to these efforts **3-3.14**, the quinazolinone precursor to sclerotigenin **3-3.15**, was also synthesized, though we were aware of the additional challenges of 7-membered ring formation and use of an aniline reactive handle for this substrate. Unsurprisingly, this substrate also failed to turn over to the desired product.

Scheme 3-3.3 Attempted deaminative cyclizations from amide-linked aminoquinazolinones to access natural product templates

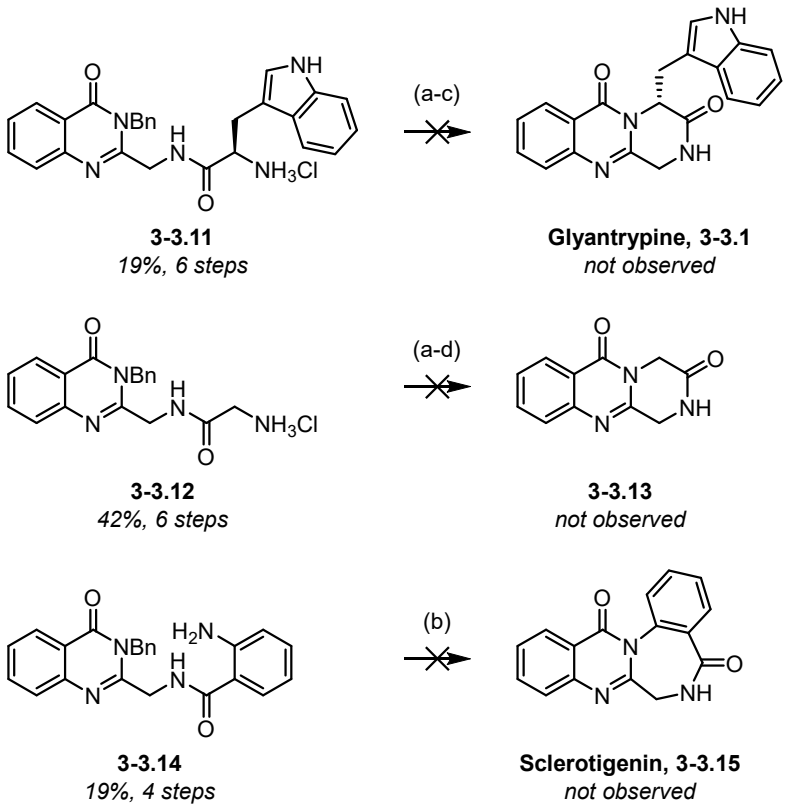

Reagents and conditions: (a) Et_3N, CH_3OH, 100°C, 1 h, microwave irradiation (b) Et_3N, CH_3OH, 150°C, 2 h, microwave irradiation (c) Et_3N, CH_3CN, 150°C, 2 h, microwave irradiation (d) Et_3N, $PhCH_3$, 150°C, 2 h, microwave irradiation.

Although disappointing in that they consisted of synthetic dead ends, these studies successfully probed the limitations of the deaminative ring-closure reaction of amidines described in **Section 3-2**. We found that the amidines resulting from amide-linked quinazolinones of type **3-3.5** do not appear to form under even vigorous heating, likely due to the preferred conformation of the amide disfavoring the rearrangement. Thus the limits of preceding rearrangement chemistry to access the amidines remains an important consideration, and this work has implications for future application of the deaminative cyclization in synthesis as new routes to forming the requisite transient amidine(s) will need to be explored. For this reason, the ring-opening polymerization-

based synthesis of the glyantrypine-type natural products was not pursued further. In the future, explorations into different solvents, or high temperature neat reactions may prove fruitful for these challenging cyclizations. Additionally, exploration of Thorpe-Ingold type effects proximal to the internal amide in compounds like **3-3.5** may sufficiently favor amidine formation by overcoming the amide conformation problem and thus driving reaction turnover.

Section 3-4: Conclusion

In this work, we successfully adapted newly developed chemistry in our group to access transient *ortho*-amidobenzamidines that proceed in a domino fashion to tetrahydropyrrolopyrazino-fused quinazolinones, an underrepresented group of small molecules within a large privileged scaffold class. Incorporation of chiral starting materials, by virtue of an asymmetric Ugi multicomponent reaction, enables control over the resulting product stereochemistry via sterics whose outcomes can be easily predicted. These outcomes were confirmed by x-ray crystallography of the reaction products, which can be obtained in up to 88% yield over four operational steps (6 reactions, 7 chemical transforms) and in an 89:11 ratio of separable diastereomers when enantiopure amine, which controls the stereochemistry at the induced stereocenter, is being used. We further explored the limits of applications for this deaminative cyclization reaction in the context of natural product total syntheses and found that entry to the requisite transient amidines can be limited by functional groups, particularly amides, in the quinazolinone intermediate's linker. This finding implies that new entries into the synthesis of such amidines could be worthwhile, enabling both ongoing antiviral medicinal chemistry programs and total synthesis.

Section 3-5: Experimental

The experimental data for this work, including starting materials, a substantial part of the substrate scope, and crystal structure of ***3-2.10e*** *have been previously reported in part by Lt. Col. Victor Jaffett in his dissertation. Materials reported here pertain only to newly synthesized compounds and investigations in total synthesis.*

General Information and Methods

Compounds not described below were purchased from commercial vendors. Analytical TLC experiments were performed on aluminum-backed Silica Gel plates (TLC Silica gel 60 F_{254}) from EMD Millipore and analyzed with 254 nm UV light using diluted samples. All compounds were characterized with the following instrumentation: Varian Unity-Inova 400 MHz NMR spectrometer (operating at 400 and 101 MHz, respectively) or a Varian Unity-Inova 500 MHz NMR spectrometer (operating at 500 and 126 MHz, respectively) in $CDCl_3$ ($CDCl_3$: $^1H = \delta$ 7.26 ppm, $^{13}C = \delta$ 77.16 ppm) or DMSO (DMSO: $CDCl_3$: $^1H = \delta$ 2.50 ppm, $^{13}C = \delta$ 39.50 ppm). The chemical shifts (δ) reported are given in parts per million (ppm) and the coupling constants (J) are in Hertz (Hz). The spin multiplicities are reported as s = singlet, br s = broad singlet, d = doublet, t = triplet, q = quartet, p = pentuplet, dd = doublet of doublet, ddd = doublet of doublet of doublet, and m = multiplet. The LC-MS analysis was performed on an Agilent 1290 Infinity II HPLC system with 1290 Infinity II Diode Array Detector and an Agilent 6120 Quadrupole LC-MS system. The analytical chromatography method utilized the following parameters: Poroshell 120 EC-C18, 1.9 μm column, UV detection wavelength = 254 nm, Flow rate = 1.0 mL/min, Gradient = 5-100% LC-MS grade Methanol over 4 min; The organic mobile phase and aqueous mobile phase contained 0.1% LC-MS grade formic acid. The mass spectrometer utilized the following parameters: an Agilent multimode source that simultaneously acquires ESI+/APCI+; Final

compounds were determined to be > 95% purity by UV-LCMS at 254 nm. Microwave irradiated (MWI) reactions were carried out using an Anton Paar Monowave 300 Microwave Synthesis Reactor or Biotage Initiator+ Fourth Generation Microwave Synthesizer. Flash chromatography separations were carried out using a Teledyne Isco CombiFlash Rf 200 purification system with silica gel columns (normal phase). High resolution mass spectra (HRMS) were performed by Analytical Instrument Center at the School of Pharmacy on an Electron Spray Injection (ESI) mass spectrometer. Melting points were measured on OptiMelt MPA100 Automated Melting Point System.

General Procedure A. *Synthesis of tetrahydropyrrolopyrazino-fused quinazolinone derivatives*

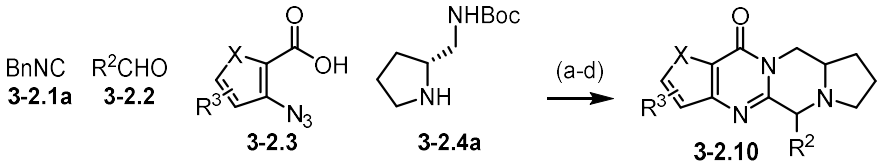

All reactions in procedure A were carried out under N_2 atmosphere in oven-dry glassware using dry, HPLC-grade solvent.

(a) To a solution of diamine **3-2.4a** (0.6 mmol, 2 equiv.) and aldehyde **3-2.2** (1.2 mmol, 4 equiv.) in CH_2Cl_2 (0.92 mL) with 4Å molecular sieve powder (50 mg) under N_2 (g) was added azido-acid **3-2.3** (0.3 mmol, 1 equiv.) as a suspension in 3:1 CH_3OH/CH_2Cl_2 (0.4 mL), stirred 10 min at rt before addition of benzyl isocyanide **3-2.1a** (150 µL, 4 equiv.) as a solution in CH_2Cl_2 (0.36 mL). The reaction was stirred at rt for 18 h, then filtered through a 0.45 µm syringe filter and concentrated to give a crude residue that was used in the next step without further manipulation.

(b) The crude residue obtained in step (a) was dissolved in $PhCH_3$ (3 mL), resin-bound triphenyl phosphine (1.4 mmol/g, 438 mg, 2 equiv.) was added and the reaction stirred at rt for 1 h. The reaction was then fitted with a reflux condenser and heated to reflux and

stirred 18 h. The reaction was filtered through celite and concentrated to give a crude residue that was used in the next step without further manipulation.

(c) The crude residue obtained in step (b) was dissolved in CH_2Cl_2 (3 mL) and cooled to 0°C before addition of a 4M HCl solution in dioxane (0.73 mL, 10 equiv.). The reaction was allowed to warm to rt and stirred 18 h before concentrating to give a crude residue that was used in the next step without further manipulation.

(d) The crude residue obtained in step (c) was dissolved in CH_3OH (3 mL), then Et_3N (3 mL, 10 equiv.) was added and the reaction heated to 100°C by microwave irradiation for 1 h. The reaction was then concentrated, redissolved in CH_2Cl_2, washed with brine (1 x 50 mL), dried over MgS_4 (s) and purified as described.

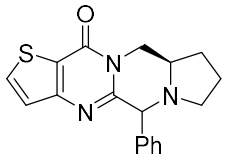

3-2.10q

(9a*R*)-5-phenyl-8,9,9a,10-tetrahydro-7*H*-pyrrolo[1',2':4,5]pyrazino[1,2-*a*]thieno[3,2-*d*]pyrimidin-12(5*H*)-one (**3-2.10q**). 3-azido-2-thiophenoic acid (49 mg, 0.29 mmol) was subjected to procedure A using benzaldehyde and purified by MPLC (12 g, 0-10% EtOAc/CH_2Cl_2, 30 mL/min) to give **3-2.10q** as a yellow oil (*trans* isomer (major): 10.7 mg, 12% yield; *cis* isomer (minor): 7.7 mg, 8% yield).

Major isomer

^{1}H NMR (400 MHz, $CDCl_3$) δ 7.79 (d, J = 5.3 Hz, 1H), 7.43 – 7.27 (m, 6H), 5.16 (s, 1H), 4.54 – 4.39 (m, 1H), 3.77 – 3.64 (m, 1H), 3.38 (dd, J = 14.0, 5.3 Hz, 1H), 3.10 (ddd, J = 9.2, 5.8, 4.1 Hz, 1H), 2.70 (q, J = 8.4 Hz, 1H), 2.13 – 1.98 (m, 1H), 1.79 (ddt, J = 9.3, 8.0, 5.3 Hz, 2H), 1.47 – 1.31 (m, 1H).

Minor isomer

^{1}H NMR (400 MHz, $CDCl_3$) δ 7.66 (d, *J* = 5.3 Hz, 1H), 7.43 – 7.28 (m, 5H), 7.11 (d, *J* = 5.3 Hz, 1H), 4.75 (dd, *J* = 13.3, 3.4 Hz, 1H), 4.47 (s, 1H), 3.61 (dd, *J* = 13.3, 10.9 Hz, 1H), 2.88 (ddd, *J* = 9.3, 7.7, 2.9 Hz, 1H), 2.78 – 2.67 (m, 1H), 2.63 (s, 1H), 2.24 – 2.13 (m, 3H). ^{13}C NMR (101 MHz, $CDCl_3$) *δ* 158.5, 156.6, 156.2, 140.9, 134.1, 129.3, 128.5, 128.0, 125.4, 72.4, 58.9, 53.9, 53.7, 48.6, 29.4, 28.8, 21.8.

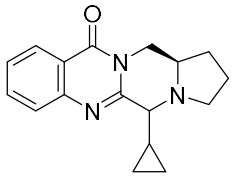

3-2.10l

(13a*R*)-5-cyclopropyl-2,3,13,13a-tetrahydro-1*H*-pyrrolo[1',2':4,5]pyrazino[2,1-*b*]quinazolin-11(5*H*)-one (**3-2.10l**). 2-azido-benzoic acid was subjected to procedure A using cyclopropylaldehyde and purified by MPLC (12 g, 20-50% EtOAc/CH_2Cl_2, 30 mL/min) to give **3-2.10l** as a yellow oil (*trans* isomer (major): 36 mg, 41% yield; *cis* isomer (minor): not isolated).

Major isomer

^{1}H NMR (400 MHz, $CDCl_3$) *δ* 8.28 (dd, *J* = 7.9, 1.5 Hz, 1H), 7.86 – 7.71 (m, 1H), 7.66 (d, *J* = 8.1 Hz, 1H), 7.45 (t, *J* = 7.3 Hz, 1H), 4.28 (dd, *J* = 14.0, 5.0 Hz, 1H), 4.06 (dd, *J* = 14.0, 6.5 Hz, 1H), 3.73 – 3.59 (m, 1H), 3.29 (d, *J* = 8.1 Hz, 1H), 3.23 (ddd, *J* = 9.0, 6.6, 4.5 Hz, 1H), 2.75 – 2.59 (m, 1H), 2.14 (ddt, *J* = 16.8, 7.0, 3.2 Hz, 1H), 1.89 – 1.79 (m, 2H), 1.50 (dq, *J* = 12.5, 8.7 Hz, 1H), 1.23 (dtd, *J* = 16.1, 8.1, 4.3 Hz, 1H), 0.78 – 0.68 (m, 1H), 0.58 (tdd, *J* = 13.5, 6.5, 4.2 Hz, 3H). ^{13}C NMR (101 MHz, $CDCl_3$) δ 162.1, 155.1, 147.5, 134.3, 127.4, 126.9, 126.5, 120.7, 67.0, 54.4, 53.3, 43.4, 30.5, 24.1, 12.2, 5.9, 3.2.

General Procedure B. *Synthesis of quinazolinone precursors **3-3.11, 3-3.12, 3-3.14***

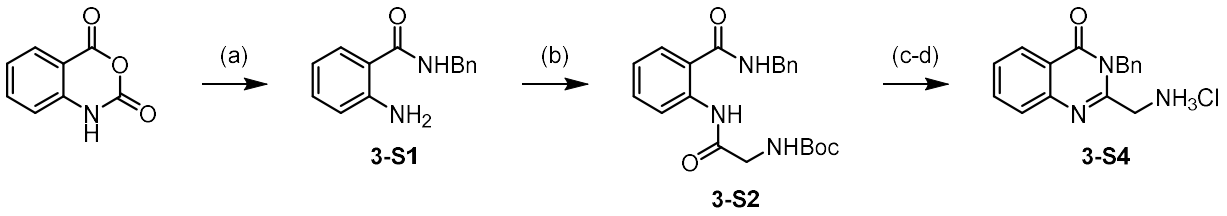

(a) To a solution of isatoic anhydride (1.6 g, 10.4 mmol, 1 equiv.) in CH_2Cl_2 (100 mL) was added benzylamine (1.1 mL, 10.0 mmol, 1 equiv.). The reaction was stirred at rt for 18 h, then partitioned with brine. The organic layer was separated and concentrated to give **3-S1** as an off-white solid (2.2 g, 97% yield). ^{1}H NMR (400 MHz, $CDCl_3$) δ 7.30-7.26 (m, 5H), 7.16 (t, J = 7.8 Hz, 1H), 6.64 (d, J = 8.3 Hz, 1H), 6.58 (t, J = 7.5 Hz, 1H), 6.49 (s, 1H), 5.37 (s, 2H), 4.54 (d, J = 5.7 Hz, 2H).

(b) To a solution of **3-S1** (893 mg, 4.0 mmol, 1 equiv.) in CH_2Cl_2 (40 mL) was added *N*-Boc glycine (1.02 g, 5.8 mmol, 1.5 equiv.) and DMAP (734 mg, 6.0 mmol, 1.5 equiv.) before cooling the reaction to 0°C. To this was added EDC*HCl (1.15 g, 6.0 mmol, 1.5 equiv.) and the reaction allowed to warm to rt and stirred 18 h. The reaction was concentrated, washed with 5% citric acid (aq.) (2 x 25 mL) and brine (3 x 50 mL), separated and the organic layers concentrated. The crude product was purified by MPLC (24 g, 0-50% EtOAc/Hexanes, 35 mL/min) to give **3-S2** as an off-white solid (876 mg, 2.3 mmol, 58% yield). ^{1}H NMR (400 MHz, $CDCl_3$) δ 11.54 (s, 1H), 8.57 (d, J = 8.5 Hz, 1H), 7.48 – 7.29 (m, 7H), 7.05 (td, J = 7.7, 1.1 Hz, 1H), 5.21 (t, J = 7.0 Hz, 1H), 4.59 (d, J = 5.6 Hz, 2H), 3.97 (d, J = 5.9 Hz, 1H), 1.48 (s, 9H).

(c) A solution of **3-S2** (753 mg, 2.0 mmol, 1.0 equiv.) in 1:1 dioxane/2.5M NaOH (aq.) (24 mL) was stirred at rt for 18 h, then partitioned with EtOAc (75 mL) and brine (100 mL). The organic layer was washed with brine (2 x 100 mL), then concentrated to give a white

solid that was used in the next step without further manipulation or characterization as **3-S3**.

(d) The crude material from step (c) was dissolved in CH_2Cl_2 (10 mL) and then a solution of 4M HCl in dioxane was added (5 mL) and the reaction stirred at rt for 18 h. The reaction was concentrated, filtered, and rinsed with CH_2Cl_2/hexanes to give **3-S4** a white solid (473 mg, 1.6 mmol, 80% over two steps). ^{1}H NMR (400 MHz, $CDCl_3$) δ 8.53 (br s, 3H), 8.23 (d, J = 8.03 Hz, 1H), 7.93 (t, J = 7.81 Hz, 1H), 7.74 (d, J = 8.3 Hz, 1H), 7.63 (t, J = 7.8 Hz, 1H), 7.40 – 7.22 (m, 5H), 5.39 (s, 2H), 4.19 (s, 2H).

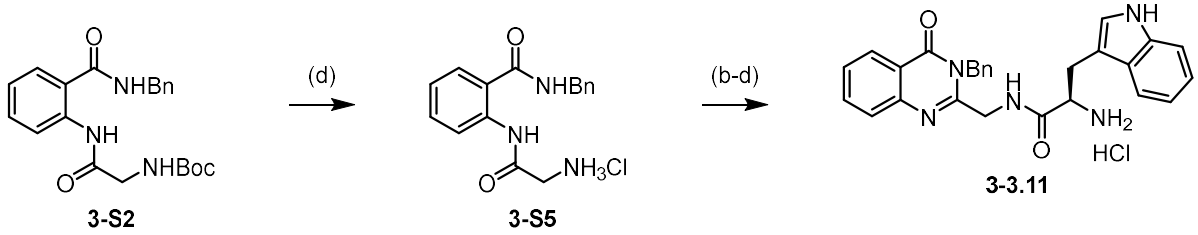

(*R*)-2-amino-*N*-((3-benzyl-4-oxo-3,4-dihydroquinazolin-2-yl)methyl)-3-(1*H*-indol-3-yl)propanamide hydrochloride (**3-3.11**). Compound **3-S2** (67 mg) was subjected to procedure B, step d to give **3-S5**, which was used without further analysis. **3-S5** was subjected to procedure B, step c using *N*-Boc-tryptophan (77 mg) and purified by MPLC (4g, 25-100% EtOAc, 20 mL/min) to give a white foam, **3-S6**, that was used without further manipulation in procedure B, steps c and d to give **3-3.11**. This was used subsequently without characterization.

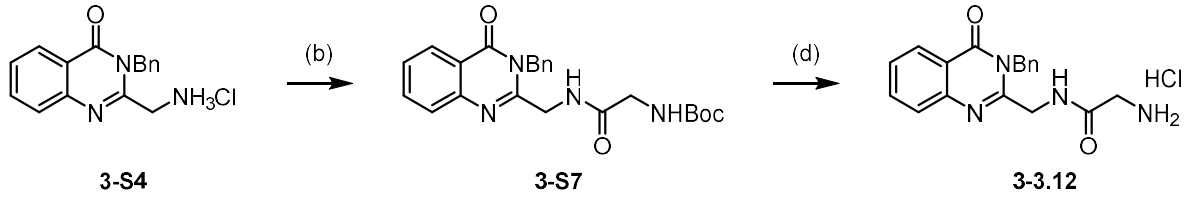

2-Amino-*N*-((3-benzyl-4-oxo-3,4-dihydroquinazolin-2-yl)methyl)acetamide (**3-3.12**). Compound **3-S3** (176 mg) was subjected to procedure B, step b to give **3-S7** (235 mg, 95% yield). ^{1}H NMR (400 MHz, $CDCl_3$) δ 8.33 (d, J = 8.0 Hz, 1H), 7.78 (t, J = 8.0 Hz, 1H), 7.66 (d, J = 8.3 Hz, 1H),

7.58 (s, 1H), 7.52 (t, *J* = 7.7 Hz, 1H), 7.29 (dt, *J* = 13.6, 6.8 Hz, 3H), 7.24 – 7.10 (m, 1H), 5.36 (s, 2H), 5.19 (d, *J* = 5.8 Hz, 1H), 4.47 (d, *J* = 4.0 Hz, 2H), 3.88 (d, *J* = 6.1 Hz, 1H), 1.46 (s, 9H).

S3-7 was subjected to procedure B, step d to give **3-3.12** as a pink-white solid. ^{1}H NMR (400 MHz, DMSO) δ 8.99 (t, *J* = 5.5 Hz, 1H), 8.21 (s, 2H), 8.19 (dd, *J* = 8.0, 1.5 Hz, 1H), 7.88 (ddd, *J* = 8.5, 7.2, 1.6 Hz, 1H), 7.71 (dd, *J* = 8.2, 1.0 Hz, 1H), 7.58 (ddd, *J* = 8.1, 7.2, 1.2 Hz, 1H), 7.35 (dd, *J* = 8.2, 6.5 Hz, 2H), 7.32 – 7.27 (m, 1H), 7.21 (dd, *J* = 7.0, 1.8 Hz, 2H), 5.40 (s, 2H), 4.49 (d, *J* = 5.5 Hz, 2H), 3.58 (q, *J* = 5.9 Hz, 2H).

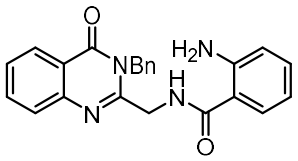

3-3.14

2-Amino-*N*-((3-benzyl-4-oxo-3,4-dihydroquinazolin-2-yl)methyl)benzamide (**3-3.14**). To a solution of **3-S3** (30 mg) in CH_3CN (1 mL) was added Et_3N (0.02 mL, 1.1 equiv.) and the reaction stirred at rt for 18 h. The reaction was poured over crushed ice and filtered to collect **3-3.14** as a white solid (15 mg, 40% yield). ^{1}H NMR (400 MHz, DMSO-d_6) *δ* 8.62 (t, *J* = 5.5 Hz, 1H), 8.19 (dd, *J* = 8.0, 1.5 Hz, 1H), 7.85 (td, *J* = 7.7, 7.2, 1.6 Hz, 1H), 7.65 (d, *J* = 8.1 Hz, 1H), 7.57 (t, *J* = 7.5 Hz, 1H), 7.50 (dd, *J* = 7.9, 1.5 Hz, 1H), 7.40 – 7.23 (m, 5H), 7.16 (dd, *J* = 7.4, 1.3 Hz, 1H), 6.70 (d, *J* = 8.0 Hz, 1H), 6.53 (t, *J* = 7.5 Hz, 1H), 6.39 (s, 2H), 5.45 (s, 2H), 4.56 (d, *J* = 5.5 Hz, 2H).

References

(1) Jaffett, V. A.; Fitz-Henley, J. N.; Khalifa, M. M.; Golden, J. E. Diastereoselective Multicomponent Synthesis of Ring-Fused Quinazolinones via Sequential Quinazolinone Rearrangement & Intramolecular Ring Closure of (Z)-Benzamidines, *In preparation*, 2020.

(2) Welsch, M. E.; Snyder, S. A.; Stockwell, B. R. Privileged Scaffolds for Library Design and Drug Discovery. *Curr. Opin. Chem. Biol.* **2010**, *14* (3), 347–361. https://doi.org/10.1016/j.cbpa.2010.02.018.

(3) Zhao, H.; Dietrich, J. Privileged Scaffolds in Lead Generation. *Expert Opin. Drug Discov.* **2015**, *10* (7), 781–790. https://doi.org/10.1517/17460441.2015.1041496.

(4) Ma, F.; Du, H. Novel Deoxyvasicinone Derivatives as Potent Multitarget-Directed Ligands for the Treatment of Alzheimer's Disease: Design, Synthesis, and Biological Evaluation. *Eur. J. Med. Chem.* **2017**, *140*, 118–127. https://doi.org/10.1016/j.ejmech.2017.09.008.

(5) Moon, T. C.; Murakami, M.; Kudo, I.; Son, K. H.; Kim, H. P.; Kang, S. S.; Chang, H. W. A New Class of COX-2 Inhibitor, Rutaecarpine from Evodia Rutaecarpa. *Inflamm. Res.* **1999**, *48* (12), 621–625. https://doi.org/10.1007/s000110050512.

(6) Cagir, A.; Jones, S. H.; Gao, R.; Eisenhauer, B. M.; Hecht, S. M. Luotonin A. A Naturally Occurring Human DNA Topoisomerase I Poison. *J. Am. Chem. Soc.* **2003**, *125* (45), 13628–13629. https://doi.org/10.1021/ja0368857.

(7) Yang, G.-Z.; Zhang, J.; Peng, J.-W.; Zhang, Z.-J.; Zhao, W.-B.; Wang, R.-X.; Ma, K.-Y.; Li, J.-C.; Liu, Y.-Q.; Zhao, Z.-M.; Shang, X.-F. Discovery of Luotonin A Analogues as Potent Fungicides and Insecticides: Design, Synthesis and Biological Evaluation Inspired by Natural Alkaloid. *Eur. J. Med. Chem.* **2020**, *194*, 112253. https://doi.org/10.1016/j.ejmech.2020.112253.

(8) He, F.; Snider, B. B. Total Synthesis of (+)-Fumiquinazoline G and (+)-Dehydrofumiquinazoline G. *Synlett* **1997**, *1997* (Sup. I), 483–484. https://doi.org/10.1055/s-1997-6137.

(9) Joshi, B. K.; Gloer, J. B.; Wicklow, D. T.; Dowd, P. F. Sclerotigenin: A New Antiinsectan Benzodiazepine from the Sclerotia of *Penicillium Sclerotigenum*. *J. Nat. Prod.* **1999**, *62* (4), 650–652. https://doi.org/10.1021/np980511n.

(10) Molina, P.; Tárraga, A.; Gonzalez-Tejero, A.; Rioja, I.; Ubeda, A.; Terencio, M. C.; Alcaraz, M. J. Inhibition of Leukocyte Functions by the Alkaloid Isaindigotone from Isatis Indigotica and Some New Synthetic Derivatives. *J. Nat. Prod.* **2001**, *64* (10), 1297–1300. https://doi.org/10.1021/np0101898.

(11) Shan, C.; Yan, J.-W.; Wang, Y.-Q.; Che, T.; Huang, Z.-L.; Chen, A.-C.; Yao, P.-F.; Tan, J.-H.; Li, D.; Ou, T.-M.; Gu, L.-Q.; Huang, Z.-S. Design, Synthesis, and Evaluation of Isaindigotone Derivatives To Downregulate *c-Myc* Transcription via Disrupting the Interaction of NM23-H2 with G-Quadruplex. *J. Med. Chem.* **2017**, *60* (4), 1292–1308. https://doi.org/10.1021/acs.jmedchem.6b01218.

(12) Hardy, L. W.; Heffernan, M. L. R.; Wu, F. X.; Spear, K. L.; Saraswat, L. D. Compounds for Treating Disorders Mediated by Metabotropic Glutamate Receptor 5, and Methods of Use Thereof. WO2011075699 (A2).

(13) Yan, G.; Zekarias, B. L.; Li, X.; Jaffett, V. A.; Guzei, I. A.; Golden, J. E. Divergent 2-Chloroquinazolin-4(3H)-One Rearrangement: Twisted-Cyclic Guanidine Formation or Ring-Fused N-Acylguanidines via a Domino Process. *Chem. – Eur. J.* **2020**, *26* (11), 2486–2492. https://doi.org/10.1002/chem.201905219.

(14) Parfitt, R. T.; Partridge, M. W.; Vipond, H. J. 562. Cyclic Amidines. Part XVI. Tetra-Azanaphtho[1,2,3-Fg]Naphthacenes. *J. Chem. Soc. Resumed* **1963**, No. 0, 3062–3066. https://doi.org/10.1039/JR9630003062.

(15) Taylor, J. E.; Bull, S. D.; Williams, J. M. J. Amidines, Isothioureas, and Guanidines as Nucleophilic Catalysts. *Chem. Soc. Rev.* **2012**, *41* (6), 2109. https://doi.org/10.1039/c2cs15288f.

(16) Jaffett, V. A.; Nerurkar, A.; Cao, X.; Guzei, I. A.; Golden, J. E. Telescoped Synthesis of C3-Functionalized (*E*)-Arylamidines Using Ugi–Mumm and Regiospecific Quinazolinone Rearrangements. *Org. Biomol. Chem.* **2019**, *17* (12), 3118–3128. https://doi.org/10.1039/C9OB00073A.

(17) Schroeder, C. E.; Neuenswander, S. A.; Yao, T.; Aubé, J.; Golden, J. E. One-Pot, Regiospecific Assembly of (E)-Benzamidines from δ- and γ-Amino Acids via an Intramolecular Aminoquinazolinone Rearrangement. *Org. Biomol. Chem.* **2016**, *14* (16), 3950–3955. https://doi.org/10.1039/C5OB02378E.

(18) Wang, Q.; Wang, D.-X.; Wang, M.-X.; Zhu, J. Still Unconquered: Enantioselective Passerini and Ugi Multicomponent Reactions. *Acc. Chem. Res.* **2018**, *51* (5), 1290–1300. https://doi.org/10.1021/acs.accounts.8b00105.

(19) Zhang, J.; Yu, P.; Li, S.-Y.; Sun, H.; Xiang, S.-H.; Wang, J. (Joelle); Houk, K. N.; Tan, B. Asymmetric Phosphoric Acid–Catalyzed Four-Component Ugi Reaction. *Science* **2018**, *361* (6407). https://doi.org/10.1126/science.aas8707.

(20) Znabet, A.; Ruijter, E.; de Kanter, F. J. J.; Köhler, V.; Helliwell, M.; Turner, N. J.; Orru, R. V. A. Highly Stereoselective Synthesis of Substituted Prolyl Peptides Using a Combination

of Biocatalytic Desymmetrization and Multicomponent Reactions. *Angew. Chem.* **2010**, *122* (31), 5417–5420. https://doi.org/10.1002/ange.201001592.

(21) Cheng, J.; Deming, T. J. Synthesis of Polypeptides by Ring-Opening Polymerization of α-Amino Acid N-Carboxyanhydrides. In *Peptide-Based Materials*; Deming, T., Ed.; Topics in Current Chemistry; Springer: Berlin, Heidelberg, 2012; pp 1–26. https://doi.org/10.1007/128_2011_173.

(22) Semple, J. E.; Sullivan, B.; Sill, K. N. Large-Scale Synthesis of α-Amino Acid-N-Carboxyanhydrides. *Synth. Commun.* **2017**, *47* (1), 53–61. https://doi.org/10.1080/00397911.2016.1249289.

(23) Fuller, W. D.; Cohen, M. P.; Shabankareh, M.; Blair, R. K.; Goodman, M.; Naider, F. R. Urethane Protected Amino Acid N-Carboxyanhydrides and Their Use in Peptide Synthesis. *J. Am. Chem. Soc.* **1990**, *112* (20), 7414–7416. https://doi.org/10.1021/ja00176a063.

(24) Daly, W. H.; Poché, D. The Preparation of N-Carboxyanhydrides of α-Amino Acids Using Bis(Trichloromethyl)Carbonate. *Tetrahedron Lett.* **1988**, *29* (46), 5859–5862. https://doi.org/10.1016/S0040-4039(00)82209-1.

(25) Wang, H.; Ganesan, A. Total Synthesis of the Fumiquinazoline Alkaloids: Solution-Phase Studies [1]. *J. Org. Chem.* **2000**, *65* (4), 1022–1030. https://doi.org/10.1021/jo9914364.

(26) Wang, H.; Ganesan, A. Total Synthesis of the Fumiquinazoline Alkaloids: Solid-Phase Studies [1]. *J. Comb. Chem.* **2000**, *2* (2), 186–194. https://doi.org/10.1021/cc9900807.

(27) Liu, J.-F.; Ye, P.; Zhang, B.; Bi, G.; Sargent, K.; Yu, L.; Yohannes, D.; Baldino, C. M. Three-Component One-Pot Total Syntheses of Glyantrypine, Fumiquinazoline F, and Fiscalin B Promoted by Microwave Irradiation [†]. *J. Org. Chem.* **2005**, *70* (16), 6339–6345. https://doi.org/10.1021/jo0508043.

(28) Chung, D.; Schroeder, C. E.; Sotsky, J.; Yao, T.; Roy, S.; Smith, R. A.; Tower, N. A.; Noah, J. W.; McKellip, S.; Sosa, M.; Rasmussen, L.; White, E. L.; Aubé, J.; Golden, J. E. ML336: Development of Quinazolinone-Based Inhibitors Against Venezuelan Equine Encephalitis Virus (VEEV). In *Probe Reports from the NIH Molecular Libraries Program*; National Center for Biotechnology Information (US): Bethesda (MD), 2010.

(29) Schroeder, C. E.; Yao, T.; Sotsky, J.; Smith, R. A.; Roy, S.; Chu, Y.-K.; Guo, H.; Tower, N. A.; Noah, J. W.; McKellip, S.; Sosa, M.; Rasmussen, L.; Smith, L. H.; White, E. L.; Aubé, J.; Jonsson, C. B.; Chung, D.; Golden, J. E. Development of (E)-2-((1,4-Dimethylpiperazin-2-Ylidene)Amino)-5-Nitro-N-Phenylbenzamide, ML336: Novel 2-Amidinophenylbenzamides as Potent Inhibitors of Venezuelan Equine Encephalitis Virus. *J. Med. Chem.* **2014**, *57* (20), 8608–8621. https://doi.org/10.1021/jm501203v.

Chapter 4 – Development of Benzoic Acid-derived Anti-Parasitic Agents

This chapter is adapted in part from works prepared or submitted for publication.[1,2] *The Toxoplasma gondii work was completed in collaboration with Prof. Laura Knoll (University of Wisconsin-Madison) and Prof. James C. Morris (Clemson University). The Trypanosoma brucei and Naegleria fowleri work was also executed in collaboration with the Morris lab. The Leishmania donovani work was executed in collaboration with Prof. Karl A. Werbovetz (The Ohio State University). Synthesis was supported in part by Soren Rozema, an undergraduate student in the Golden lab.*

Section 4-1: Introduction

Discovery and development of new drugs for infectious diseases caused by parasites remain important areas of investigation due to continued unmet medical need. The subject continues to be a research focus of the Golden group, conducted in collaboration with experts in parasite biology. This chapter discusses the medicinal chemistry optimization of a series of benzoic acid derivatives against several parasitic threats to human health. These include *Toxoplasma gondii*, which is a leading cause of foodborne illness, hospitalizations, and death in the developed world; *Trypanosoma brucei*, which causes human African sleeping sickness; and *Leishmania donovani*, which is responsible for visceral leishmaniasis (a disease also known as *kala-azar*).[3–5]

The compounds described in this chapter are derived from a series of benzamidobenzoic acids ("**BABA**s") developed by our group over the course of a substantial medicinal chemistry campaign targeting *T. brucei* parasites (see **Section 4-2**).[4,6,7] The campaign was focused on identifying selective inhibitors of *T. brucei* hexokinase 1 (TbHK1), an enzyme integral to that

parasite's metabolism during the acute stage of human infection.[8] These inhibitors act by inhibiting the parasite enzymatic machinery selectively over the most closely related human homolog enzyme, human glucokinase (hGlk) or human hexokinase 4 (HK IV). Further, it was shown that the compounds inhibit the enzyme non-competitively with respect to the enzyme's substrate, ATP.[4,6,7] Because the *T. brucei* hexokinase catalyzes the flux-control step of glycolysis, and because *T. brucei* relies exclusively on glycolysis for energy production in its bloodstream form, inhibition of TbHK1 led to arrest of the downstream pathway and subsequent parasite killing.[4] Although the related kinetoplastid *Leishmania major* is less metabolically reliant on glycolysis compared to *T. brucei*, its hexokinase (LmHK1) shares 61% sequence homology with TbHK1.[9] The team recognized that inhibiting *L. major* glycolysis might provide a window of therapeutic synergy with other agents, thereby reducing or eliminating the need for problematic drugs upon which the current standards of care rely (see **Section 4-5**).[4,10] Assessment of the benzamidobenzoic acids originally designed as inhibitors of *T. brucei* hexokinase 1 revealed hit-level inhibition (IC_{50} < 10 μM) of LmHK1.[4] Though we observed comparatively less potency against LmHK1 than for TbHK1, the data suggested that improved multi-parasite inhibition might be possible from this template through further structural refinement.

Since then, the Golden group has continued to investigate the benzamidobenzoic acid template to improve properties that limited these exploratory compounds from further drug development. These efforts, described in this chapter, have resulted in compounds with improved physicochemical and ADME (absorption, distribution, metabolism, and excretion) characteristics and desirable whole parasite growth inhibition despite a loss of activity against the original kinase target. This suggests discovery of an as-yet unidentified and novel mode of action for this family of molecules. When these compounds were tested broadly against more phylogenetically distant

parasites, we discovered significant inhibitory activity beyond kinetoplastids with differentiated structure-activity relationships, which has further intensified our interest in the development and optimization of this chemical series. This scaffold-centric, multi-pathogen approach - as opposed to the pathogen-centric, multi-scaffold approach that is typical of a traditional drug discovery program - has recently been coined "parasite hopping", and represents a sub-strategy of the broader concept of compound repurposing.[11–13]

Compound repurposing refers generally to a strategy wherein known compounds (often approved drugs) are deployed against a disease or target other than the one(s) for which they were originally designed.[12,13] This can dramatically abbreviate the discovery workflow and drug development timeline by taking advantage of previously-established safety information.[13] In a "parasite hopping" approach, compounds developed for activity against one organism may also show activity against another parasite, although additional structural optimization of the chemical scaffold may be required. The required motifs for activity may also diverge between the parasites of interest.

A recent example from the Ferrins group found lead compounds with distinct activity against three protozoan pathogens by screening derivatives of **NEU-1953**, an inhibitor of *T. brucei* and itself the result of multiple rounds of optimization for anti-parasitic activity following repurposing of the human EGFR tyrosine kinase inhibitor lapatinib.[11,12] While all share a substantial portion of the central aminoquinoline core, divergent structure-activity relationships (SAR) for each parasite enabled tuning of the scaffold to optimize activity against either *Plasmodium falciparum* (**NEU-4439**, *P. falciparum* EC_{50} = 0.19 μM), which causes malaria, *Trypanosoma cruzi* (**NEU-5535**, *T. cruzi* EC_{50} = 0.33 μM), which causes Chagas disease, or *Leishmania major* (**NEU-2213**, *L. major* EC_{50} = 0.73 μM), which causes cutaneous leishmaniasis

(**Figure 4-1.1**).[11] The differentiated structure-activity requirements meant that potency improvements for a given structural modification were parasite-specific: **NEU-5535** has high potency against its optimized target *T. cruzi* (EC_{50} = 0.33 μM) but not against *L. major* (EC_{50} > 15 μM), and the *L. major*-specialized **NEU-2213** is similarly potent against its target (EC_{50} = 0.73 μM) but impotent against *T. cruzi* (EC_{50} > 15 μM).[11] Meanwhile the original compound, **NEU-1953**, is comparatively weak against both *T. cruzi* (EC_{50} = 6.0 μM) and *L. major* (EC_{50} > 15 μM) but highly potent against *T. brucei* (EC_{50} = 0.43 μM) and *P. falciparum* (EC_{50} = 0.026 μM).[11] Importantly, desirable physicochemical and ADME properties intrinsic to the core motif of the original parent compound **NEU-1953** were generally retained in the optimized analogs.[11]

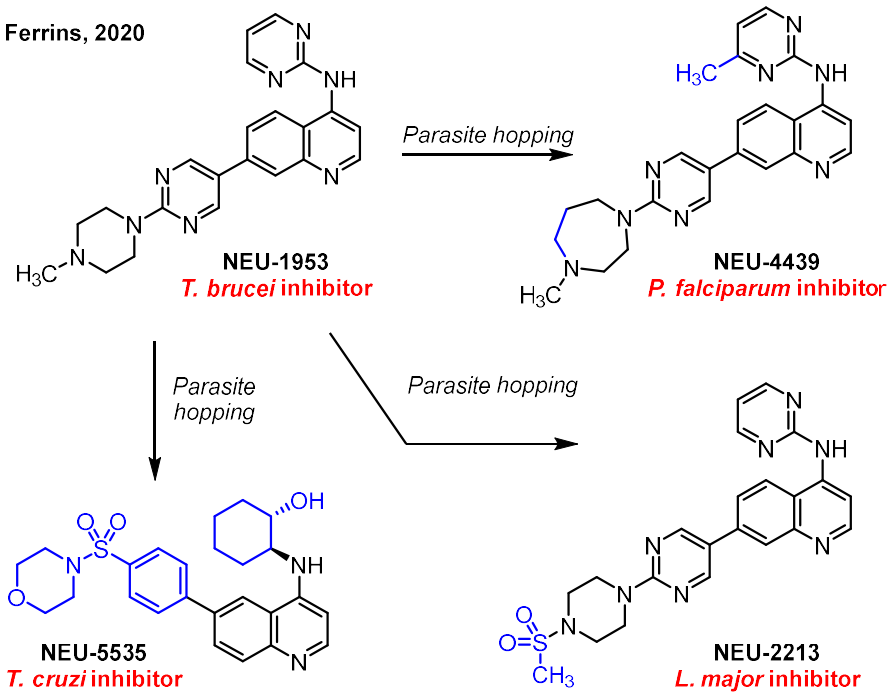

Figure 4-1.1 Selected examples of parasite hopping for discovery of new anti-parasitics. Blue highlights indicate structural differences conferring parasite specificity as dictated by divergent structure-activity relationships.

In some cases, the broad spectrum of activity observed when parasite hopping with a particular scaffold may occur by virtue of targeting relatively conserved biological pathways with a shared level of importance to pathogenicity or parasite survival, though this is not always clearly established at the outset. Importantly, the biological targets of a compound need not be known for a parasite hopping approach to be effective, and even phylogenetically distant pathogens can be similarly susceptible to a family of chemical matter. The work in this chapter exemplifies such target-agnostic and phylogenetically distant parasite hopping successes in a number of important eukaryotic pathogens responsible for human disease, namely *Toxoplasma gondii* (toxoplasmosis), *Trypanosoma brucei* (human African trypanosomiasis, "human African sleeping sickness", "HAT"), *Leishmania donovani* (visceral leishmaniasis, "kala-azar"), and *Naegleria fowleri* (primary amoebic meningoencephalitis, "brain-eating amoeba"). The divergent structure-activity and structure-property relationships of this series against each of the pathogens will be discussed, as well as synthetic challenges and improvements.

Section 4-2: Benzamidobenzoic acids as an anti-parasitic scaffold

Prior to my involvement, a collection of benzamidobenzoic acids (**BABA**s) was developed by the Golden group and representative examples were established as inhibitors of *T. brucei* hexokinase 1 (TbHK1).[4,6,7] TbHK1 catalyzes the flux-control step of glycolysis in *T. brucei*, a pathway upon which the parasite is metabolically reliant during acute infection.[4] It was expected that inhibition of this enzyme would arrest the downstream pathway and lead to parasite death.[4] Following a high-throughput screen of more than 220,000 molecules, the singleton hit compound 4-chloro-2-(4-methoxybenzamido)benzoic acid (**4-2.1**) was identified with weak inhibition of the target enzyme *in vitro* and no efficacy against whole *T. brucei* parasites.[6] Medicinal chemistry optimization yielded 4-(4-(*tert*-butyl)benzamido-6-chloro-[1,1'-biphenyl]-3-carboxylic acid,

BABA 1, which featured submicromolar TbHK1 inhibition, good selectivity over human glucokinase (hGlk), low mammalian cell (IMR90) toxicity, and growth inhibition of whole bloodstream form (BSF) *T. brucei* parasites (**Scheme 4-2.1**).[4] Subsequent screening of **BABA 1** revealed inhibition of the homologous enzyme (*L. major* hexokinase, LmHK1) in *Leishmania major*, which causes cutaneous leishmaniasis. Despite a 6-fold reduction in potency for LmHK1, this outcome nonetheless established the potential for parasite hopping using the benzamidobenzoic acid template. [4,14]

Scheme 4-2.1 Development of **BABA 1** as a parasite glycolytic inhibitor[4,6,7]

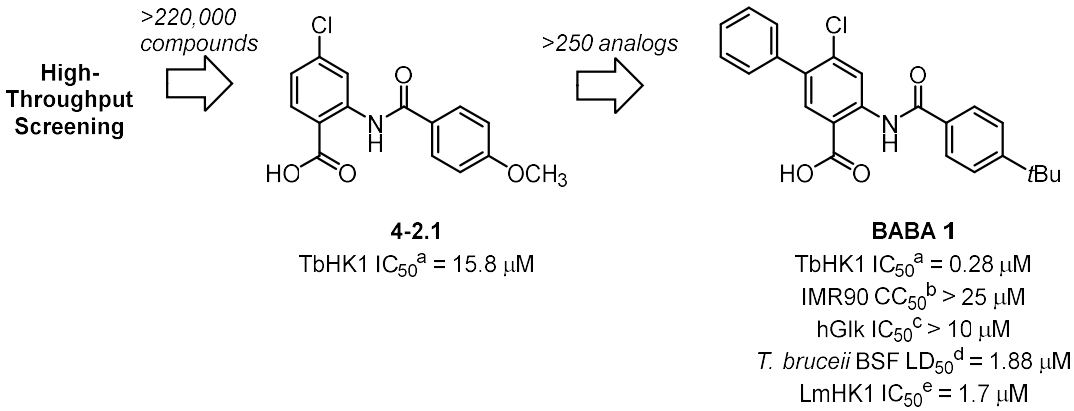

[a]TbHK1: *Trypanosoma brucei* hexokinase 1, IC_{50}: half-maximal inhibitory concentration; [b]IMR90: human fetal lung cells, CC_{50}: half-maximal cytotoxic concentration; [c]hGlk: human glucokinase; [d]BSF: bloodstream form, LD_{50}: half-maximal lethal concentration; [d]LmHK1: *Leishmania major* hexokinase 1.

Section 4-3: Benzamidopicolinic acids as improved BABA surrogates

As discussed in the previous section, the benzamidobenzoic acids (culminating in **BABA 1**) were discovered and developed as inhibitors of kinetoplastid parasite glycolysis, especially focused on *T. brucei* with some adventitious inhibition of *L. major*.[4,6,7] Despite exciting milestones in potency and selectivity for an enzymatic target and efficacy in whole parasites, which were important to establishing the proof-of-concept for hexokinase-mediated parasite inhibition, further

development of these compounds in a drug discovery context was impaired by high lipophilicity ($LogD_{7.4}$ > 5.0) resulting in poor physicochemical and ADME properties.[1,4] Nonetheless, the benzamidobenzoic acid series represented a collection of novel chemical probes that might serve as a template from which better anti-parasitic agents could be derived.

To overcome the physicochemical and ADME limitations, a "methine-to-nitrogen atom switch" modification of the **BABA** core was implemented. In some parasites, such as *T. brucei*, the glycolytic enzymes are localized to a specialized subcellular compartment called the glycosome.[15] The glycosomal environment is slightly acidic (pH ~ 6), which can cause some small molecules with basic residues to be sequestered as ionized species in the organelle.[16,17] Experimental results suggest sequestration can be as high as 15-fold greater than theoretically predicted.[18] As such, the incorporation of a nitrogen atom into the scaffold was anticipated to offer some benefit in this respect, depending on its placement within the molecule. Moreover, the introduction of a nitrogen atom into the scaffold, if tolerated, would be expected to reduce lipophilicity and enhance solubility, both of which were liabilities for the **BABA** series.[4,19] With these considerations in mind, and knowing that an expedient synthesis for rapid assessment called for minimal alterations to the existing routes used to access the compounds, we opted to incorporate the nitrogen atom into the benzoic acid moiety of the benzamidobenzoic acid template. Using **BABA 1** as a test case afforded benzamidopicolinic acid derivative **BDGR 6001** (*Note: compounds arising from medicinal chemistry optimization in the Golden group are assigned unique numerical monikers of type "**BDGR** ####" based on their structure to enable tracking; compounds are referred to here and in subsequent sections by assigned "BDGR numbers"*). Comparison of the calculated and measured properties of **BABA 1** and **BDGR 6001** is illustrative of the effect of a methine-to-nitrogen atom substitution ("CH-to-N atom switch") in this scaffold:

lipophilicity was reduced by 1-2 log units, kinetic solubility in phosphate-buffered saline (PBS) more than doubled, and 15% more of the compound remained after 1 h exposure to mouse microsomes. These improvements were achieved without reducing membrane permeability significantly (**Scheme 4-3.1**).

Scheme 4-3.1 Effects of methine-to-nitrogen atom exchange in the **BABA** core on physicochemical properties and compound stability

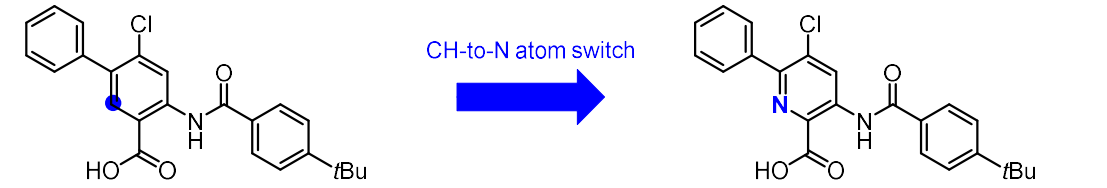

BABA 1
cLogD (pH 5.0-7.4)[a]: 6.75 - 5.42
Solubility (PBS 1X, pH 7.4)[b]: 2.7 µM
Microsomal stability[c]: 69.2%
Permeability (PAMPA)[d]: 6.7 Pe (10^{-6} cm/s)

BDGR 6001
cLogD (pH 5.0-7.4)[a]: 5.18 - 4.32
Solubility (PBS 1X, pH 7.4)[b]: 6.4 µM
Microsomal stability[c]: 85.1%
Permeability (PAMPA)[d]: 5.4 Pe (10^{-6} cm/s)

[a]cLogD: calculated partition coefficient octanol/water using ACD/LogD v8.07; [b]Kinetic aqueous solubility at pH 7.4, PBS: phosphate-buffered saline; [c]Microsomal stability: Percent compound remaining in mouse microsomes after 1 h; [d]PAMPA: parallel artificial membrane permeability assay.

With a nitrogen-containing analog of **BABA 1** in hand (**BDGR 6001**), along with evidence that desired physicochemical properties had improved, we sought to test the compounds against *T. brucei* hexokinase 1 and the whole parasite to see if activity was altered. Given that we had observed growth inhibition against *L. major* in the benzamidobenzoic acid parent series[4,6,7], we also sought to expand our screening panel to include other parasites for opportunistic development. As a result, we were able to evaluate members of the **BABA** series, as well as **BDGR 6001** and related analogs, against *Toxoplasma gondii*, *Trypanosoma brucei*, *Leishmania donovani*, and *Naegleria fowleri* parasites.

Section 4-4: Picolinic acid derived dual stage inhibitors of *Toxoplasma gondii*

The apicoplast parasite *Toxoplasma gondii* is a leading cause for food-borne illness, hospitalizations, and death in the developed world and is estimated to affect 30-50% of the human population worldwide.[3,20–22] The disease, toxoplasmosis, affects 60% of the U.S. population and is characterized by lifelong, chronic infection in immune-competent individuals and disease resurgence with potentially fatal complications in fetuses and immune-compromised patients.[3,20,23–25] Acute *T. gondii* infection is typically contracted through consumption of contaminated food or water, and occurs while the parasite is in its rapidly growing tachyzoite form.[24,26,27] The standard of care for acute infection is a synergistic combination of antifolate drugs, pyrimethamine and sulfadiazine (**Figure 4-4.1**).[28,29]

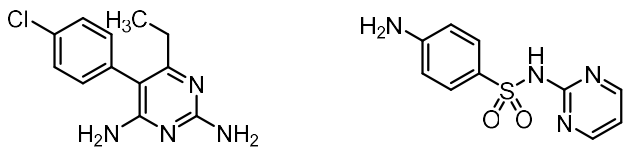

Pyrimethamine Sulfadiazine

Figure 4-4.1 Structure of current standard of care drugs for toxoplasmosis.

Unfortunately, significant side effects and resistance have been reported with use of these drugs.[30–34] After the infamous Turing Pharmaceuticals incident in 2015, during which the price of pyrimethamine increased more than 55-fold overnight, concerns regarding access to these drugs has also become an important concern.[35,36]

Robust host immune response and/or challenge by chemotherapeutics induces parasite differentiation from the proliferating tachyzoite stage to the cyst-dwelling bradyzoite stage, against which current treatments are ineffective.[24–26,37–40] Failure of current treatments against bradyzoites and the resulting inability to clear parasitic infection completely in patients results in lifelong

opportunistic chronic infection with significant risk of resurgence in immunocompromised individuals.[41] While immunocompetent individuals who become infected are typically asymptomatic or may suffer self-limiting flu-like illness, ocular lesions have been reported and maternal infection during pregnancy can lead to miscarriage or visual or motor disabilities in newborns.[42–45] Despite new development and drug repurposing efforts, clearing the bradyzoite stage of the parasite continues to be a major challenge in the battle against *T. gondii*.[25,33,37,39,46–62]

Given that the activity of the **BABA** series in *T. brucei* hinged on inhibition of a metabolically critical glycolytic enzyme, the rationale for repurposing the benzamidobenzoic acids towards *T. gondii* extended beyond the optimism that must necessarily accompany broad, opportunistic screening efforts. For example, efforts targeting glycolytic pathways in *Plasmodium falciparum*, which causes malaria and is also an apicoplast parasite, have recently met with some success.[63–65] A key factor of this approach relied on parasite dependence on glycolysis during life stage(s) relevant to host infection.[6,7,63–71] In the case of *T. gondii*, the bradyzoite form of the parasite that characterizes chronic infection relies exclusively on glycolysis for energy metabolism.[24,26,37,72,73] Despite this known metabolic vulnerability of bradyzoites, therapeutic approaches targeting *T. gondii* glycolysis have not been described. Furthermore, we were unsure if the picolinic acid derivatives would behave similarly.

Nonetheless, in light of recent successes for such a strategy in campaigns against other protozoan parasites with glycolysis-dependent infectious stages, we anticipated that a parasite hopping approach using a collection of known glycolytic inhibitors with evidence of broader-spectrum activity might provide an opportunity to develop more effective *T. gondii* therapeutics.[6,7,63,65–69] As discussed in preceding sections, a series of benzamidobenzoic acids were previously identified as glycolytic inhibitors of *Trypanosoma brucei*.[4,6,7] Although the potential

for successful parasite hopping to the relatively closely-related kinetoplastid *Leishmania major* had been demonstrated, assessment against the more phylogenetically-distant, apicoplast parasite *T. gondii* had not been explored.

To this end, seven benzamidobenzoic acids were assayed by parasitologists in Prof. Laura Knoll's lab at the University of Wisconsin-Madison for *in vitro* growth inhibition of *T. gondii* tachyzoites and bradyzoites at a single concentration of 10 μM. Human foreskin fibroblast host cells were infected with parasite, then exposed to compound for 48 h before addition of [^{3}H]-uracil and incubation for 24 h. Incorporated uracil was assessed by scintillation counter and served as a measure of replication, a proxy for parasite growth. The growth inhibitory effect of each compound was normalized to a DMSO negative control and compared to pyrimethamine as a positive control (tachyzoites only). Excitingly, we observed substantial growth inhibition against both parasite forms across the compound set, with the best dual stage growth inhibition demonstrated by **BABA 1**. In contrast to pyrimethamine, which inhibited tachyzoite growth (98.0%) but not bradyzoite growth (0%), **BABA 1** gave robust inhibition of both tachyzoites (99.6%) and bradyzoites (96.7%) (**Table 4-4.1**).

Table 4-4.1 Percent *in vitro* growth inhibition of *T. gondii* tachyzoites and bradyzoites by selected benzamidobenzoic acids at a single concentration of 10 μM

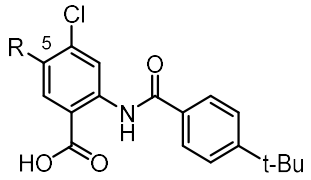

Compound	R =	cLogD 7.4[a]	Tachyzoite % Growth Inhibition[b]	Bradyzoite % Growth Inhibition[b]
DMSO	-	-	0.0	0.0
Pyrimethamine	-	3.1	98.0	0.0
BABA 1	Ph	5.4	99.6	96.7
BABA 2	F	4.0	81.0	89.1
BABA 3	2-F-Ph	5.9	92.0	94.7
BABA 4	2-thiophenyl	5.2	96.9	95.9
BABA 5	3-OCH_3-Ph	5.2	91.7	98.4
BABA 6	3-CF_3-Ph	6.4	99.7	96.4
BABA 7	4-Cl-Ph	6.0	94.1	98.7

[a]Calculated partition coefficient octanol/water at pH 7.4 using ACD/LogD v8.07; [b]Average of at least three independent experiments; DMSO: dimethyl sulfoxide (control).

Although the set of **BABA** compounds at initial screening was small, it was curated primarily to assess a variety of changes on the benzoic acid ring where structure activity relationships (SAR) in *T. brucei* had been most permissive. The rationale was that detection of permissive SAR in *T. gondii* would enable refinement to less lipophilic compounds. Since aryl substitution at the C5 position of the benzoic acid ring accounted for a substantial portion of lipophilicity, assessing SAR tolerance at that position became important. For example, exchange of a phenyl group in **BABA 1** for a fluorine atom in **BABA 2** leads to a > 10-fold reduction in calculated lipophilicity (> 1-unit change in cLogD). Indeed, we observed broad tolerance for substitution changes at this position, with comparable levels of growth inhibition for the aryl substituted analogs **BABA 1** and **BABA 3-7**, and only slightly reduced activity (~10%) in the

fluorine-substituted analog **BABA 2**. This suggested that alteration of the **BABA** scaffold towards less lipophilic compounds might be tolerated.

Based on these results, we anticipated that a series of benzamidopicolinic acid analogs might perform well in the same assessment. These desired compounds were synthesized with the intent of surveying structure-activity relationships of a series with reduced lipophilicity and improved physicochemical properties compared to the **BABA** series, though the synthetic approach was refined. The benzamidobenzoic acids had generally been prepared by a route wherein an appropriately substituted methyl 2-aminobenzoate of type **4-4.1** was diversified at C5 of the benzoic acid ring system by Suzuki or other coupling, followed by benzoylation and ester hydrolysis to give the **BABA** scaffold (**Scheme 4-4.1**).[4]

Scheme 4-4.1 Synthetic route to benzamidobenzoic acid (**BABA**) series

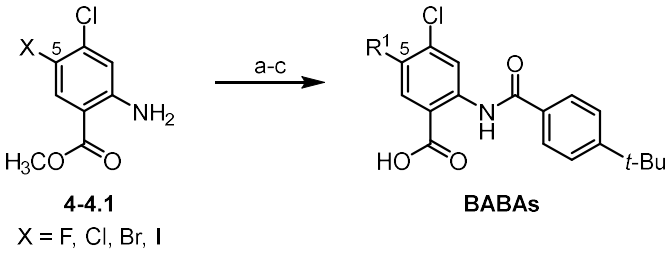

4-4.1
X = F, Cl, Br, I

BABAs

Reagents and conditions: (a) Coupling conditions, 21-92% (b) 4-*t*BuBzCl, CH_3CN, 150°C, 1 h, 25-95%; (c) LiOH, 3:2 THF/H_2O, rt, 18 h, 15-93%.

To generate the desired benzamidopicolinic acids and analogs, a similar approach was adopted, however, several important changes were made to the synthesis that enabled this work. First, the order of steps was modified such that Suzuki coupling (**Scheme 4-4.2**, step c), if used, was conducted after formation of the benzamide (**Scheme 4-4.2**, step b). This overcame problems with selectivity between the 6-Br and 5-Cl groups during Suzuki coupling in the synthesis of **BDGR 6001** (**Scheme 4-4.2**).

Scheme 4-4.2 Synthesis of benzamidopicolinic and benzamidonicotinic acids

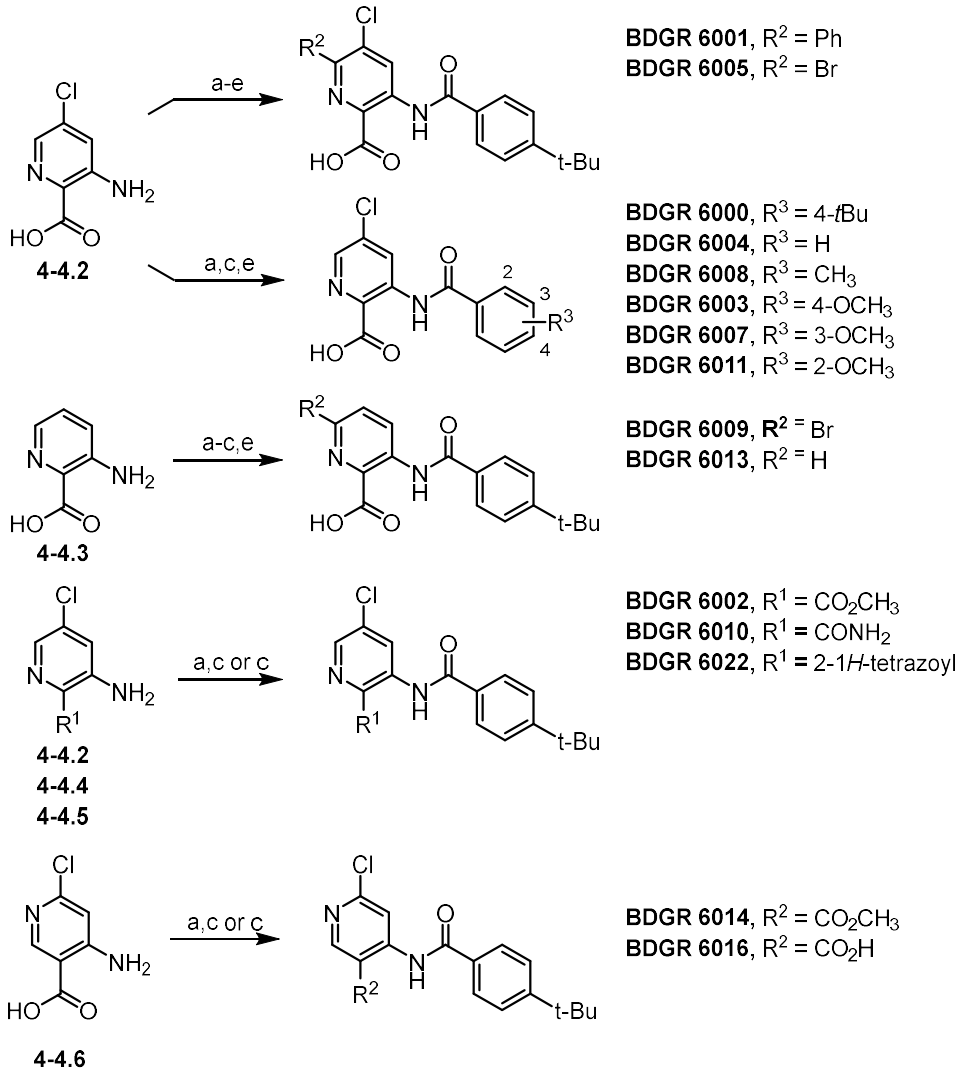

Reagents and conditions: (a) 2.0M TMS-diazomethane in hexanes, 1:4 CH_3OH/CH_2Cl_2, rt, 18 h, 42-76%; (b) 2.6 M Br_2 in AcOH, 2M H_2SO_4, rt, 4-72 h, 51-55%; (c) ArCOCl, Et_3N or iPr_2EtN, THF or CH_3CN, rt-150°C, 6-94%; (d) $PhB(OH)_2$, Na_2CO_3, $Pd(PPh)_3Cl_2$, 10:1 CH_3CN/H_2O, 100°C, 0.5 h, 67%; (e) 1.3 M aq. LiOH, 3:2 THF/H_2O, rt, 12-48 h, 31-93%.

Second, improvements were made to the synthesis of methyl 3-amino-5-chloropicolinate **4-4.7**, a key building block for many of the benzamidopicolinic acids (**Scheme 4-4.3**). To access **4-4.7** cheaply, expediently, and to obviate the subsequent use of highly toxic TMS-diazomethane during esterification, I developed an efficient alternative to the initial route. This was achieved by synthesizing **4-4.7** over two steps from commercially available 3-nitro-5-chloropicolinonitrile **4-**

4.8, which circumvented the need for the expensive picolinic acid **4-4.2** that was purchased during the initial discovery route. This resulted in a 99% material cost reduction and enabled synthesis of the key building block **4-4.7** at 20-fold the original scale with only a single net additional step (**Scheme 4-4.3**).

Scheme 4-4.3 Route modifications for scale-up

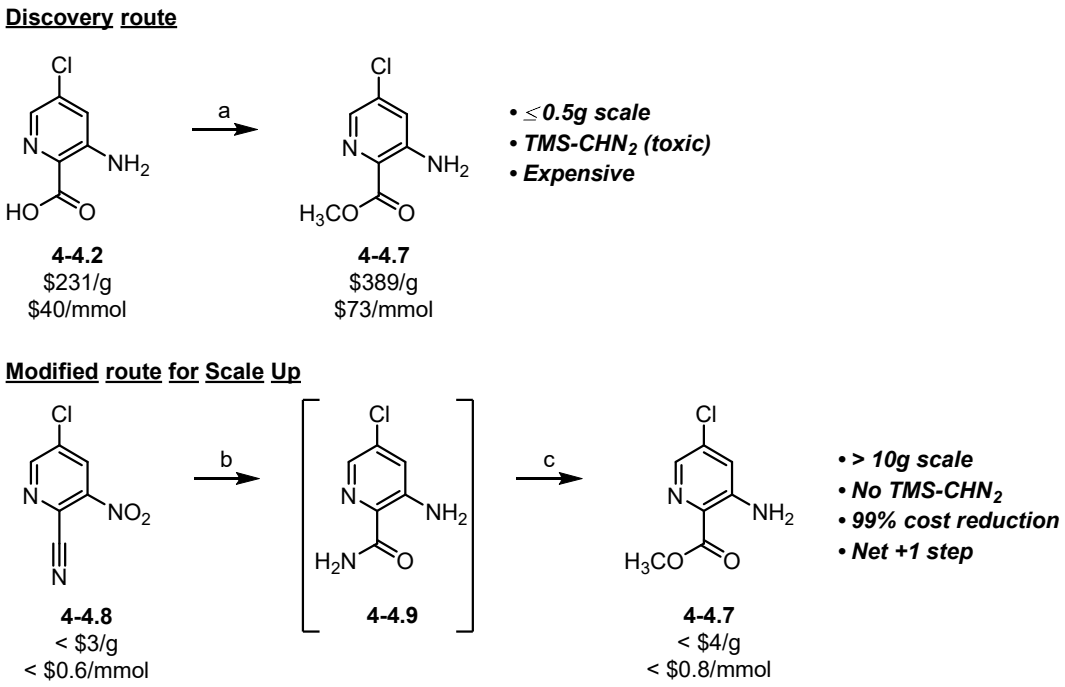

Reagents and conditions: (a) 2.0M TMS-diazomethane in hexanes, 1:4 CH_3OH/CH_2Cl_2, rt, 18 h, 55%; (b) $FeCl_3{*}6H_2O$, 65% N_2H_2 (aq), charcoal, CH_3OH, reflux, 1-2 h; (c) 1:10 H_2SO_4/CH_3OH, 100°C, 48 h, 73% over two steps.

With 14 benzamidopicolinic acids and 2 benzamidonicotinic acids in hand, the compounds were screened by our collaborators in the Knoll lab. This revealed strong *in vitro* anti-parasitic activity across the collection, with 10 of 16 compounds (63%) displaying at least 70% growth inhibition of both stages of *T. gondii* at 10μM. As a result, these compounds were further assayed in dose-response format to assess potency. They were also assayed to measure toxicity to the human foreskin fibroblast (HFF) host cells.

BDGR 6001 represented the most structurally comparable nitrogenated analog to **BABA 1**, as the only modification to the structure was the methine-to-nitrogen atom switch. As a substantial amount of undesired lipophilicity can be attributed to the C6-aryl substitution on the benzamidopicolinic acid, a feature inherited from the parent compound **BABA 1**, we sought to investigate whether such functionality in the nitrogenated series was required for activity in *T. gondii* (**Table 4-4.2**). We were encouraged to find that removal of substitution altogether from the C6- position of the pyridyl ring system of **BDGR 6001**, as shown in **BDGR 6000,** afforded a two-fold increase in potency against tachyzoites and maintained comparable activity against bradyzoites. Maintaining the C5-Cl substituent was preferable to its removal, as shown by the differences in potency and selectivity index between **BDGR 6000** and **BDGR 6013**. Neither of the benzamidonicotinic acid analogs **BDGR 6014** or **BDGR 6016** were superior to their benzamidopicolinic acid counterparts. The benzamidonicotinic acid motif was therefore not explored further. We also observed some cytotoxicity against the host cells with a selectivity index between parasite and host cells of about 5-10 for these analogs. **BDGR 6000** was selected as a new benchmark compound despite **BDGR 6001** having a higher selectivity index in both tachyzoites and bradyzoites, primarily in an effort to reduce lipophilicity (a more extensive comparison of the profiles for both compounds is available in **Table 4-4.6**).

Table 4-4.2 Potency of derivatives with changes to the pyridyl ring

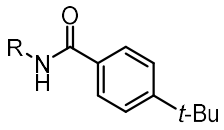

BDGR	R =	Tachyzoite EC_{50} (μM)[a]	Tachyzoite SI[b]	Bradyzoite EC_{50} (μM)[a]	Bradyzoite SI[b]	HFF CC_{50} (μM)[c]
6001	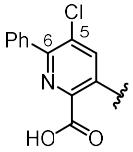	0.56 ± 0.10	86.1	0.41 ± 0.11	117.6	48.2
6005	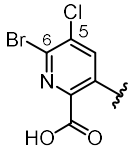	3.85 ± 0.27	> 13.0	4.09 ± 0.33	> 12.2	> 50
6009	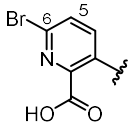	5.14 ± 0.22	> 9.7	3.96 ± 3.22	> 12.6	> 50
6000	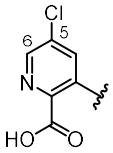	0.24 ± 0.04	10.4	0.35 ± 0.01	7.1	2.5
6013	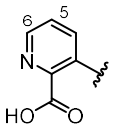	1.11 ± 1.34	8.1	2.16 ± 0.59	4.2	9.0
6016	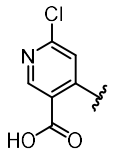	> 10	-	> 10	-	23.6
6014	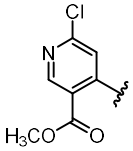	1.69 ± 0.37	> 29.6	> 10	-	> 50

[a]EC_{50}: half-maximal inhibitory concentration; [b]SI: selectivity index = CC_{50}/EC_{50}; [c]HFF: human foreskin fibroblast, CC_{50}: half-maximal toxicity concentration. All values are an average of at least three independent experiments.

Next, we explored the necessity of the acid functional group on the pyridyl ring for the benzamidopicolinic acids (**Table 4-4.3**). Compared to the new benchmark compound **BDGR 6000**, changes to the acid functional group to a non-acidic group were not well tolerated. **BDGR 6010** featured exchange of the carboxylic acid in **BDGR 6000** for a primary amide. The primary amide is isosteric in terms of contributions from a carbonyl functional group but is not acidic under physiological conditions. The amide containing analog **BDGR 6010** was characterized by loss of activity in both parasite forms. **BDGR 6002**, which contained an ester functional group in place of the acid, appeared to be active. However, rapid hydrolysis to the acid was expected under the assay conditions, especially at the elevated pH and temperature used to induce tachyzoite differentiation to bradyzoites. Our interpretation was that acidic functionality at the picolinic position was still required, but the result suggested that forming an ester prodrug that is hydrolyzed to the acid *in vivo* might be tolerated. The acidic carboxylic acid isostere 1*H*-tetrazole enabled **BDGR 6022** to retain some activity against both stages of *T. gondii*, however, an increase in toxicity precluded this compound from further investigation (**Table 4-4.3**).

Table 4-4.3 Potency of benzamidopicolinic acid derivatives with replacement of the acid motif

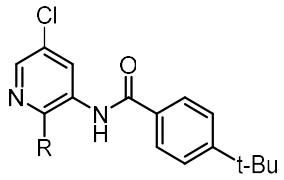

BDGR	R =	Tachyzoite EC_{50} (μM)[a]	Tachyzoite SI[b]	Bradyzoite EC_{50} (μM)[a]	Bradyzoite SI[b]	HFF CC_{50} (μM)[c]
6000		0.24 ± 0.04	10.4	0.35 ± 0.01	7.1	2.5
6002	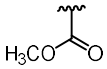	0.43 ± 0.01	> 116.3	0.57 ± 0.09	> 87.7	> 50
6010		> 10[d]	-	> 10	-	> 50
6022		0.80 ± 0.29	1.5	2.45 ± 1.32	0.5	1.2

[a]EC_{50}: half-maximal inhibitory concentration; [b]SI: selectivity index = CC_{50}/EC_{50}; [c]HFF: human foreskin fibroblast, CC_{50}: half-maximal toxicity concentration; [d]Average of two independent experiments, all other values are an average of at least three independent experiments.

With an improved understanding of the structure-activity requirements of the picolinic acid portion of the scaffold, we turned our attention to the benzamide system (**Table 4-4.4**). Substitutions were selected in a further attempt to reduce lipophilicity, in particular through exchange of the *tert*-butyl group for a smaller alkyl group like methyl, as in **BDGR 6008**, or more polar functionality such a methoxy group in **BDGR 6003**, **6007**, and **6011**. Unfortunately, none of the alternate substitution patterns retained the desired level of potency, though reduced toxicity was occasionally observed. As the selectivity indices remained comparable, the *tert*-butyl group of **BDGR 6000** remained the preferred substituent for the benzamide portion of the scaffold, suggesting that hydrophobic interactions with that portion of the molecule are particularly important for activity.

Table 4-4.4 Potency of benzamidopicolinic acids with substitution changes on the benzamide ring

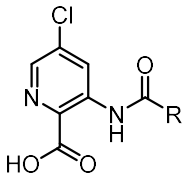

BDGR	R =	Tachyzoite EC_{50} (μM)[a]	Tachyzoite SI[b]	Bradyzoite EC_{50} (μM)[a]	Bradyzoite SI[b]	HFF CC_{50} (μM)[c]
6000	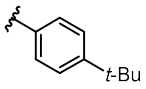	0.24 ± 0.04	10.4	0.35 ± 0.01	7.1	2.5
6004		2.42 ± 0.38	> 20.7	4.47 ± 0.48	> 11.2	> 50
6008	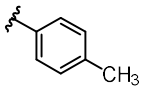	1.48 ± 0.12	12.3	1.10 ± 0.54	16.5	18.2
6003	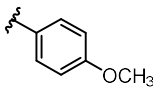	7.10 ± 0.79	> 7.0	2.41 ± 2.07	> 20.7	> 50
6007	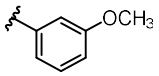	1.82 ± 0.60	> 27.5	6.20 ± 1.86[d]	> 8.1	> 50
6011	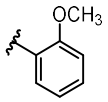	3.50 ± 0.61	> 14.3	4.91 ± 3.32	> 10.2	> 50

[a]EC_{50}: half-maximal inhibitory concentration; [b]SI: selectivity index = CC_{50}/EC_{50}; [c]HFF: human foreskin fibroblast, CC_{50}: half-maximal toxicity concentration; [d]Average of two independent experiments, all other values are an average of at least three independent experiments.

In addition to the potency and selectivity of a compound, other attributes such as solubility, stability, and permeability are vital parameters that determine the likely advancement of a molecule in a drug discovery pipeline. In preparation for potential studies *in vivo*, **BABA 1** and **BDGR 6000-6002** were selected for a comparative assessment of key properties that inform the tractability of pre-clinical development and additional study in *in vivo* models. (**Table 4-4.6**).

These compounds were selected because they had the best potency and selectivity, and we anticipated that significant differences in physicochemical properties would determine selection of a candidate for further advancement. We found that solubility of **BDGR 6000**, the carboxylic acid containing compound without an aryl substitution at the C6-position, was at least 5-fold better than that of the other compounds (33 μM vs. < 6.5 μM). Furthermore, its microsomal and plasma stability were among the best of the set, and it maintained moderate membrane permeability. Taken together, the compound profile for **BDGR 6000** appeared to be the best.

In preparation for potential studies *in vivo*, and to further improve the solubility of **BDGR 6000**, we undertook screening of formulations for the compound. Over 35 formulations were screened and included excipients such as methanol, ethanol, DMSO, Tween80, PEG_{400}, and Captisol at various ratios and concentrations. None was satisfactory, giving visible amounts of precipitate or incomplete dissolution in our hands. During this process, we observed that formulation of **BDGR 6000** as its sodium salt **BDGR 6015** afforded greatly improved solubility and qualitative dissolution behavior. We were pleased to find that it displayed a comparatively improved physicochemical profile to the parent acid **BDGR 6000** while retaining the anti-parasitic activity. The result that **BDGR 6015** demonstrated a 5-fold improvement in aqueous kinetic solubility and a 25% increase in microsomal stability was especially important (**Table 4-4.6**).

Table 4-4.6 Comparison of activity and property profiles for selected compounds

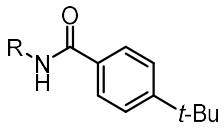

R =	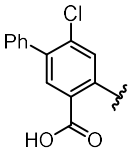	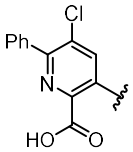	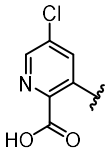	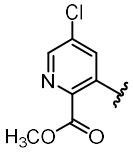	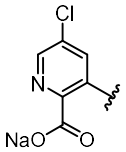
Compound	**BABA 1**	**BDGR 6001**	**BDGR 6000**	**BDGR 6002**	**BDGR 6015**
Tachyzoite EC_{50} (μM)[a]	0.46 ± 0.01	0.56 ± 0.10	0.24 ± 0.04	0.43 ± 0.01	0.32 ± 0.02
Tachyzoite SI[b]	> 108.7	86.1	10.4	>116.3	6.6
Bradyzoite EC_{50} (μM)[a]	0.99 ± 0.09	0.41 ± 0.11	0.35 ± 0.01	0.57 ± 0.09	0.23 ± 0.01
Bradyzoite SI[b]	> 50.5	117.6	7.1	> 87.7	9.1
HFF CC_{50} (μM)[c]	> 50	48.2	2.5	> 50	2.1
$LogD_{7.4}$[d]	5.4	3.9	2.7	5.3	2.6
Solubility (μM)[e]	2.7	6.4	33	< 1.6	164
Microsomal Stability[f]	69.2%	85.1%	75.4%	2.7%	100%
Plasma Stability[g]	100%	97.1%	98.4%	24.7%	88.1%
BBB PAMPA[h]	6.7	5.4	6.9	ND	ND

[a]EC_{50}: half-maximal inhibitory concentration; [b]SI: selectivity index = CC_{50}/EC_{50}; [c]HFF: human foreskin fibroblast, CC_{50}: half-maximal toxicity concentration; [d]Experimentally determined; [e]Kinetic aqueous solubility at pH 7.4; [f]Mouse microsomes, percent parent remaining after 1 h exposure; [g]Mouse plasma, percent parent remaining after 2 h exposure; [h]BBB PAMPA, Pe (10^{-6} cm/s); ND = not determined. All values are an average of three independent experiments.

Given the improved compound profile, **BDGR 6015** was selected for a snapshot pharmacokinetic experiment in mice to assess plasma and brain exposure of the compound (experiment performed by Wuxi Apptech). Male Balb/C mice were administered 15 mg/kg of compound via intraperitoneal (IP) injection as a clear solution. Plasma concentrations were assessed at 30 min and 2 h post administration, and brain exposure was measured at the 2 h timepoint. Terminal mean plasma and brain exposure (AUC_{2h} = 7883 ng/mL and AUC_{2h} = 816 ng/g, respectively) were determined, affording a brain-to-plasma (B/P) ratio of 0.1. These values translate to 22 μM in plasma and 2.3 μM in brain at 2 h post administration without correction for protein binding.

Although these concentrations are higher than the EC_{50} value for **BDGR 6015** against either tachyzoites or bradyzoites, it does not account for the percentage of compound that is bound to protein, which can drastically lower the effective concentration available physiologically. A further concern was that despite the increased solubility obtained by formation of the sodium salt in our hands, the compound required formulation using a cyclodextrin when it was used at a contract research organization for the pharmacokinetic studies. Rates of complexation/de-complexation from the cyclodextrin impact the effective concentration of a compound *in vivo;* therefore, additional work is needed to better understand the tissue exposure of **BDGR 6015**.[74] Furthermore, cyclodextrins do not cross the blood brain barrier, and thus the brain exposure values may be artificially low. While the pharmacokinetic results for sodium salt **BDGR 6015** could be interpreted optimistically – detected plasma concentrations were almost 100-fold that of the EC_{50} and brain exposure was detected despite a non-CNS penetrant formulation – further work is needed to improve solubility and/or refine the formulation, as well as to understand the extent of protein binding for our compound.

To evaluate if **BDGR 6015** could be advanced to an acute or chronic murine model of *T. gondii* infection, several factors were considered. First, frequent IP dosing of mice is challenging over an extended treatment window; therefore, a compound would maximally be dosed twice daily under these conditions. Given the pharmacokinetic snapshot, a twice daily regimen was unlikely to provide the requisite compound exposure to expect success. Second, *T. gondii* infected mice launch a robust immunological response that renders them especially susceptible to inherent toxicities of any compound. *In vivo* candidate compounds must therefore demonstrate a comfortable margin between inhibitory and cytotoxic concentrations, preferably with selectivity indices > 10. Unfortunately, **BDGR 6015** possesses a selectivity index below 10 for both tachyzoites and bradyzoites. Third, sufficient exposure, especially in brain tissue that is known to harbor encysted bradyzoites, is essential for a candidate compound. The snapshot pharmacokinetic study suggested inadequate compound concentrations in the brain, though this conclusion is confounded by formulation using a cyclodextrin. Although **BDGR 6015** demonstrated exposure at a low dose in both plasma and brain, we determined that *in vivo* assessment was premature given these limitations.

Further study in an *in vivo* model of disease remains a future goal towards which additional improvements in the selectivity and bioavailability of these compounds will need to be made. Nonetheless, these dual stage *T. gondii* inhibitors culminating in **BDGR 6015** represent an important advancement in the development of effective therapeutics because they provide a new probe compound with *in vitro* efficacy. We expect that future efforts will further improve the profile of this series, enabling efficacy studies in animal models and mode of action identification.

A biological target of the picolinic acids is currently unknown. While we have yet to test these compounds in a comparable *T. gondii* enzymatic assay, the benzamidobenzoic acids from

which these nitrogenated analogs were derived are inhibitors of the *T. brucei* parasite glycolytic enzyme hexokinase 1 (TbHK1).[4] *T. gondii* possesses a single copy of its hexokinase (*T. gondii* hexokinase, TgHK), which has recently been classified as essential for parasite fitness during infection.[23,75–77] Notably, like *T. brucei* parasites, *T. gondii* bradyzoites are glycolysis-dependent. Metabolic arrest may be a potentially common therapeutic intervention, though this remains to be determined. As will be discussed in **Section 4-5**, the benzamidopicolinic acids appear to act in a non-hexokinase-mediated manner in *T. brucei*. Nonetheless, our ability to design derivatives from a prior glycolytic inhibitor series in one parasite to inhibit another phylogenetically distant, but glycolysis-dependent, pathogen is a successful demonstration of the power of a "parasite hopping" approach for the development of novel anti-parasitic agents.

Section 4-5: Discovery and development of *Trypanosoma brucei* inhibitors based on the picolinic acid scaffold

The parasite *Trypanosoma brucei*, specifically the subspecies *T. b. gambiense* and *T. b. rhodesiense*, is responsible for human African trypanosomiasis (HAT), a potentially fatal disease also known as "human African sleeping sickness".[4,6,7,78] The parasite is transmitted by the bite of the tsetse fly during a blood meal, and infection progresses from an initial hemolymphatic stage to parasite invasion of the CNS, which marks the neurological stage in late disease.[78] Infection is almost invariably fatal if left untreated.[4,78] Although treatments exist for *T. brucei* infection, they are limited by adverse side effects (pentamidine, suramin), toxicity to patient subgroups (melarsoprol), specificity to parasite subspecies or disease stage (pentamidine, suramin, eflornithine), cumbersome administration routes (pentamidine, suramin, eflornithine, nifurtimox), and/or emerging pathogen resistance (melarsoprol) (**Figure 4-5.1**).[79] As such, new therapeutic options for *T. brucei* infection are urgently needed.

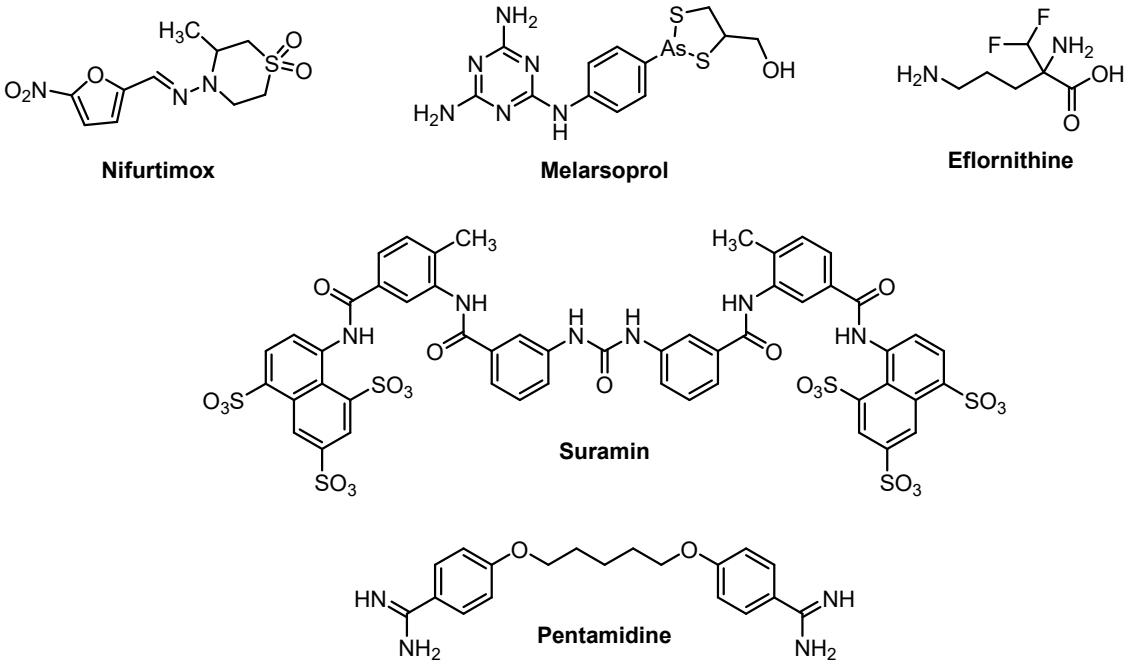

Figure 4-5.1 Current treatments for *T. brucei* infection.[79]

As reviewed previously in this chapter, our group recently developed benzamidobenzoic acids (**BABA** compound series) as anti-trypanosomal agents that act by inhibiting the parasite hexokinase (TbHK1).[4,6,7] We later discovered that compounds in this series had activity against multiple parasites (see **Section 4-1** and **Section 4-2**). Follow-on medicinal chemistry optimization led to a benzamidopicolinic acid series (via a methine-to-nitrogen atom switch) in a bid to improve physicochemical properties, especially lipophilicity and aqueous solubility (see **Section 4-3**). Anti-*T. gondii* activity was identified in the benzamidobenzoic and benzamidopicolinic acids, enabling development of a probe compound, sodium salt **BDGR 6015**, that displayed inhibition of both tachyzoite and bradyzoites in tissue culture and had improved solubility and microsomal stability over its benzamidobenzoic acid progenitors (see **Section 4-4**). In parallel to those efforts, we sought to leverage the benzamidopicolinic acid scaffold to identify anti-trypanosomal agents with superior physicochemical and ADME profiles for further medicinal chemistry development.

To this end, a collection of 16 benzamidopicolinic and 3 benzamidonicotinic acid derivatives were screened against TbHK1 and whole *T. brucei* bloodstream form (BSF) parasites at a concentration of 10 μM (**Table 4-5.1**). For the enzymatic assay, compounds were incubated with recombinant TbHK1 before measuring TbHK1 activity using a secondary reporter assay.[4] A counter-assay without TbHK1 was used to correct for any background inhibition by our compounds on the reporter itself.[4] Whole parasite inhibition was measured by exposing bloodstream form (BSF) *T. brucei* parasites to compound for 72 h at 37°C, then measuring cell viability via a fluorescent reporter. Compounds with > 50% inhibition at 10 μM were advanced to assay in dose response format to determine an EC_{50} and counter screened for cytotoxicity against human foreskin fibroblasts (HFF). This revealed anti-trypanosomal activity in the low micromolar range for the picolinic acid series. Furthermore, all tested picolinic acid analogs had TbHK1 IC_{50} values greater than 10 μM, indicating that the mode of action for whole parasite growth inhibition was unlikely to be TbHK1 mediated.

We observed that structure activity relationships for the series in *T. brucei* were divergent from the trends in *T. gondii*, signaling potential for further parasite-specific refinement on this scaffold against an unknown target. For instance, substitution on the pyridyl ring was more broadly tolerated in *T. brucei*, with a C6-Br substituent contributing to improved selectivity for **BDGR 6005** and **BDGR 6009** compared to the corresponding analogs **BDGR 6000** and **BDGR 6013**, which lacked the bromine atom. The benzamidonicotinic acid derivatives were inactive with the notable exception of **BDGR 6014**, which demonstrated an improved selectivity index despite reduced potency against *T. brucei* and an ester in place of the acid functional group. The corresponding acid **BDGR 6016** was inactive, suggesting other structural changes might accommodate loss of an acidic group and that the acid alone was insufficient for activity.

Table 4-5.1 Potency of benzamidopicolinic acids with substitution changes on the pyridyl ring

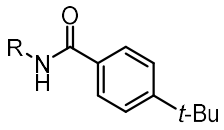

BDGR	R =	BSF *T. brucei* LD_{50} (μM)[a]	BSF *T. brucei* SI[b]	HFF CC_{50} (μM)[c]
6001	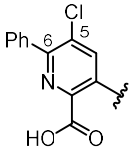	9.13 ± 1.35	5.3	48.2
6005	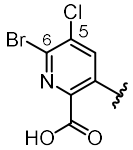	3.15 ± 1.29	> 15.9	> 50
6009	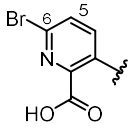	2.61 ± 0.37	> 19.2	> 50
6000	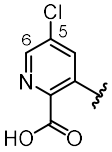	2.08 ± 0.31	1.2	2.5
6013	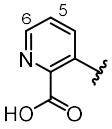	3.42 ± 0.38	2.6	9.0
6016	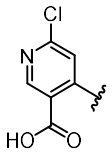	> 10	-	23.6
6014	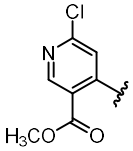	8.11 ± 1.17	> 6.2	> 50
6026	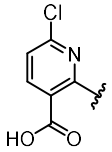	> 10	-	> 50

[a]BSF: bloodstream form, LD_{50}: half-maximal lethal concentration; [b]SI: selectivity index = CC_{50}/LD_{50}; [c]HFF: human foreskin fibroblast, CC_{50}: half-maximal toxicity concentration. All values are an average of at least three independent experiments.

Toxicity to the host cells (HFFs) was too high, and selectivity indices therefore too low, to draw meaningful conclusions regarding the structure-activity requirements at the C2 position of the pyridyl ring, where the acid functional group is attached in **BDGR 6000** (**Table 4-5.2**). No activity was detected for analogs without an acidic functional group, such as ester **BDGR 6002** or amide **BDGR 6010**.

Table 4-5.2 Potency of benzamidopicolinic acid derivatives with replacement of the acid motif

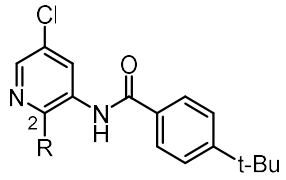

BDGR	R =	BSF *T. brucei* LD_{50} (µM)[a]	BSF *T. brucei* SI[b]	HFF CC_{50} (µM)[c]
6000		2.08 ± 0.31	1.2	2.5
6025		9.91 ± 0.76	1.6	15.4
6002	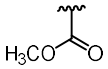	> 10	-	> 50
6010		> 10	-	> 50
6022		5.39 ± 1.45	0.39	1.2
6015		1.89 ± 0.37	1.1	2.1
6042		> 10	-	> 50

[a]BSF: bloodstream form, LD_{50}: half-maximal lethal concentration; [b]SI: selectivity index = CC_{50}/LD_{50}; [c]HFF: human foreskin fibroblast, CC_{50}: half-maximal toxicity concentration. All values are an average of at least three independent experiments.

Attempts to exchange the 4-*tert*-butyl group on the benzamide ring were detrimental to potency against BSF *T. brucei* parasites, with no activity detected for the other substitution patterns

surveyed. However, toleration for the isosteric aromatic system thiophenyl in place of the benzene ring was observed via **BDGR 6033**, which by virtue of reduced toxicity improved the selectivity profile by approximately 10-fold (**Table 4-5.3**).

Table 4-5.3 Potency of picolinic acid derivatives with changes to the benzamide ring

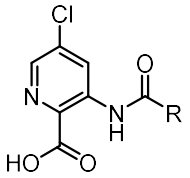

BDGR	R =	BSF *T. brucei* LD_{50} (μM)[a]	BSF *T. brucei* SI[b]	HFF CC_{50} (μM)[c]
6000	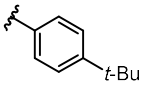	2.08 ± 0.31	1.2	2.5
6004		> 10	-	> 50
6008	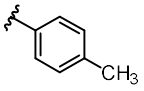	> 5[d]	-	18.2
6003	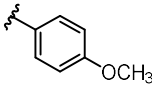	> 10	-	> 50
6007	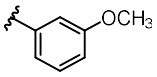	> 10	-	> 50
6011	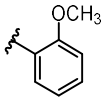	> 10	-	> 50
6033	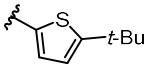	3.77 ± 0.33	13.3	> 50

[a]BSF: bloodstream form, LD_{50}: half-maximal lethal concentration; [b]SI: selectivity index = CC_{50}/LD_{50}; [c]HFF: human foreskin fibroblast, CC_{50}: half-maximal toxicity concentration; [d]This value requires additional testing to resolve but initial assessments indicated an IC_{50} > 5 μM. All values are an average of at least three independent experiments.

Taken together, the data indicated further investigation was warranted to better understand the new structure-activity requirements at play with the ultimate goals of improving the selectivity and physicochemical profile of this chemical series in *T. brucei*. To this end, four new picolinic acid derivatives were prepared to explore the effect of alterations to the linker region between the two aryl systems. This proved fruitful, as a variety of linkers corresponding to different lengths and chemical functionality were tolerated (**Table 4-5.5**).

Table 4-5.5 Potency of picolinic acid derivatives with various linker functional groups

BDGR	Structure	BSF *T. brucei* LD_{50} (µM)[a]	BSF *T. brucei* SI[b]	HFF CC_{50} (µM)[c]
6000	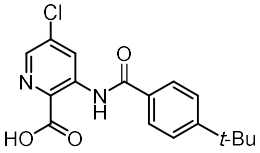	2.08 ± 0.31	1.2	2.5
6035	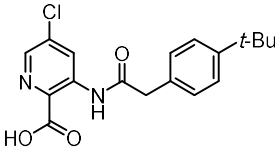	7.14[d]	> 7.0	> 50
6049	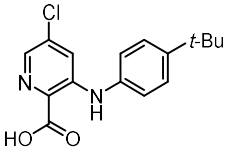	0.59[d]	26.6	15.7
6023	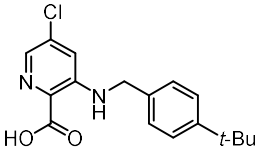	0.43 ± 0.10	53.9	22.9
6047	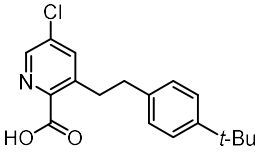	TBD	TBD	> 50

[a]BSF: bloodstream form, LD_{50}: half-maximal lethal concentration; [b]SI: selectivity index = CC_{50}/LD_{50}; [c]HFF: human foreskin fibroblast, CC_{50}: half-maximal toxicity concentration; TBD: to be determined; [d]Due to a technical problem with the assay during initial data collection, additional testing is required to resolve a standard deviation for the LD_{50} value. All values are an average of at least three independent experiments.

Extending the amide group by one methylene unit from the 4-*tert*-butylphenyl ring in **BDGR 6035** gave 3-fold reduced potency but > 6-fold greater selectivity compared to the previous leading compound **BDGR 6015** (sodium salt). Alternatively, excision of the carbonyl (i.e., shortening the linker to consist of only a single nitrogen atom) afforded **BDGR 6049** and resulted in a > 3-fold increase in potency. The greatest improvement was obtained with **BDGR 6023**, which featured reduction of the benzamide functionality to a simple benzylamine. This resulted in a simultaneous increase in potency (BSF LD_{50} = 0.43 μM) and reduction in toxicity (HFF CC_{50} = 22.9 μM) such that the selectivity index improved over 20-fold compared to **BDGR 6015**.

Several analogs were also made featuring multiple scaffold modifications in tandem. This is done routinely in medicinal chemistry programs for more expedient syntheses or to capitalize on a structurally similar intermediate (and/or serendipitous byproduct) being generated in the course of accessing other analogs, and can provide SAR information in multiple dimensions more quickly. For example, the derivatives **BDGR 6040**, **6041**, **6050** and **6052** were generated to further probe the effect of linker chemistry, especially in the absence of an acidic functional group on the pyridyl ring (**Table 4-5.6**). Excitingly, **BDGR 6040** and **6052** featuring an *N*-hydroxyamide linker were extremely potent (*T. brucei* LD_{50} = 0.57 μM and < 0.16 μM, respectively) despite featuring the non-acidic ester functionality on the pyridyl ring system, and in the case of **BDGR 6042** absent the 4-*tert*-butyl group that was required in the amide linker-containing series (see **Table 4-5.3**). The *N*-hydroxyamides were also non-toxic (HFF CC_{50} > 50 μM), leading to the best selectivity indices (SI = 87.9 and 312.5, for **BDGR 6040** and **6052**, respectively) observed up to this point.

N-hydroxyamides are much more acidic than their *N*-H amide counterparts (calculated pKa = 7.5 for *N*-hydroxyamide **BDGR 6040** vs calculated pKa = 15.5 for the corresponding *N*-H amide analog **BDGR 6002** at 25°C), which we hypothesized might compensate for the lack of an

ionizable group in that region of the molecule due to the linker's close proximity.[80] Increased linker acidity contributing to potency would explain the observation that **BDGR 6042** (without the 4-*tert*-butyl group, whose linker is expected to be more acidic) is more potent than **BDGR 6040**. This was significant because it suggested that removal or replacement of the aryl carboxylic acid, which tends to improve membrane permeability and CNS tissue exposure by reducing compound polarity, might be tolerated with appropriate changes in the linker to make up for the missing functionality. Two examples of "scaffold hop" compounds, wherein a structural alteration yields a new class of compounds distinct from the parent molecule, were also explored but did not display activity against *T. brucei*: **BDGR 6053** is an example of the pyrido[3,2-*d*]pyrimidine-2,4-diones, a well-known privileged scaffold, while **BDGR 6055** is the first example, to our knowledge, of a benzo[4,5]oxazolo[3,2-*a*]pyrido[3,2-*d*]pyrimidin-12-one heterocyclic ring system (**Table 4-5.6**).

Table 4-5.6 Potency of derivatives with multiple simultaneous modifications to structure

BDGR	Structure	BSF *T. brucei* LD_{50} (µM)[a]	BSF *T. brucei* SI[b]	HFF CC_{50} (µM)[c]
6034	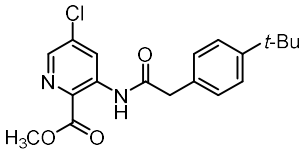	> 10	-	> 50
6032	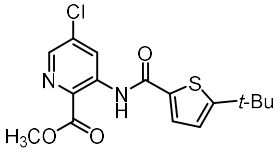	6.4 ± 2.8	26.6	> 50
6040	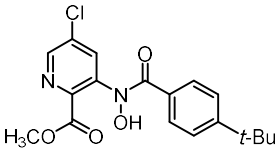	0.57 ± 0.03	87.9	> 50
6041	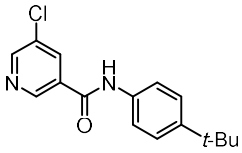	> 10	-	> 50
6050	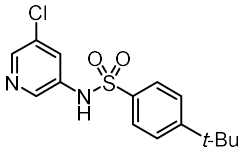	TBD	TBD	15.4
6052	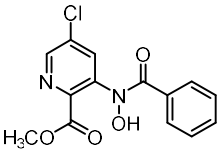	< 0.16	> 312.5	> 50
6053	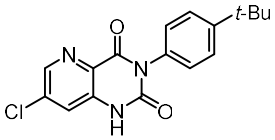	> 10	-	> 50
6055	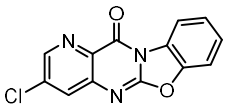	TBD	TBD	> 50

[a]BSF: bloodstream form, LD_{50}: half-maximal lethal concentration; [b]SI: selectivity index = CC_{50}/LD_{50}; [c]HFF: human foreskin fibroblast, CC_{50}: half-maximal toxicity concentration; TBD: to be determined. All values are an average of at least three independent experiments.

We determined that the most promising direction for further investigation lay in new linker chemistries, especially with a goal to obviate the requirement for a carboxylic acid functional group on the pyridyl ring and/or the highly lipophilic 4-*tert*-butyl group of the benzamide system. Removing the carboxylic acid group was expected to improve membrane permeability and subsequent CNS exposure, while precluding an aryl 4-*tert*-butyl group would enable further reduction in lipophilicity while avoiding a potential metabolic liability.[80,81] Evaluation of the best compounds solely on the basis of potency and selectivity suggested scaffolds with an *N*-hydroxyamide linker (exemplified by **BDGR 6040** and **6052**) or an *N*-H benzylamine linker (**BDGR 6023**) should be explored further, however, consideration of other important properties in pre-clinical development such as solubility, microsomal stability, plasma stability, and plasma protein binding revealed otherwise.

The *N*-hydroxyamide linker-containing compound **BDGR 6040** was poorly stable in microsomes (10.3% remaining after 1 hour), as was the sulfonamide-linker compounds **BDGR 6050** (0% remaining after 1 hour). Both **BDGR 6040** and **BDGR 6050** also suffered from poor solubility (< 1.6 μM in aqueous buffer at pH 7.4). The benzylamine-linked compound **BDGR 6023** was more soluble (83.9 μM), slightly more stable in microsomes (37.3% remaining after 1 hour) and had good plasma stability (92.5% remaining after 2 hours). This meant that in addition to superior potency and selectivity against *T. brucei*, **BDGR 6023** had greater than 2.5-fold improved solubility compared to the benzamidopicolinic acid parent compound **BDGR 6000**, and comparable plasma stability. We reasoned that if the microsomal stability of **BDGR 6023** could be improved by further scaffold optimization, a substantially better compound might be obtained (**Table 4-5.7**).

Table 4-5.7 Comparison of physicochemical and ADME properties for compounds with different linker chemistry

BDGR	Structure	Solubility (μM)[a]	Microsomal Stability[b]	Plasma Stability[c]	Plasma Protein Binding[d]
6000	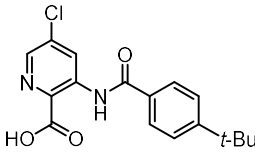	33	75.4%	98.4%	ND
6023	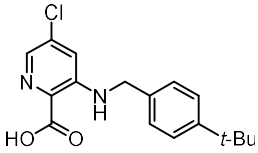	83.9	37.3%	92.5%	99.1%
6040	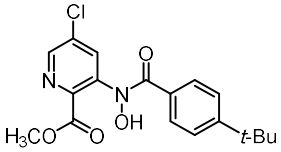	< 1.6	10.3%	ND	ND
6050	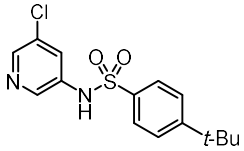	< 1.6	0%	ND	ND
6055	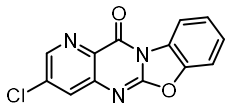	8.3	7.2%	100%	ND

[a]Kinetic aqueous solubility at pH 7.4; [b]Mouse microsomes, percent parent remaining after 1 h exposure; [c]Mouse plasma, percent parent remaining after 2 h exposure; [d]Mouse plasma, percent bound after 4 h; ND: not determined. All values are an average of at least three independent experiments.

The novel heterocyclic system represented by **BDGR 6055** was also evaluated in terms of these physicochemical and ADME parameters to better understand its potential as a secondary scaffold series. Given its poor microsomal stability and comparatively low solubility, in combination with incomplete information regarding its anti-parasitic activity, it was not explored further.

Based on these data, a benzylamine-linked series of analogs based on the **BDGR 6023** template was chosen for further investigation. To enable efficient analog generation in the

benzylamine linker series, the synthetic route to these compounds required significant retooling. In the initial discovery route, **BDGR 6023** was generated in an analogous way as described in **Section 4-4** for the benzamidopicolinic acids, namely by use of the 3-amino-5-chloro methyl picolinate building block **4-5.1** as a nucleophile. This synthetic approach was adequate for generating benzamide-linked compounds such as **BDGR 6000** because the exceptionally reactive acyl chloride building blocks (e.g., **4-5.2**) compensated for the poor nucleophilicity of **4-5.1**, but gave mediocre yields with less electrophilic building blocks like the 4-*tert*-butyl benzyl bromide **4-5.3** used to make **BDGR 6023**. To overcome this challenge, we adopted a Buchwald-Hartwig amination paradigm for the syntheses, wherein the pyridyl building block **4-5.4** could act as the electrophile and an amine (e.g., **4-5.5**) could act as the nucleophile. This better aligned the innate electronic nature of each starting material with the reactivity we desired from it, and enabled synthesis from commercially available 3-bromo-5-chloro picolinic acid in the same number of steps. Importantly, analogs such as **BDGR 6057**, which were inaccessible via other chemistry, could be generated with good overall efficiency (**Scheme 4-5.1**).

Scheme 4-5.1 Adjusted synthetic approach for synthesis of benzylamine-based analogs

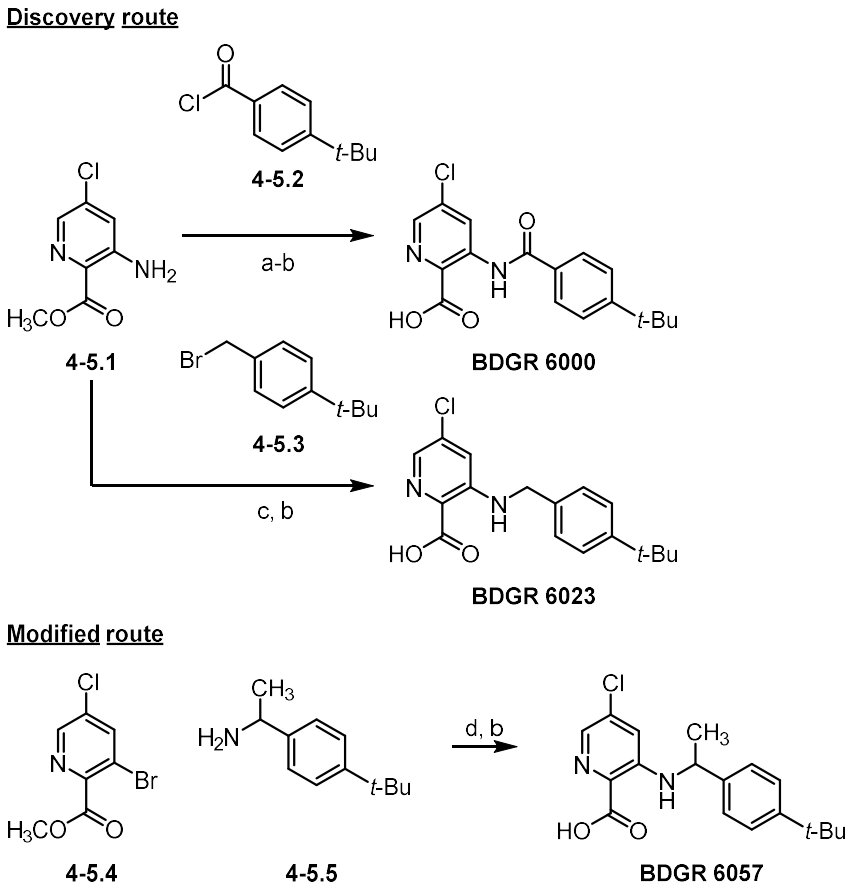

Reagents and conditions: (a) CH_3CN, 150°C, 1 h, 51%; (b) 1.3 M aq. LiOH, 3:2 THF/H_2O, rt, 18 h, 71-92%; (c) *i*Pr_2EtN, CH_3CN, 85°C, 48 h, 36%; (d) $Pd_2(dba)_3$, Xantphos, Cs_2CO_3, $PhCH_3$, 85°C, 18 h, 79%.

Initially, scale up of this route beyond 1.5 mmol (250 mg) scale proved problematic due to the formation of a small amount of an unknown impurity (**A**, ~ 3% by mass) in batches of **4-5.4** that heavily attenuated the subsequent Buchwald-Hartwig coupling reactions (**Figure 4-5.3**). We found that trituration of the contaminated batch of **4-5.4** obtained via TMS-diazomethane esterification at 10 mmol (2.3 g) scale with toluene as an anti-solvent, followed by filtration sequentially through 0.45 µm and 0.1 µm filters, gave a batch of material (**B**) that could be converted smoothly via Buchwald-Hartwig coupling in good yield across a range of amine

substrates. Ultimately, an uncontaminated batch of material (**C**) could be obtained by using a Fischer reaction for esterification exceeding 1.5 mmol (250 mg) scale.

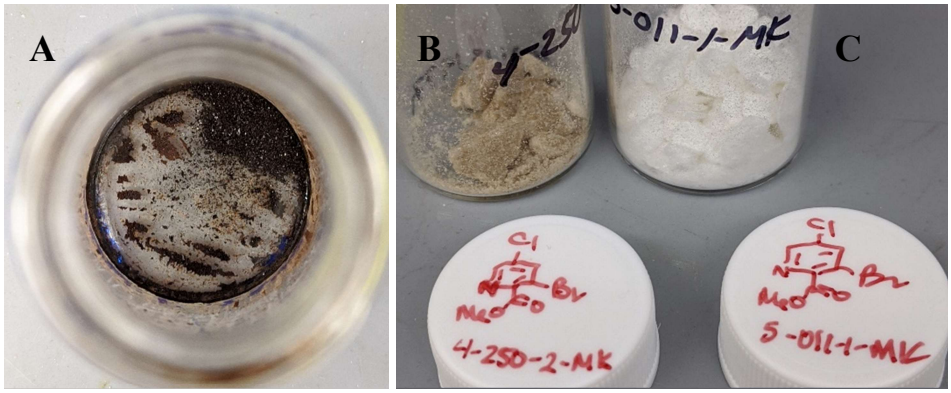

Figure 4-5.3 (**A**) Unidentified impurity in batches of **4-5.4** formed by TMS-diazomethane esterification at 10 mmol (2.3 g) scale (**B**) Batch of **4-5.4** after toluene trituration and filtration (**C**) Batch of **4-5.4** formed by Fischer esterification at 10 mmol (2.3 g) scale.

With the synthetic route to our desired scaffold greatly enabled, we set out to probe the structure-activity requirements of the benzylamine-linked template. We sought to improve on **BDGR 6023**, especially by increasing microsomal stability. Reduction in plasma protein binding and/or further improving the selectivity index towards *T. brucei* would also be valuable outcomes in the structural optimization of this series. To this end, 5 benzylamine-linked picolinic acids were generated to explore modifications to the pyridyl ring system. Of the changes explored, only removal of the C5-Cl substituent in **BDGR 6045** was tolerated, and even this was accompanied by a deterioration in selectivity by virtue of increased toxicity towards human foreskin fibroblasts (HFFs) (**Table 4-5.8**).

Table 4-5.8 Potency of benzylamine-linked analogs with changes to the pyridyl ring

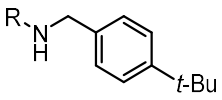

BDGR	Structure	BSF *T. brucei* LD_{50} (μM)[a]	BSF *T. brucei* SI[b]	HFF CC_{50} (μM)[c]
6023	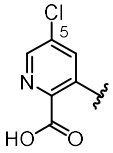	0.43 ± 0.1	53.9	22.9
6038	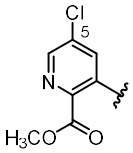	TBD	TBD	28.5
6039	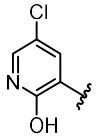	> 10	-	> 50
6043	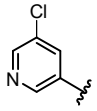	> 10	-	37.1
6045	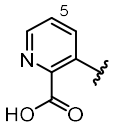	0.56 ± 0.16	13.0	7.28
6051	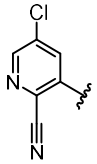	> 10	-	> 50

[a]BSF: bloodstream form, LD_{50}: half-maximal lethal concentration; [b]SI: selectivity index = CC_{50}/LD_{50}; [c]HFF: human foreskin fibroblast, CC_{50}: half-maximal toxicity concentration; TBD: to be determined. All values are an average of at least three independent experiments.

A variety of amines were used to generate eight analogs that featured alterations to the 4-*tert*-butylbenzyl group and installation of functional groups at the benzylic position that were expected to block oxidation, a common metabolic pathway that might account for microsomal

instability. Unfortunately, due to the covid-19 pandemic, screening is not completed and the anti-parasitic activity for these compounds remains to be determined. The two examples for which data was obtained (**BDGR 6044** and **BDGR 6054**) were inferior to the parent compound **BDGR 6023** (**Table 4-5.9**).

Table 4-5.9 Potency and physicochemical/ADME properties of analogs with changes to the benzylamine system

Structure	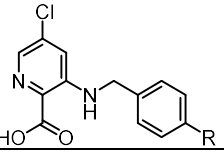						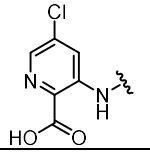		
R =	*t*-Bu	CH_3	H	OCH_3	F	CF_3	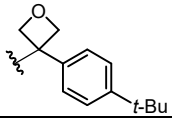	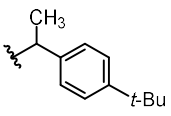	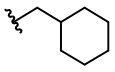
BDGR	**6000**	**6044**	**6048**	**6058**	**6059**	**6060**	**6056**	**6057**	**6054**
BSF *T. brucei* LD_{50} (µM)[a]	0.43	> 10	TBD	TBD	TBD	TBD	TBD	TBD	2.1
BSF *T. brucei* SI[b]	53.9	TBD	TBD	TBD	TBD	TBD	TBD	TBD	23.8
HFF CC_{50} (µM)[c]	22.9	TBD	> 50	25	20	12.5	19.5	9.47	> 50
Solubility[d] (µM)	83.9	ND	ND	178	164	174	140	121	ND
Microsomal Stability (%)[e]	37.3	ND	ND	73.3	69.1	81.0	37.2	76.0	ND
Plasma Stability (%)[f]	92.5	ND	ND	82.9	81.2	67.2	78.1	83.5	ND
Plasma Protein Binding (%)[g]	99.1	ND	ND	98.4	98.9	Inc.	99.0	Inc.	ND

[a]BSF: bloodstream form, LD_{50}: half-maximal lethal concentration; [b]SI: selectivity index = CC_{50}/LD_{50}; [c]HFF: human foreskin fibroblast, CC_{50}: half-maximal toxicity concentration; [d]Kinetic aqueous solubility at pH 7.4; [e]Mouse microsomes, percent parent remaining after 1 h exposure; [f]Mouse plasma, percent parent remaining after 2 h exposure; [g]Mouse plasma, percent bound after 4 h; ND: not determined; TBD: to be determined; Inc: data inconclusive, may indicate 100% bound. All values are an average of at least three independent experiments.

Nonetheless, **BDGR 6056-6060** were concurrently assessed for physicochemical and ADME properties, which was successfully completed. This showed that improved solubility and stability could be achieved by alteration of the aryl substituent (**BDGR 6058-6060**), and/or blocking of the benzylic position with a methyl group (**BDGR 6057**). Plasma stability was slightly reduced for all the new analogs, and plasma protein binding was largely unchanged.

Although additional work remains to determine the anti-*T. brucei* activity of some of the latest benzylamino-linked picolinic acid analogs, important physicochemical and ADME improvements in this series of compounds has been demonstrated. The newest benzylaminopicolinic acids with changes to the 4-*tert*-butyl group and/or blocking groups at the benzylic position feature improved potency, selectivity, solubility, and stability over preceding compounds derived from the **BABA** template. They also appear to act in a non-TbHK1 mediated manner, suggesting a novel mode of action to be elucidated in the future. Nonetheless, this work in developing *T. brucei* inhibitors with improved physicochemical and ADME profiles further demonstrates the utility of the **BABA** scaffold as a starting point for development of new anti-infective agents.

Section 4-6: Discovery and development of *Leishmania donovani* inhibitors based on the picolinic acid scaffold

T. brucei shares a phylogenetic family with several other parasites that cause important neglected diseases in humans. The *Leishmania* species *L. major* causes cutaneous leishmaniasis and *L. donovani* causes visceral leishmaniasis (also known as "*kala-azar*"), which is potentially fatal without treatment.[82] The parasite is transmitted via the bite of female sandflies, and is estimated to cause up to 2 million infections with 70,000 deaths each year.[83] Leishmaniasis diseases have a number of treatments in use today, but they suffer from significant toxicity/side effects (pentavalent antimony compounds, amphotericin B, pentamidine, paromomycin), variable parasite sensitivity (pentavalent antimony compounds, pentamidine, paromomycin), barriers to administration/patient compliance (non-liposomal amphotericin B, pentamidine), contraindication in pregnant patients (meltifosine), and developing parasite resistance (pentavalent antimony compounds, meltifosine) (**Figure 4-5.2**).[82–84] Better therapeutics against *Leishmania* parasites therefore remain an important unmet medical need.

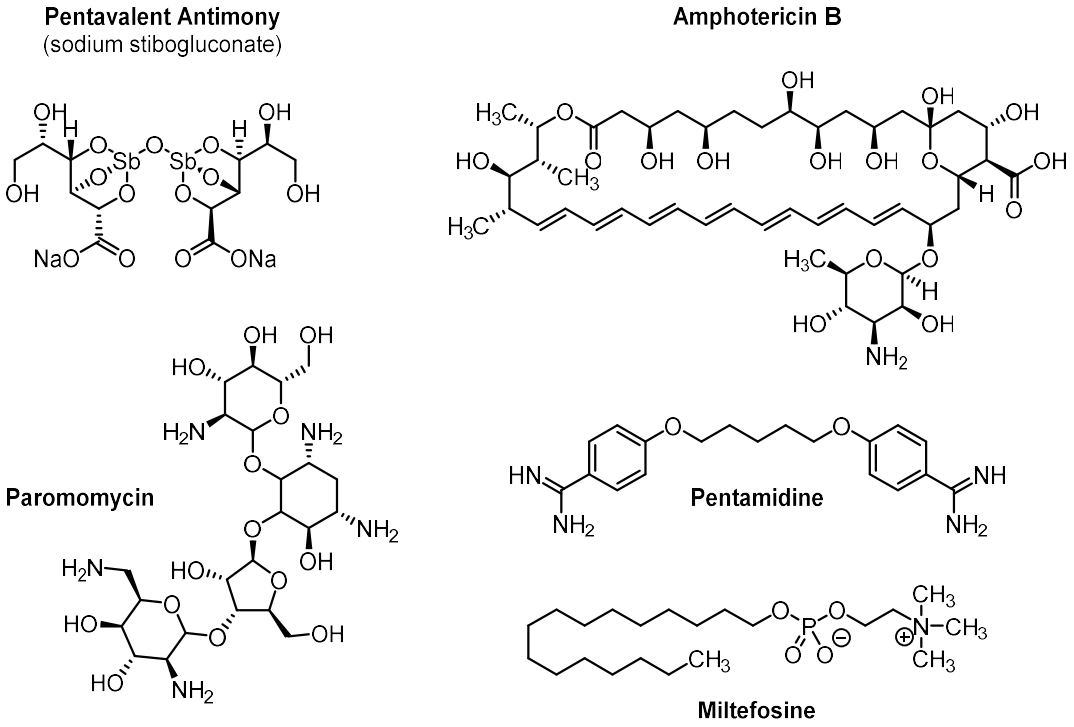

Figure 4-5.2 Current treatments for *L. donovani* infection.[82–84]

As reviewed previously in this chapter, our group recently developed benzamidobenzoic acids (**BABA** compound series) as anti-trypanosomal agents that act by inhibiting the parasite hexokinase (TbHK1).[4,6,7] We later discovered that compounds in this series had activity against multiple parasites, which provided an opportunity to adopt a parasite hopping approach to discovery of novel anti-parasitics (see **Section 4-1** and **Section 4-2**). Follow-on medicinal chemistry optimization led to a benzamidopicolinic acid series (via a carbon-to-nitrogen atom switch) in a bid to improve the compounds' physicochemical properties, especially lipophilicity and aqueous solubility (see **Section 4-3**). Better compound profiles for pre-clinical development were achieved in this new series, albeit in the context of anti-*T. gondii*, rather than anti-*T. brucei*, activity (see **Section 4-4**). Building on the improvements in profile achieved against *T. gondii*, we repurposed the benzamidopicolinic acid series to identify non-TbHK1 dependent inhibitors of *T.*

brucei. This led to development of benzylamine-linked derivatives that featured divergent structure activity relationships and improved physicochemical and ADME properties compared to previous compound series (see **Section 4-5**). Concurrently to those efforts in *T. brucei*, we explored repurposing the benzamidopicolinic acid series from our *T. gondii* work, as well as selected examples from the benzylamine-linked analogs derived in our *T. brucei* campaign, to identify potential anti-leishmanial agents for further medicinal chemistry development; the results of that work are described in this section.

Due to the lower-throughput nature of the *L. donovani* assays compared to *T. brucei* assays, significant curation of the compound set must be exercised. A subset of 20 picolinic and nicotinic acid derivatives from those described in **Section 4-4** were screened against *L. donovani* axenic amastigotes, the intracellular stage of the parasite, as well as against the host macrophage cells (J774) to gauge mammalian cellular toxicity in a relevant cell line. To determine anti-parasitic activity, host macrophage cells were infected overnight with *L. donovani* parasites, then exposed to compound for 72 h at 37°C before the percentage of infected cells was determined microscopically and compared to a vehicle-only control.[85] A similar process using uninfected cells was used to measure compound toxicity.[85] Macrophages are more sensitive to compound toxicity than human foreskin fibroblasts (HFFs), and are the target of amastigote invasion, so although HFF toxicity was also assessed for these compounds (see **Section 4-4** or **Section 4-5**), only the J774 data is presented here.

The prototypical benzamidopicolinic acid **BDGR 6000** was potent against axenic amastigotes with a selectivity index of about 10. Changes to the pyridyl ring did not improve this: introduction of a bromine substituent in **BDGR 6005** reduced potency by 45-fold, although removal of the chlorine substituent was allowed, with no significant change to potency or

selectivity in **BDGR 6013** by comparison. The benzamidonicotinic acids **BDGR 6016** and **6026** were not active against *L. donovani* axenic amastigotes (**Table 4-6.1**).

Table 4-6.1 Potency of derivatives with changes to the pyridyl ring

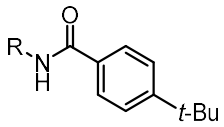

BDGR	R =	Amastigote EC_{50} (μM)[a]	SI[b]	Macrophage CC_{50} (μM)[c]
6000	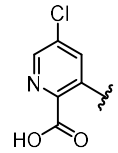	0.18 ± 0.05	10.4	1.88 ± 0.10
6005	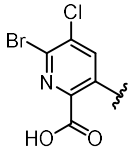	8.12 ± 1.70	> 3.1	> 25
6009	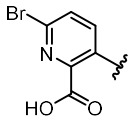	> 12.5	-	> 25
6013	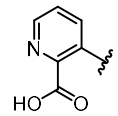	0.21 ± 0.04	12.7	2.59 ± 0.43
6016	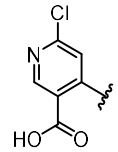	> 12.5	-	ND
6026	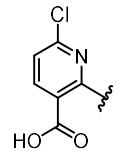	> 12.5	-	ND

[a]EC_{50}: half-maximal inhibitory concentration; [b]SI: [c]CC_{50}: half-maximal toxicity concentration; SI: selectivity index = CC_{50}/EC_{50}; ND: not determined. All values are average of at least three independent experiments.

Changes to the acidic functional group were also investigated. This revealed that an acidic group was required at this position for activity in *L. donovani*: non-acidic analogs **BDGR 6010**, **6025**, and **6042** were all inactive, and the ester compound **BDGR 6002** was more toxic against the host cells than it was active against the parasite. Notably, that the tetrazole isostere in **BDGR 6022** did not significantly degrade selectivity as was observed in the *T. gondii* or *T. brucei* campaigns (**Table 4-6.2**).

Table 4-6.2 Potency of benzamidopicolinic acid derivatives with replacement of the acid motif

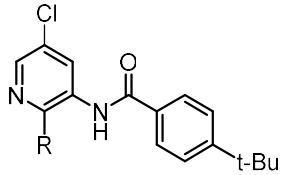

BDGR	R =	Amastigote EC_{50} (μM)[a]	SI[b]	Macrophage CC_{50} (μM)[c]
6000		0.18 ± 0.05	10.4	1.88 ± 0.10
6025		> 12.5	-	ND
6002	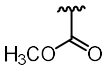	8.51 ± 0.05	0.4	2.86 ± 0.27
6010		> 12.5	-	ND
6022		0.80 ± 0.07	11.4	9.10 ± 1.13
6015		0.20 ± 0.03	12.9	2.58 ± 1.20
6042		> 12.5	-	ND

[a]EC_{50}: half-maximal inhibitory concentration; [b]SI: [c]CC_{50}: half-maximal toxicity concentration; SI: selectivity index = CC_{50}/EC_{50}; ND: not determined. All values are average of at least three independent experiments.

Alteration to the benzamide portion of the molecule were much more broadly tolerated in *L. donovani* than in *T. brucei*. Although no significant breakthroughs in terms of potency or selectivity were realized in this series of compounds, this divergent SAR and wide tolerance was encouraging in terms of the prospects for future work on this scaffold in the context of *L. donovani* (**Table 4-6.3**).

Table 4-6.3 Potency of benzamidopicolinic acids with changes to the benzamide ring

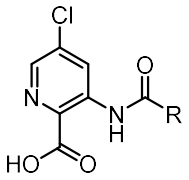

BDGR	R =	Amastigote EC_{50} (μM)[a]	SI[b]	Macrophage CC_{50} (μM)[c]
6000	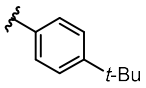	0.18 ± 0.05	10.4	1.88 ± 0.10
6004		2.02 ± 0.17	6.4	12.89 ± 3.63
6008	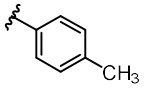	0.54 ± 0.09	9.7	5.26 ± 1.61
6003	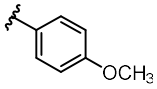	1.14 ± 0.12	10.2	11.59 ± 0.81
6007	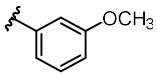	1.41 ± 0.34	11.9	16.63 ± 5.27
6011	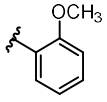	3.05 ± 0.61	5.7	17.34 ± 1.43
6033	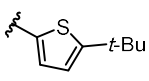	0.22 ± 0.02	7.2	1.62 ± 0.36

[a]EC_{50}: half-maximal inhibitory concentration; [b]SI: [c]CC_{50}: half-maximal toxicity concentration; SI: selectivity index = CC_{50}/EC_{50}. All values are average of at least three independent experiments.

Investigation of the linker chemistries revealed that benzylamine-linked **BDGR 6023** was a better compound than its benzamido precursor **BDGR 6000** in *L. donovani*, in a similar manner as was found in *T. brucei*. Macrophage toxicity was reduced by 10-fold in **BDGR 6023** without substantially altering the potency against amastigotes, resulting in a 3-fold selectivity improvement (**Table 4-6.4**).

Table 4-6.4 Potency of picolinic acid derivatives with various linker functional groups

BDGR	Structure	Amastigote EC_{50} (μM)[a]	SI[b]	Macrophage CC_{50} (μM)[c]
6000	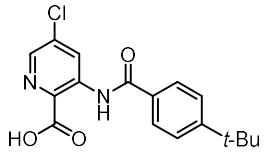	0.18 ± 0.05	10.4	1.88 ± 0.10
6023	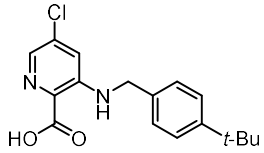	0.31 ± 0.06	33.4	10.48 ± 6.59
6035	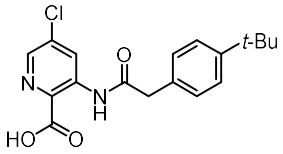	3.31 ± 0.10	2.5	8.42 ± 2.03

[a]EC_{50}: half-maximal inhibitory concentration; [b]SI: [c]CC_{50}: half-maximal toxicity concentration; SI: selectivity index = CC_{50}/EC_{50}. All values are average of at least three independent experiments.

Work in this project is ongoing, as advancements in the benzylamine series in the context of *T. brucei* have indicated further optimization on the scaffold is possible and we have already observed divergent SAR between the *T. brucei* and *L. donovani*. Important differences in the *L. donovani* activity requirements include much greater permissibility in the benzamide portion of the scaffold, though it remains to be seen if this permissibility extends to the benzylamine analog set. Combined with what we currently know regarding the improvements to microsomal stability

that can be obtained by alteration of the benzylamine moiety in **BDGR 6023** (see **Section 4-5**), this permissible SAR may enable significant improvements to physicochemical and ADME properties without compromising potency and selectivity. We expect that future work in this series will involve screening of more benzylamine-linked analogs to elaborate on the structure-activity relationship information. This will enable us to capitalize on the physicochemical and ADME improvements and refine a more potent and selective *L. donovani* inhibitor that benefits from advancements in solubility and stability for the scaffold.

Section 4-7: Discovery of *N. fowleri* glucokinase inhibitors based on the benzamidobenzoic, benzamidopicolinic, and benzylaminopicolinic acid templates

The benzamidobenzoic acids (**BABA**s) developed in our group as inhibitors of kinetoplastid glycolysis have since become a rich source for new anti-parasitic optimization after evidence for parasite hopping potential was established.[4,6,7] Although **BABA 1** (and its analogs) possessed unfavorable physicochemical properties (e.g., high lipophilicity, poor aqueous solubility) that posed a significant challenge to further advancement in a drug development context, the scaffold represented an important starting point for bioactive chemical matter in our efforts to discover novel anti-parasitic agents. The history of the **BABA** scaffold, as well as recent work in the refinement of new derivatives towards *T. gondii* (see **Section 4-4**), *T. brucei* (see **Section 4-5**), and *L. donovani* (see **Section 4-6**) have been described earlier in this chapter. Those efforts have enabled discovery of benzamidopicolinic acids and benzylaminopicolinic acids with superior physicochemical and ADME properties that enable further pre-clinical optimization towards improved anti-infectives. Meanwhile, continued investigation of the parasite hopping potential for

the **BABA** scaffold through broader screening revealed analogs of **BABA 1** with anti-amoebic properties.[2]

We recently demonstrated that the analogs **BABA 8-13** inhibit (IC_{50} < 10μM) the hexokinase of *Naegleria fowleri* (NfGlck), a glycolysis-dependent pathogen known colloquially as the "brain eating amoeba".[2] Infection by *N. fowleri* leads to primary amebic meningoencephalitis ("PAM"), which although rare is characterized by a 99% mortality rate and no known cure.[86] Discovery of *N. fowleri* inhibition by a *T. brucei*-optimized scaffold was significant, due to the phylogenetic distance between the parasites involved in the "hopping" approach. The kinetoplastids *T. brucei* and *L. major* (the two parasites for which an initial parasite hopping approach using the **BABA** template appeared tractable) are relatively closely related, being members of different genera in the family Trypanosomatidae, but *N. fowleri* is comparatively distant, being of the phylum Percolozoa rather than Euglenozoa.[86,87] The *N. fowleri* glucokinase shares less than 30% sequence homology with the kinetoplastid glucokinases.[2] Activity against both kinetoplastids and *N. fowleri* was therefore an exciting opportunity. Comparison of the anti-parasitic activity of various **BABA** analogs showed the divergent structure-activity requirements of the scaffold in these parasites (**Table 4-7.1**). **BABA 8** shows inhibition against the hexokinase of all three parasites, while **BABA 9-13** inhibit NfGlck more strongly than either TbHK1 or LmHK1, and **BABA 1** is potent against TbHK1 and LmHK1 but not NfGlck.[2,4]

Table 4-7.1 Activity of selected benzamidobenzoic acids against hexokinases of glycolysis-dependent pathogenic parasites[2,4]

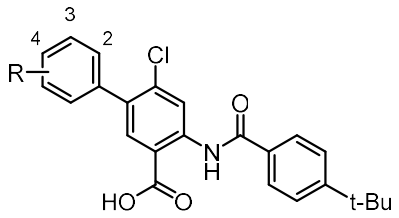

BABA 1, 8-13

Compound	R =	TbHK1 IC_{50} (μM)[a]	LmHK1 IC_{50} (μM)[b]	NfGlck IC_{50} (μM)[c]
BABA 1	H	0.28	1.70	> 10
BABA 8	3-Cl	2.70	1.70	6.5
BABA 9	3-NO_2	> 10	ND	9.3
BABA 10	3-Cl, 4-F	> 10	ND	5.9
BABA 11	3,4-*di*Cl	> 10	ND	2.9
BABA 12	4-CF_3	> 10	ND	6.0
BABA 13	4-OCF_3	> 10	ND	5.0

[a]TbHK1: *Trypanosoma brucei* hexokinase 1; [b]LmHK1: *Leishmania major* hexokinase 1; [c]NfGlck: *Naegleria fowleri* glucokinase; IC_{50}: half-maximal inhibitory concentration; ND: not determined. All values are average of at least three independent experiments.

Discovery of NfGlck inhibition occurred during the course of a structural and enzymatic elucidation effort by our collaborators in which a crystal structure of the enzyme was obtained.[2] Subsequent efforts, which are ongoing, have been focused on obtaining a co-crystal structure of our small molecule inhibitors bound to the enzyme in order to identify the binding site and enable rational- or structure-based compound design. In the meantime, the nitrogenated derivatives of the **BABA** template were screened for NfGlck and whole parasite inhibition (**Table 4-7.2**). For the enzymatic assay, compounds were incubated with recombinant NfGlck before measuring enzymatic activity using a secondary reporter assay.[2] A counter-assay without NfGlck was used to correct for any background inhibition by our compounds on the reporter itself.[2] Whole parasite inhibition was measured by exposing *N. fowleri* trophozoites to compound or vehicle for 48 h at

37°C, then monitoring cultures visually by cell imaging.[2] Compounds were screened at a single concentration of 10 μM against the *N. fowleri* glucokinase (NfGlck), and those with > 50% inhibition against the enzyme were further assayed in dose response format to obtain an IC_{50} and then evaluated against the whole parasite. We found only low levels of NfGlck inhibition (< 50% at 10 μM) for the benzamidopicolinic acids **BDGR 6000**, **6001**, and **6015**, but were pleased to find more substantial inhibition in the case of the benzylamine-linked derivative **BDGR 6023**, with low micromolar IC_{50} values and a selectivity index of almost 3.

Table 4-7.2 Potency of selected benzamido- and benzylamino- picolinic acids

BDGR	Structure	NfGlck % growth inhibition (10 μM)[a]	NfGlck IC_{50} (μM)[b]	*N. fowleri* EC_{50} (μM)[c]	SI[d]	HFF CC_{50} (μM)[e]
6000	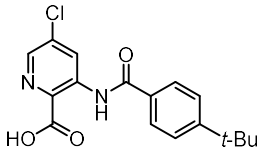	49.2 ± 4.1	8.73 ± 0.53	ND	-	2.5
6001	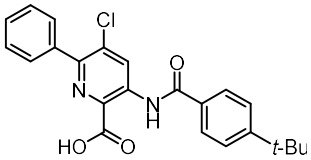	35.7 ± 12.2	> 10	ND	-	48.2
6015	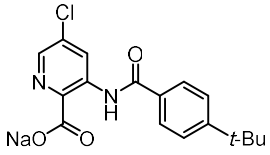	39.6 ± 5.1	> 10	ND	-	2.1
6023	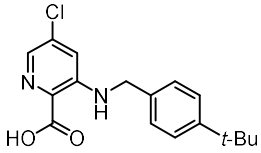	65.0 ± 1.7	6.31 ± 0.26	8.1 ± 0.90	2.8	22.9

[a]NfGlck: *N. fowleri* glucokinase; [b]IC_{50}: half-maximal inhibitory concentration, [c]*N. fowleri*: *Naegleria fowleri,* EC_{50}: half-maximal effective concentration; SI: selectivity index = CC_{50}/EC_{50}; CC_{50}: half-maximal cytotoxic concentration. All values are an average of at least three independent experiments.

In sum, hit-level potency (IC_{50} < 10 μM) was detected against both the enzyme NfGlck, and more significantly, the whole parasite *N. fowleri*. Additional optimization will be required to improve selectivity for the parasite and to further understand the structure activity relationships at play. We anticipate that analogs in the benzylamine-linked picolinic acid series (examples of which have been discussed in **Section 4-5**, but have not yet been tested in *N. fowleri*) will help us to further refine this scaffold in the context of *N. fowleri* and potentially identify better inhibitors for use in the development of new therapeutics.

Section 4-8: Conclusions

Our group's work in identifying benzamidobenzoic acid (**BABA**) small molecules that inhibit kinetoplastid glycolysis in a hexokinase-dependent manner has led to the development of inhibitors along a broad pathogen spectrum using a parasite hopping approach (**Fig. 4-8.1**). The **BABA** series displayed anti-parasitic activity against kinetoplastid pathogens *Trypanosoma brucei* (human African sleeping sickness) and *Leishmania major* (cutaneous leishmaniasis) but was limited by high lipophilicity and concomitantly poor solubility and physiologically relevant stability (see **Section 4-2**). By using the **BABA** template as a starting point despite limitations in the compound series' physicochemical and ADME properties, we identified that the scaffold also had activity against another kinetoplastid, *Leishmania donovani* (visceral leishmaniasis), the apicoplast pathogen *Toxoplasma gondii* (toxoplasmosis), and the amoeba *Naegleria fowleri* (primary amoebic meningoencephalitis).

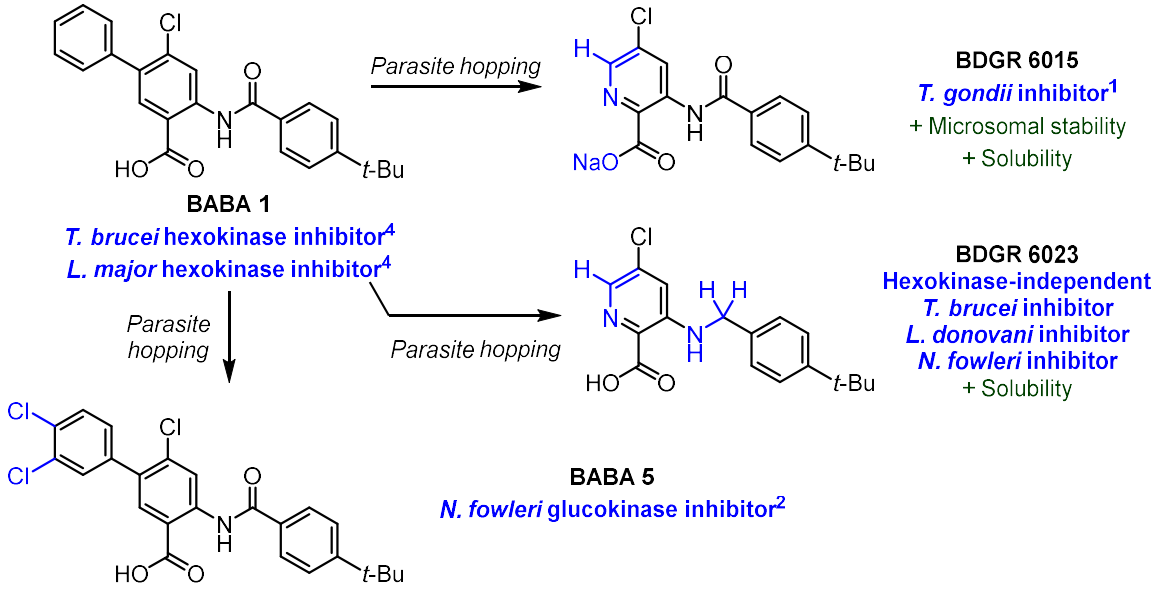

Figure 4-8.1 Summary of results in our parasite hopping approach using the **BABA** template. Blue highlights indicate structural differences conferring parasite specificity as dictated by divergent structure-activity relationships.

Medicinal chemistry efforts focusing on reducing the lipophilicity of the **BABA** template resulted in a benzamidopicolinic acid series that featured improved solubility and microsomal stability (see **Section 4-3**). The structure-activity relationship for the benzamidopicolinic acid scaffold was explored in *T. gondii*, leading to a compound that retained activity against both *T. gondii* tachyzoites and bradyzoites without compromising physicochemical and ADME needs. Several advancements in the synthesis of such compounds were developed that enabled routine scale-up in a safer and more cost-effective manner. We thus developed a new set of probe compounds for the study of *T. gondii* (see **Section 4-4**).

Further investigation revealed that the benzamidopicolinic acids also possessed hexokinase-independent inhibitory activity against kinetoplastids, making them anti-trypanosomal compounds with a new, and as-yet unidentified, mode of action compared to the parent **BABA** series (see **Section 4-5**). Follow-up medicinal chemistry led to a benzylamine-linked picolinic acid

derivative with better activity but poor microsomal stability. Improvements to the synthetic route for the benzylamine-linked template enabled access to analogs designed to overcome this microsomal stability limitation and revealed divergent structure-activity relationships for the compounds in *T. brucei* and *L. donovani* (see **Sections 4-5** and **4-6**). The new analogs also featured improved microsomal stability and solubility. Future work will be focused on delineating SAR with the objective of improving compound the profile further.

Advancements in other parasite campaigns often benefitted other efforts, as was the case with building upon the **BABA** activity observed against *N. fowleri*. By identifying screening candidates from benzamido picolinic and benzylamino picolinic acids with improved physicochemical and ADME properties from our *T. gondii*, *T. brucei*, and *L. donovani* efforts, we quickly arrived at a benzylamino picolinic acid scaffold with hit-level potency against a newly identified enzyme target and whole parasite activity. Work in this area is ongoing, but the power of the parasite hopping approach in this context is evident in the compound profile improvements achieved over just a handful (< 10) compounds screened to date (see **Section 4-7**).

The collective result of our parasite hopping efforts from the **BABA** scaffold was development of differentiated picolinic acid derivatives with improved physicochemical profiles and anti-parasitic activity in a number of important eukaryotic pathogens responsible for human disease, namely *T. gondii*, *T. brucei*, *L. donovani*, and *N. fowleri* (**Figure 4-8.1**). As is common in parasite hopping, the compounds displayed divergent structure-activity relationships in different pathogens and could be optimized towards a given parasite. The optimization efforts benefited from the physicochemical and ADME advantages inherent to the improved picolinic acid-derived scaffolds. Increasing potency via pathogen-specific SAR enabled increases in compound selectivity, and future work will be focused on additional improvements to advance the drug discovery workflow.

Section 4-9: Experimental

The experimental data has been adapted from work prepared for publication with minimal modification.[1]

Assay of compounds against *Toxoplasma gondii* tachyzoites: The assay employed was modified from Pfefferkorn *et al*.[1] Confluent monolayers of Human Foreskin Fibroblast (HFF-1) were infected with 2 x 10^5 ME49 tachyzoites for 4 hours, then new media (DMEM; Gibco 21013024, plus 10% FBS; Gibco 26140079) was added containing different compounds to evaluate potential growth inhibition. In the negative control, only DMSO (Santa Cruz, 67-58-5) was added. As a positive control for parasite growth inhibition, pyrimethamine (Sigma, P7771) was used at 1μM. Parasites were grown for 48 hours, and then 1 μCi of [^{3}H] (Moraveck, MT 512) uracil was added in each well. After additional 24 hours, monolayers were quenched by adding 1 mL ice-cold 0.6 N (10%) Trichloroacetic acid (TCA; Merck, 100807) to the existing medium and incubated at 4 °C for 1 hour to fix the monolayer. TCA was removed and properly discarded, and the plates were washed with tap water for at least 4 hours. After the wash was added 500 mL of 1 M NaOH (Honeywell, 35256) per well, and the plates were gently shaken for one hour at room temperature. 4 ml of Scintillation fluid (RPI, 111167) was added to each vial. Then each vial received 400 mL of sample for each well, and after overnight incubation, [^{3}H] was measured.

Assay of compounds against *Toxoplasma gondii* bradyzoites: Tachyzoites were differentiated into bradyzoite for 4 days in RPMI (Gibco, 31800089) pH 8.1, as previously described.[2] After differentiation, the growth assay was performed similarly to the one described for tachyzoites; however, 10 μCi of [3H] uracil was used per well instead.

Cytotoxicity assay of compounds in HFF cells: 1000 human foreskin fibroblasts cells per well were plated in a 384 well plate. The cells were treated with a single compound at eight concentrations in duplicate, for 72 hours. Following treatment, 20 uL of CellTiterGLO reagent was added per well and submitted to a plate reader to assess toxicity.

In vitro blood brain barrier parallel artificial membrane permeability assay (BBB PAMPA): A 96-well filter plate and the donor plate was used, along with the following reagents: porcine polar brain lipid (PBL), clonidine, theophylline, Verapamil, hydrocortisone, DMSO, PBS, Dodecane. Procedure: The 96-well filter plate (catalog no. MAIPN4550) and the donor plate (catalog no. MATRNPS50) were both purchased from Millipore. The porcine polar brain lipid (PBL) was purchased from Avanti Polar Lipids (catalog no. 141101P). Dodecane and DMSO were obtained from Sigma-Aldrich. Verapamil, clonidine, hydrocortisone, and theophylline were purchased from Sigma-Aldrich and used as positive control. Tested compounds were dissolved in DMSO at 5 mg/mL as stock solutions, which were diluted in PBS to make a final solution (final concentration 25 μg/mL). The PBL was dissolved in dodecane as 20 mg/mL PBL solution. A 350 μL final solution was added to the donor well, the filter membrane of the filter plate was coated with 4 μL of PBL solution, and then the filter plate well was filled with 150 μL of PBS. The filter plate was carefully put on the donor plate to form a "sandwich" with tested compounds solution on the bottom, artificial lipid membrane in the middle, and the acceptor PBS on the top. The sandwich was incubated at room temperature for 18 h. The donor plate was removed after incubation. The solution from donor and filter wells were carefully transferred into the HPLC vials. The concentration ratios were determined by HPLC. Every sample was analyzed in triplicate. The P_e (cm/s) was obtained by the following equations:

$$P_e = -\frac{V_{dp}V_{fp}}{st(V_{dp} + V_{fp})}\ln\left(1 - \frac{[drug]_{fp}}{[drug]_{ref}}\right)$$

$$[drug]_{ref} = \frac{[drug]_{dp} \times 350 + [drug]_{fp} \times 150}{500}$$

where V_{dp} (mL) = volume of the donor plate (0.35 mL), V_{fp} (mL) = volume of the filter plate (0.15 mL), $[drug]_{fp}$ = compound concentration (area under the curve of the compound peak in the HPLC plot) of the filter plate, $[drug]_{dp}$ = compound concentration (area under the curve of the compound peak in the HPLC plot) of the donor plate, s (cm^2) = membrane area (0.28 cm^2), and t (s) = incubation time (64,800 s).

Reagents/supplies were sourced as follows:

Reagent/Supply	Vendor	Catalog No.
96-well filter plate	EMD Millipore	MATRNPS50
96-well donor plate	EMD Millipore	MAIPN4550
PBL	Avanti Polar Lipids	141101P
PBS	Thermal Fisher	10010-031
Dodecane	Sigma-Aldrich	297879-100ML
DMSO	Sigma-Aldrich	D8418-500ML
Verapamil hydrochloride	Sigma-Aldrich	PHR1131-1G
Clonidine hydrochloride	Sigma-Aldrich	C7897-100MG
Hydrocortisone	Sigma-Aldrich	H4001-1G
Theophylline	Sigma-Aldrich	T1633-50G

Kinetic Solubility assessment: *Media prep:* The phosphate buffer was prepared (pH at 7.4). The preparation of 50 mM NaH_2PO_4 in water (pH 4.50): 6.06 g of $NaH_2PO_4{\cdot}2H_2O$ was dissolved in 778 mL of water in a 1000 mL volumetric flask, and the measured pH was 4.50. Separately, 50 mM Na_2HPO_4 in water (pH 9.35) was prepared by dissolving 6.48 g of Na_2HPO_4 in 914 mL of water in a 1000 mL volumetric flask, and the pH measured was 9.35. The preparation of 50 mM phosphate buffer pH 7.4 was completed by adding 15 mL of 50 mM Na_2HPO_4 in water (pH 9.35)

into a 50 mL tube, and then adjusting pH to 7.4 with 50 mM NaH_2PO_4 in water (pH 4.50). *Procedure:* Compound (10 mM in DMSO,10 µL) was added into lower chambers of a Whatman miniuniprep vial (Miniuniprep (PTFE filter media with polypropylene housing, cat. no. UN203NPUORG, GE Halthcare Whatman), and then 490 µL of buffer at pH 7.4 was added into lower chamber of the Whatman miniuniprep vial. The solubility sample was vortexed for at least 2 minutes. The miniuniprep vial was agitated on a Barnstead shaker for 24 h at RT at the speed of 800 rpm, and then centrifuged 20 min (eg.4000 rpm). The miniuniprep was compressed to prepare the filtrate for injection into HPLC system to calculate the concentration with standard curve. The positive controls, amiodarone hydrochloride, carbamazepine, and chloramphenicol, were included in the analysis.

In vitro plasma stability assay: Pooled frozen plasma from a CD-1 mouse was thawed in a water bath at 37 ℃ prior to experiment. Plasma was centrifuged at 4000 rpm for 5 min and the clots were removed if any. The pH was adjusted to 7.4 ± 0.1 if required. Preparation of compound and positive control: 1 mM intermediate solution was prepared by diluting 10 µL of the stock solution with 90 µL DMSO; 1 mM intermediate of positive control Propantheline was prepared by diluting 10 µL of the stock solution with 90 µL ultrapure water. 100 µM dosing solution was prepared by diluting 10 µL of the intermediate solution (1 mM) with 90 µL DMSO. 98 µL of blank plasma was spiked with 2 µL of dosing solution (100 µM) to achieve 2 µM of the final concentration in duplicate and samples were Incubated at 37 ℃ in a water bath. At each time point (0,10, 30, 60 and 120 min), 400 µL of stop solution (200 ng/mL tolbutamide and 200 ng/mL Labetalol in 50% ACN/MeOH) was added to precipitate protein and mixed thoroughly. Centrifuged sample plates at 4,000 rpm for 10 min. An aliquot of supernatant (50 µL) was transferred from each well and mixed with 100 µL ultrapure water. The samples were agitated via shaker at 800 rpm for about 10

min before submitting to LC-MS/MS analysis. The % remaining of test compound after incubation in plasma was calculated using following equation: % Remaining= 100 x (PAR at appointed incubation time / PAR at T0 time) where PAR is the peak area ratio of analyte versus internal standard (IS). Propantheline bromide was used as reference compound in this assay.

In vitro mouse microsomal stability assay: Intermediate solution: 5 µL of compound stock solution (10 mM in dimethyl sulfoxide (DMSO)) was diluted with 495 µL of methanol (MeOH) (intermediate solution concentration: 100 µM, 99% MeOH). Working solution: 50 µL of compound intermediate solution (100 µM) were diluted with 450 µL of 100 mM potassium phosphate buffer (working solution concentration: 10 µM, 9.9% MeOH). NADPH Cofactor Preparation: NADPH powder: β-Nicotinamide adenine dinucleotide phosphate reduced form, tetrasodium salt; NADPH·4Na (Vendor: Chem-Impex International, Cat. No. 00616). The appropriate amount of NADPH powder was weighed and diluted into a 10 mM $MgCl_2$ solution (working solution concentration: 10 unit/mL; final concentration in reaction system: 1 unit/mL). Liver Microsomes Preparation: CD-1 Mouse (MLM, Cat No. BQM1000, Lot No. MIC255036 from Biopredic). The appropriate concentrations of microsome working solutions were prepared in 100 mM potassium phosphate buffer. Stop Solution Preparation: Cold (4°C) acetonitrile (ACN) containing 100 ng/mL tolbutamide and 100 ng/mL labetalol as internal standards (IS) was used as the stop solution. Using an Apricot automation workstation, 10 µL/well of compound working solution were added to all 96-well reaction plates except the blank (T0, T5, T10, T20, T30, T60, and NCF60). An Apricot automation workstation was used to add 80 µL/well of microsome solution to all reaction plates (Blank, T0, T5, T10, T20, T30, T60, and NCF60). All reaction plates containing mixtures of compound and microsomes were pre-incubated at 37 °C for 10 minutes. An Apricot automation workstation was used to add 10 µL/well of 100 mM potassium phosphate

buffer to reaction plate NCF60. Reaction plate NCF60 was incubated at 37 °C, and timer 1 was started. After pre-incubation, an Apricot automation workstation was used to add 10 µL/well of NADPH regenerating system to every reaction plate except NCF60 (Blank, T0, T5, T10, T20, T30, and T60) to start the reaction. The reaction plates were incubated at 37°C, and timer 2 was started. An Apricot automation workstation was used to add 300 µL/well of stop solution to each reaction plate at its appropriate end time point to terminate the reaction. Each plate was sealed and shaken for 10 minutes. After shaking, each plate was centrifuged at 4000 rpm and 4°C for 20 minutes. During centrifugation, an Apricot automation workstation was used to add 300 µL/well of HPLC grade water to eight new 96-well plates. After centrifugation, an Apricot automation workstation was used to transfer 100 µL of supernatant from each reaction plate to its corresponding bioanalysis plate. Each bioanalysis plate was sealed and shaken for 10 minutes prior to LC-MS/MS analysis. The equation of first order kinetics was used to calculate T1/2 and CLint(mic) (µL/min/mg). Controls used in the analysis included testosterone, diclofenac, and propafenone.

Snapshot pharmacokinetic analysis of compound 23: Six fed, male Balb/c Mouse and 6 in 1 internal standard (Labetalol & tolbutamide & Verapamil & dexamethasone & glyburide & Celecoxib 100 ng/mL for each) in acetonitrile were used for this study. Each mouse was administered a single IP dose of 15 mg/kg (formulation: 3 mg/ml in 12% SBE-β-CD, clear solution). Plasma samples were evaluated 30 min and 120 min. Brain homogenate of each mouse was analyzed at 120 min. For plasma and brain homogenate samples: Brain homogenate was prepared by homogenizing brain with 5 volumes (w:v) of homogenizing solution (PBS (pH=7.4) buffer : MeOH (v:v, 2:1)). An aliquot of 20 µL sample, calibration standard, quality control, dilute quality control, single blank and double blank samples were added to the 1.5 mL tube; each sample (except the double blank) was quenched with 200 µL IS solution respectively (double blank sample

was quenched with 200 µL ACN), and then the mixture was vortex-mixed well (at least 15 s) with vortexer and centrifuged for 15 min at 12000 g, 4 ℃; 5 µL the supernatant were directly injected for LC-MS/MS analysis. Dilution factor: an aliquot of 2 µL sample was added with 18 µL blank plasma. Samples were analyzed by LC-MS/MS.

Assay of compounds against *Trypanosoma brucei* hexokinase 1: Experiments were performed as previously reported.[4]

Assay of compounds against whole parasite *Trypanosoma brucei* bloodstream form: Experiments were performed as previously reported.[4]

Assay of compounds against *Leishmania donovani* axenic amastigotes: Experiments were performed as previously reported.[85]

Cytotoxicity assay of compounds in human macrophage cells (J774): Experiments were performed as previously reported.[85]

Assay of compounds against *N. fowleri* glucokinase: Experiments were performed as previously reported.[2]

Assay of compounds against *N. fowleri* whole parasite (trophozoites): Experiments were performed using a modified procedure to the one previously reported.[2] *N. fowleri* trophozoites were seeded in a treated 24-well white plate at a concentration of $1*10^4$cells/mL. Compounds were serially diluted and added to wells. Plate was incubated at 37°C for 48 hours. Plate was removed from incubator and allowed to sit at RT for 10 minutes. CTGlo reagent was added to each well and the ATP bioluminescence signal was measured at 490nm using a BioTek Synergy H1 plate reader. Prism was used to determine resulting EC_{50} values and standard deviation of the triplicate.

In vitro mouse plasma protein binding assay:

Plasma/Matrix and Dialysis Membrane Preparation:

1) The dialysis membrane strips were soaked in ultra-pure water at room temperature for approximately 1 hour. Each membrane strip containing 2 membranes was separated and soaked in 20:80 ethanol/water (v/v) for approximately 20 minutes, after which they were ready for use or were stored in the solution at 2-8°C for up to a month. Prior to the experiment, the membrane was rinsed and soaked for 20 minutes in ultra-pure water

2) On the day of experiment, the plasma was thawed by running under cold tap water and centrifuged at 3220 rpm for 5 minutes to remove any clots. The pH value of the resulting plasma was checked. Only plasma with pH value within 7.0-8.0 could be used

Buffer Preparation:

1) A basic solution was made by dissolving 64.44g $Na_2HPO_4 \cdot 12H_2O$ and 15.66g NaCl in 1.8L deionized water.
2) An acidic solution was made by dissolving 7.8g $NaH_2PO_4 \cdot 2H_2O$ and 4.39g NaCl in 0.5L deionized water.
3) The basic solution was titrated with the acidic solution to pH 7.3~7.5. Titrated solution was stored at 4°C for up to 1 month.

Stop Solution Preparation:

1) An aliquot of internal standard stock solution was added to a solution of methanol:acetonitrile (50:50, v:v) to obtain a solution of concentration 200 ng/mL tolbutamide, 200 ng/mL labetalol, and 50 ng/mL metformin

Test Compound and Control Compound Preparation:

1) Test compound and control compound were dissolved in dimethyl sulfoxide (DMSO) to achieve 10 mM stock solutions

2) Working solutions (400 μM) of test compound and control compound were prepared by diluting 10 μL of stock solutions with 240 μL of DMSO

3) Loading matrix solutions (2 μM) of test compound and control compound were prepared by diluting 5 μL of working solutions with 995 μL of blank matrix

Dialysis Procedure:

1) To prepare the loading matrix containing the test compound or control compound, aliquots of test compound working solutions or control compound working solution were spiked into blank matrix to achieve final test concentrations. The concentration of organic solvent in the final solutions were no more than 1% (normally 0.5%). The samples were mixed thoroughly before the next step

2) To prepare the time zero (T0) samples to be used for recovery determination, 50 μL aliquots of loading matrix were transferred in triplicate to the sample collection plate. The samples were immediately matched with opposite blank buffer to obtain a final volume of 100 μL of 1:1 matrix/dialysis buffer (v/v) in each well. 500 μL of stop solution were added to these T0 samples. They were then stored at 2-8°C pending further processes along with other post-dialysis samples

3) To load the dialysis device, an aliquot of 150 μL of the loading matrix was transferred to the donor side of each dialysis well in triplicate, and 150 μL of the dialysis buffer was loaded to the receiver side of the well. The dialysis plate was placed in a humidified incubator at 37 °C with 5% CO_2 on a shaking platform that rotated slowly (about 100 rpm) for 4 hours

4) At the end of the dialysis, aliquots of 50 µL of samples were taken from both the buffer side and the matrix side of the dialysis device. These samples were transferred into new 96-well plates (the sample collection plates). Each sample was mixed with an equal volume of opposite blank matrix (buffer or matrix) to reach a final volume of 100 µL of 1:1 matrix/dialysis buffer (v/v) in each well. All samples were further processed by adding 500 µL of stop solution containing internal standards. The mixture was vortexed and centrifuged at 4000 rpm for about 20 minutes. An aliquot of 100 µL of supernatant of all the samples was then removed for LC-MS/MS analysis

5) The single blank samples were prepared by transferring 50 µL of blank matrix to a 96 well plate and adding 50 µL of blank PBS buffer to each well. The blank plasma must match the species of plasma used in the plasma side of the well. Then the matrix-matched samples were further processed by adding 500 µL of stop solution containing internal standards, following the same sample processing method as the dialysis samples.

Data Calculation:

The % Unbound, % Bound, and % Recovery values were calculated using the following equations:

$$\%Unbound = 100 \times \frac{[F]}{[T]}$$

$$\%Bound = 100 \times \left(1 - \frac{[F]}{[T]}\right)$$

$$\%Recovery = 100 \times \left(\frac{[F] + [T]}{[\bar{T}_0]}\right)$$

Where [F] is the analyte concentration or peak area ratio of analyte/internal standard on the buffer (receiver) side of the membrane, [T] is the analyte concentration or peak area ratio of analyte/internal standard on the plasma (donor) side of the membrane, and [T_0] is the analyte concentration or the peak area ratio of analyte/internal standard in the plasma sample at time zero.

Reagents/supplies were sourced as follows:

Reagent/Supply	Vendor	Catalog No.
HTD 96 a/b dialysis membrane strips	HT Dialysis LLC	Cat # 1101
96-well polypropylene plate (2.2 mL/well)	Apricot	DWP-22-96-SQ-U-C-L
96-well equilibrium dialysis plate (Model 96b)	HT Dialysis LLC	Cat # 1006
CD-1 Mouse plasma	Beijing Vital River Laboratory Animal Technology Co., Ltd	Lot # 20190116-14
Warfarin	Stru Chem	SC-16139 Lot # 20141222

Synthetic procedures and characterization for compounds 1-23

General Information. Commercial reagents (3-amino-5-chloropicolinic acid, 3-aminopicolinic acid, 5-chloro-3-nitropicolinonitrile, 5-chloropyridin-3-amine, 4-amino-6-chloronicotinic acid, 2-amino-6-chloronicotinic acid, methyl 2-amino-5-bromo-4-chlorobenzoate, all boronic acids, and all benzoyl chlorides) and solvents were used as received. All thin layer chromatography was performed using precoated silica gel 60 F_{254} plates (EMD Millipore). Flash chromatography separations were carried out using a Teledyne ISCO CombiFlash Rf 200 purification system (MPLC) with silica gel columns. Purity of all final compounds was confirmed by HPLC/MS analysis on an Agilent 1290 LCMS and determined to be ≥ 95% AUC at 254 nm or 218 nm. ^{1}H and ^{13}C nuclear magnetic resonance (NMR) spectra were recorded on a Varian Unity-Inova 400 MHz NMR Spectrometer (operating at 400, 376, and 101 MHz, respectively) or a Varian Unity-Inova 500 MHz NMR Spectrometer (operating at 500, 470, and 126 MHz, respectively) or Bruker Ascend 400 MHz Spectrometer (operating at 400, 376, and 101 MHz, respectively) in $CDCl_3$, MeOD, or DMSO-d_6. The chemical shifts (δ) reported are given in parts per million (ppm). The signal splitting patterns were described as s = singlet, d = doublet, t = triplet, q = quartet, p = pentuplet, dd = doublet of doublet, dt = doublet of triplet, td = triplet of doublet, tt = triplet of triplet, ddd = doublet of doublet of doublet, br = broad and m = multiplet, with coupling constants (J) in hertz (Hz). The LC-MS analysis was performed on an Agilent 1290 Infinity II HPLC system with 1290 Infinity II Diode Array Detector and an Agilent 6120 Quadrupole LC-MS system. The analytical chromatography method utilized the following parameters: Poroshell 120 EC-C18, 1.9 μm column, UV detection wavelength = 254 nm, Flow rate = 1.0 mL/min, Gradient = 5-100% LC-MS grade Methanol over 4 min; The organic mobile phase and aqueous mobile phase contained 0.1% LC-MS grade formic acid. The purity analysis of some compounds was performed

on Waters Prep LC-150 HPLC system with Waters 2545 Binary Gradient Module Pump, and Waters 2998 Photodiode Array Detector. The analytical chromatography method utilized the following parameters: XBridge® C18, 4.6 x 50 mm, 3.5 µm column; UV detection wavelength = 254 nm, Flow rate = 1.0 mL/min, Gradient = 5-100% HPLC grade Methanol over 10 min. The organic mobile phase and aqueous mobile phase contained 0.1% HPLC grade ammonium chloride. The mass spectrometer utilized the following parameters: an Agilent multimode source that simultaneously acquires ESI+/APCI+. High resolution mass spectra (HRMS) were performed by the Analytical Instrument Center at the School of Pharmacy on a Bruker MaXis 4G mass spectrometer. Chemical nomenclature was generated using ChemBioDraw Ultra version 14.0. Calculated cLogD and cLogP values were obtained using MarvinSketch version 18.25, ChemAxon: Budapest, Hungary, 2018 or ACD/LogD version 8.07, Advanced Chemistry Development, Inc., Toronto, ON, Canada, 2004.

Syntheses of compounds **BABA 1-13** have been previously reported.[2,4] Intermediates **4-S1a-c** and **4-S2a-b** have been previously reported via alternative synthetic routes.[88,89] 3-(4-(*tert*-Butyl)phenyl)oxetan-3-amine hydrochloride was synthesized by adapting a published procedure.[90] Spectral data for known compounds that were resynthesized matched reported values. All final compounds were assessed for purity by LCMS/UV and determined to be $\geq$ 95% prior to assessments.

General Procedure A. *Esterification of picolinic and nicotinic acids*.

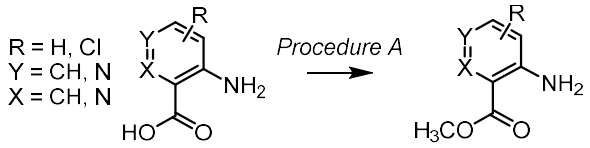

4-S1a-c

To a solution of the corresponding acid (1 equiv.) in 1:4 MeOH/CH_2Cl_2 (0.1M) was added dropwise a solution of TMS-diazomethane (2M in hexanes, 2 equiv.) and the reaction stirred at rt for 18 h. The reaction was then concentrated and purified as indicated give the title compound.

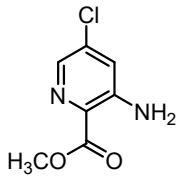

4-S1a

3-Amino-5-chloropicolinic acid (251 mg, 1.5 mmol) was subjected to procedure A, then purified by MPLC (4g SiO_2, 0-25% EtOAc, 30 mL/min) to give methyl 3-amino-5-chloropicolinate **4-S1a** as a yellow solid (149 mg, 0.8 mmol, 55% yield). Characterization matched literature report.[88]

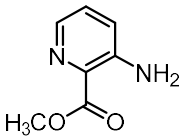

4-S1b

3-Aminopicolinic acid (499 mg, 3.6 mmol) was subjected to procedure A, then purified by MPLC (12g SiO_2, 0-100% EtOAc/Hexanes, 30 mL/min) to give methyl 3-aminopicolinate **4-S1b** as a white solid (232 mg, 1.5 mmol, 42% yield). Characterization matched literature report.[88]

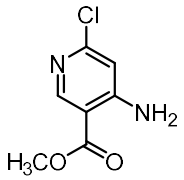

4-S1c

4-Amino-6-chloronicotinic acid was subjected to procedure A, then purified by MPLC (4g SiO_2, 0-25% EtOAc/Hexanes, 20 mL/min) to give methyl 4-amino-6-chloronicotinate **4-S1c** as a white solid (83 mg, 0.45 mmol, 76% yield). Characterization matched literature report.[89]

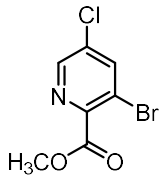

4-S1d

3-Bromo-5-chloropicolinic acid (2.30 g, 9.7 mmol) was subjected to procedure A, then triturated with toluene and filtered sequentially through a 0.45μm, then 0.10 μm syringe filter. The filtrate was concentrated to give **4-S1d** as a light tan solid (1.61 g, 6.4 mmol, 66% yield). ^{1}H NMR (400 MHz, $CDCl_3$) δ 8.56 (d, J = 2.1 Hz, 1H), 8.03 (d, J = 2.1 Hz, 1H), 4.00 (s, 3H).

Alternatively, to a solution of 3-bromo-5-chloropicolinic acid (1.05 g, 4.5 mmol) in methanol (0.23M) was added concentrated H_2SO_4 (2 mL). The reaction vessel was sealed in a screwcap flask and placed behind a blast shield, heated to 110°C, and stirred 18 h. The reaction was then cooled to rt, neutralized to pH 7 with sat. $NaHCO_3$ (aq) and filtered to collect **4-S1d** as a white solid (892 mg, 3.6 mmol, 80% yield). ^{1}H NMR (400 MHz, $CDCl_3$) δ 8.57 (d, J = 2.0 Hz, 1H), 8.04 (d, J = 2.0 Hz, 1H), 4.01 (s, 3H).

General Procedure B. *Bromination of methyl 3-amino picolinates*.

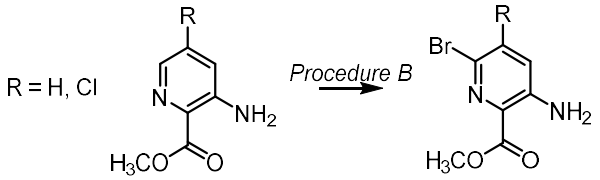

4-S1a-b **4-S2a-b**

To a suspension of the corresponding methyl 3-amino picolinate in water (0.5M) was added 2M H_2SO_4 (aq) (10 mL/mmol, 20 equiv.) and this was stirred until the starting material was dissolved. To the reaction solution was then added 2.6M Br_2 (AcOH) solution dropwise (0.4 mL/mmol, 1 equiv.), and the mixture stirred at rt for 18 h. The pH was then adjusted to 12 using 1M NaOH (aq) and the resulting precipitate collected by filtration.

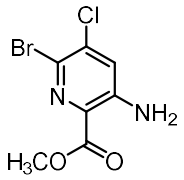

4-S2a

4-S1a (369 mg, 1.98 mmol) was subjected to general procedure B to give methyl 3-amino-6-bromo-5-chloropicolinate **4-S2a** as an off-white solid (268 mg, 1.0 mmol, 51% yield). Characterization matched literature report.[88]

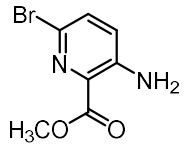

4-S2b

4-S1b (23 mg, 0.15 mmol) was subjected to general procedure B, then purified by MPLC (4g SiO_2, 25% EtOAc/Hexanes, 20 mL/min) to give methyl 3-amino-6-bromopicolinate **4-S2b** as a white solid (91 mg, 0.40 mmol, 55% yield). Characterization matched literature report.[88]

General Procedures C-1 and C-2. *Amide coupling of (hetero)aryl amine building blocks to give benzamido compounds.*

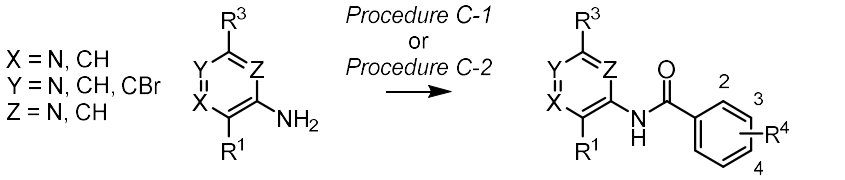

4-S3a-i
BDGR 6002, 6010, 6022, 6014, 6016
BDGR 6025-6026, 6032, 6034, 6042

Procedure C-1: To a solution of the corresponding (hetero)aryl amine (1 equiv.) in CH_3CN (1M) was added the corresponding benzoyl chloride (1.1 equiv.), then Et_3N or *i*Pr_2EtN as indicated (2.2 equiv.), and the reaction stirred at rt for 18 h. The reaction mixture was then diluted with EtOAc and washed with 1M HCl (aq) (2 x 10 mL), the organic layer separated, dried over $MgSO_4$ (s), concentrated, and purified as indicated to give the title compound.

Procedure C-2: To a G10 microwave vial equipped with stir bar was added the corresponding (hetero)aryl amine (1 equiv.) in CH_3CN (0.06M) and the corresponding benzoyl chloride (1.1 equiv.). The vessel was sealed and heated to 150°C by microwave irradiation with stirring for 1 hour. The reaction mixture was then treated as indicated to give the title compound.

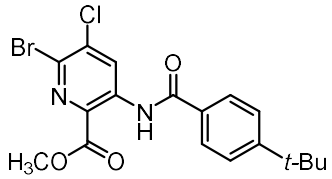

4-S3a

4-S2a (399 mg, 1.5 mmol) was subjected to procedure C-2 using 4-(*tert*-butyl)benzoyl chloride, then concentrated and purified by MPLC (12g SiO_2, 0-25% EtOAc, 30 mL/min) to give methyl 6-

bromo-3-(4-(tert-butyl)benzamido)-5-chloropicolinate **S3a** as a white solid (371 mg, 0.87 mmol, 58% yield). ^{1}H NMR (400 MHz, $CDCl_3$) δ 11.89 (s, 1H), 9.56 (s, 1H), 7.96 (d, J = 8.5 Hz, 2H), 7.57 (d, J = 8.5 Hz, 2H), 4.06 (s, 3H), 1.37 (s, 9H).

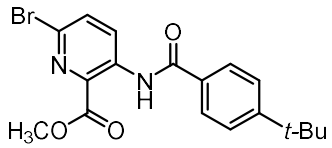

4-S3b

4-S2b (15 mg, 0.07 mmol) was subjected to procedure C-2 using 4-(*tert*-butyl)benzoyl chloride, then the reaction was diluted with CH_2Cl_2, washed with sat. $NaHCO_3$ (aq) (3 x 10 mL), brine (1 x 10 mL), separated and dried over $MgSO_4$ (s), then purified by MPLC (4g SiO_2, 0-10% EtOAc/Hexanes, 20 mL/min) to give methyl 6-bromo-3-(4-(tert-butyl)benzamido)picolinate **4-S3b** as a white solid (8 mg, 0.02 mmol, 30% yield). ^{1}H NMR (400 MHz, $CDCl_3$) δ 11.90 (s, 1H), 9.36 (d, J = 9.0 Hz, 1H), 7.96 (dd, J = 8.5, 1.6 Hz, 2H), 7.57-7.54 (m, 3H), 4.06 (s, 3H), 1.37 (s, 9H).

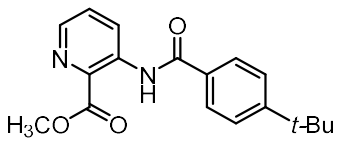

4-S3c

4-S1b (40 mg, 0.26 mmol) was subjected to procedure C-1 using 4-(*tert*-butyl)benzoyl chloride and *i*Pr_2EtN, then purified by MPLC (4g SiO_2, 0-25% EtOAc/Hexanes, 20 mL/min) to give methyl 3-(4-(tert-butyl)benzamido)picolinate **S3c** as a brown oil (73 mg, 0.23 mmol, 89% yield). ^{1}H NMR (400 MHz, $CDCl_3$) δ 11.87 (s, 1H), 9.27 (d, J = 8.6 Hz, 1H), 8.38 (d, J = 4.4 Hz, 1H), 7.92 (d, J = 7.0 Hz, 2H), 7.50 (d, J = 7.1 Hz, 2H), 7.47 (t, J = 4.5 Hz, 1H), 4.01 (s, 3H), 1.31 (s, 9H).

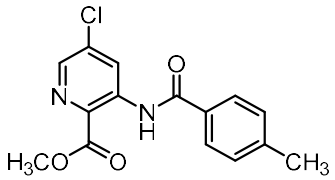

4-S3d

4-S1a (29 mg, 0.16 mmol) was subjected to procedure C-2 using 4-methylbenzoyl chloride. The reaction mixture was filtered to collect methyl 5-chloro-3-(4-methylbenzamido)picolinate **S3d** as a white solid (20 mg, 0.06 mmol, 41% yield). ^{1}H NMR (400 MHz, $CDCl_3$) δ 11.95 (s, 1H), 9.45 (d, J = 2.2 Hz, 1H), 8.38 (d, J = 2.2 Hz, 1H), 7.93 (d, J = 8.2 Hz, 2H), 7.35 (d, J = 8.0 Hz, 2H), 4.08 (s, 3H), 2.45 (s, 3H).

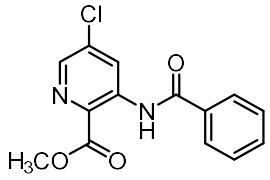

4-S3e

4-S1a (35 mg, 0.19 mmol) was subjected to procedure C-2 using benzoyl chloride. The reaction mixture was filtered to collect methyl 3-benzamido-5-chloropicolinate **4-S3e** as an off-white solid (25 mg, 0.09 mmol, 47% yield). ^{1}H NMR (400 MHz, $CDCl_3$) δ 12.01 (s, 1H), 9.46 (d, J = 2.2 Hz, 1H), 8.40 (d, J = 2.2 Hz, 1H), 8.05-8.03 (m, 2H), 7.62-7.54 (m, 3H), 4.08 (s, 3H).

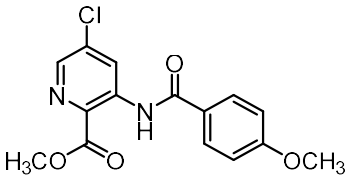

4-S3f

4-S1a (38 mg, 0.20 mmol) was subjected to procedure C-2 using 4-methoxybenzoyl chloride. The reaction mixture was filtered to collect methyl 5-chloro-3-(4-methoxybenzamido)picolinate **4-S3f** as a white solid (27 mg, 0.09 mmol, 43% yield). ^{1}H NMR (400 MHz, $CDCl_3$) δ 11.92 (s, 1H), 9.44

(d, *J* = 2.2 Hz, 1H), 8.37 (d, *J* = 2.2 Hz, 1H), 8.01 (d, *J* = 8.9 Hz, 2H), 7.04 (d, *J* = 9.0 Hz, 2H), 4.08 (s, 3H), 3.90 (s, 3H).

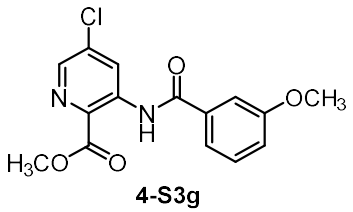

4-S3g

4-S1a (39 mg, 0.20 mmol) was subjected to procedure C-2 using 3-methoxybenzoyl chloride. The reaction mixture was filtered to collect a white solid, which was purified by MPLC (4g SiO_2, 0-50% EtOAc/Hexanes, 20 mL/min) to give methyl 5-chloro-3-(3-methoxybenzamido)picolinate **4-S3g** as a white solid (48 mg, 0.15 mmol, 72% yield). ^{1}H NMR (400 MHz, $CDCl_3$) δ 12.00 (s, 1H), 9.44 (d, *J* = 2.2 Hz, 1H), 8.39 (d, *J* = 2.2 Hz, 1H), 7.60-7.58 (m, 2H), 7.46 (t, *J* = 8.2 Hz, 1H), 7.15 (ddd, *J* = 8.3, 2.4, 1.2 Hz, 1H), 4.08 (s, 3H), 3.91 (s, 3H).

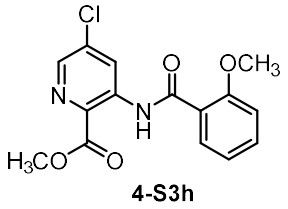

4-S3h

4-S1a was subjected to procedure C-2 using 2-methoxybenzoyl chloride. The reaction mixture was filtered to collect methyl 5-chloro-3-(2-methoxybenzamido)picolinate **4-S3h** as an off-white solid (18 mg, 0.06 mmol, 38% yield). ^{1}H NMR (500 MHz, $CDCl_3$) δ 12.36 (s, 1H), 9.51 (d, *J* = 2.2 Hz, 1H), 8.36 (d, *J* = 2.2 Hz, 1H), 8.21 (dd, *J* = 7.9, 1.8 Hz, 1H), 7.54 (ddd, *J* = 8.8, 7.4, 1.9 Hz, 1H), 7.12 (dd, *J* = 8.0, 7.2 Hz, 1H), 7.06 (d, *J* = 8.3 Hz, 1H), 4.13 (s, 3H), 4.04 (s, 3H).

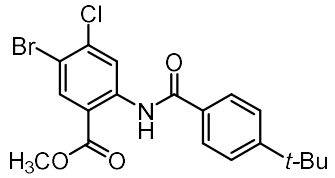

4-S3i

Methyl 2-amino-5-bromo-4-chlorobenzoate was subjected to general procedure C-2 using 4-(*tert*-butyl)benzoyl chloride, then filtered to give methyl 5-bromo-2-(4-(tert-butyl)benzamido)-4-chlorobenzoate **4-S3i** as a light brown solid (1.6 g, 3.8 mmol, 50% yield). ^{1}H NMR (400 MHz, $CDCl_3$) δ 11.94 (s, 1H), 9.20 (s, 1H), 8.29 (s, 1H), 7.95 (d, J = 8.8 Hz, 1H), 7.55 (d, J = 8.8 Hz, 1H), 3.98 (s, 3H), 1.36 (s, 7H).

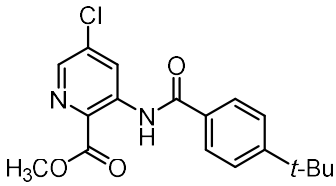

Methyl 3-(4-(tert-butyl)benzamido)-5-chloropicolinate (**BDGR 6002**).

4-S1a (95 mg, 0.51 mmol) was subjected to procedure C-2 using 4-(*tert*-butyl)benzoyl chloride. The reaction mixture was filtered, and the filtrate concentrated and redissolved in CH_2Cl_2. The organic layer was washed with sat. $NaHCO_3$ (aq) (3 x 10 mL), brine (1 x 10 mL), separated and dried over $MgSO_4$ (s), then purified by MPLC (4g SiO_2, 0-50% EtOAc/Hexanes, 20 mL/min) to give **BDGR 6002** as a white solid (90 mg, 0.26 mmol, 51% yield). ^{1}H NMR (500 MHz, $CDCl_3$) δ 11.97 (s, 1H), 9.46 (d, J = 2.2 Hz, 1H), 8.38 (d, J = 2.2 Hz, 1H), 7.97 (d, J = 8.5 Hz, 2H), 7.57 (d, J = 8.5 Hz, 2H), 4.08 (s, 3H), 1.37 (s, 9H). ^{13}C NMR (126 MHz, $CDCl_3$) δ 168.0, 166.4, 156.6, 142.5, 140.2, 137.2, 131.0, 129.8, 127.9, 127.5, 126.2, 53.6, 35.3, 31.3. HRMS (ESI-QTOF) m/z: $[M + H]^+$ Calcd for $C_{18}H_{20}N_2O_3^+$ 347.1157; Found: 347.1157. HPLC Purity ≥ 96%.

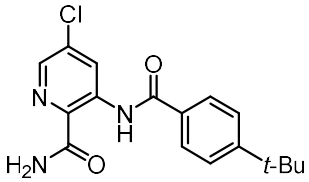

3-(4-(*tert*-Butyl)benzamido)-5-chloropicolinamide (**BDGR 6010**).

5-chloro-3-nitropicolinonitrile (187 mg, 1.0 mmol, 1 equiv.) was dissolved in MeOH (10 mL) before the addition of $FeCl_3$*$6H_2O$ (25 mg, 0.09 mmol, 0.09 equiv.) and activated charcoal (45 mg, 3.8 mmol, 3 equiv.). The reaction flask was fitted with reflux condenser, heated to reflux, and stirred 10 min before the dropwise addition of hydrazine monohydrate (0.2 mL, 4.1 mmol, 4 equiv.). The reaction was stirred at reflux for 1 hour, then cooled to rt, filtered through celite, concentrated, and purified by MPLC (4g SiO_2, 0-50% EtOAc/Hexanes, 20 mL/min) to give 3-amino-5-chloropicolinamide **4-S4a** as a white solid (76 mg, 0.44 mmol, 44% yield). Characterization matched literature report.[91]

4-S4a (66 mg, 0.43 mmol) was subjected to procedure C-2 using 4-(*tert*-butyl)benzoyl chloride. The reaction was filtered to give **BDGR 6010** as a green solid (85 mg, 0.27 mmol, 63% yield). ^{1}H NMR (500 MHz, $CDCl_3$) δ 12.91 (s, 1H), 9.44 (d, J = 2.2 Hz, 1H), 8.20 (d, J = 1.9 Hz, 1H), 8.06 (br s, 1H), 7.98 (d, J = 8.3 Hz, 2H), 7.54 (d, J = 8.4 Hz, 2H), 5.71 (br s, 1H), 1.36 (s, 9H). ^{13}C NMR (126 MHz, $CDCl_3$) δ 169.6, 166.6, 156.3, 141.0, 139.5, 136.5, 131.2, 130.8, 127.9, 127.5, 126.0, 35.2, 31.3. HRMS (ESI-QTOF) m/z: $[M + H]^+$ Calcd for $C_{17}H_{19}ClN_3O_2^+$ 332.11603; Found: 332.1156. HPLC Purity ≥ 98%.

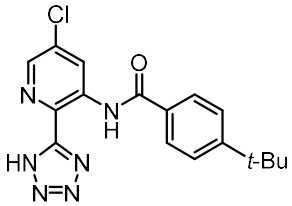

4-(*tert*-Butyl)-N-(5-chloro-2-(*1H*-tetrazol-5-yl)pyridin-3-yl)benzamide (**BDGR 6022**).

5-chloro-3-nitropicolinonitrile (1.8 g, 9.6 mmol, 1 equiv.) was dissolved in *n*-BuOH (25 mL) before the addition of zinc chloride (1.3 g, 9.9 mmol, 1 equiv.) and sodium azide (0.83 g, 13 mmol, 1.2 equiv.). The reaction mixture was heated to 110°C with vigorous stirring for 1.5 h, then cooled to rt and concentrated to a cream residue. The residue was redissolved in 1M NaOH (aq) (50 mL) and stirred 20 min before filtering. The filter cake was washed with water (2 x 25 mL). The resulting filtrate was acidified with concentrated HCl until a precipitate formed (pH 6), this was collected to give 5-chloro-3-nitro-2-(1H-tetrazol-5-yl)pyridine **4-S5a** as a brown solid (1.4 g, 6.1 mmol, 63% yield), used without purification.

4-S5a (223 mg, 0.99 mmol, 1 equiv.) was dissolved in MeOH (10 mL) before the addition of $FeCl_3$*$6H_2O$ (21 mg, 0.08 mmol, 0.07 equiv.) and activated charcoal (37 mg, 3.1 mmol, 3 equiv.). The mixture was heated to reflux and stirred 10 min before the dropwise addition of hydrazine monohydrate (0.2 mL, 4.1 mmol, 4 equiv.). The reaction was stirred at reflux for 4 hours, then cooled to rt, filtered through celite, concentrated, and triturated with MeOH to give 5-chloro-2-(1H-tetrazol-5-yl)pyridin-3-amine **4-S6a** as a green/off-white solid (67 mg, 0.34 mmol, 35% yield). ^{1}H NMR (400 MHz, $CDCl_3$) δ 7.99 (d, J = 2.0 Hz, 1H), 7.44 (d, J = 2.1 Hz, 1H), 7.01 (br s, 2H).

4-S6a (31 mg, 0.16 mmol) was subjected to procedure C-1 using 4-(*tert*-butyl)benzoyl chloride and *i*Pr_2EtN, then purified by MPLC (4g SiO_2, 0-10% EtOAc/Hexanes, 20 mL/min) to give **BDGR 6022** as an off-white solid (16 mg, 0.05 mmol, 30% yield). ^{1}H NMR (500 MHz, MeOD) δ 9.36 (d, J = 2.1 Hz, 1H), 8.47 (d, J = 2.2 Hz, 1H), 8.13 (d, J = 8.5 Hz, 2H), 7.66 (d, J = 8.4 Hz, 2H), 1.40 (s, 9H). ^{13}C NMR (126 MHz, MeOD) δ ^{13}C NMR (MHz,) δ 168.0, 157.9, 156.0, 144.0, 137.2, 135.3, 132.0, 130.4, 128.7, 128.3, 127.1, 36.0, 31.5. HRMS (ESI-QTOF) m/z: $[M + H]^+$ Calcd for $C_{17}H_{18}ClN_6O^+$ 357.1225; Found: 357.12260. HPLC Purity ≥ 95%.

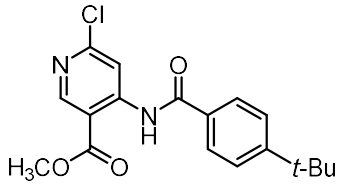

Methyl 4-(4-(tert-butyl)benzamido)-6-chloronicotinate (**BDGR 6014**).

4-S1c (48 mg, 0.25 mmol) was subjected to procedure C-1 using 4-(*tert*-butyl)benzoyl chloride and *i*Pr$_2$EtN, then purified by MPLC (4g SiO_2, 0-25% EtOAc/Hexanes, 20 mL/min) to give **BDGR 6014** as an off-white solid (83 mg, 0.24 mmol, 94% yield). ^{1}H NMR (500 MHz, $CDCl_3$) δ 12.09 (s, 1H), 8.98 (s, 1H), 8.94 (s, 1H), 7.97 (d, J = 8.5 Hz, 2H), 7.57 (d, J = 8.5 Hz, 2H), 4.02 (s, 3H), 1.37 (s, 9H). ^{13}C NMR (101 MHz, $CDCl_3$) δ 168.1, 166.2, 157.6, 156.9, 152.7, 149.6, 130.7, 127.6, 126.2, 113.8, 110.0, 53.1, 35.3, 31.3. HRMS (ESI-QTOF) m/z: [M - H]$^-$ Calcd for $C_{18}H_{18}ClN_2O_3^-$ 345.1011; Found: 345.1009. HPLC Purity ≥ 98%.

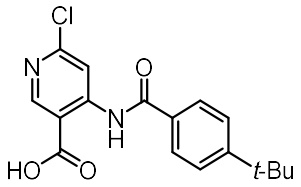

4-(4-(*tert*-Butyl)benzamido)-6-chloronicotinic acid (**BDGR 6016**).

4-Amino-6-chloronicotinic acid (25 mg, 0.15 mmol) was subjected to procedure C-1 using 4-(*tert*-butyl)benzoyl chloride and *i*Pr$_2$EtN, then purified by MPLC (4g SiO_2, 0-10% EtOAc/Hexanes, 20 mL/min) to give **BDGR 6016** as a white solid (9 mg, 0.03 mmol, 20% yield). ^{1}H NMR (500 MHz, $CDCl_3$) δ 9.20 (s, 1H), 8.24 (d, J = 8.3 Hz, 2H), 7.57 (s, 1H), 7.56 (d, J = 8.3 Hz, 2H), 1.38 (s, 9H). ^{13}C NMR (126 MHz, $CDCl_3$) δ ^{13}C NMR (126 MHz,) δ 162.5, 158.6, 158.6, 157.5, 154.8, 152.0, 129.3, 126.3, 126.2, 120.6, 112.0, 35.5, 31.2. HRMS (ESI-QTOF) m/z: [M - H]$^-$ Calcd for $C_{17}H_{16}ClN_2O_3^-$ 331.0855; Found: 331.0848. HPLC Purity ≥ 96%.

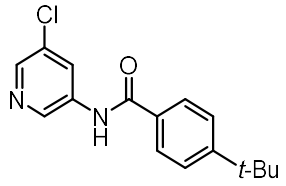

4-(*tert*-Butyl)-N-(5-chloropyridin-3-yl)benzamide (**BDGR 6025**).

5-chloropyridin-3-amine (25 mg, 0.19 mmol) was subjected to procedure C-1 using 4-(*tert*-butyl)benzoyl chloride and *i*Pr_2EtN, then purified by MPLC (4g SiO_2, 0-30% EtOAc/Hexanes, 20 mL/min) to give **BDGR 6025** as an off-white solid (35 mg, 0.12 mmol, 63% yield). ^{1}H NMR (400 MHz, $CDCl_3$) δ 8.58 – 8.39 (m, 2H), 8.33 (t, J = 2.0 Hz, 1H), 8.04 (s, 1H), 7.91 – 7.75 (m, 2H), 7.60 – 7.44 (m, 2H), 1.35 (s, 9H). ^{13}C NMR (101 MHz, $CDCl_3$) δ 166.1, 156.5, 144.0, 138.9, 135.7, 132.4, 131.0, 127.3, 127.2, 126.1, 35.3, 31.3. HRMS (ESI-QTOF) m/z: $[M + H]^+$ Calcd for $C_{16}H_{18}ClN_2O^+$ 289.1102; Found: 289.1094. HPLC Purity ≥ 98%.

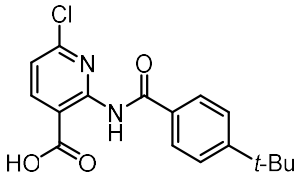

2-(4-(*tert*-Butyl)benzamido)-6-chloronicotinic acid (**BDGR 6026**).

2-Amino-6-chloronicotinic acid (173 mg, 1.0 mmol) was subjected to procedure C-1 using 4-(*tert*-butyl)benzoyl chloride and Et_3N, then purified by MPLC (4g SiO_2, 50-100% EtOAc/Hexanes, 20 mL/min) to give **BDGR 6026** as a white solid (20 mg, 0.06 mmol, 6% yield). ^{1}H NMR (400 MHz, DMSO-d_6) δ 11.71 (s, 1H), 8.25 (d, J = 9.0 Hz, 1H), 7.93 (d, J = 9.1 Hz, 2H), 7.58 (d, J = 9.0 Hz, 2H), 7.38 (d, J = 10.1 Hz, 1H), 1.32 (s, 9H). ^{13}C NMR (101 MHz, DMSO-d_6) δ 167.5, 164.9, 155.9, 151.37, 151.35, 143.0, 131.5, 128.1, 126.0, 120.1, 118.0, 35.3, 31.4. HRMS (ESI-QTOF) m/z: $[M - H]^-$ Calcd for $C_{17}H_{18}ClN_2O_3^+$ 333.1001; Found: 333.0990. HPLC Purity ≥ 99%.

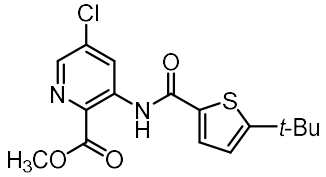

Methyl 3-(5-(*tert*-butyl)thiophene-2-carboxamido)-5-chloropicolinate (**BDGR 6032**).

4-S1a (38 mg, 0.20 mmol) was subjected to procedure C-1 using 5-(*tert*-butyl)thiophene-2-carbonyl chloride and Et_3N in THF. The reaction mixture was filtered to collect a tan solid, which was then purified by MPLC (4g SiO_2, 0-10% EtOAc/Hexanes, 20 mL/min) to give **BDGR 6032** as a yellow oil that solidified (38 mg, 0.11 mmol, 54% yield). ^{1}H NMR (400 MHz, $CDCl_3$) δ 11.81 (s, 1H), 9.33 (d, J = 2.2 Hz, 1H), 8.35 (d, J = 2.2 Hz, 1H), 7.63 (d, J = 3.9 Hz, 1H), 6.92 (d, J = 3.9 Hz, 1H), 4.07 (s, 3H), 1.43 (s, 9H). ^{13}C NMR (101 MHz, $CDCl_3$) δ 168.0, 166.0, 161.2, 142.4, 140.1, 137.2, 135.4, 129.6, 129.5, 127.7, 123.0, 53.6, 35.4, 32.4. HPLC Purity ≥ 95%.

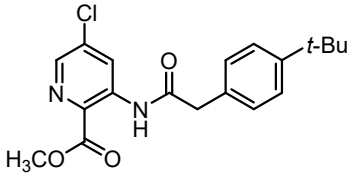

Methyl 3-(2-(4-(*tert*-butyl)phenyl)acetamido)-5-chloropicolinate (**BDGR 6034**).

4-S1a (113 mg, 0.61 mmol) was subjected to procedure C-1 using 2-(4-(*tert*-butyl)phenyl)acetyl chloride and *i*Pr_2EtN in THF. The reaction mixture was filtered, and the filtrate washed with sat. 1M NaOH (aq) (3 x 20 mL), brine (1 x 20 mL), and separated. The aqueous layer was back-extracted with CH_2Cl_2 (3 x 10 mL) and the organic layers combined, dried over $MgSO_4$ (s), then purified by MPLC (4g SiO_2, 0-25% EtOAc/Hexanes, 20 mL/min) to give **BDGR 6034** as a light brown solid (40 mg, 0.11 mmol, 18% yield). ^{1}H NMR (400 MHz, $CDCl_3$) δ 10.96 (s, 1H), 9.24 (d, J = 2.1 Hz, 1H), 8.31 (d, J = 2.2 Hz, 1H), 7.42 (d, J = 8.3 Hz, 2H), 7.29 (d, J = 8.4 Hz, 2H), 3.94

(s, 3H), 3.76 (s, 2H), 1.33 (s, 9H). ^{13}C NMR (101 MHz, $CDCl_3$) δ 171.3, 167.3, 150.2, 142.5, 139.5, 137.0, 130.5, 129.3, 127.8, 126.2, 53.3, 45.4, 34.7, 31.5. HPLC Purity ≥ 95%.

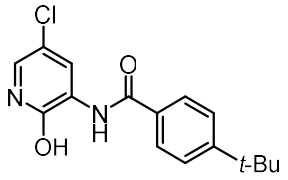

4-(*tert*-Butyl)-N-(5-chloro-2-hydroxypyridin-3-yl)benzamide (**BDGR 6042**).

3-Amino-5-chloropyridin-2-ol (50 mg, 0.35 mmol) was subjected to procedure C-1 using 4-(*tert*-butyl)benzoyl chloride and *i*Pr$_2$EtN in THF. The reaction mixture was diluted with EtOAc, washed with 1M HCl (aq) (2 x 10 mL), 1M NaOH (aq) (2 x 10 mL), and separated. The organic layer was dried over $MgSO_4$ (s) and purified by MPLC (4g SiO_2, 0-25% EtOAc/Hexanes, 20 mL/min) to give **BDGR 6042** as a pink solid (16 mg, 0.05 mmol, 15% yield). ^{1}H NMR (400 MHz, $CDCl_3$) δ 12.67 (s, 1H), 9.03 (s, 1H), 8.72 (d, J = 2.6 Hz, 1H), 7.88 (d, J = 8.5 Hz, 2H), 7.54 (d, J = 8.5 Hz, 2H), 7.16 (d, J = 2.6 Hz, 1H), 1.37 (s, 9H). ^{13}C NMR (101 MHz, $CDCl_3$) δ 165.9, 157.8, 156.3, 131.1, 129.9, 127.3, 126.0, 125.0, 124.0, 115.4, 35.2, 31.3. HPLC Purity ≥ 95%.

General Procedure D. *Alkylation of 3-amino pyridyl building blocks to give benzylamine-linked compounds*.

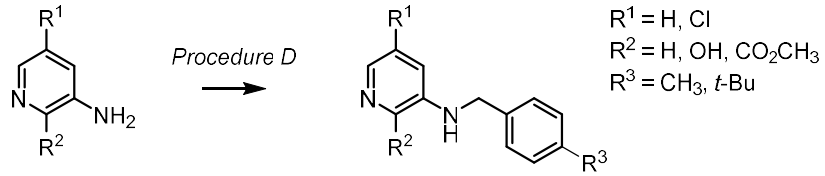

4-S7a-b
BDGR 6038-6039, 6043

To a solution of the corresponding pyridyl amine (1 equiv.) in CH_3CN (0.1M) was added the corresponding benzyl bromide (1.2 equiv.), then *i*Pr_2EtN (0, 1.2, or 2.2 equiv. as indicated), and the reaction stirred at the indicated temperature for the specified time. The reaction mixture was then concentrated and purified as indicated to give the title compound.

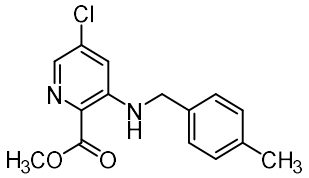

Methyl 5-chloro-3-((4-methylbenzyl)amino)picolinate (**4-S7a**).

4-S1a (37 mg, 0.20 mmol) was subjected to procedure D using 4-methylbenzyl bromide and 1.2 equiv. of *i*Pr_2EtN at 150° for 1 h with microwave irradiation. The reaction was purified by MPLC (4g SiO_2, 0-25% EtOAc/Hexanes, 20 mL/min) to give **4-S7a** as a white solid (13 mg, 0.04 mmol, 22% yield). ^{1}H NMR (400 MHz, $CDCl_3$) δ 8.20 (s, 1H), 7.91 (d, J = 2.3 Hz, 1H), 7.24 – 7.13 (m, 4H), 7.02 (s, 1H), 4.37 (d, J = 5.5 Hz, 2H), 3.96 (s, 3H), 2.34 (s, 3H).

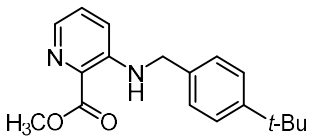

Methyl 3-((4-(*tert*-butyl)benzyl)amino)picolinate (**4-S7b**).

4-S1b (70 mg, 0.46 mmol) was subjected to procedure D using 4- *tert*-butylbenzyl bromide and 1.2 equiv. of *i*Pr_2EtN at 60° for 24 h. The reaction was purified by MPLC (4g SiO_2, 10-25% EtOAc/Hexanes, 20 mL/min) to give **4-S7b** as a yellow oil (52 mg, 0.18 mmol, 41% yield). ^{1}H NMR (400 MHz, $CDCl_3$) δ 8.12 (t, J = 5.5 Hz, 1H), 8.01 (d, J = 4.0 Hz, 1H), 7.37 (d, J = 8.1 Hz, 2H), 7.31 – 7.19 (m, 3H), 7.05 (d, J = 8.6 Hz, 2H), 4.42 (d, J = 5.6 Hz, 2H), 3.97 (s, 3H), 1.31 (s, 9H).

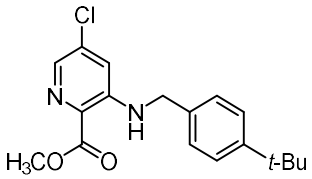

Methyl 3-((4-(*tert*-butyl)benzyl)amino)-5-chloropicolinate (**BDGR 6038**).

4-S1a (24 mg, 0.13 mmol) was subjected to procedure D using 4-*tert*-butylbenzyl bromide and 1.2 equiv. of *i*Pr_2EtN at 85° for 42 h. The reaction was concentrated, dissolved with EtOAc (15 mL), washed with 1M NaOH (aq) (3 x 10 mL) and brine (1 x 10 mL), dried over $MgSO_4$ (s), and then purified by MPLC (4g SiO_2, 10-15% EtOAc/Hexanes, 20 mL/min) to give **BDGR 6038** as a yellow oil that solidified (60 mg, 0.18 mmol, 36% yield). ^{1}H NMR (400 MHz, $CDCl_3$) δ 8.19 (t, J = 4.6 Hz, 1H), 7.92 (d, J = 2.0 Hz, 1H), 7.39 (d, J = 8.4 Hz, 2H), 7.26 (d, J = 8.3 Hz, 2H), 7.06 (d, J = 2.1 Hz, 1H), 4.38 (d, J = 5.5 Hz, 1H), 3.96 (s, 3H), 1.32 (s, 9H). ^{13}C NMR (101 MHz, $CDCl_3$) δ 168.0, 150.9, 148.3, 136.9, 135.6, 134.1, 127.0, 126.04, 125.94, 118.9, 52.7, 46.5, 34.7, 31.5. HPLC Purity ≥ 99%.

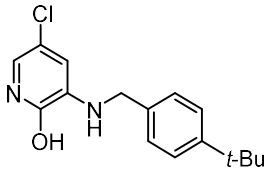

3-((4-(*tert*-Butyl)benzyl)amino)-5-chloropyridin-2-ol (**BDGR 6039**).

3-Amino-5-chloropyridin-2-ol (52 mg, 0.36 mmol) was subjected to procedure D using 4-*tert*-butylbenzyl bromide without base at rt for 48 h, then 60°C for 1 h. The reaction was filtered, and the collected solid purified by MPLC (4g SiO_2, 25-50% EtOAc/Hexanes, 20 mL/min) to give **BDGR 6039** as an off-white solid (23 mg, 0.08 mmol, 22% yield). ^{1}H NMR (400 MHz, $CDCl_3$) δ 11.46 (s, 1H), 7.38 (d, J = 8.3 Hz, 2H), 7.27 (d, J = 8.6 Hz, 4H), 6.68 (d, J = 2.4 Hz, 1H), 6.22 (d,

J = 2.4 Hz, 1H), 5.39 (s, 1H), 4.27 (s, 2H), 1.33 (s, 9H). ^{13}C NMR (101 MHz, $CDCl_3$) δ 157.8, 150.8, 139.0, 134.5, 127.4, 125.8, 116.3, 115.6, 109.3, 47.1, 34.7, 31.5. HPLC Purity ≥ 95%.

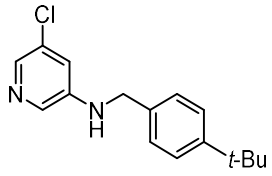

N-(4-(*tert*-butyl)benzyl)-5-chloropyridin-3-amine (**BDGR 6043**).

3-Amino-5-chloropyridine (31 mg, 0.24 mmol) was subjected to procedure D using 4-*tert*-butylbenzyl bromide without base at 85°C for 18 h. The reaction was concentrated and purified by MPLC (4g SiO_2, 0-20% CH_3OH/CH_2Cl_2, 20 mL/min) to give the **BDGR 6043** hydrobromide salt as a tan foam (41 mg, 0.11 mmol, 48% yield). ^{1}H NMR (400 MHz, $CDCl_3$) δ 9.00 (s, 1H), 7.87 (s, 1H), 7.73 (s, 1H), 7.43 (d, *J* = 8.1 Hz, 2H), 7.38 (d, *J* = 8.0 Hz, 2H), 6.98 (s, 2H), 5.63 (s, 2H), 1.25 (s, 9H). ^{13}C NMR (101 MHz, $CDCl_3$) δ ^{13}C NMR (101 MHz, $CDCl_3$) δ 153.6, 149.3, 135.2, 129.4, 129.0, 128.9, 127.7, 126.8, 126.7, 65.3, 34.9, 31.3. HPLC Purity ≥ 95%.

General Procedure E. *Buchwald-Hartwig amination of 3-bromo pyridyl building blocks*.

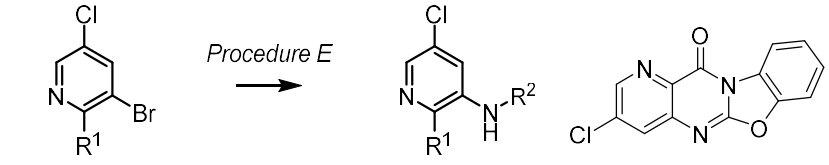

R^1 = CN, CO_2CH_3

4-S7c-j
BDGR 6051

BDGR 6055

To a solution of the corresponding pyridyl bromide (1 equiv.) in CH_3CN, toluene, or dioxane (0.25M) was added $Pd_2(dba)_3$ (5 mol%), XantPhos (10 mol%), and Cs_2CO_3 (1.4 equiv.) before heating to the specified temperature for 5 min. Upon observation of a color change, the corresponding amine (1.1 equiv.) was added and the reaction was stirred and heated at the same

temperature for 18 h. The reaction was then concentrated and purified as indicated to give the title compound.

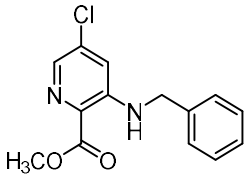

Methyl 3-(benzylamino)-5-chloropicolinate (**4-S7c**).

4-S1d (60 mg, 0.24 mmol) was subjected to procedure E using benzylamine in dioxane at reflux, then purified by MPLC (4g SiO_2, 0-25% EtOAc, 20 mL/min) to give **4-S7c** as an off-white solid (14 mg, 0.05 mmol, 22% yield). ^{1}H NMR (400 MHz, $CDCl_3$) δ 8.25 (t, J = 5.7 Hz, 1H), 7.91 (s, 1H), 7.38 – 7.28 (m, 5H), 7.01 (s, 1H), 4.42 (d, J = 5.6 Hz, 2H), 3.96 (s, 3H).

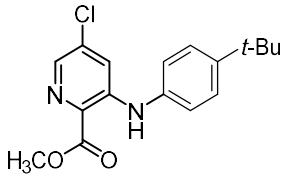

Methyl 3-((4-(*tert*-butyl)phenyl)amino)-5-chloropicolinate (**4-S7d**).

4-S1d (67 mg, 0.27 mmol) was subjected to procedure E using 4-*tert*-butylaniline in CH_3CN at reflux, then purified by MPLC (4g SiO_2, 0-25% EtOAc, 20 mL/min) to give **4-S7d** as an orange semisolid (65 mg, 0.21 mmol, 77% yield). ^{1}H NMR (400 MHz, $CDCl_3$) δ 9.44 (s, 1H), 7.98 (d, J = 2.0 Hz, 1H), 7.47 (d, J = 2.0 Hz, 1H), 7.43 (d, J = 8.7 Hz, 2H), 7.15 (d, J = 8.6 Hz, 2H), 4.00 (s, 3H), 1.35 (s, 9H).

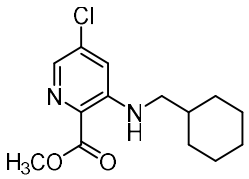

Methyl 5-chloro-3-((cyclohexylmethyl)amino)picolinate (**4-S7e**).

4-S1d (59 mg, 0.23 mmol) was subjected to procedure E using cyclohexylamine in dioxane at reflux, then purified by MPLC (4g SiO_2, 0-10% EtOAc, 20 mL/min) to give **4-S7e** as colorless oil that was used as a crude mixture without further manipulation.

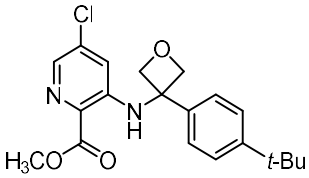

Methyl 3-((3-(4-(*tert*-butyl)phenyl)oxetan-3-yl)amino)-5-chloropicolinate (**4-S7f**).

4-S1d (62 mg, 0.25 mmol) was subjected to procedure E using 3-(4-(*tert*-butyl)phenyl)oxetan-3-amine hydrochloride in toluene at 85°C, then purified by MPLC (4g SiO_2, 0-20% EtOAc, 20 mL/min) to give **4-S7f** as colorless oil (34 mg, 0.09 mmol, 36% yield). ^{1}H NMR (400 MHz, $CDCl_3$) δ 8.76 (s, 1H), 7.92 (d, J = 2.5 Hz, 1H), 7.47 (d, J = 8.8 Hz, 2H), 7.40 (d, J = 8.2 Hz, 2H), 6.15 (d, J = 2.6 Hz, 1H), 4.99 (d, J = 6.7 Hz, 2H), 4.94 (d, J = 6.0 Hz, 2H), 4.01 (s, 3H), 1.31 (s, 9H).

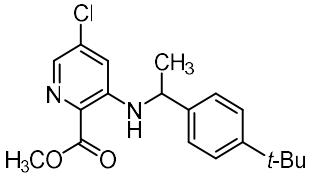

Methyl 3-((1-(4-(*tert*-butyl)phenyl)ethyl)amino)-5-chloropicolinate (**4-S7g**).

4-S1d (59 mg, 0.24 mmol) was subjected to procedure E using 1-(4-(*tert*-butyl)phenyl)ethan-1-amine in toluene at 85°C, then purified by MPLC (4g SiO_2, 0-10% EtOAc, 20 mL/min) to give **4-S7g** as a yellow oil (65 mg, 0.19 mmol, 79% yield). ^{1}H NMR (400 MHz, $CDCl_3$) δ 8.25 (d, J = 6.1 Hz, 1H), 7.84 (d, J = 1.9 Hz, 1H), 7.34 (d, J = 8.3 Hz, 2H), 7.22 (d, J = 8.6 Hz, 2H), 6.86 (d, J = 1.8 Hz, 1H), 4.49 (t, J = 6.6 Hz, 1H), 3.97 (s, 3H), 1.58 (d, J = 6.7 Hz, 3H), 1.29 (s, 9H).

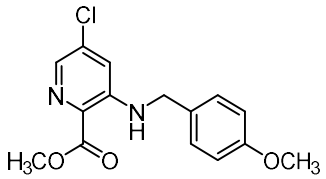

Methyl 5-chloro-3-((4-methoxybenzyl)amino)picolinate (**4-S7h**).

4-S1d (62 mg, 0.25 mmol) was subjected to procedure E using (4-methoxyphenyl)methanamine in toluene at 85°C, then purified by MPLC (4g SiO_2, 0-30% EtOAc, 20 mL/min) to give **4-S7h** as an off-white solid (40 mg, 0.13 mmol, 52% yield). ^{1}H NMR (400 MHz, $CDCl_3$) δ 8.14 (t, J = 5.6 Hz, 1H), 7.89 (d, J = 2.0 Hz, 1H), 7.23 (d, J = 8.7 Hz, 2H), 7.01 (d, J = 2.0 Hz, 1H), 6.88 (d, J = 8.6 Hz, 2H), 4.32 (d, J = 5.4 Hz, 2H), 3.94 (s, 3H), 3.78 (s, 3H).

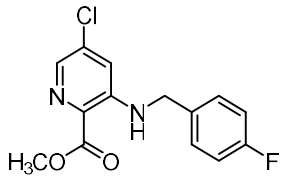

Methyl 5-chloro-3-((4-fluorobenzyl)amino)picolinate (**4-S7i**).

4-S1d (62 mg, 0.25 mmol) was subjected to procedure E using (4-fluorophenyl)methanamine in toluene at 85°C, then purified by MPLC (4g SiO_2, 0-25% EtOAc, 20 mL/min) to give **4-S7i** as an off-white solid (55 mg, 0.19 mmol, 75% yield). ^{1}H NMR (400 MHz, $CDCl_3$) δ 8.23 (t, J = 5.6 Hz, 1H), 7.93 (d, J = 2.0 Hz, 1H), 7.35 – 7.22 (m, 2H), 7.05 (t, J = 8.6 Hz, 2H), 6.99 (d, J = 2.0 Hz, 1H), 4.39 (d, J = 5.6 Hz, 2H), 3.96 (s, 3H).

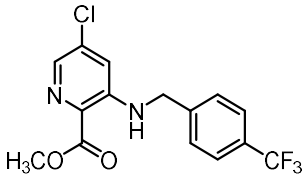

Methyl 5-chloro-3-((4-(trifluoromethyl)benzyl)amino)picolinate (**4-S7j**).

4-S1d (62 mg, 0.25 mmol) was subjected to procedure E using (4-(trifluoromethyl)phenyl)methanamine in toluene at 85°C, then purified by MPLC (4g SiO_2, 0-25% EtOAc, 20 mL/min) to give **4-S7j** as a light yellow solid (62 mg, 0.18 mmol, 72% yield). ^{1}H NMR

(400 MHz, $CDCl_3$) δ ^{1}H NMR (400 MHz, $CDCl_3$) δ 8.34 (d, J = 5.9 Hz, 1H), 7.95 (s, 1H), 7.63 (d, J = 7.9 Hz, 2H), 7.45 (d, J = 7.9 Hz, 2H), 6.95 (s, 1H), 4.51 (d, J = 5.7 Hz, 2H), 3.98 (s, 3H).

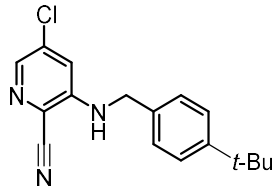

3-((4-(*tert*-Butyl)benzyl)amino)-5-chloropicolinonitrile (**BDGR 6051**).

3-Bromo-5-chloropicolinonitrile (212 mg, 0.98 mmol) was subjected to procedure E using 4-*tert*-butylbenzylamine in CH_3CN, then purified by MPLC (4g SiO_2, 0-5% EtOAc, 20 mL/min) to give **BDGR 6051** as a white solid (44 mg, 0.14 mmol, 14% yield). ^{1}H NMR (400 MHz, $CDCl_3$) δ 7.92 (d, J = 1.9 Hz, 1H), 7.41 (d, J = 8.3 Hz, 2H), 7.26 (d, J = 8.2 Hz, 2H), 7.03 (d, J = 1.9 Hz, 1H), 5.09 (t, J = 5.3 Hz, 1H), 4.37 (d, J = 5.4 Hz, 2H), 1.33 (s, 9H). ^{13}C NMR (101 MHz, $CDCl_3$) δ 151.5, 147.9, 138.3, 136.8, 133.07, 127.3, 126.3, 118.0, 116.9, 115.7, 47.1, 34.8, 31.4. HPLC Purity ≥ 96%.

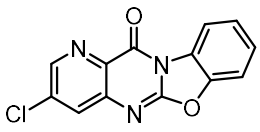

3-Chloro-12*H*-benzo[4,5]oxazolo[3,2-*a*]pyrido[3,2-*d*]pyrimidin-12-one (**BDGR 6055**).

4-S1d (62 mg, 0.25 mmol) was subjected to procedure E using benzo[*d*]oxazol-2-amine in toluene at 85°C, then purified by MPLC (4g SiO_2, 0-30% EtOAc, 20 mL/min) to give **BDGR 6055** as a white solid (23 mg, 35% yield). ^{1}H NMR (400 MHz, $CDCl_3$) δ 8.79 (d, J = 2.2 Hz, 1H), 8.53 (dd, J = 7.6, 1.7 Hz, 1H), 8.09 (d, J = 2.2 Hz, 1H), 7.59 – 7.45 (m, 3H). ^{13}C NMR (101 MHz, $CDCl_3$) δ ^{13}C NMR (101 MHz, $CDCl_3$) δ 156.9, 152.8, 147.7, 145.3, 145.1, 137.1, 134.0, 133.5, 127.6, 126.4, 125.8, 116.6, 111.1. HPLC Purity ≥ 99%.

General Procedure F. Suzuki coupling of (hetero)aryl benzamido bromide esters to give 6-substituted (hetero)aryl benzamido methyl esters.

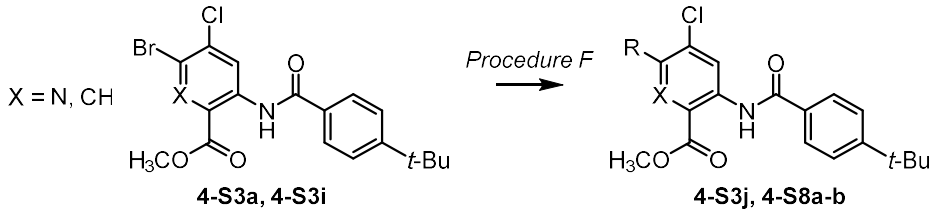

To a G4 microwave vial equipped with stir bar was added the corresponding (hetero)aryl bromide (1 equiv.), corresponding boronic acid (1.2 equiv.), bis(triphenylphosphine)palladium dichloride (0.1 equiv.), and sodium carbonate (1.5 equiv.) before addition of a 10:1 (v/v) CH_3CN/H_2O solution (0.1M). The vessel was sealed and heated at 100-150°C by microwave irradiation with stirring for 30 min. Upon cooling to room temperature, the reaction was diluted with EtOAc (5 mL) and washed with water (2 x 5 mL) and brine (2 x 5 mL). The organic layer was separated and dried over MgSO4 (s), filtered, and concentrated. The resulting crude material was purified as indicated to give the title compound.

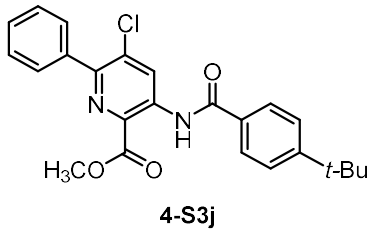

4-S3a (47 mg, 0.11 mmol) was subjected to procedure F using phenylboronic acid (20 mg, 0.16 mmol) at 100°C, then purified by MPLC (4g SiO_2, 0-5% EtOAc, 20 mL/min) to give methyl 3-(4-(tert-butyl)benzamido)-5-chloro-6-phenylpicolinate **4-S3j** as a white solid (31 mg, 0.07 mmol, 67%

yield). ^{1}H NMR (400 MHz, $CDCl_3$) δ 11.95 (s, 1H), 9.54 (s, 1H), 8.00 (d, J = 8.5 Hz, 2H), 7.78-7.76 (m, 2H), 7.58 (d, J = 8.1 Hz, 2H), 7.49-7.41 (m, 3H), 4.04 (s, 3H), 1.38 (s, 9H).

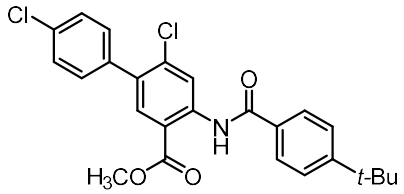

4-S8a

4-S3i (50 mg, 0.12 mmol) was subjected to procedure F using 4-chlorophenylboronic acid (20 mg, 0.14 mmol, 1.2 equiv.) at 150°C, then purified by MPLC (4g SiO_2, 0-2% EtOAc/Hexanes over 10 min, 20 mL/min) to give methyl 4-(4-(*tert*-butyl)benzamido)-4',6-dichloro-[1,1'-biphenyl]-3-carboxylate **4-S8a** (27 mg, 0.07 mmol, 49% yield). Used without analysis.

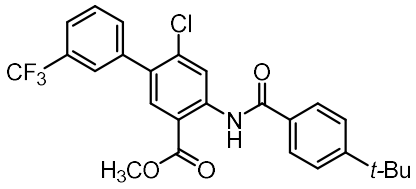

4-S8b

4-S3i (50 mg, 0.12 mmol) was subjected to procedure F using 3-(trifluoromethyl)phenylboronic acid (27 mg, 0.14 mmol, 1.2 equiv.) at 150°C, then purified by MPLC (4g SiO_2, 0-5% EtOAc/Hexanes over 10 min, 20 mL/min) to give methyl 4-(4-(tert-butyl)benzamido)-6-chloro-3'-trifluoromethyl-[1,1'-biphenyl]-3-carboxylate **4-S8b** (35 mg, 0.07 mmol, 61% yield). Used without analysis.

General Procedure G. *Hydrolysis of (hetero)aryl methyl esters to give (hetero)aryl acid compounds*.

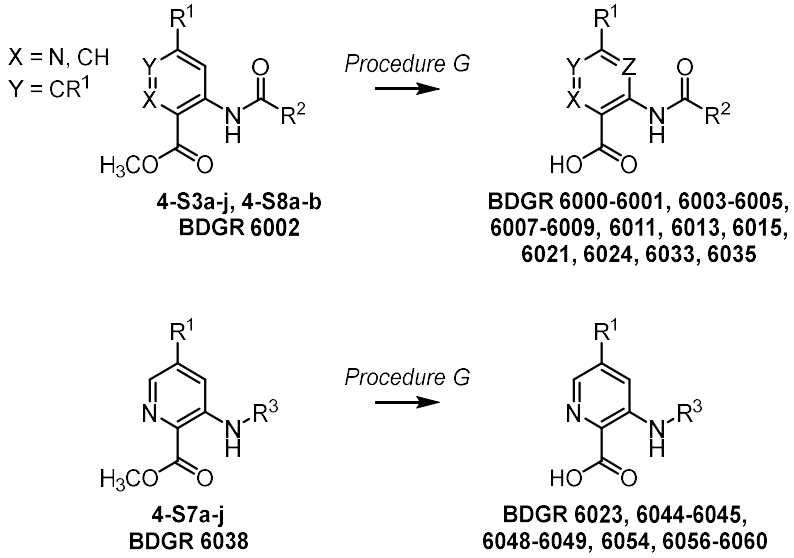

To a 1-dram vial equipped with stir bar was added the corresponding methyl ester (1 equiv.) as a solution in THF (0.1M). 1.3M LiOH (aq) solution (7 equiv.) was added and the solution stirred at rt for 18 h. The reaction mixture was then acidified with 1M HCl (aq) to pH 2 and the resulting precipitate isolated by vacuum filtration to give the title compound.

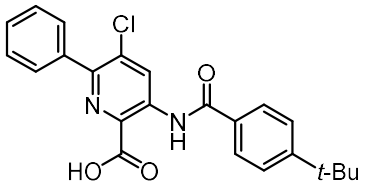

3-(4-(*tert*-Butyl)benzamido)-5-chloro-6-phenylpicolinic acid (**BDGR 6001**).

4-S7j (31 mg, 0.07 mmol) was subjected to procedure G to give **BDGR 6001** as a white solid (21 mg, 0.05 mmol, 70% yield). ^{1}H NMR (400 MHz, DMSO-d_6) δ 11.95 (s, 1H), 9.22 (s, 1H), 7.98-7.83 (m, 2H), 7.73 (d, J = 7.1 Hz, 2H), 7.67-7.62 (m, 2H), 7.55-7.47 (m, 3H), 1.33 (s, 9H). ^{13}C NMR (101 MHz, DMSO-d_6) δ 168.4, 165.3, 155.8, 149.0, 137.2, 136.8, 132.6, 132.5, 130.8, 129.3,

129.1, 128.9, 128.1, 127.1, 126.0, 34.9, 30.9. HRMS (ESI-QTOF) m/z: [M - H]$^-$ Calcd for $C_{23}H_{20}ClN_2O_3^-$ 407.1168; Found: 407.1156. HPLC Purity ≥ 98%.

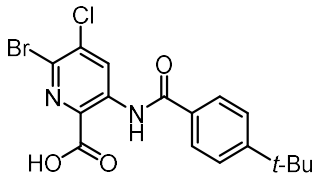

6-Bromo-3-(4-(*tert*-butyl)benzamido)-5-chloropicolinic acid (**BDGR 6005**).

4-S3a (50 mg, 0.12 mmol) was subjected to procedure G to give **BDGR 6005** as a white solid (16 mg, 0.04 mmol, 31% yield). ^{1}H NMR (400 MHz, $CDCl_3$) δ 11.87 (s, 1H), 9.67 (s, 1H), 7.97 (d, J = 8.2 Hz, 2H), 7.56 (d, J = 8.4 Hz, 2H), 1.37 (s, 9H). ^{13}C NMR (126 MHz, $CDCl_3$) δ 166.4, 165.6, 157.1, 149.5, 138.9, 131.9, 131.7, 130.2, 127.6, 126.3, 35.3, 31.2. HRMS (ESI-QTOF) m/z: [M - H]$^-$ Calcd for $C_{17}H_{15}BrClN_2O_3^-$ 410.9939; Found: 410.9930. HPLC Purity ≥ 95%.

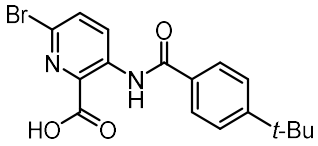

6-Bromo-3-(4-(*tert*-butyl)benzamido)picolinic acid (**BDGR 6009**).

4-S3b (8 mg, 0.02 mmol) was subjected to procedure G to give **BDGR 6009** as a white solid (6 mg, 0.02 mmol, 80% yield). ^{1}H NMR (500 MHz, DMSO-d_6) δ 11.92 (s, 1H), 9.43 (d, J = 9.0 Hz, 1H), 7.97 (d, J = 8.5 Hz, 2H), 7.60 (d, J = 9.0 Hz, 1H), 7.55 (d, J = 8.6 Hz, 2H), 1.36 (s, 9H). ^{13}C NMR (126 MHz, $CDCl_3$) δ 166.4, 156.8, 142.4, 139.2, 138.9, 132.4, 132.0, 130.8, 130.6, 127.6, 126.2, 35.3, 31.2. HRMS (ESI-QTOF) m/z: [M - H]$^-$ Calcd for $C_{17}H_{16}BrN_2O_3^-$ 375.0350; Found: 375.0344. HPLC Purity ≥ 97%.

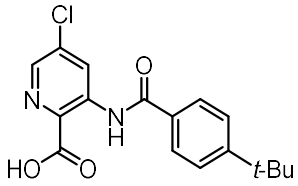

3-(4-(*tert*-Butyl)benzamido)-5-chloropicolinic acid (**BDGR 6000**).

BDGR 6002 (41 mg, 0.12 mmol) was subjected to general procedure G to give **BDGR 6000** as a white solid (36 mg, 0.11 mmol, 92% yield). ^{1}H NMR (500 MHz, $CDCl_3$) δ 11.94 (s, 1H), 9.52 (d, J = 2.1 Hz, 1H), 8.25 (d, J = 2.1 Hz, 1H), 7.98 (d, J = 8.5 Hz, 2H), 7.56 (d, J = 8.5 Hz, 2H), 1.37 (s, 9H). ^{13}C NMR (126 MHz, $CDCl_3$) δ 166.6, 166.5, 156.9, 140.9, 139.9, 138.6, 130.5, 128.6, 128.0, 127.6, 126.2, 35.3, 31.3. HRMS (ESI-QTOF) m/z: [M - H]$^-$ Calcd for $C_{17}H_{16}ClN_2O_3^-$ 331.0855; Found: 331.0844. HPLC Purity ≥ 95%.

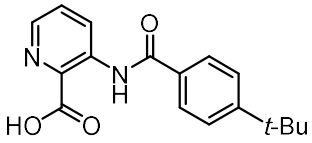

3-(4-(*tert*-Butyl)benzamido)picolinic acid (**BDGR 6013**).

4-S3c (36 mg, 0.12 mmol) was subjected to procedure G to give **BDGR 6013** as a white solid (26 mg, 0.09 mmol, 77% yield).^{1}H NMR (500 MHz, $CDCl_3$) δ 11.97 (s, 1H), 9.43 (d, J = 8.6 Hz, 1H), 8.31 (d, J = 4.4 Hz, 1H), 8.00 (d, J = 8.0 Hz, 2H), 7.65 (dd, J = 8.7, 4.5 Hz, 1H), 7.56 (d, J = 8.0 Hz, 2H), 1.37 (s, 9H). ^{13}C NMR (126 MHz, $CDCl_3$) δ 167.0, 166.6, 156.5, 141.2, 139.8, 130.8, 130.04, 129.95, 129.8, 127.5, 126.1, 35.2, 31.2. HRMS (ESI-QTOF) m/z: [M - H]$^-$ Calcd for $C_{17}H_{17}N_2O_3^-$ 297.1245; Found: 297.1241. HPLC Purity ≥ 97%.

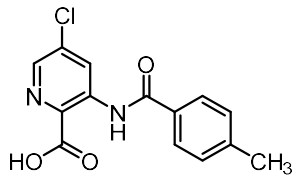

5-Chloro-3-(4-methylbenzamido)picolinic acid (**BDGR 6008**).

4-S3d (20 mg, 0.07 mmol) was subjected to procedure G to give **BDGR 6008** as a white solid (17 mg, 0.06 mmol, 92% yield). ^{1}H NMR (400 MHz, $CDCl_3$) δ 11.94 (s, 1H), 9.52 (d, J = 2.0 Hz, 1H), 8.25 (d, J = 2.1 Hz, 1H), 7.94 (d, J = 7.9 Hz, 2H), 7.34 (d, J = 7.8 Hz, 2H), 2.45 (s, 3H). ^{13}C NMR (126 MHz, $CDCl_3$) δ 166.7, 166.5, 143.9, 140.9, 139.9, 138.6, 130.5, 129.9, 128.6, 128.0, 127.7, 21.8. HRMS (ESI-QTOF) m/z: $[M - H]^-$ Calcd for $C_{14}H_{10}ClN_2O_3^-$ 289.03854; Found: 289.0378. HPLC Purity ≥ 99%.

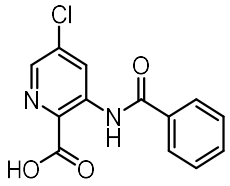

3-Benzamido-5-chloropicolinic acid (**BDGR 6004**).

4-S3e (18 mg, 0.06 mmol) was subjected to procedure G to give **BDGR 6004** as a white solid (16 mg, 0.06 mmol, 93% yield). ^{1}H NMR (400 MHz, $CDCl_3$) δ 11.99 (s, 1H), 9.52 (d, J = 2.0 Hz, 1H), 8.27 (d, J = 2.0 Hz, 1H), 8.11 – 7.97 (m, 2H), 7.76 – 7.45 (m, 3H). ^{13}C NMR (126 MHz, $CDCl_3$) δ 166.7, 166.5, 141.1, 139.8, 138.7, 133.3, 133.1, 129.2, 128.7, 128.1, 127.7. HRMS (ESI-QTOF) m/z: $[M - H]^-$ Calcd for $C_{13}H_8ClN_2O_3^-$ 275.0229; Found: 275.0219. HPLC Purity ≥ 98%.

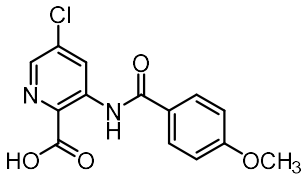

5-Chloro-3-(4-methoxybenzamido)picolinic acid (**BDGR 6003**).

4-S3f (22 mg, 0.07 mmol) was subjected to procedure G to give **BDGR 6003** as a tan solid (14 mg, 0.05 mmol, 67% yield). ^{1}H NMR (400 MHz, $CDCl_3$) δ 11.89 (s, 1H), 9.50 (d, J = 2.1 Hz, 1H),

8.24 (d, J = 2.0 Hz, 1H), 8.02 (d, J = 8.9 Hz, 2H), 7.03 (d, J = 8.8 Hz, 2H), 3.90 (s, 3H). ^{13}C NMR (126 MHz, $CDCl_3$) δ 166.8, 166.0, 163.5, 140.8, 140.0, 138.6, 129.8, 128.5, 127.9, 125.6, 114.5, 55.7. HRMS (ESI-QTOF) m/z: $[M - H]^-$ Calcd for $C_{14}H_{10}ClN_2O_4^-$ 305.0335; Found: 305.0328. HPLC Purity ≥ 95%.

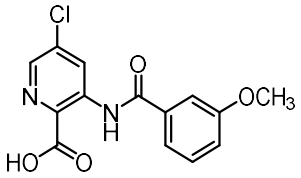

5-Chloro-3-(3-methoxybenzamido)picolinic acid (**BDGR 6007**).

4-S3g (29 mg, 0.09 mmol) was subjected to procedure G to give **BDGR 6007** as an off-white solid (24 mg, 0.08 mmol, 87% yield). ^{1}H NMR (400 MHz, $CDCl_3$) δ 9.50 (d, J = 2.0 Hz, 1H), 8.27 (d, J = 2.0 Hz, 1H), 7.63 – 7.55 (m, 2H), 7.45 (t, J = 8.0 Hz, 1H), 7.15 (dd, J = 8.1, 2.5 Hz, 1H), 3.90 (s, 3H). ^{13}C NMR (126 MHz, $CDCl_3$) δ 166.6, 166.4, 160.3, 141.1, 139.7, 138.7, 134.7, 130.3, 128.6, 128.1, 119.7, 119.6, 112.5, 55.7. HRMS (ESI-QTOF) m/z: $[M - H]^-$ Calcd for $C_{14}H_{10}ClN_2O_4^-$ 305.0335; Found: 305.0326. HPLC Purity ≥ 95%.

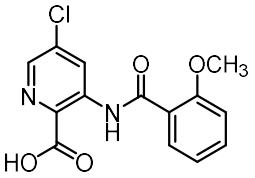

5-Chloro-3-(2-methoxybenzamido)picolinic acid (**BDGR 6011**).

4-S3h (18 mg, 0.06 mmol) was subjected to procedure G to give **BDGR 6011** as a white solid (13 mg, 0.04 mmol, 68% yield). ^{1}H NMR (500 MHz, $CDCl_3$) δ 12.55 (s, 1H), 11.32 (br s, 1H), 9.67 (s, 1H), 8.23 (s, 2H), 8.20 (s, 1H), 7.55 (t, J = 7.8 Hz, 1H), 7.12 (t, J = 7.5 Hz, 1H), 7.06 (d, J = 8.4 Hz, 1H), 4.13 (s, 3H). ^{13}C NMR (126 MHz, $CDCl_3$) δ 165.6, 165.2, 158.1, 140.5, 139.6, 138.1,

134.5, 132.8, 129.9, 128.8, 121.3, 121.1, 111.6, 55.8. HRMS (ESI-QTOF) m/z: $[M - H]^-$ Calcd for $C_{14}H_{10}ClN_2O_4^-$ 305.0335; Found: 305.0322. HPLC Purity ≥ 98%.

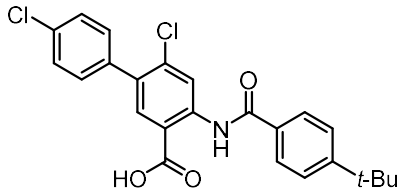

4-(4-(*tert*-Butyl)benzamido)-4',6-dichloro-[1,1'-biphenyl]-3-carboxylic acid (**BDGR 6021**).

4-S8a (27 mg, 0.07 mmol) was subjected to procedure G to give **BDGR 6021** as an off-white solid (19 mg, 0.04 mmol, 57% yield). ^{1}H NMR (400 MHz, DMSO-d_6) δ 12.23 (s, 1H), 8.97 (s, 1H), 8.01 (s, 1H), 7.91 (d, J = 8.5 Hz, 2H), 7.63 (d, J = 8.6 Hz, 2H), 7.58 – 7.48 (m, 4H), 1.33 (s, 9H). ^{13}C NMR (101 MHz, DMSO-d_6) δ 169.1, 164.8, 155.6, 141.2, 136.7, 136.3, 133.5, 132.9, 132.7, 131.2, 131.1, 128.4, 127.0, 125.9, 120.4, 115.7, 34.8, 30.8. HRMS (ESI-QTOF) m/z: $[M - H]^-$ Calcd for $C_{24}H_{20}Cl_2NO_3^-$ 440.0826; Found: 440.0818. HPLC Purity ≥ 96%.

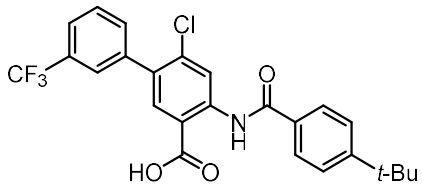

4-(4-(*tert*-Butyl)benzamido)-6-chloro-3'-(trifluoromethyl)-[1,1'-biphenyl]-3-carboxylic acid (**BDGR 6024**).

4-S8b (35 mg, 0.07 mmol) was subjected to procedure G to give **BDGR 6024** as an off-white solid (26 mg, 0.06 mmol, 86% yield). ^{1}H NMR (400 MHz, Acetone -d_6) δ 12.36 (s, 1H), 9.23 (s, 1H), 8.21 (s, 1H), 7.99 (d, J = 8.3 Hz, 2H), 7.88 – 7.70 (m, 4H), 7.65 (d, J = 8.2 Hz, 2H), 1.37 (s, 9H). ^{13}C NMR (101 MHz, Acetone -d_6) δ 165.1, 165.0, 155.9, 142.6, 142.4, 139.2, 137.9, 133.9, 133.4, 132.7, 131.6 (d, J = 5.1 Hz), 130.1 (d, J = 32.2 Hz), 129.3, 127.2, 126.1 (q, J = 3.9 Hz), 125.9,

124.6 (q, J = 4.1 Hz), 124.3 (d, J = 271.6 Hz) 120.6 (d, J = 5.3 Hz), 34.7, 30.5. HRMS (ESI-QTOF) m/z: [M - H]$^-$ Calcd for $C_{25}H_{20}ClF_3NO_3^-$ 474.1089; Found: 474.1084. HPLC Purity ≥ 95%.

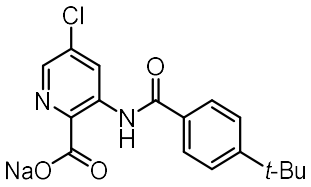

Sodium 3-(4-(*tert*-butyl)benzamido)-5-chloropicolinate (**BDGR 6015**).

To a solution of **BDGR 6002** (1.0 g, 2.9 mmol, 1 equiv.) in THF (25 mL) was added 1M NaOH (aq) (2.9 mL, 1 equiv.) and stirred at rt for 18 h. The reaction was then concentrated to give **BDGR 6015** as a white solid (1.0 g, 2.8 mmol, 97% yield). ^{1}H NMR (400 MHz, DMSO-d_6) δ 15.64 (s, 1H), 9.11 (d, J = 2.4 Hz, 1H), 8.21 (d, J = 2.3 Hz, 1H), 7.94 (d, J = 8.5 Hz, 2H), 7.58 (d, J = 8.5 Hz, 2H), 1.33 (s, 9H). ^{13}C NMR (126 MHz, DMSO-d_6) δ 167.6, 165.3, 155.0, 140.2, 140.1, 138.3, 131.7, 131.1, 127.1, 125.6, 125.1, 34.7, 30.9. HRMS (ESI-QTOF) m/z: [M - H]$^-$ Calcd for $C_{17}H_{16}ClN_2O_3^-$ 331.0855; Found: 331.0846. HPLC Purity ≥ 96%.

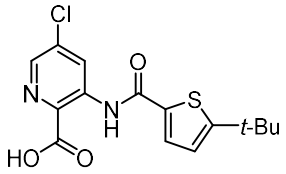

3-(5-(*tert*-Butyl)thiophene-2-carboxamido)-5-chloropicolinic acid (**BDGR 6033**).

BDGR 6032 (21 mg, 0.06 mmol) was subjected to procedure G to give **BDGR 6033** as a yellow solid (17 mg, 0.05 mmol, 82% yield). ^{1}H NMR (400 MHz, DMSO) δ 11.78 (s, 1H), 9.40 (d, J = 0.9 Hz, 1H), 8.24 (s, 1H), 7.66 (d, J = 2.4 Hz, 1H), 6.92 (d, J = 2.4 Hz, 1H), 1.43 (s, 9H). ^{13}C NMR (101 MHz, DMSO) δ 166.7, 166.5, 161.3, 140.8, 139.8, 138.6, 134.8, 130.1, 128.4, 127.7, 123.2, 35.4, 32.4. HPLC Purity ≥ 97%.

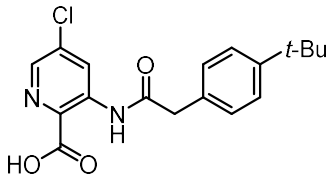

3-(2-(4-(*tert*-Butyl)phenyl)acetamido)-5-chloropicolinic acid (**BDGR 6035**).

BDGR 6034 (20 mg, 0.06 mmol) was subjected to procedure G to give **BDGR 6035** as an off-white solid (11 mg, 0.03 mmol, 57% yield). ^{1}H NMR (400 MHz, DMSO) δ 11.03 (s, 1H), 9.30 (d, J = 2.0 Hz, 1H), 8.19 (d, J = 2.1 Hz, 1H), 7.41 (d, J = 7.8 Hz, 2H), 7.30 (d, J = 8.0 Hz, 2H), 3.76 (s, 2H), 1.32 (s, 9H). ^{13}C NMR (101 MHz, DMSO) δ 171.5, 166.0, 150.9, 140.9, 139.3, 138.4, 130.3, 129.2, 128.6, 127.9, 126.2, 45.3, 34.7, 31.5. HPLC Purity ≥ 96%.

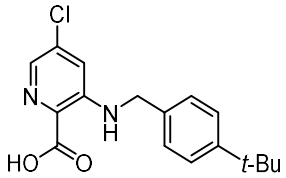

3-((4-(*tert*-Butyl)benzyl)amino)-5-chloropicolinic acid (**BDGR 6023**).

BDGR 6038 (42 mg, 0.13 mmol) was subjected to procedure G to give **BDGR 6023** as a white solid (34 mg, 0.11 mmol, 84% yield). ^{1}H NMR (400 MHz, DMSO) δ 9.90 (t, J = 5.8 Hz, 1H), 7.58 (s, 1H), 7.37 (d, J = 7.9 Hz, 2H), 7.26 (d, J = 8.0 Hz, 2H), 7.04 (s, 1H), 4.33 (d, J = 5.8 Hz, 2H), 1.27 (s, 9H). ^{13}C NMR (126 MHz, DMSO) δ 170.0, 149.9, 147.5, 136.7, 136.3, 132.8, 131.8, 127.4, 125.8, 117.5, 45.7, 34.7, 31.7. HPLC Purity ≥ 97%.

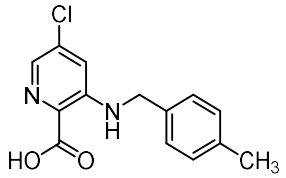

5-Chloro-3-((4-methylbenzyl)amino)picolinic acid (**BDGR 6044**).

4-S7a (42 mg, 0.13 mmol) was subjected to procedure G to give **BDGR 6044** as a white solid (5 mg, 0.02 mmol, 38% yield). ^{1}H NMR (400 MHz, DMSO) δ 8.23 (s, 1H), 7.74 (s, 1H), 7.18 (q, J = 7.9 Hz, 4H), 7.04 (s, 1H), 4.41 (d, J = 5.7 Hz, 2H), 2.35 (s, 3H). ^{13}C NMR (101 MHz, DMSO) δ 166.9, 147.5, 137.9, 137.7, 134.0, 133.8, 129.8, 127.0, 124.6, 119.6, 46.4, 21.3. HPLC Purity ≥ 95%.

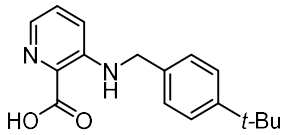

3-((4-(*tert*-Butyl)benzyl)amino)picolinic acid (**BDGR 6045**).

4-S7b (53 mg, 0.18 mmol) was subjected to procedure G to give **BDGR 6045** as a pale yellow solid (41 mg, 0.14 mmol, 80% yield). ^{1}H NMR (400 MHz, DMSO) δ 8.22 (s, 1H), 7.82 (d, J = 4.3 Hz, 1H), 7.36 (d, J = 8.1 Hz, 2H), 7.32 – 7.20 (m, 4H), 7.08 (d, J = 8.6 Hz, 1H), 4.44 (d, J = 5.8 Hz, 2H), 1.31 (s, 9H). ^{13}C NMR (101 MHz, $CDCl_3$) δ 166.6, 150.6, 147.5, 134.4, 132.3, 128.9, 127.0, 126.8, 125.9, 122.1, 46.3, 34.6, 31.5. HPLC Purity ≥ 97%.

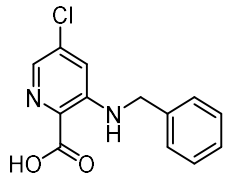

3-(Benzylamino)-5-chloropicolinic acid (**BDGR 6048**).

4-S7c (14 mg, 0.05 mmol) was subjected to procedure G to give **BDGR 6048** as an off-white solid (10 mg, 0.04 mmol, 78% yield). ^{1}H NMR (400 MHz, $CDCl_3$) δ 8.27 (s, 1H), 7.75 (s, 1H), 7.47 – 7.23 (m, 5H), 7.04 (s, 1H), 4.46 (s, 2H). ^{13}C NMR (101 MHz, $CDCl_3$) δ 166.9, 147.5, 138.0, 136.9, 134.1, 129.2, 127.9, 127.0, 124.6, 119.6, 46.6. HPLC Purity ≥ 99%.

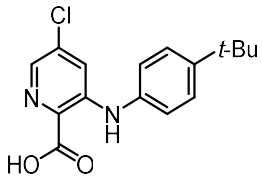

3-((4-(*tert*-Butyl)phenyl)amino)-5-chloropicolinic acid (**BDGR 6049**).

4-S7d (58 mg, 0.18 mmol) was subjected to procedure G to give **BDGR 6049** as a yellow solid (43 mg, 0.14 mmol, 78% yield). ^{1}H NMR (400 MHz, $CDCl_3$) δ 9.43 (s, 1H), 7.82 (s, 1H), 7.50 (s, 1H), 7.43 (d, J = 6.6 Hz, 2H), 7.16 (d, J = 5.3 Hz, 2H), 1.35 (s, 9H). ^{13}C NMR (101 MHz, $CDCl_3$) δ 166.9, 149.3, 145.9, 137.8, 135.5, 135.2, 126.9, 124.7, 123.9, 120.9, 34.7, 31.5. HPLC Purity ≥ 99%.

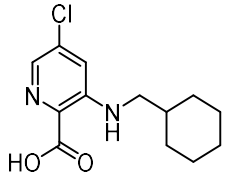

5-Chloro-3-((cyclohexylmethyl)amino)picolinic acid (**BDGR 6054**).

4-S7e (14 mg, 0.05 mmol) was subjected to procedure G to give **BDGR 6054** as an off-white solid (10 mg, 0.04 mmol, 78% yield). ^{1}H NMR (400 MHz, DMSO-d_6) δ 9.56 (t, J = 5.2 Hz, 1H), 7.51 (s, 1H), 7.00 (s, 1H), 2.93 (t, J = 6.1 Hz, 2H), 1.86 – 1.47 (m, 6H), 1.30 – 1.08 (m, 3H), 1.05 – 0.91 (m, 2H). ^{13}C NMR (126 MHz, DMSO-d6) δ 169.7, 147.7, 132.5, 131.0, 116.4, 48.7, 37.5, 31.1, 26.6, 26.0. HPLC Purity ≥ 95%.

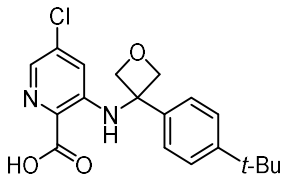

3-((3-(4-(*tert*-Butyl)phenyl)oxetan-3-yl)amino)-5-chloropicolinic acid (**BDGR 6056**).

4-S7f (34 mg, 0.09 mmol) was subjected to procedure G to give **BDGR 6056** as a white solid (24 mg, 0.07 mmol, 74% yield). ^{1}H NMR (400 MHz, DMSO-d$_6$) δ 8.90 (s, 1H), 7.90 (d, J = 1.9 Hz, 1H), 7.49 (d, J = 8.5 Hz, 2H), 7.44 (d, J = 8.4 Hz, 2H), 6.19 (d, J = 2.0 Hz, 1H), 4.94 (d, J = 6.6 Hz, 2H), 4.85 (d, J = 6.6 Hz, 2H), 1.27 (s, 9H). ^{13}C NMR (101 MHz, DMSO-d$_6$) δ 169.0, 150.5, 145.5, 137.9, 135.1, 135.0, 127.8, 126.2, 125.4, 119.5, 82.6, 59.3, 34.7, 31.6. HPLC Purity ≥ 95%.

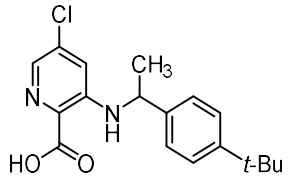

3-((1-(4-(*tert*-Butyl)phenyl)ethyl)amino)-5-chloropicolinic acid (**BDGR 6057**).

4-S7g (65 mg, 0.19 mmol) was subjected to procedure G to give **BDGR 6057** as an off-white solid (45 mg, 0.13 mmol, 71% yield). ^{1}H NMR (400 MHz, DMSO-d$_6$) δ 8.36 (d, J = 7.2 Hz, 1H), 7.82 (d, J = 1.9 Hz, 1H), 7.37 (d, J = 8.0 Hz, 2H), 7.29 (d, J = 8.1 Hz, 2H), 7.17 (d, J = 1.9 Hz, 1H), 4.79 (p, J = 6.8 Hz, 1H), 1.47 (d, J = 6.6 Hz, 3H), 1.25 (s, 9H). ^{13}C NMR (101 MHz, DMSO-d$_6$) δ 168.7, 149.5, 146.8, 140.6, 135.3, 133.7, 126.0, 125.5, 125.4, 119.3, 50.6, 34.2, 31.1, 24.1. HPLC Purity ≥ 96%.

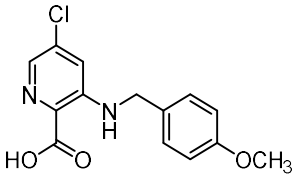

5-Chloro-3-((4-methoxybenzyl)amino)picolinic acid (**BDGR 6058**).

4-S7h (21 mg, 0.07 mmol) was subjected to procedure G to give **BDGR 6058** as a white solid (12 mg, 0.04 mmol, 63% yield). ^{1}H NMR (400 MHz, DMSO-d$_6$) δ 8.28 (t, J = 5.8 Hz, 1H), 7.84 (d, J = 2.0 Hz, 1H), 7.33 – 7.24 (m, 2H), 6.92 (d, J = 8.6 Hz, 2H), 4.42 (d, J = 5.0 Hz, 2H), 3.73 (s, 3H).

^{13}C NMR (101 MHz, DMSO-d$_6$) δ 168.4, 158.5, 147.5, 135.4, 133.5, 129.9, 128.5, 126.0, 118.8, 114.0, 55.0, 44.8. HPLC Purity ≥ 95%.

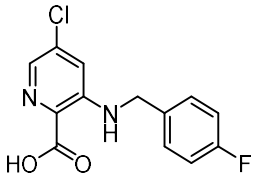

5-Chloro-3-((4-fluorobenzyl)amino)picolinic acid (**BDGR 6059**).

4-S7i (25 mg, 0.08 mmol) was subjected to procedure G to give **BDGR 6059** as an off-white solid (16 mg, 0.05 mmol, 69% yield). ^{1}H NMR (400 MHz, DMSO-d$_6$) δ 8.37 (t, J = 6.0 Hz, 1H), 7.85 (d, J = 1.9 Hz, 1H), 7.39 (dd, J = 8.4, 5.6 Hz, 2H), 7.28 (d, J = 2.0 Hz, 1H), 7.18 (t, J = 8.8 Hz, 2H), 4.51 (d, J = 5.6 Hz, 2H). ^{19}F NMR (376 MHz, DMSO-d$_6$) δ -115.59. ^{13}C NMR (101 MHz, DMSO-d$_6$) δ 168.9, 161.8 (d, J = 242.8 Hz), 147.9, 135.9, 134.9 (d, J = 2.9 Hz), 134.1, 129.6 (d, J = 8.3 Hz), 126.7, 119.3, 115.9 (d, J = 21.5 Hz), 45.0. HPLC Purity ≥ 95%.

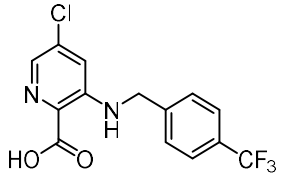

5-Chloro-3-((4-(trifluoromethyl)benzyl)amino)picolinic acid (**BDGR 6060**).

4-S7j (30 mg, 0.09 mmol) was subjected to procedure G to give **BDGR 6060** as a yellow solid (11 mg, 0.07 mmol, 75% yield). ^{1}H NMR (400 MHz, DMSO-d$_6$) δ 8.49 (t, J = 6.3 Hz, 1H), 7.86 (d, J = 2.1 Hz, 1H), 7.72 (d, J = 8.0 Hz, 2H), 7.55 (d, J = 8.0 Hz, 2H), 7.25 (d, J = 2.2 Hz, 1H), 4.66 (d, J = 6.0 Hz, 2H). ^{19}F NMR (376 MHz, DMSO-d$_6$) δ -60.83. ^{13}C NMR (101 MHz, DMSO-d$_6$) δ 168.4, 147.4, 143.5, 135.4, 133.9, 127.73 (q, J = 31.8 Hz), 127.68, 126.4, 125.5 (q, J = 3.5 Hz), 124.3 (d, J = 271.9 Hz), 118.8, 44.7. HPLC Purity ≥ 97%.

General Procedure H: *Peptide couplings to produce alternatively linked pyridyl species*.

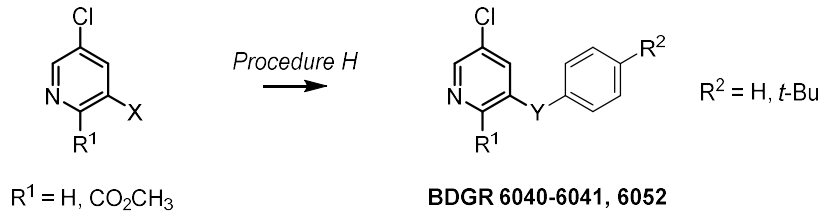

To a solution of the corresponding pyridyl compound (1.0 equiv) in CH_2Cl_2 (0.05M) was added the substituted phenyl compound (1.2 equiv), EDC*HCl (1.5 equiv), and HOBt or DMAP (1.5 equiv) before stirring at rt for the indicated time. The reaction was concentrated and purified as indicated to give the title compound.

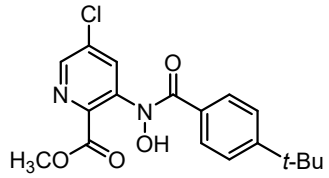

Methyl 3-(4-(*tert*-butyl)-*N*-hydroxybenzamido)-5-chloropicolinate (**BDGR 6040**).

Methyl 5-chloro-3-(hydroxyamino)picolinate (32 mg, 0.16 mmol) was subjected to procedure H using 4-*tert*-butylbenzoic acid and HOBt for 18 h and purified by MPLC (4g SiO_2, 0-10% EtOAc/Hexanes, 20 mL/min) to give **BDGR 6040** as a white solid (40 mg, 0.11 mmol, 69% yield). ^{1}H NMR (400 MHz, $CDCl_3$) δ 11.31 (s, 1H), 8.25 (d, J = 2.1 Hz, 1H), 8.06 (d, J = 8.5 Hz, 2H), 7.61 (d, J = 2.1 Hz, 1H), 7.55 (d, J = 8.5 Hz, 2H), 4.05 (s, 3H), 1.37 (s, 9H). ^{13}C NMR (101 MHz, $CDCl_3$) δ 166.6, 165.4, 158.5, 147.6, 141.1, 137.0, 129.8, 128.1, 126.1, 124.2, 122.9, 53.3, 35.5, 31.2. HPLC Purity ≥ 94%.

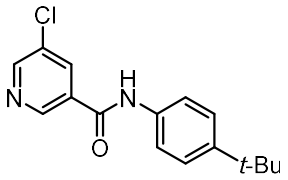

N-(4-(*tert*-butyl)phenyl)-5-chloronicotinamide (**BDGR 6041**).

5-Chloronicotinic acid (41 mg, 0.26 mmol) was subjected to procedure H using 4-*tert*-butylaniline and DMAP for 5 h and purified by MPLC (4g SiO_2, 0-25% EtOAc/Hexanes, 20 mL/min) to give **BDGR 6041** as a white solid (62 mg, 0.20 mmol, 82% yield). ^{1}H NMR (400 MHz, $CDCl_3$) δ 8.93 (d, J = 1.8 Hz, 1H), 8.72 (d, J = 2.4 Hz, 1H), 8.18 (t, J = 2.1 Hz, 1H), 7.87 (s, 1H), 7.53 (d, J = 8.3 Hz, 2H), 7.40 (d, J = 8.6 Hz, 2H), 1.33 (s, 9H). ^{13}C NMR (101 MHz, $CDCl_3$) δ 162.5, 151.6, 148.7, 145.5, 135.2, 134.6, 132.8, 132.0, 126.2, 120.5, 34.7, 31.5. HPLC Purity ≥ 97%.

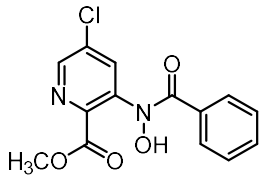

Methyl 5-chloro-3-(*N*-hydroxybenzamido)picolinate (**BDGR 6052**).

Methyl 5-chloro-3-(hydroxyamino)picolinate (7 mg, 0.04 mmol) was subjected to procedure H using benzoic acid and HOBt for 18 h and purified by MPLC (4g SiO_2, 0-10% EtOAc/Hexanes, 20 mL/min) to give **BDGR 6052** as a white solid (6 mg, 0.02 mmol, 58% yield). ^{1}H NMR (400 MHz, $CDCl_3$) δ 11.37 (s, 1H), 8.26 (s, 0H), 8.13 (d, J = 7.2 Hz, 2H), 7.75 – 7.46 (m, 4H), 4.05 (s, 2H). ^{13}C NMR (101 MHz, $CDCl_3$) δ 166.6, 165.4, 147.4, 141.2, 137.0, 134.4, 129.9, 129.1, 128.1, 127.1, 123.0, 53.3. HPLC Purity ≥ 97%.

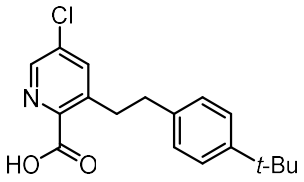

3-(4-(*tert*-Butyl)phenethyl)-5-chloropicolinic acid (**BDGR 6047**).

To a solution of diisopropylamine (0.21 mL, 1.5 mmol, 1.5 equiv) in dry THF (5 mL) at -78°C was added *n*-butyllithium (2.5M solution in hexanes, 0.65 mL, 1.6 mmol, 1.6 equiv.) and stirred 1 minute before addition of a solution of 5-chloro-3-methylpicolinic acid (168 mg, 0.98 mmol, 1.0 equiv.) and Et_3N (0.14 mL, 1.0 mmol, 1.0 equiv.) in dry THF (5 mL). To the resulting indigo colored solution was added 4-*tert*-butylbenzyl bromide (0.18 mL, 0.98 mmol, 1.0 equiv) and the reaction was stirred and warmed to rt over 18 h. The reaction was quenched with a solution of acetyl chloride (0.14 mL) in ethanol (3 mL) and then filtered to collect a white solid. This crude material was dissolved in EtOAc, washed with 1M HCl (aq) (2 x 20 mL), brine (1 x 20 mL), and dried over $MgSO_4$ (s) before purifying by MPLC (4g SiO_2, 0-10% CH_3OH/CH_2Cl_2, 20 mL/min) to give **BDGR 6047** as a white solid (186 mg, 0.59 mmol, 60% yield). ^{1}H NMR (400 MHz, $CDCl_3$) δ 8.41 (d, J = 2.2 Hz, 1H), 7.55 (d, J = 2.2 Hz, 1H), 7.32 (d, J = 8.3 Hz, 2H), 7.15 (d, J = 8.3 Hz, 2H), 3.53 – 3.39 (m, 2H), 2.96 – 2.87 (m, 2H), 1.32 (s, 9H). ^{13}C NMR (101 MHz, $CDCl_3$) δ 163.3, 149.4, 144.7, 142.7, 141.2, 140.6, 137.6, 136.3, 128.4, 125.5, 36.3, 35.3, 34.6, 31.5. HPLC Purity ≥ 96%.

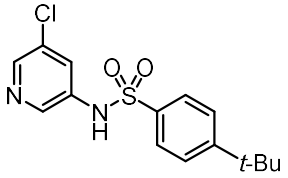

4-(*tert*-Butyl)-*N*-(5-chloropyridin-3-yl)benzenesulfonamide (**BDGR 6050**).

To a solution of 3-bromo-5-chloropyridine (56 mg, 0.29 mmol, 1.2 equiv.) in CH_3CN (3 mL) was added 4-*tert*-butylbenzenesulfonamide (43 mg, 0.20 mmol, 1.0 equiv) and K_2CO_3 (81 mg, 0.59 mmol, 2.5 equiv) before sparging with N_2 (g) for 5 min. To the sparged reaction mixture was added CuI (5 mg, 10 mol%) and 1,2-dimethylethylenediamine (0.01 mL, 0.5 equiv.) and the reaction as heated to 130°C for 15 min by microwave irradiation. The reaction was filtered and then purified by MPLC (4g SiO_2, 0-10% EtOAc/CH_2Cl_2, 20 mL/min) to give **BDGR 6050** as a white solid (40 mg, 0.12 mmol, 61% yield). ^{1}H NMR (400 MHz, DMSO-d_6) δ 10.88 (s, 1H), 8.30 (d, J = 2.0 Hz, 1H), 8.26 (d, J = 2.1 Hz, 1H), 7.74 (d, J = 8.5 Hz, 2H), 7.62 (d, J = 8.3 Hz, 2H), 7.56 (d, J = 2.1 Hz, 1H), 1.26 (s, 9H). ^{13}C NMR (101 MHz, DMSO-d_6) δ 156.5, 143.2, 139.0, 136.1, 135.6, 130.9, 126.5, 126.5, 125.7, 34.9, 30.7. HPLC Purity ≥ 99%.

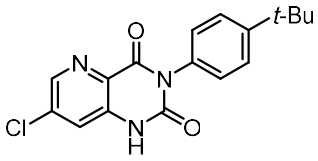

3-(4-(*tert*-Butyl)phenyl)-7-chloropyrido[3,2-*d*]pyrimidine-2,4(1*H*,3*H*)-dione (**BDGR 6053**).

To a solution of **4-S1a** (44 mg, 0.23 mmol, 1 equiv.) in CH_2Cl_2 (2.5 mL) was added Et_3N (0.10 mL, 0.72 mmol, 3.0 equiv.) followed by phosgene (15 wt% solution in toluene, 0.18 mL, 0.25 mmol, 1.0 equiv.). The reaction mixture was stirred 20 min at rt, then 4-*tert*-butylaniline (0.04 mL, 0.25 mmol, 1.0 equiv.) was added and the reaction was stirred at rt for 18 h. The reaction was diluted with hexanes (2.5 mL) and filtered to collect an off-white solid, which was purified by MPLC (4g SiO_2, 25-50% EtOAc/Hexanes, 20 mL/min) to give **BDGR 6053** as a white solid (16 mg, 0.04 mmol, 16% yield). ^{1}H NMR (400 MHz, DMSO-d_6) δ 11.74 (s, 1H), 8.53 (d, J = 2.9 Hz, 1H), 7.67 (d, J = 3.0 Hz, 1H), 7.51 (d, J = 8.1 Hz, 2H), 7.24 (d, J = 8.1 Hz, 2H), 1.35 (s, 9H). ^{13}C

NMR (101 MHz, DMSO-d_6) δ 160.7, 151.1, 150.2, 143.6, 138.2, 135.7, 133.4, 130.7, 128.8, 126.2, 122.9, 34.9, 31.6. HPLC Purity ≥ 97%.

References

(1) Khalifa, M. M.; Martorelli Di Genova, B.; McAlpine, S. G.; Rozema, S. D.; Monaghan, N. P.; Morris, J. C.; Knoll, L., J.; Golden, J. E. Dual Stage Picolinic Acid Derived Inhibitors of Toxoplasma Gondii, *Submitted*, 2020.

(2) Milanes, J. E.; Suryadi, J.; Abendroth, J.; Voorhis, W. C. V.; Barrett, K. F.; Dranow, D. M.; Phan, I. Q.; Patrick, S. L.; Rozema, S. D.; Khalifa, M. M.; Golden, J. E.; Morris, J. C. Enzymatic and Structural Characterization of the Naegleria Fowleri Glucokinase. *Antimicrob. Agents Chemother.* **2019**, *63* (5). https://doi.org/10.1128/AAC.02410-18.

(3) Dubey, J. P.; Lindsay, D. S.; Speer, C. A. Structures of Toxoplasma Gondi Tachyzoites, Bradyzoites, and Sporozoites and Biology and Development of Tissue Cysts. *Clin. Microbiol. Rev.* **1998**, *11* (2), 267–299. https://doi.org/10.1128/CMR.11.2.267.

(4) Flaherty, D. P.; Harris, M. T.; Schroeder, C. E.; Khan, H.; Kahney, E. W.; Hackler, A. L.; Patrick, S. L.; Weiner, W. S.; Aubé, J.; Sharlow, E. R.; Morris, J. C.; Golden, J. E. Optimization and Evaluation of Antiparasitic Benzamidobenzoic Acids as Inhibitors of Kinetoplastid Hexokinase 1. *ChemMedChem* **2017**, *12* (23), 1994–2005. https://doi.org/10.1002/cmdc.201700592.

(5) van Griensven, J.; Diro, E. Visceral Leishmaniasis. *Infect. Dis. Clin. North Am.* **2012**, *26* (2), 309–322. https://doi.org/10.1016/j.idc.2012.03.005.

(6) Sharlow, E.; Golden, J. E.; Dodson, H.; Morris, M.; Hesser, M.; Lyda, T.; Leimgruber, S.; Schroeder, C. E.; Flaherty, D. P.; Weiner, W. S.; Simpson, D.; Lazo, J. S.; Aubé, J.; Morris, J. C. Identification of Inhibitors of Trypanosoma Brucei Hexokinases. In *Probe Reports from the NIH Molecular Libraries Program*; National Center for Biotechnology Information (US): Bethesda (MD), 2010.

(7) Sharlow, E. R.; Lyda, T. A.; Dodson, H. C.; Mustata, G.; Morris, M. T.; Leimgruber, S. S.; Lee, K.-H.; Kashiwada, Y.; Close, D.; Lazo, J. S.; Morris, J. C. A Target-Based High Throughput Screen Yields Trypanosoma Brucei Hexokinase Small Molecule Inhibitors with Antiparasitic Activity. *PLoS Negl. Trop. Dis.* **2010**, *4* (4), e659. https://doi.org/10.1371/journal.pntd.0000659.

(8) Jones, A. J.; Avery, V. M. Future Treatment Options for Human African Trypanosomiasis. *Expert Rev. Anti Infect. Ther.* **2015**, *13* (12), 1429–1432. https://doi.org/10.1586/14787210.2015.1094374.

(9) Umasankar, P. K.; Jayakumar, P. C.; Shouche, Y. S.; Patole, M. S. Molecular Characterization of the Hexokinase Gene From Leishmania Major. *J. Parasitol.* **2005**, *91* (6), 1504–1509. https://doi.org/10.1645/GE-502R1.1.

(10) de Menezes, J. P. B.; Guedes, C. E. S.; Petersen, A. L. de O. A.; Fraga, D. B. M.; Veras, P. S. T. Advances in Development of New Treatment for Leishmaniasis https://www.hindawi.com/journals/bmri/2015/815023/ (accessed May 20, 2020). https://doi.org/10.1155/2015/815023.

(11) Singh, B.; Bernatchez, J. A.; McCall, L.-I.; Calvet, C. M.; Ackermann, J.; Souza, J. M.; Thomas, D.; Silva, E. M.; Bachovchin, K. A.; Klug, D. M.; Jalani, H. B.; Bag, S.; Buskes, M. J.; Leed, S. E.; Roncal, N. E.; Penn, E. C.; Erath, J.; Rodriguez, A.; Sciotti, R. J.; Campbell, R. F.; McKerrow, J.; Siqueira-Neto, J. L.; Ferrins, L.; Pollastri, M. P. Scaffold and Parasite Hopping: Discovery of New Protozoal Proliferation Inhibitors. *ACS Med. Chem. Lett.* **2020**, *11* (3), 249–257. https://doi.org/10.1021/acsmedchemlett.9b00453.

(12) Klug, D. M.; Gelb, M. H.; Pollastri, M. P. Repurposing Strategies for Tropical Disease Drug Discovery. *Bioorg. Med. Chem. Lett.* **2016**, *26* (11), 2569–2576. https://doi.org/10.1016/j.bmcl.2016.03.103.

(13) Talevi, A.; Bellera, C. L. Challenges and Opportunities with Drug Repurposing: Finding Strategies to Find Alternative Uses of Therapeutics. *Expert Opin. Drug Discov.* **2020**, *15* (4), 397–401. https://doi.org/10.1080/17460441.2020.1704729.

(14) Alrajhi, A. A.; Ibrahim, E. A.; De Vol, E. B.; Khairat, M.; Faris, R. M.; Maguire, J. H. Fluconazole for the Treatment of Cutaneous Leishmaniasis Caused by Leishmania Major. *N. Engl. J. Med.* **2002**, *346* (12), 891–895. https://doi.org/10.1056/NEJMoa011882.

(15) Bakker, B. M.; Michels, P. A. M.; Opperdoes, F. R.; Westerhoff, H. V. Glycolysis in Bloodstream Form Trypanosoma Brucei Can Be Understood in Terms of the Kinetics of the Glycolytic Enzymes. *J. Biol. Chem.* **1997**, *272* (6), 3207–3215. https://doi.org/10.1074/jbc.272.6.3207.

(16) Lin, S.; Morris, M. T.; Ackroyd, P. C.; Morris, J. C.; Christensen, K. A. Peptide-Targeted Delivery of a PH Sensor for Quantitative Measurements of Intraglycosomal PH in Live Trypanosoma Brucei. *Biochemistry* **2013**, *52* (21), 3629–3637. https://doi.org/10.1021/bi400029m.

(17) Kazmi, F.; Hensley, T.; Pope, C.; Funk, R. S.; Loewen, G. J.; Buckley, D. B.; Parkinson, A. Lysosomal Sequestration (Trapping) of Lipophilic Amine (Cationic Amphiphilic) Drugs in Immortalized Human Hepatocytes (Fa2N-4 Cells). *Drug Metab. Dispos.* **2013**, *41* (4), 897–905. https://doi.org/10.1124/dmd.112.050054.

(18) Duvvuri, M.; Krise, J. P. A Novel Assay Reveals That Weakly Basic Model Compounds Concentrate in Lysosomes to an Extent Greater Than PH-Partitioning Theory Would Predict. *Mol. Pharm.* **2005**, *2* (6), 440–448. https://doi.org/10.1021/mp050043s.

(19) Pennington, L. D.; Moustakas, D. T. The Necessary Nitrogen Atom: A Versatile High-Impact Design Element for Multiparameter Optimization. *J. Med. Chem.* **2017**, *60* (9), 3552–3579. https://doi.org/10.1021/acs.jmedchem.6b01807.

(20) Kamau, E.; Meehan, T.; Lavine, M. D.; Arrizabalaga, G.; Wilson, G. M.; Boyle, J. A Novel Benzodioxole-Containing Inhibitor of Toxoplasma Gondii Growth Alters the Parasite Cell Cycle. *Antimicrob. Agents Chemother.* **2011**, *55* (12), 5438–5451. https://doi.org/10.1128/AAC.00455-11.

(21) Murata, Y.; Sugi, T.; Weiss, L. M.; Kato, K. Identification of Compounds That Suppress Toxoplasma Gondii Tachyzoites and Bradyzoites. *PLOS ONE* **2017**, *12* (6), e0178203. https://doi.org/10.1371/journal.pone.0178203.

(22) Scallan, E.; Hoekstra, R. M.; Angulo, F. J.; Tauxe, R. V.; Widdowson, M.-A.; Roy, S. L.; Jones, J. L.; Griffin, P. M. Foodborne Illness Acquired in the United States—Major Pathogens - Volume 17, Number 1—January 2011 - Emerging Infectious Diseases Journal - CDC. https://doi.org/10.3201/eid1701.p11101.

(23) Saito, T.; Maeda, T.; Nakazawa, M.; Takeuchi, T.; Nozaki, T.; Asai, T. Characterisation of Hexokinase in Toxoplasma Gondii Tachyzoites. *Int. J. Parasitol.* **2002**, *32* (8), 961–967. https://doi.org/10.1016/S0020-7519(02)00059-0.

(24) Gross, U.; Bohne, W.; Soête, M.; Dubremetz, J. F. Developmental Differentiation between Tachyzoites and Bradyzoites of Toxoplasma Gondii. *Parasitol. Today* **1996**, *12* (1), 30–33. https://doi.org/10.1016/0169-4758(96)80642-9.

(25) Asai, T.; Takeuchi, T.; Diffenderfer, J.; Sibley, L. D. Identification of Small-Molecule Inhibitors of Nucleoside Triphosphate Hydrolase in Toxoplasma Gondii. *Antimicrob. Agents Chemother.* **2002**, *46* (8), 2393–2399. https://doi.org/10.1128/AAC.46.8.2393-2399.2002.

(26) Bohne, W.; Holpert, M.; Gross, U. Stage Differentiation of the Protozoan Parasite Toxoplasma Gondii. *Immunobiology* **1999**, *201* (2), 248–254. https://doi.org/10.1016/S0171-2985(99)80065-5.

(27) Pittman, K. J.; Knoll, L. J. Long-Term Relationships: The Complicated Interplay between the Host and the Developmental Stages of Toxoplasma Gondii during Acute and Chronic Infections. *Microbiol. Mol. Biol. Rev.* **2015**, *79* (4), 387–401. https://doi.org/10.1128/MMBR.00027-15.

(28) Peters, P. J.; Thigpen, M. C.; Parise, M. E.; Newman, R. D. Safety and Toxicity of Sulfadoxine/Pyrimethamine. *Drug Saf.* **2007**, *30* (6), 481–501. https://doi.org/10.2165/00002018-200730060-00003.

(29) Pissinate, K.; dos Santos Martins-Duarte, É.; Schaffazick, S. R.; de Oliveira, C. P.; Vommaro, R. C.; Guterres, S. S.; Pohlmann, A. R.; de Souza, W. Pyrimethamine-Loaded Lipid-Core Nanocapsules to Improve Drug Efficacy for the Treatment of Toxoplasmosis. *Parasitol. Res.* **2014**, *113* (2), 555–564. https://doi.org/10.1007/s00436-013-3715-6.

(30) Macy, E.; Poon K-Y, T. Self-Reported Antibiotic Allergy Incidence and Prevalence: Age and Sex Effects. *Am. J. Med.* **2009**, *122* (8), 778.e1-778.e7. https://doi.org/10.1016/j.amjmed.2009.01.034.

(31) Wulf, N. R.; Matuszewski, K. A. Sulfonamide Cross-Reactivity: Is There Evidence to Support Broad Cross-Allergenicity? *Am. J. Health. Syst. Pharm.* **2013**, *70* (17), 1483–1494. https://doi.org/10.2146/ajhp120291.

(32) Fung, H. B.; Kirschenbaum, H. L. Treatment Regimens for Patients with Toxoplasmic Encephalitis. *Clin. Ther.* **1996**, *18* (6), 1037–1056. https://doi.org/10.1016/S0149-2918(96)80059-2.

(33) Montazeri, M.; Sharif, M.; Sarvi, S.; Mehrzadi, S.; Ahmadpour, E.; Daryani, A. A Systematic Review of In Vitro and In Vivo Activities of Anti-Toxoplasma Drugs and Compounds (2006–2016). *Front. Microbiol.* **2017**, *8*. https://doi.org/10.3389/fmicb.2017.00025.

(34) Montazeri, M.; Mehrzadi, S.; Sharif, M.; Sarvi, S.; Tanzifi, A.; Aghayan, S. A.; Daryani, A. Drug Resistance in Toxoplasma Gondii. *Front. Microbiol.* **2018**, *9*. https://doi.org/10.3389/fmicb.2018.02587.

(35) Pollack, A. Drug Goes From $13.50 a Tablet to $750, Overnight. *The New York Times*. September 20, 2015.

(36) Essential Medicines in the United States — Why Access Is Diminishing | NEJM http://www.nejm.org/doi/10.1056/NEJMp1601559 (accessed May 20, 2020).

(37) Denton, H.; Roberts, C. W.; Alexander, J.; Thong, K.; Coombs, G. H. Enzymes of Energy Metabolism in the Bradyzoites and Tachyzoites of Toxoplasma Gondii. *FEMS Microbiol. Lett.* **1996**, *137* (1), 103–108. https://doi.org/10.1111/j.1574-6968.1996.tb08090.x.

(38) Denkers, E. Y.; Gazzinelli, R. T. Regulation and Function of T-Cell-Mediated Immunity during Toxoplasma Gondii Infection. *Clin. Microbiol. Rev.* **1998**, *11* (4), 569–588. https://doi.org/10.1128/CMR.11.4.569.

(39) Neville, A. J.; Zach, S. J.; Wang, X.; Larson, J. J.; Judge, A. K.; Davis, L. A.; Vennerstrom, J. L.; Davis, P. H. Clinically Available Medicines Demonstrating Anti-Toxoplasma Activity. *Antimicrob. Agents Chemother.* **2015**, *59* (12), 7161–7169. https://doi.org/10.1128/AAC.02009-15.

(40) Konstantinovic, N.; Guegan, H.; Stäjner, T.; Belaz, S.; Robert-Gangneux, F. Treatment of Toxoplasmosis: Current Options and Future Perspectives. *Food Waterborne Parasitol.* **2019**, *15*, e00036. https://doi.org/10.1016/j.fawpar.2019.e00036.

(41) Meireles, L. R.; Ekman, C. C. J.; Andrade Jr, H. F. de; Luna, E. J. de A.; Meireles, L. R.; Ekman, C. C. J.; Andrade Jr, H. F. de; Luna, E. J. de A. Human Toxoplasmosis Outbreaks And The Agent Infecting Form. Findings From A Systematic Review. *Rev. Inst. Med. Trop. São Paulo* **2015**, *57* (5), 369–376. https://doi.org/10.1590/S0036-46652015000500001.

(42) Park, Y.-H.; Nam, H.-W. Clinical Features and Treatment of Ocular Toxoplasmosis. *Korean J. Parasitol.* **2013**, *51* (4), 393–399. https://doi.org/10.3347/kjp.2013.51.4.393.

(43) McAuley, J. B. Congenital Toxoplasmosis. *J. Pediatr. Infect. Dis. Soc.* **2014**, *3* (suppl_1), S30–S35. https://doi.org/10.1093/jpids/piu077.

(44) Neu, N.; Duchon, J.; Zachariah, P. TORCH Infections. *Clin. Perinatol.* **2015**, *42* (1), 77–103. https://doi.org/10.1016/j.clp.2014.11.001.

(45) Tenter, A. M.; Heckeroth, A. R.; Weiss, L. M. Toxoplasma Gondii: From Animals to Humans. *Int. J. Parasitol.* **2000**, *30* (12), 1217–1258. https://doi.org/10.1016/S0020-7519(00)00124-7.

(46) Vidadala, R. S. R.; Rivas, K. L.; Ojo, K. K.; Hulverson, M. A.; Zambriski, J. A.; Bruzual, I.; Schultz, T. L.; Huang, W.; Zhang, Z.; Scheele, S.; DeRocher, A. E.; Choi, R.; Barrett, L. K.; Siddaramaiah, L. K.; Hol, W. G. J.; Fan, E.; Merritt, E. A.; Parsons, M.; Freiberg, G.; Marsh, K.; Kempf, D. J.; Carruthers, V. B.; Isoherranen, N.; Doggett, J. S.; Van Voorhis, W. C.; Maly, D. J. Development of an Orally Available and Central Nervous System (CNS) Penetrant *Toxoplasma Gondii* Calcium-Dependent Protein Kinase 1 (*Tg* CDPK1) Inhibitor with Minimal Human Ether-a-Go-Go-Related Gene (HERG) Activity for the Treatment of

Toxoplasmosis. *J. Med. Chem.* **2016**, *59* (13), 6531–6546. https://doi.org/10.1021/acs.jmedchem.6b00760.

(47) Vidadala, R. S. R.; Golkowski, M.; Hulverson, M. A.; Choi, R.; McCloskey, M. C.; Whitman, G. R.; Huang, W.; Arnold, S. L. M.; Barrett, L. K.; Fan, E.; Merritt, E. A.; Van Voorhis, W. C.; Ojo, K. K.; Maly, D. J. 7H-Pyrrolo[2,3-d]Pyrimidin-4-Amine-Based Inhibitors of Calcium-Dependent Protein Kinase 1 Have Distinct Inhibitory and Oral Pharmacokinetic Characteristics Compared with 1H-Pyrazolo[3,4-d]Pyrimidin-4-Amine-Based Inhibitors. *ACS Infect. Dis.* **2018**, *4* (4), 516–522. https://doi.org/10.1021/acsinfecdis.7b00224.

(48) Welsch, M. E.; Zhou, J.; Gao, Y.; Yan, Y.; Porter, G.; Agnihotri, G.; Li, Y.; Lu, H.; Chen, Z.; Thomas, S. B. Discovery of Potent and Selective Leads against *Toxoplasma Gondii* Dihydrofolate Reductase via Structure-Based Design. *ACS Med. Chem. Lett.* **2016**, *7* (12), 1124–1129. https://doi.org/10.1021/acsmedchemlett.6b00328.

(49) Simpson, C.; Jones, N. G.; Hull-Ryde, E. A.; Kireev, D.; Stashko, M.; Tang, K.; Janetka, J. W.; Wildman, S. A.; Zuercher, W. J.; Schapira, M.; Hui, R.; Janzen, W.; Sibley, L. D. Identification of Small Molecule Inhibitors That Block the Toxoplasma Gondii Rhoptry Kinase ROP18. *ACS Infect. Dis.* **2016**, *2* (3), 194–206. https://doi.org/10.1021/acsinfecdis.5b00102.

(50) Heaslip, A. T.; Leung, J. M.; Carey, K. L.; Catti, F.; Warshaw, D. M.; Westwood, N. J.; Ballif, B. A.; Ward, G. E. A Small-Molecule Inhibitor of T. Gondii Motility Induces the Posttranslational Modification of Myosin Light Chain-1 and Inhibits Myosin Motor Activity. *PLOS Pathog.* **2010**, *6* (1), e1000720. https://doi.org/10.1371/journal.ppat.1000720.

(51) Lourido, S.; Zhang, C.; Lopez, M. S.; Tang, K.; Barks, J.; Wang, Q.; Wildman, S. A.; Shokat, K. M.; Sibley, L. D. Optimizing Small Molecule Inhibitors of Calcium-Dependent Protein

Kinase 1 to Prevent Infection by Toxoplasma Gondii. *J. Med. Chem.* **2013**, *56* (7), 3068–3077. https://doi.org/10.1021/jm4001314.

(52) Brown, K. M.; Suvorova, E.; Farrell, A.; McLain, A.; Dittmar, A.; Wiley, G. B.; Marth, G.; Gaffney, P. M.; Gubbels, M. J.; White, M.; Blader, I. J. Forward Genetic Screening Identifies a Small Molecule That Blocks Toxoplasma Gondii Growth by Inhibiting Both Host- and Parasite-Encoded Kinases. *PLOS Pathog.* **2014**, *10* (6), e1004180. https://doi.org/10.1371/journal.ppat.1004180.

(53) Leesombun, A.; Iijima, M.; Umeda, K.; Kondoh, D.; Pagmadulam, B.; Abdou, A. M.; Suzuki, Y.; Ohba, S.-I.; Isshiki, K.; Kimura, T.; Kubota, Y.; Sawa, R.; Nihei, C.-I.; Nishikawa, Y. Metacytofilin Is a Potent Therapeutic Drug Candidate for Toxoplasmosis. *J. Infect. Dis.* **2020**, *221* (5), 766–774. https://doi.org/10.1093/infdis/jiz501.

(54) Liu, S.; Wu, M.; Hua, Q.; Lu, D.; Tian, Y.; Yu, H.; Cheng, L.; Chen, Y.; Cao, J.; Hu, X.; Tan, F. Two Old Drugs, NVP-AEW541 and GSK-J4, Repurposed against the Toxoplasma Gondii RH Strain. *Parasit. Vectors* **2020**, *13* (1), 242. https://doi.org/10.1186/s13071-020-04094-2.

(55) Alday, P. H.; Doggett, J. S. Drugs in development for toxoplasmosis: advances, challenges, and current status https://www.dovepress.com/drugs-in-development-for-toxoplasmosis-advances-challenges-and-current-peer-reviewed-fulltext-article-DDDT (accessed May 20, 2020). https://doi.org/10.2147/DDDT.S60973.

(56) Radke, J. B.; Burrows, J. N.; Goldberg, D. E.; Sibley, L. D. Evaluation of Current and Emerging Antimalarial Medicines for Inhibition of *Toxoplasma Gondii* Growth in Vitro. *ACS Infect. Dis.* **2018**, *4* (8), 1264–1274. https://doi.org/10.1021/acsinfecdis.8b00113.

(57) Radke, J. B.; Carey, K. L.; Shaw, S.; Metkar, S. R.; Mulrooney, C.; Gale, J. P.; Bittker, J. A.; Hilgraf, R.; Comer, E.; Schreiber, S. L.; Virgin, H. W.; Perez, J. R.; Sibley, L. D. High

Throughput Screen Identifies Interferon γ-Dependent Inhibitors of *Toxoplasma Gondii* Growth. *ACS Infect. Dis.* **2018**, *4* (10), 1499–1507. https://doi.org/10.1021/acsinfecdis.8b00135.

(58) Hopper, A. T.; Brockman, A.; Wise, A.; Gould, J.; Barks, J.; Radke, J. B.; Sibley, L. D.; Zou, Y.; Thomas, S. Discovery of Selective *Toxoplasma Gondii* Dihydrofolate Reductase Inhibitors for the Treatment of Toxoplasmosis. *J. Med. Chem.* **2019**, *62* (3), 1562–1576. https://doi.org/10.1021/acs.jmedchem.8b01754.

(59) Dittmar, A. J.; Drozda, A. A.; Blader, I. J. Drug Repurposing Screening Identifies Novel Compounds That Effectively Inhibit Toxoplasma Gondii Growth. *mSphere* **2016**, *1* (2). https://doi.org/10.1128/mSphere.00042-15.

(60) Zhang, J. L.; Si, H. F.; Shang, X. F.; Zhang, X. K.; Li, B.; Zhou, X. Z.; Zhang, J. Y. New Life for an Old Drug: In Vitro and in Vivo Effects of the Anthelmintic Drug Niclosamide against Toxoplasma Gondii RH Strain. *Int. J. Parasitol. Drugs Drug Resist.* **2019**, *9*, 27–34. https://doi.org/10.1016/j.ijpddr.2018.12.004.

(61) McFarland, M. M.; Zach, S. J.; Wang, X.; Potluri, L.-P.; Neville, A. J.; Vennerstrom, J. L.; Davis, P. H. Review of Experimental Compounds Demonstrating Anti-Toxoplasma Activity. *Antimicrob. Agents Chemother.* **2016**, *60* (12), 7017–7034. https://doi.org/10.1128/AAC.01176-16.

(62) Dunay, I. R.; Gajurel, K.; Dhakal, R.; Liesenfeld, O.; Montoya, J. G. Treatment of Toxoplasmosis: Historical Perspective, Animal Models, and Current Clinical Practice. *Clin. Microbiol. Rev.* **2018**, *31* (4). https://doi.org/10.1128/CMR.00057-17.

(63) Harris, M. T.; Walker, D. M.; Drew, M. E.; Mitchell, W. G.; Dao, K.; Schroeder, C. E.; Flaherty, D. P.; Weiner, W. S.; Golden, J. E.; Morris, J. C. Interrogating a Hexokinase-

Selected Small-Molecule Library for Inhibitors of Plasmodium Falciparum Hexokinase. *Antimicrob. Agents Chemother.* **2013**, *57* (8), 3731–3737. https://doi.org/10.1128/AAC.00662-13.

(64) Harris, M. T.; Mitchell, W. G.; Morris, J. C. Targeting Protozoan Parasite Metabolism: Glycolytic Enzymes in the Therapeutic Crosshairs http://www.ingentaconnect.com/content/ben/cmc/2014/00000021/00000015/art00002 (accessed May 12, 2020).

(65) Davis, M. I.; Patrick, S. L.; Blanding, W. M.; Dwivedi, V.; Suryadi, J.; Golden, J. E.; Coussens, N. P.; Lee, O. W.; Shen, M.; Boxer, M. B.; Hall, M. D.; Sharlow, E. R.; Drew, M. E.; Morris, J. C. Identification of Novel Plasmodium Falciparum Hexokinase Inhibitors with Antiparasitic Activity. *Antimicrob. Agents Chemother.* **2016**, *60* (10), 6023–6033. https://doi.org/10.1128/AAC.00914-16.

(66) Chambers, J. W.; Fowler, M. L.; Morris, M. T.; Morris, J. C. The Anti-Trypanosomal Agent Lonidamine Inhibits Trypanosoma Brucei Hexokinase 1. *Mol. Biochem. Parasitol.* **2008**, *158* (2), 202–207. https://doi.org/10.1016/j.molbiopara.2007.12.013.

(67) Verlinde, C. L. M. J.; Hannaert, V.; Blonski, C.; Willson, M.; Périé, J. J.; Fothergill-Gilmore, L. A.; Opperdoes, F. R.; Gelb, M. H.; Hol, W. G. J.; Michels, P. A. M. Glycolysis as a Target for the Design of New Anti-Trypanosome Drugs. *Drug Resist. Updat.* **2001**, *4* (1), 50–65. https://doi.org/10.1054/drup.2000.0177.

(68) Kalel, V. C.; Emmanouilidis, L.; Dawidowski, M.; Schliebs, W.; Sattler, M.; Popowicz, G. M.; Erdmann, R. Inhibitors of Glycosomal Protein Import Provide New Leads against Trypanosomiasis. *Microb. Cell* **2017**, *4* (7), 229–232. https://doi.org/10.15698/mic2017.07.581.

(69) Walsh, M. J.; Brimacombe, K. R.; Vásquez-Valdivieso, M. G.; Auld, D. S.; Simeonov, A.; Morgan, H. P.; Fothergill-Gilmore, L. A.; Michels, P. A. M.; Walkinshaw, M. D.; Shen, M.; Boxer, M. B. Identification of Selective Inhibitors of Phosphofructokinase as Lead Compounds Against Trypanosomiasis. In *Probe Reports from the NIH Molecular Libraries Program*; National Center for Biotechnology Information (US): Bethesda (MD), 2010.

(70) Olszewski, K. L.; Llinás, M. Central Carbon Metabolism of Plasmodium Parasites. *Mol. Biochem. Parasitol.* **2011**, *175* (2), 95–103. https://doi.org/10.1016/j.molbiopara.2010.09.001.

(71) Opperdoes, F. R.; Michels, P. A. M. Enzymes of Carbohydrate Metabolism as Potential Drug Targets. *Int. J. Parasitol.* **2001**, *31* (5), 482–490. https://doi.org/10.1016/S0020-7519(01)00155-2.

(72) Lyons, R. E.; McLeod, R.; Roberts, C. W. Toxoplasma Gondii Tachyzoite–Bradyzoite Interconversion. *Trends Parasitol.* **2002**, *18* (5), 198–201. https://doi.org/10.1016/S1471-4922(02)02248-1.

(73) Skariah, S.; McIntyre, M. K.; Mordue, D. G. Toxoplasma Gondii: Determinants of Tachyzoite to Bradyzoite Conversion. *Parasitol. Res.* **2010**, *107* (2), 253–260. https://doi.org/10.1007/s00436-010-1899-6.

(74) Carneiro, S. B.; Costa Duarte, F. Í.; Heimfarth, L.; Siqueira Quintans, J. de S.; Quintans-Júnior, L. J.; Veiga Júnior, V. F. da; Neves de Lima, Á. A. Cyclodextrin–Drug Inclusion Complexes: In Vivo and In Vitro Approaches. *Int. J. Mol. Sci.* **2019**, *20* (3), 642. https://doi.org/10.3390/ijms20030642.

(75) Fleige, T.; Fischer, K.; Ferguson, D. J. P.; Gross, U.; Bohne, W. Carbohydrate Metabolism in the Toxoplasma Gondii Apicoplast: Localization of Three Glycolytic Isoenzymes, the

Single Pyruvate Dehydrogenase Complex, and a Plastid Phosphate Translocator. *Eukaryot. Cell* **2007**, *6* (6), 984–996. https://doi.org/10.1128/EC.00061-07.

(76) Gajria, B.; Bahl, A.; Brestelli, J.; Dommer, J.; Fischer, S.; Gao, X.; Heiges, M.; Iodice, J.; Kissinger, J. C.; Mackey, A. J.; Pinney, D. F.; Roos, D. S.; Stoeckert, C. J.; Wang, H.; Brunk, B. P. ToxoDB: An Integrated Toxoplasma Gondii Database Resource. *Nucleic Acids Res.* **2008**, *36* (suppl_1), D553–D556. https://doi.org/10.1093/nar/gkm981.

(77) Sidik, S. M.; Huet, D.; Ganesan, S. M.; Huynh, M.-H.; Wang, T.; Nasamu, A. S.; Thiru, P.; Saeij, J. P. J.; Carruthers, V. B.; Niles, J. C.; Lourido, S. A Genome-Wide CRISPR Screen in Toxoplasma Identifies Essential Apicomplexan Genes. *Cell* **2016**, *166* (6), 1423-1435.e12. https://doi.org/10.1016/j.cell.2016.08.019.

(78) Ponte-Sucre, A. An Overview of Trypanosoma Brucei Infections: An Intense Host–Parasite Interaction. *Front. Microbiol.* **2016**, *7*. https://doi.org/10.3389/fmicb.2016.02126.

(79) Human African Trypanosomiasis – Current Treatments and the Drug Pipeline. *Infectious Diseases Hub*, 2017.

(80) Lassalas, P.; Gay, B.; Lasfargeas, C.; James, M. J.; Tran, V.; Vijayendran, K. G.; Brunden, K. R.; Kozlowski, M. C.; Thomas, C. J.; Smith, A. B.; Huryn, D. M.; Ballatore, C. Structure Property Relationships of Carboxylic Acid Isosteres. *J. Med. Chem.* **2016**, *59* (7), 3183–3203. https://doi.org/10.1021/acs.jmedchem.5b01963.

(81) Westphal, M. V.; Wolfstädter, B. T.; Plancher, J.-M.; Gatfield, J.; Carreira, E. M. Evaluation of *Tert*-Butyl Isosteres: Case Studies of Physicochemical and Pharmacokinetic Properties, Efficacies, and Activities. *ChemMedChem* **2015**, *10* (3), 461–469. https://doi.org/10.1002/cmdc.201402502.

(82) Fersing, C.; Basmaciyan, L.; Boudot, C.; Pedron, J.; Hutter, S.; Cohen, A.; Castera-Ducros, C.; Primas, N.; Laget, M.; Casanova, M.; Bourgeade-Delmas, S.; Piednoel, M.; Sournia-Saquet, A.; Belle Mbou, V.; Courtioux, B.; Boutet-Robinet, É.; Since, M.; Milne, R.; Wyllie, S.; Fairlamb, A. H.; Valentin, A.; Rathelot, P.; Verhaeghe, P.; Vanelle, P.; Azas, N. Nongenotoxic 3-Nitroimidazo[1,2-a]Pyridines Are NTR1 Substrates That Display Potent in Vitro Antileishmanial Activity. *ACS Med. Chem. Lett.* **2019**, *10* (1), 34–39. https://doi.org/10.1021/acsmedchemlett.8b00347.

(83) Seifert, K. Structures, Targets and Recent Approaches in Anti-Leishmanial Drug Discovery and Development. *Open Med. Chem. J.* **2011**, *5* (1). https://doi.org/10.2174/1874104501105010031.

(84) Croft, S. L.; Sundar, S.; Fairlamb, A. H. Drug Resistance in Leishmaniasis. *Clin. Microbiol. Rev.* **2006**, *19* (1), 111–126. https://doi.org/10.1128/CMR.19.1.111-126.2006.

(85) Wang, M. Z.; Zhu, X.; Srivastava, A.; Liu, Q.; Sweat, J. M.; Pandharkar, T.; Stephens, C. E.; Riccio, E.; Parman, T.; Munde, M.; Mandal, S.; Madhubala, R.; Tidwell, R. R.; Wilson, W. D.; Boykin, D. W.; Hall, J. E.; Kyle, D. E.; Werbovetz, K. A. Novel Arylimidamides for Treatment of Visceral Leishmaniasis. *Antimicrob. Agents Chemother.* **2010**, *54* (6), 2507–2516. https://doi.org/10.1128/AAC.00250-10.

(86) Grace, E.; Asbill, S.; Virga, K. Naegleria Fowleri: Pathogenesis, Diagnosis, and Treatment Options. *Antimicrob. Agents Chemother.* **2015**, *59* (11), 6677–6681. https://doi.org/10.1128/AAC.01293-15.

(87) Hughes, A. L.; Piontkivska, H. Phylogeny of Trypanosomatidae and Bodonidae (Kinetoplastida) Based on 18S RRNA: Evidence for Paraphyly of Trypanosoma and Six

Other Genera. *Mol. Biol. Evol.* **2003**, *20* (4), 644–652. https://doi.org/10.1093/molbev/msg062.

(88) Bell, M. G.; Cao, G.; Escribano, A. M.; Fernandez, M. C.; Mantlo, N. B.; Nava, E. M. M. D. L.; Herranz, A. I. M.; Mayhugh, D. R.; Wang, X. Compounds and Methods for Treating Dyslipidemia. WO2005097805A1, October 20, 2005.

(89) Luk, K.-C. 1,6- and 1,8-Naphthyridines. US20120184562A1, July 19, 2012.

(90) Hamzik, P. J.; Brubaker, J. D. Reactions of Oxetan-3-Tert-Butylsulfinimine for the Preparation of Substituted 3-Aminooxetanes. *Org. Lett.* **2010**, *12* (5), 1116–1119. https://doi.org/10.1021/ol100119e.

(91) Zhou, Z.-L.; Navratil, J. M.; Cai, S. X.; Whittemore, E. R.; Espitia, S. A.; Hawkinson, J. E.; Tran, M.; Woodward, R. M.; Weber, E.; Keana, J. F. W. Synthesis and SAR of 5-, 6-, 7- and 8-Aza Analogues of 3-Aryl-4-Hydroxyquinolin-2(1H)-One as NMDA/Glycine Site Antagonists. *Bioorg. Med. Chem.* **2001**, *9* (8), 2061–2071. https://doi.org/10.1016/S0968-0896(01)00115-8.

Appendix I: Publications and Presentations

Publications

1. **Khalifa**, **M. M.**[§]; Martorelli di Genova, B.[§]; McAlpine, S. G.; Rozema, S. D.; Monaghan, N. P.; Morris, J. C.; Knoll, L. J.; Golden, J. E. Dual Stage Picolinic Acid Derived Inhibitors of *Toxoplasma gondii*. Submitted (*ACS Med. Chem. Lett.*), [§]equal contributors.

2. Antoniou, C.; Burnette, K.; Christensen-Quick, A.; Lewinska, M.; Ji, Y.; **Khalifa**, **M. M.**, Nikolaou, A.; Srivastava, P.; Hollingsworth, B. A.; van Rhijn, N.; Saurabh, S.; Konstantinides, N.; Heim, A. B.; Moore, E. B.; Strong, M.; Kosanic, A.; Kirshner, S. M.; Halder, A.; Waiho, K. Seeking Career Clarity. *Science* **2020**, *368*(6486), 26-28.

3. **Khalifa**, **M. M.**[§]; Philkhana, S. C.[§]; Golden, J. E. Synthesis of Ring-Fused, *N*-Substituted 4-Quinolinones Using pK_a-Guided, Base-Promoted Annulations with Isatoic Anhydrides: Total Synthesis of Penicinotam. *J. Org. Chem.* **2020**, *85*(2), 464-481. [§]equal contributors.

4. Milanes, J. E.; Suryadi, J.; Abendroth, J.; Van Voorhis, W. C.; Barrett, K. F.; Dranow, D. M.; Phan, I. Q.; Patrick, S. P.; Rozema, S. D.; **Khalifa**, **M. M.**; Golden, J. E.; Morris, J. C. Enzymatic and Structural Characterization of the *Naegleria fowleri* Glucokinase. *Antimicrob. Agents Chemother.*, **2019**, *63*(5), e02410-18.

5. Fitz-Henley, J. N. [§]; Jaffett, V. A. [§]; **Khalifa**, **M. M.**; Guzei, I. A.; Golden, J. E. Diastereoselective Multicomponent Synthesis of Pyrrolopyrazinoquinazolinones via a Cascading Quinazolinone Rearrangement/Intramolecular Ring Closure of (*Z*)-Benzamidines. *In preparation*, [§]equal contributors.

6. **Khalifa, M. M.**; Monaghan, N. P.; Werbovetz, K.; Morris, J. C.; Golden, J. E. Development of Picolinic Acid Derivatives as Inhibitors of Kinetoplastid Parasites *Trypanosoma brucei* and *Leishmania donovani*. *In preparation*.

7. Milanes, J. E.; Suryadi, J.; Monaghan, N. P.; Harding, E.; Morrissey, C-L.; Morris, C.; Rozema, S. D.; **Khalifa**, **M. M.**; Golden, J. E.; Kassu, M.; Manetsch, R.; Phan, I. Q.; Morris, J. C. Comparison of glucokinases from the pathogenic free-living amoeba *Acanthamoeba castellani* and *Balamuthia mandrillaris*. *In preparation*.

8. **Khalifa**, **M. M.**; Bodner, M. J.; Berglund, J. A.; Haley, M. M. Synthesis of *N*-substituted Aryl Amidines by Strong Base Activation of Amines. *Tetrahedron Lett.*, **2015**, *56*(27), 4109-4111.

9. Siboni, R. B.; Bodner, M. J.; **Khalifa**, **M. M.**; Docter, A. G.; Choi, J. Y.; Nakamori, M.; Haley, M. M.; Berglund, J. A. Biological Efficacy and Toxicity of Diamidines in Myotonic Dystrophy Type 1 Models. *J. Med. Chem.*, **2015**, *58*(15), 5770-5780.

10. Vonnegut, C. L.; Shonkweiler, A. M.; **Khalifa**, **M. M.**; Zakharov, L. N.; Johnson, D. W.; Haley, M. M. Facile Synthesis and Properties of 2-λ5-Phosphaquinolines and 2-λ5-Phosphaquinolin-2-ones. *Angew. Chem. Int. Ed.*, **2015**, *54*(45), 13318-13322.

Oral Presentations

1. *Convergent Annulative Platform for the Synthesis of Ring-fused Quinolones*, Khalifa, M. M.; Philkhana, S.C.; Golden, J.E. Pharmaceutics Graduate Research Meeting (PGSRM), University of Wisconsin-Madison, Madison WI. June 13-15, 2019
2. *Convergent Annulative Platform for the Synthesis of Ring-fused Quinolones*, Khalifa, M. M.; Philkhana, S.C.; Golden, J.E. Medicinal Chemistry Meeting-in-Miniature (MIKIW), University of Kansas, Lawrence KS. April 12-14, 2019

3. *Synthesis of N-Substituted Aryl Amidines by Strong Base Activation of Amines*, Khalifa, M. M.; Bodner, M. J.; Berglund, J. A.; Haley, M. M. Robert D. Clark Honors College Senior Thesis Defense, University of Oregon, Eugene OR. Sep 11, 2014
4. *Alkaline Synthesis of Amidines – Studying a New Method for Accessing a Pharmaceutically Relevant Functional Group*, Khalifa, M. M.; Bodner, M. J.; Berglund, J. A.; Haley, M. M. Multiple venues:
    a. SuperNova Talks, University of Oregon, Eugene OR. May 29, 2014
    b. Center for Teaching and Learning's Undergraduate Research Fellowship Talks, University of Oregon, Eugene OR. May 27, 2014
    c. University of Oregon Undergraduate Research Symposium, University of Oregon, Eugene, OR. May 15, 2014
5. *Alkaline Synthesis of Amidines – Exploring a New Approach to Accessing a Pharmaceutically Relevant Functional Group*, Khalifa, M. M.; Bodner, M. J.; Berglund, J. A.; Haley, M. M. Annual Biomedical Research Conference for Minority Students, Gaylord Opryland, Nashville TN. Nov 14, 2013

6. *Alkaline Synthesis of Amidines – A New Approach to Accessing a Biologically Relevant Functional Group*, Khalifa, M. M.; Bodner, M. J.; Berglund, J. A.; Haley, M. M. University of Oregon Summer Program for Undergraduate Research Symposium, University of Oregon, Eugene OR. Aug 16, 2013

Poster Presentations

1. *Discovery and Development of Benzoic acid Derivatives as Multistage Inhibitors of Toxoplasma gondii*, Khalifa, M. M.; Martorelli di Genova, B.; Rozema, S.D.; Garfoot, A.; Knoll, L. J.; Golden, J.E. Multiple venues:
    a. [*Accepted; cancelled due to COVID-19*] Medicinal Chemistry Meeting-in-Miniature (MIKIW), University of Wisconsin-Madison, Madison WI. April 17-19, 2020
    b. [*Accepted; cancelled due to COVID-19*] American Chemical Society Spring 2020 National Meeting & Exposition - Division of Medicinal Chemistry General Poster Session, Philadelphia PA. Mar 22-26, 2020
    c. Pharmaceutical Sciences Division Research Day, University of Wisconsin-Madison, Madison WI. Feb 7, 2020
    d. Parasitology & Vector Biology Training Grant Annual Meeting, University of Wisconsin-Madison, Madison WI. Sep 10, 2019
    e. Symposium Honoring the Career of Prof. Richard E. Peterson, University of Wisconsin-Madison, Madison WI. Aug 16, 2019
    f. Pharmaceutics Graduate Student Research Meeting (PGSRM), University of Wisconsin-Madison, Madison WI. June 13-15, 2019
    g. Pharmaceutical Sciences Division Retreat, University of Wisconsin-Madison, Madison WI. May 13, 2019
    h. Perlman Symposium, University of Wisconsin-Madison, Madison WI. April 26, 2019
2. *Convergent Annulative Platform for the Synthesis of Ring-Fused Quinolinones,* Khalifa, M. M.; Philkhana, S. C.; Golden, J. E. Multiple venues:
    a. 46th National Organic Symposium, University of Indiana, Bloomington IN. June 24, 2019

b. Pharmaceutical Sciences Division Research Day, University of Wisconsin-Madison, Madison WI. Feb 8, 2019

3. *Progress Towards an Efficient Annulative Cascade Affording Natural Product Inspired 2-3-Dihydropyrrolo[3,4-b]quinolin-1,9-diones and Derivatives,* Khalifa, M. M.; Golden, J. E. Multiple venues:
   a. Pharmaceutics Graduate Student Research Meeting (PGSRM), University of Minnesota, Minneapolis MN. June 7-9, 2018
   b. Pharmaceutical Sciences Graduate Student Retreat, University of Wisconsin-Madison, Madison WI. May 18, 2018
   c. Graduate Student-Faculty Liaison Committee Annual Poster Session, University of Wisconsin-Madison, Madison WI. May 10, 2018
   d. Medicinal Chemistry Meeting-in-Miniature (MIKI), University of Illinois Chicago, Chicago IL. April 6-8, 2018
4. *Alkaline Synthesis of Amidines – A New Approach to Accessing a Biologically Relevant Functional Group*, Khalifa, M. M.; Bodner, M. J.; Berglund, J. A.; Haley, M. M. University of Oregon Summer Program for Undergraduate Research Symposium, University of Oregon, Eugene OR. August 15, 2013
5. *Alkaline Synthesis of Amidines – New Methodology for the Preparation of Medicinally Relevant Small Molecules*, Khalifa, M. M.; Bodner, M. J.; Berglund, J. A.; Haley, M. M. University of Oregon Undergraduate Research Symposium, University of Oregon, Eugene OR. May 16, 2013

Appendix II: Copies of NMR Spectra

Spectra of Compounds in Chapter 2

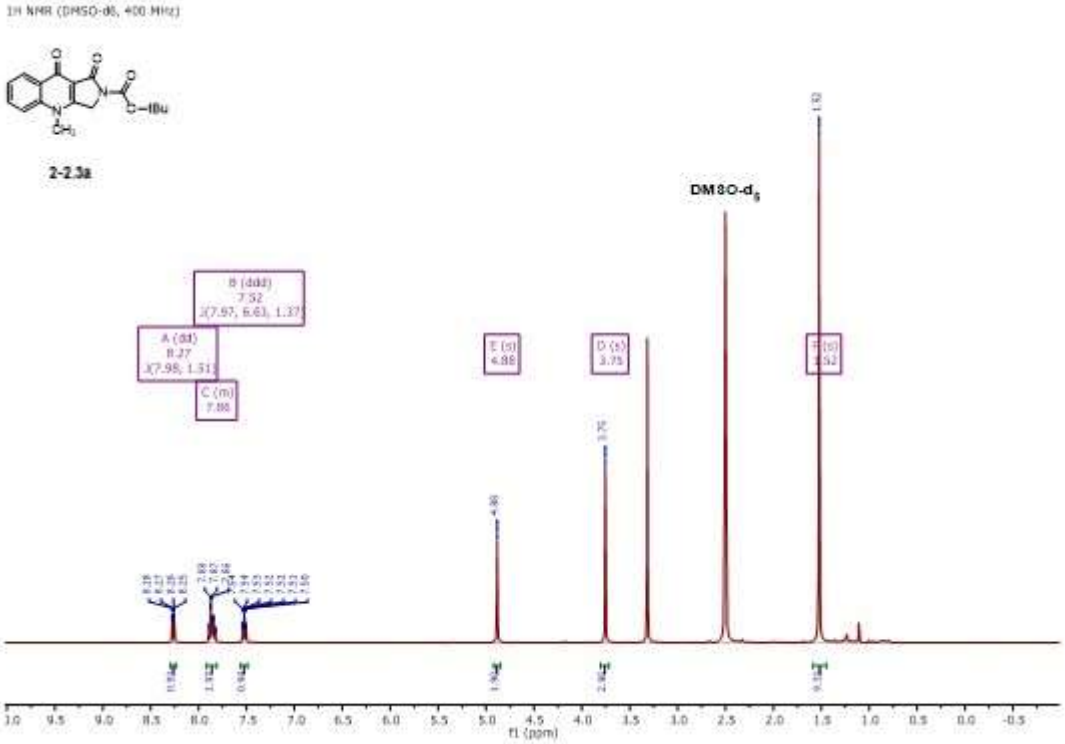

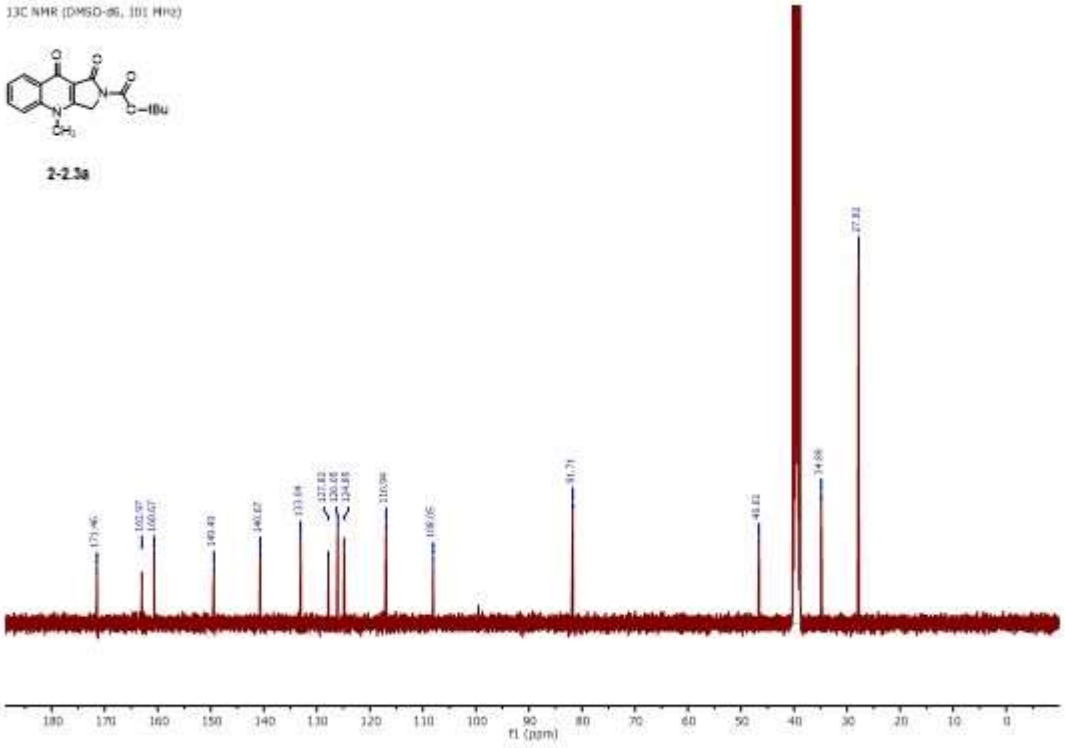

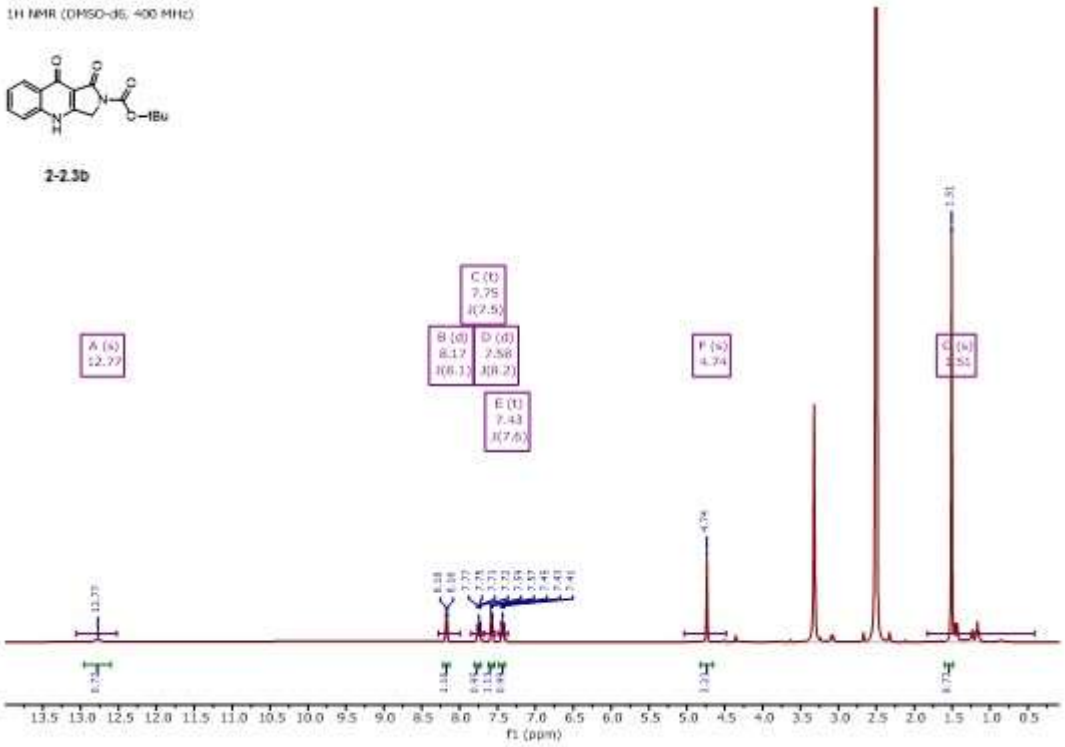
1H NMR (DMSO-d6, 400 MHz)
2-2.3b
A (s)
12.77
B (d)
8.17
J(8.1)
C (t)
7.75
J(7.5)
D (d)
7.58
J(8.2)
E (t)
7.43
J(7.6)
F (s)
4.74
G (s)
1.51
f1 (ppm)

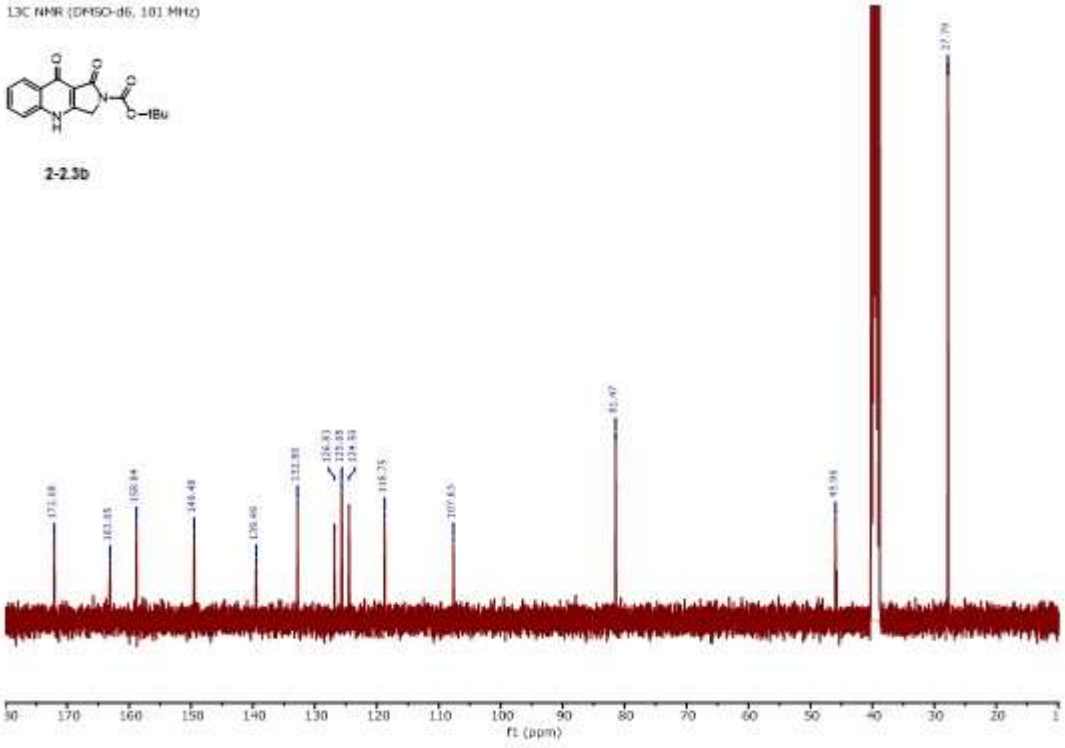
13C NMR (DMSO-d6, 101 MHz)
2-2.3b
f1 (ppm)

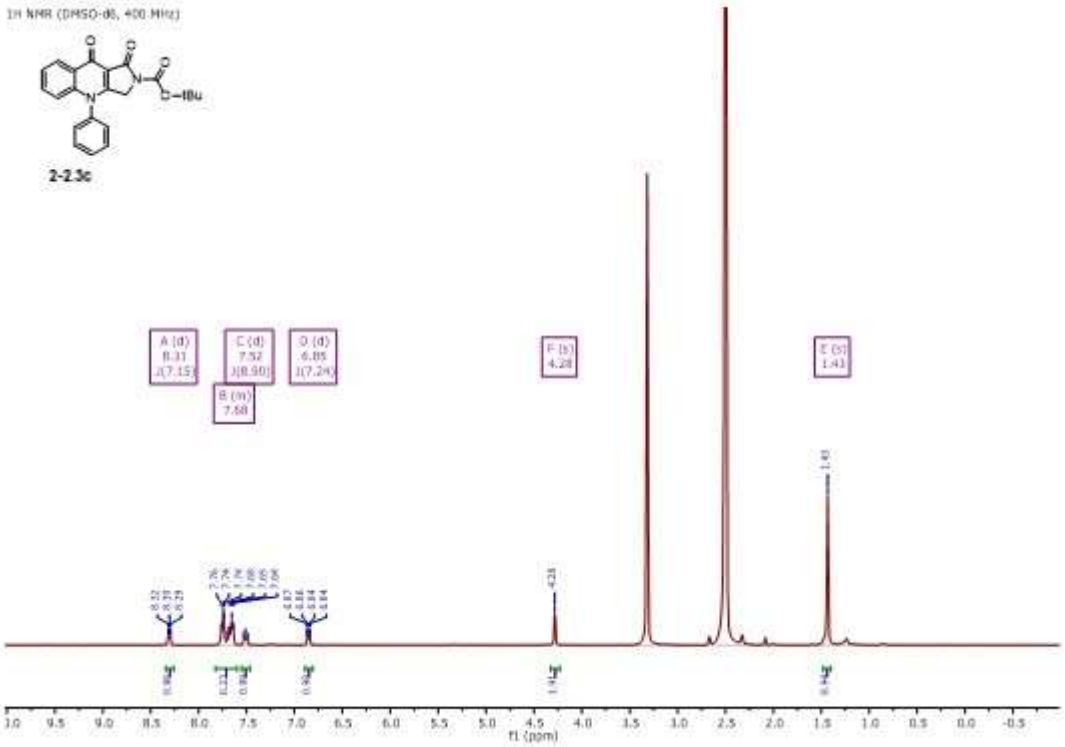
1H NMR (DMSO-d6, 400 MHz)
2-2.3c
A (d)
8.31
J(7.15)
B (m)
7.68
C (d)
7.52
J(8.90)
D (d)
6.85
J(7.24)
F (s)
4.28
E (s)
1.43
f1 (ppm)

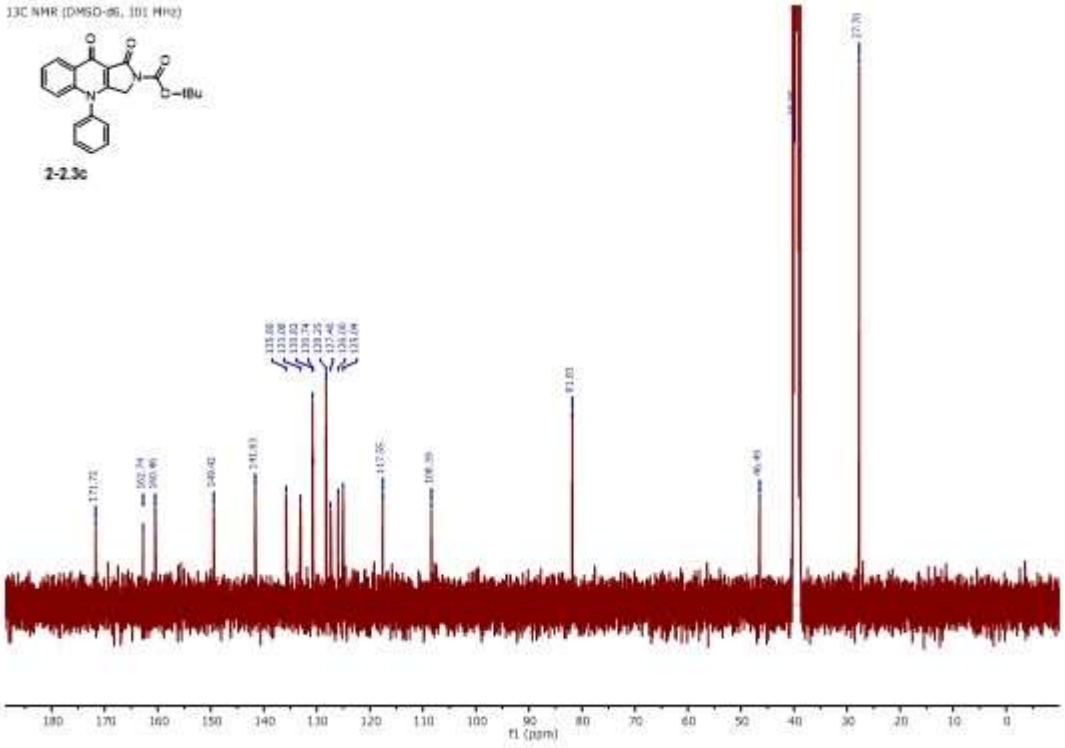
13C NMR (DMSO-d6, 101 MHz)
2-2.3c
f1 (ppm)

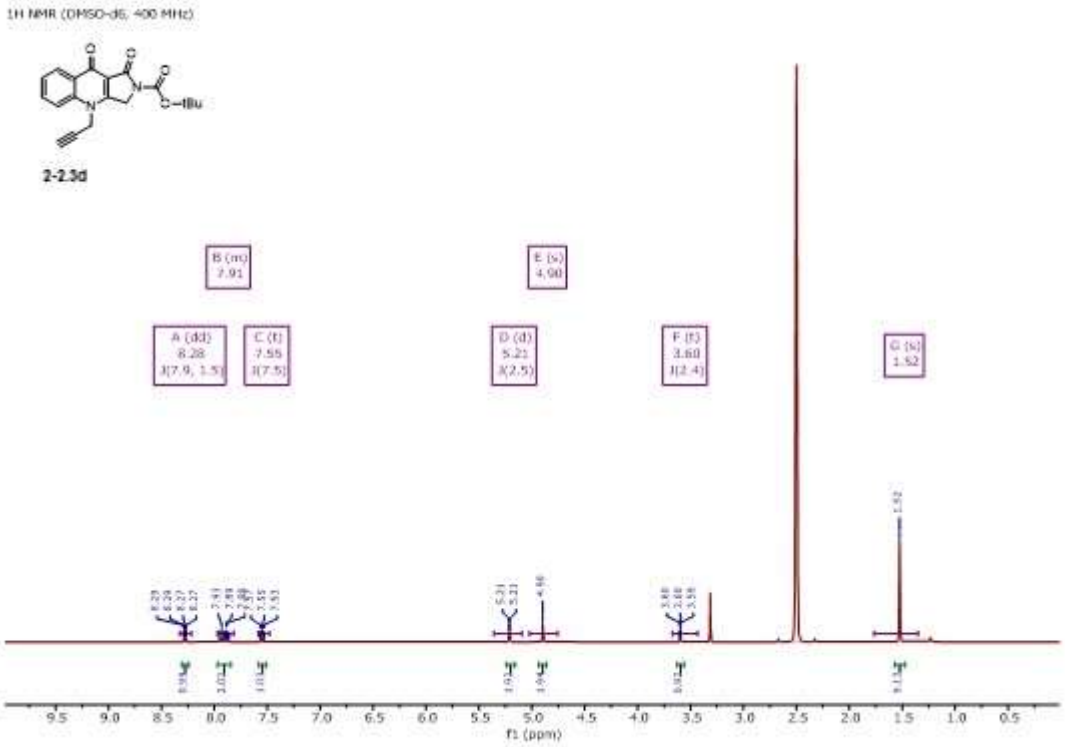
1H NMR (DMSO-d6, 400 MHz)
2-2.3d
B (m)
7.91
E (s)
4.90
A (dd)
8.28
J(7.9, 1.5)
C (t)
7.55
J(7.5)
D (d)
5.21
J(2.5)
F (t)
3.60
J(2.4)
G (s)
1.52
f1 (ppm)

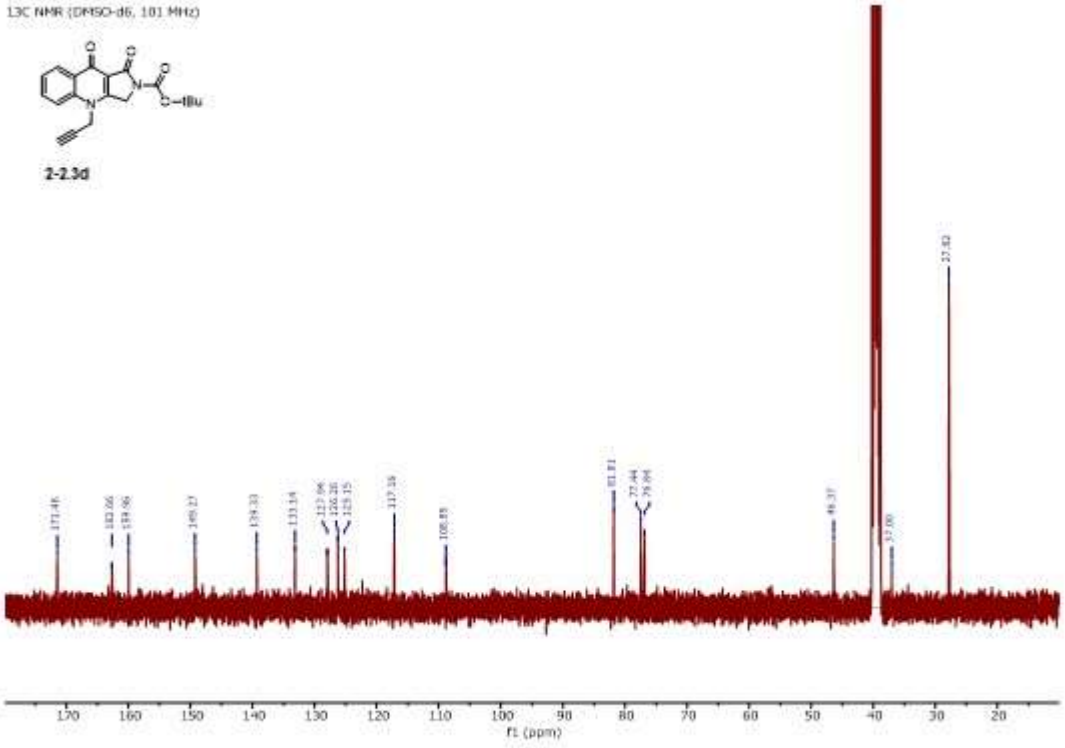
13C NMR (DMSO-d6, 101 MHz)
2-2.3d
f1 (ppm)

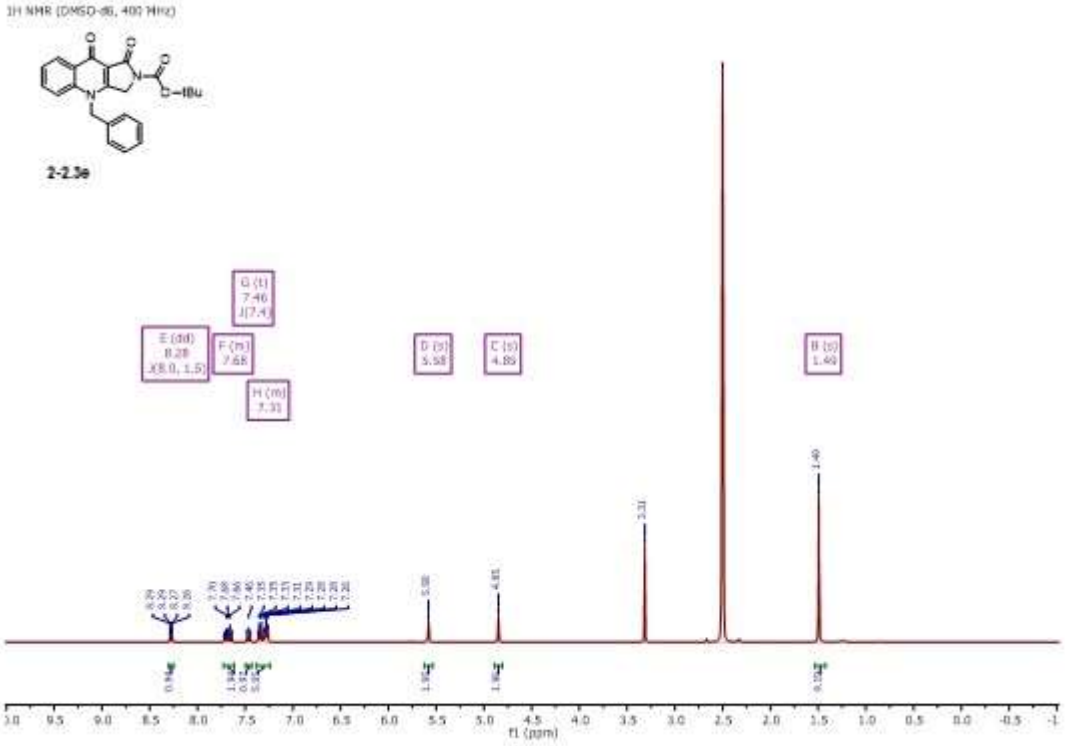
1H NMR (DMSO-d6, 400 MHz)
2-2.3e
G (t) 7.46 J(7.4
E (dd) 8.28 J(8.0, 1.5)
F (m) 7.68
H (m) 7.31
D (s) 5.58
C (s) 4.85
B (s) 1.40
2.51
f1 (ppm)

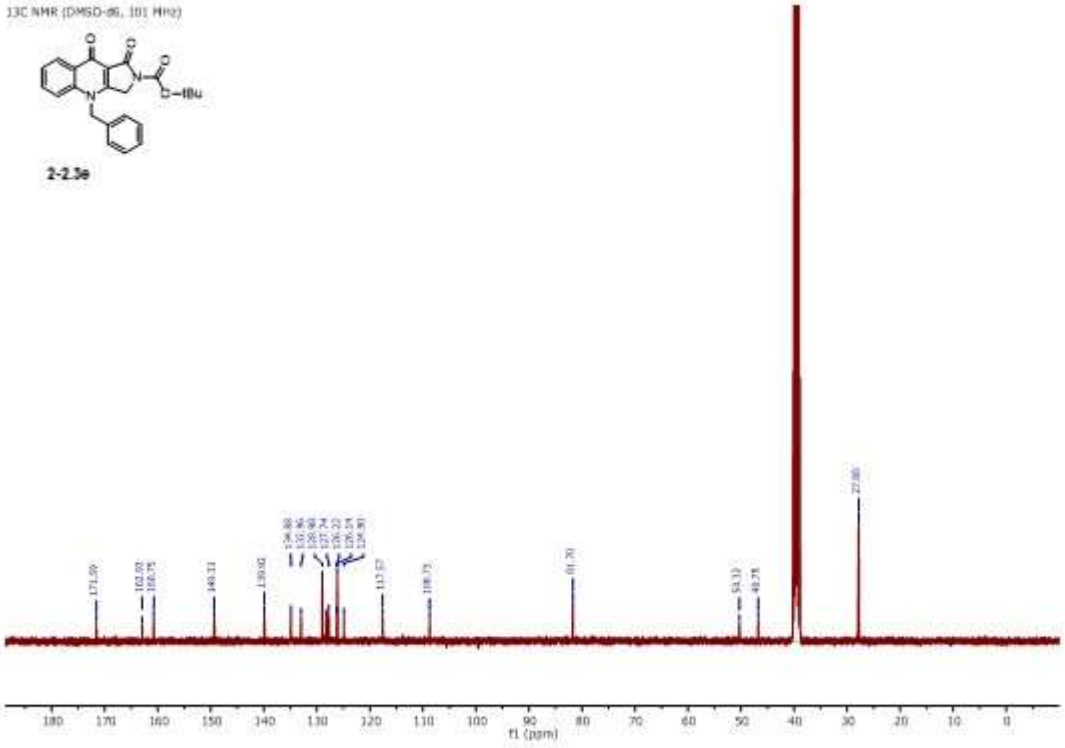
13C NMR (DMSO-d6, 101 MHz)
2-2.3e
171.99
162.93
160.75
149.11
139.60
117.57
108.75
81.70
53.13
48.78
27.80
f1 (ppm)

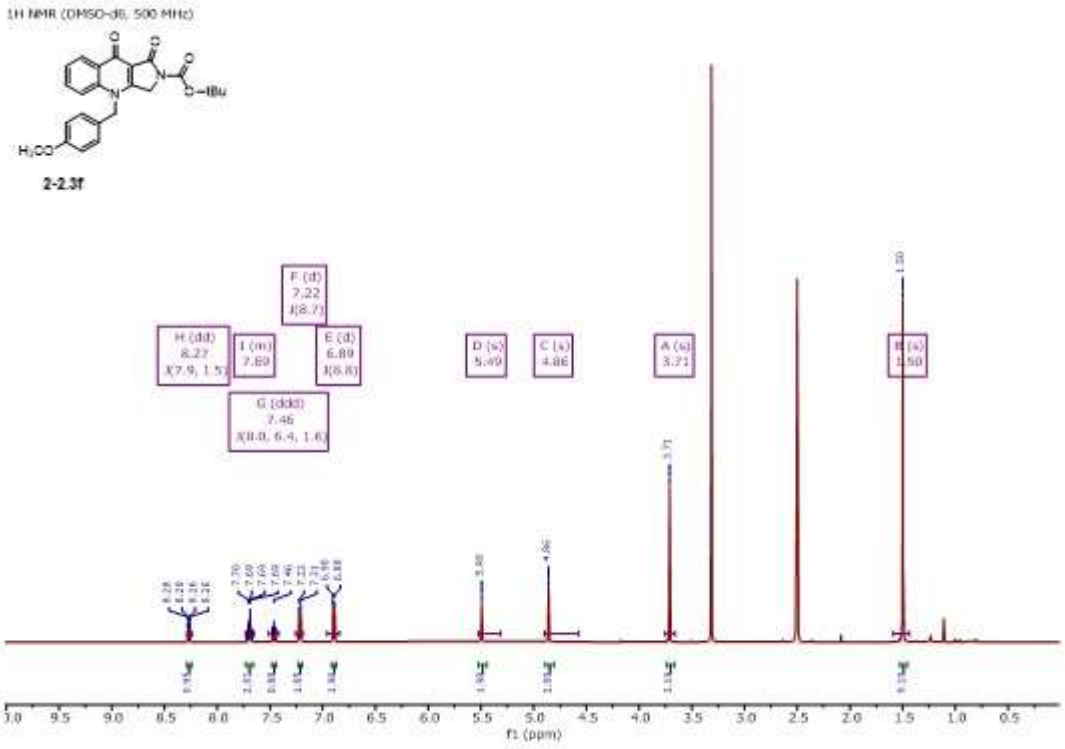
1H NMR (DMSO-d6, 500 MHz)
2-2.3f
F (d)
7.22
J(8.7)
H (dd)
8.27
J(7.9, 1.5)
I (m)
7.69
E (d)
6.89
J(8.6)
G (ddd)
7.46
J(8.0, 6.4, 1.6)
D (s)
5.49
C (s)
4.86
A (s)
3.71
B (s)
1.50
f1 (ppm)

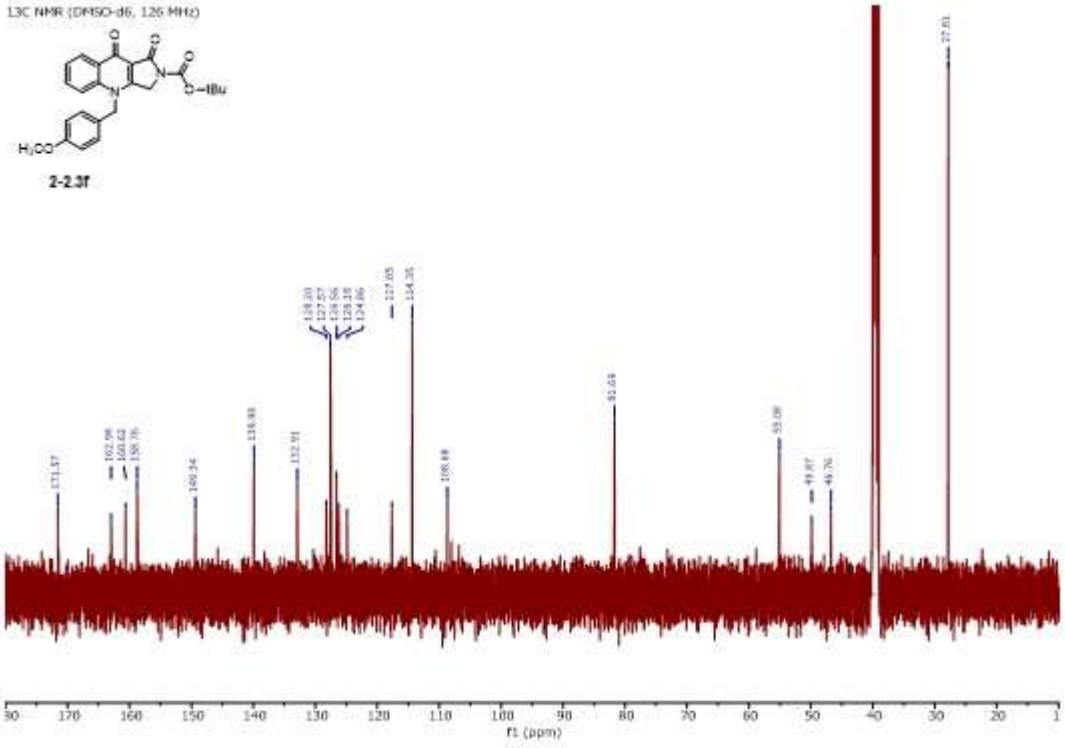
13C NMR (DMSO-d6, 126 MHz)
2-2.3f
f1 (ppm)

1H NMR (DMSO-d6, 400 MHz)

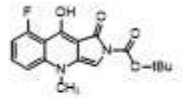

2-2.3h

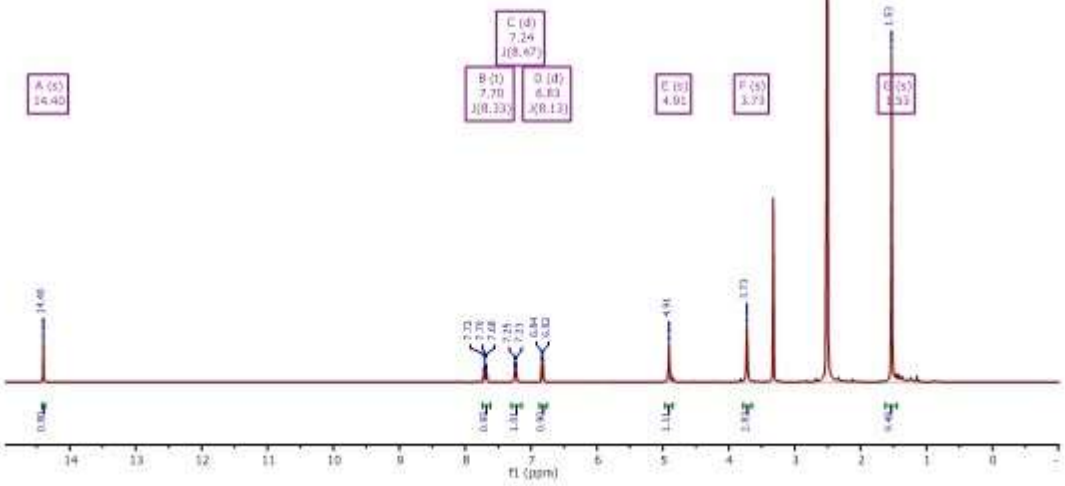

19F NMR (DMSO-d6, 376 MHz)

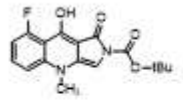

2-2.3h

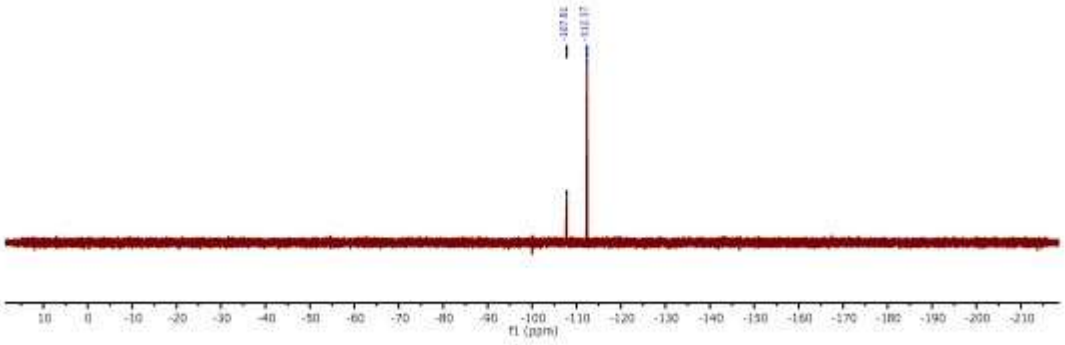

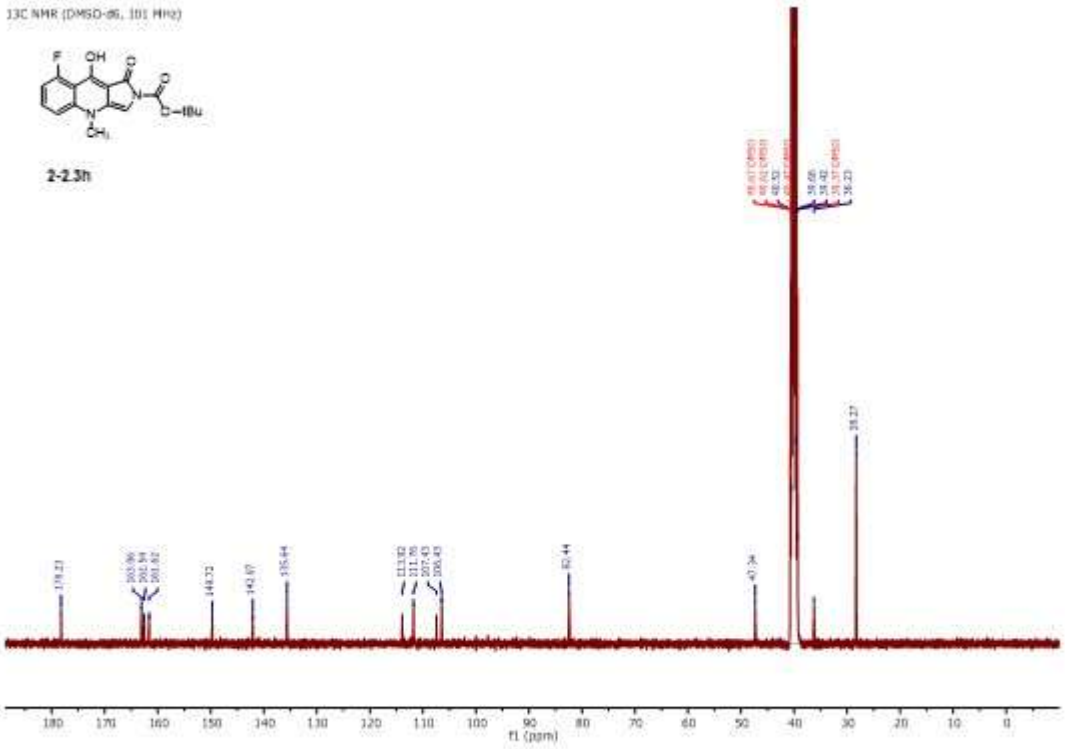
13C NMR (DMSO-d6, 101 MHz)
2-2.3h
f1 (ppm)

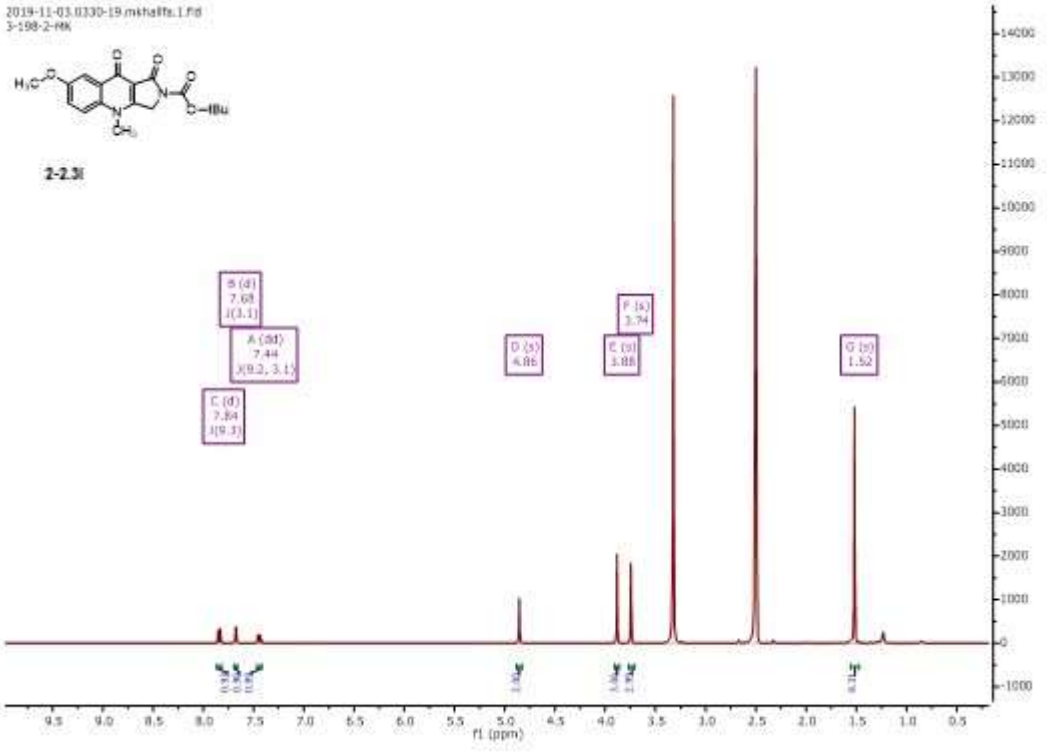
2019-11-03.0330-19.mkhalfa.1.fid
3-198-2-MK
2-2.3i
f1 (ppm)

13C NMR (DMSO-d6, 101 MHz)

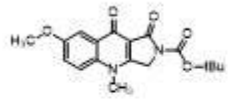

2-2.3I

1H NMR (DMSO-d6, 400 MHz)

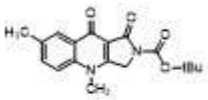

2-2.3J

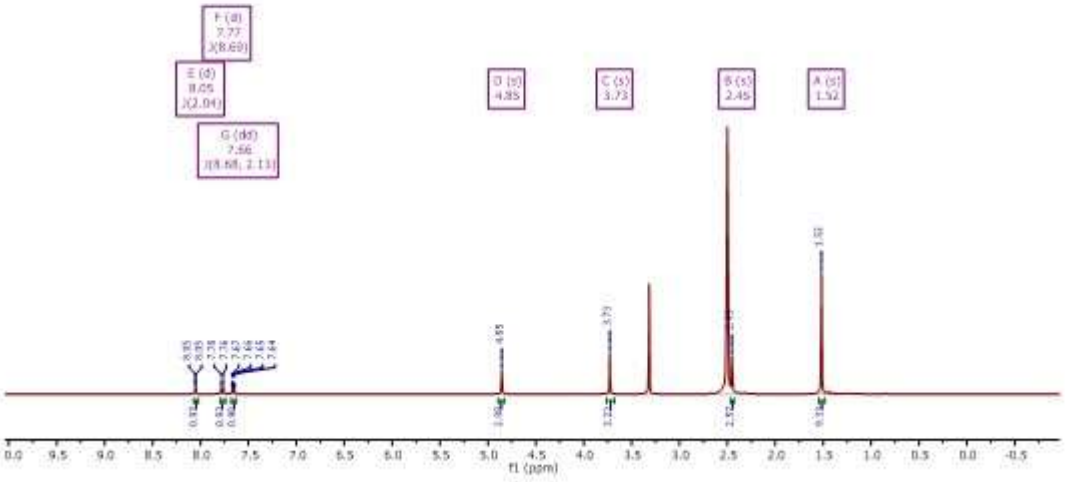

13C NMR (DMSO-d6, 101 MHz)

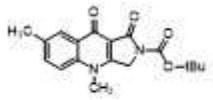

2-2.3j

1H NMR (DMSO-d6, 400 MHz)

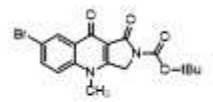

2-2.3k

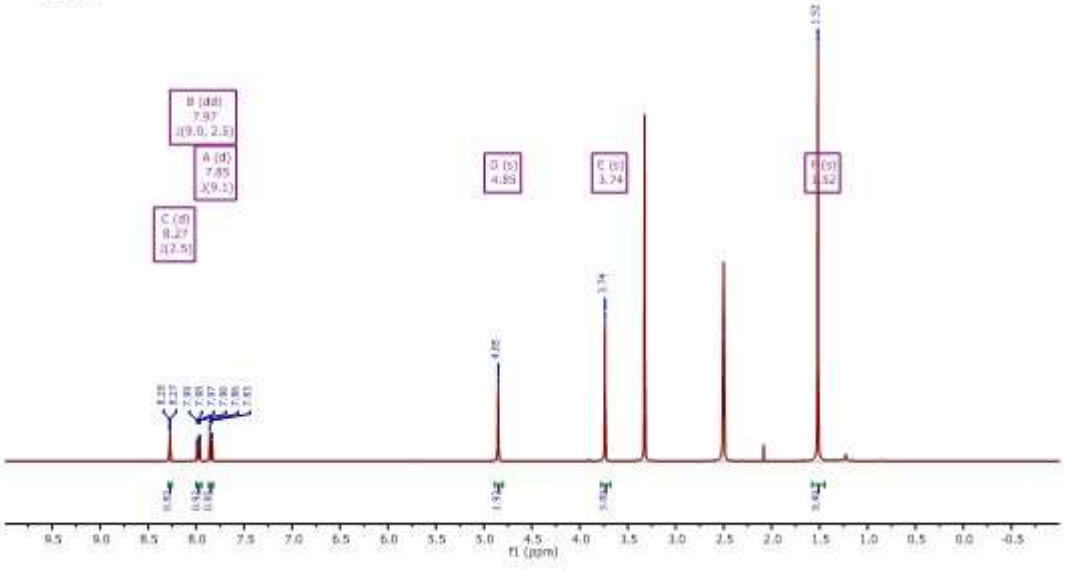

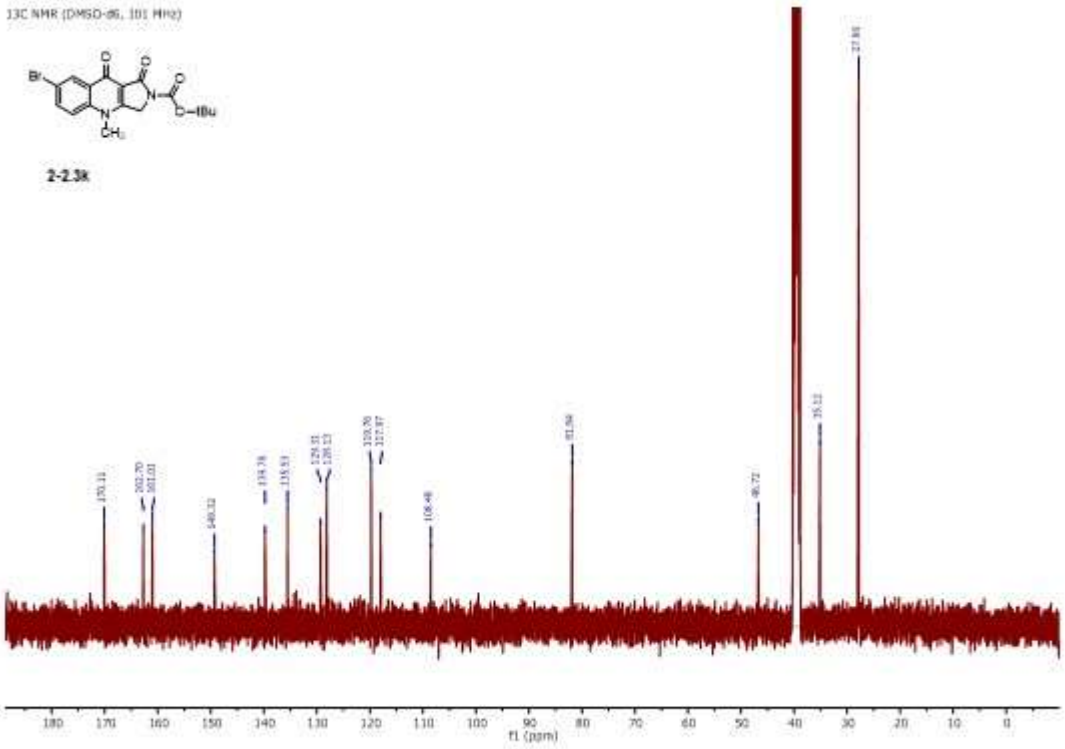
13C NMR (DMSO-d6, 101 MHz)
2-2.3k
f1 (ppm)

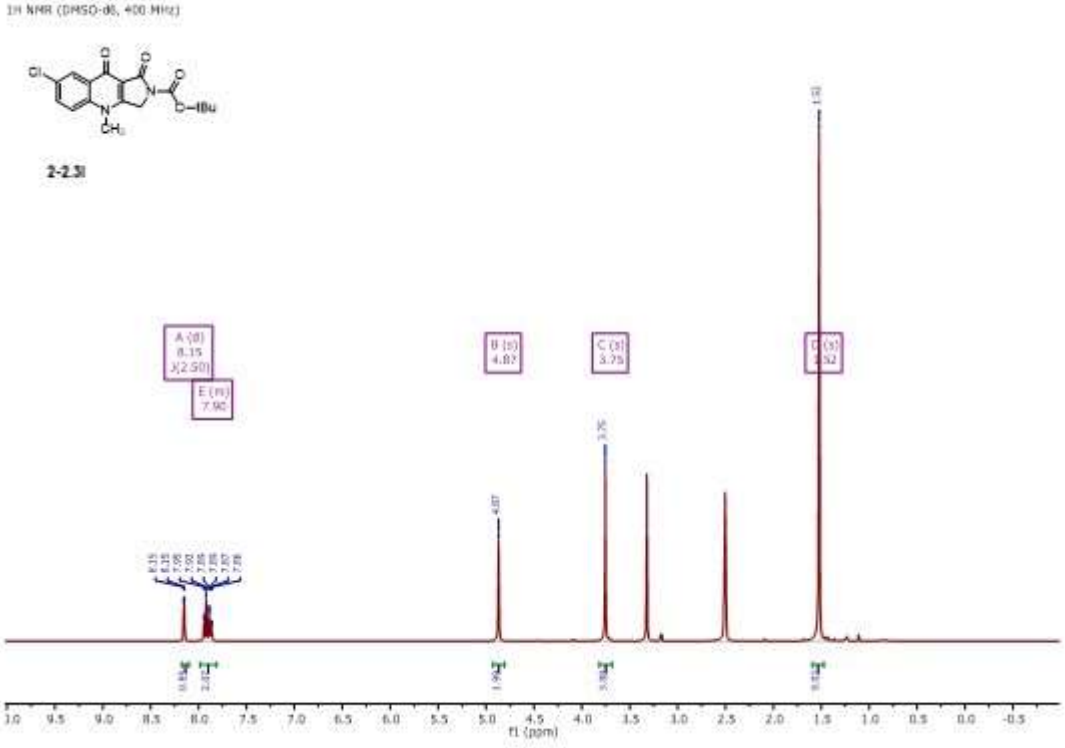
1H NMR (DMSO-d6, 400 MHz)
2-2.3l
f1 (ppm)

13C NMR (DMSO-d6, 101 MHz)

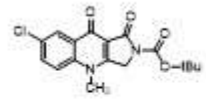

2-2.3l

1H NMR (DMSO-d6, 400 MHz)

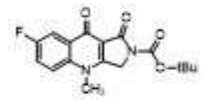

2-2.3m

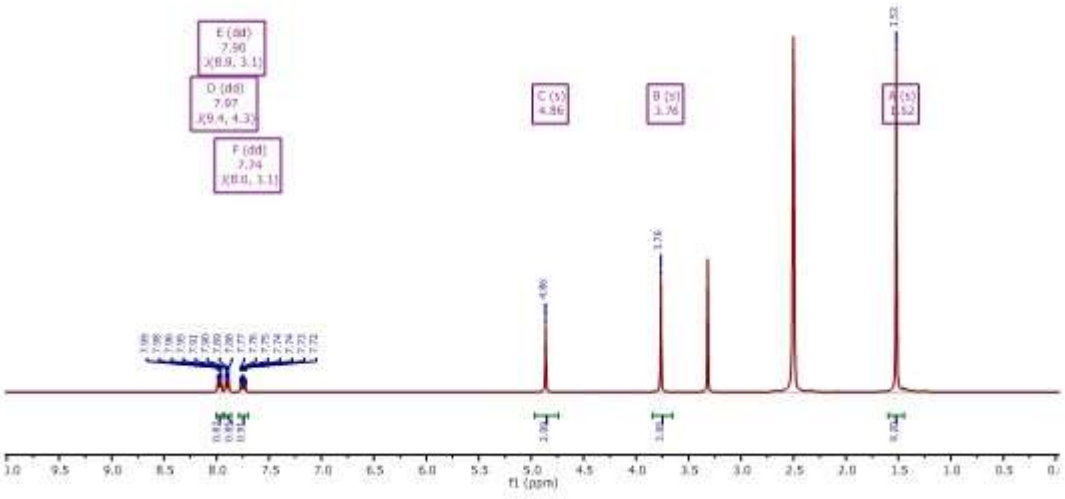

19F NMR (DMSO-d6, 376 MHz)

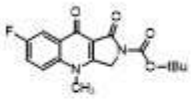

2-2.3m

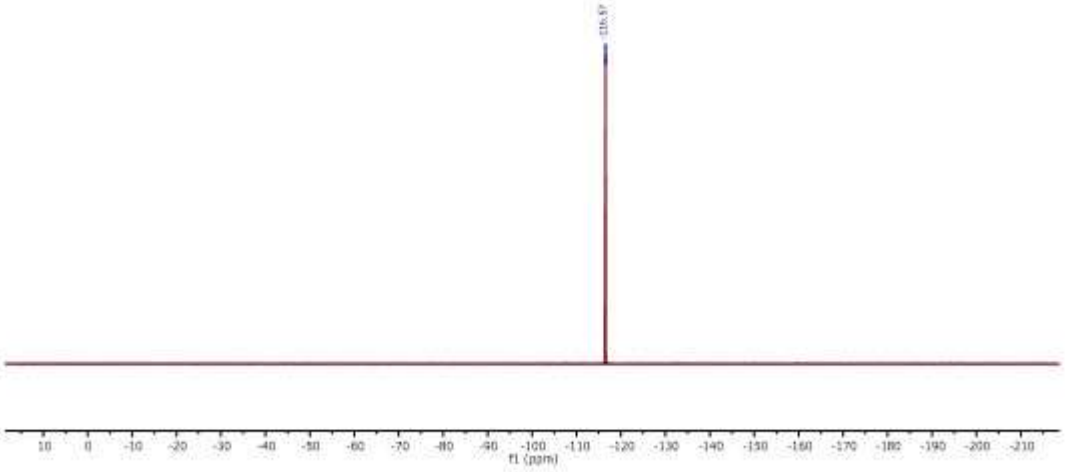

13C NMR (DMSO-d6, [illegible])

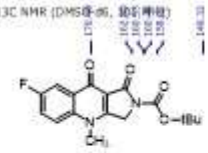

2-2.3m

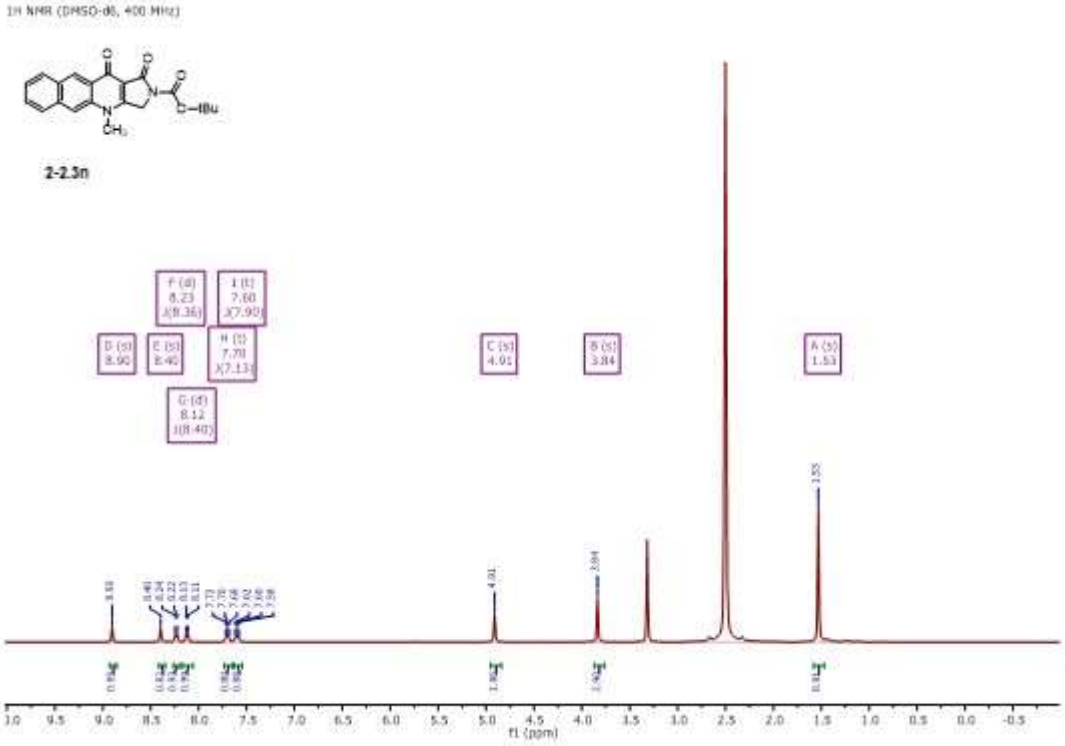
1H NMR (DMSO-d6, 400 MHz)
2-2.3n
F (d) 8.23 J(8.36)
I (t) 7.60 J(7.90)
D (s) 8.90
E (s) 8.40
H (t) 7.70 J(7.13)
G (d) 8.12 J(8.40)
C (s) 4.01
B (s) 3.84
A (s) 1.53
f1 (ppm)

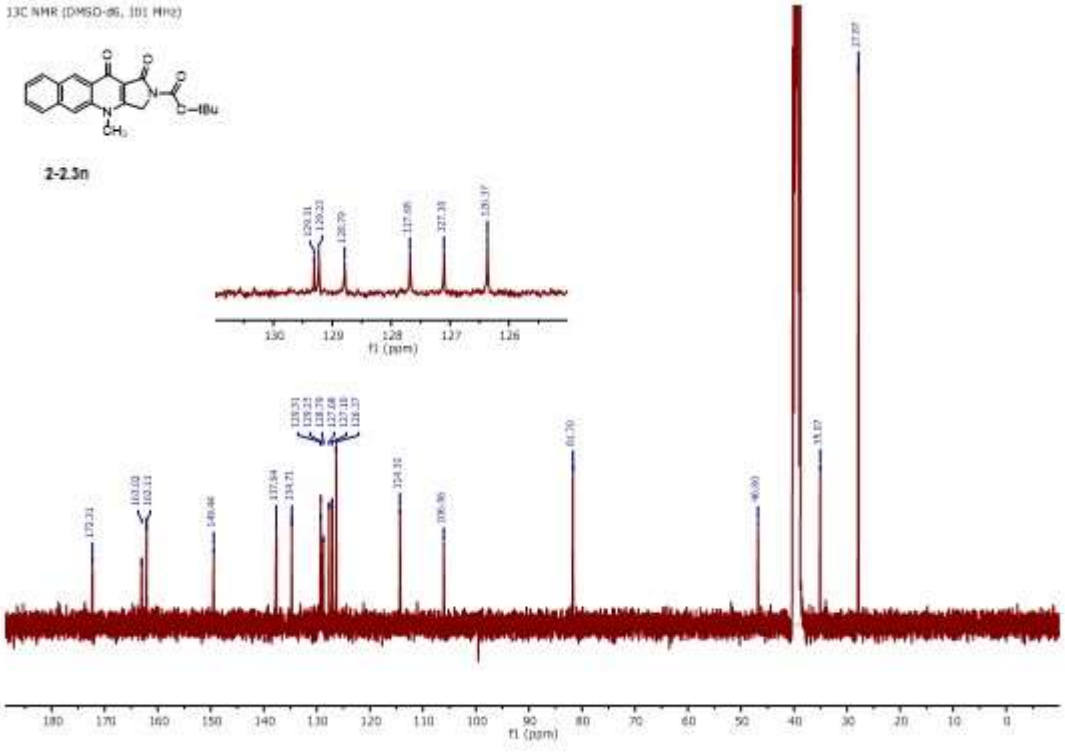
13C NMR (DMSO-d6, 101 MHz)
2-2.3n
f1 (ppm)

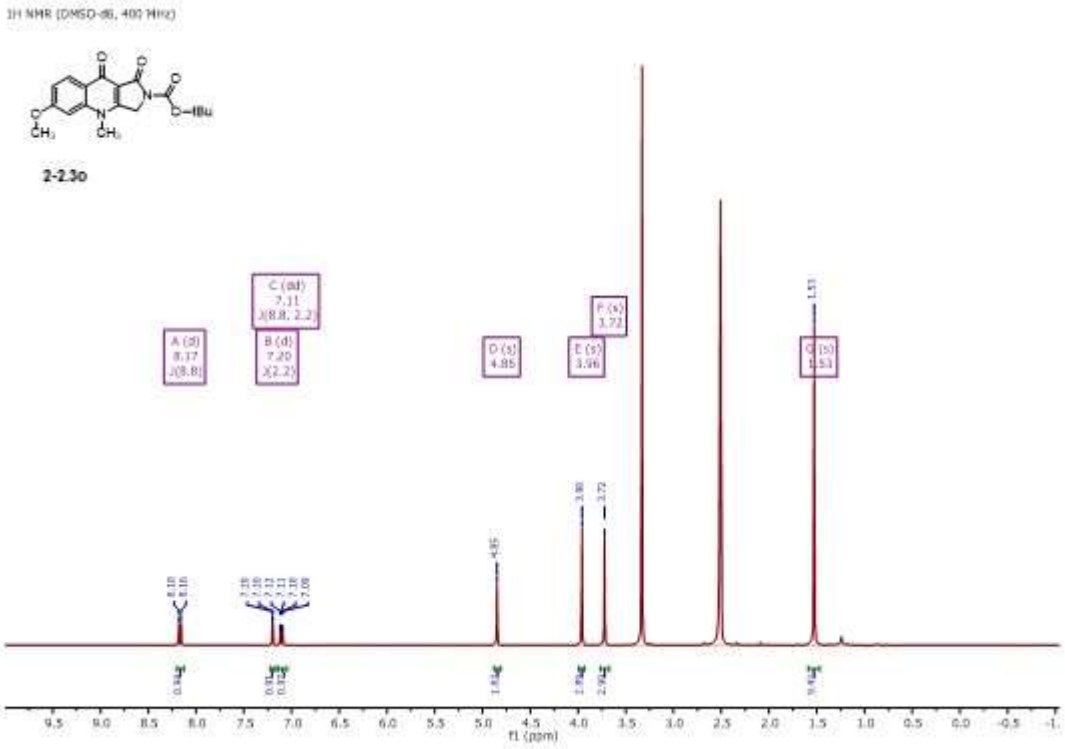
1H NMR (DMSO-d6, 400 MHz)
2-2.3o
A (d) 8.17 J(8.8)
B (d) 7.20 J(2.2)
C (dd) 7.11 J(8.8, 2.2)
D (s) 4.85
E (s) 3.96
F (s) 3.72
G (s) 1.53
f1 (ppm)

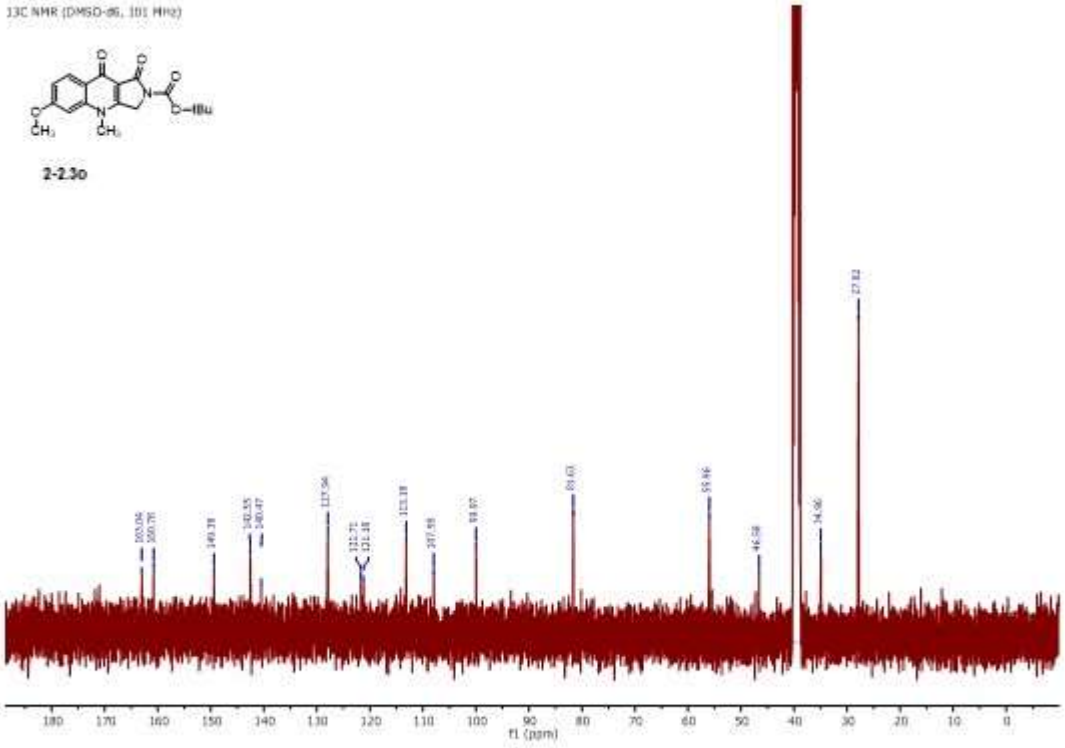
13C NMR (DMSO-d6, 101 MHz)
2-2.3o
f1 (ppm)

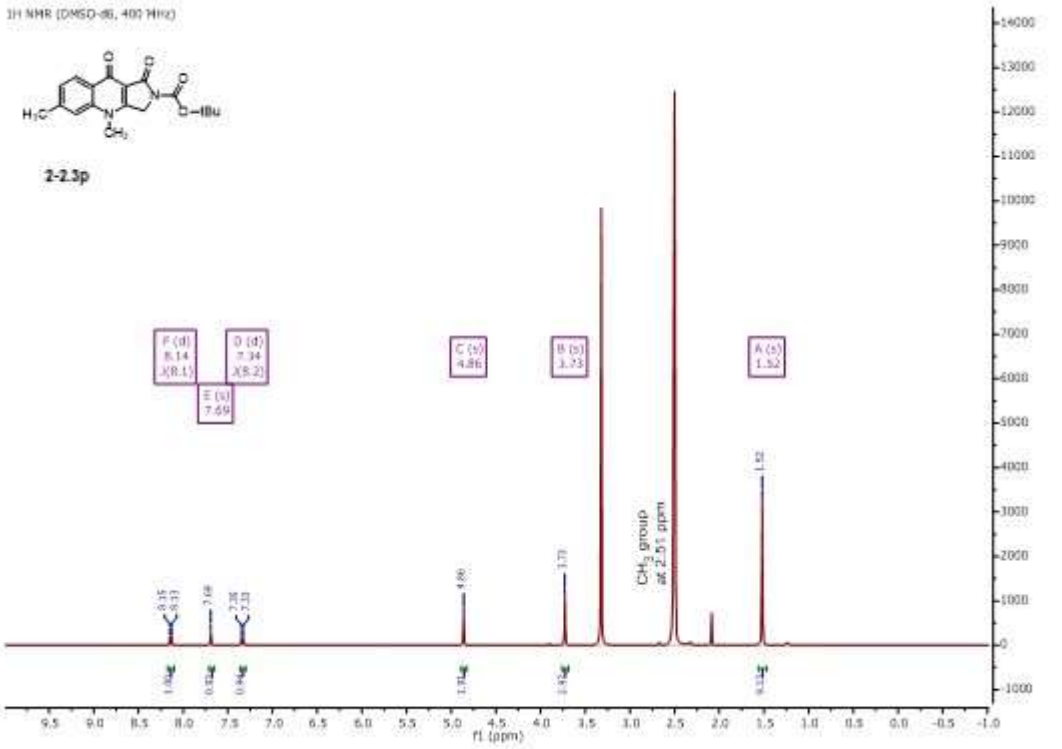
1H NMR (DMSO-d6, 400 MHz)
2-2.3p
F (d) 8.14 J(8.1)
D (d) 7.34 J(8.2)
E (s) 7.69
C (s) 4.86
B (s) 3.73
A (s) 1.52
CH3 group at 2.51 ppm
f1 (ppm)

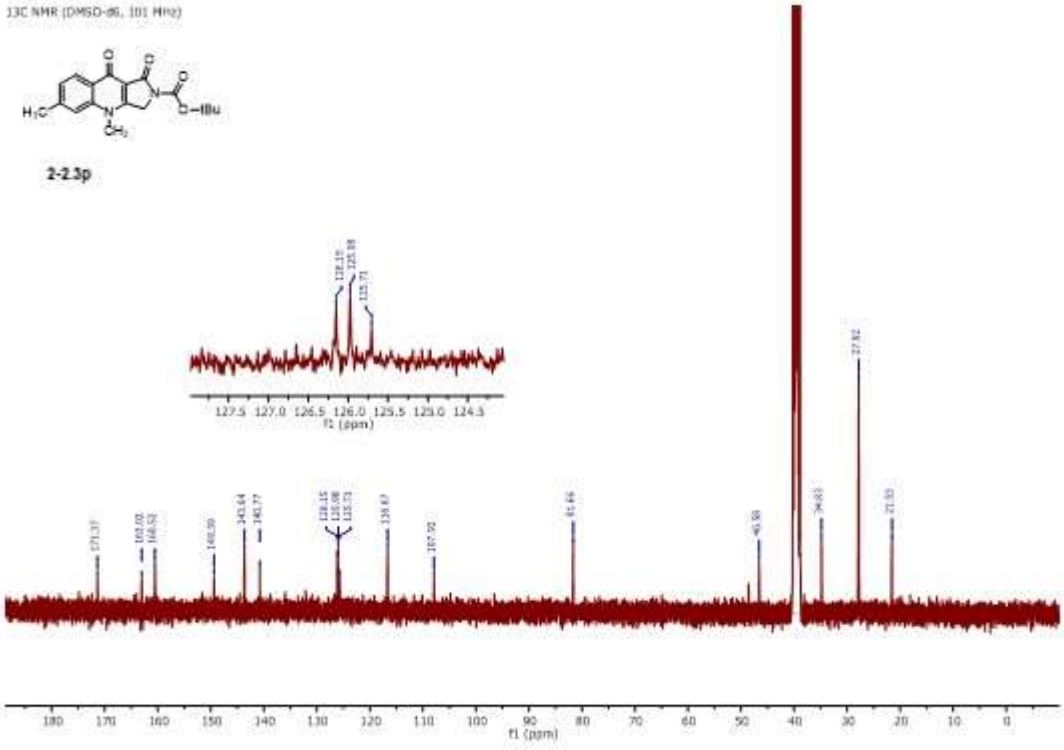
13C NMR (DMSO-d6, 101 MHz)
2-2.3p
f1 (ppm)

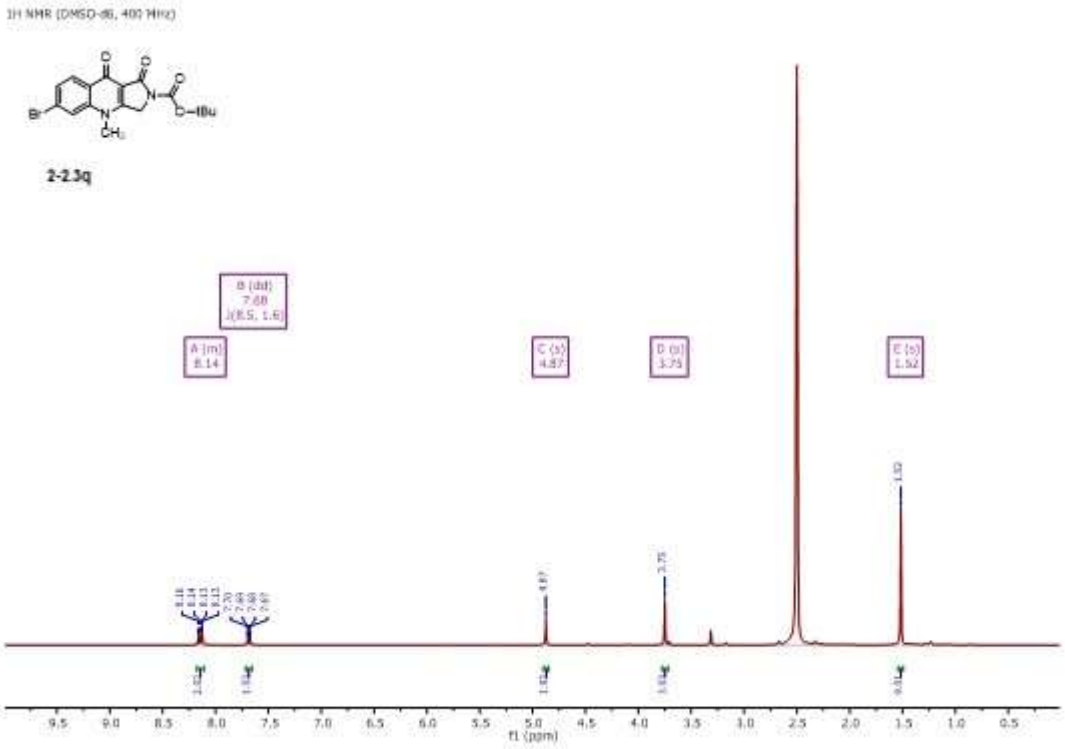
1H NMR (DMSO-d6, 400 MHz)
2-2.3q
B (dd)
7.68
J(8.5, 1.6)
A (m)
8.14
C (s)
4.87
D (s)
3.75
E (s)
1.52
f1 (ppm)

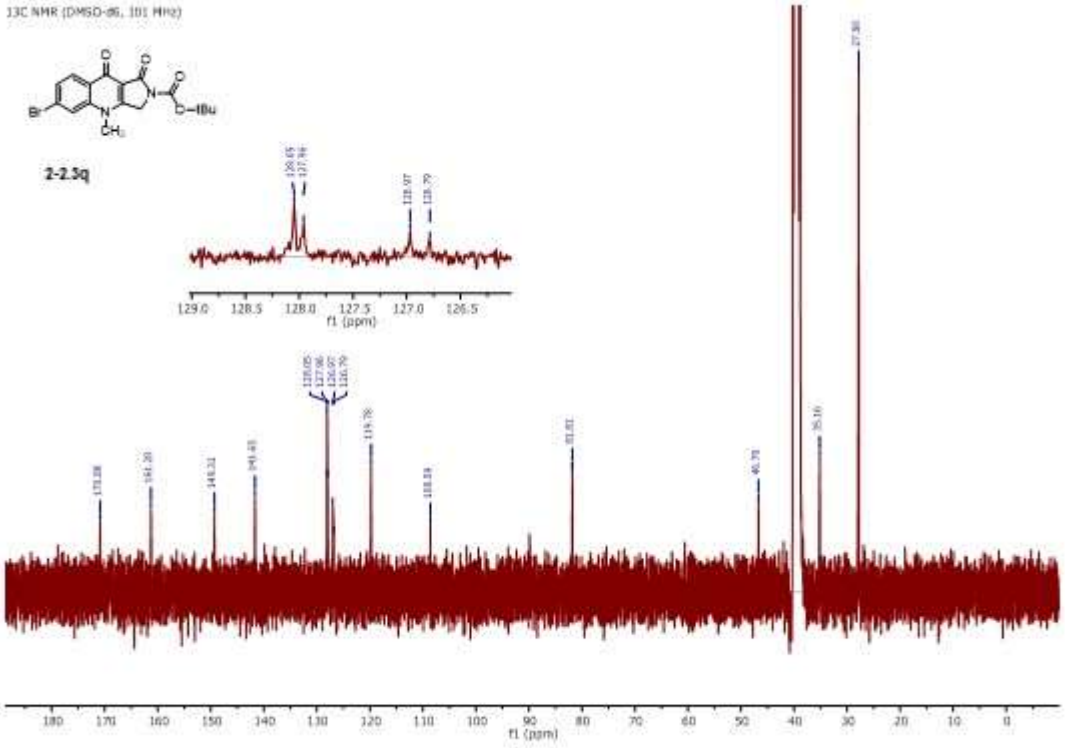
13C NMR (DMSO-d6, 101 MHz)
2-2.3q
f1 (ppm)

1H NMR (DMSO-d6, 400 MHz)

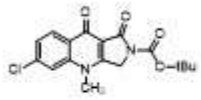

2-2.3r

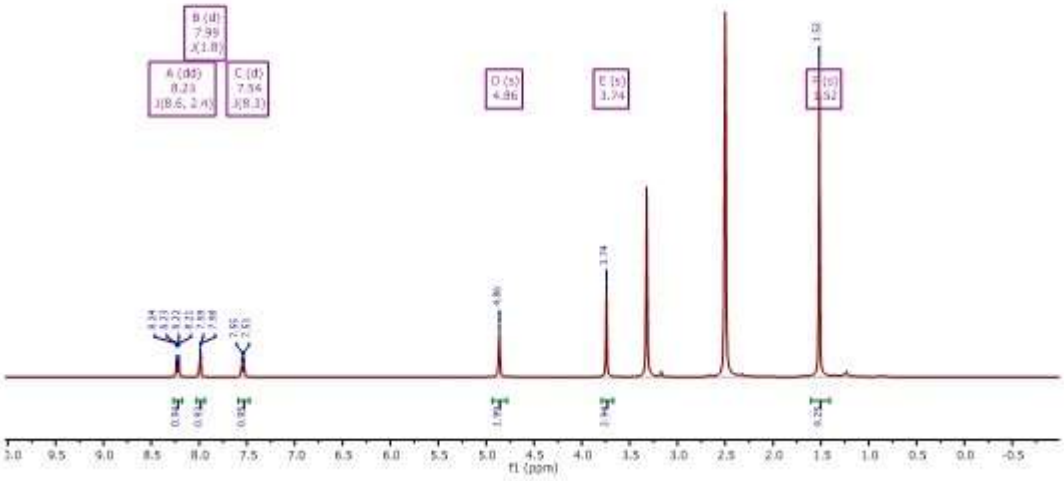

13C NMR (DMSO-d6, 101 MHz)

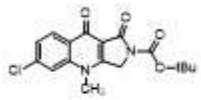

2-2.3r

1H NMR (DMSO-d6, 400 MHz)

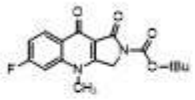

2-2.3s

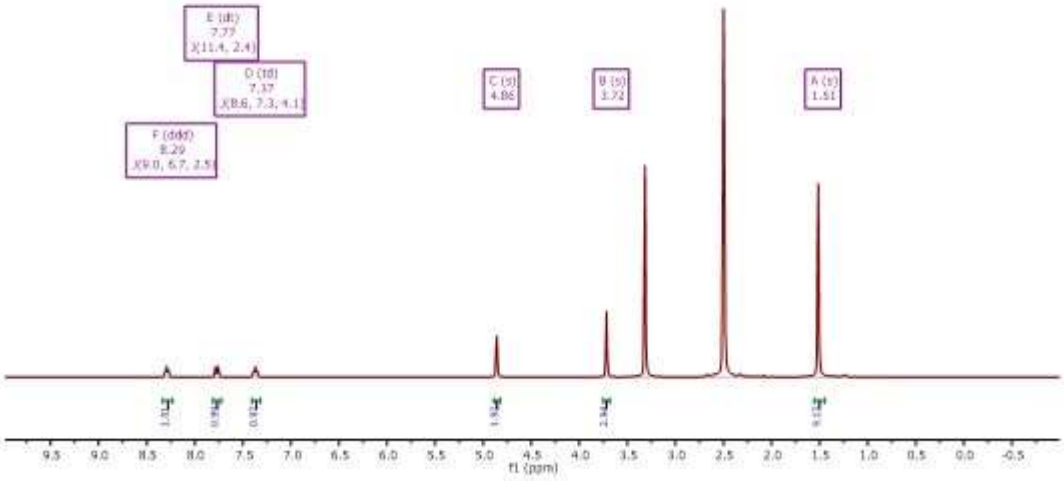

19F NMR (DMSO-d6, 376 MHz)

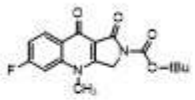

2-2.3s

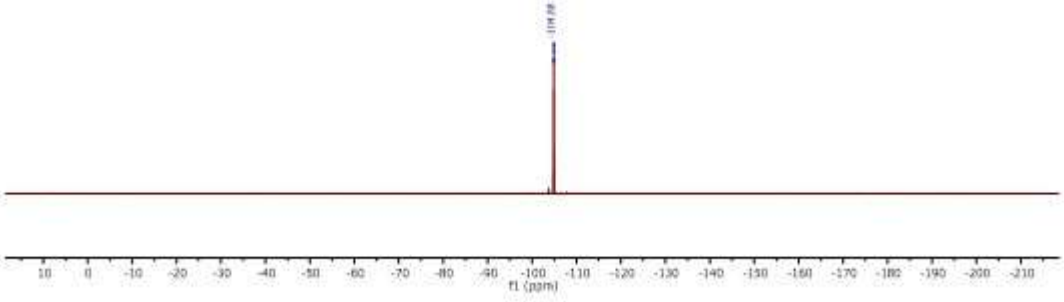

13C NMR (DMSO-d6, 101 MHz)

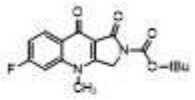

2-2.3s

1H NMR (DMSO-d6, 400 MHz)

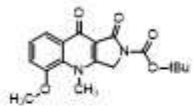

2-2.3t

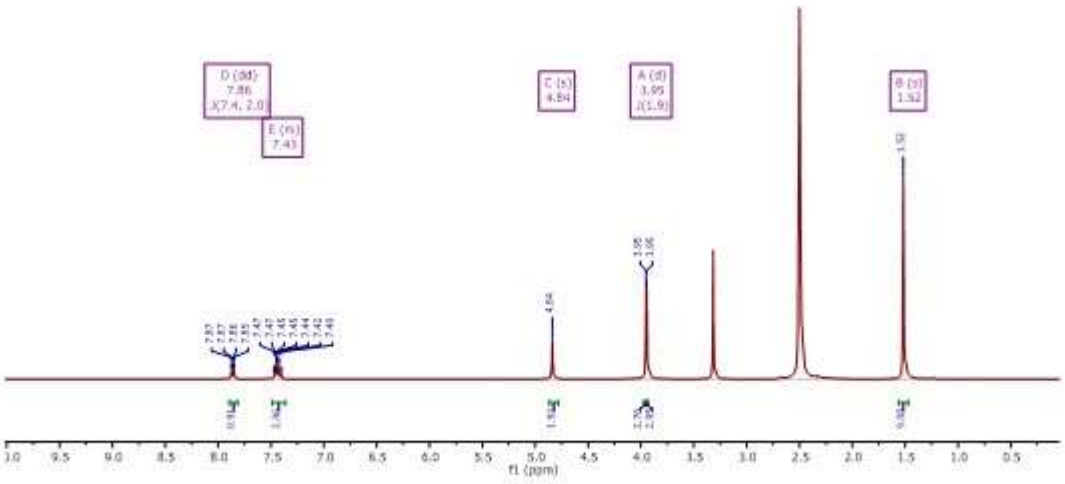

13C NMR (DMSO-d6, 101 MHz)

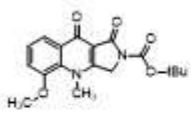

2-2.3t

1H NMR (DMSO-d6, 400 MHz)

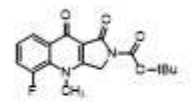

2-2.3u

19F NMR (DMSO-d6, 376 MHz)

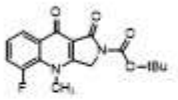

2-2.3u

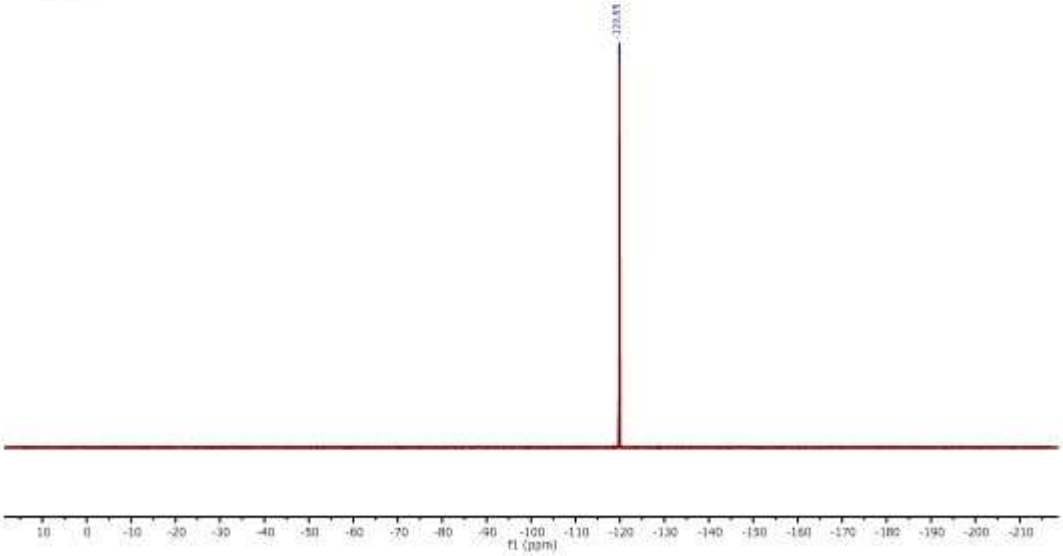

13C NMR (DMSO-d6, 101 MHz)

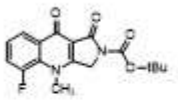

2-2.3u

1H NMR (DMSO-d6, 400 MHz)

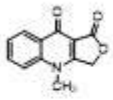

2-2.17

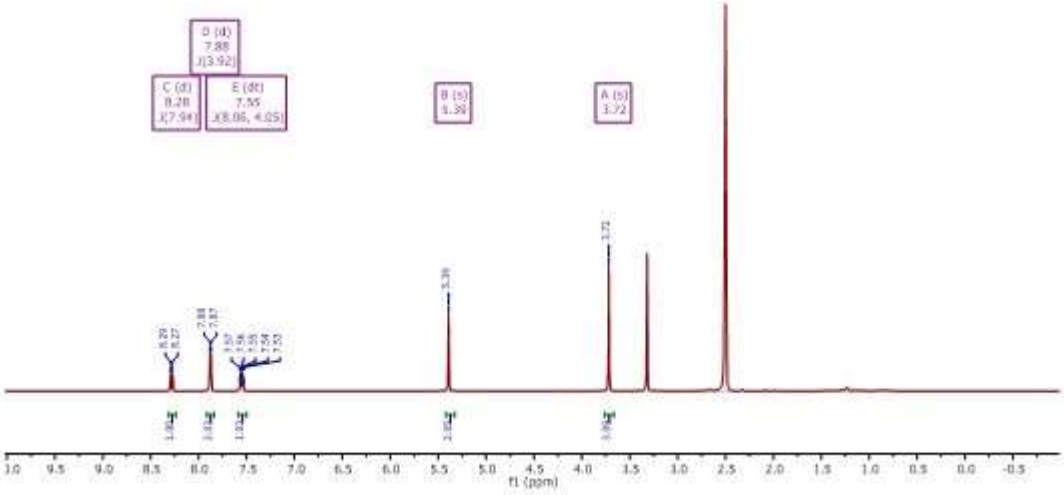

13C NMR (DMSO-d6, 101 MHz)

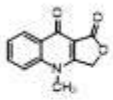

2-2.17

1H NMR (400 MHz, DMSO-d6)

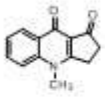

2-2.19

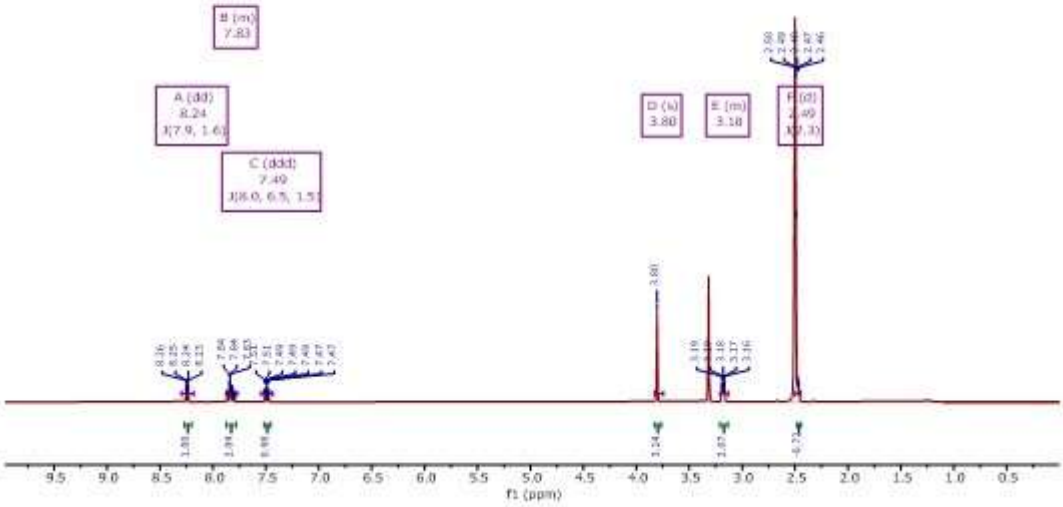

13C NMR (101 MHz, DMSO-d6)

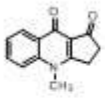

2-2.19

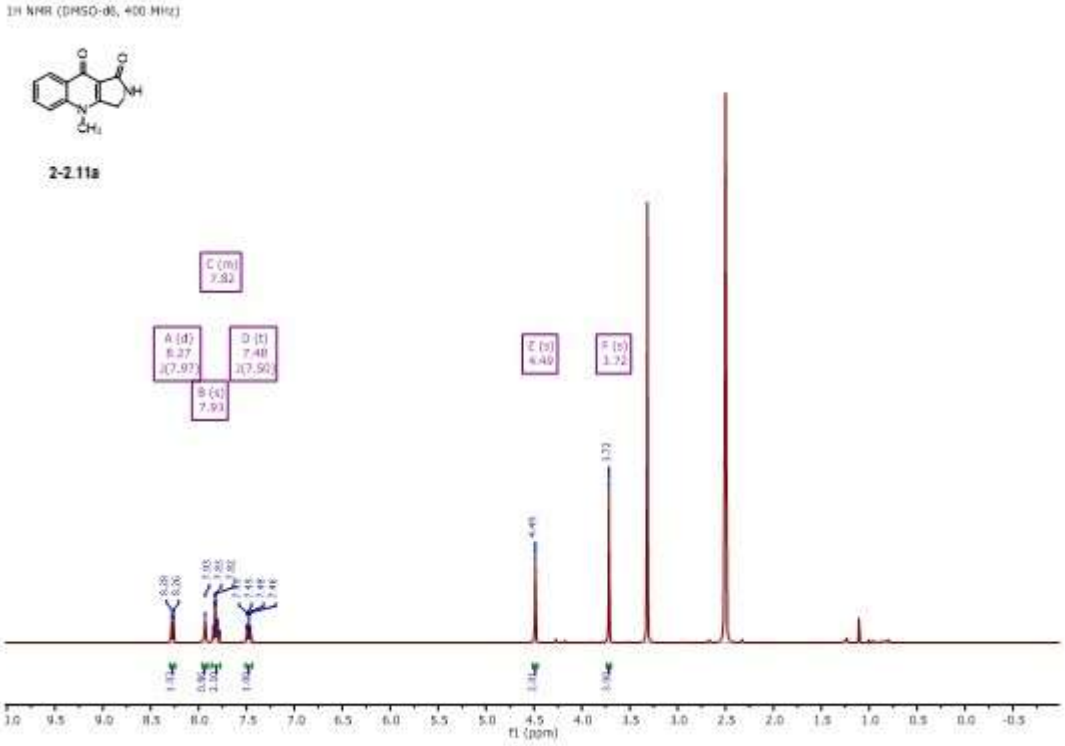
1H NMR (DMSO-d6, 400 MHz)
2-2.11a
C (m)
7.82
A (d)
8.27
J(7.97)
B (s)
7.93
D (t)
7.48
J(7.50)
E (s)
4.49
F (s)
3.72
f1 (ppm)

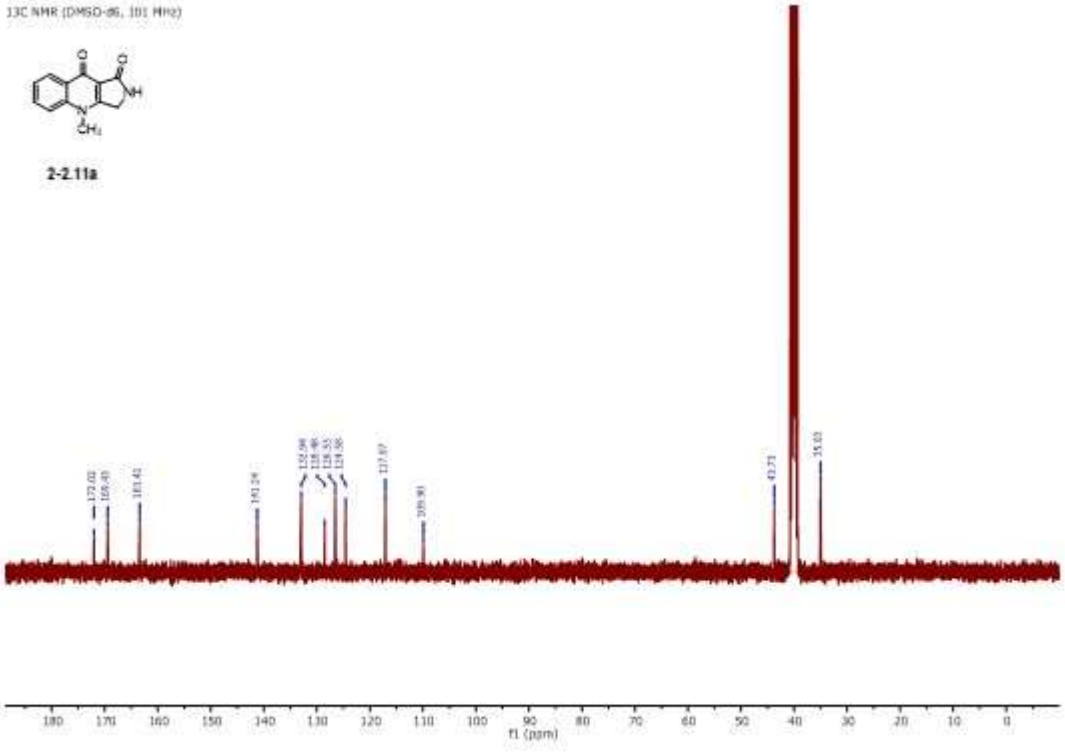
13C NMR (DMSO-d6, 101 MHz)
2-2.11a
f1 (ppm)

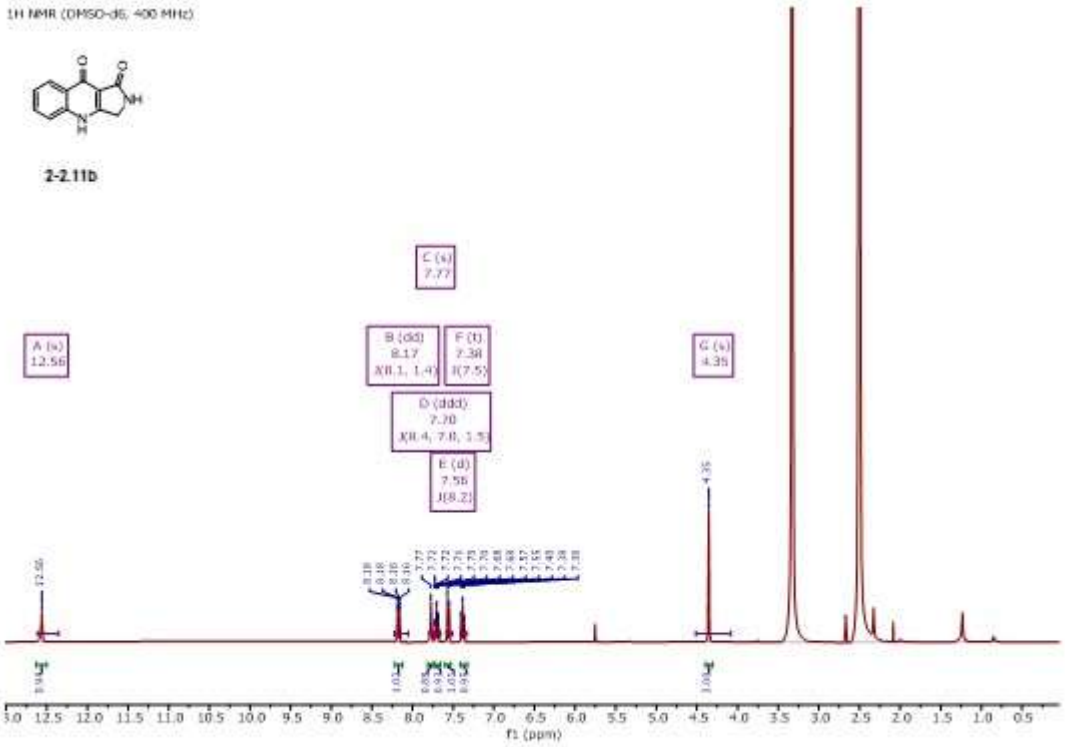
1H NMR (DMSO-d6, 400 MHz)
2-2.11b
A (s) 12.56
B (dd) 8.17 J(8.1, 1.4)
C (s) 7.77
D (ddd) 7.70 J(8.4, 7.0, 1.5)
E (d) 7.55 J(8.2)
F (t) 7.38 J(7.5)
G (s) 4.35
f1 (ppm)

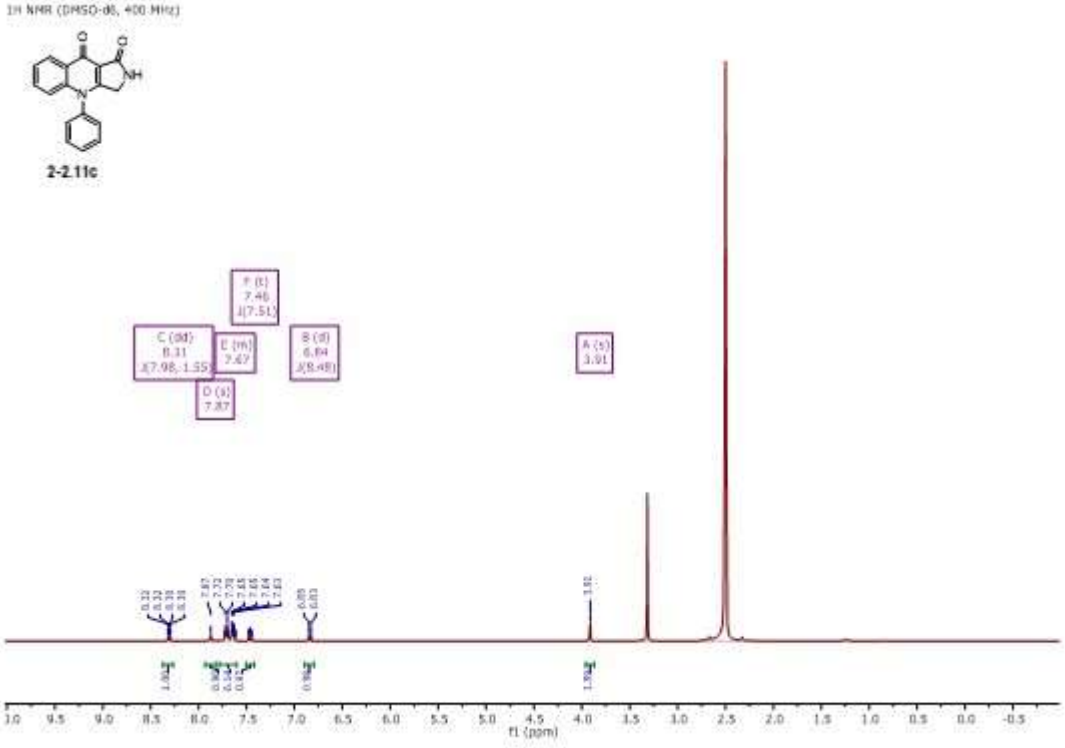
1H NMR (DMSO-d6, 400 MHz)
2-2.11c
A (s) 3.91
B (d) 6.84 J(8.48)
C (dd) 8.31 J(7.98, 1.55)
D (s) 7.87
E (m) 7.67
F (t) 7.46 J(7.51)
f1 (ppm)

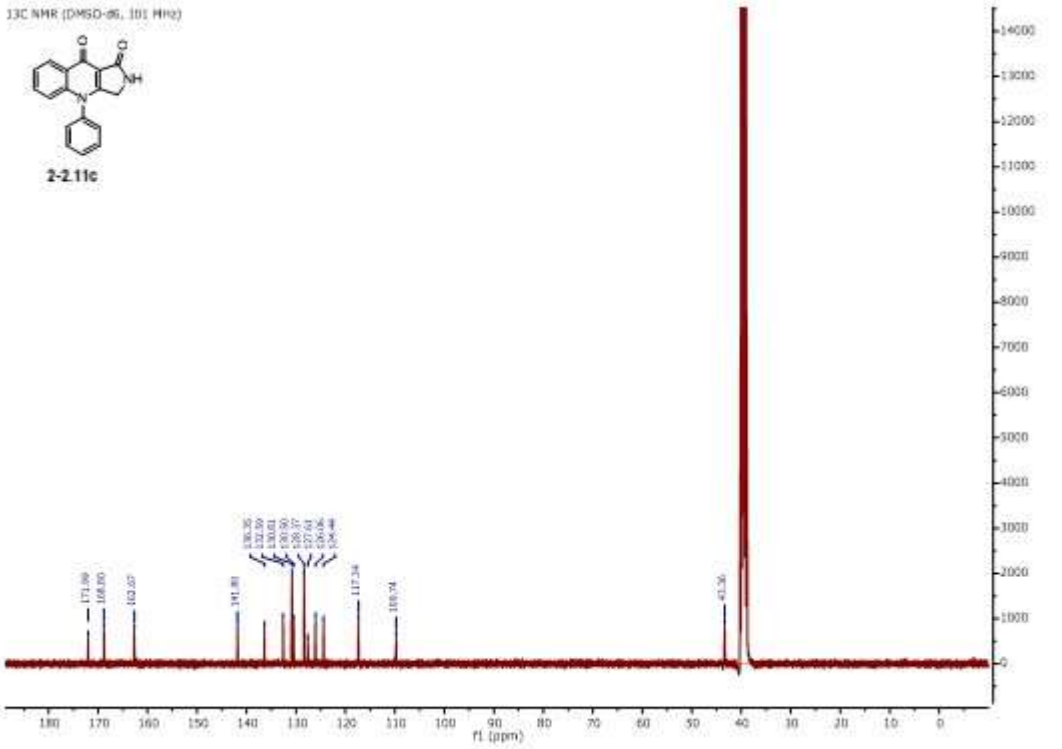
13C NMR (DMSO-d6, 101 MHz)
2-2.11c
f1 (ppm)

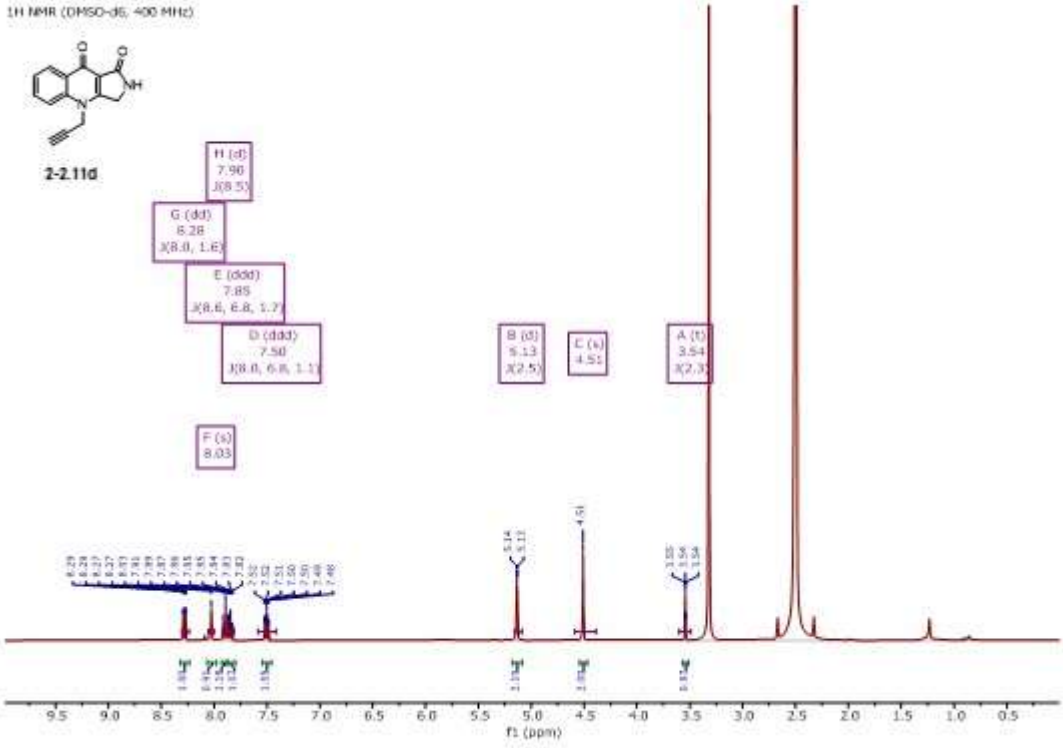
1H NMR (DMSO-d6, 400 MHz)
2-2.11d
H (d)
7.96
J(8.5)
G (dd)
8.28
J(8.0, 1.6)
E (ddd)
7.85
J(8.6, 6.8, 1.7)
D (ddd)
7.50
J(8.0, 6.8, 1.1)
F (s)
8.03
B (d)
5.13
J(2.5)
C (s)
4.51
A (t)
3.54
J(2.3)
f1 (ppm)

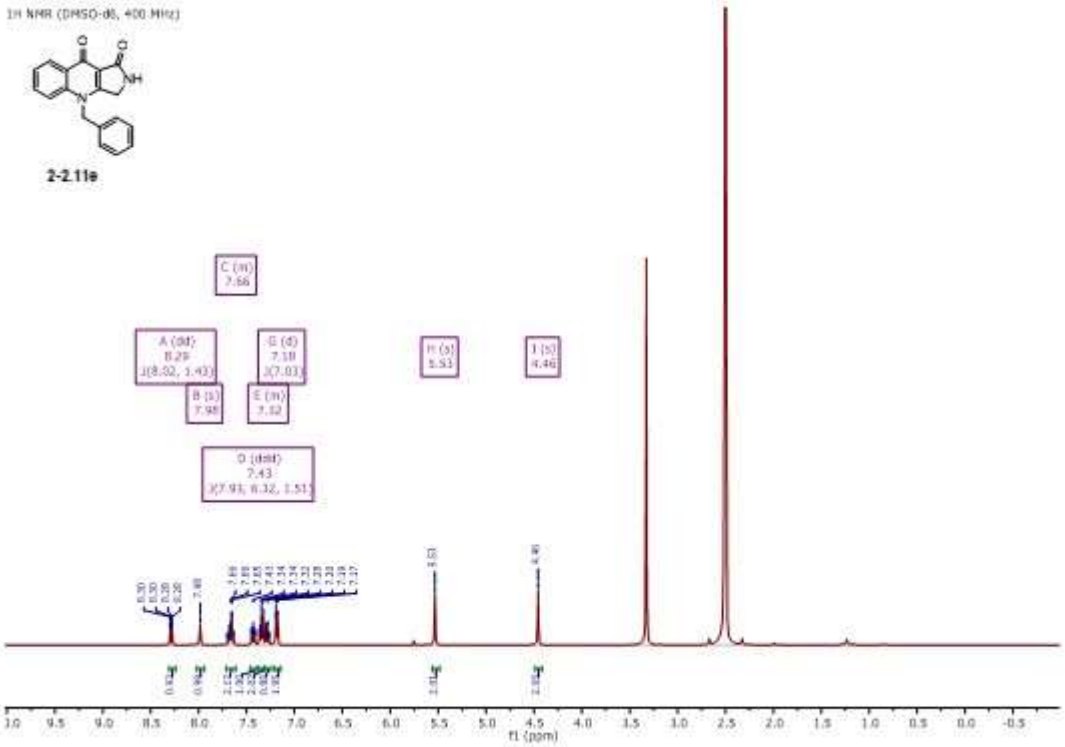
1H NMR (DMSO-d6, 400 MHz)
2-2.11e
f1 (ppm)

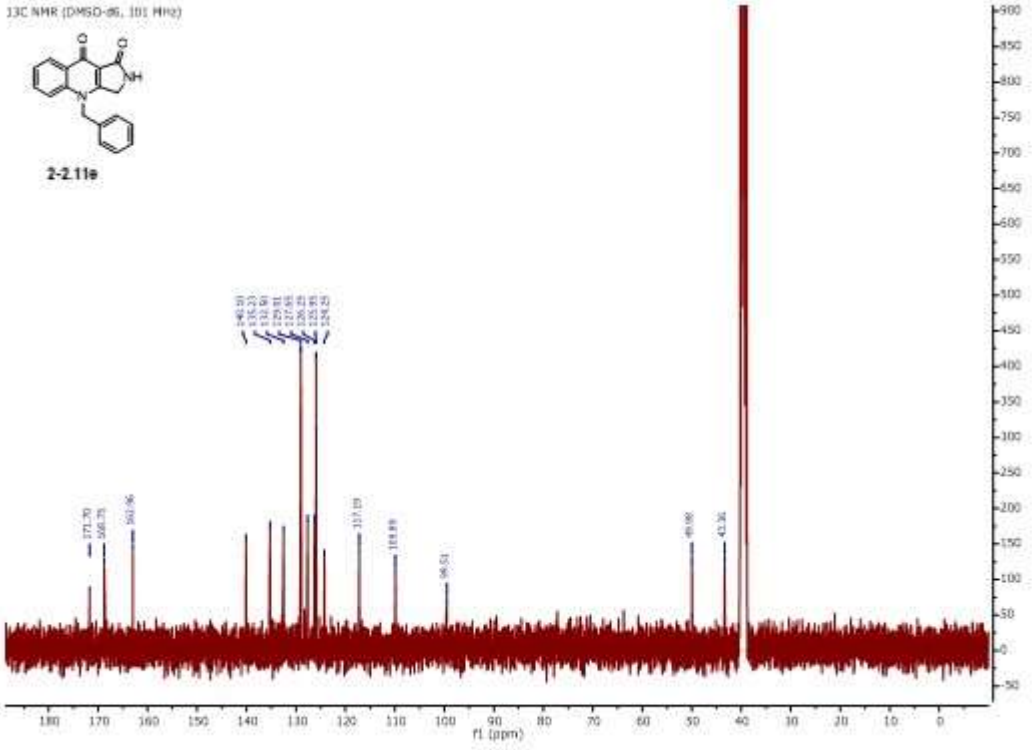
13C NMR (DMSO-d6, 101 MHz)
2-2.11e
f1 (ppm)

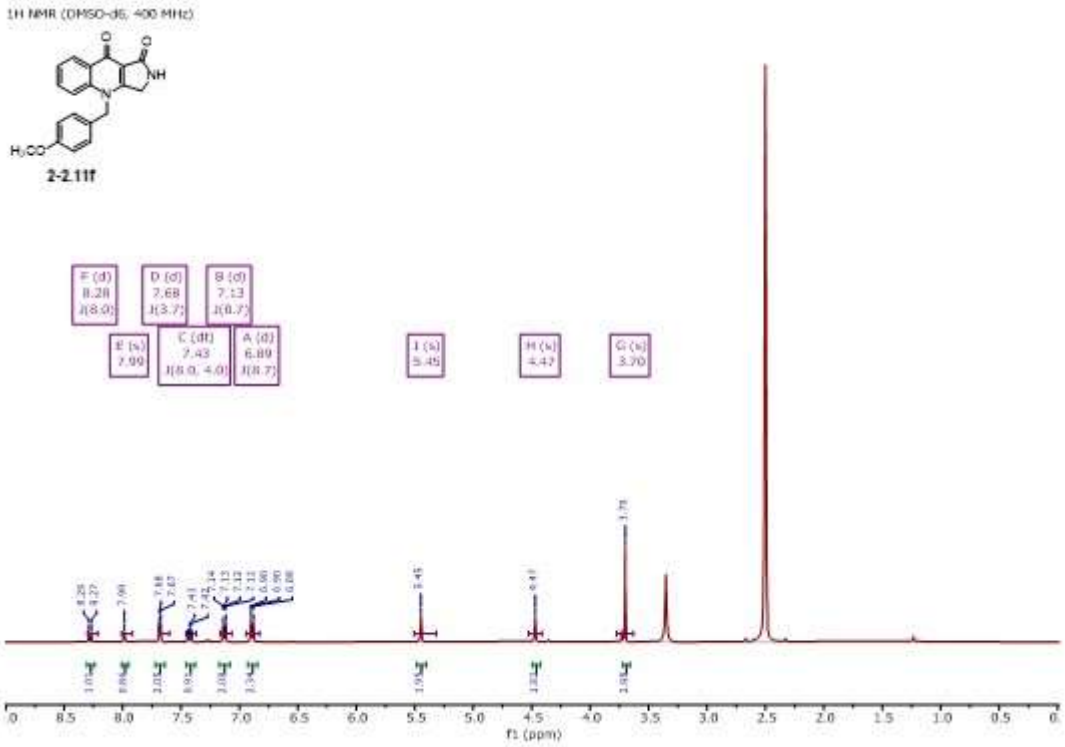
1H NMR (DMSO-d6, 400 MHz)
2-2.11f
F (d) 8.28 J(8.0)
D (d) 7.68 J(3.7)
B (d) 7.13 J(8.7)
E (s) 7.99
C (dt) 7.43 J(8.0, 4.0)
A (d) 6.89 J(8.7)
I (s) 5.45
H (s) 4.47
G (s) 3.70
f1 (ppm)

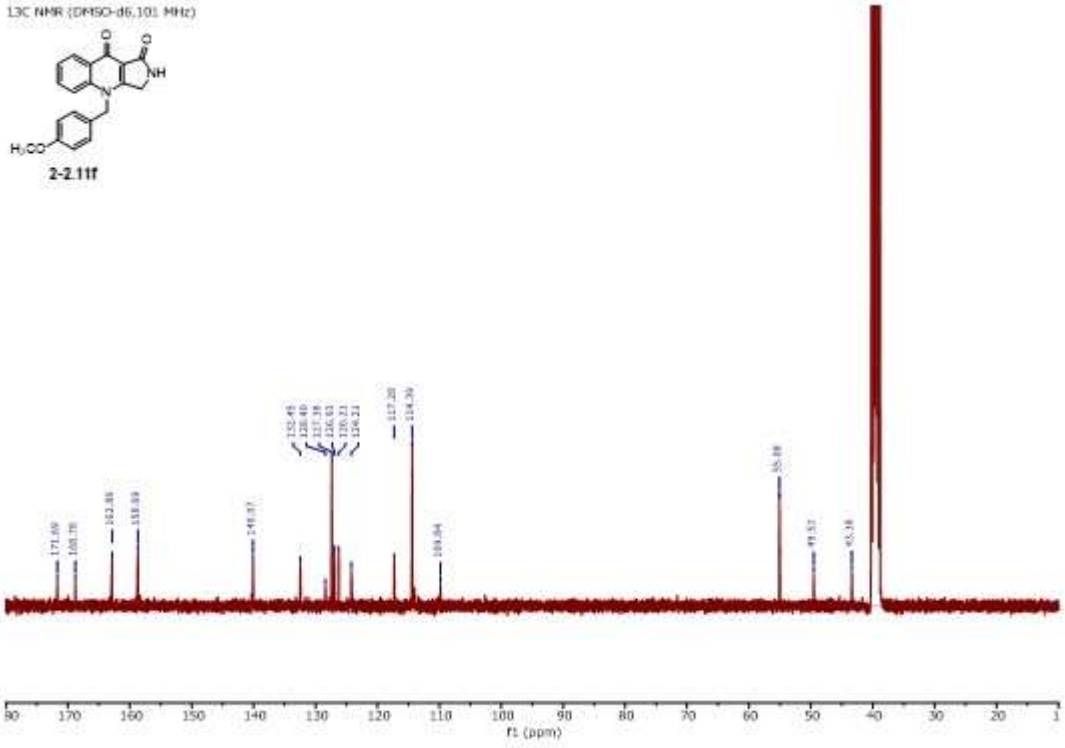
13C NMR (DMSO-d6,101 MHz)
2-2.11f
f1 (ppm)

1H NMR (DMSO-d6, 400 MHz)

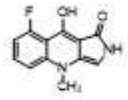

2-2.11h

19F NMR (DMSO-d6, 376 MHz)

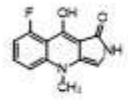

2-2.11h

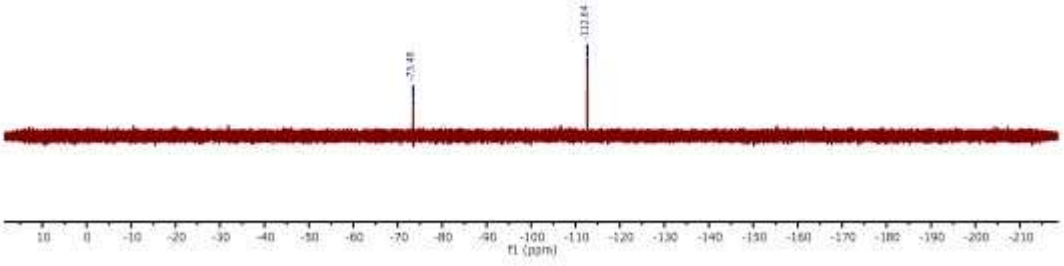

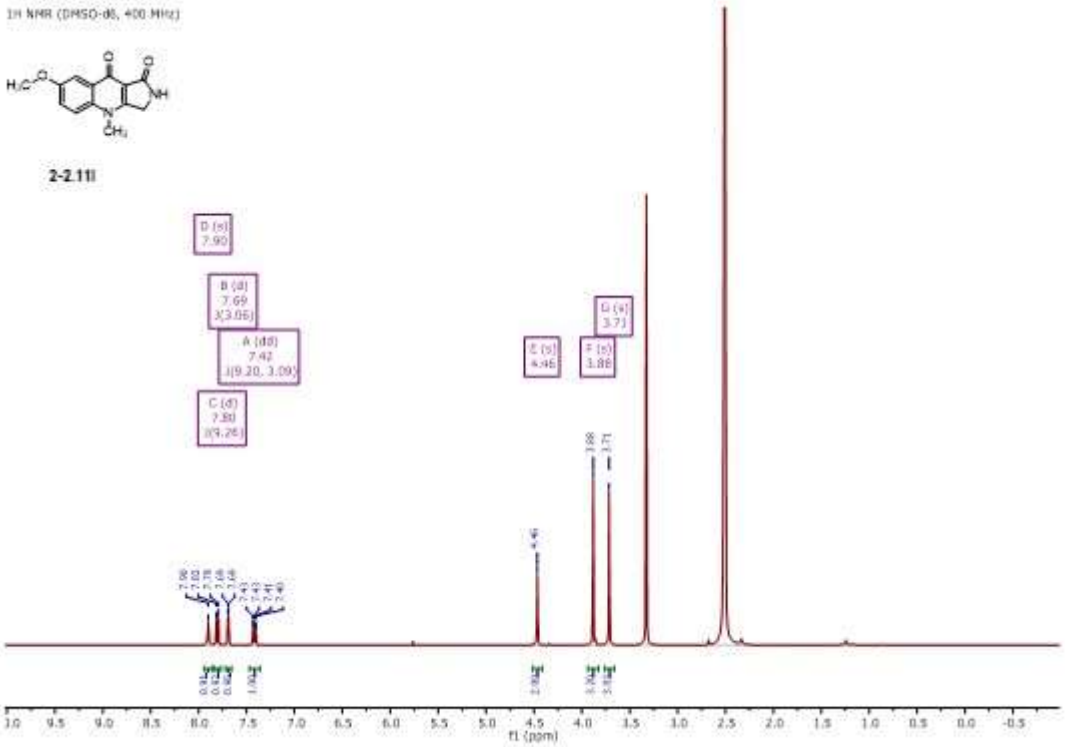
1H NMR (DMSO-d6, 400 MHz)
2-2.11l
D (s)
7.90
B (dd)
7.69
J(3.06)
A (dd)
7.42
J(9.20, 3.09)
C (d)
7.30
J(9.26)
G (s)
3.71
E (s)
4.46
F (s)
3.88
f1 (ppm)

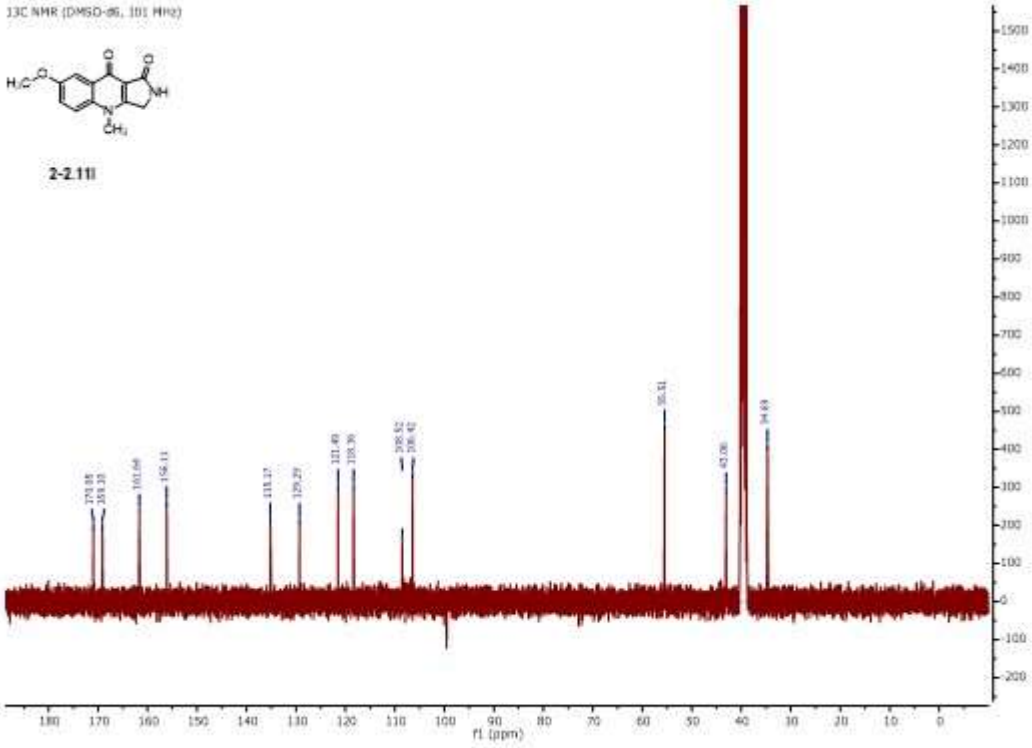
13C NMR (DMSO-d6, 101 MHz)
2-2.11l
f1 (ppm)

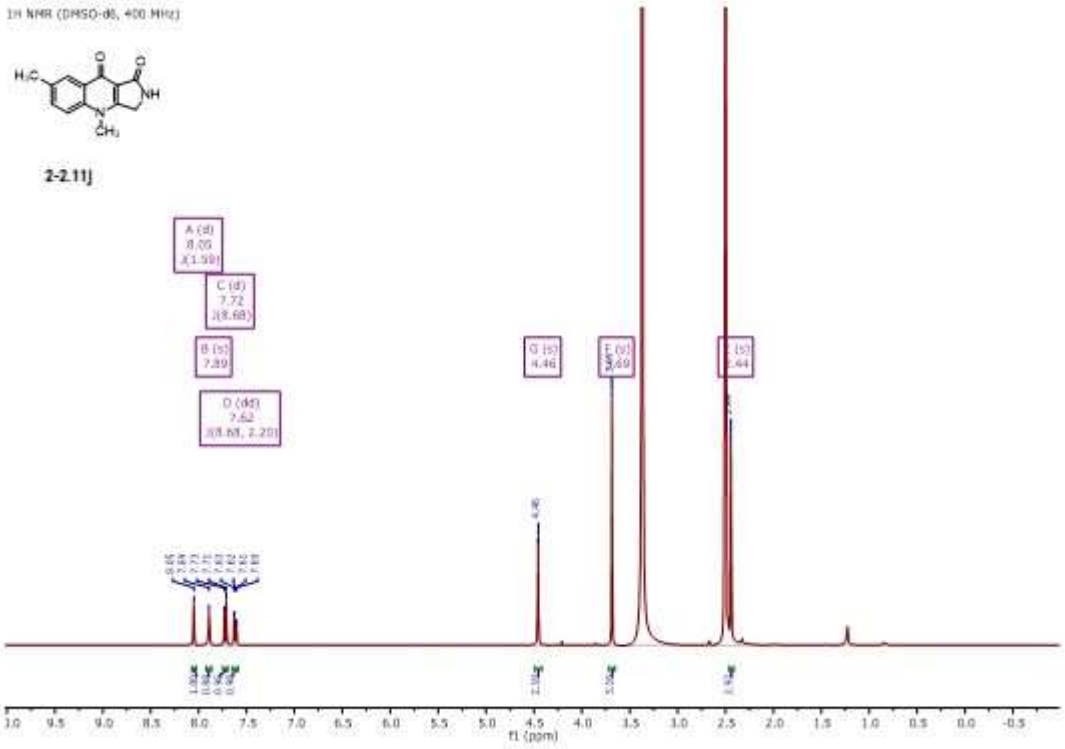
1H NMR (DMSO-d6, 400 MHz)
2-2.11J
A (d)
8.05
J(1.59)
C (d)
7.72
J(8.68)
B (s)
7.89
D (dd)
7.62
J(8.68, 2.20)
G (s)
4.46
F (s)
3.69
E (s)
2.44
f1 (ppm)

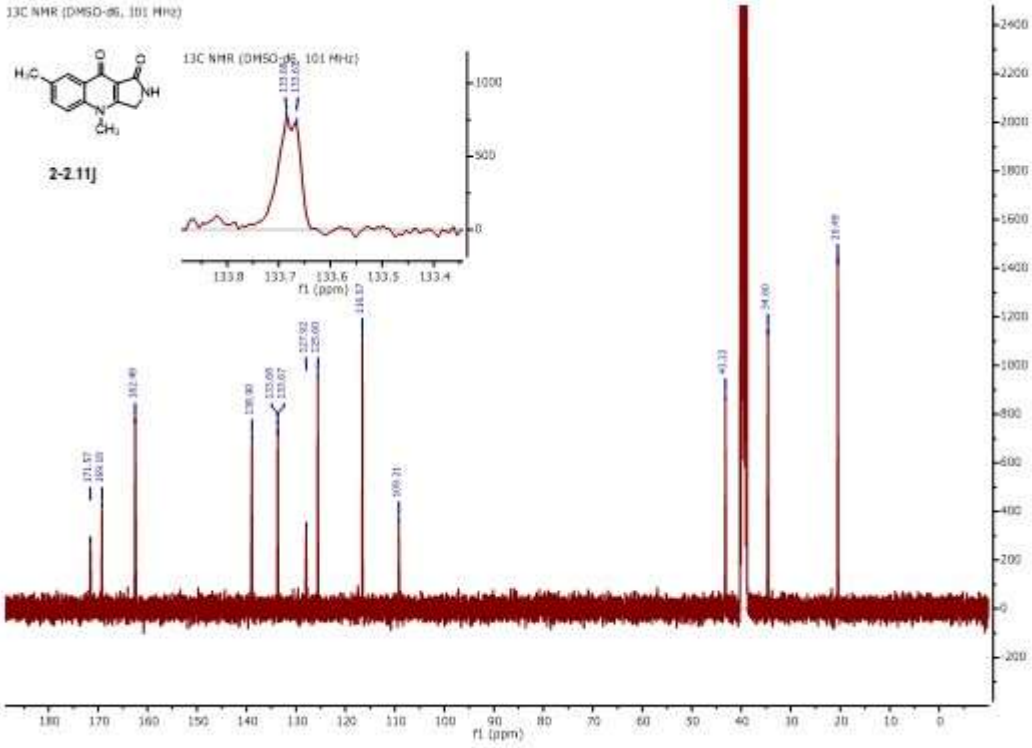
13C NMR (DMSO-d6, 101 MHz)
2-2.11J
13C NMR (DMSO-d6, 101 MHz)
f1 (ppm)

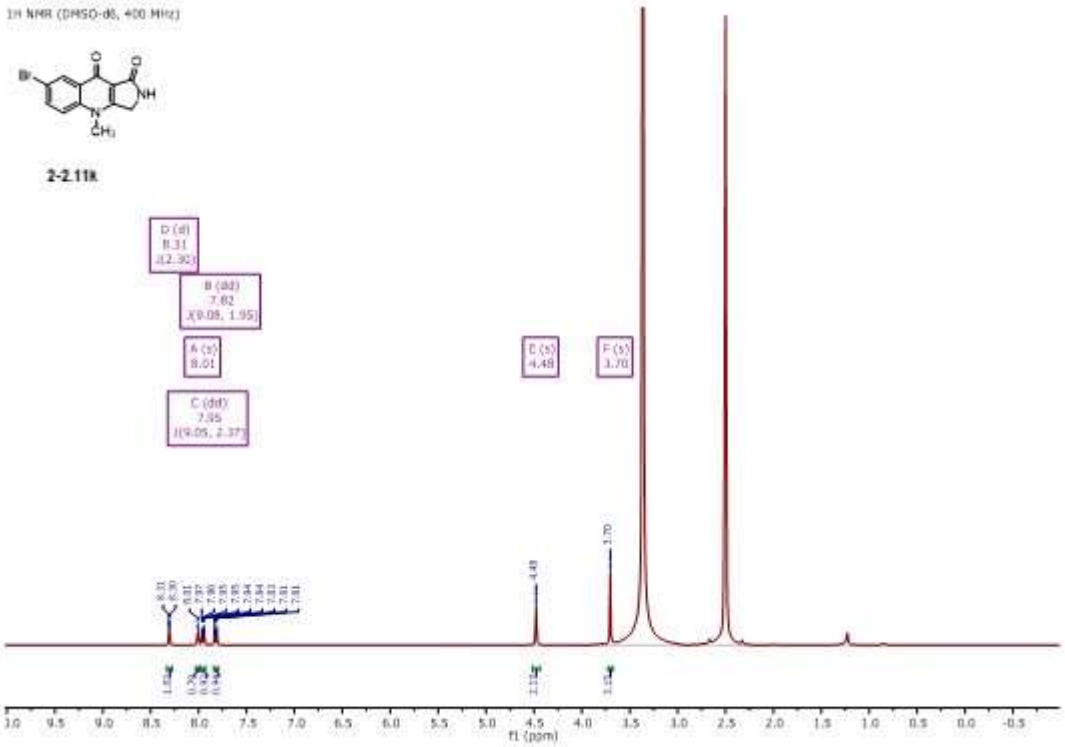
1H NMR (DMSO-d6, 400 MHz)
2-2.11k
D (d)
8.31
J(2.30)
B (dd)
7.82
J(9.09, 1.95)
A (s)
8.01
C (dd)
7.95
J(9.05, 2.37)
E (s)
4.48
F (s)
3.70
f1 (ppm)

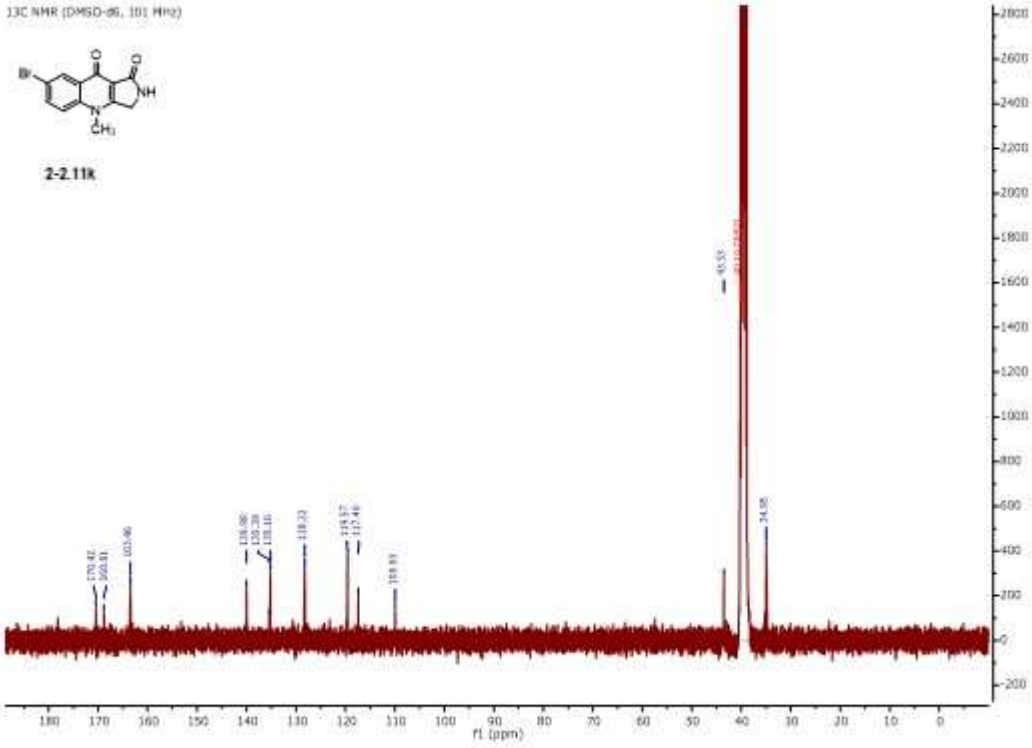
13C NMR (DMSO-d6, 101 MHz)
2-2.11k
f1 (ppm)

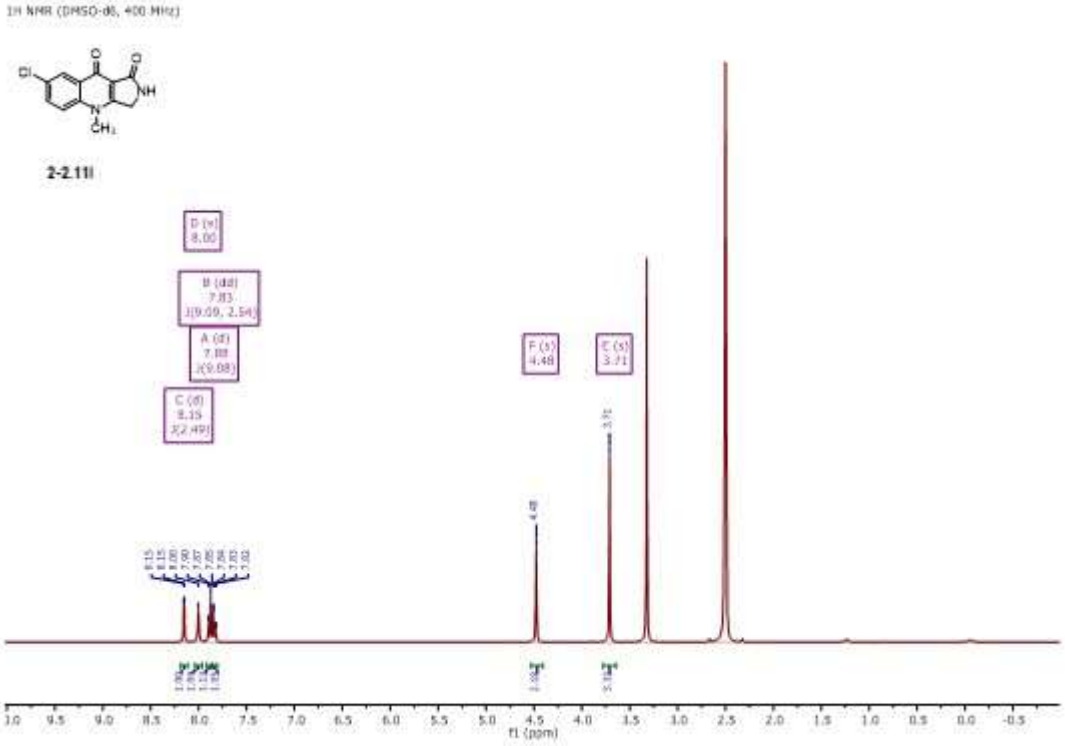
1H NMR (DMSO-d6, 400 MHz)
2-2.11l
D (s)
8.00
B (dd)
7.83
J(9.09, 2.54)
A (d)
7.88
J(9.08)
C (d)
8.15
J(2.49)
F (s)
4.48
E (s)
3.71
f1 (ppm)

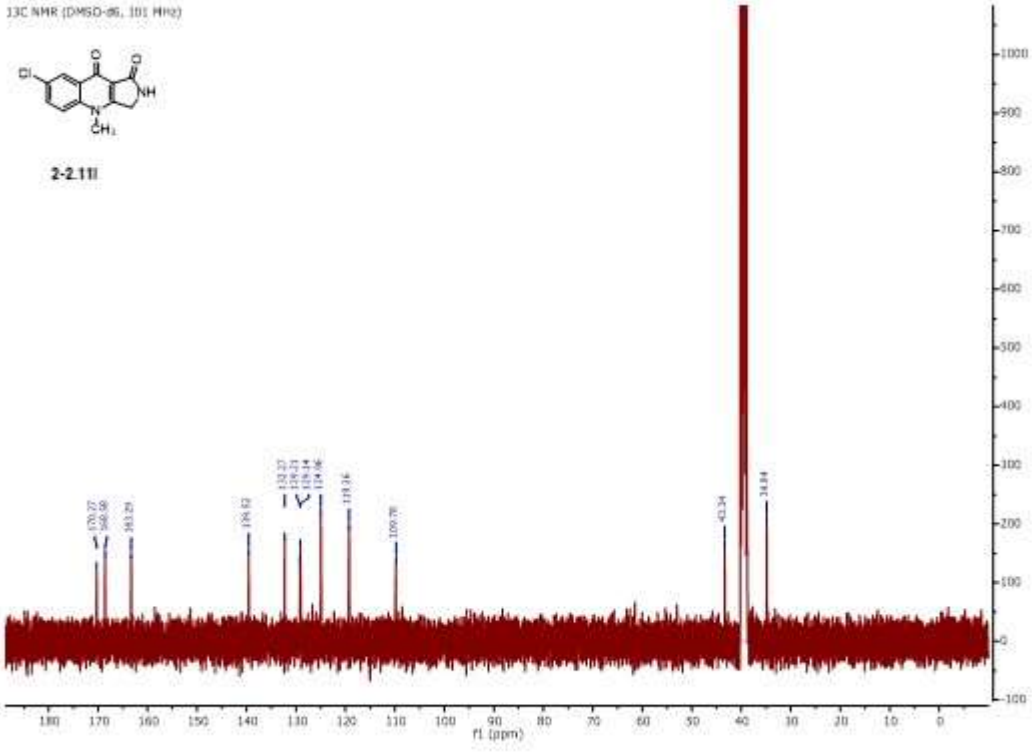
13C NMR (DMSO-d6, 101 MHz)
2-2.11l
f1 (ppm)

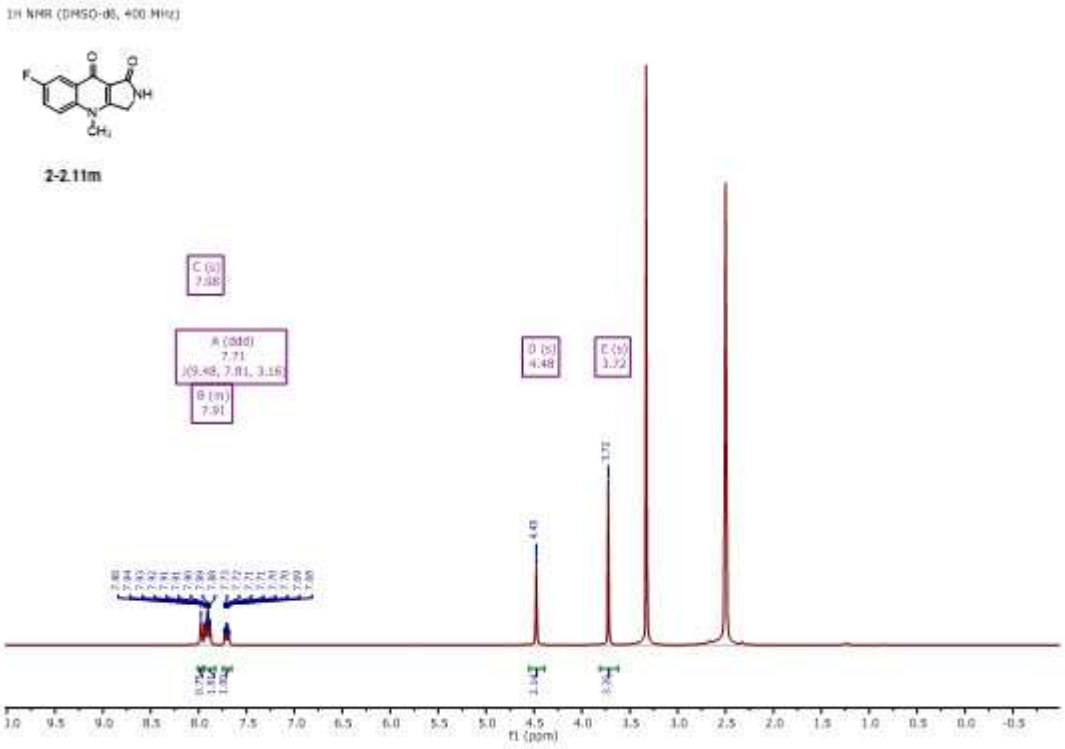
1H NMR (DMSO-d6, 400 MHz)
2-2.11m
C (s)
7.98
A (ddd)
7.71
J(9.48, 7.81, 3.16)
B (m)
7.91
D (s)
4.48
E (s)
3.72
f1 (ppm)

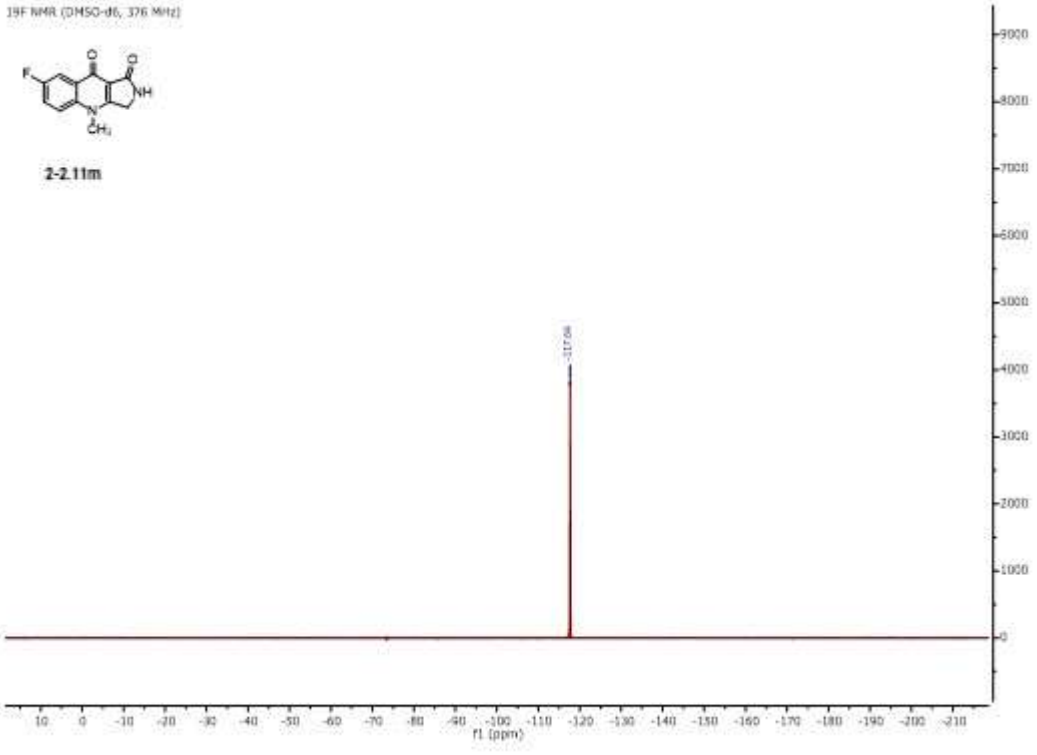
19F NMR (DMSO-d6, 376 MHz)
2-2.11m
-117.06
f1 (ppm)

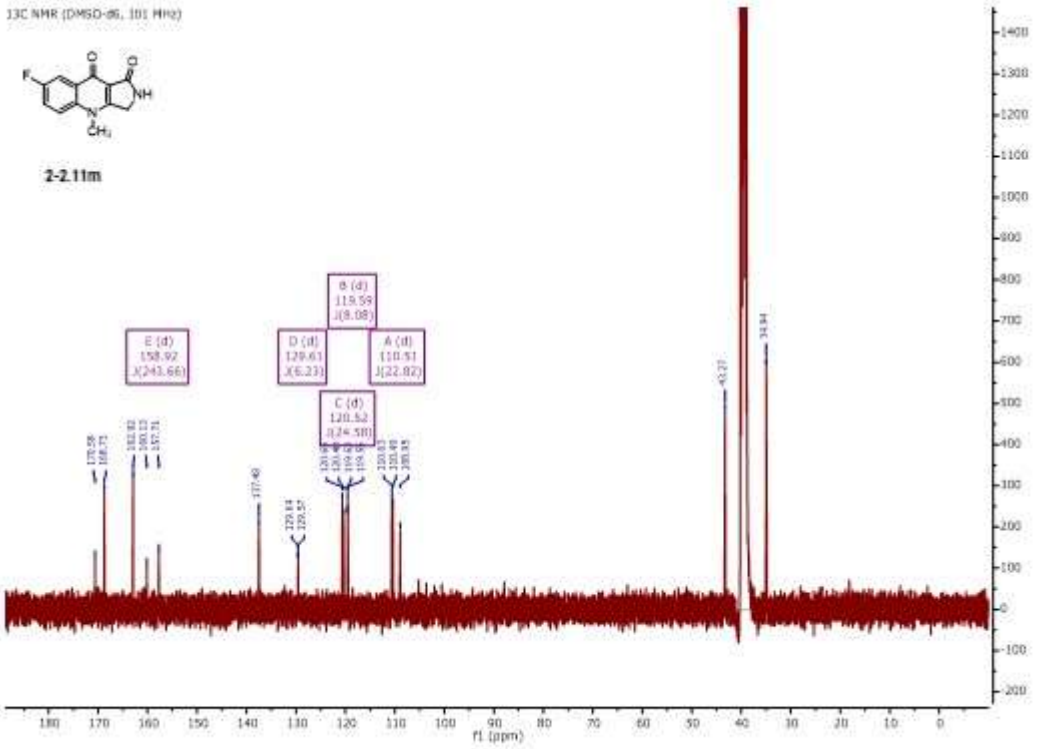
13C NMR (DMSO-d6, 101 MHz)
2-2.11m
f1 (ppm)

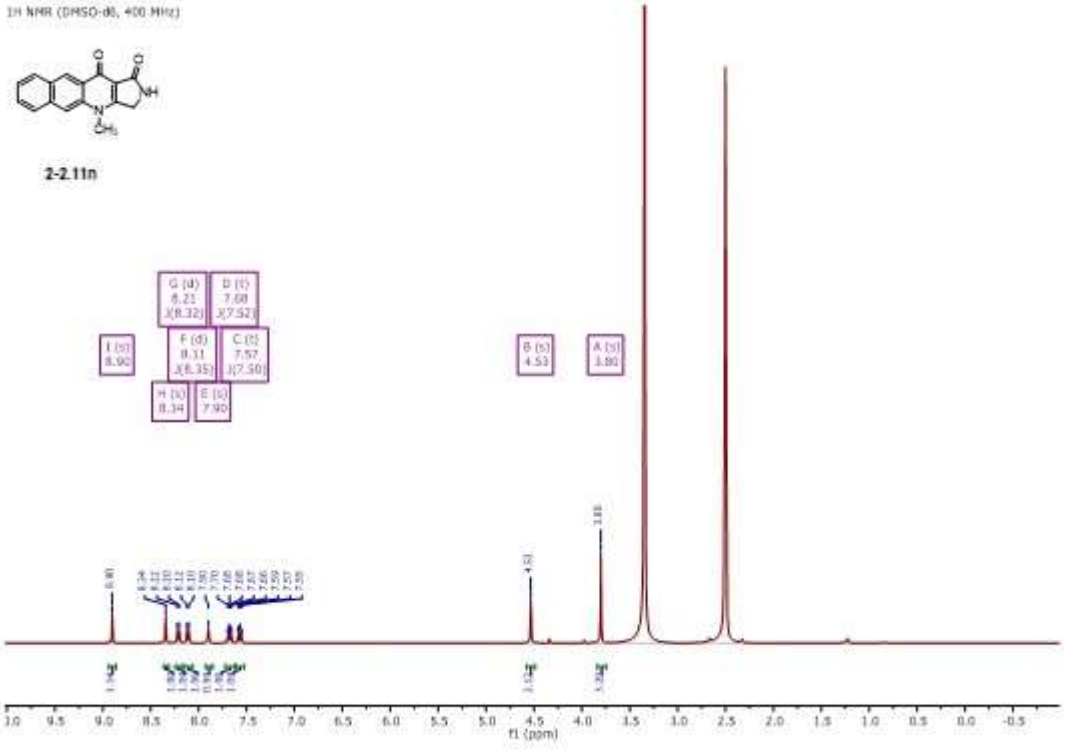
1H NMR (DMSO-d6, 400 MHz)
2-2.11n
f1 (ppm)

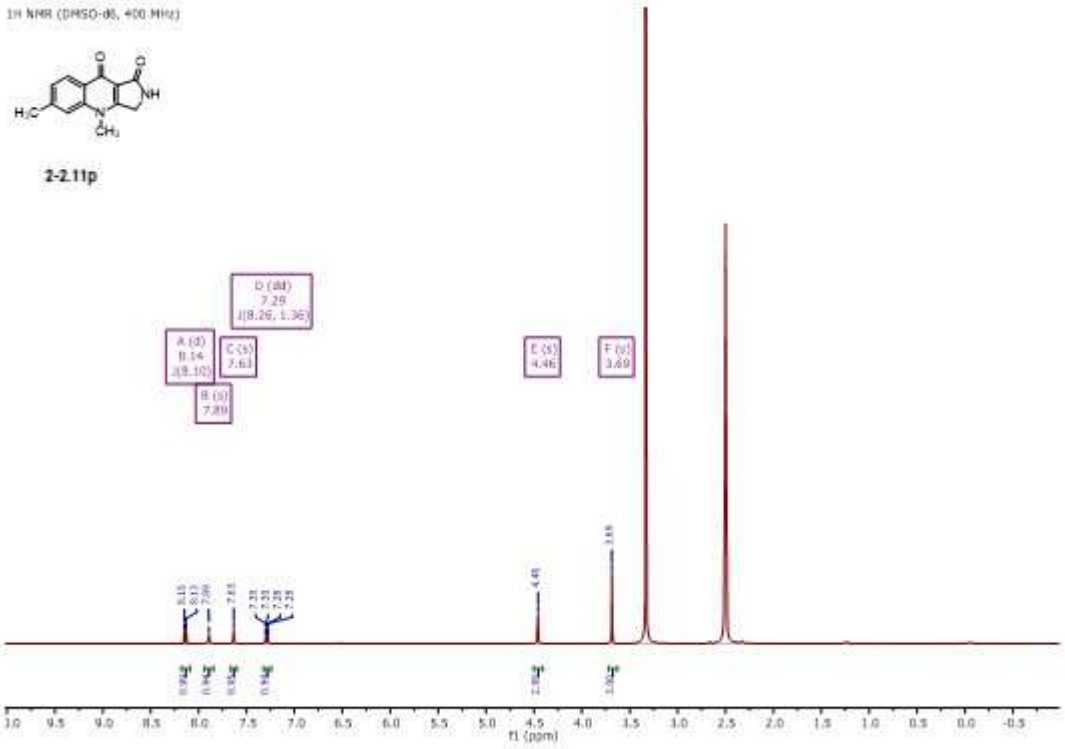
1H NMR (DMSO-d6, 400 MHz)
2-2.11p
f1 (ppm)

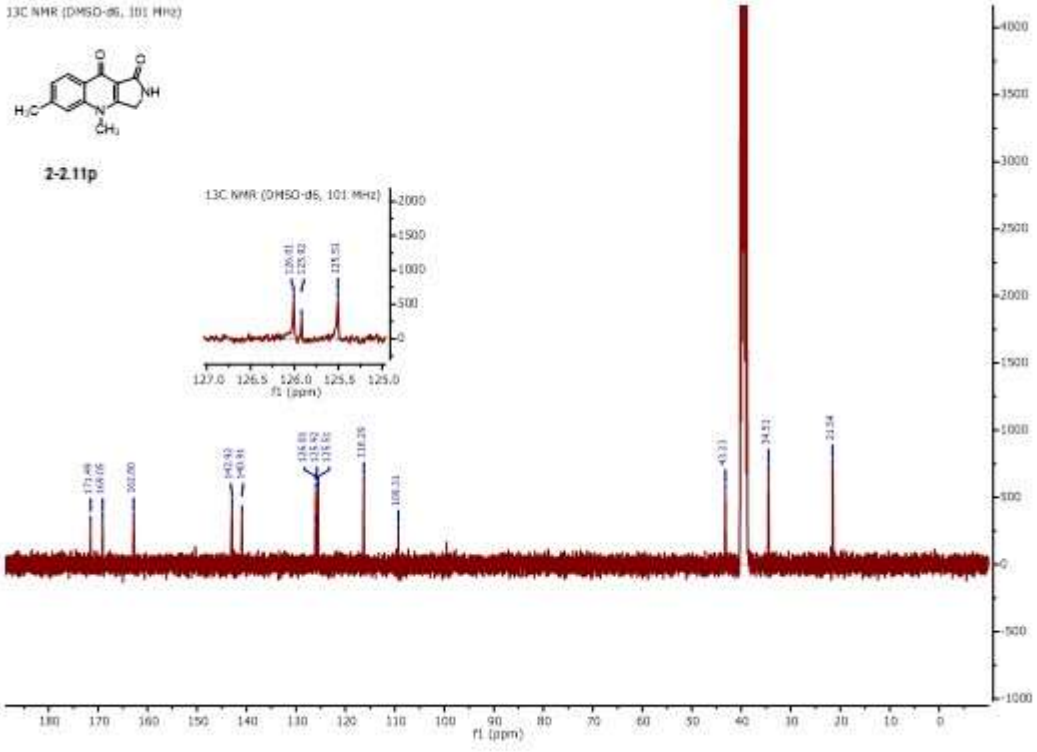
13C NMR (DMSO-d6, 101 MHz)
2-2.11p
13C NMR (DMSO-d6, 101 MHz)
f1 (ppm)

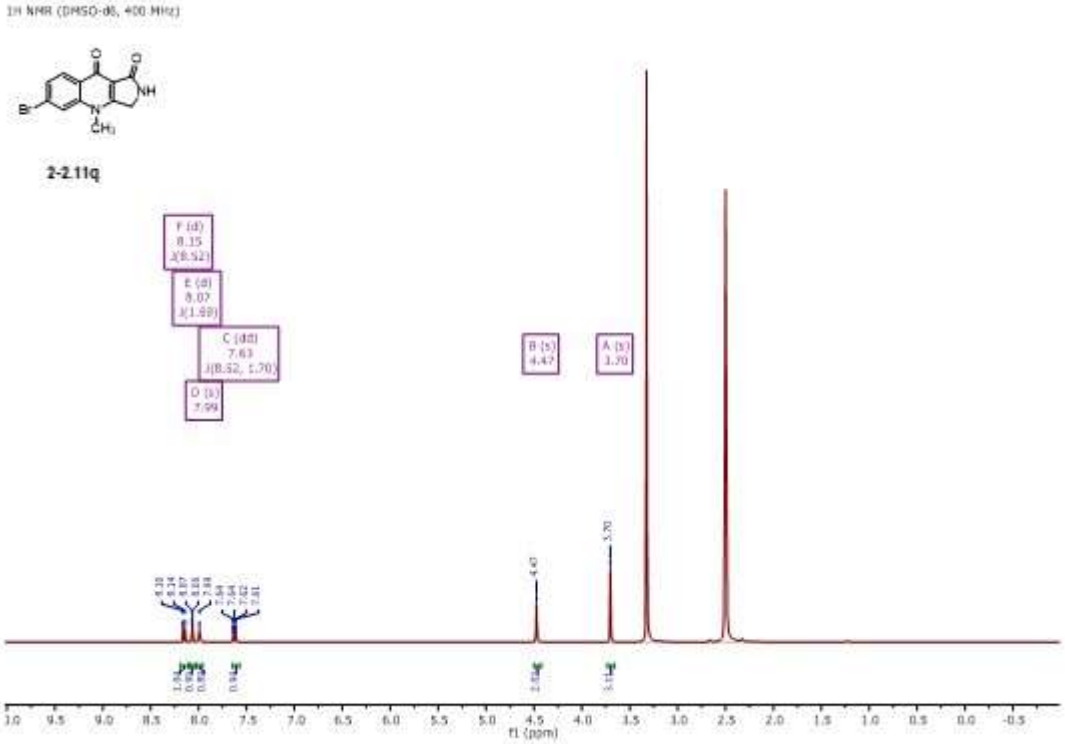
1H NMR (DMSO-d6, 400 MHz)
2-2.11q
F (d)
8.15
J(8.52)
E (d)
8.07
J(1.99)
C (dd)
7.63
J(8.52, 1.70)
D (s)
7.99
B (s)
4.47
A (s)
1.70
f1 (ppm)

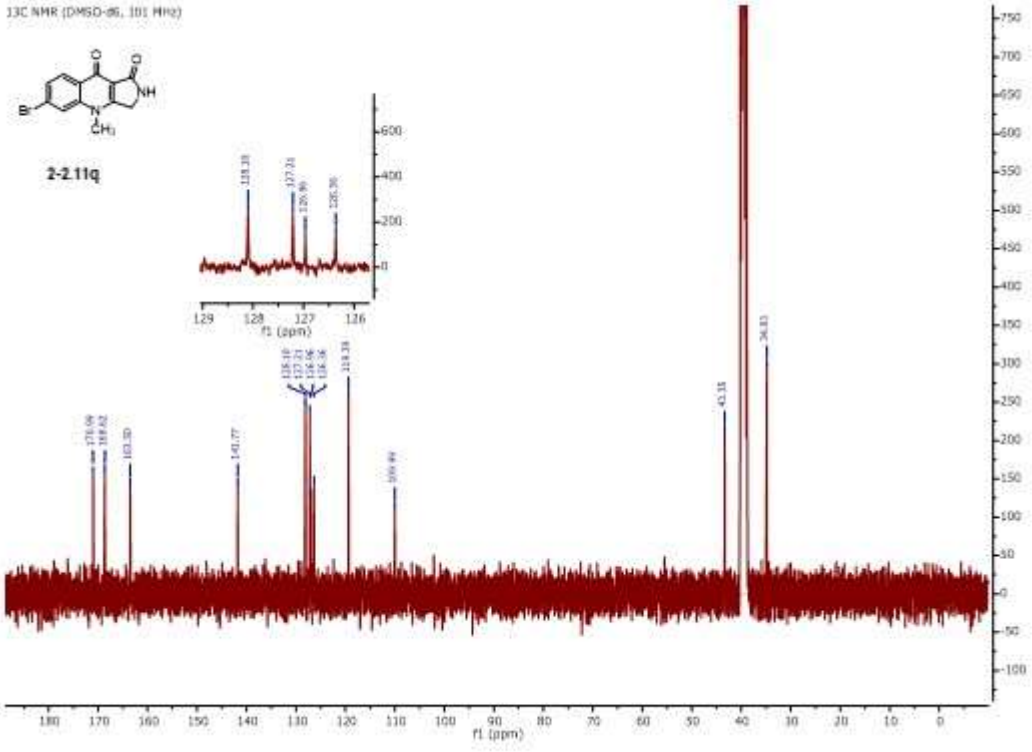
13C NMR (DMSO-d6, 101 MHz)
2-2.11q
f1 (ppm)

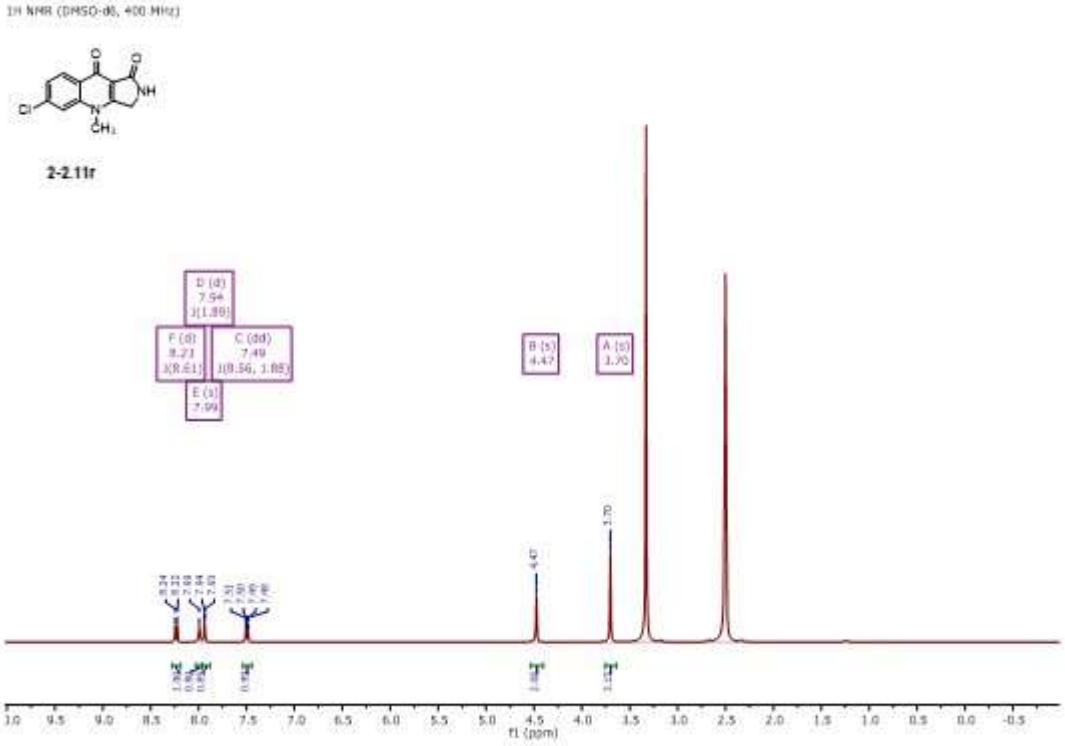
1H NMR (DMSO-d6, 400 MHz)
2-2.11r
D (d)
7.54
J(1.88)
F (d)
8.23
J(8.61)
C (dd)
7.49
J(8.56, 1.88)
E (s)
7.99
B (s)
4.47
A (s)
3.70
f1 (ppm)

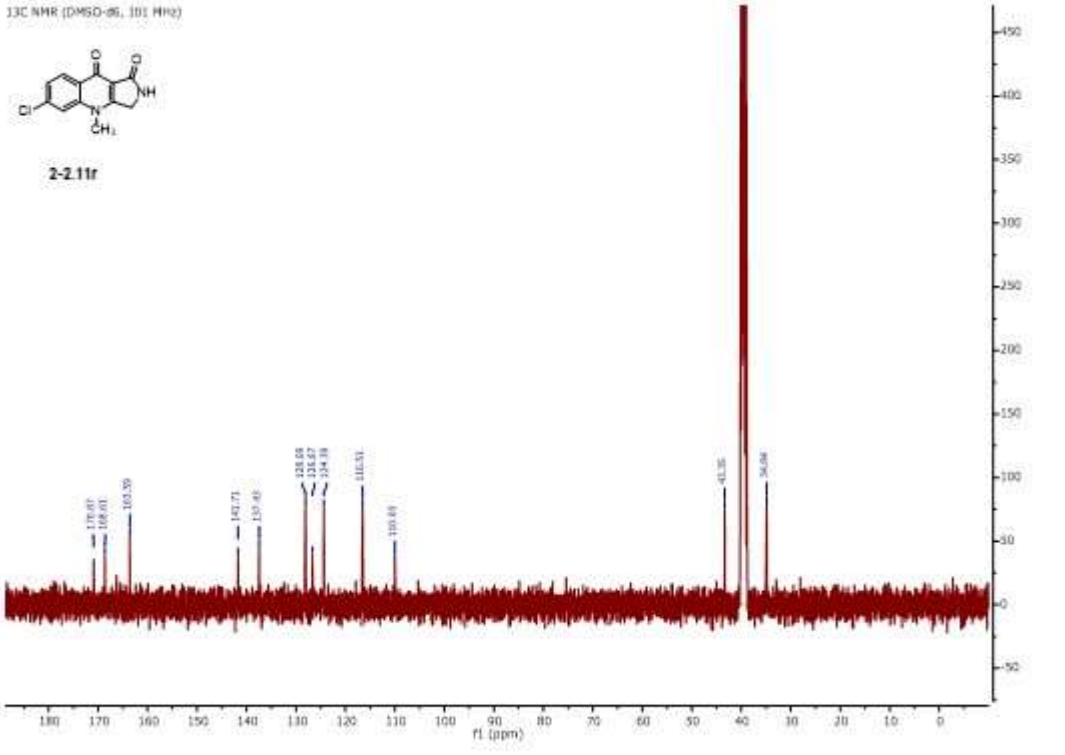
13C NMR (DMSO-d6, 101 MHz)
2-2.11r
f1 (ppm)

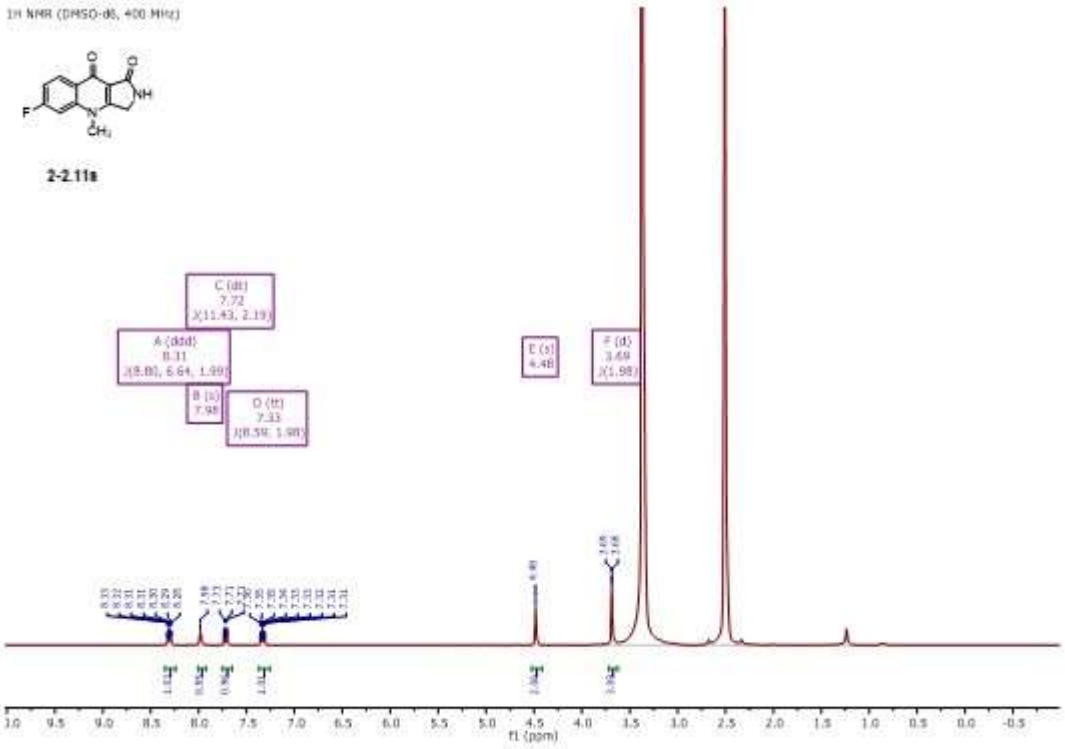
1H NMR (DMSO-d6, 400 MHz)
2-2.11s
C (dt)
7.72
J(11.43, 2.19)
A (ddd)
8.11
J(8.80, 6.64, 1.99)
B (s)
7.98
D (ft)
7.33
J(8.59, 1.98)
E (s)
4.48
F (d)
3.69
J(1.98)
f1 (ppm)

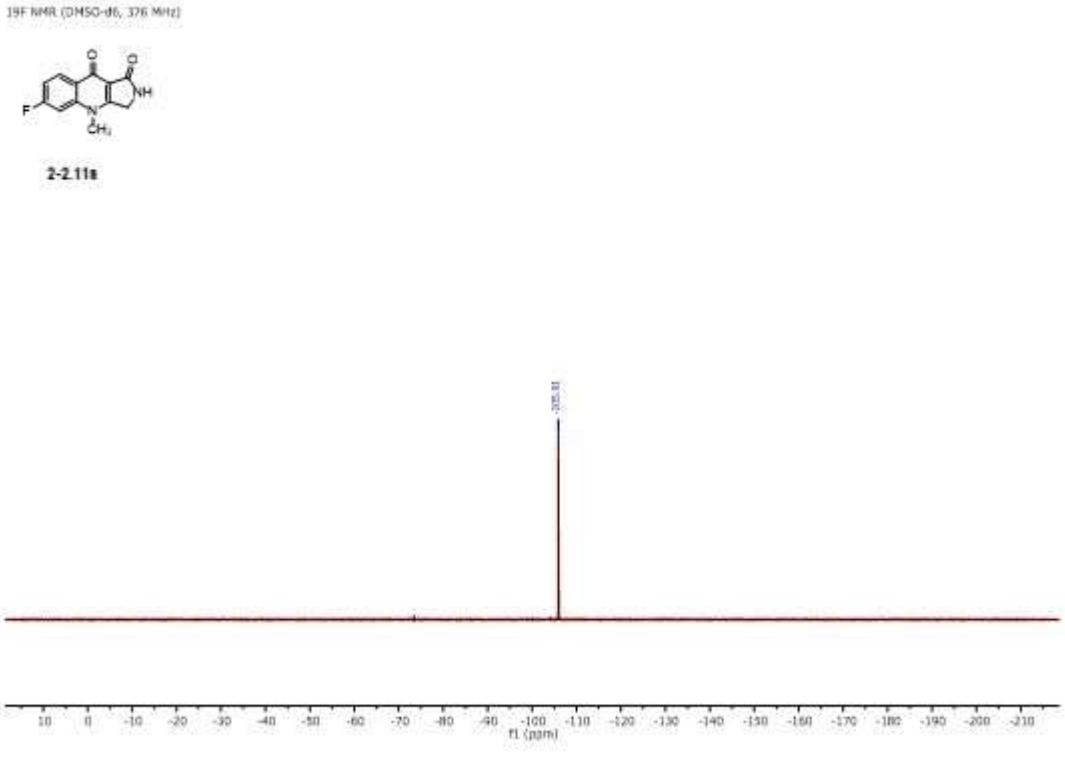
19F NMR (DMSO-d6, 376 MHz)
2-2.11s
f1 (ppm)

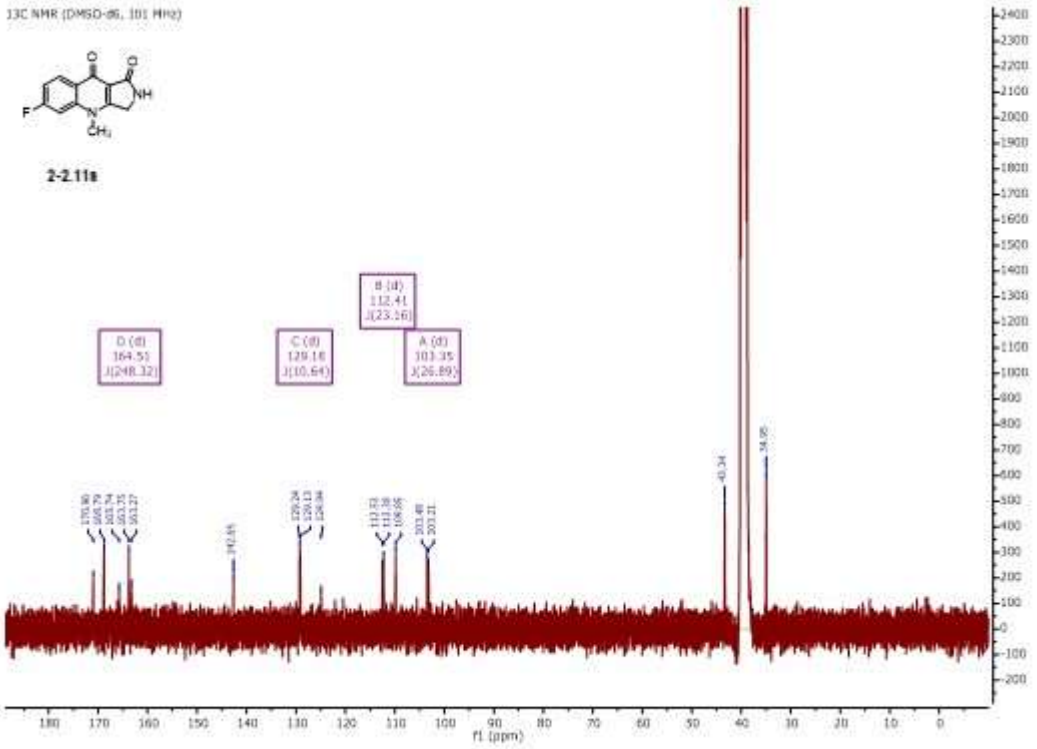
13C NMR (DMSO-d6, 101 MHz)
2-2.11s
D (d)
164.51
J(248.32)
C (d)
129.16
J(10.64)
B (d)
112.41
J(23.16)
A (d)
103.35
J(26.89)
f1 (ppm)

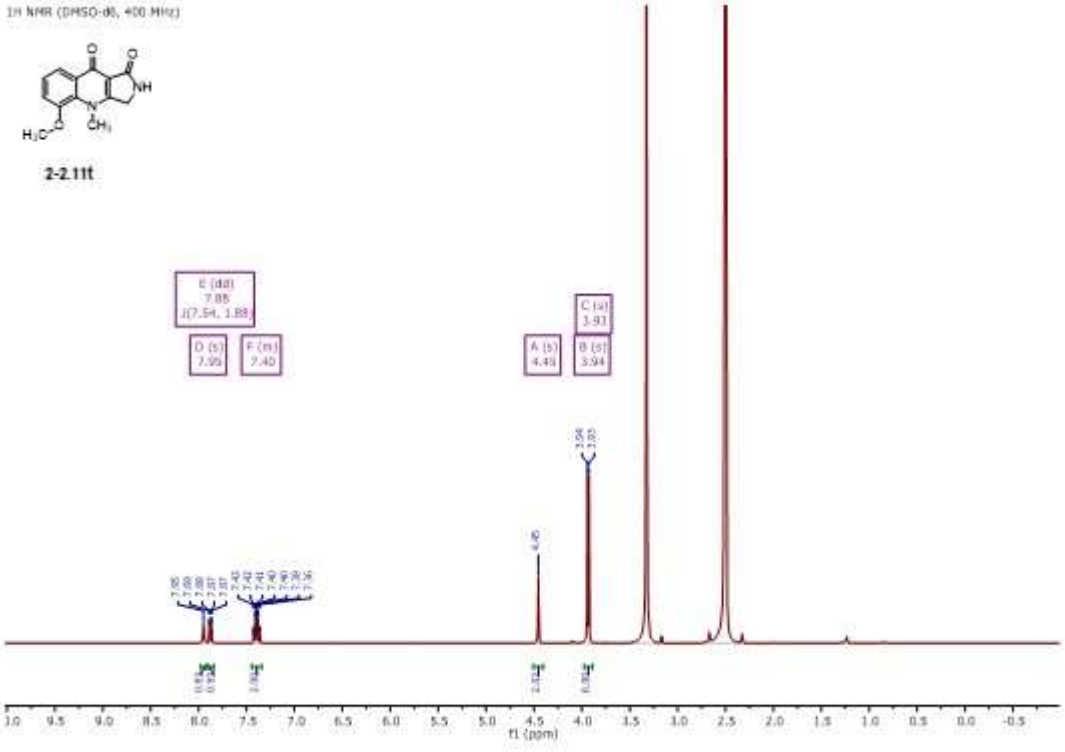
1H NMR (DMSO-d6, 400 MHz)
2-2.11t
E (dd)
7.88
J(7.54, 1.88)
D (s)
7.99
F (m)
7.40
A (s)
4.48
C (s)
3.97
B (s)
3.94
f1 (ppm)

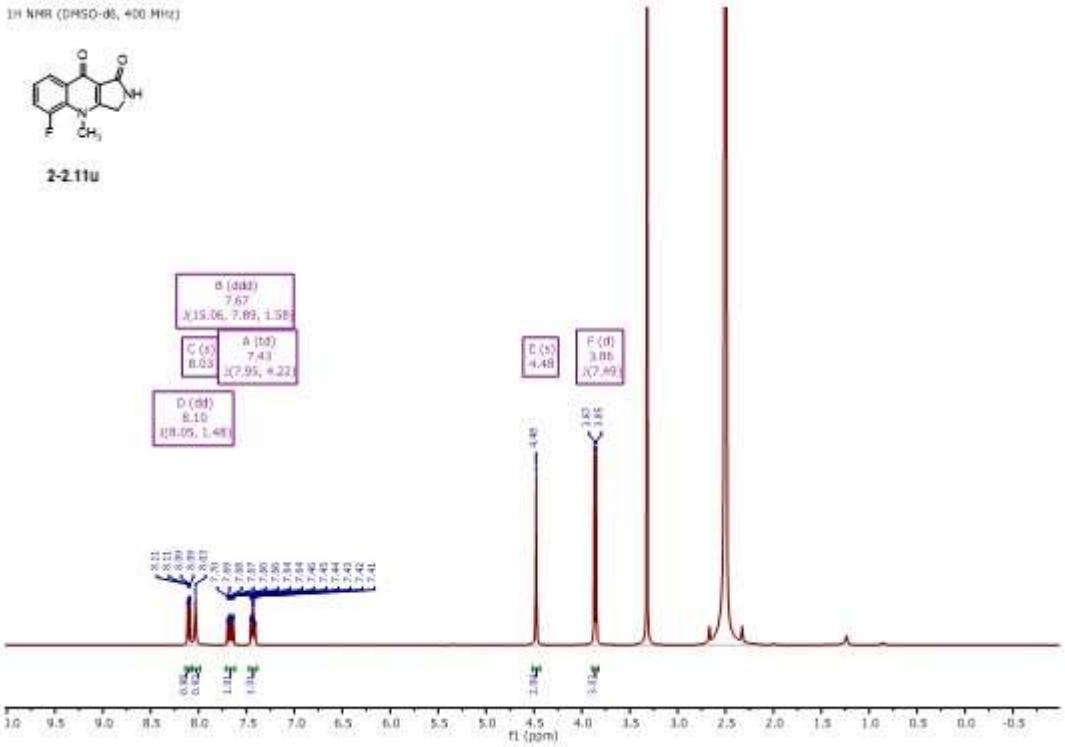
1H NMR (DMSO-d6, 400 MHz)
2-2.11u
B (ddd)
7.67
J(15.06, 7.89, 1.58)
C (s)
8.03
A (td)
7.43
J(7.95, 4.22)
D (dd)
8.10
J(8.05, 1.48)
E (s)
4.48
F (d)
3.86
J(7.49)
4.48
3.86
f1 (ppm)

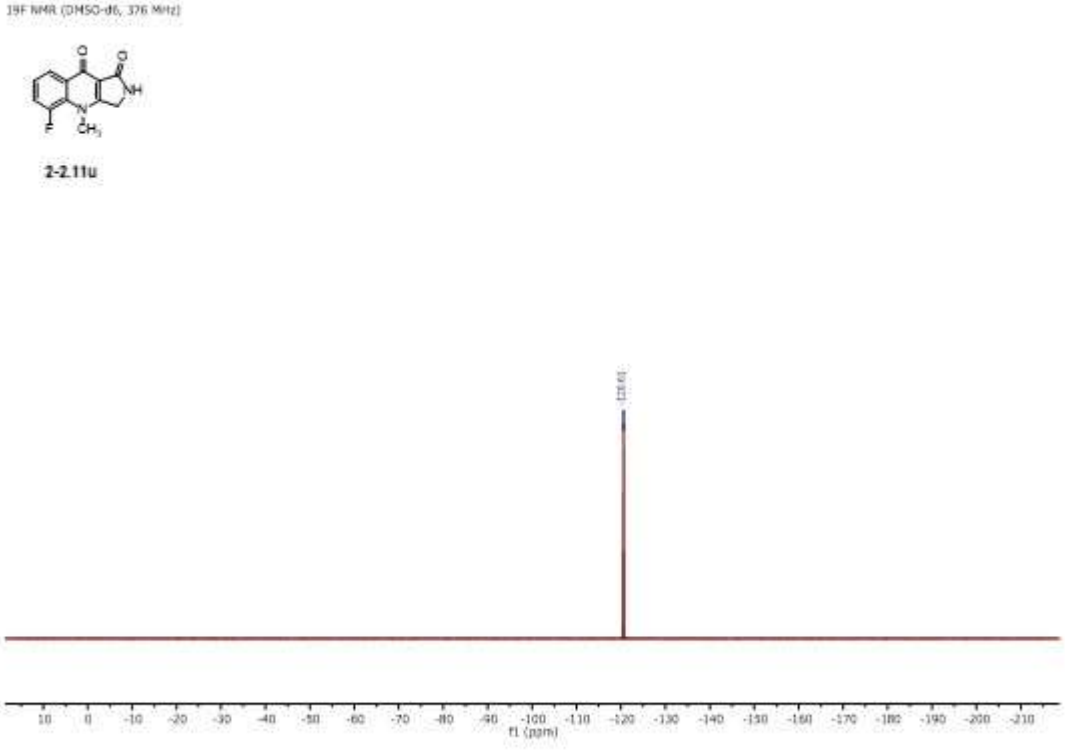
19F NMR (DMSO-d6, 376 MHz)
2-2.11u
-120.41
f1 (ppm)

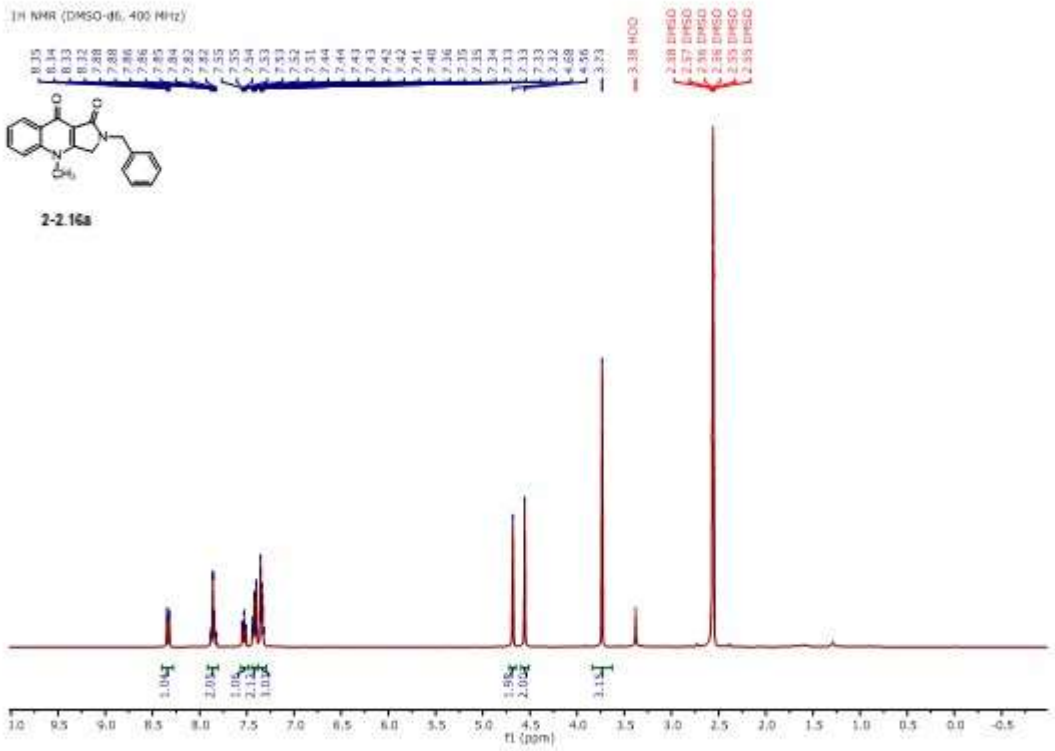
1H NMR (DMSO-d6, 400 MHz)
2-2.16a
f1 (ppm)

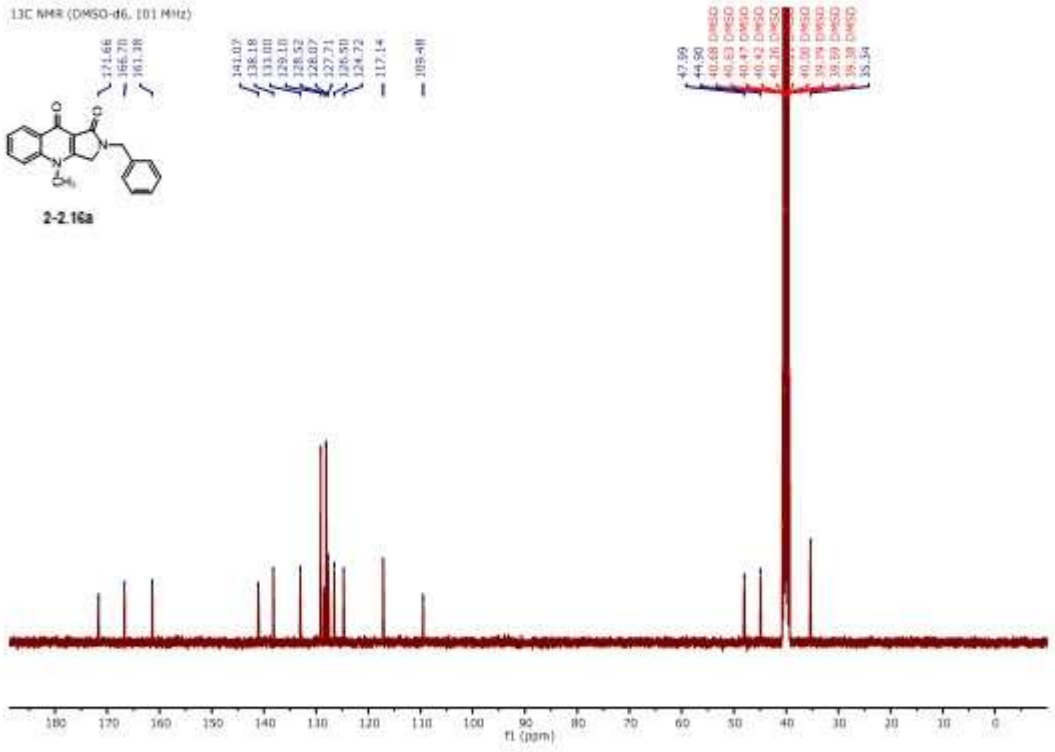
13C NMR (DMSO-d6, 101 MHz)
2-2.16a
f1 (ppm)

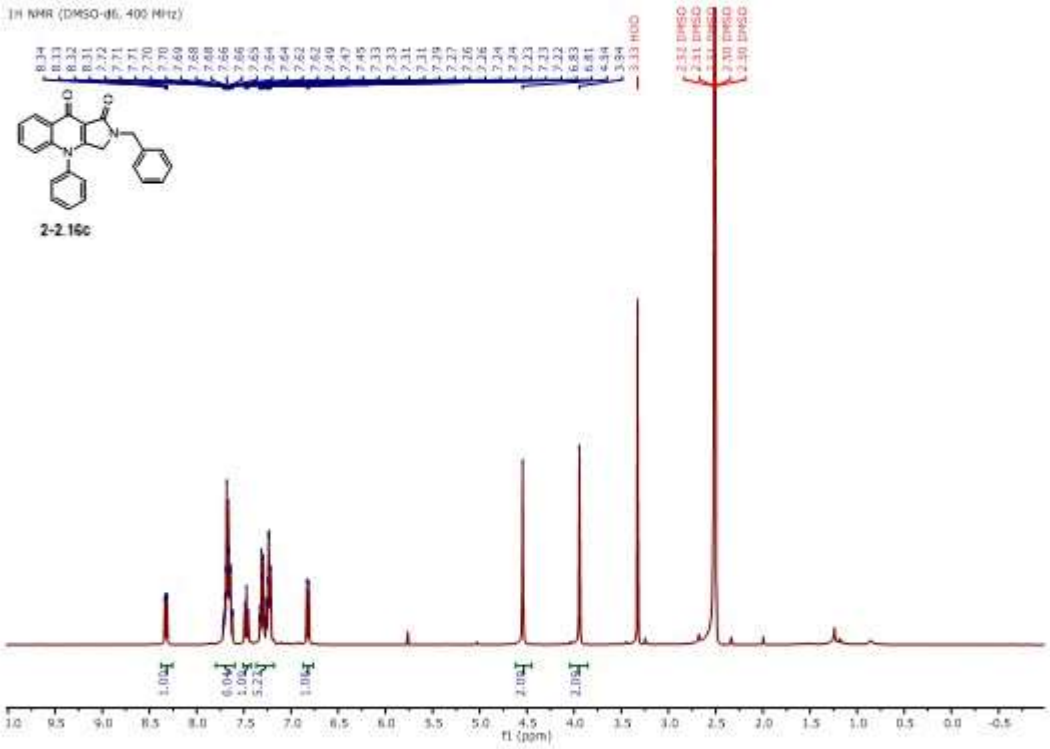
1H NMR (DMSO-d6, 400 MHz)
2-2.16c
f1 (ppm)

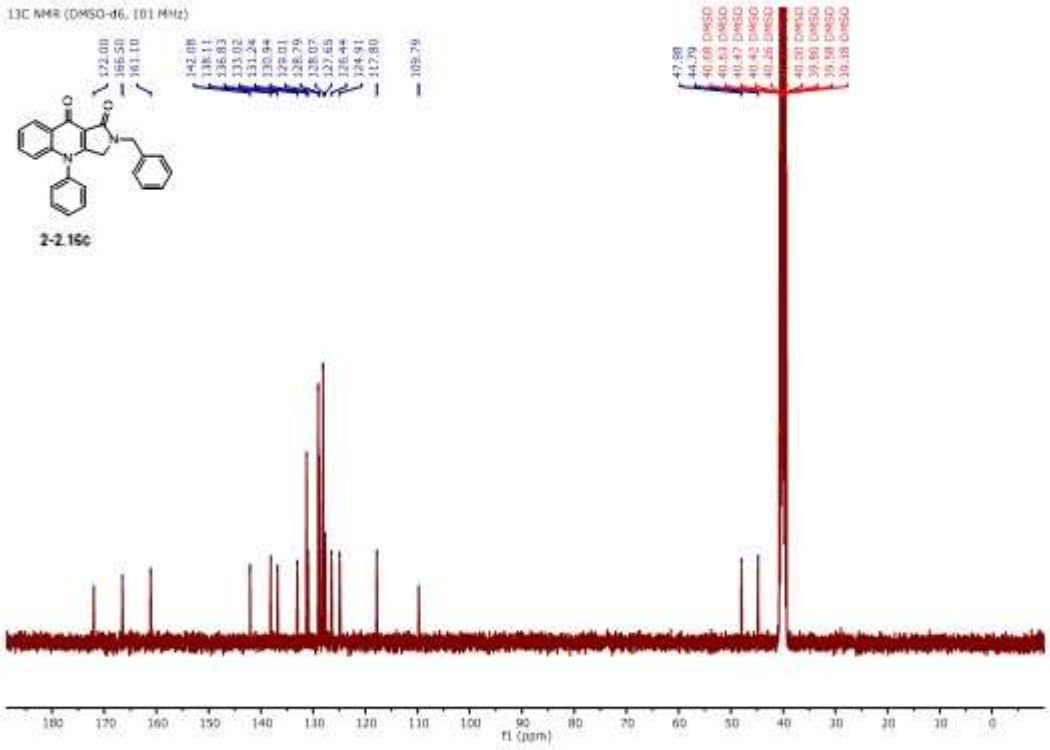
13C NMR (DMSO-d6, 101 MHz)
2-2.16c
f1 (ppm)

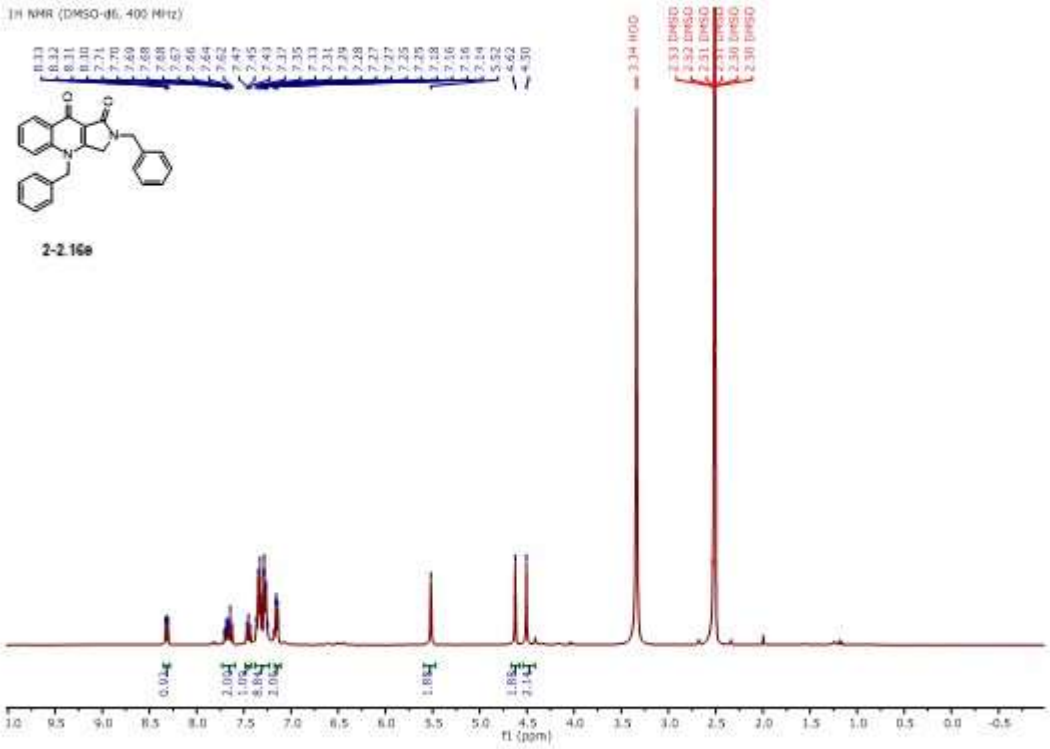
1H NMR (DMSO-d6, 400 MHz)
2-2.16e
f1 (ppm)

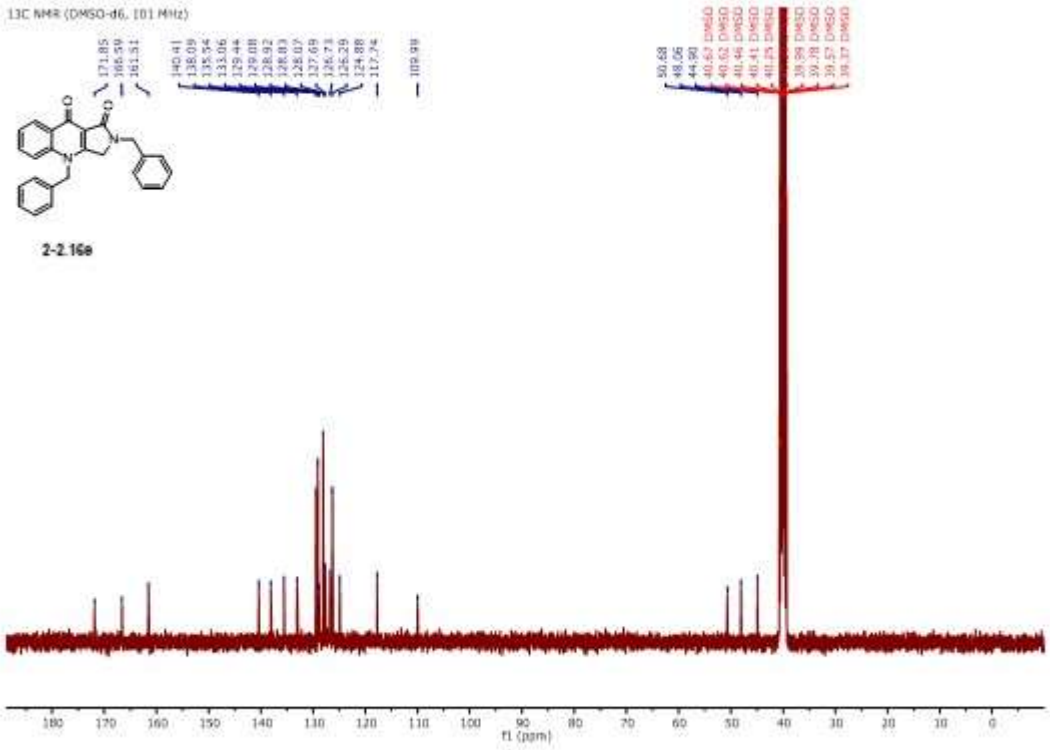
13C NMR (DMSO-d6, 101 MHz)
2-2.16e
f1 (ppm)

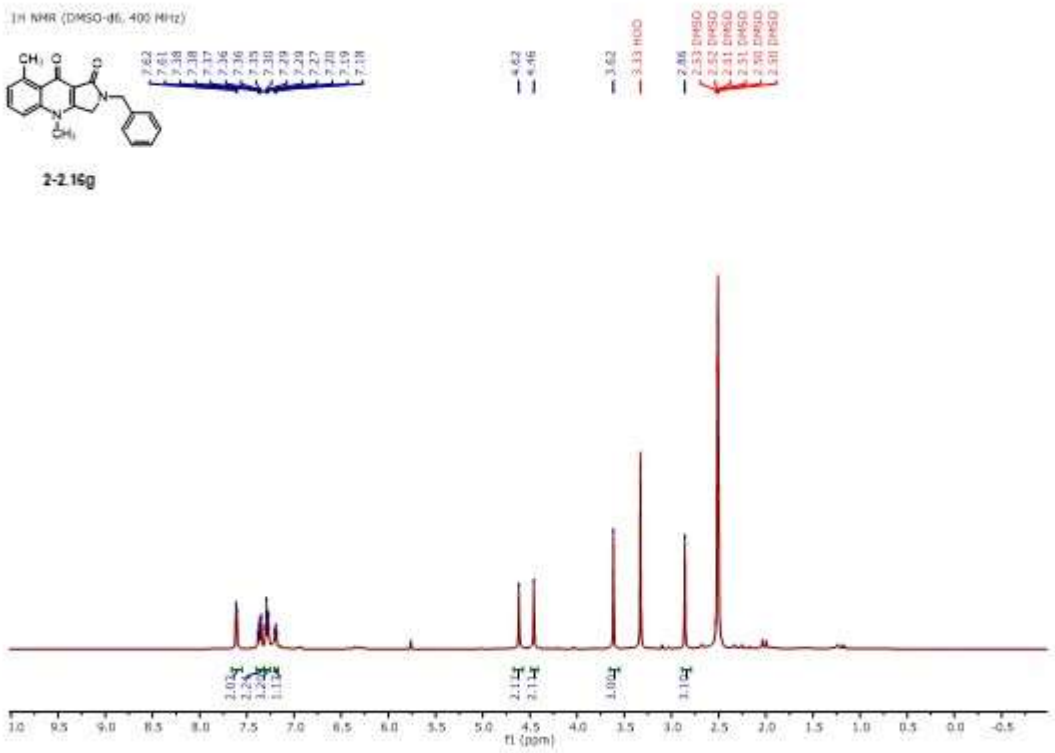
1H NMR (DMSO-d6, 400 MHz)
2-2.16g
f1 (ppm)

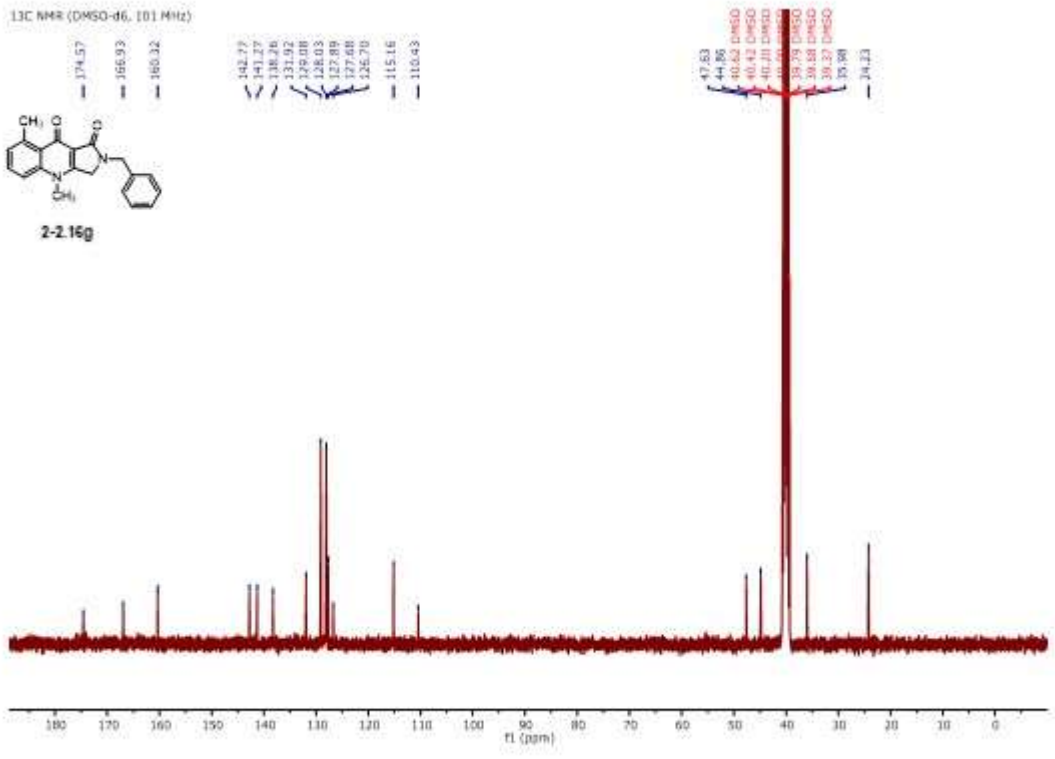
13C NMR (DMSO-d6, 101 MHz)
2-2.16g
f1 (ppm)

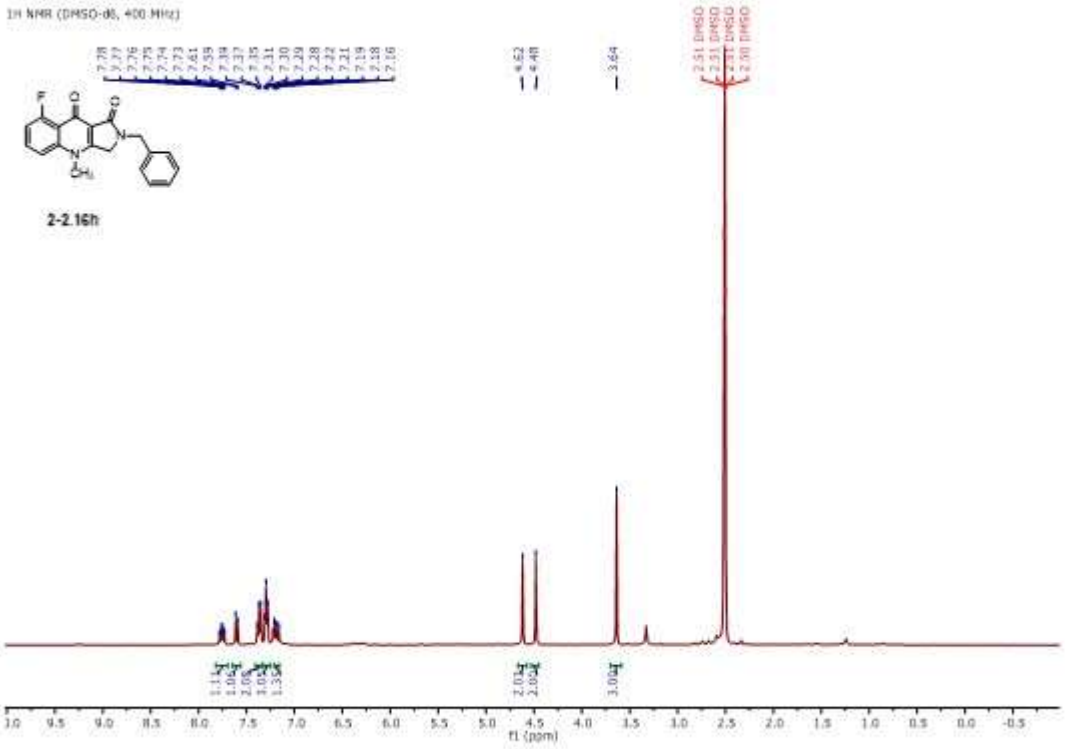
1H NMR (DMSO-d6, 400 MHz)
2-2.16h
f1 (ppm)

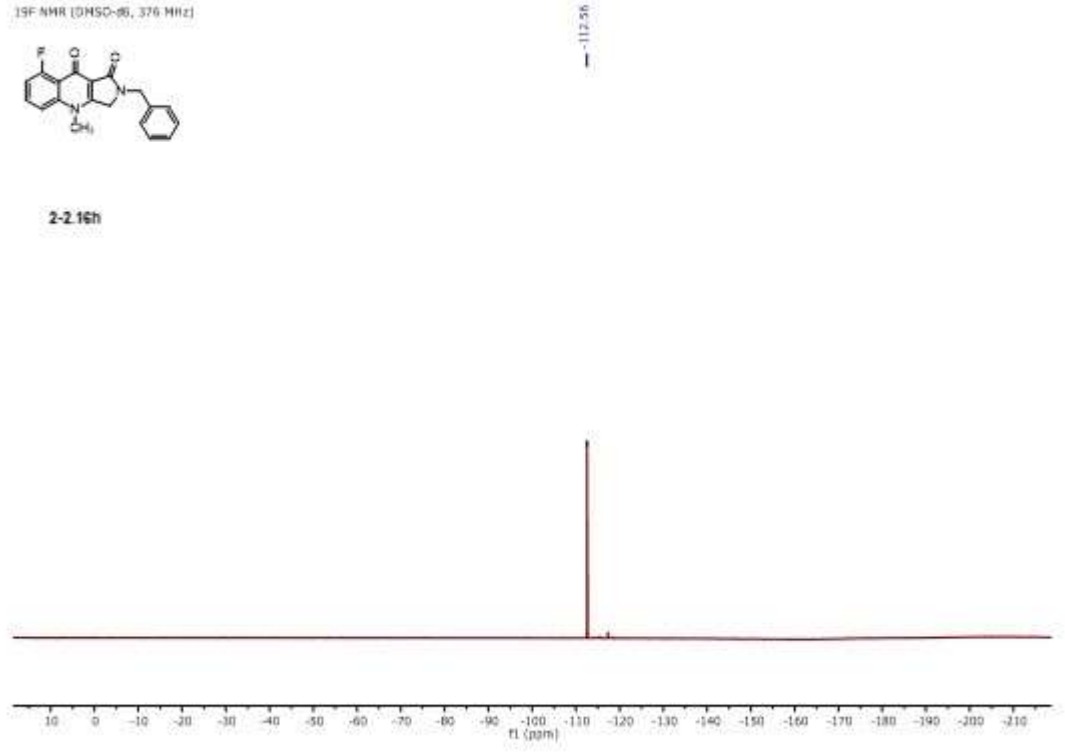
19F NMR (DMSO-d6, 376 MHz)
2-2.16h
f1 (ppm)

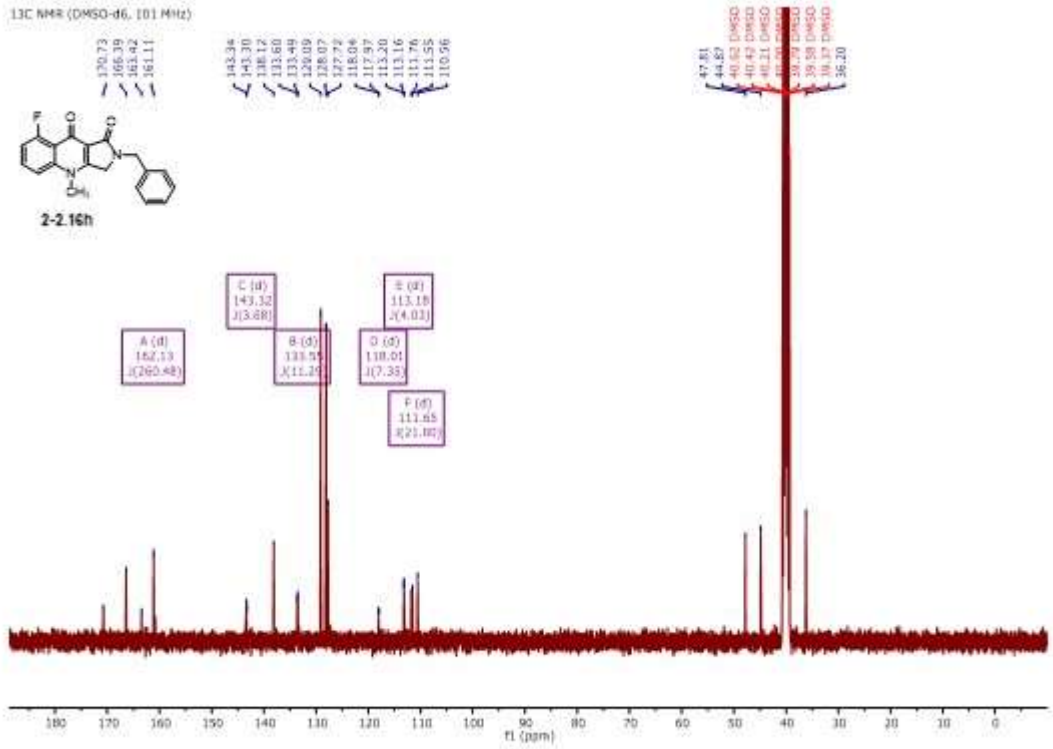
13C NMR (DMSO-d6, 101 MHz)
2-2.16h
f1 (ppm)

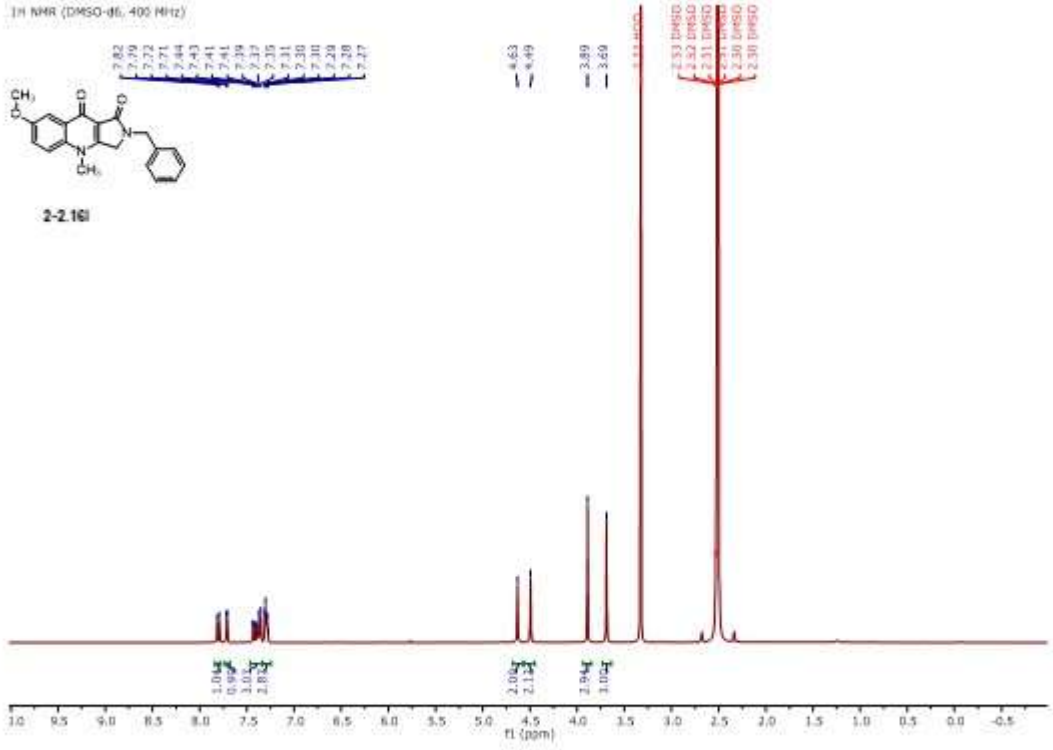
1H NMR (DMSO-d6, 400 MHz)
2-2.16l
f1 (ppm)

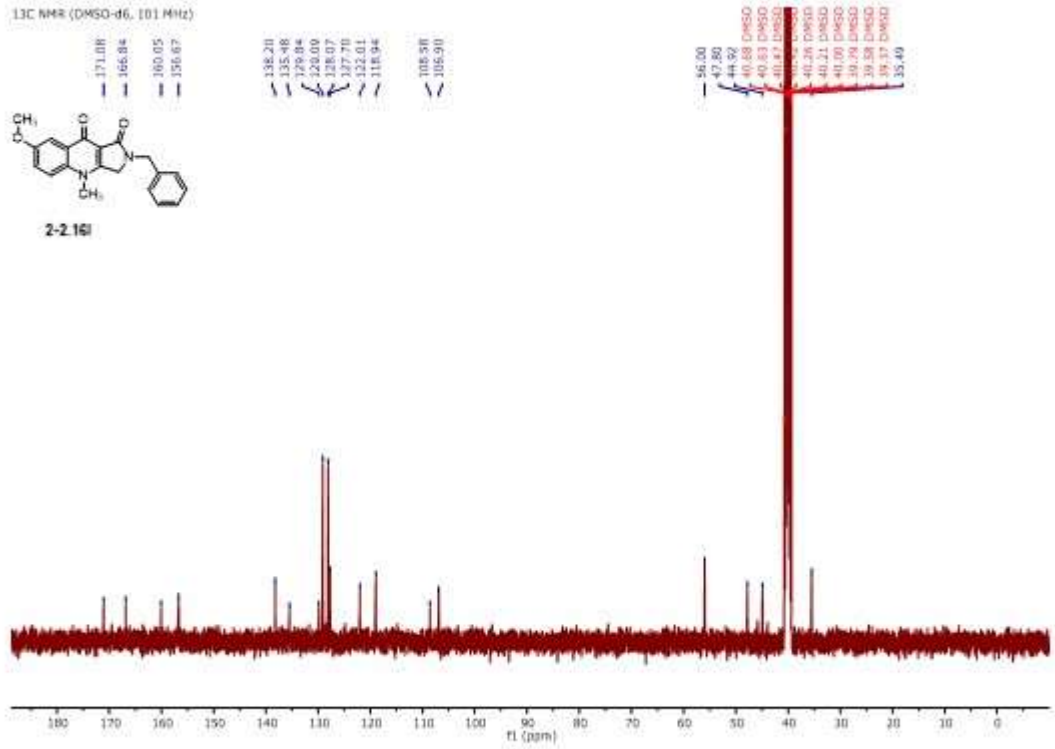
13C NMR (DMSO-d6, 101 MHz)
2-2.16I
f1 (ppm)

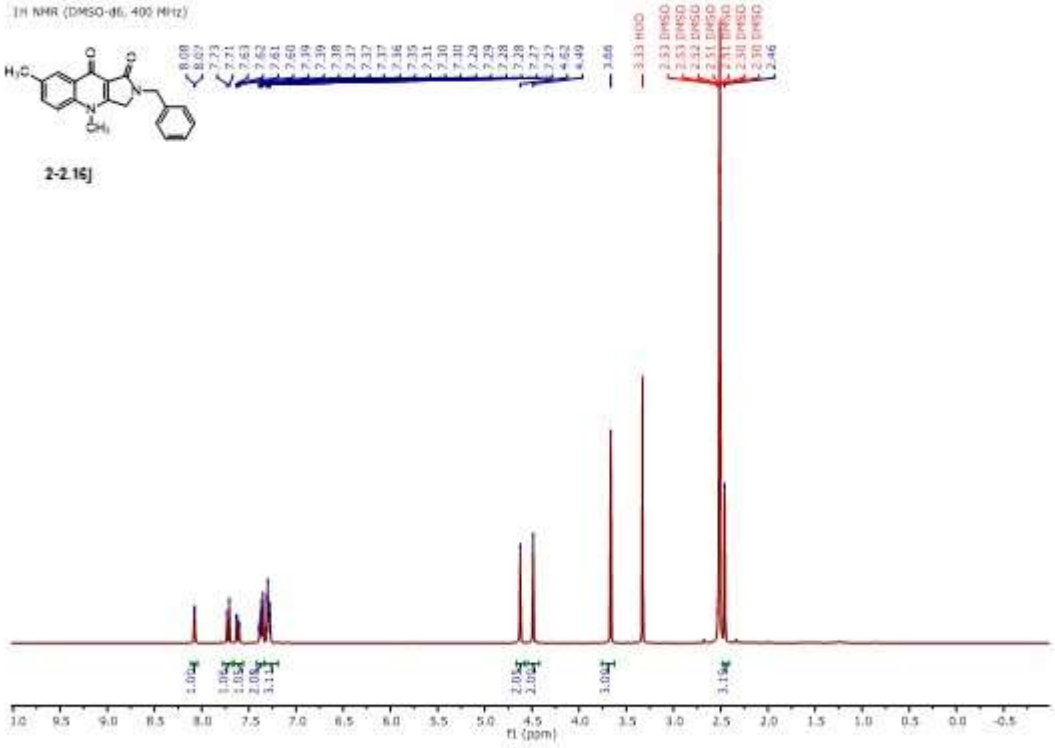
1H NMR (DMSO-d6, 400 MHz)
2-2.16J
f1 (ppm)

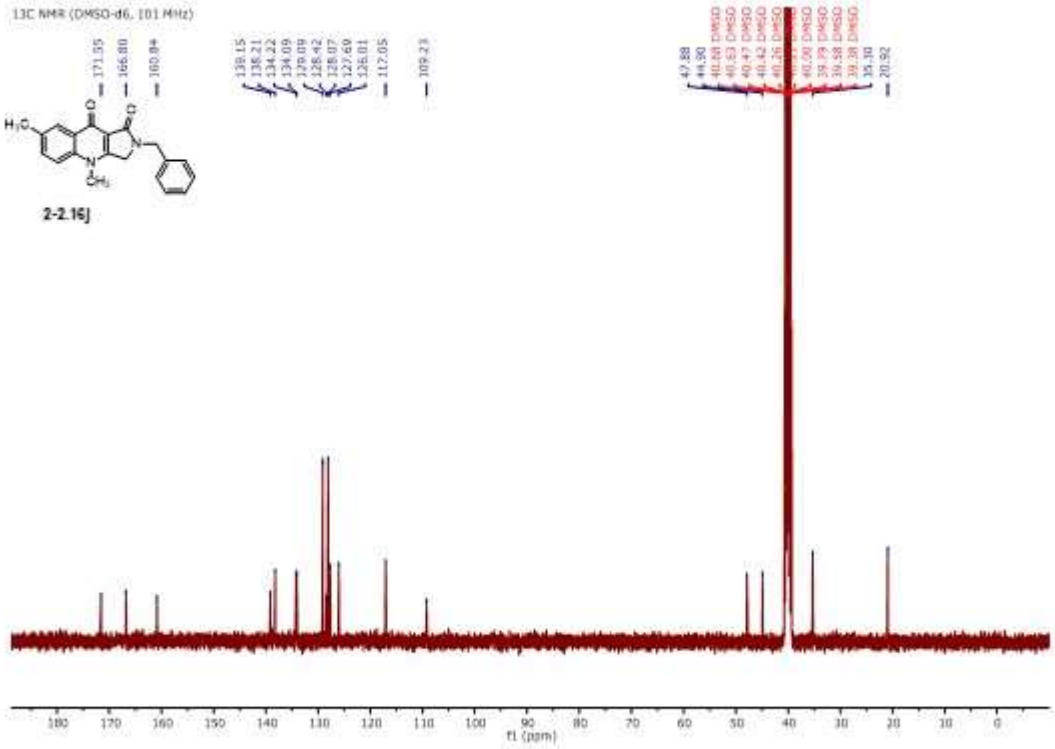
13C NMR (DMSO-d6, 101 MHz)
171.55
166.80
160.84
138.15
136.21
134.22
134.09
129.09
128.42
128.07
127.60
126.01
112.05
109.23
47.88
44.90
40.00 DMSO
39.79 DMSO
39.58 DMSO
39.38 DMSO
35.30
20.92
2-2.16J
f1 (ppm)

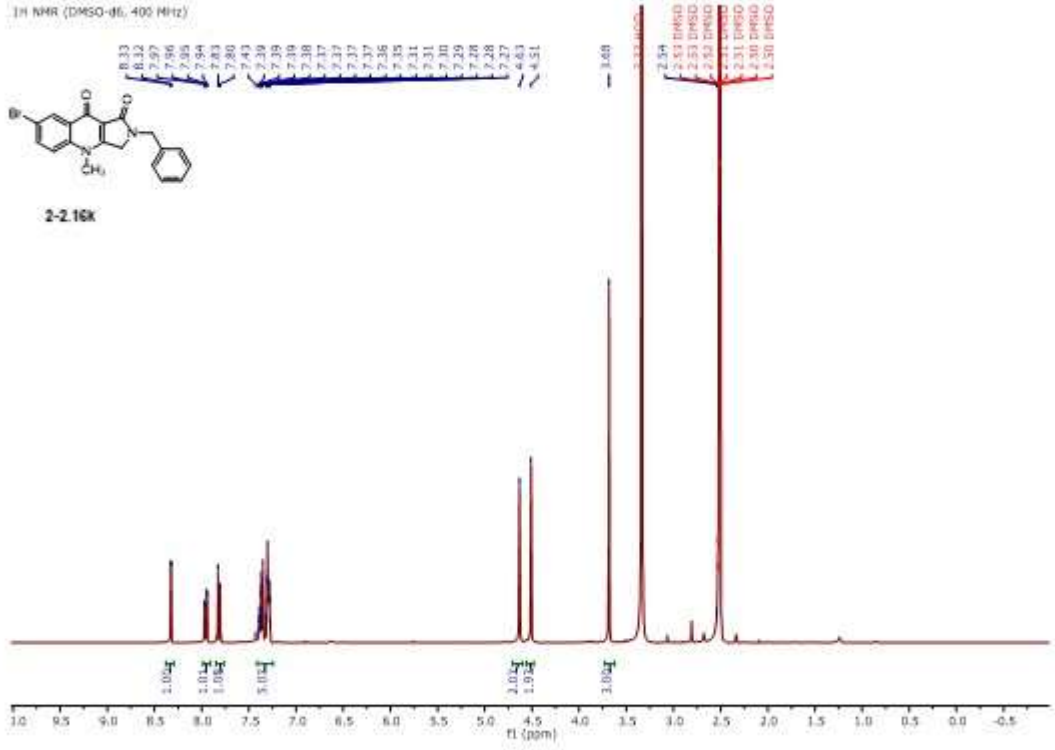
1H NMR (DMSO-d6, 400 MHz)
8.33
8.32
7.97
7.96
7.95
7.94
7.83
7.80
7.43
7.39
7.39
7.39
7.38
7.37
7.37
7.37
7.37
7.36
7.35
7.31
7.31
7.30
7.29
7.28
7.28
7.27
4.63
4.51
3.48
2.54
2.53 DMSO
2.53 DMSO
2.52 DMSO
2.31 DMSO
2.30 DMSO
2.30 DMSO
2.30 DMSO
2.30 DMSO
2-2.16K
f1 (ppm)

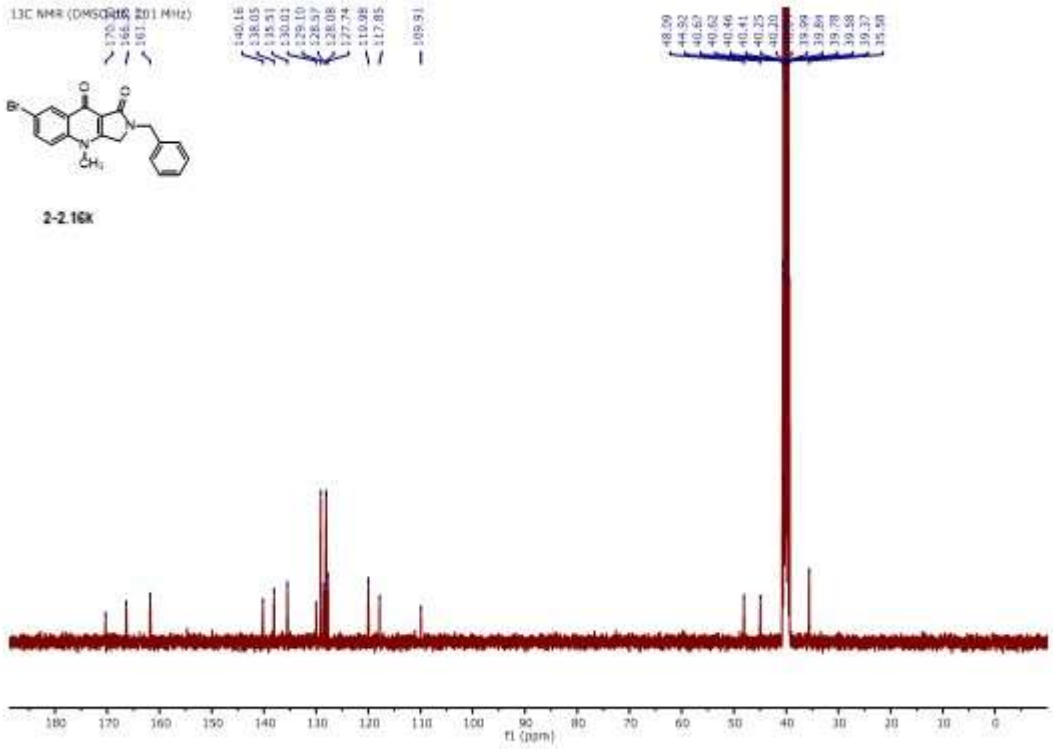
13C NMR (DMSO-d6, 201 MHz)
2-2.16k
f1 (ppm)

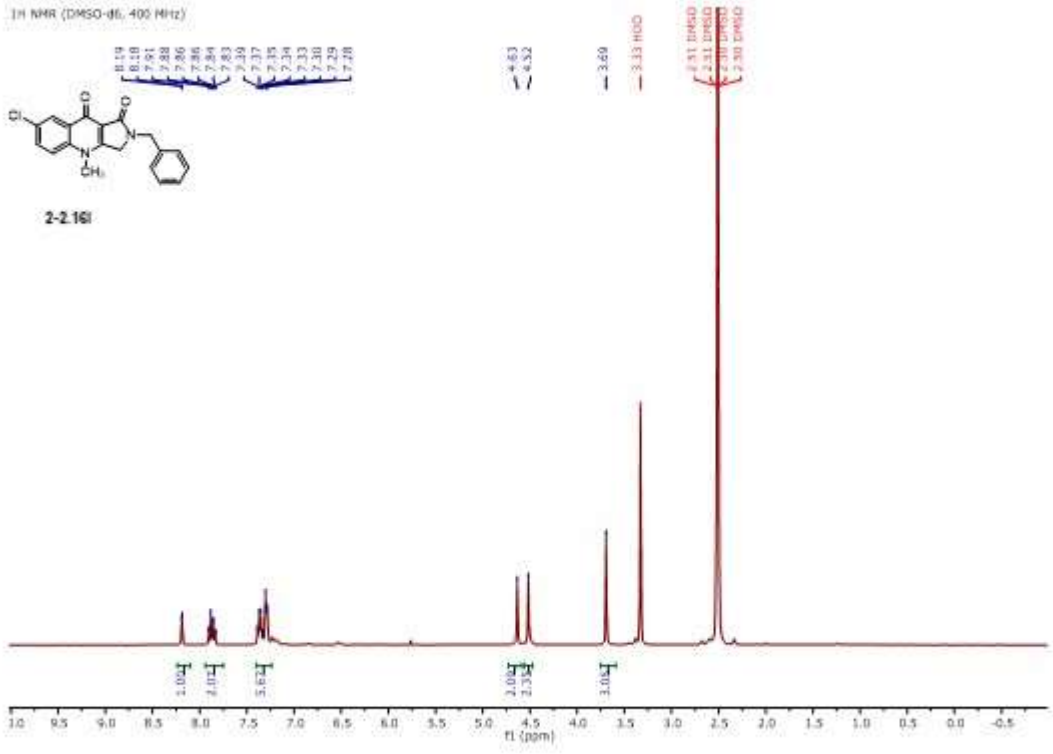
1H NMR (DMSO-d6, 400 MHz)
2-2.16l
f1 (ppm)

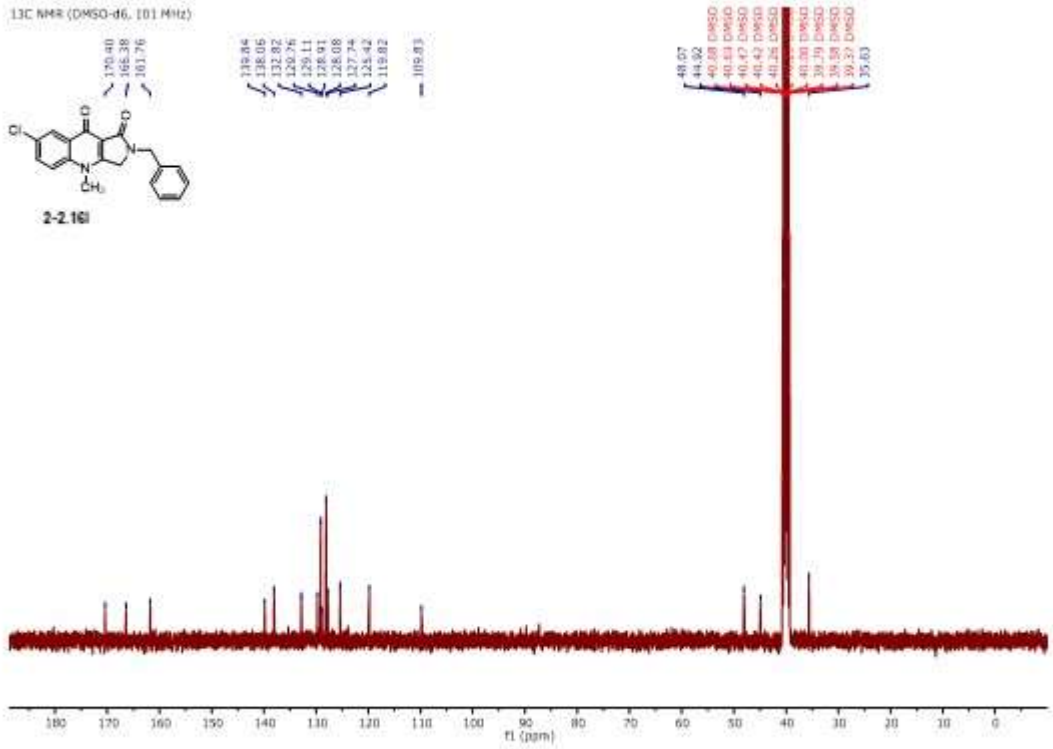
13C NMR (DMSO-d6, 101 MHz)
2-2.16l
f1 (ppm)

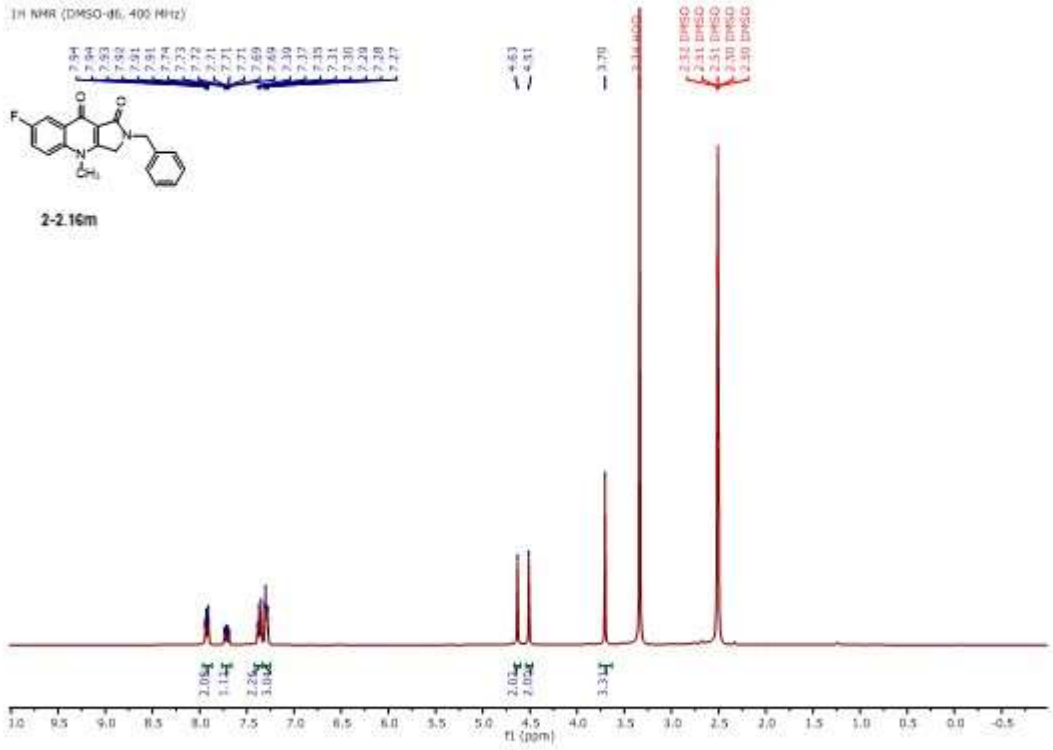
1H NMR (DMSO-d6, 400 MHz)
2-2.16m
f1 (ppm)

19F NMR (DMSO-d6, 376 MHz)

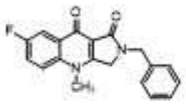

2-2.16m

13C NMR (DMSO-d6, 101 MHz)

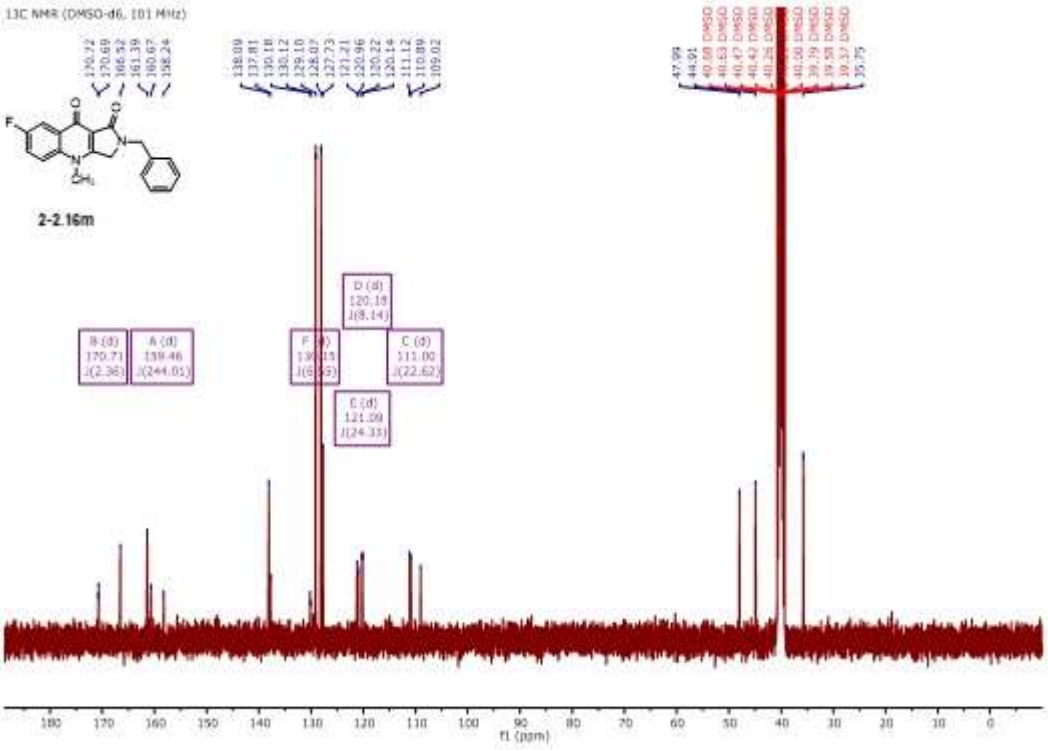

2-2.16m

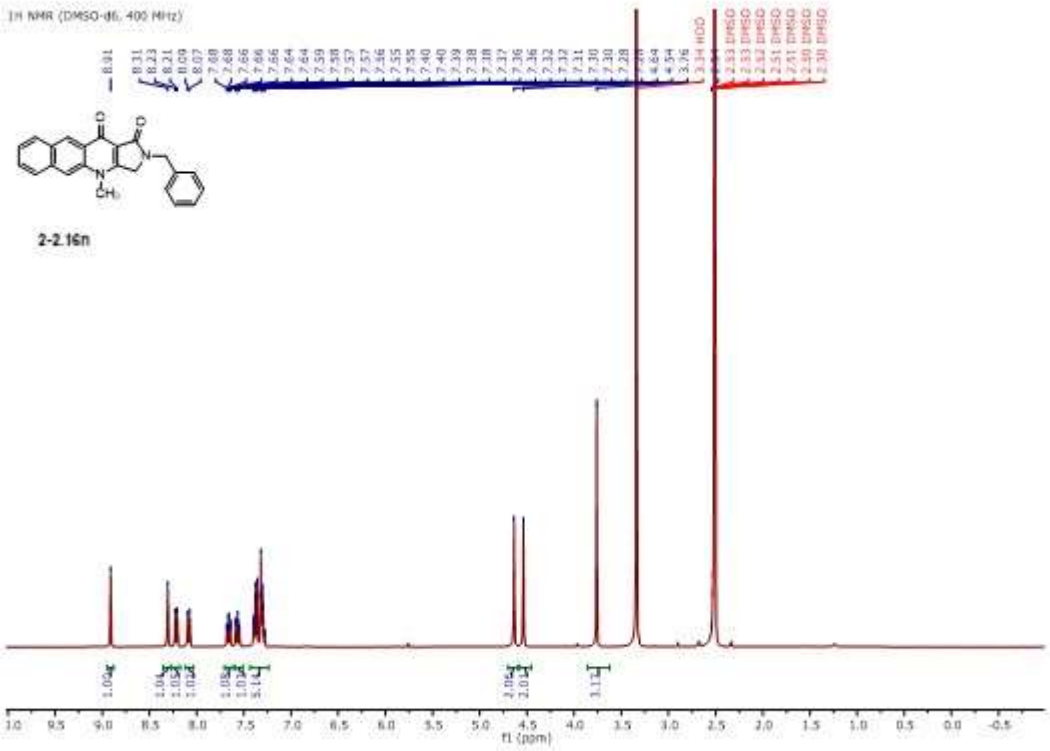
1H NMR (DMSO-d6, 400 MHz)
2-2.16n
f1 (ppm)

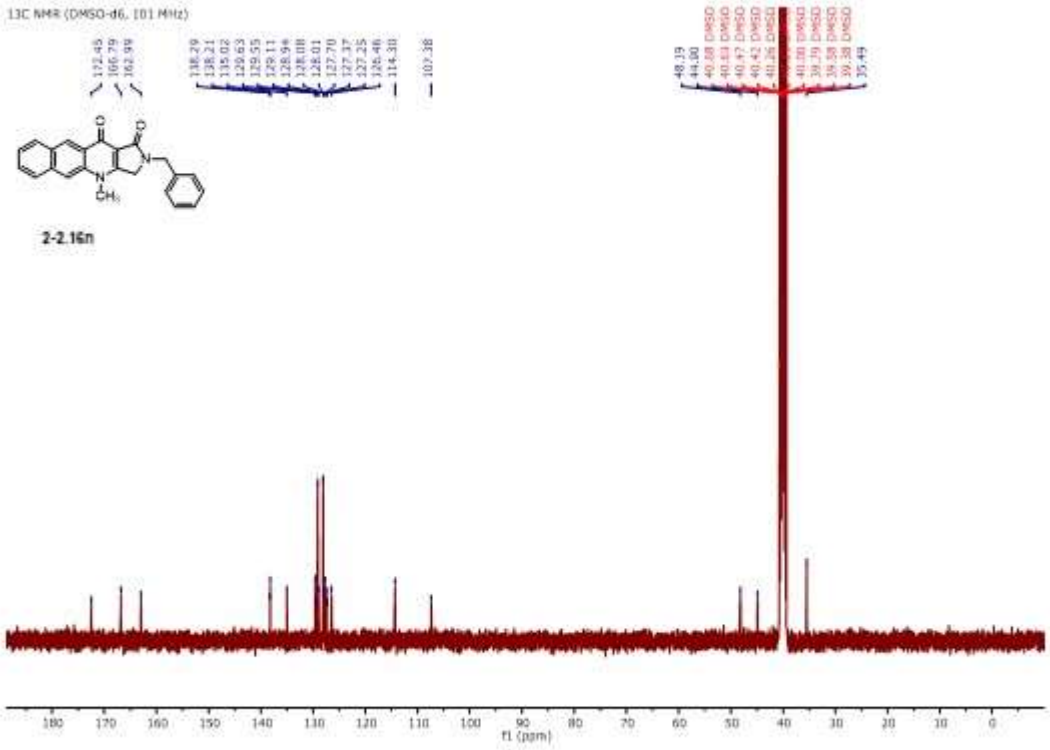
13C NMR (DMSO-d6, 101 MHz)
2-2.16n
f1 (ppm)

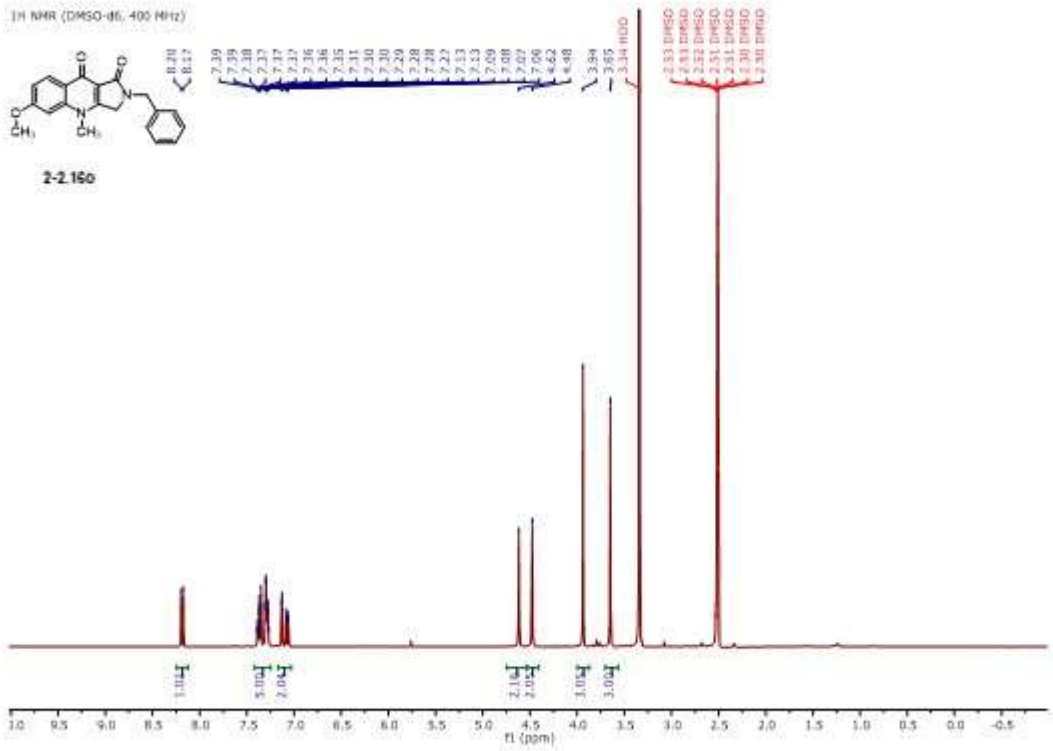
1H NMR (DMSO-d6, 400 MHz)
2-2.160
f1 (ppm)

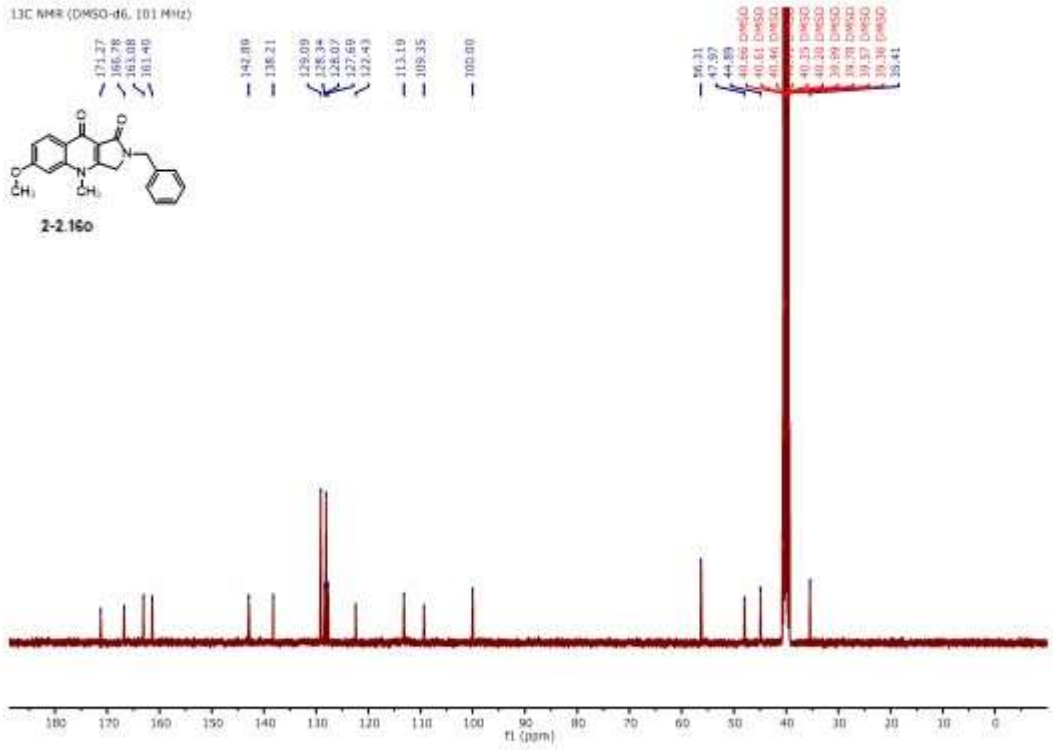
13C NMR (DMSO-d6, 101 MHz)
2-2.160
f1 (ppm)

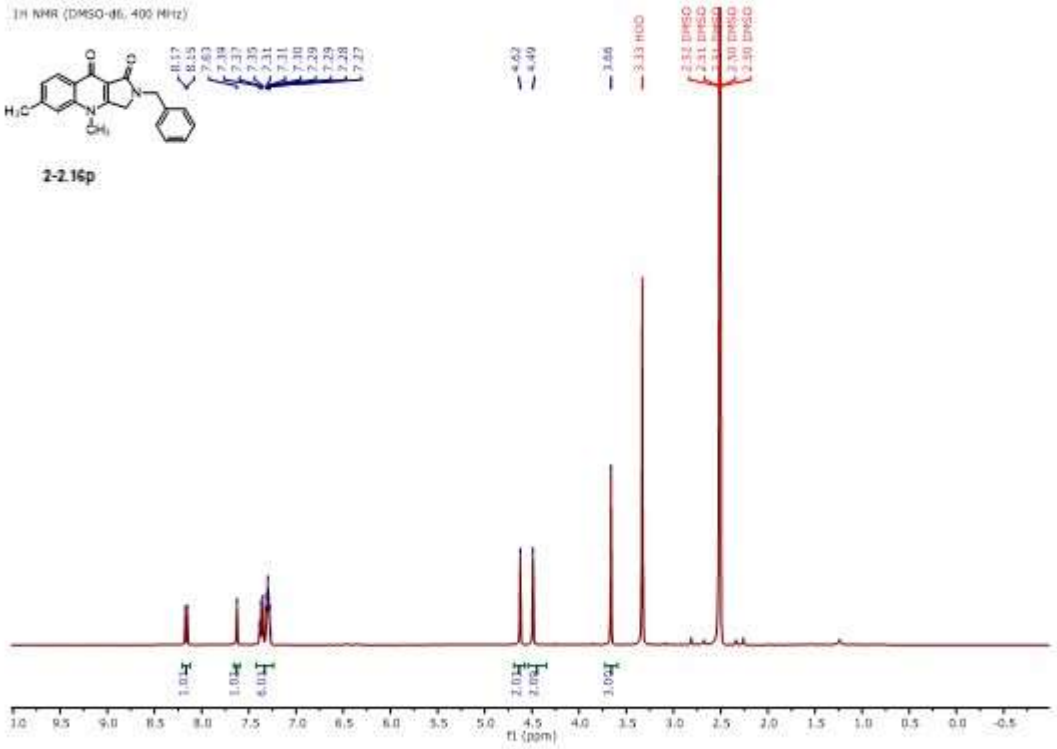
1H NMR (DMSO-d6, 400 MHz)
2-2.16p
f1 (ppm)

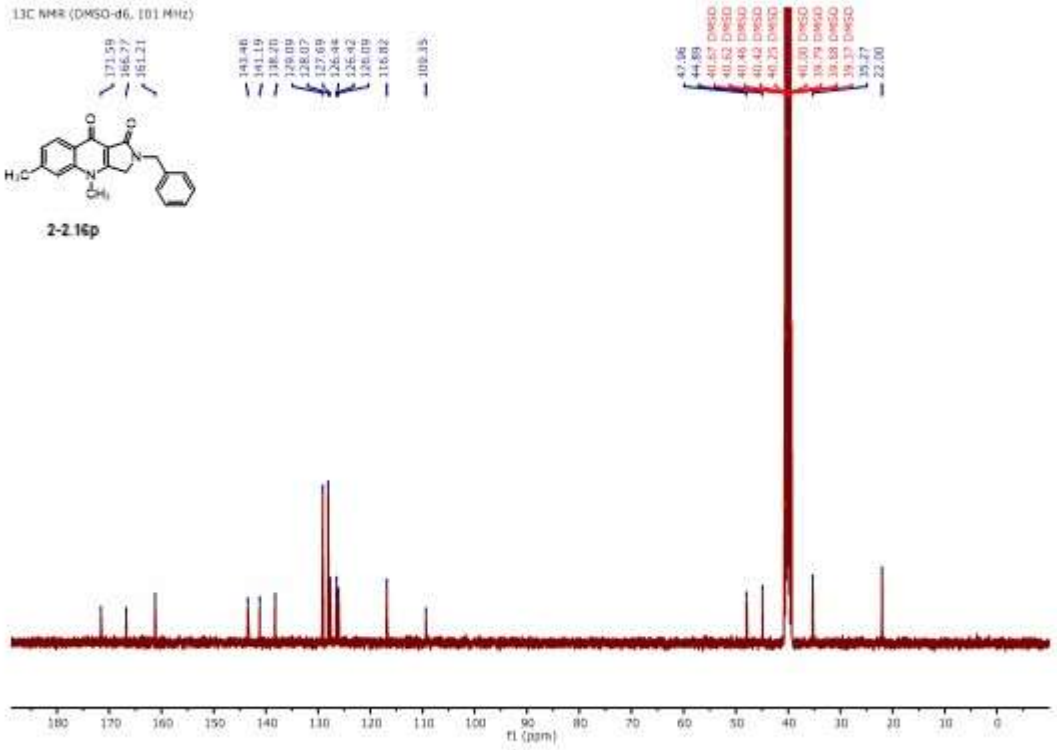
13C NMR (DMSO-d6, 101 MHz)
2-2.16p
f1 (ppm)

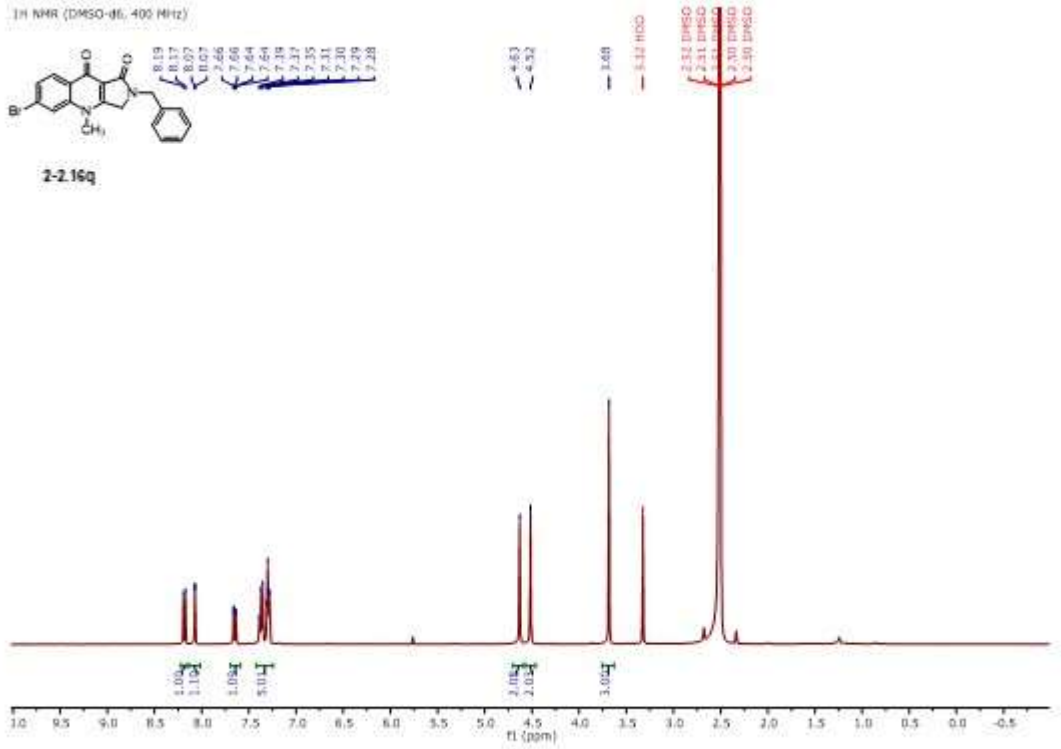
1H NMR (DMSO-d6, 400 MHz)
2-2.16q
8.19
8.17
8.07
8.05
7.66
7.64
7.39
7.37
7.35
7.31
7.30
7.29
7.28
4.63
4.52
3.68
3.32 HDO
2.52 DMSO
2.51 DMSO
2.50 DMSO
2.49 DMSO
1.00
1.02
1.09
5.01
2.05
2.03
3.02
f1 (ppm)

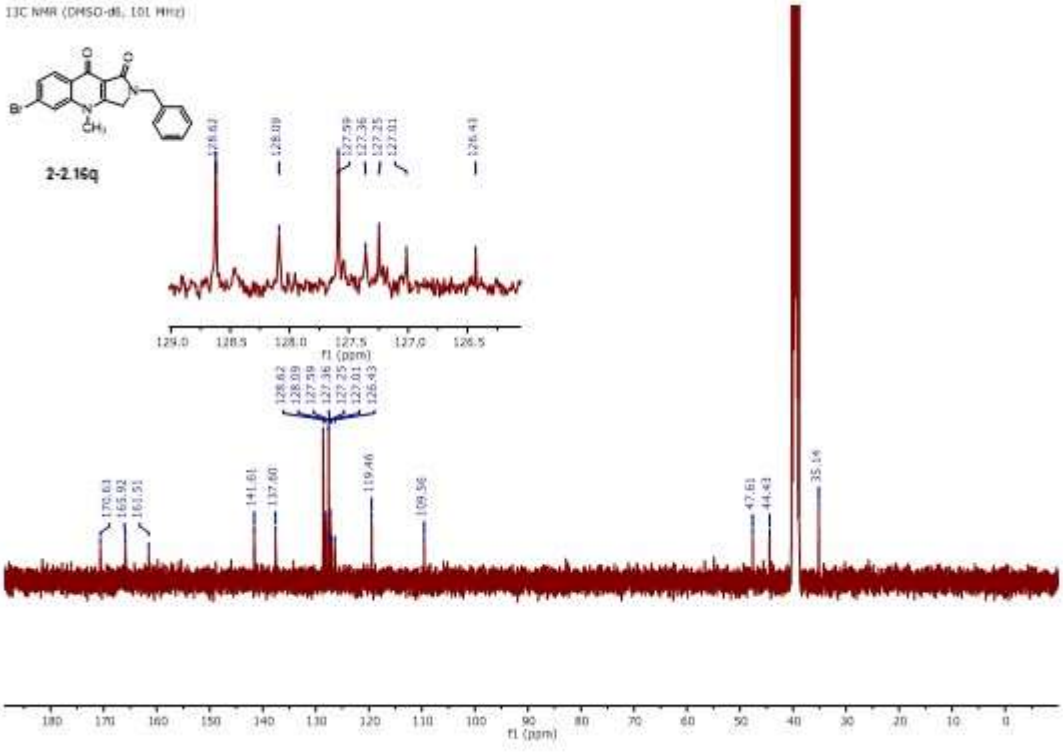
13C NMR (DMSO-d6, 101 MHz)
2-2.16q
128.62
128.09
127.59
127.36
127.25
127.01
126.43
f1 (ppm)
170.63
165.92
161.51
141.61
137.60
119.46
109.56
47.61
44.43
35.14
f1 (ppm)

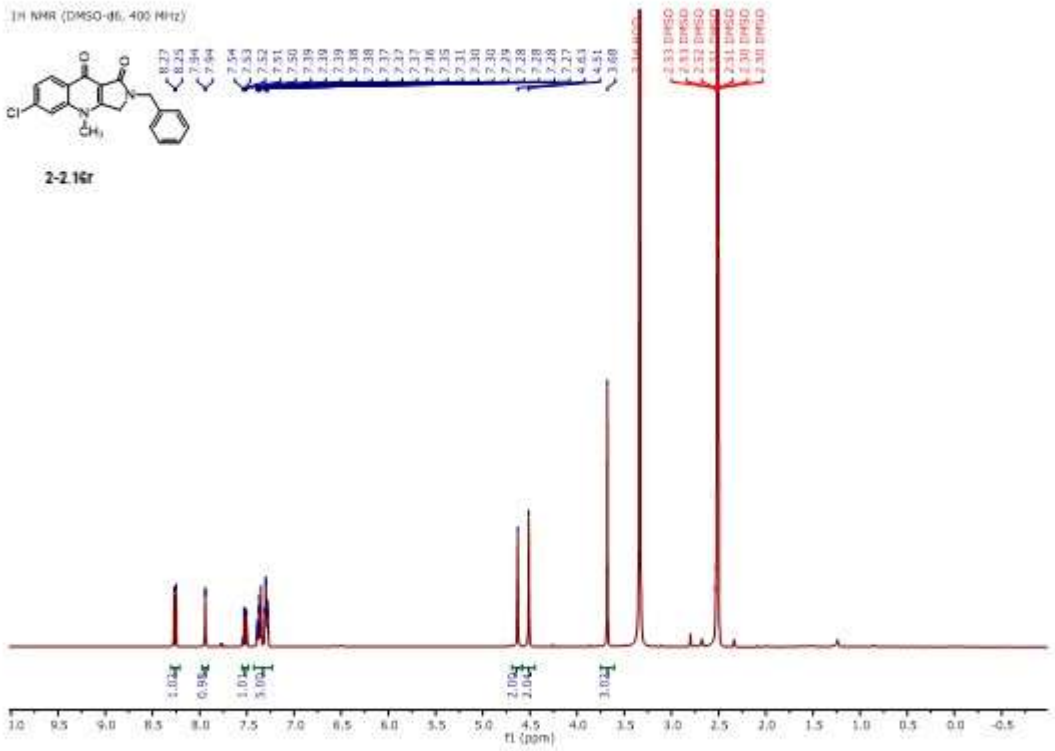
1H NMR (DMSO-d6, 400 MHz)
2-2.16r
f1 (ppm)

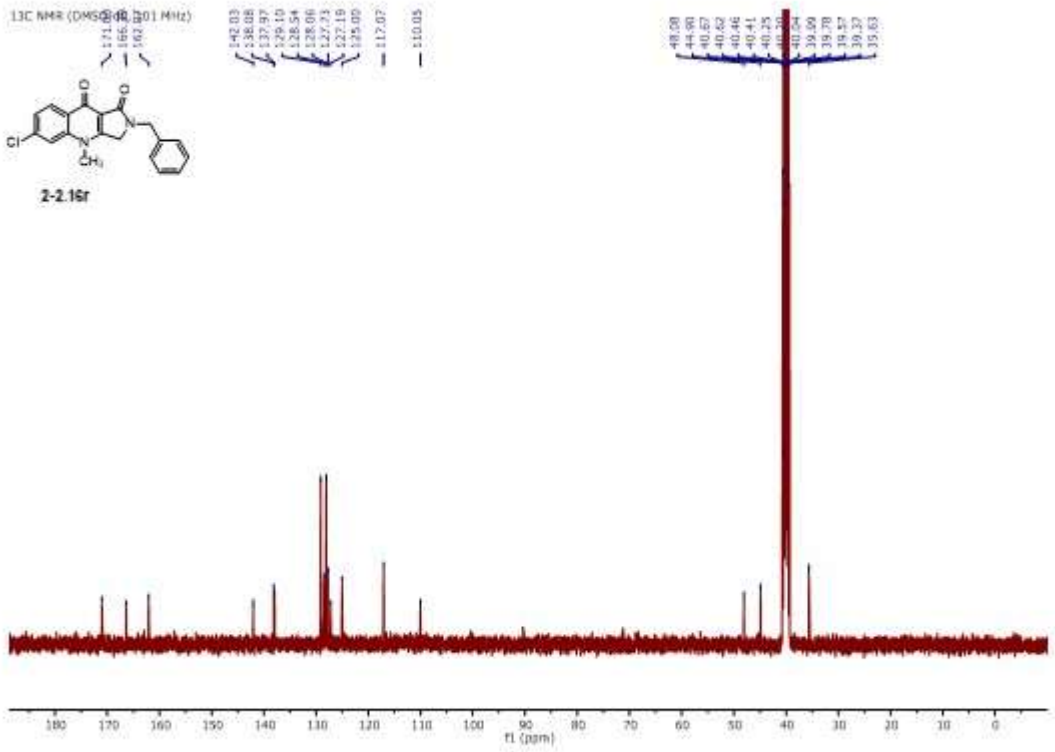
13C NMR (DMSO-d6, 101 MHz)
2-2.16r
f1 (ppm)

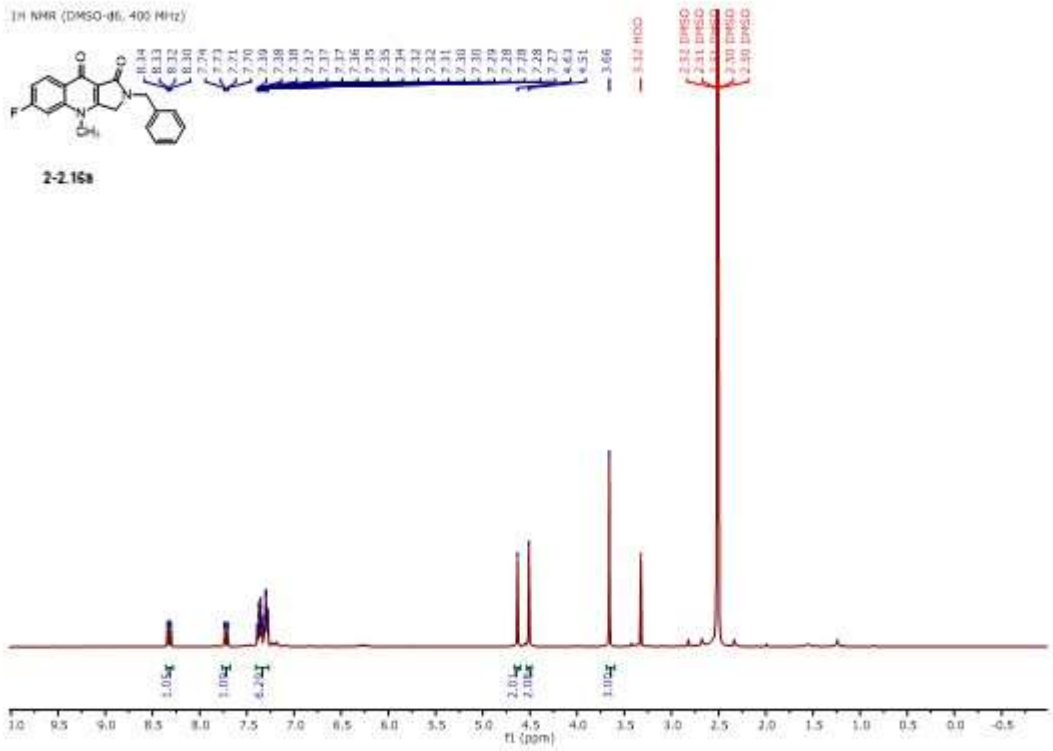
1H NMR (DMSO-d6, 400 MHz)
2-2.16a
f1 (ppm)

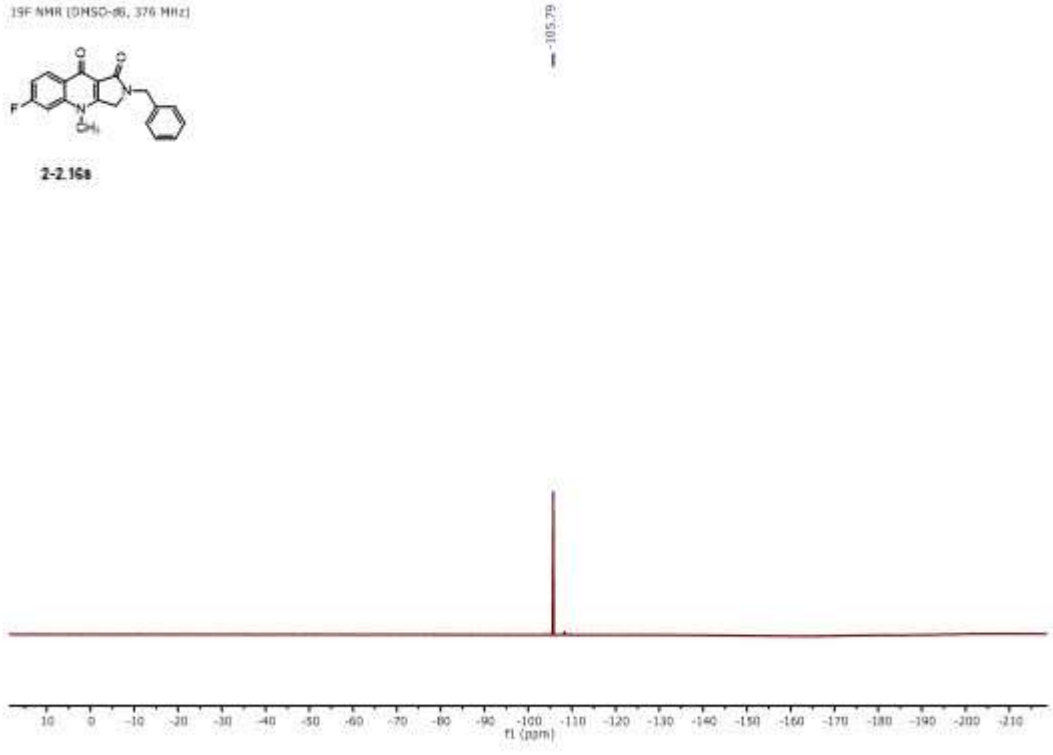
19F NMR (DMSO-d6, 376 MHz)
-105.79
2-2.16a
f1 (ppm)

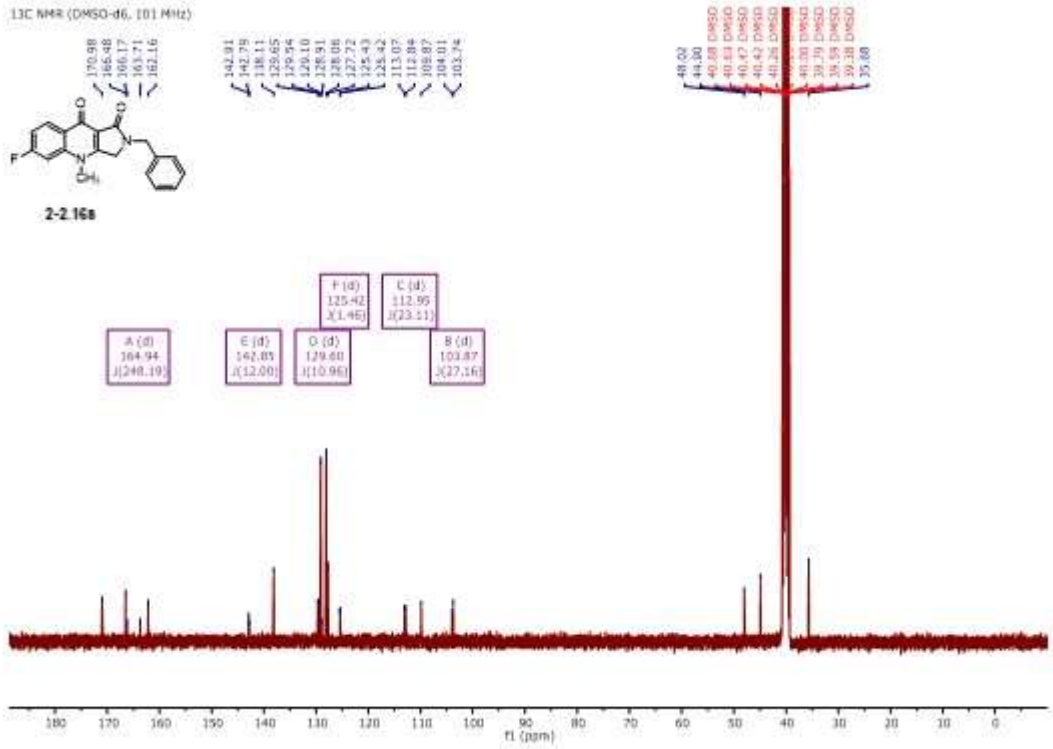
13C NMR (DMSO-d6, 101 MHz)
2-2.16s
A (d)
164.94
J(248.19)
E (d)
142.85
J(12.00)
D (d)
129.60
J(10.96)
F (d)
125.42
J(1.46)
C (d)
112.95
J(23.11)
B (d)
103.87
J(27.16)
f1 (ppm)

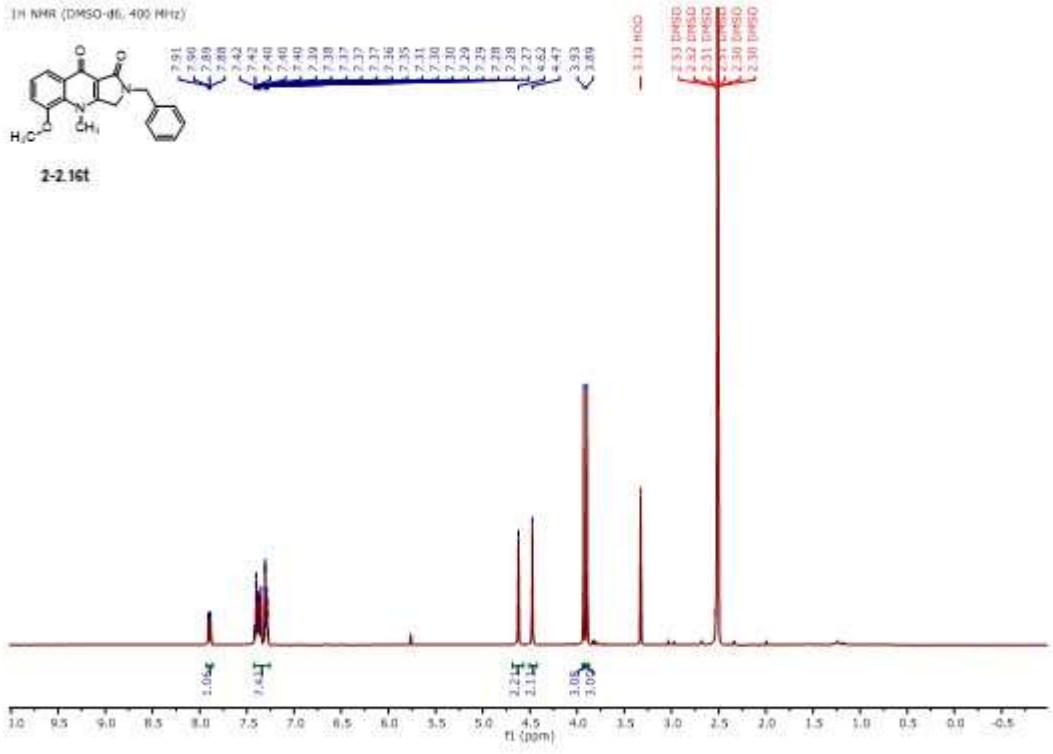
1H NMR (DMSO-d6, 400 MHz)
2-2.16t
f1 (ppm)

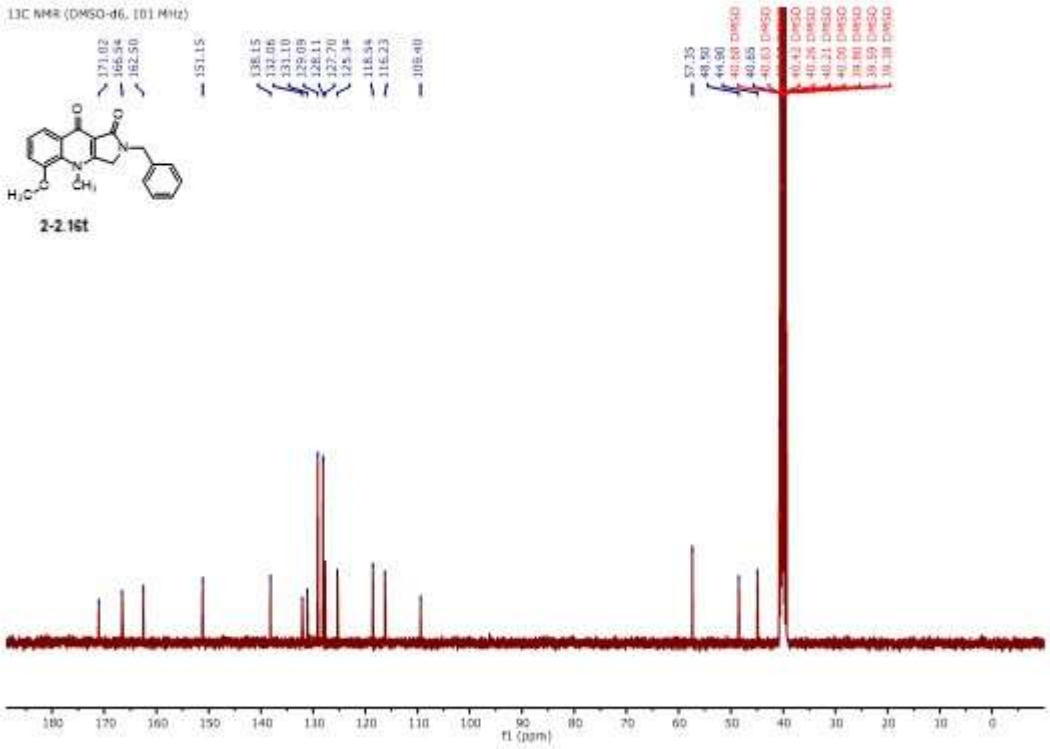
13C NMR (DMSO-d6, 101 MHz)
2-2.16t
f1 (ppm)

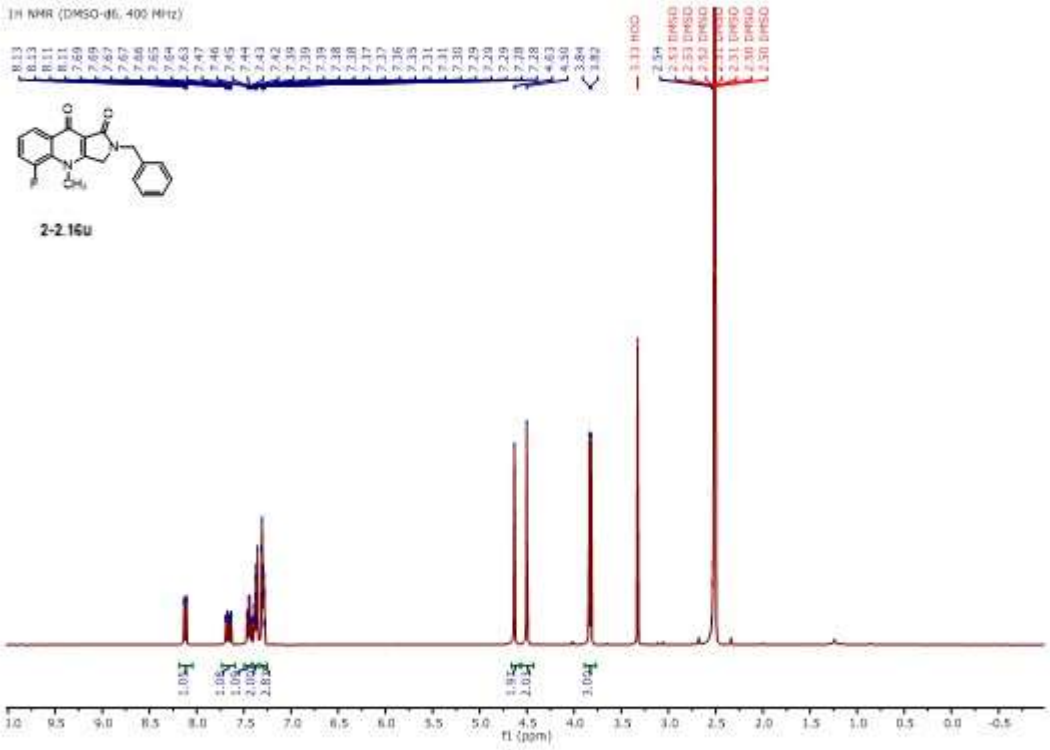
1H NMR (DMSO-d6, 400 MHz)
2-2.16u
f1 (ppm)

19F NMR (DMSO-d6, 376 MHz)

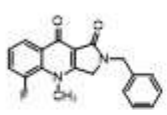

2-2.16u

13C NMR (DMSO-d6, 101 MHz)

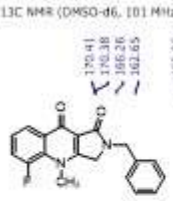

2-2.16u

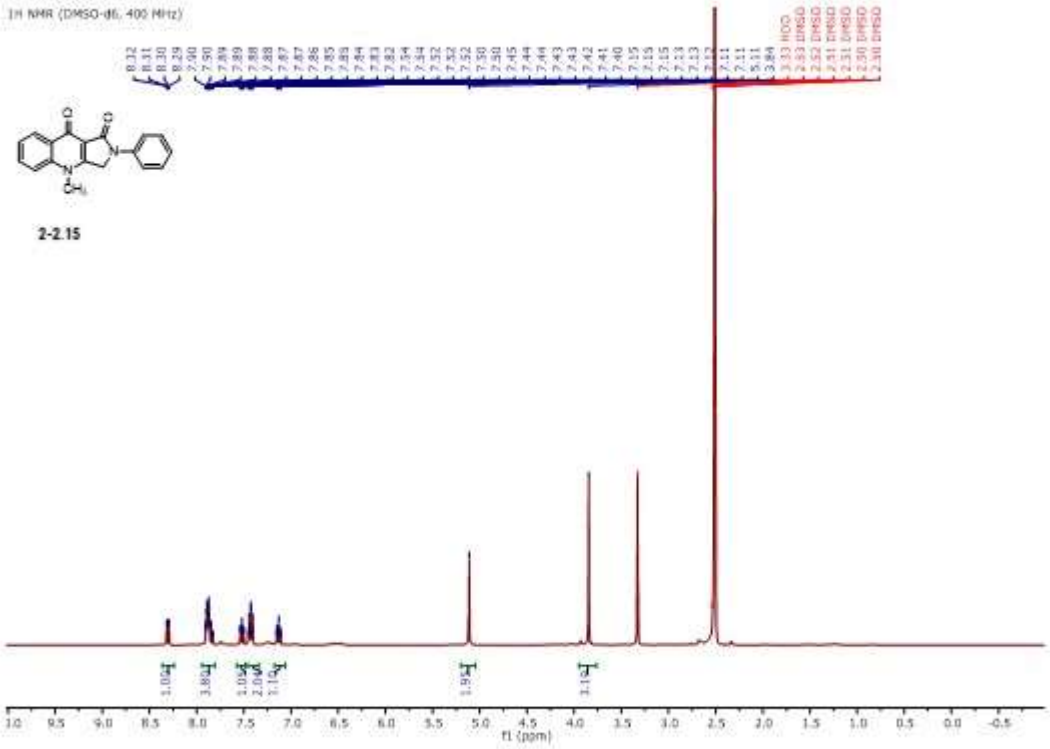
1H NMR (DMSO-d6, 400 MHz)
2-2.15
f1 (ppm)

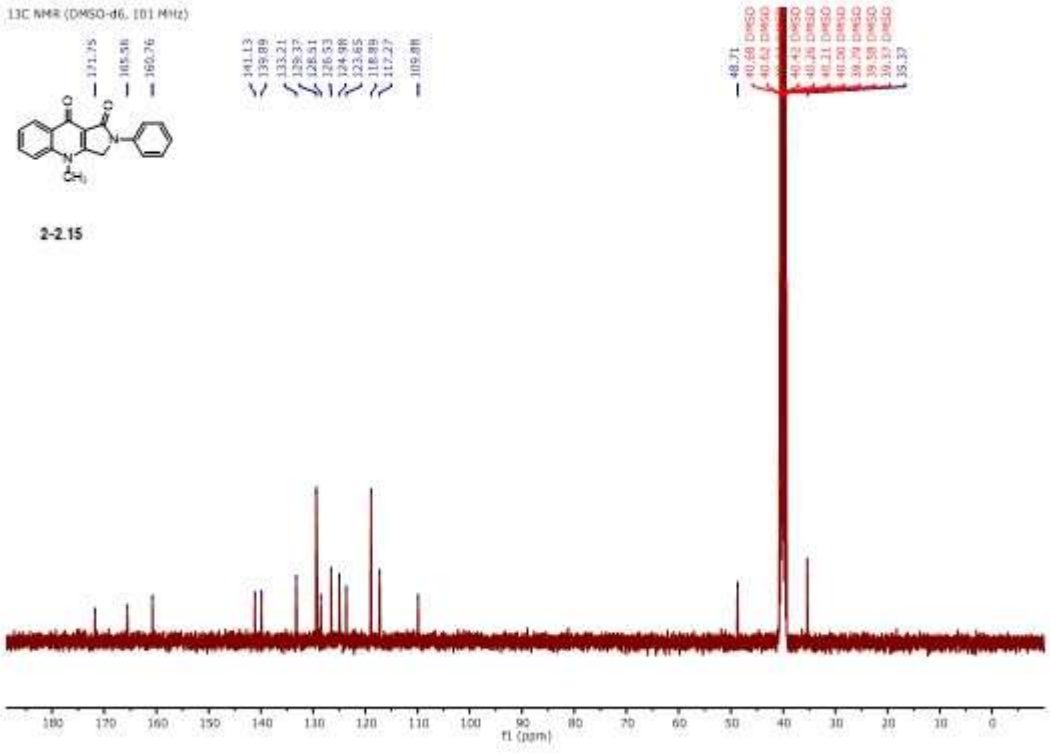
13C NMR (DMSO-d6, 101 MHz)
2-2.15
f1 (ppm)

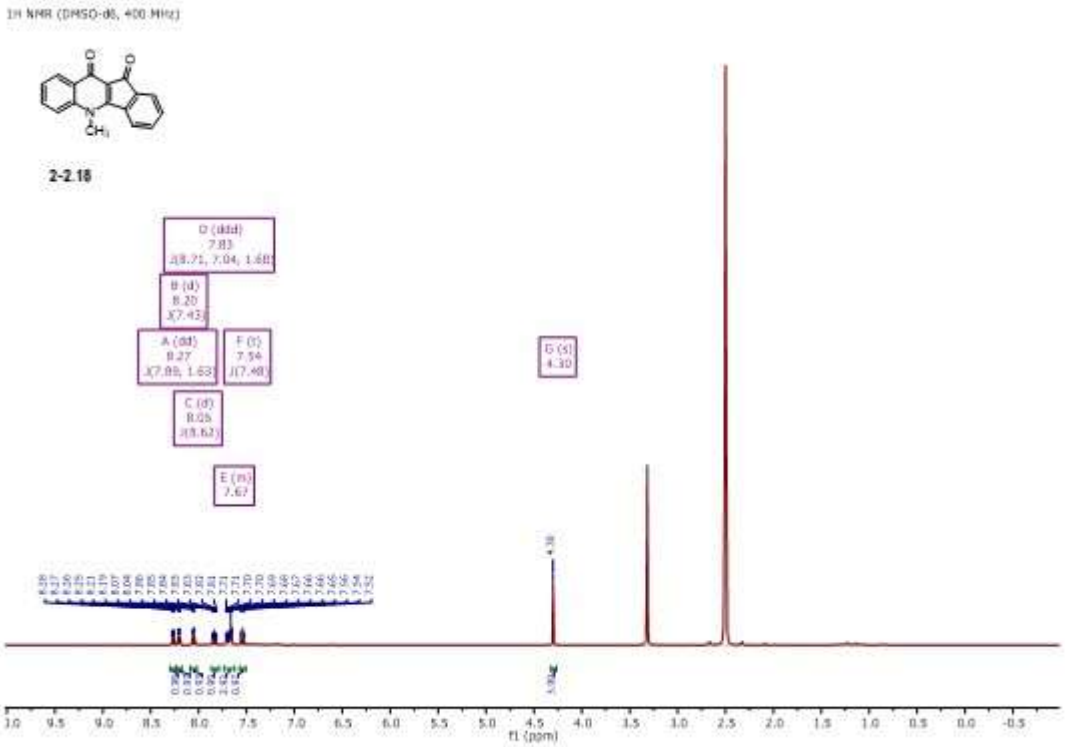
1H NMR (DMSO-d6, 400 MHz)
2-2.18
D (ddd)
7.83
J(8.71, 7.04, 1.68)
B (d)
8.20
J(7.43)
A (dd)
8.27
J(7.89, 1.63)
F (t)
7.56
J(7.48)
C (d)
8.05
J(8.62)
E (m)
7.67
G (s)
4.30
f1 (ppm)

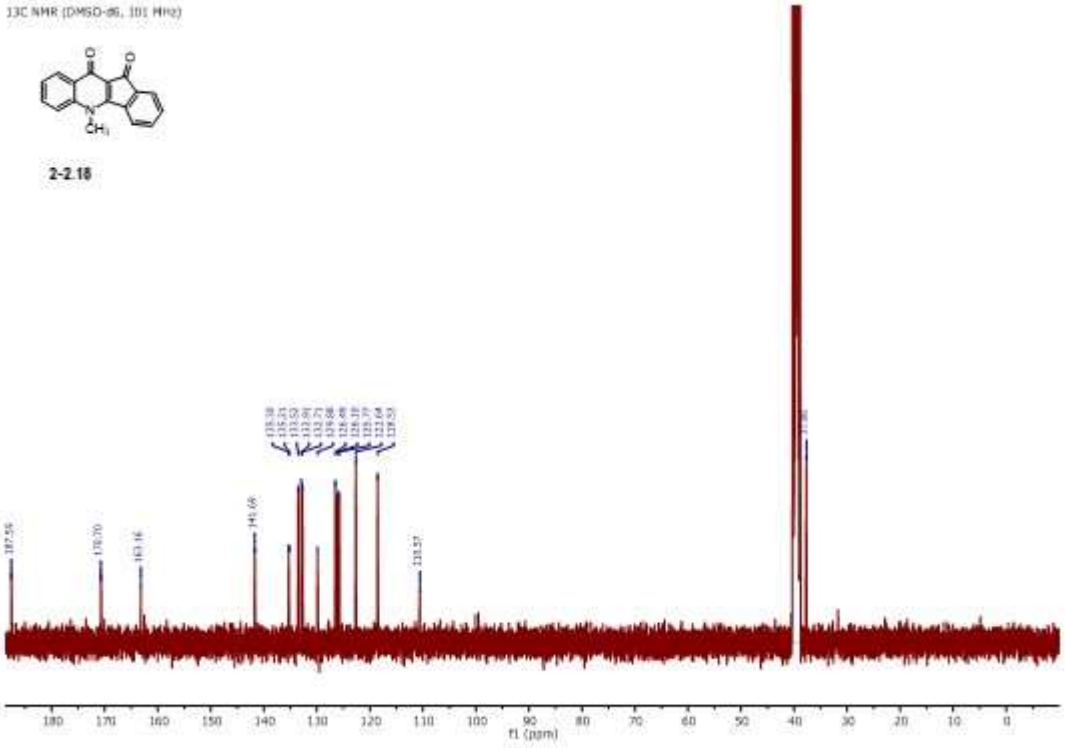
13C NMR (DMSO-d6, 101 MHz)
2-2.18
187.55
176.70
161.16
145.69
135.57
f1 (ppm)

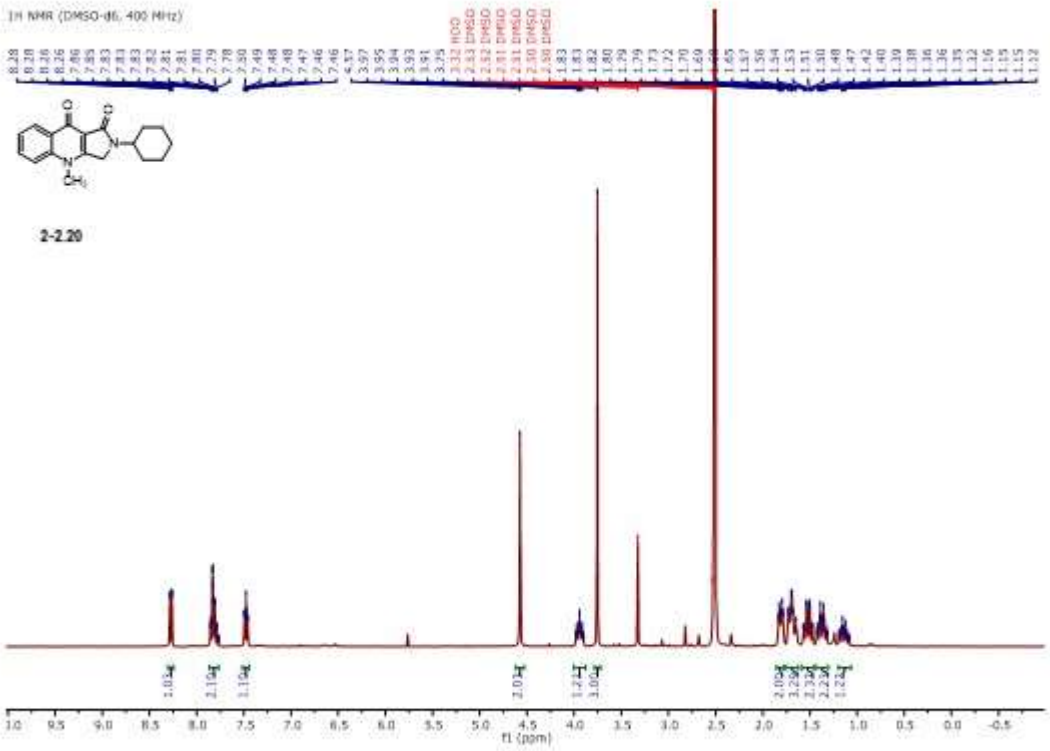
1H NMR (DMSO-d6, 400 MHz)
2-2.20
f1 (ppm)

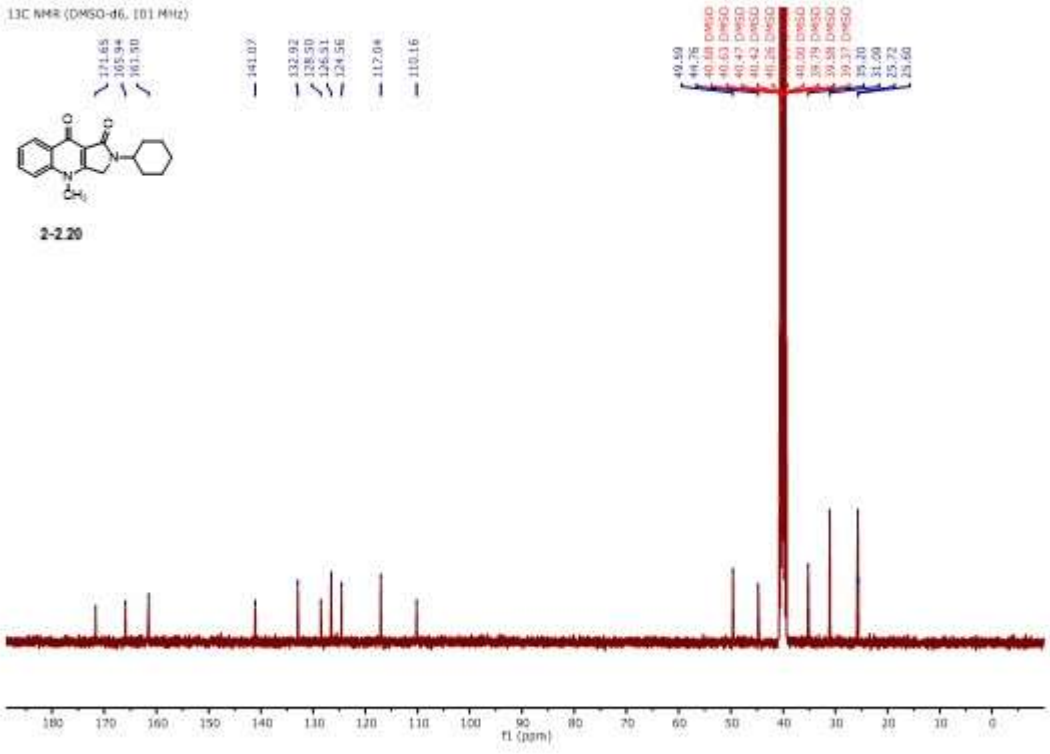
13C NMR (DMSO-d6, 101 MHz)
2-2.20
f1 (ppm)

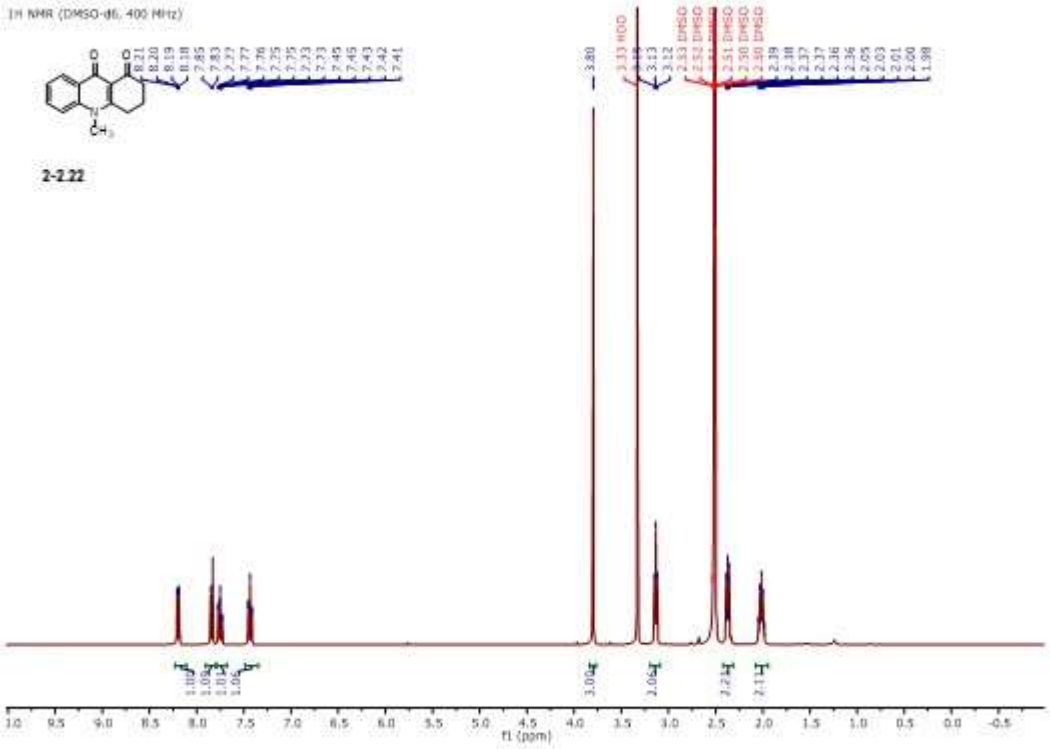
1H NMR (DMSO-d6, 400 MHz)
2-2.22
f1 (ppm)

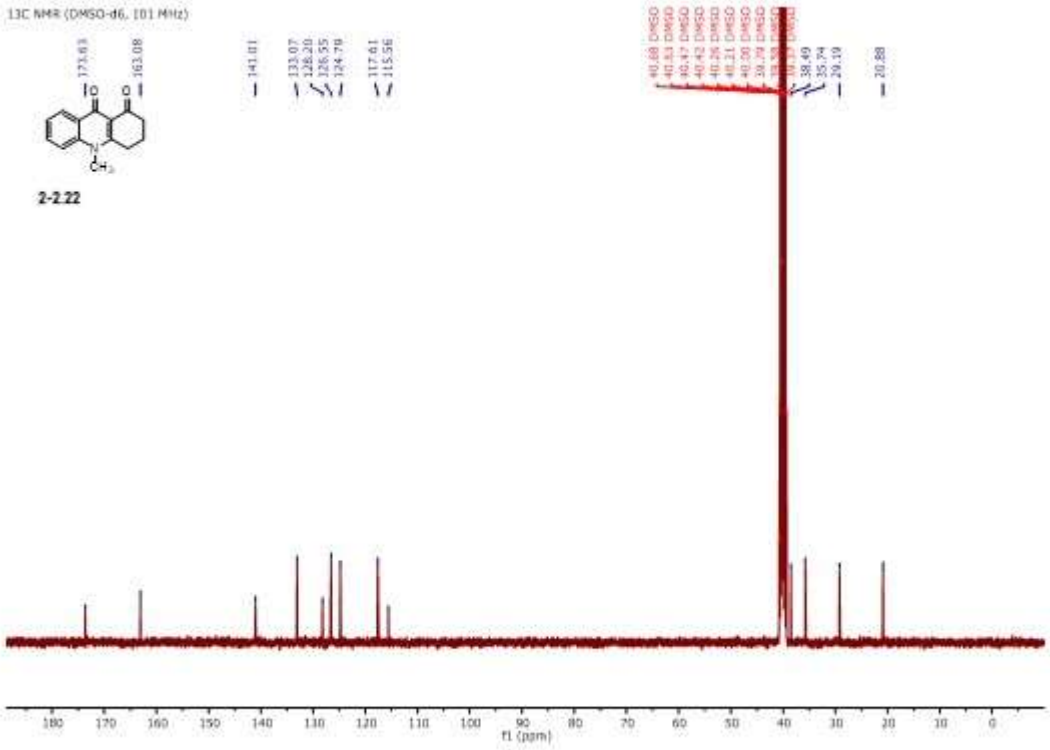
13C NMR (DMSO-d6, 101 MHz)
2-2.22
f1 (ppm)

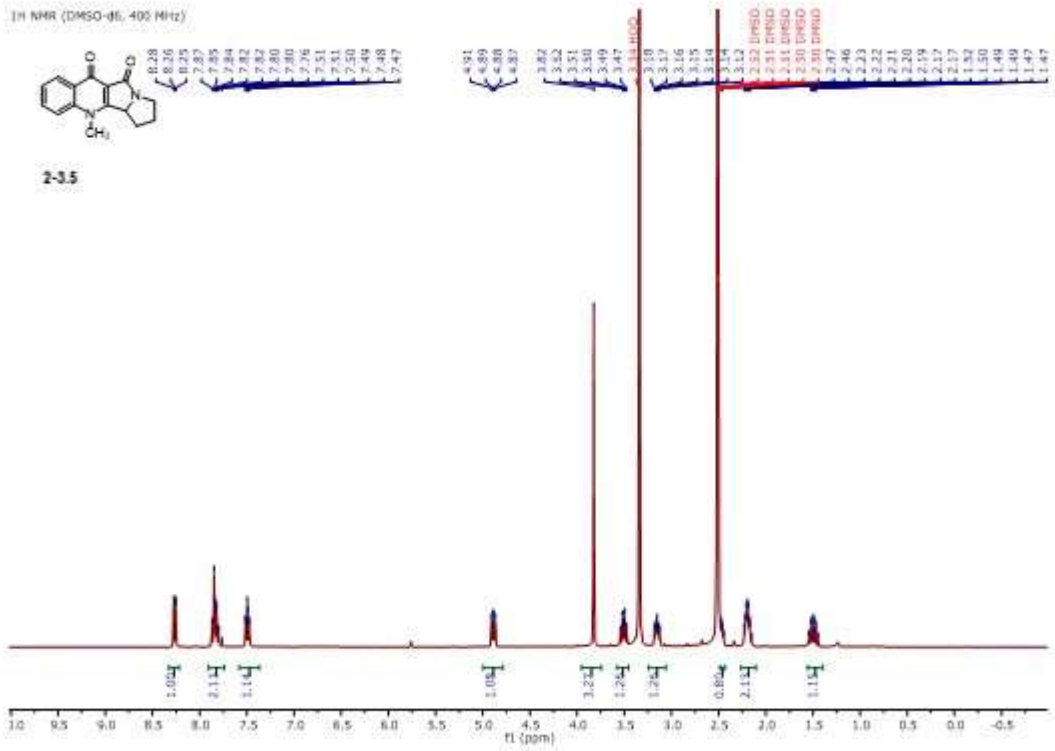
1H NMR (DMSO-d6, 400 MHz)
2-3.5
f1 (ppm)

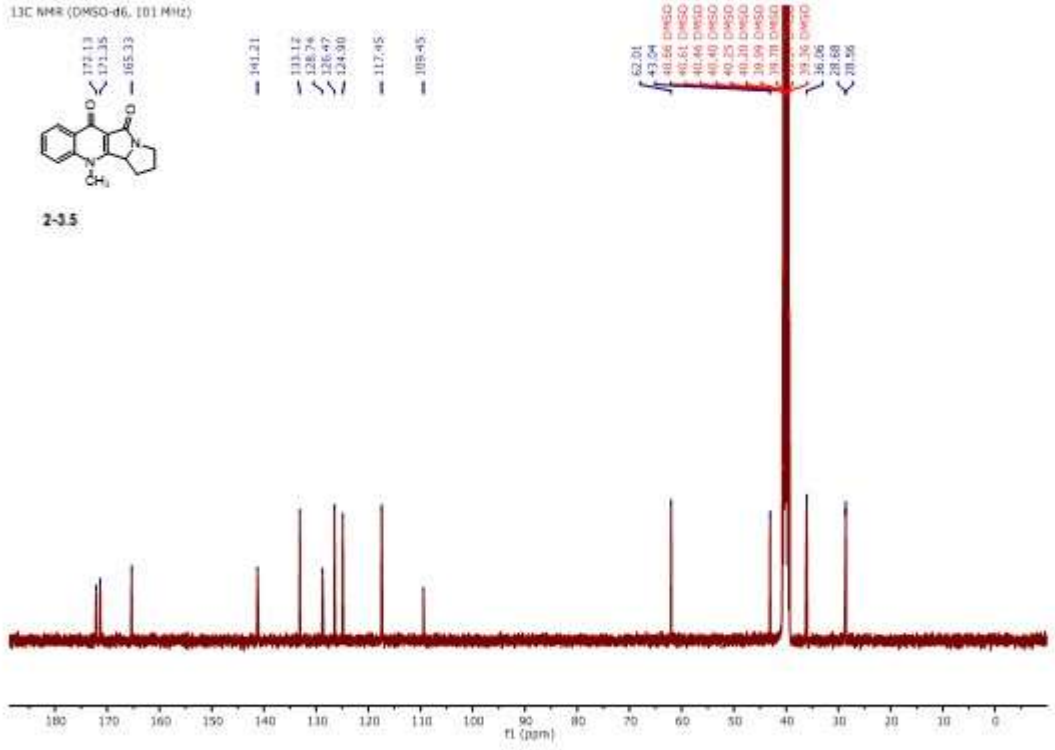
13C NMR (DMSO-d6, 101 MHz)
2-3.5
f1 (ppm)

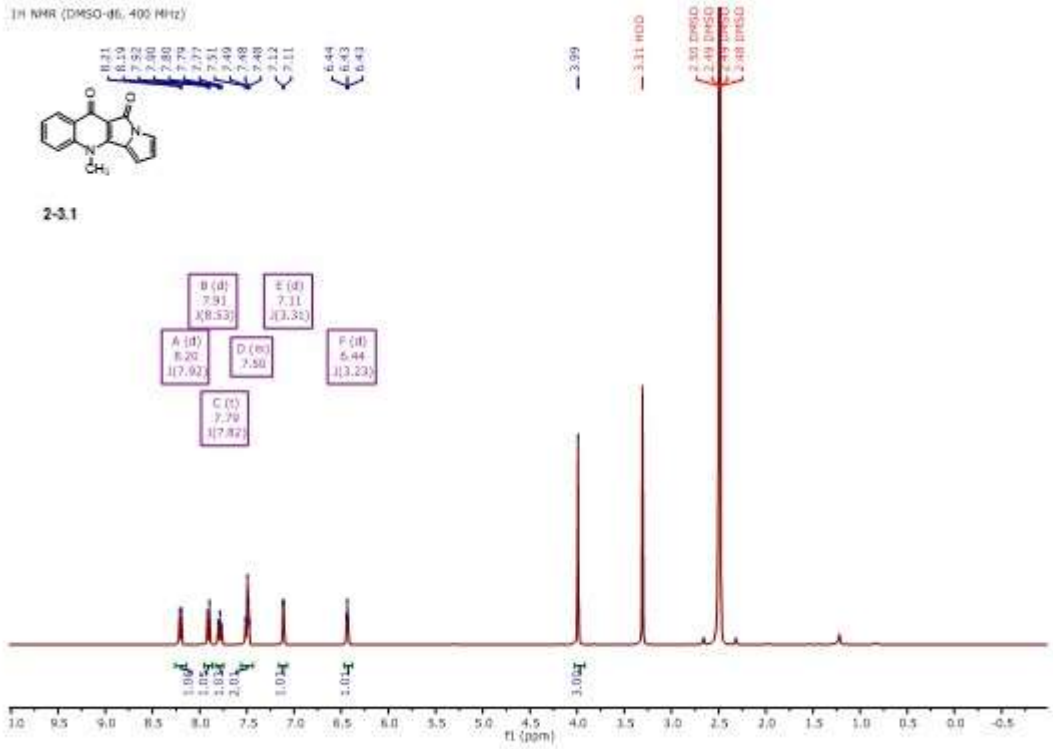
1H NMR (DMSO-d6, 400 MHz)
2-3.1
f1 (ppm)

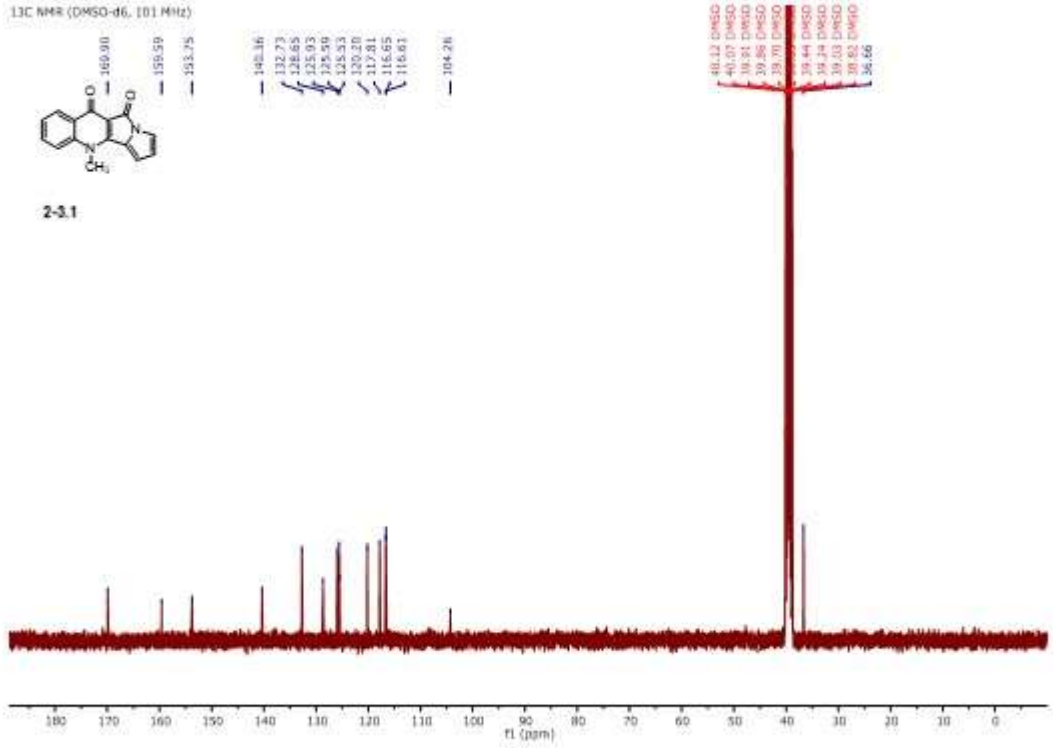
13C NMR (DMSO-d6, 101 MHz)
2-3.1
f1 (ppm)

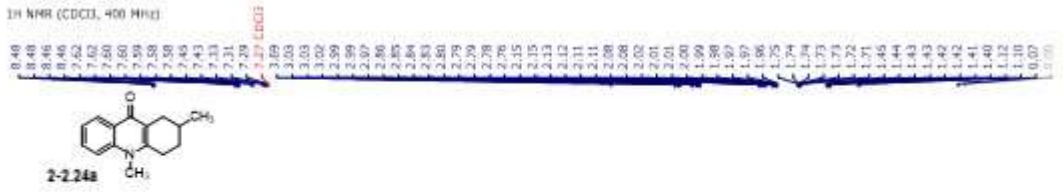
1H NMR (CDCl3, 400 MHz)
2-2.24a

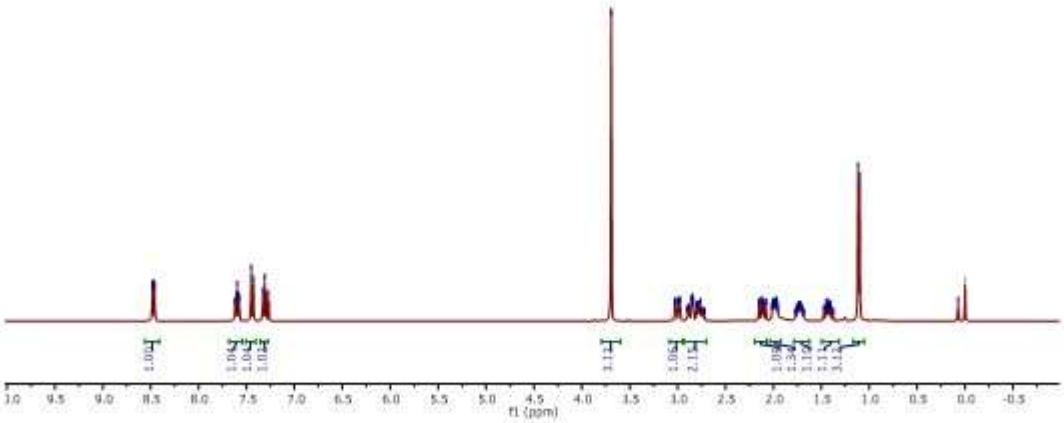
f1 (ppm)

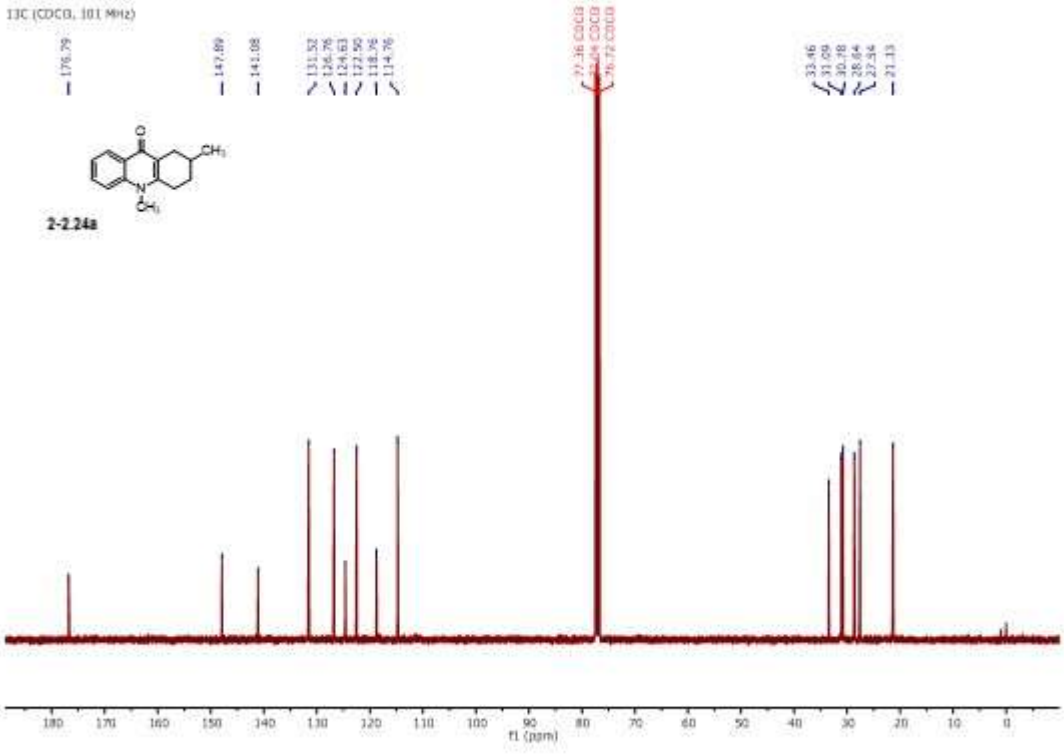
13C (CDCl3, 101 MHz)
2-2.24a
f1 (ppm)

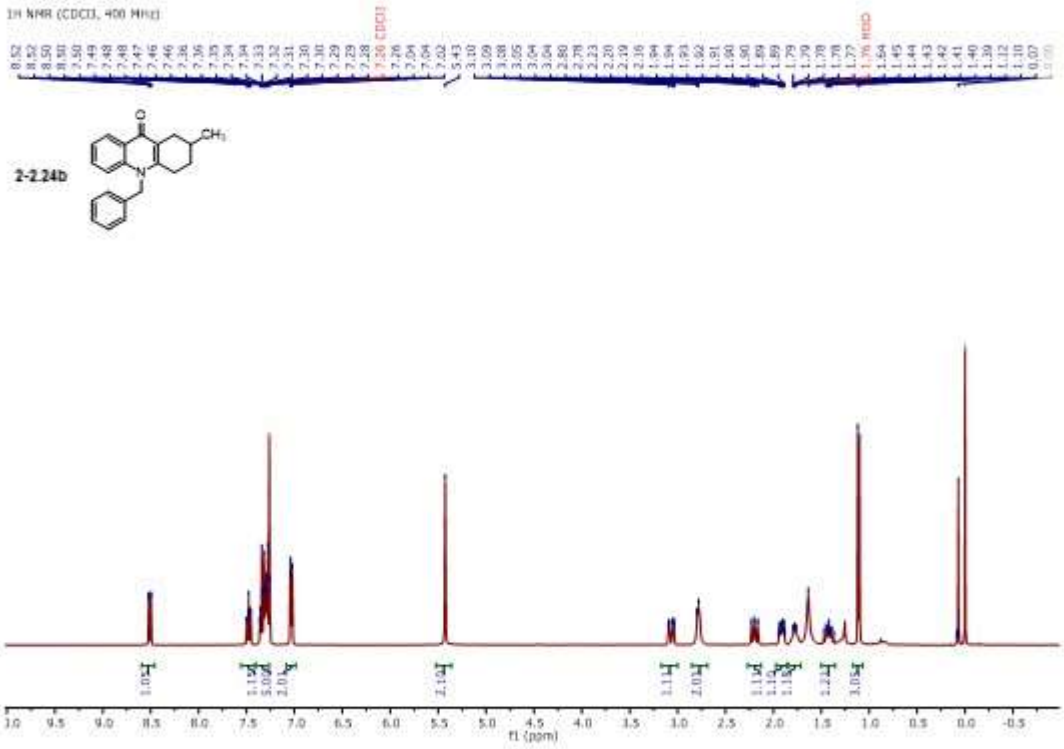
1H NMR (CDCl3, 400 MHz)
2-2.24b
f1 (ppm)

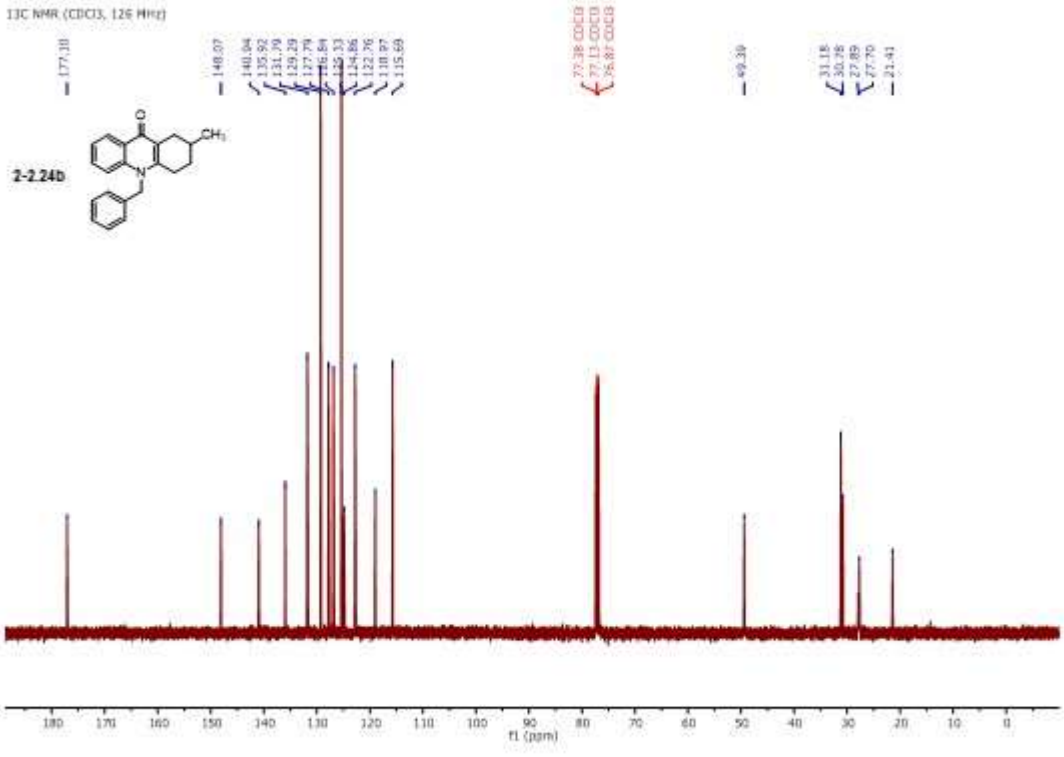
13C NMR (CDCl3, 126 MHz)
2-2.24b
f1 (ppm)

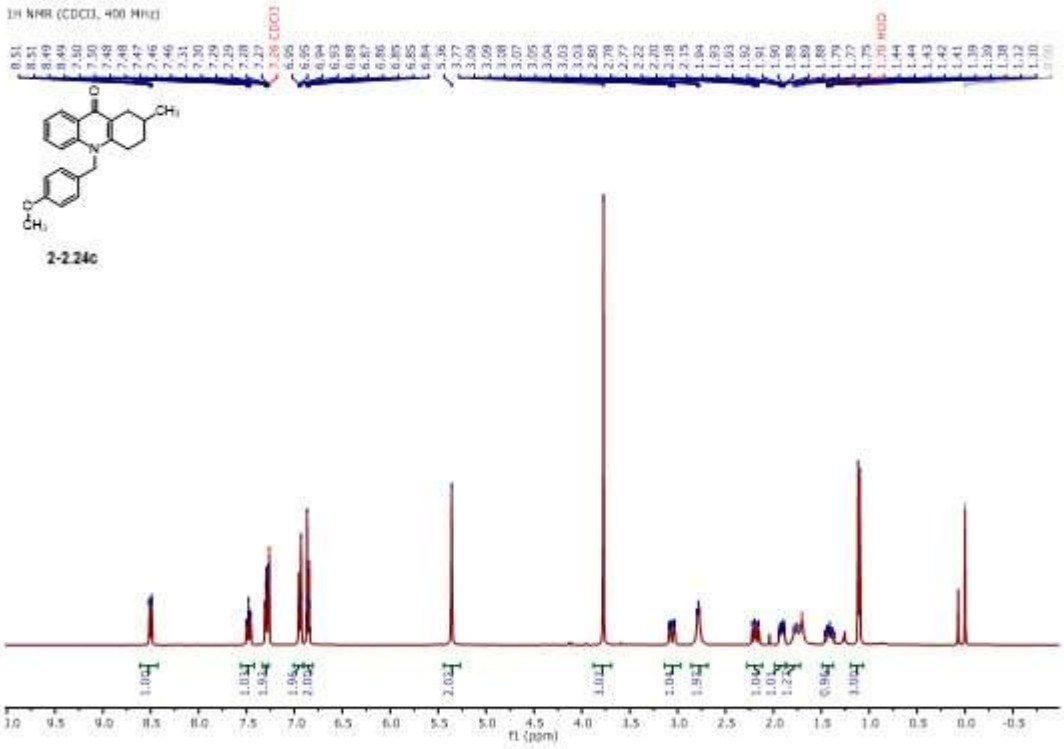
1H NMR (CDCl3, 400 MHz)
2-2.24c
f1 (ppm)

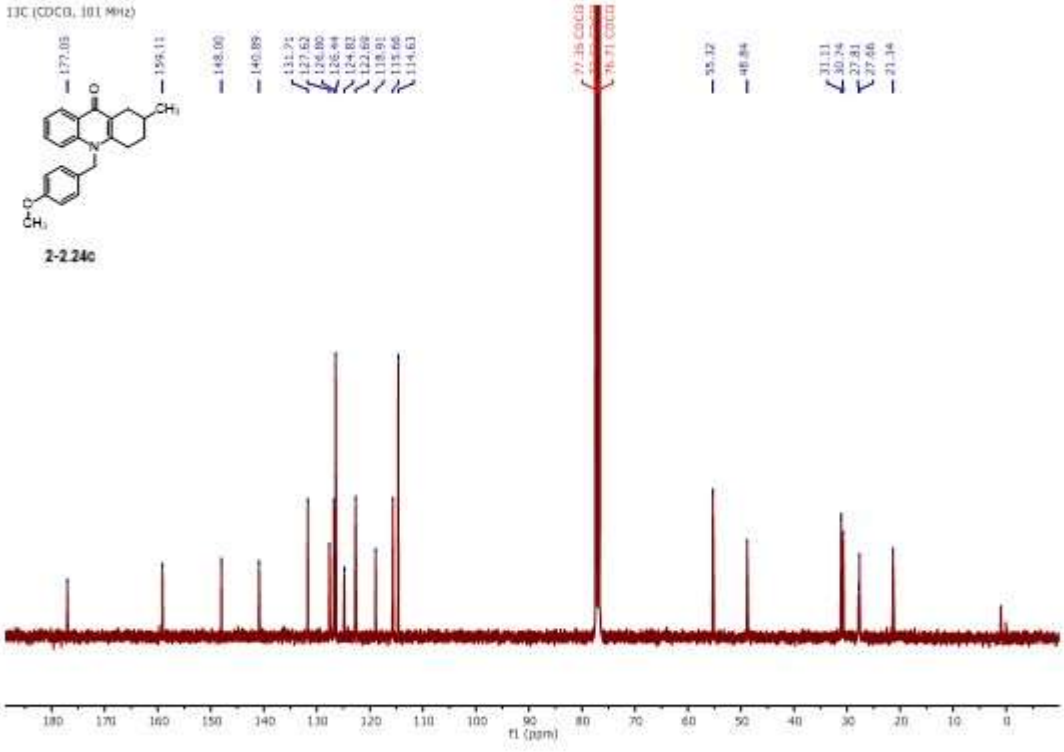
13C (CDCl3, 101 MHz)
2-2.24c
f1 (ppm)

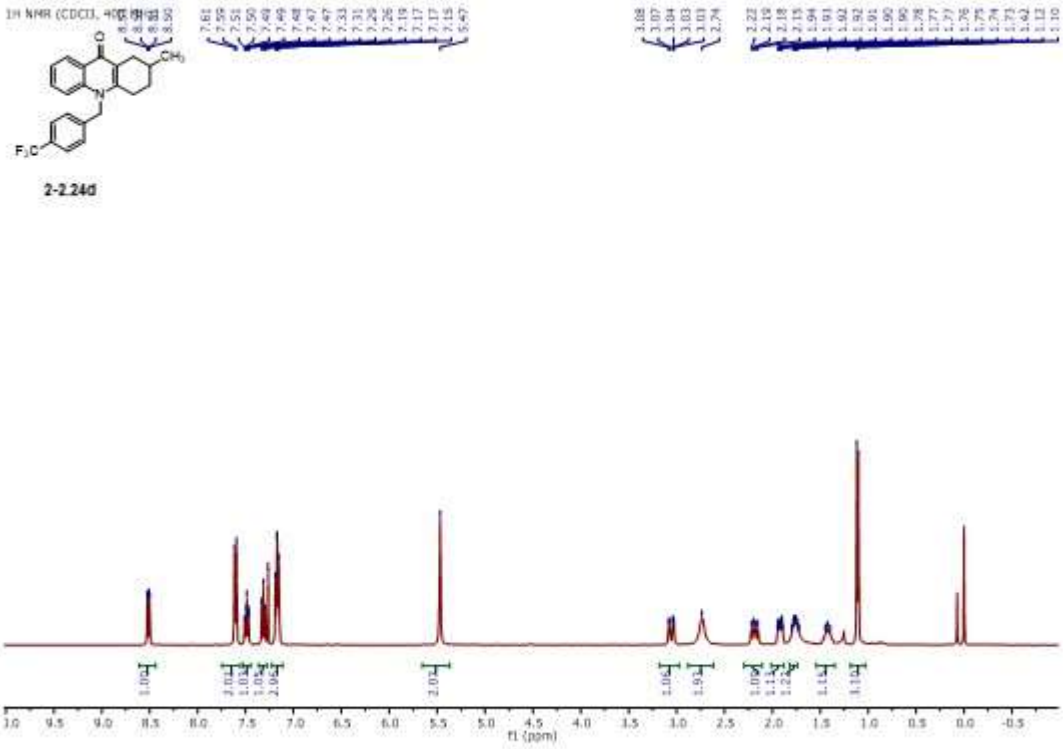
1H NMR (CDCl3, 400 MHz)
2-2.24d
1.00
2.02
1.03
1.05
2.05
2.07
1.06
1.93
1.09
1.13
1.02
1.15
3.10
f1 (ppm)

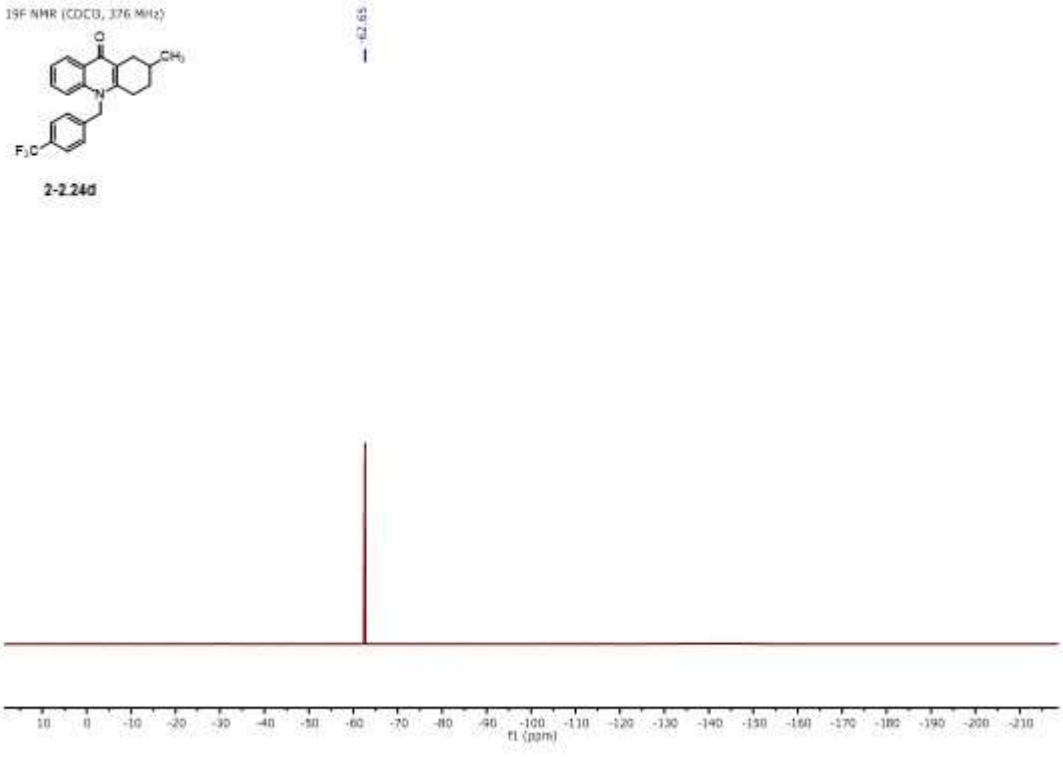
19F NMR (CDCl3, 376 MHz)
-62.65
2-2.24d
f1 (ppm)

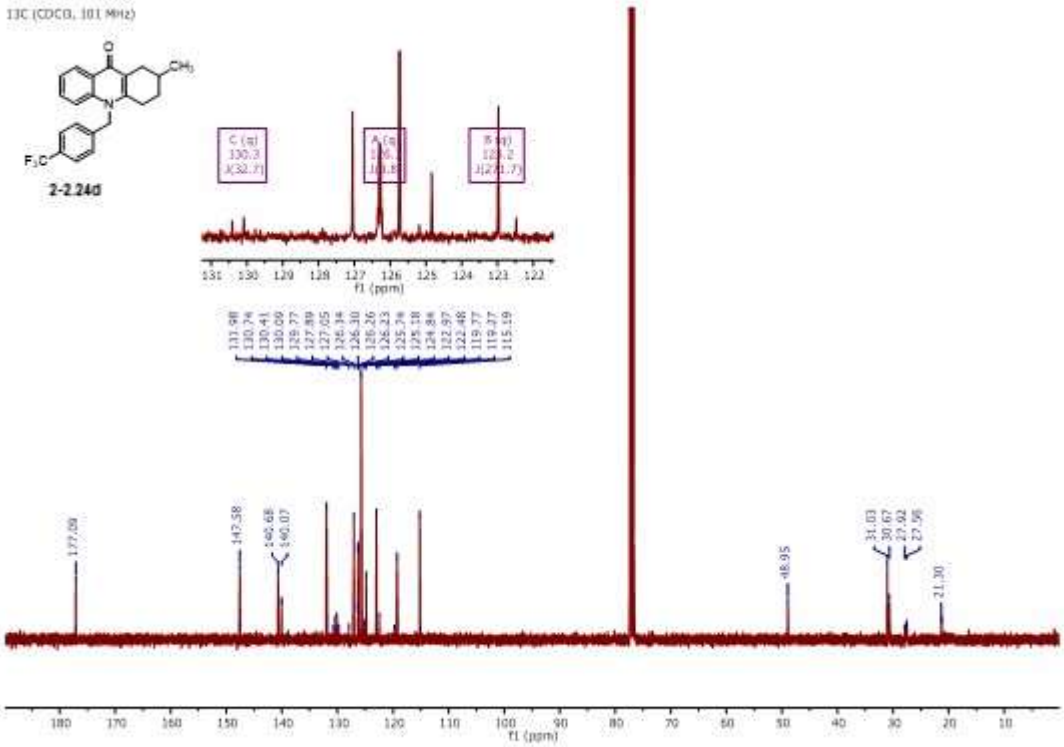
13C (CDCl3, 101 MHz)
2-2.24d
f1 (ppm)

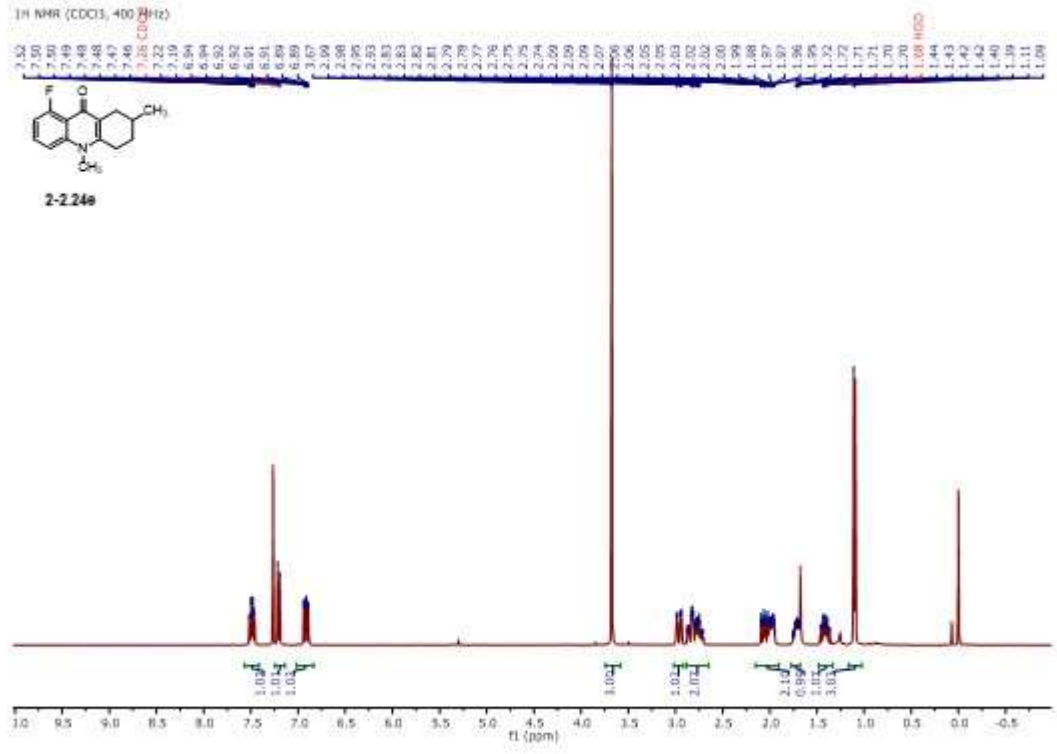
1H NMR (CDCl3, 400 MHz)
2-2.24e
f1 (ppm)

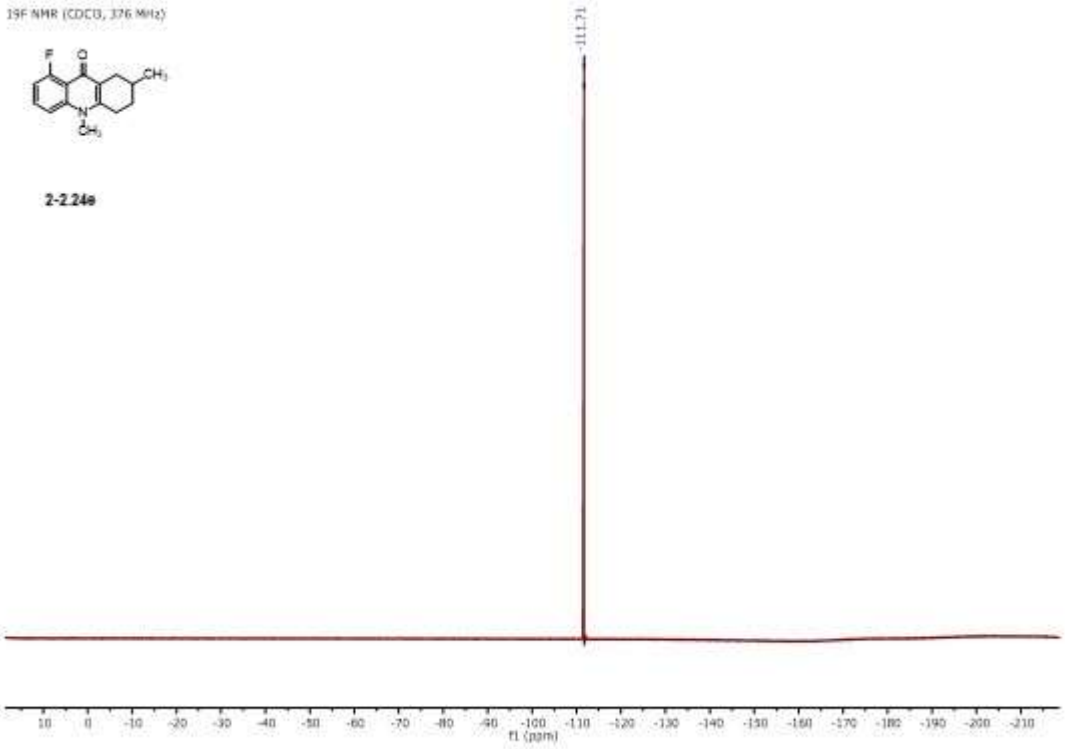
19F NMR (CDCl3, 376 MHz)
-111.71
2-2.24e
f1 (ppm)

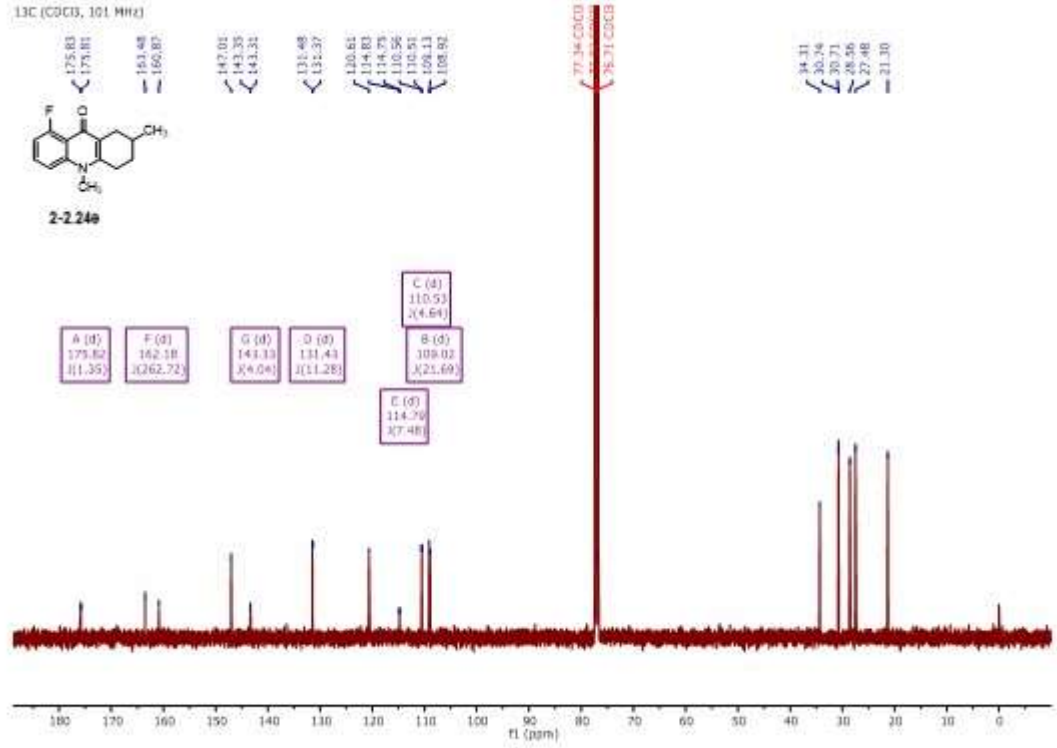
13C (CDCl3, 101 MHz)
175.83
175.81
163.48
160.87
147.01
143.35
143.31
131.48
131.37
120.61
114.83
114.75
110.96
110.51
109.13
108.92
77.34 CDCl3
76.71 CDCl3
34.31
30.74
30.71
28.56
27.48
21.30
2-2.24e
A (d)
179.82
J(1.35)
F (d)
162.18
J(262.72)
G (d)
143.33
J(4.04)
D (d)
131.43
J(11.28)
C (d)
110.53
J(4.64)
B (d)
109.02
J(21.69)
E (d)
114.79
J(7.48)
f1 (ppm)

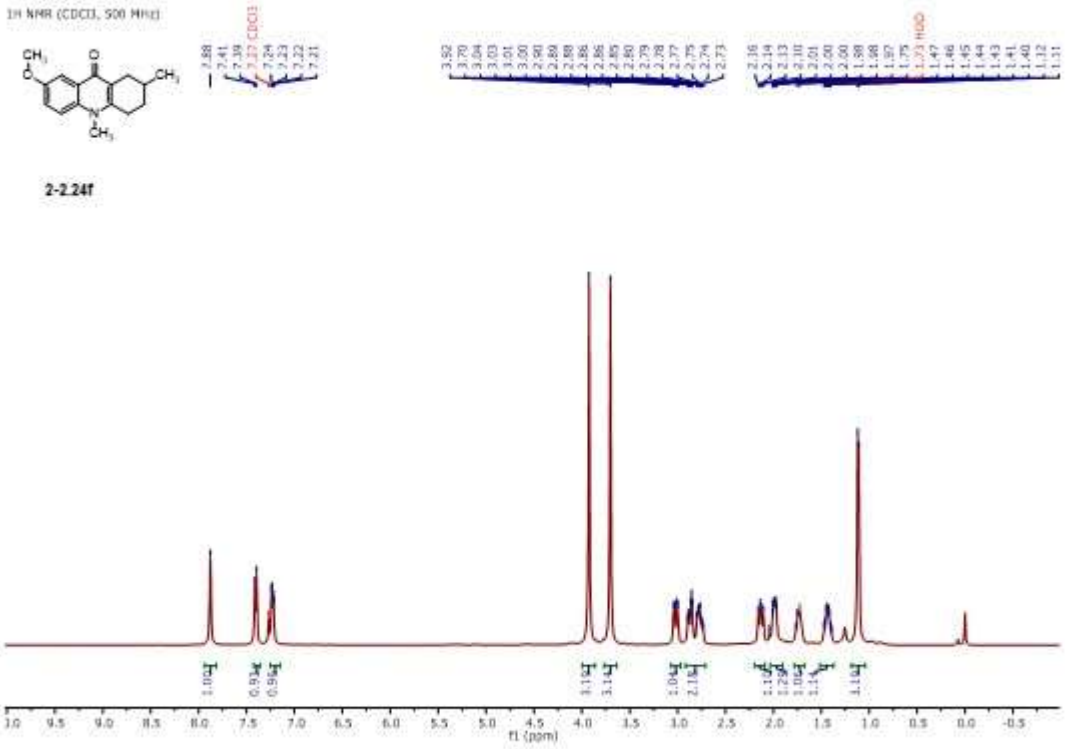
1H NMR (CDCl3, 500 MHz)
2-2.24f
fl (ppm)

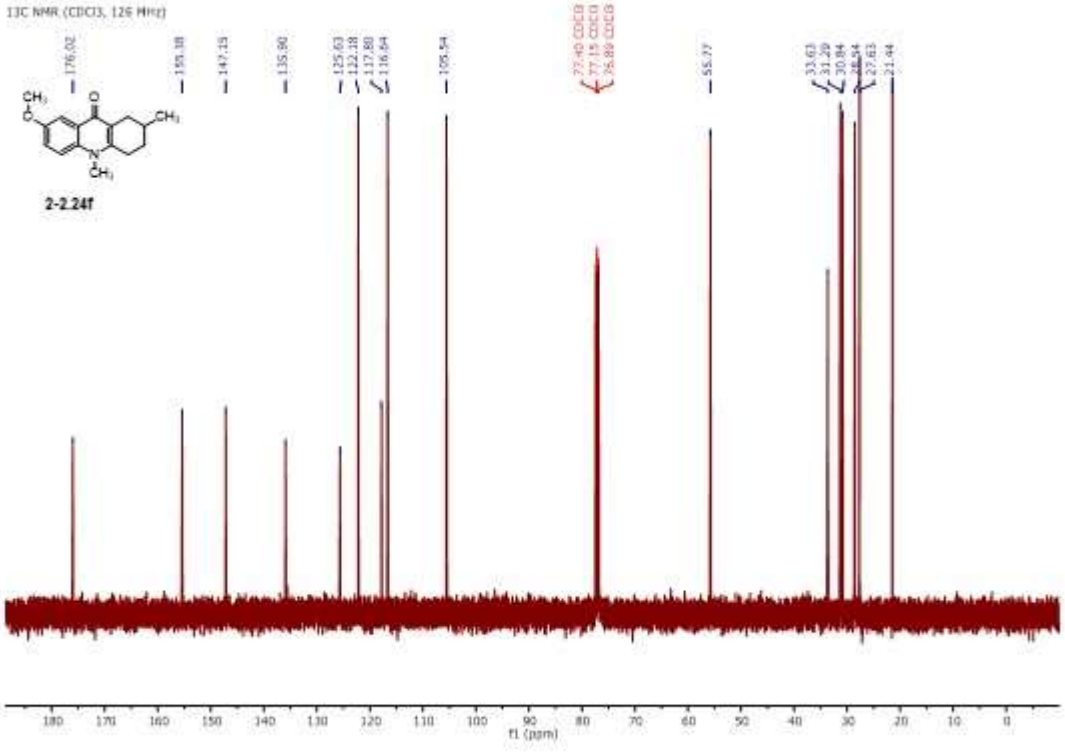
13C NMR (CDCl3, 126 MHz)
2-2.24f
fl (ppm)

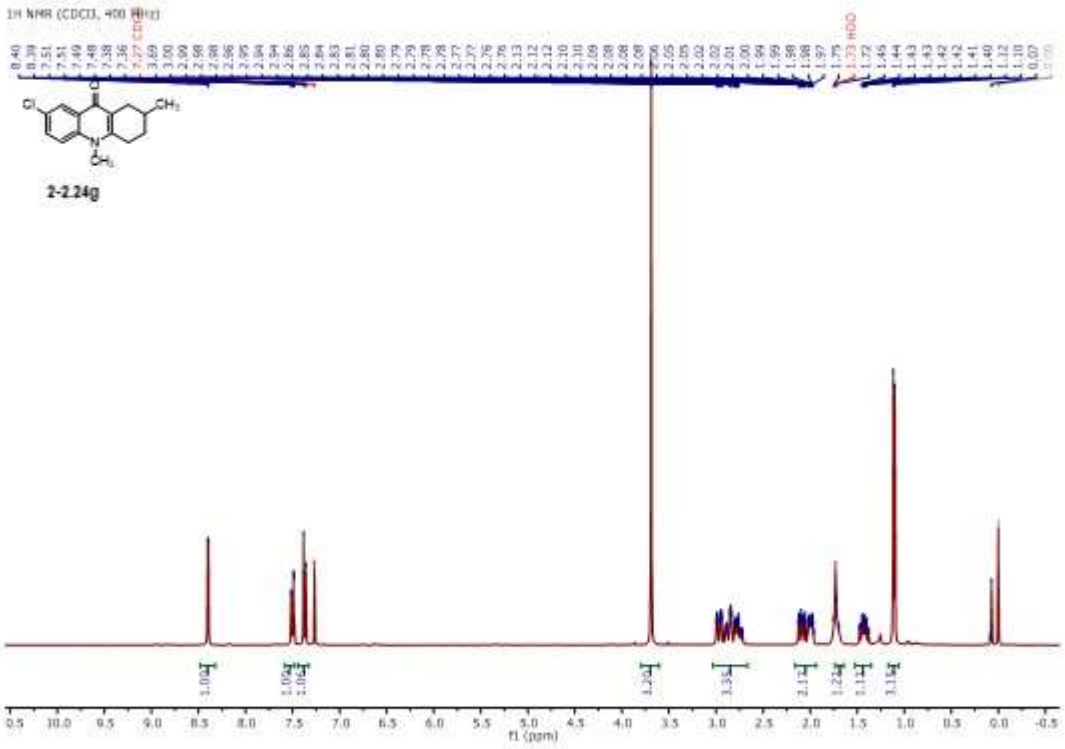
1H NMR (CDCl3, 400 MHz)
2-2.24g
f1 (ppm)

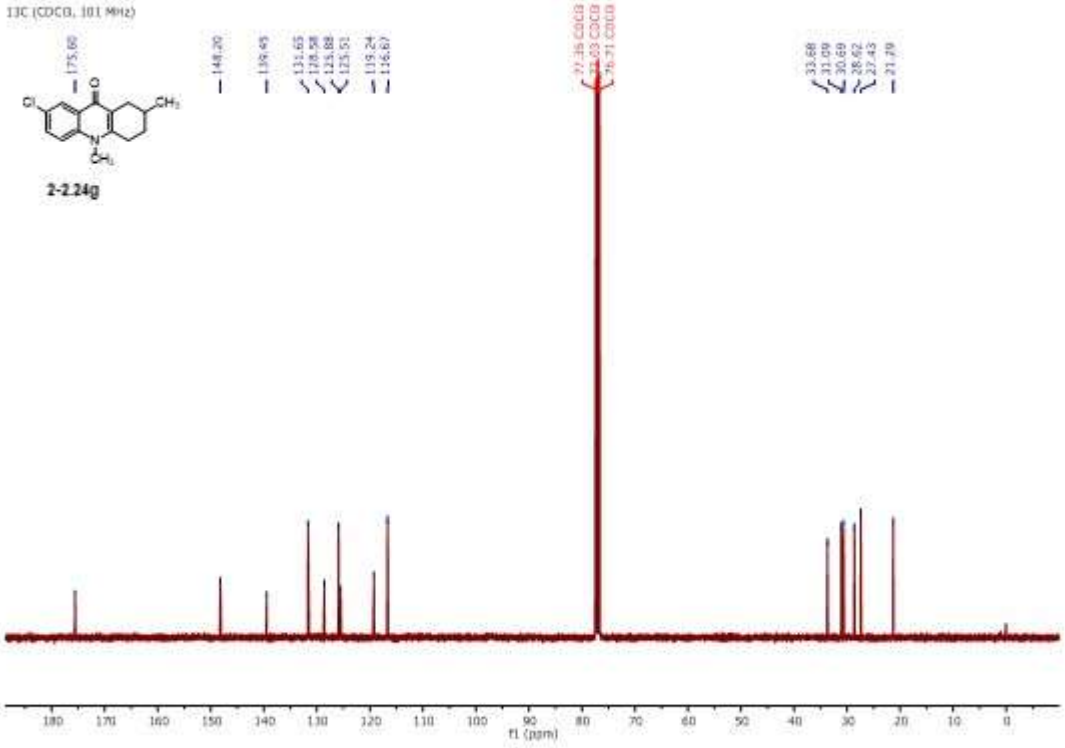
13C (CDCl3, 101 MHz)
2-2.24g
f1 (ppm)

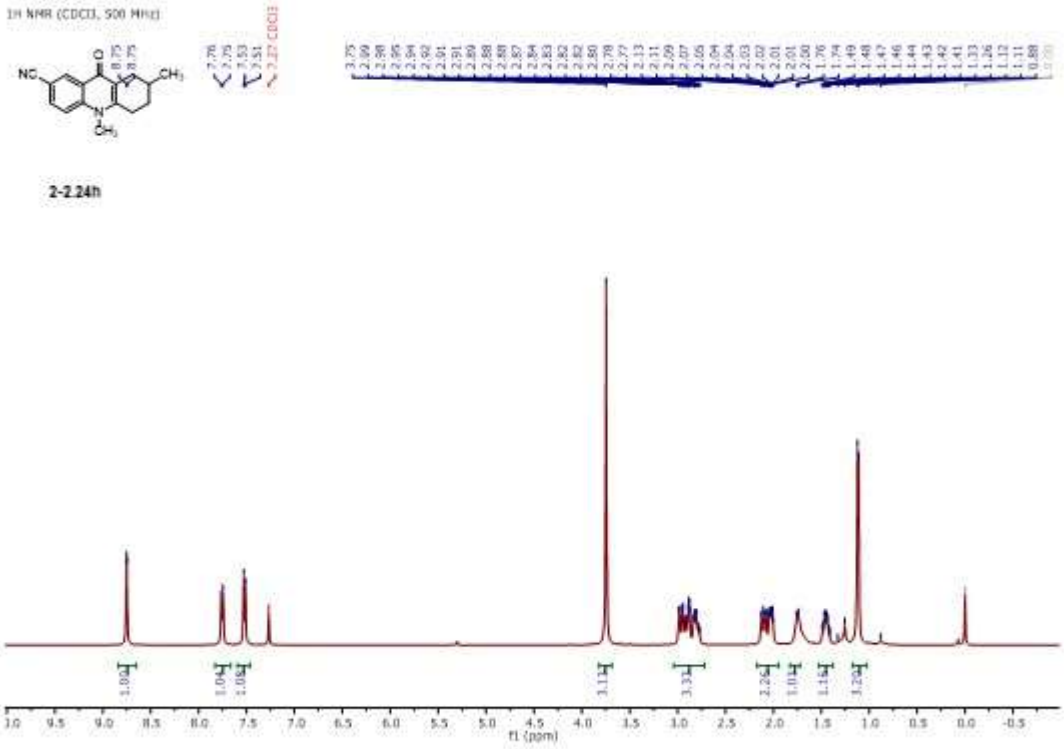
1H NMR (CDCl3, 500 MHz)
2-2.24h
f1 (ppm)

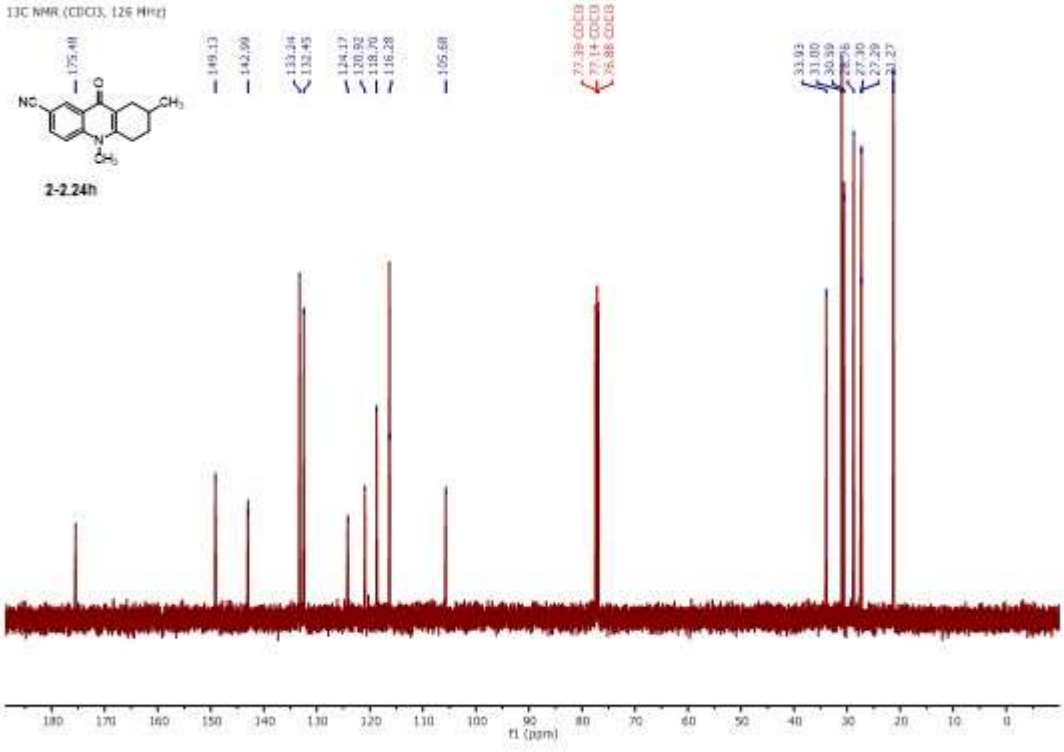
13C NMR (CDCl3, 126 MHz)
2-2.24h
f1 (ppm)

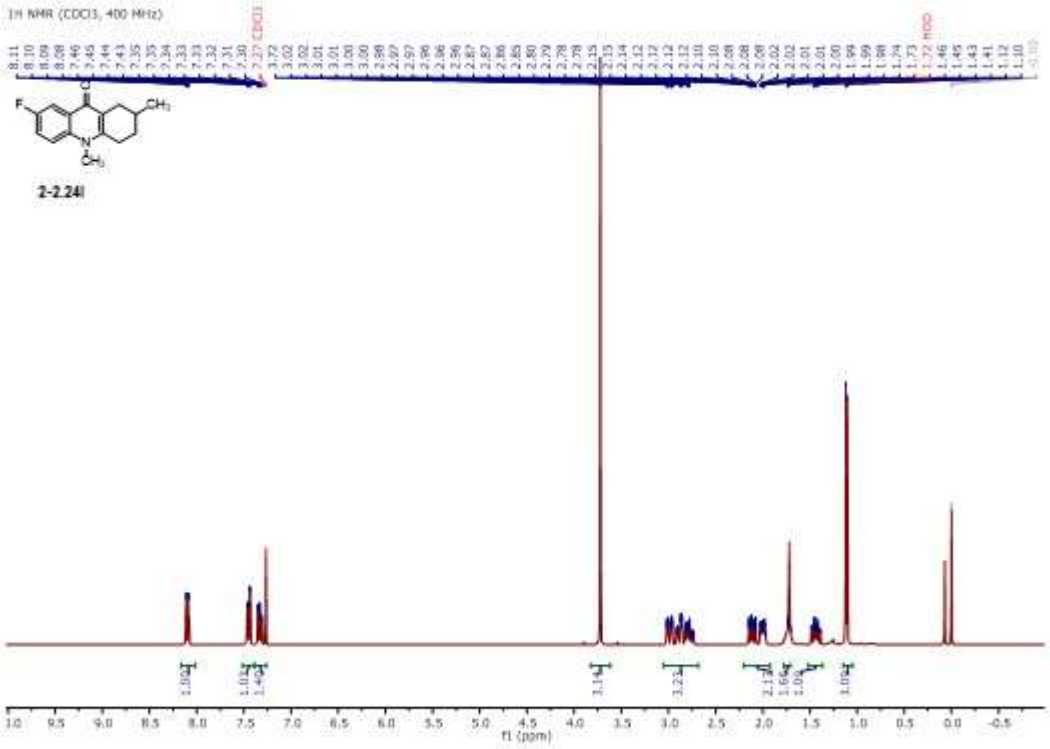
1H NMR (CDCl3, 400 MHz)
F
O
CH3
N
CH3
2-2.24l
f1 (ppm)

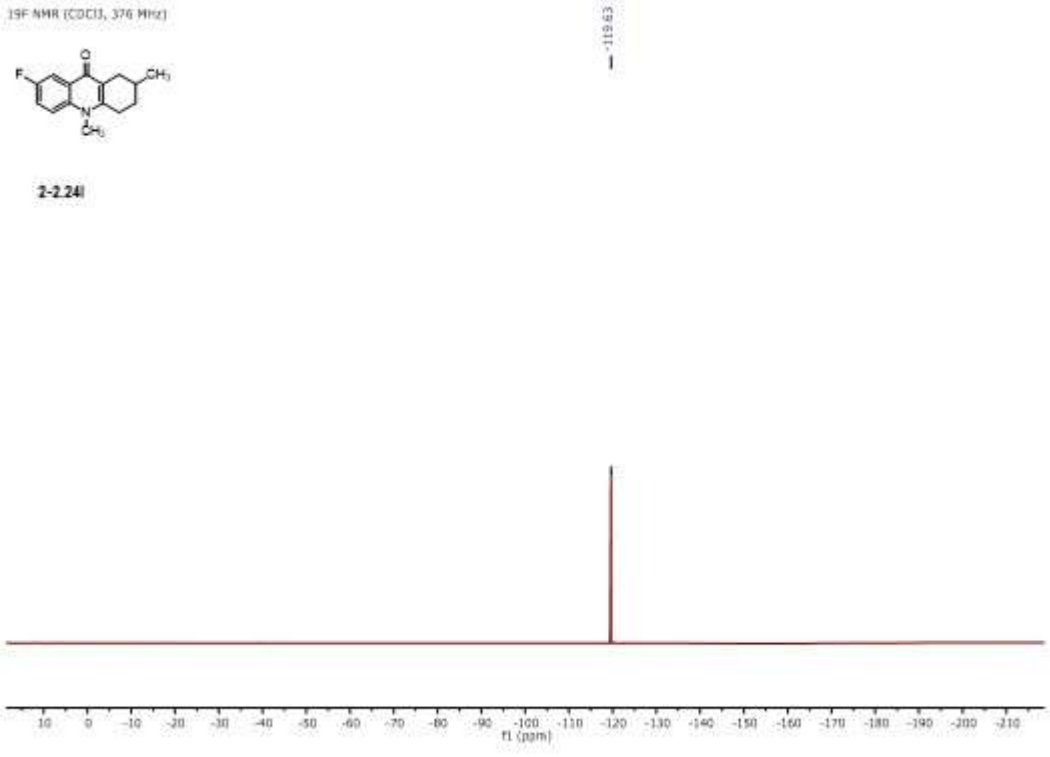
19F NMR (CDCl3, 376 MHz)
-119.63
F
O
CH3
N
CH3
2-2.24l
f1 (ppm)

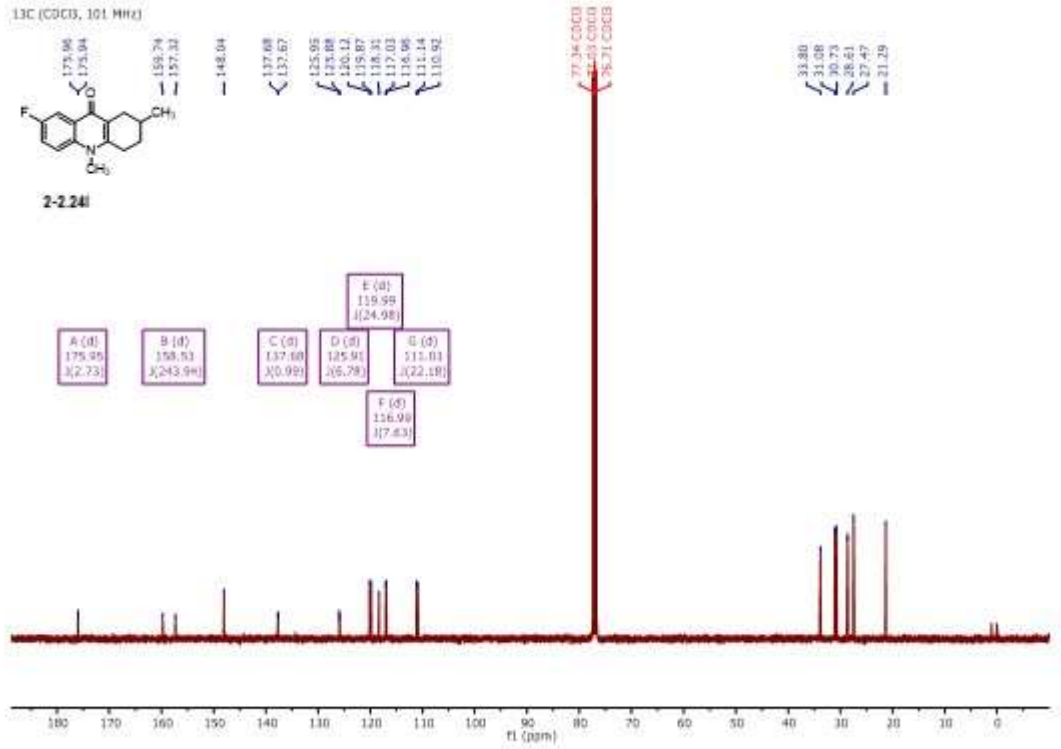
13C (CDCl3, 101 MHz)
2-2.24l
A (d)
175.95
J(2.73)
B (d)
158.53
J(243.99)
C (d)
137.68
J(0.99)
D (d)
125.91
J(6.78)
E (d)
119.99
J(24.98)
F (d)
116.98
J(7.63)
G (d)
111.03
J(22.18)
77.36 CDCl3
77.03 CDCl3
76.71 CDCl3
f1 (ppm)

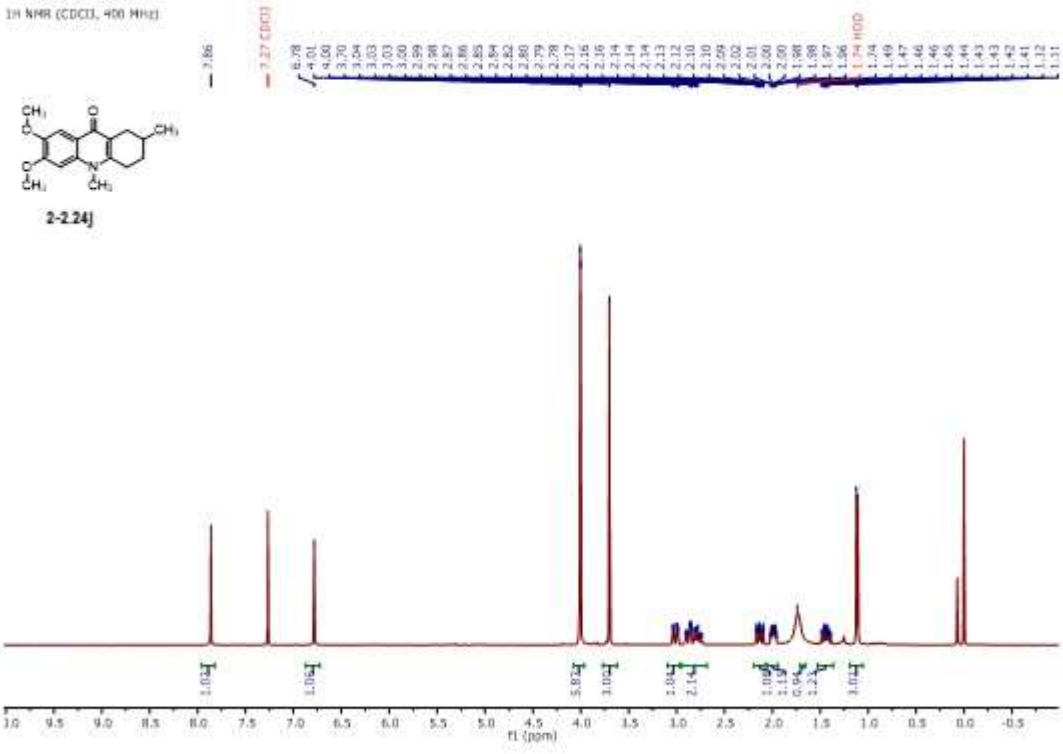
1H NMR (CDCl3, 400 MHz)
7.86
7.27 CDCl3
1.74 HOD
2-2.24j
1.00
1.00
5.87
3.00
1.00
2.14
1.09
1.15
0.94
1.25
3.00
f1 (ppm)

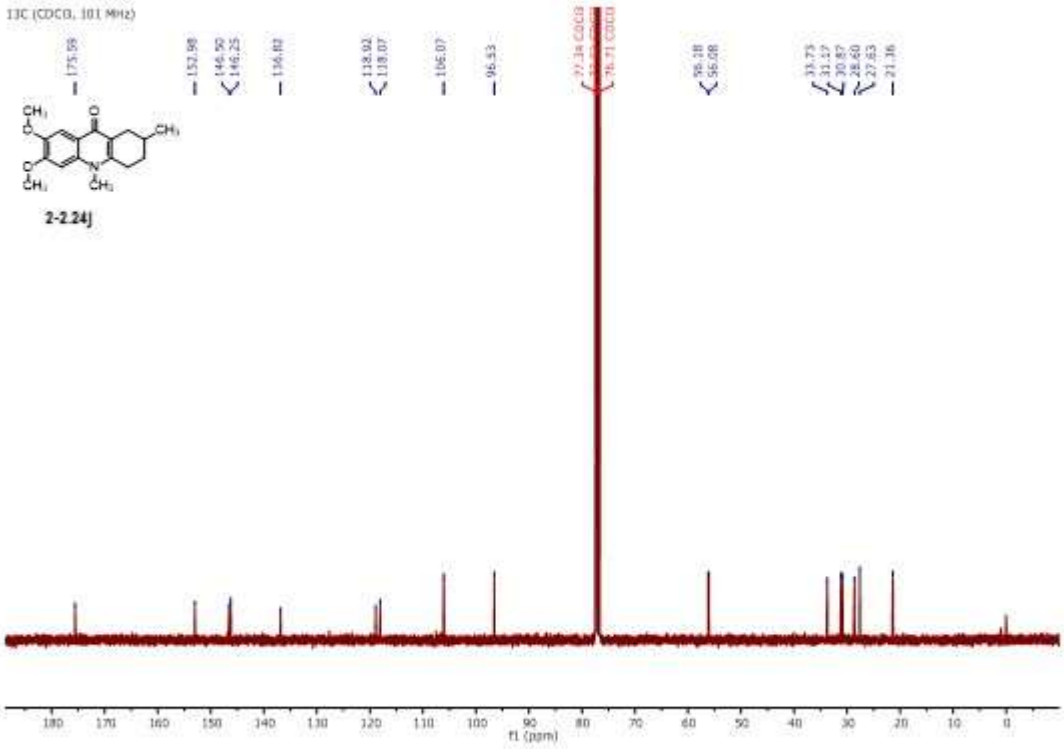
13C (CDCl3, 101 MHz)
175.59
152.98
146.50
146.25
136.83
118.92
118.07
106.07
96.53
77.34 CDCl3
76.71 CDCl3
56.18
56.08
33.73
31.17
30.87
28.60
27.83
21.36
2-2.24J
f1 (ppm)

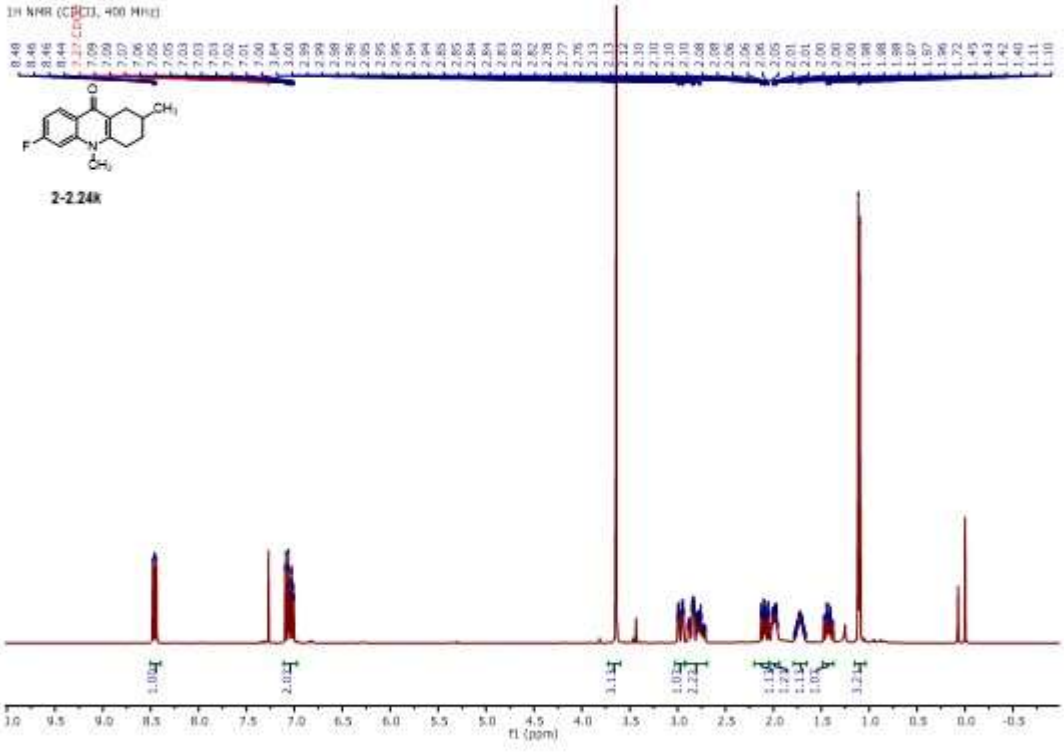
1H NMR (CDCl3, 400 MHz)
7.27 CDCl3
2-2.24K
f1 (ppm)

19F NMR (CDCl3, 376 MHz)

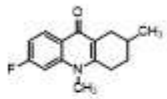

2-2.24k

13C (CDCl3, 101 MHz)

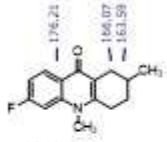

2-2.24k

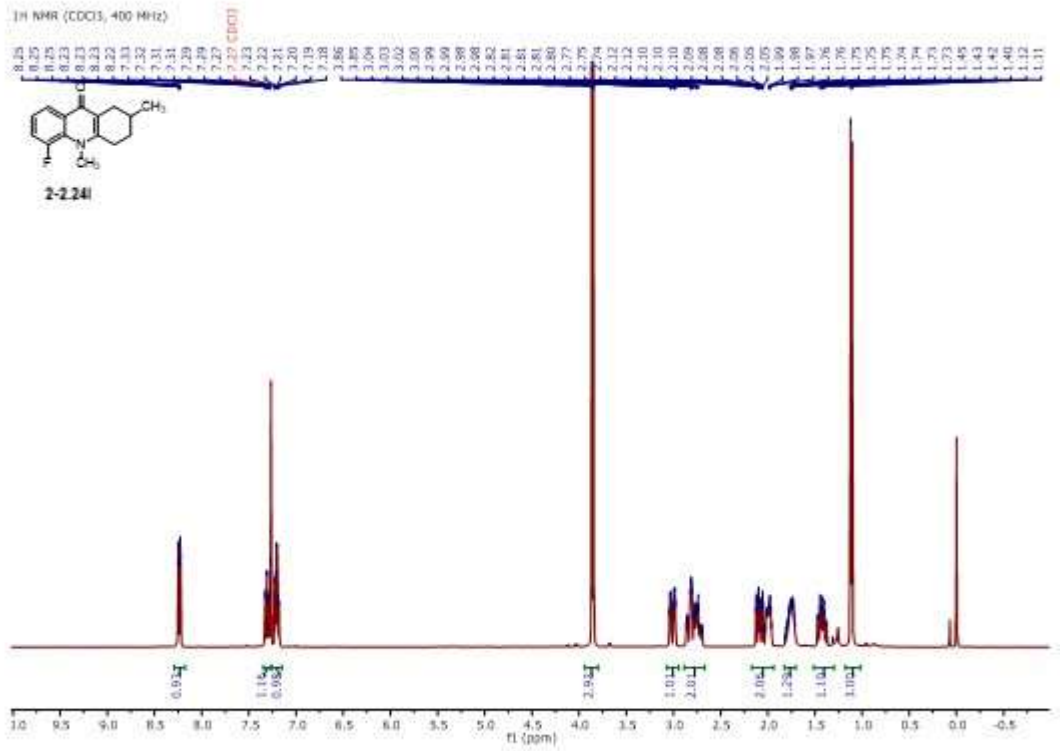
1H NMR (CDCl3, 400 MHz)
2-2.24l
f1 (ppm)

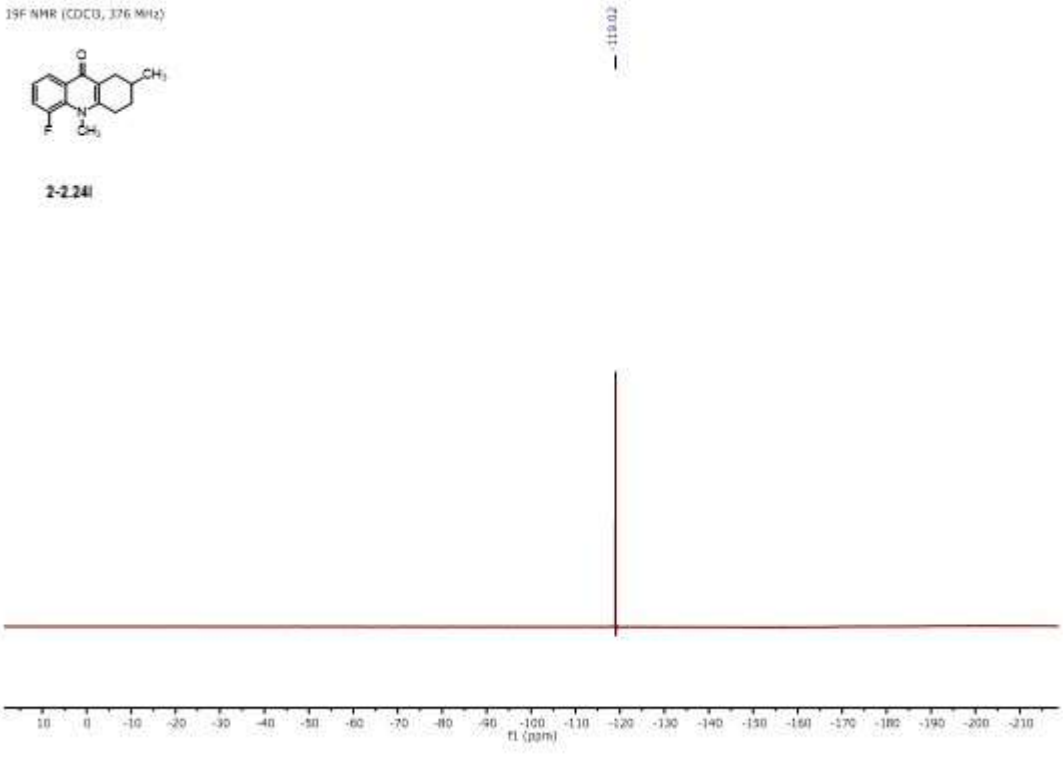
19F NMR (CDCl3, 376 MHz)
-119.02
2-2.24l
f1 (ppm)

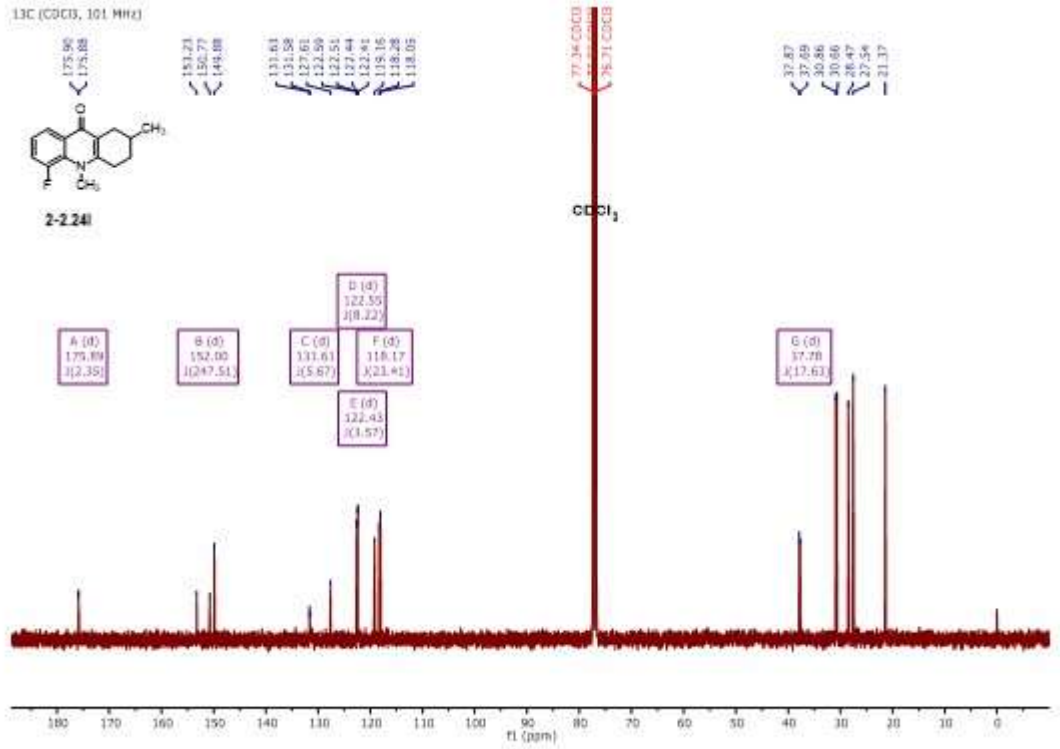
13C (CDCl3, 101 MHz)
2-2.24l
CDCl3
f1 (ppm)

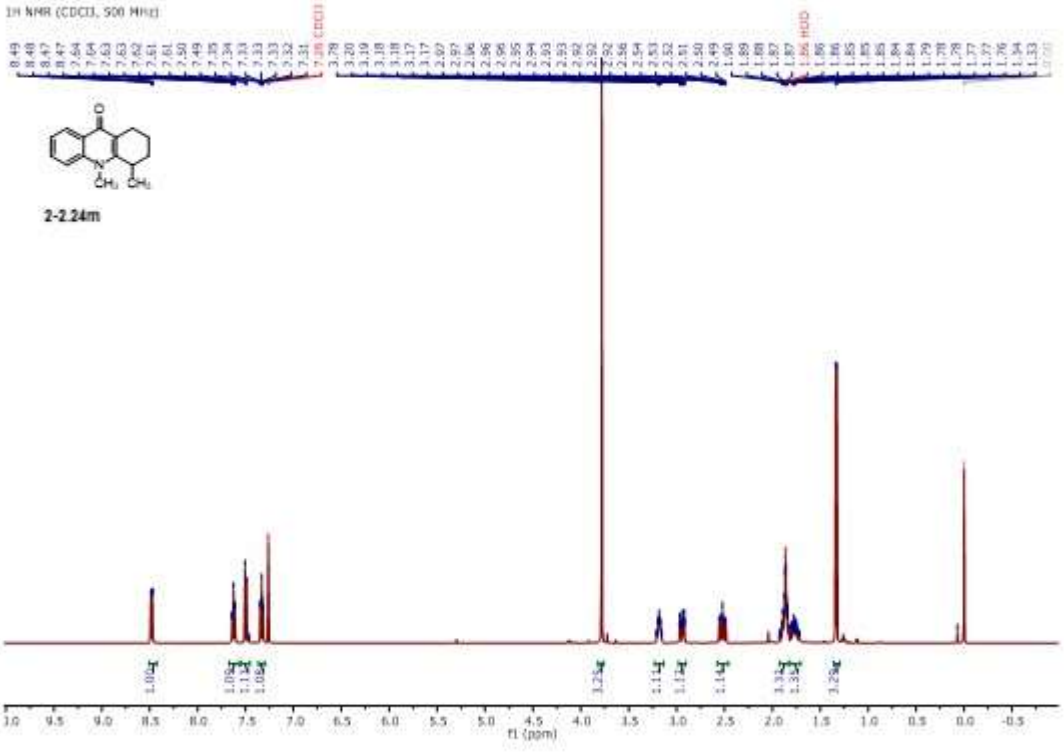
1H NMR (CDCl3, 500 MHz)
2-2.24m
f1 (ppm)

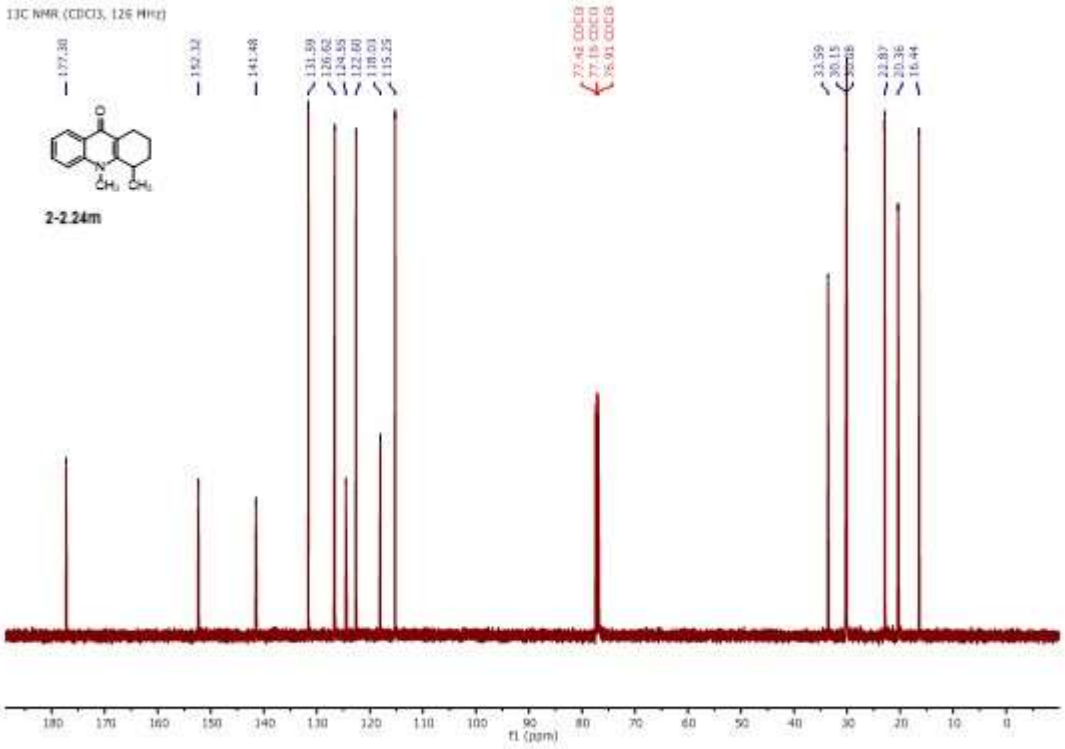
13C NMR (CDCl3, 126 MHz)
177.30
152.32
141.48
131.59
126.62
124.55
122.60
118.01
115.25
77.42 CDCl3
77.15 CDCl3
76.91 CDCl3
33.59
30.15
22.87
20.36
16.44
2-2.24m
f1 (ppm)

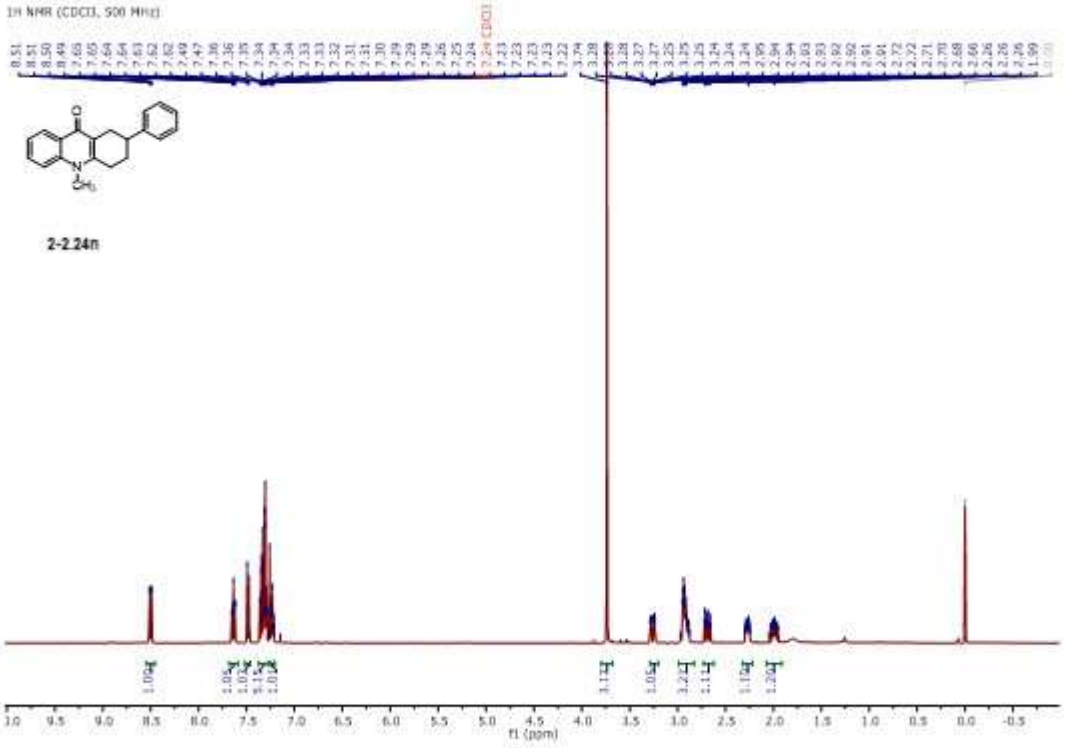
1H NMR (CDCl3, 500 MHz)
7.24 CDCl3
2-2.24n
f1 (ppm)

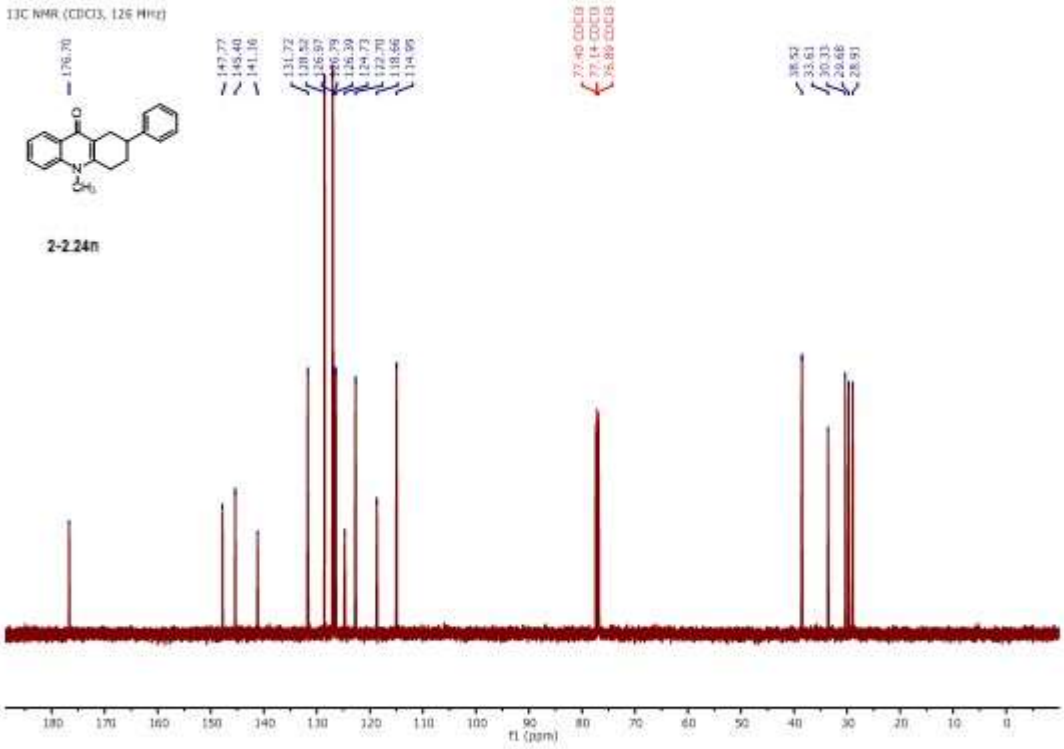
13C NMR (CDCl3, 126 MHz)
2-2.24n
f1 (ppm)

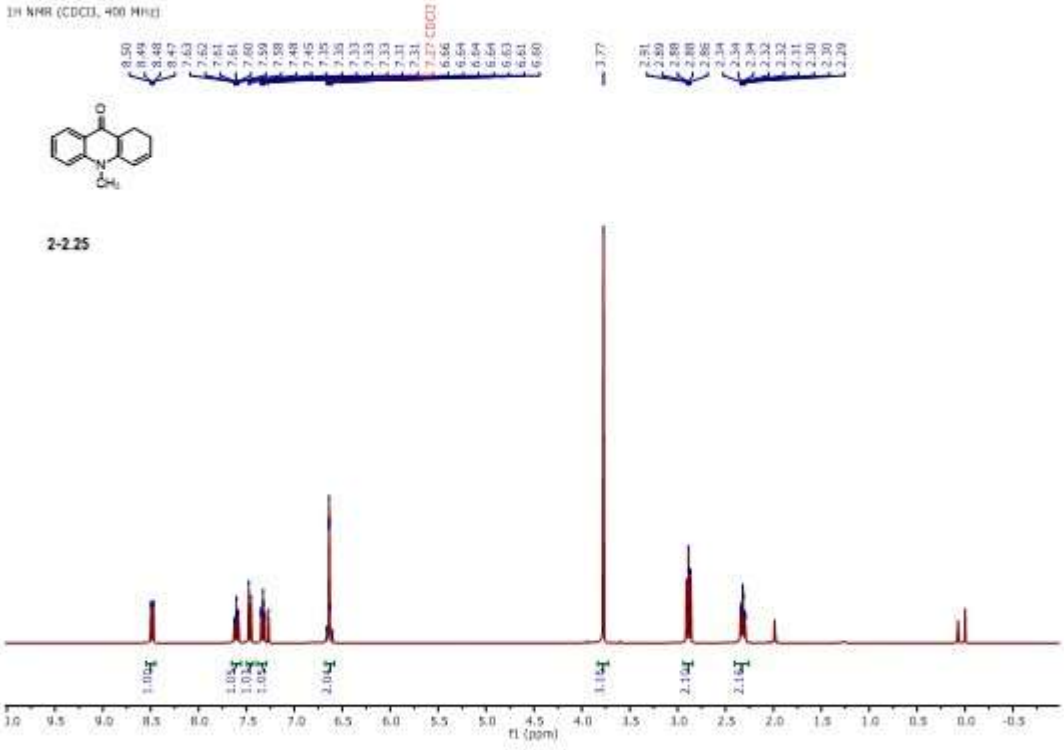
1H NMR (CDCl3, 400 MHz)
2-2.25
f1 (ppm)

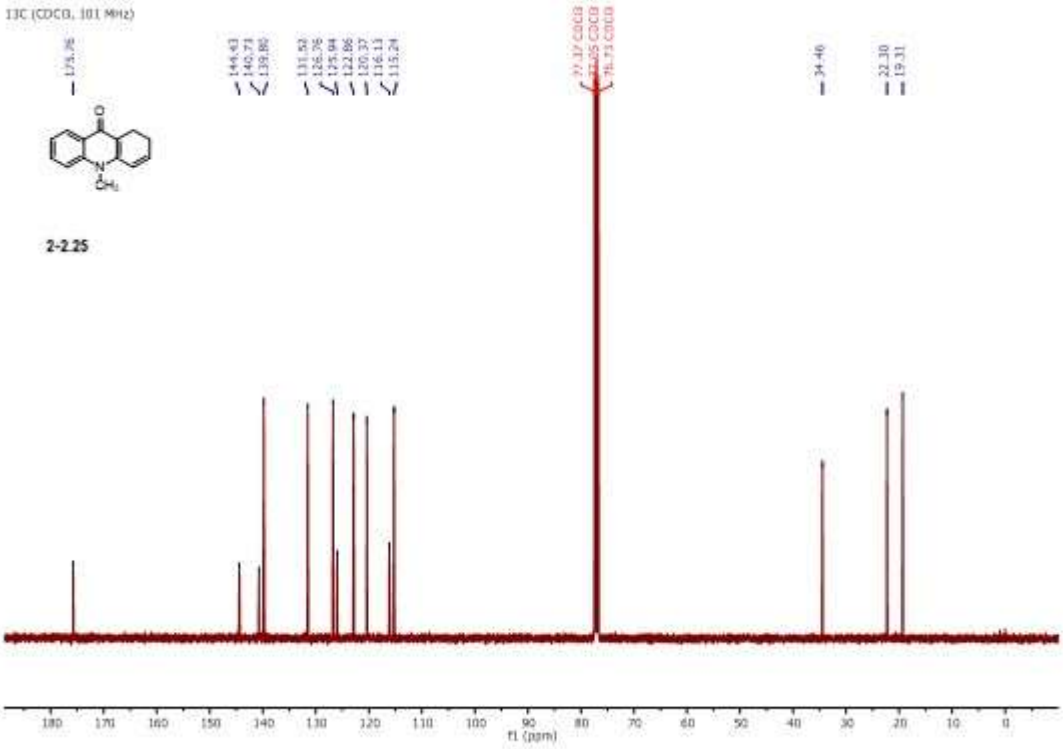
13C (CDCl3, 101 MHz)
175.76
144.43
140.73
139.80
131.52
126.76
125.94
122.86
120.37
116.13
115.24
77.32 CDCl3
77.05 CDCl3
76.73 CDCl3
34.46
22.30
19.31
f1 (ppm)

2-2.25

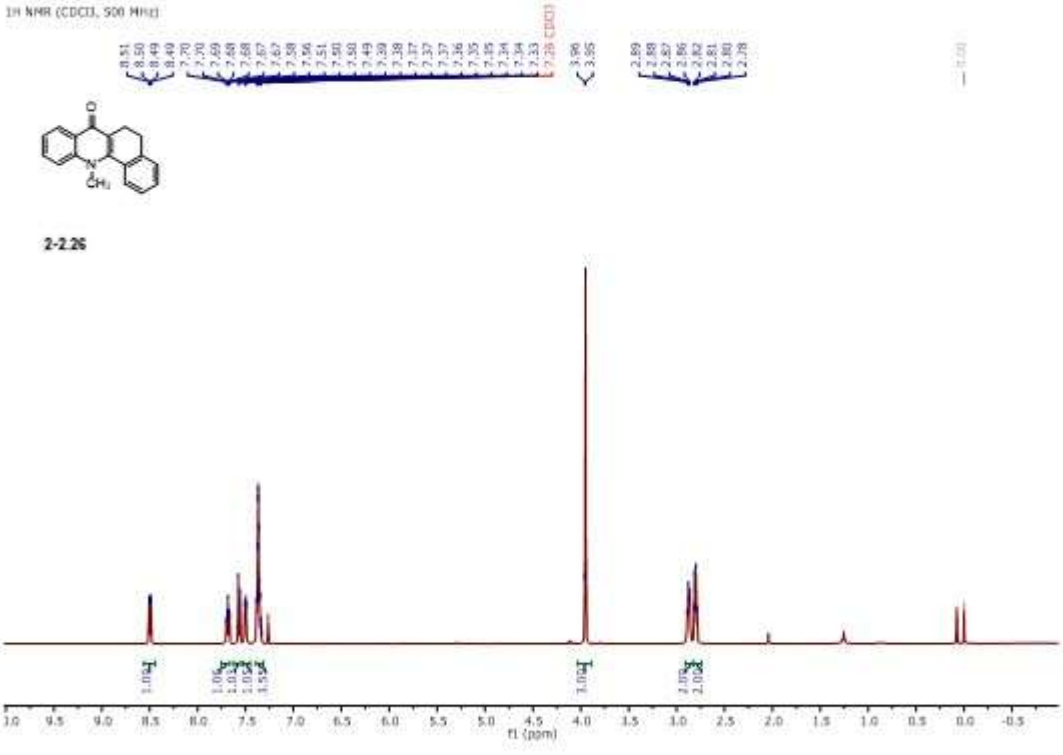
1H NMR (CDCl3, 500 MHz)
8.51
8.50
8.49
8.49
7.70
7.70
7.69
7.68
7.68
7.68
7.67
7.67
7.58
7.56
7.51
7.50
7.50
7.49
7.39
7.38
7.37
7.37
7.37
7.36
7.35
7.35
7.34
7.34
7.33
7.26 CDCl3
3.96
3.95
2.89
2.88
2.87
2.86
2.82
2.81
2.80
2.78
f1 (ppm)

2-2.26

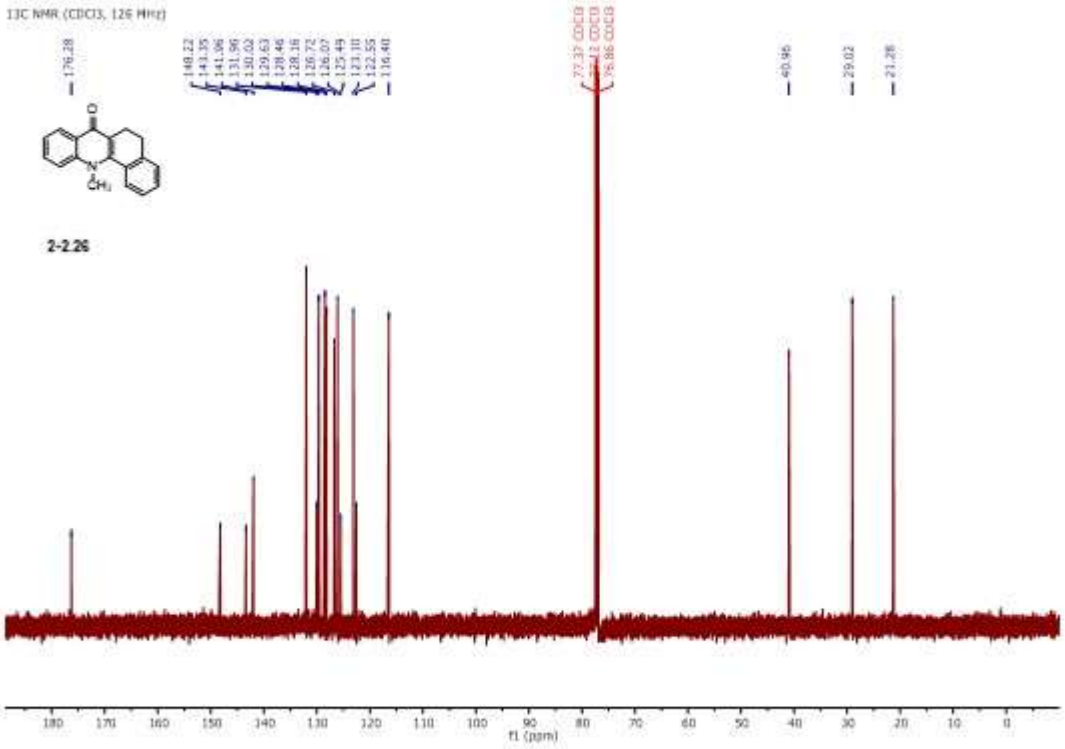
13C NMR (CDCl3, 126 MHz)
176.28
148.22
143.35
141.96
131.96
130.02
129.63
128.46
128.16
126.72
126.07
125.49
123.10
122.55
116.40
77.37 CDCl3
77.12 CDCl3
76.86 CDCl3
40.96
29.02
21.28
f1 (ppm)

2-2.26

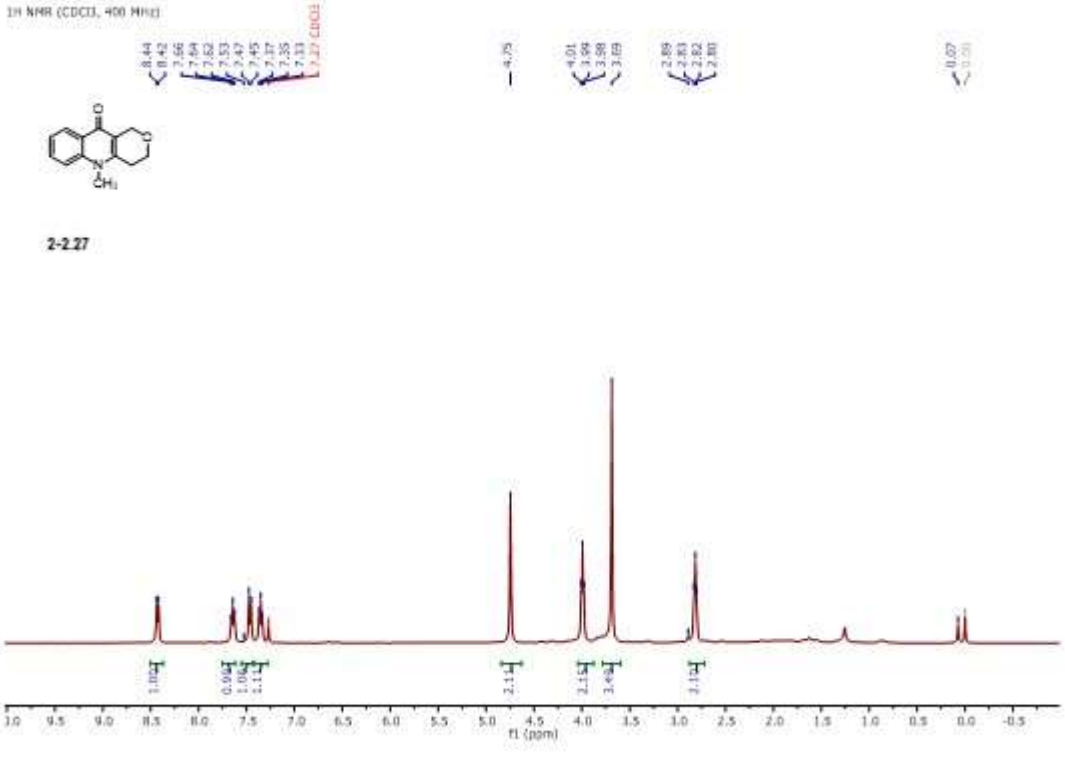
1H NMR (CDCl3, 400 MHz)
8.44
8.42
7.66
7.64
7.62
7.53
7.47
7.45
7.37
7.35
7.33
7.27 CDCl3
4.75
4.01
3.99
3.98
3.69
2.89
2.83
2.82
2.80
0.07
f1 (ppm)

2-2.27

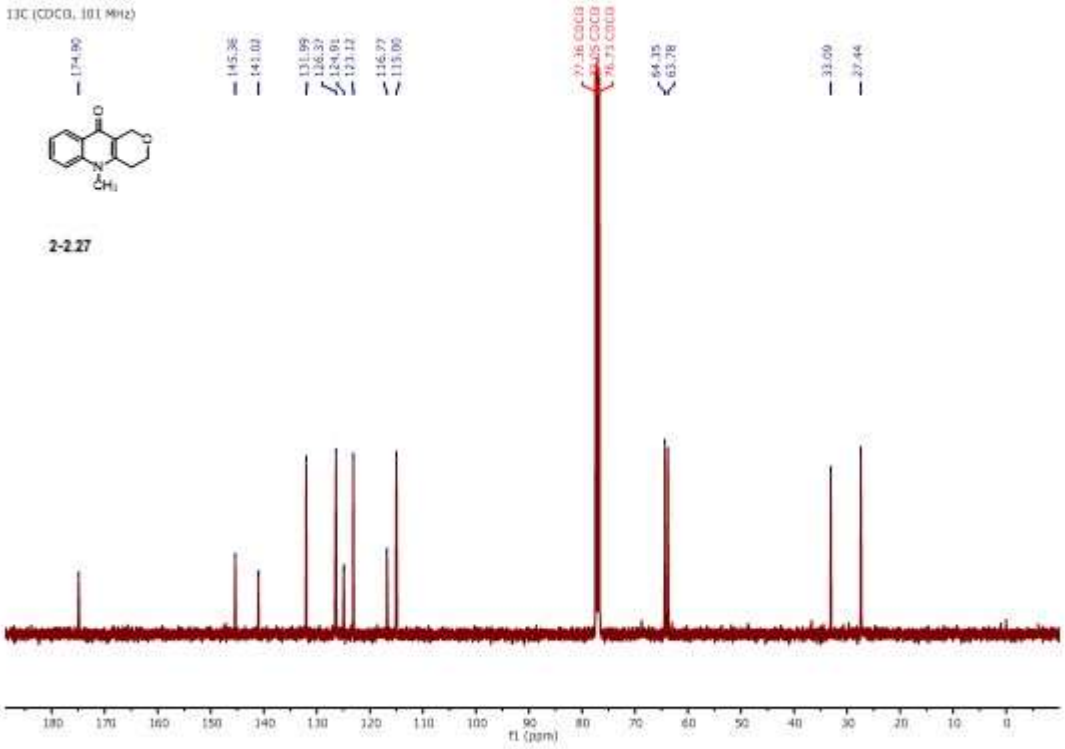
13C (CDCl3, 101 MHz)
2-2.27
f1 (ppm)

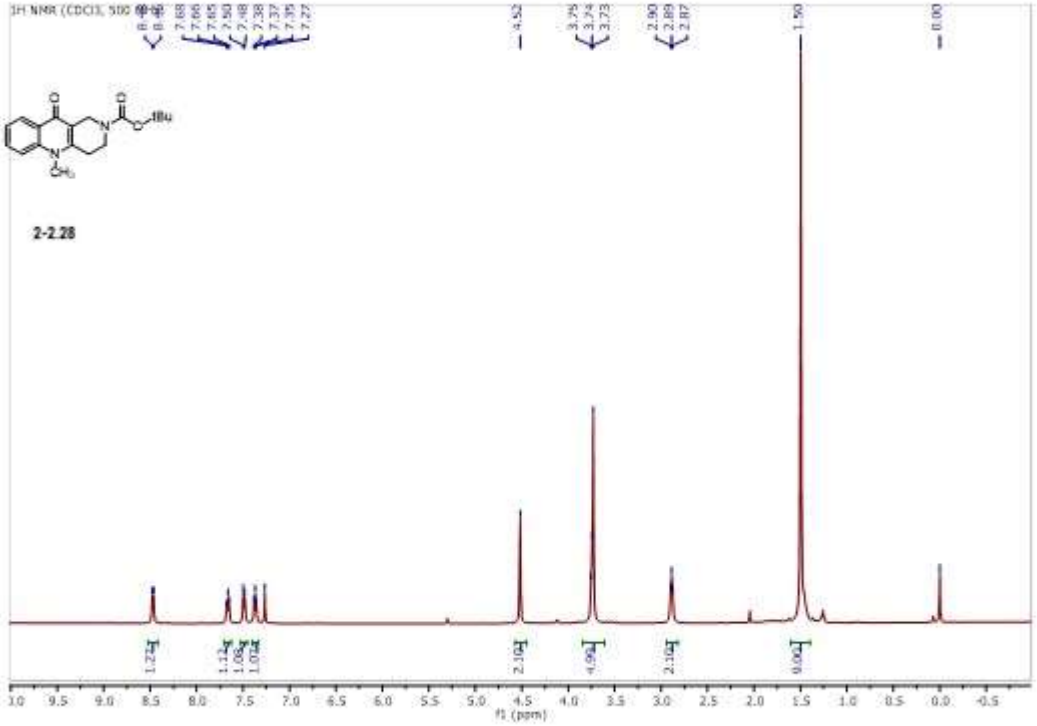
1H NMR (CDCl3, 500
2-2.28
f1 (ppm)

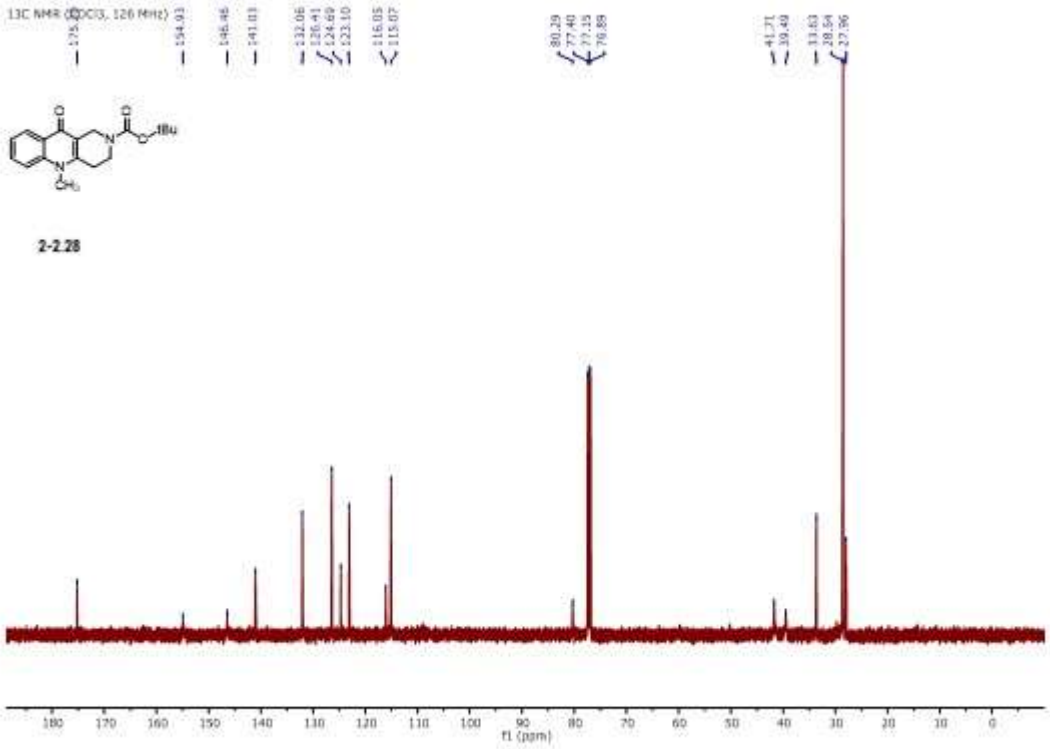
13C NMR (CDCl3, 126 MHz)
175.
164.93
146.46
141.03
132.06
126.41
124.69
123.10
116.05
115.07
80.29
77.40
77.15
76.89
41.71
39.49
13.63
28.54
27.96
2-2.28
f1 (ppm)

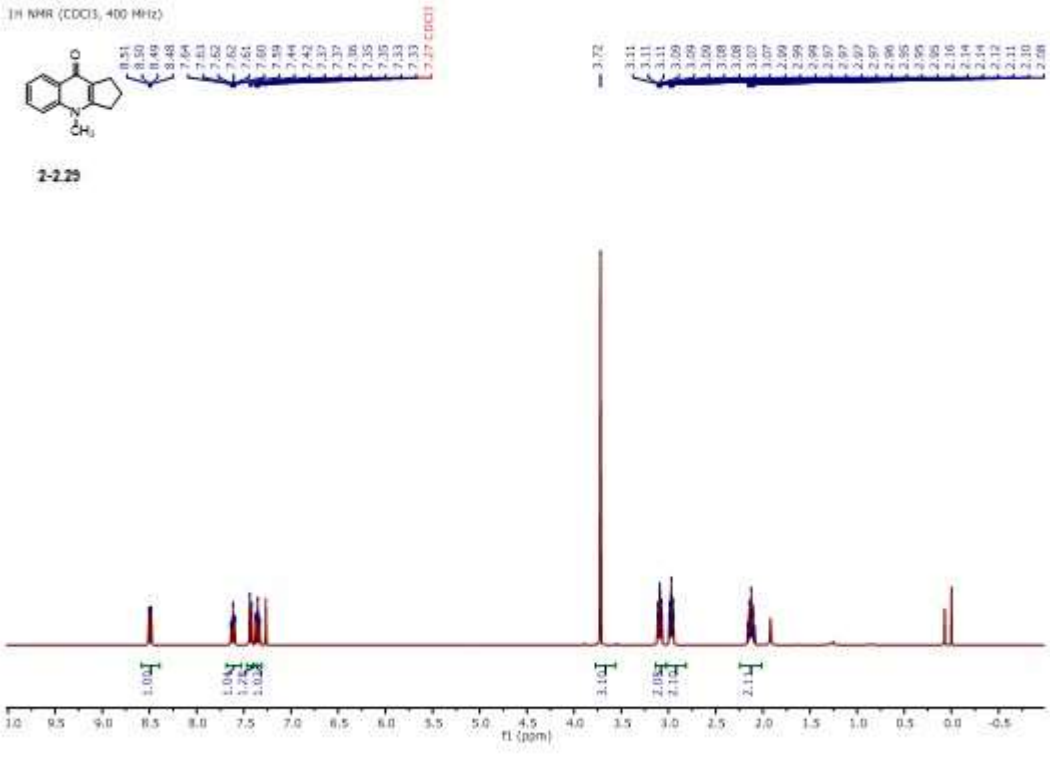
1H NMR (CDCl3, 400 MHz)
8.51
8.50
8.49
8.48
7.64
7.63
7.62
7.61
7.60
7.59
7.44
7.42
7.37
7.37
7.36
7.35
7.35
7.33
7.33
7.27 CDCl3
3.72
3.11
3.11
3.09
3.09
3.00
3.00
3.08
3.08
3.07
3.07
2.99
2.99
2.98
2.98
2.97
2.97
2.97
2.97
2.96
2.95
2.95
2.95
2.16
2.14
2.14
2.12
2.12
2.11
2.10
2.08
2-2.29
1.04
1.04
1.25
2.03
3.14
2.05
2.14
2.14
f1 (ppm)

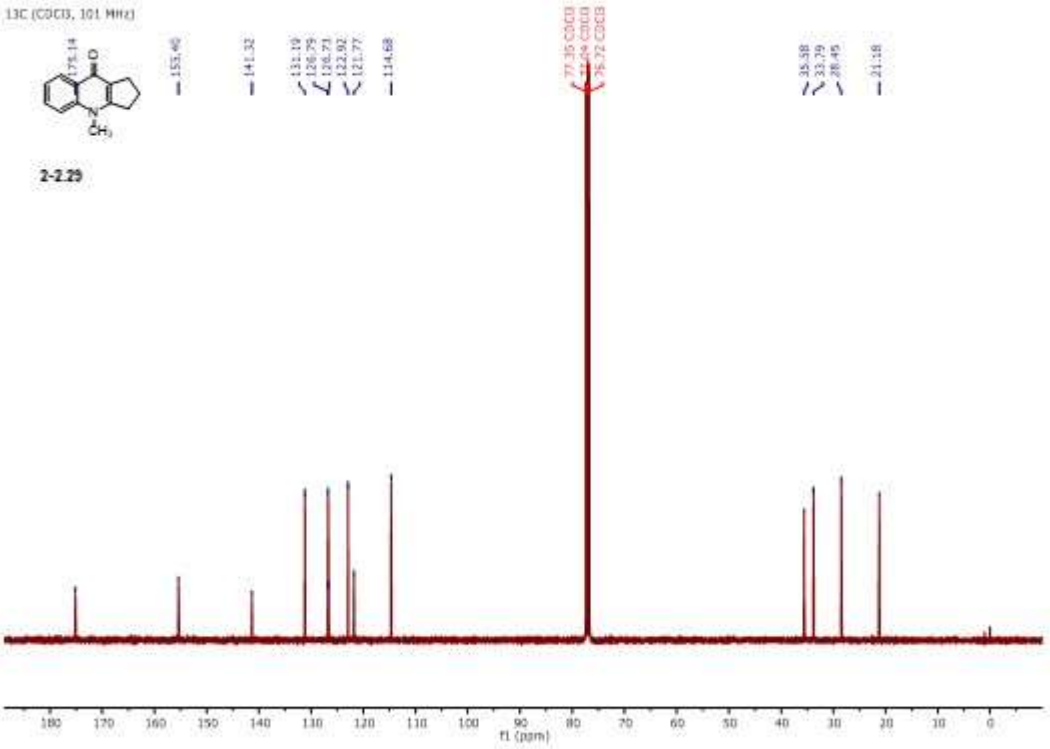
13C (CDCl3, 101 MHz)
175.14
155.40
141.32
131.19
126.79
126.73
122.92
121.77
114.68
77.35 CDCl3
77.04 CDCl3
76.72 CDCl3
35.58
33.79
28.45
21.18
f1 (ppm)

2-2.29

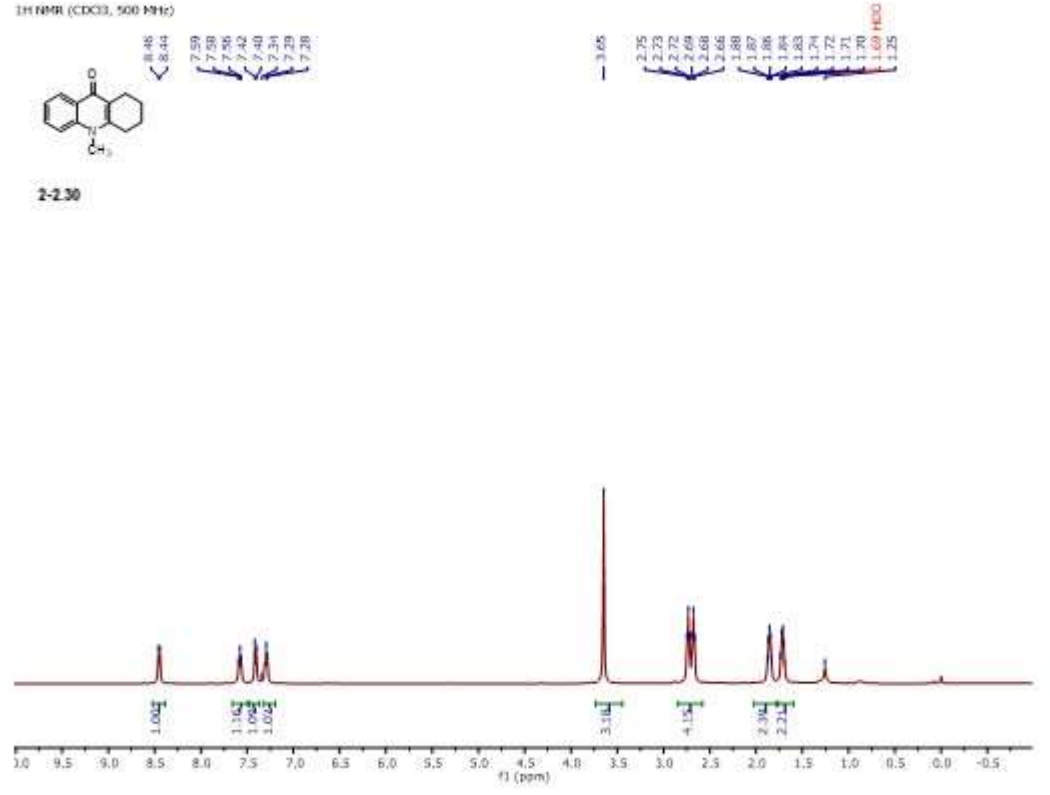
1H NMR (CDCl3, 500 MHz)
8.46
8.44
7.59
7.58
7.56
7.42
7.40
7.31
7.29
7.28
3.65
2.75
2.73
2.72
2.69
2.68
2.66
1.88
1.87
1.86
1.84
1.83
1.74
1.72
1.71
1.70
1.69 H2O
1.25
f1 (ppm)

2-2.30

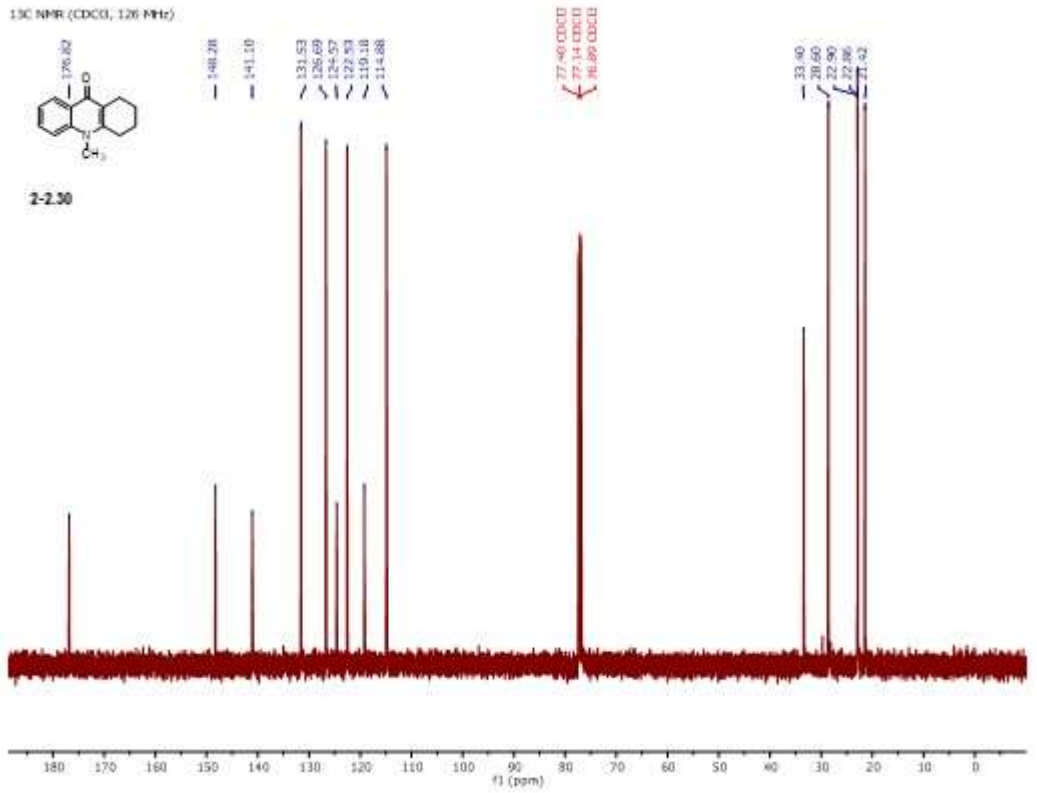
13C NMR (CDCl3, 126 MHz)
2-2.30
f1 (ppm)

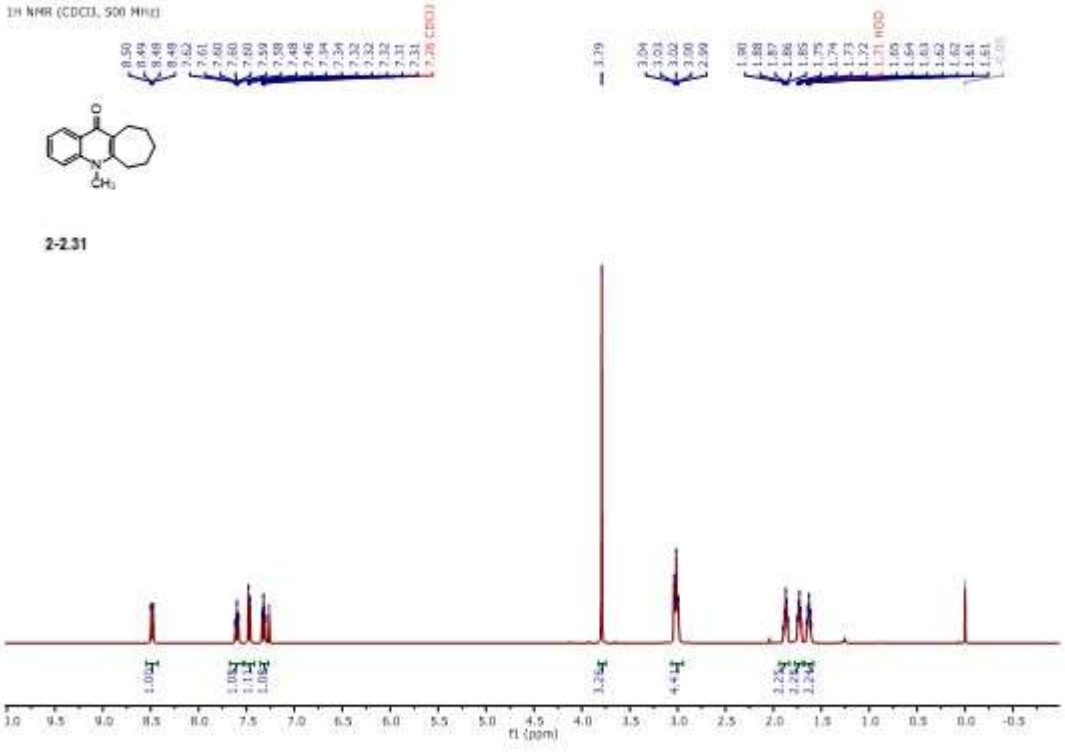
1H NMR (CDCl3, 500 MHz)
2-2.31
f1 (ppm)

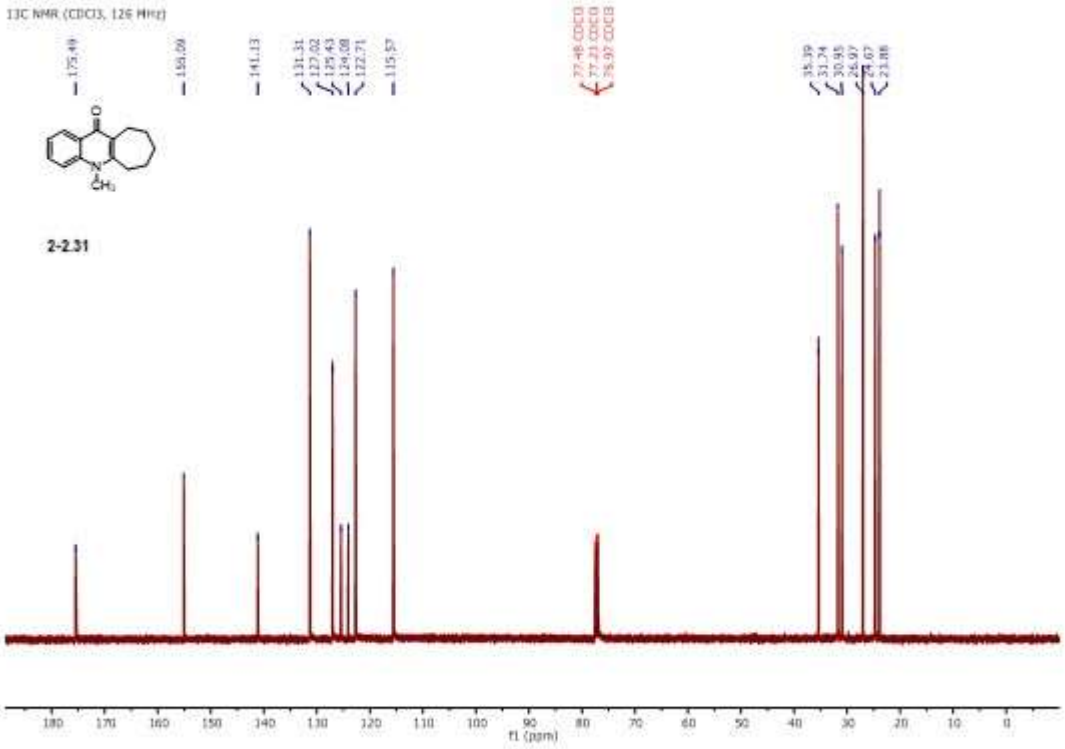
13C NMR (CDCl3, 126 MHz)
175.49
159.09
141.13
131.31
127.02
125.43
124.08
122.71
115.57
77.48 CDCl3
77.23 CDCl3
76.97 CDCl3
35.39
31.24
30.95
26.97
24.67
23.88
O
N
CH3
2-2.31
180
170
160
150
140
130
120
110
100
90
80
70
60
50
40
30
20
10
0
f1 (ppm)

Spectra of Compounds in Chapter 3

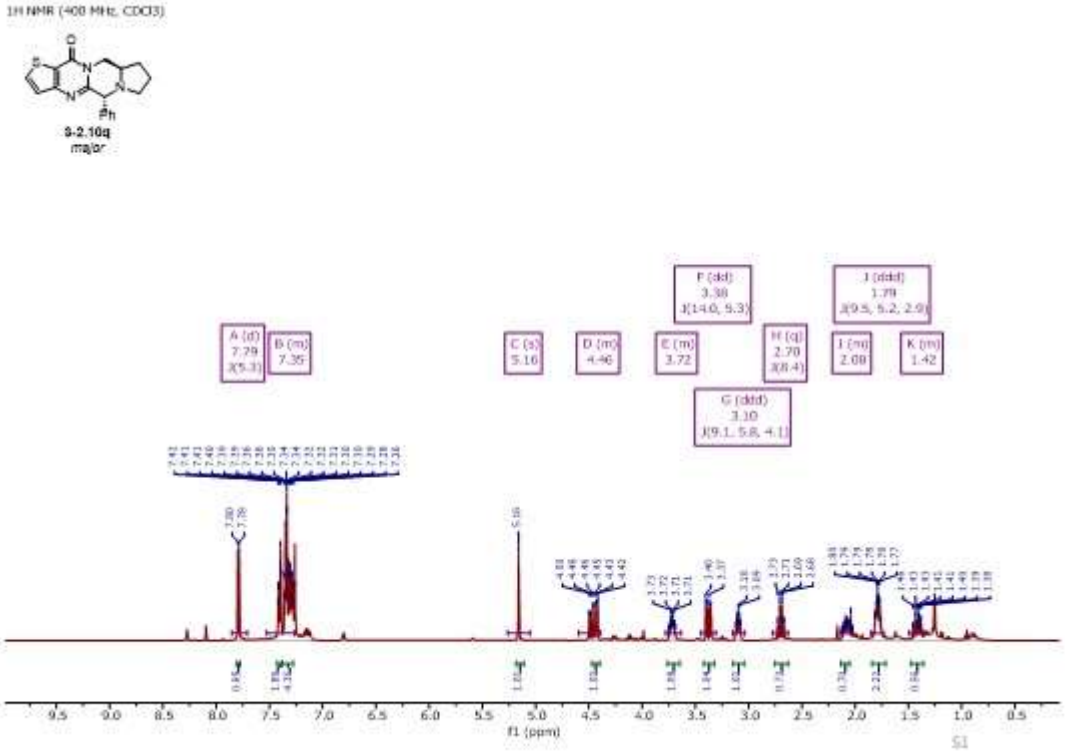

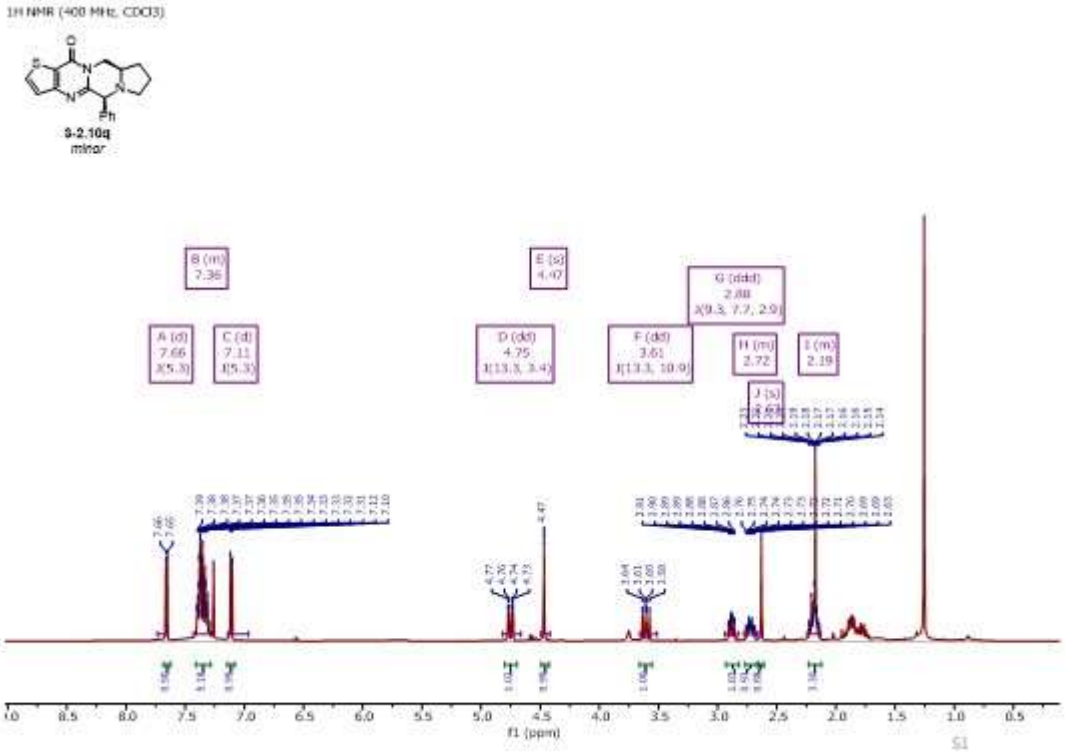

13C NMR (101 MHz, CDCl3)

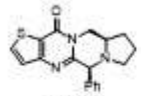

3-2.10q
minor

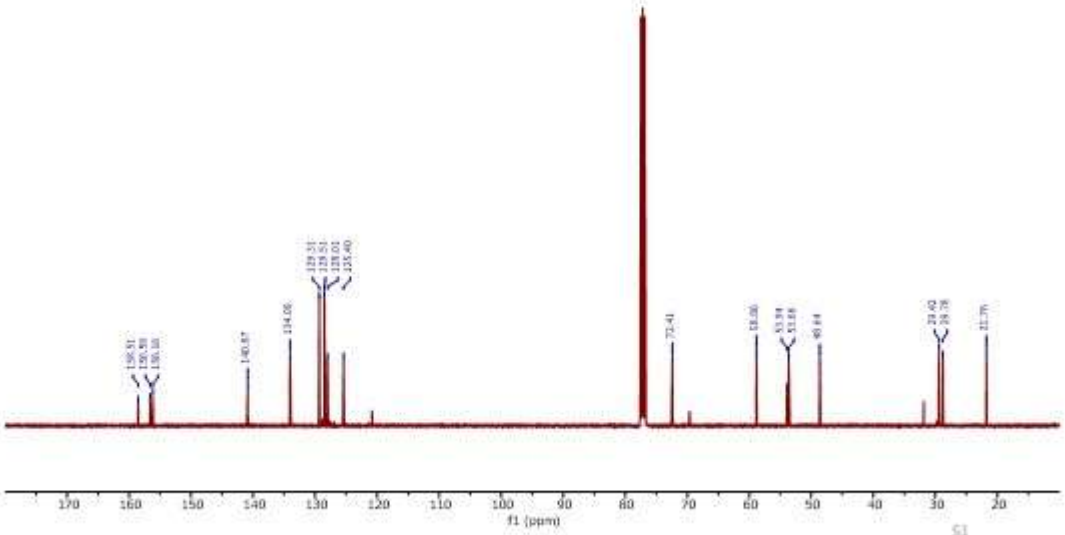

1H NMR (400 MHz, CDCl3)

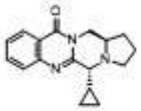

3-2.10l
major

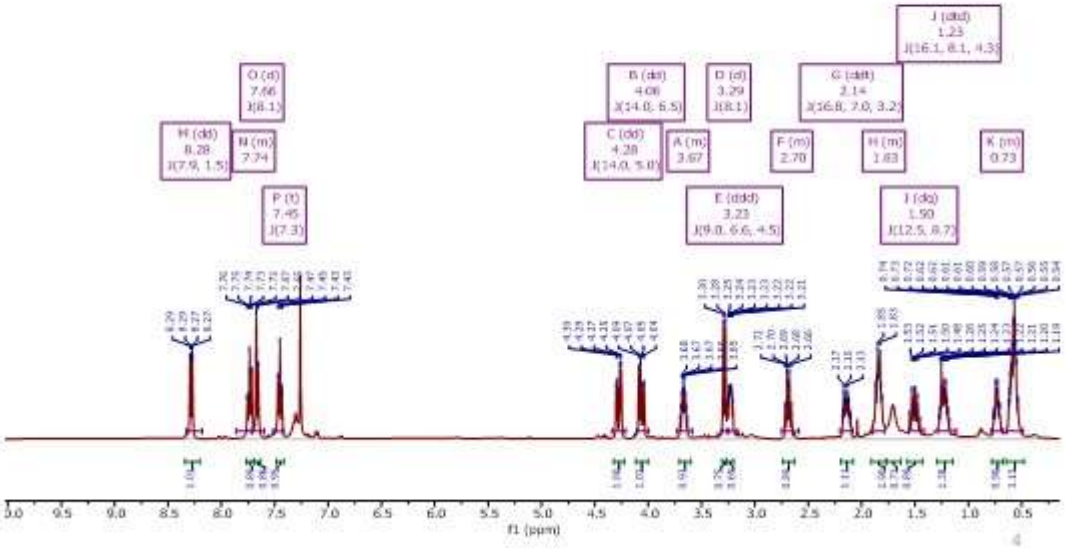

13C NMR (101 MHz, CDCl3)

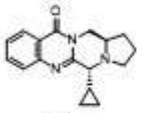

3-2.10l
mg/or

1H NMR (400 MHz, DMSO-d6)

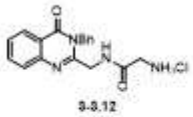

3-3.12

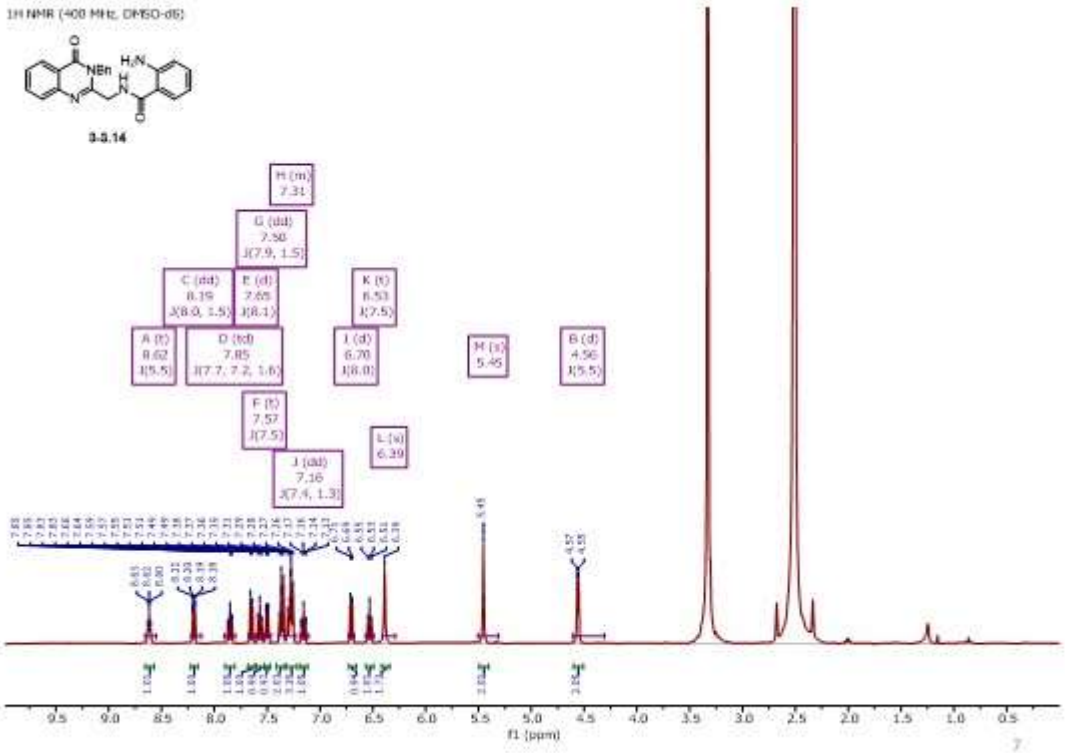
1H NMR (400 MHz, DMSO-d6)
3.3.14
H (m)
7.31
G (dd)
7.50
J(7.9, 1.5)
C (dd)
8.19
J(8.0, 1.5)
E (d)
7.65
J(8.1)
K (t)
6.53
J(7.5)
A (t)
8.62
J(5.5)
D (td)
7.85
J(7.7, 7.2, 1.6)
I (d)
6.70
J(8.0)
M (s)
5.45
B (d)
4.56
J(5.5)
F (t)
7.57
J(7.5)
L (s)
6.39
J (dd)
7.16
J(7.4, 1.3)
f1 (ppm)

Spectra of Compounds in Chapter 4

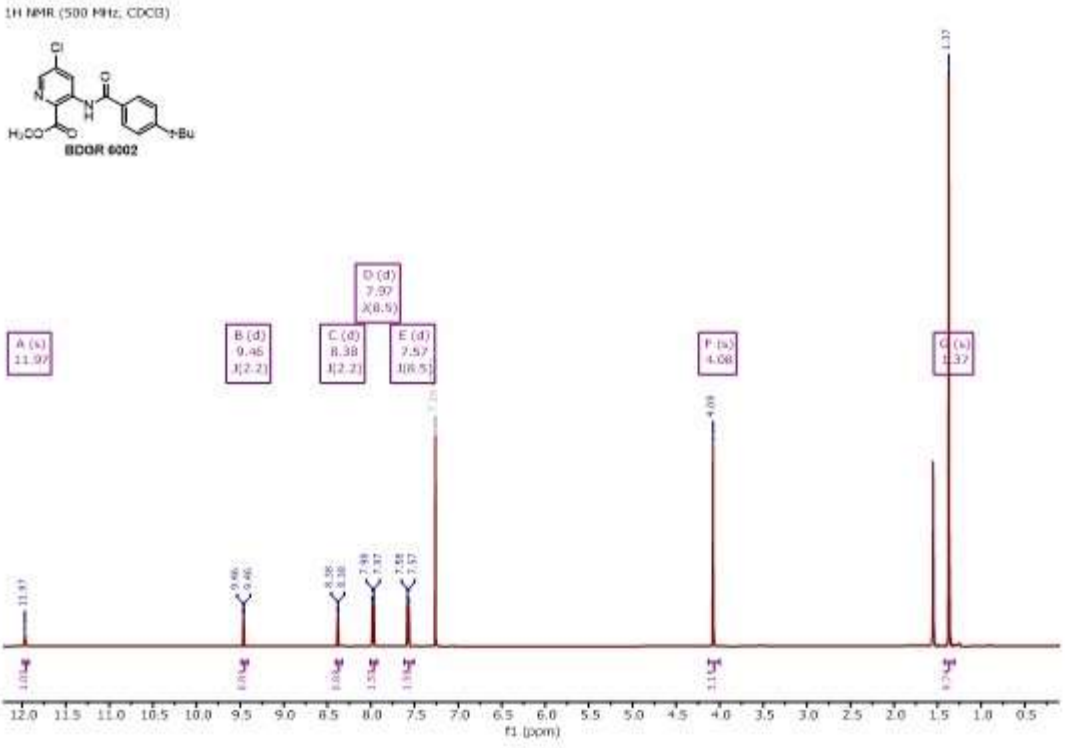

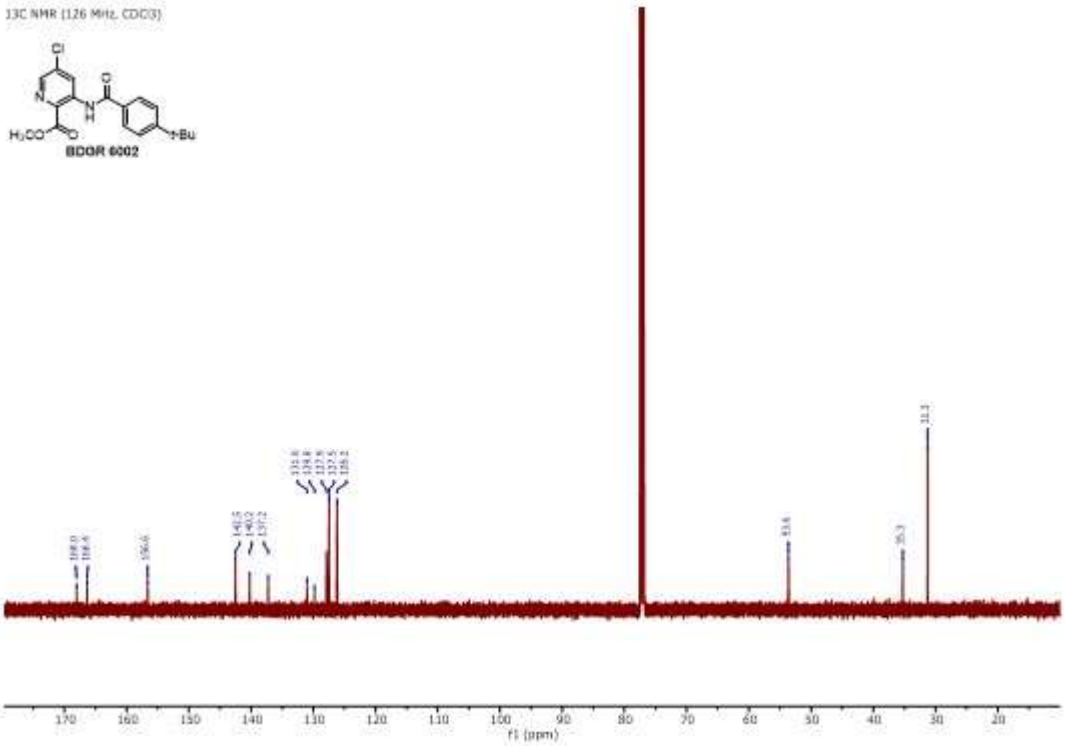

1H NMR (500 MHz, CDCl3)

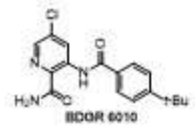

13C NMR (126 MHz, CDCl3)

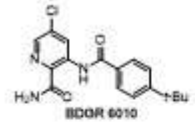

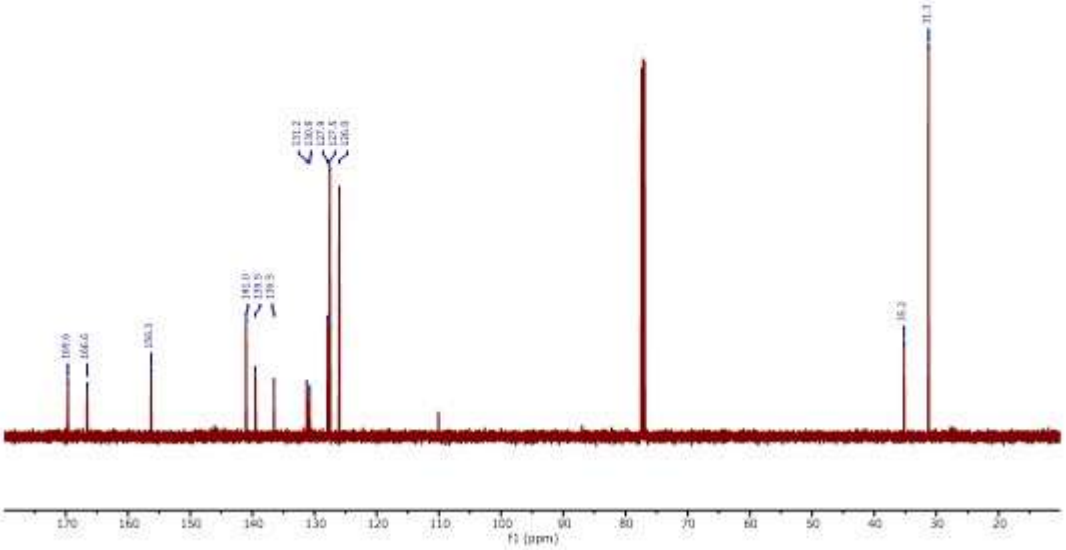

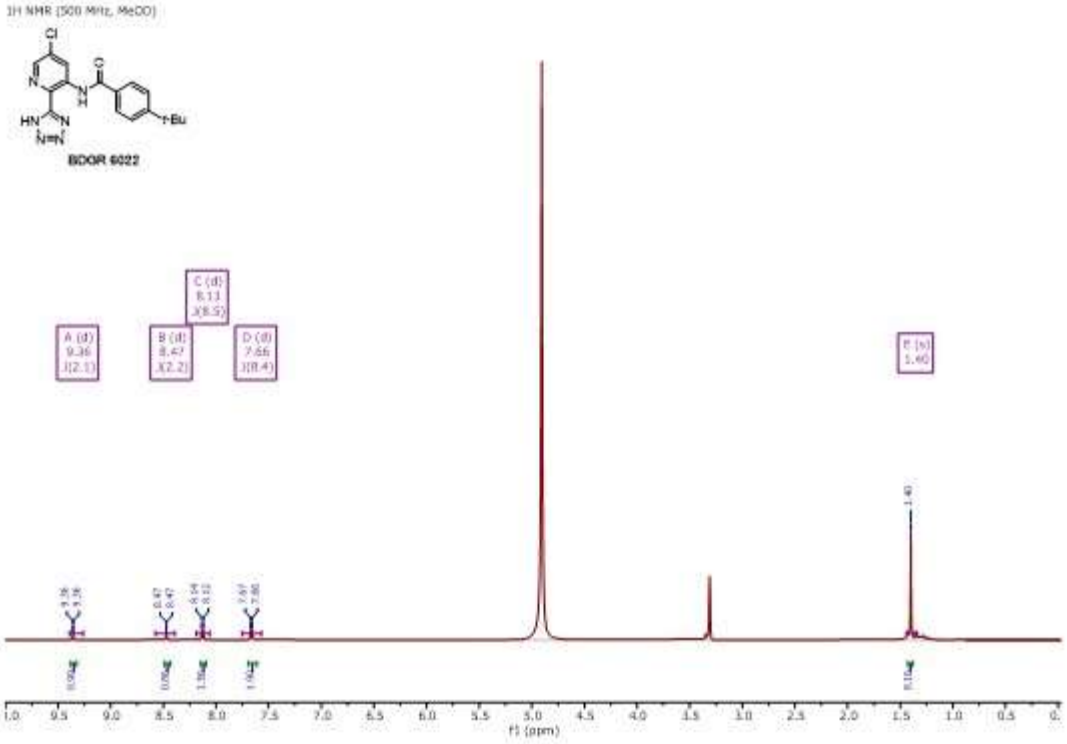
1H NMR (500 MHz, MeOD)
BDGR 6022
A (d)
9.36
J(2.1)
B (d)
8.47
J(2.2)
C (d)
8.13
J(8.5)
D (d)
7.66
J(8.4)
E (s)
1.40
f1 (ppm)

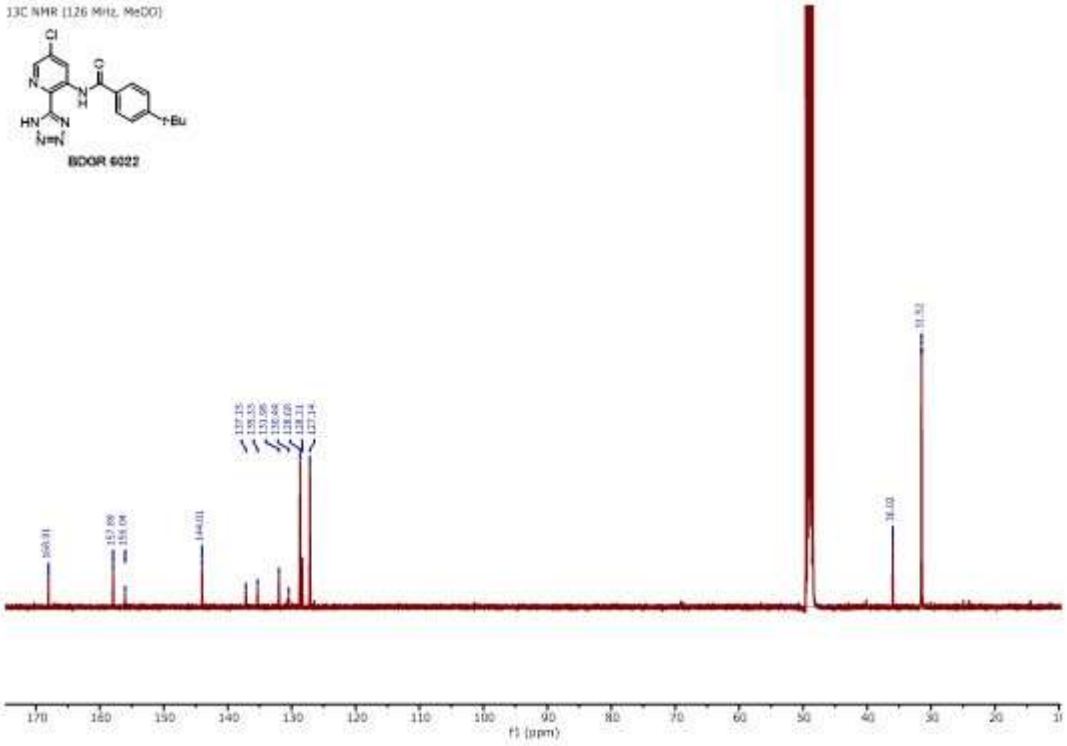
13C NMR (126 MHz, MeOD)
BDGR 6022
f1 (ppm)

1H NMR (500 MHz, CDCl3)

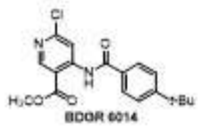

BDGR 6014

13C NMR (101 MHz, CDCl3)

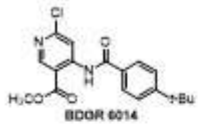

BDGR 6014

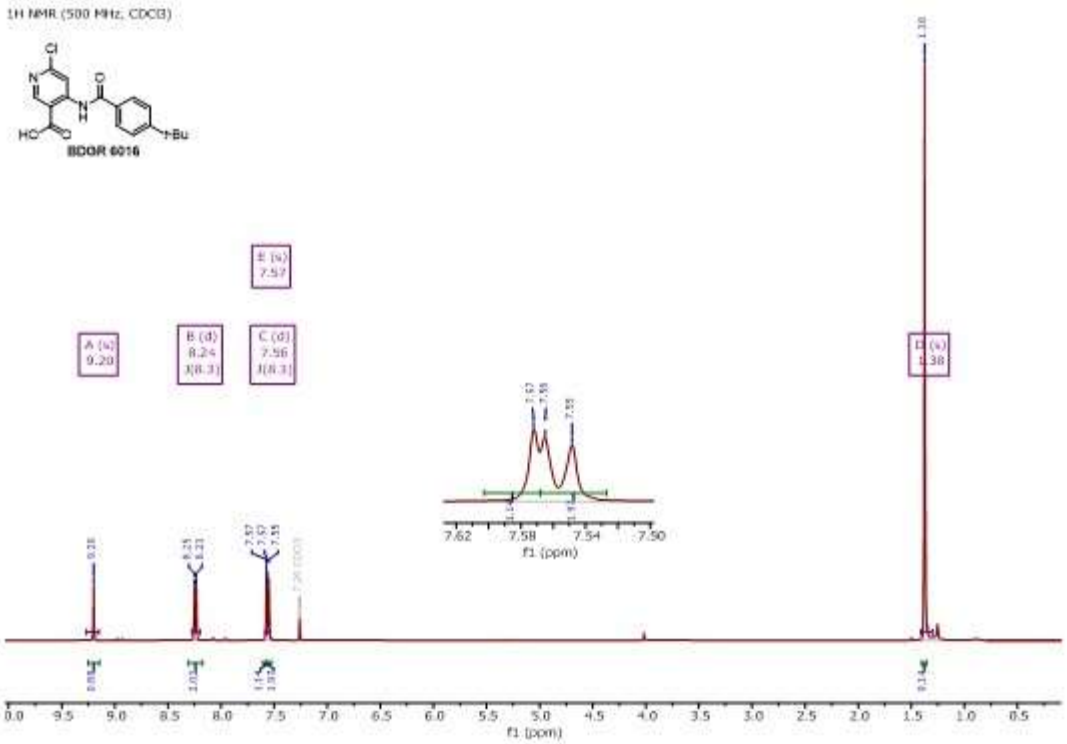
1H NMR (500 MHz, CDCl3)
BDGR 6016
A (s) 9.20
B (d) 8.24 J(8.3)
C (d) 7.56 J(8.3)
D (s) 1.38
f1 (ppm)

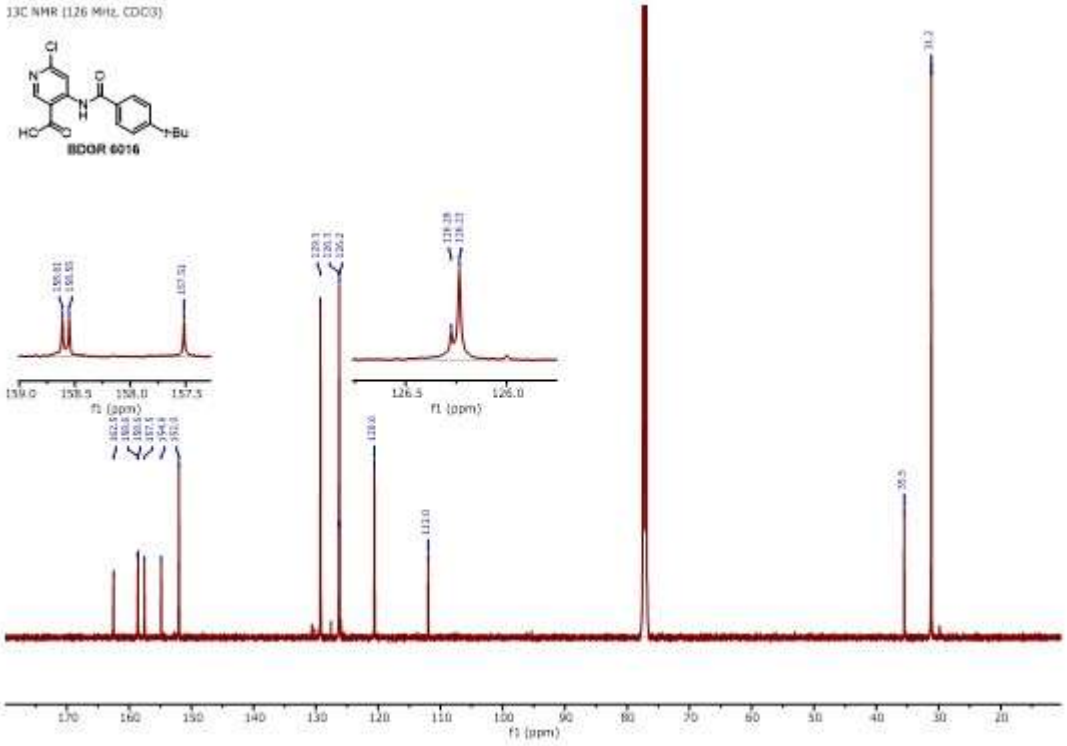
13C NMR (126 MHz, CDCl3)
BDGR 6016
f1 (ppm)

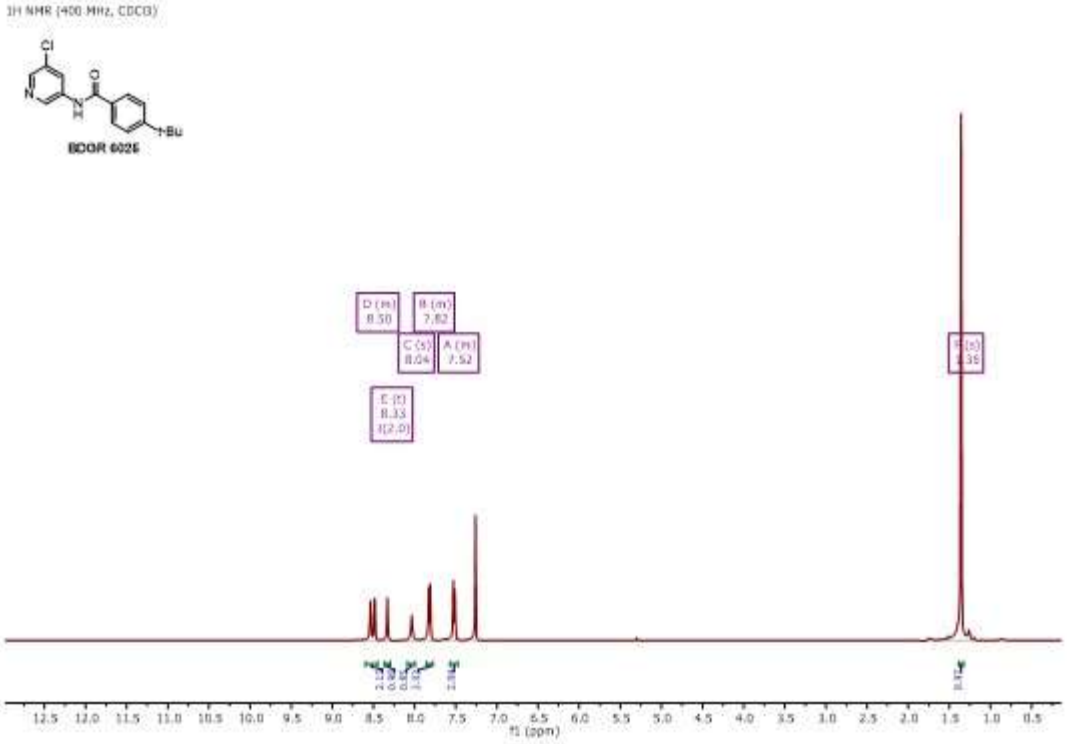
1H NMR (400 MHz, CDCl3)
BDGR 6025
D (m) 8.50
B (m) 7.82
C (s) 8.04
A (m) 7.52
E (t) 8.33 J(2.0)
f1 (ppm)

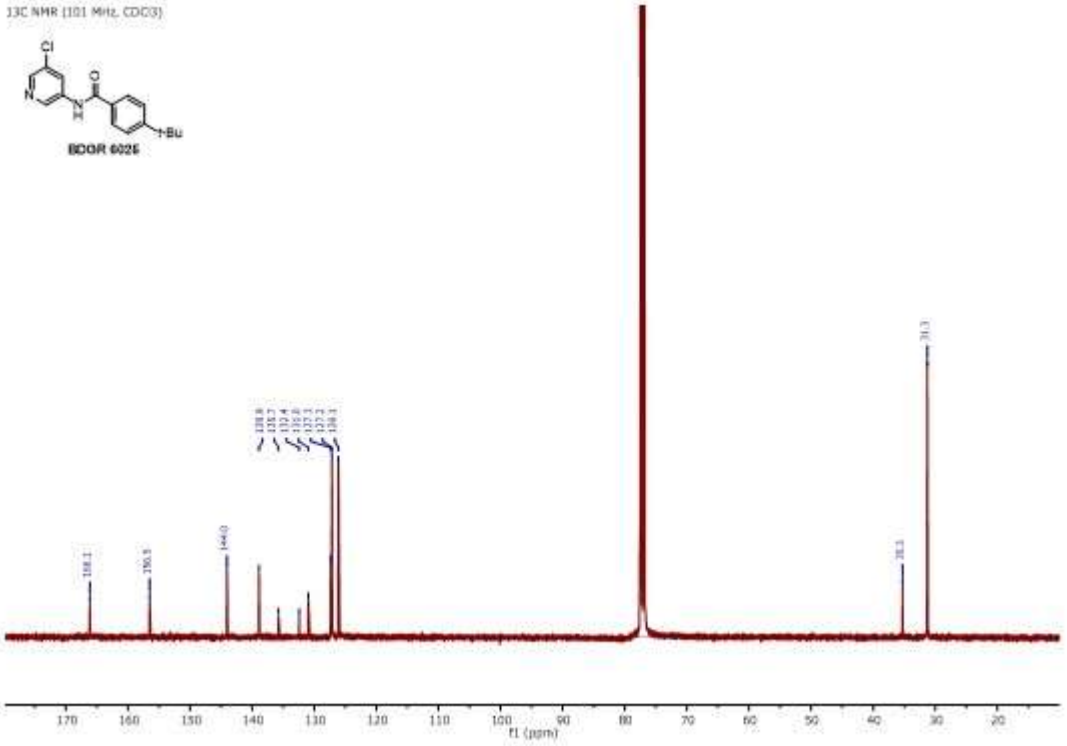
13C NMR (101 MHz, CDCl3)
BDGR 6025
f1 (ppm)

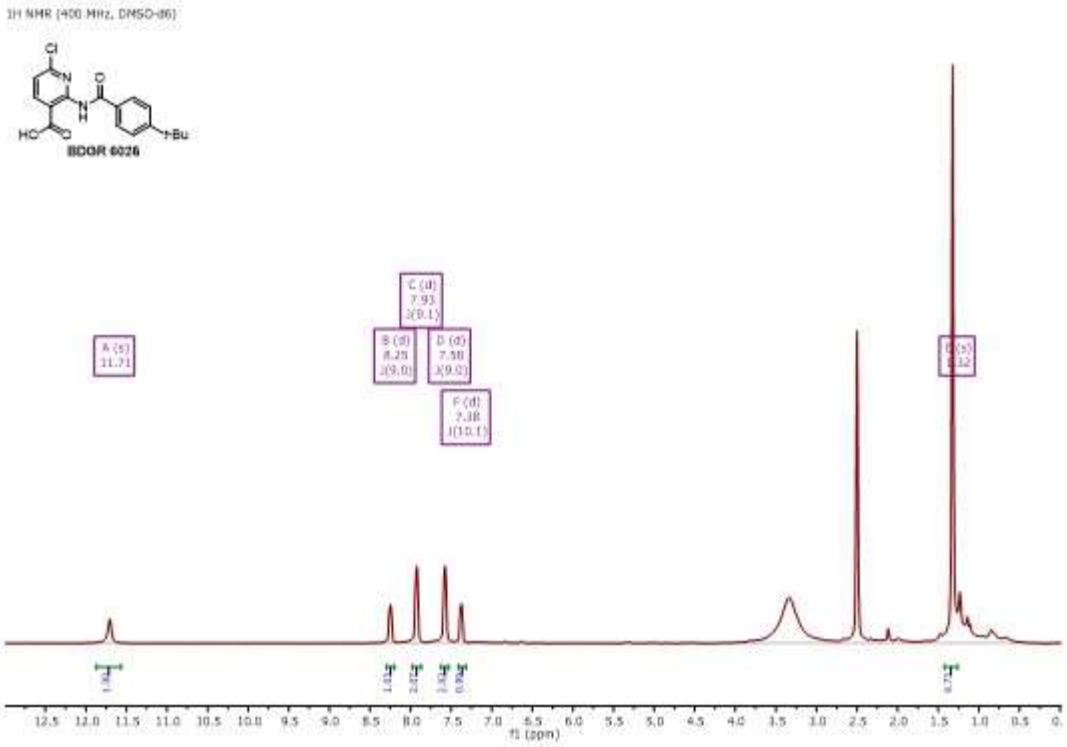
1H NMR (400 MHz, DMSO-d6)
BDGR 6026
A (s)
11.71
C (d)
7.93
J(9.1)
B (d)
8.25
J(9.0)
D (d)
7.58
J(9.0)
F (d)
7.38
J(10.1)
f1 (ppm)

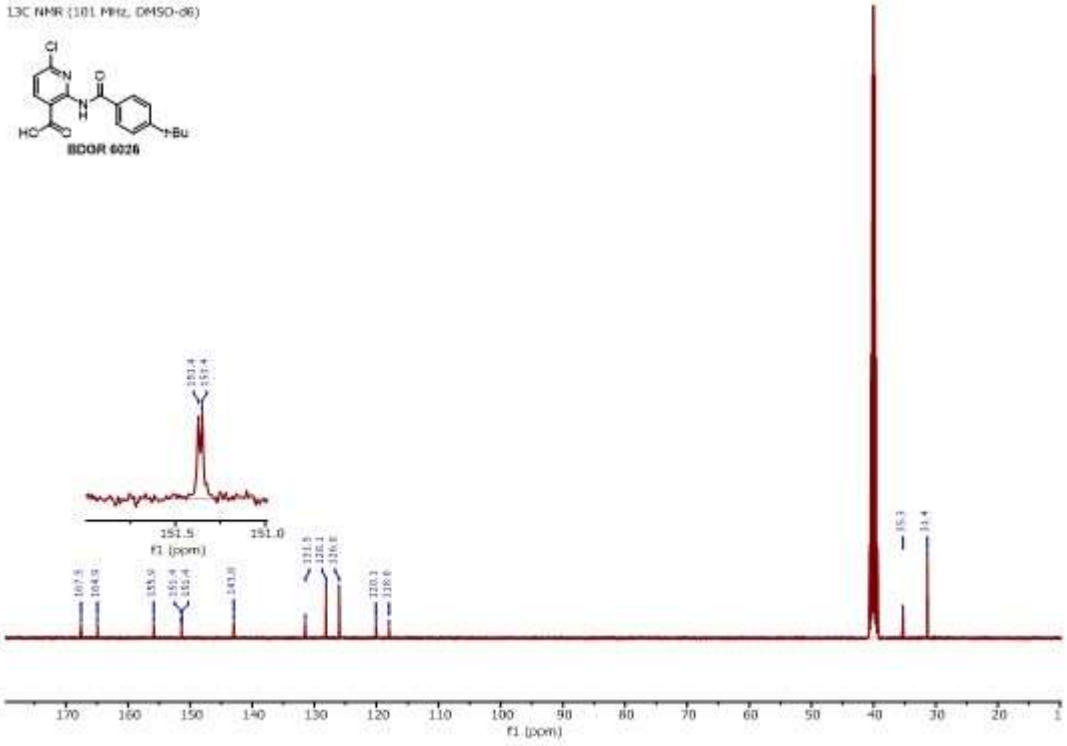
13C NMR (101 MHz, DMSO-d6)
BDGR 6026
f1 (ppm)

1H NMR (400 MHz, CDCl3)

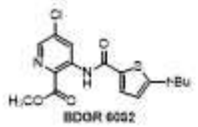

BDGR 6032

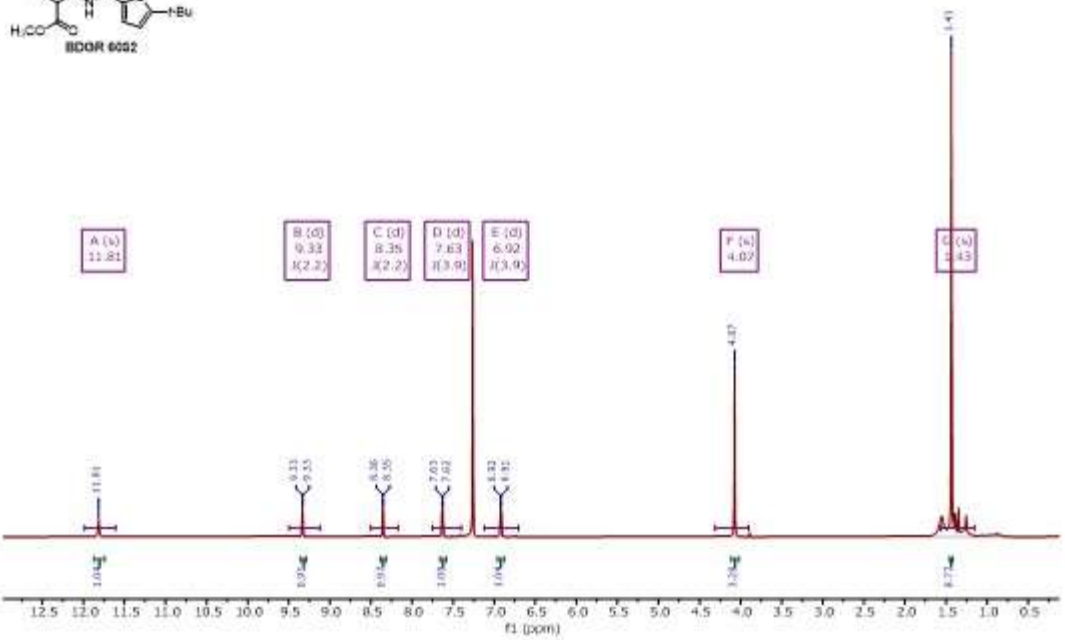

13C NMR (101 MHz, CDCl3)

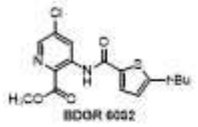

BDGR 6032

1H NMR (400 MHz, CDCl3)

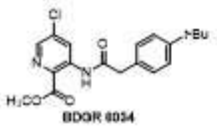

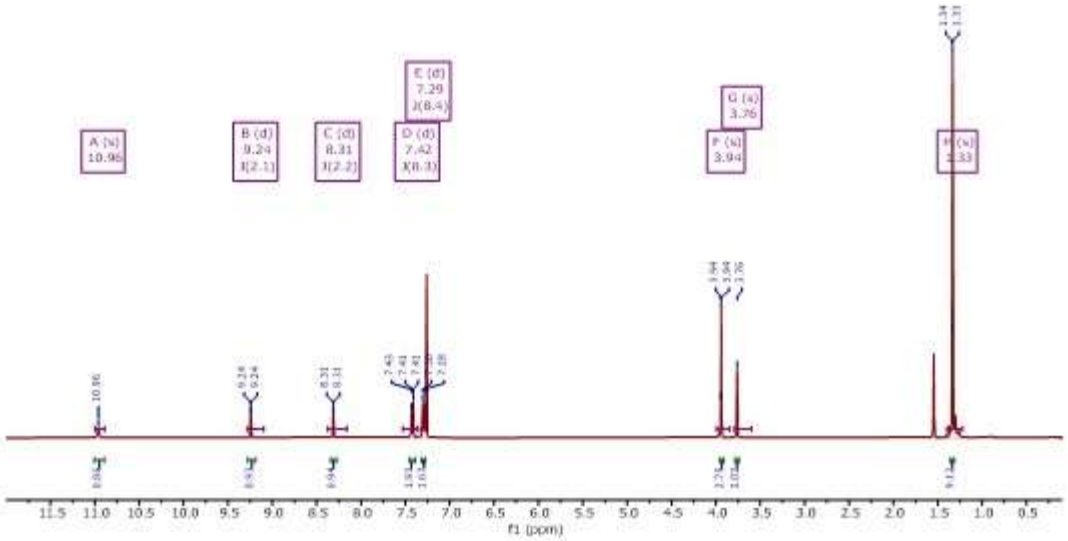

13C NMR (101 MHz, CDCl3)

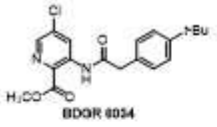

1H NMR (400 MHz, CDCl3)

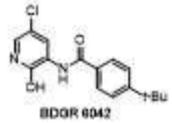

BDQR 6042

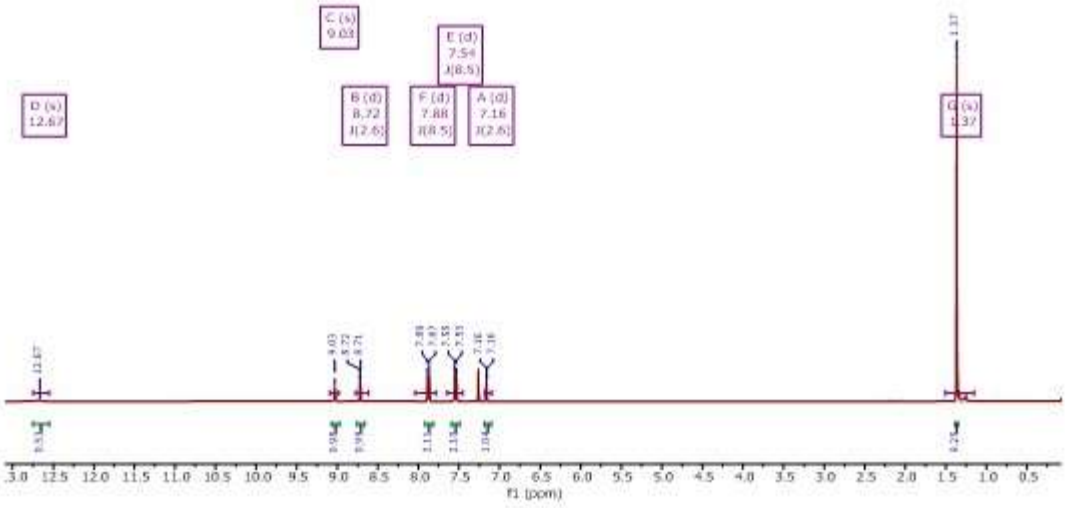

13C NMR (101 MHz, CDCl3)

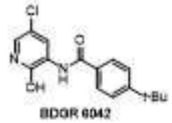

BDQR 6042

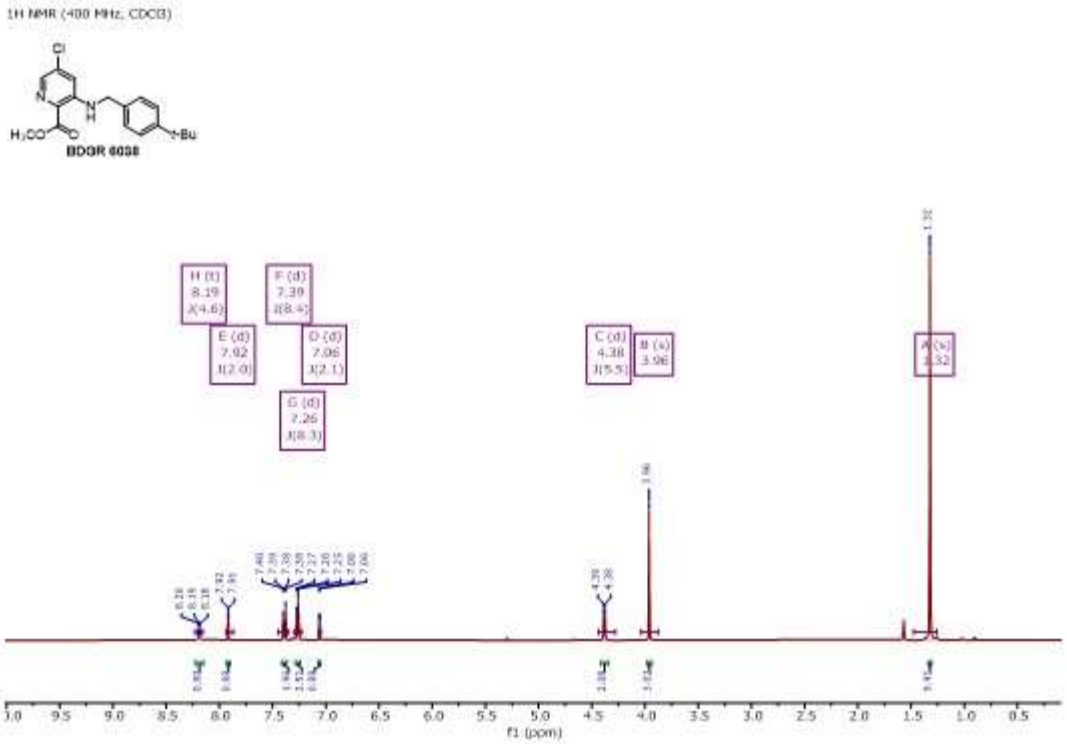
1H NMR (400 MHz, CDCl3)
BDGR 6038
H (t) 8.19 J(4.6)
F (d) 7.39 J(8.4)
E (d) 7.92 J(2.0)
D (d) 7.06 J(2.1)
G (d) 7.26 J(8.3)
C (d) 4.38 J(5.5)
B (s) 3.96
A (s) 1.32
f1 (ppm)

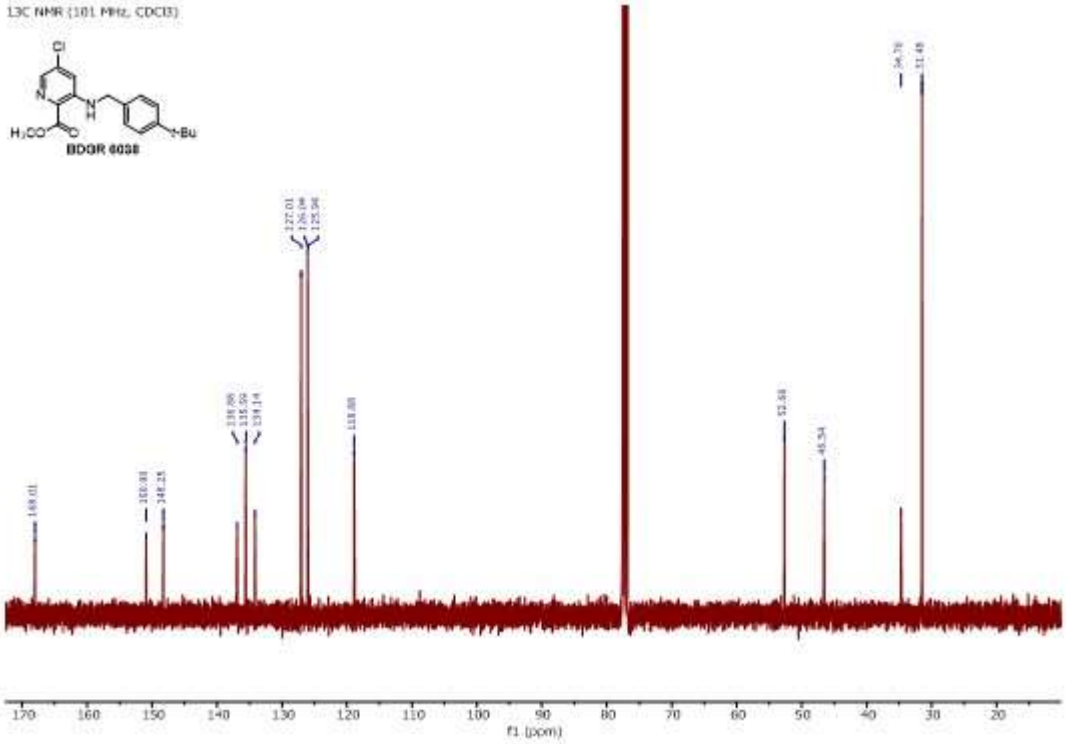
13C NMR (101 MHz, CDCl3)
BDGR 6038
f1 (ppm)

1H NMR (400 MHz, CDCl3)

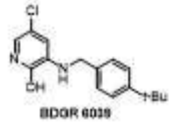

BDQR 6039

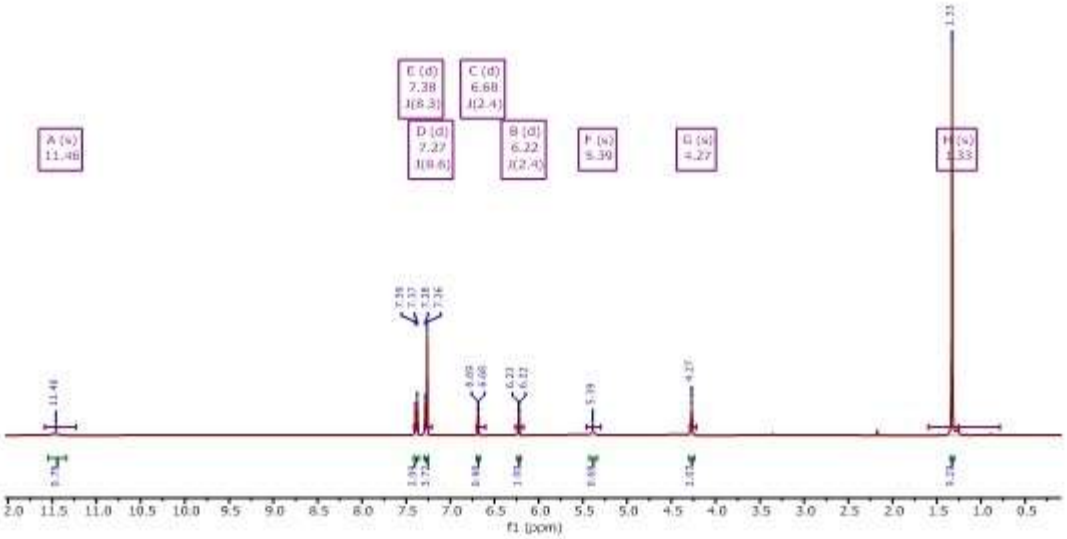

13C NMR (101 MHz, CDCl3)

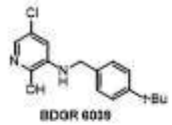

BDQR 6039

1H NMR (400 MHz, CDCl3)

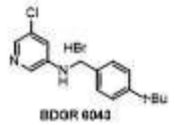

BDQR 6043

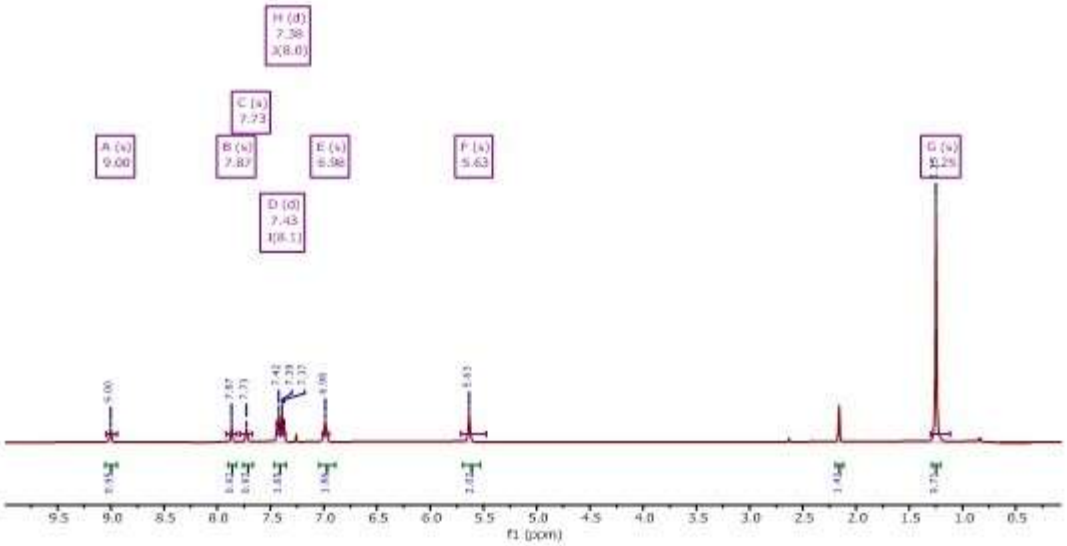

13C NMR (101 MHz, CDCl3)

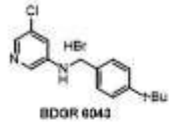

BDQR 6043

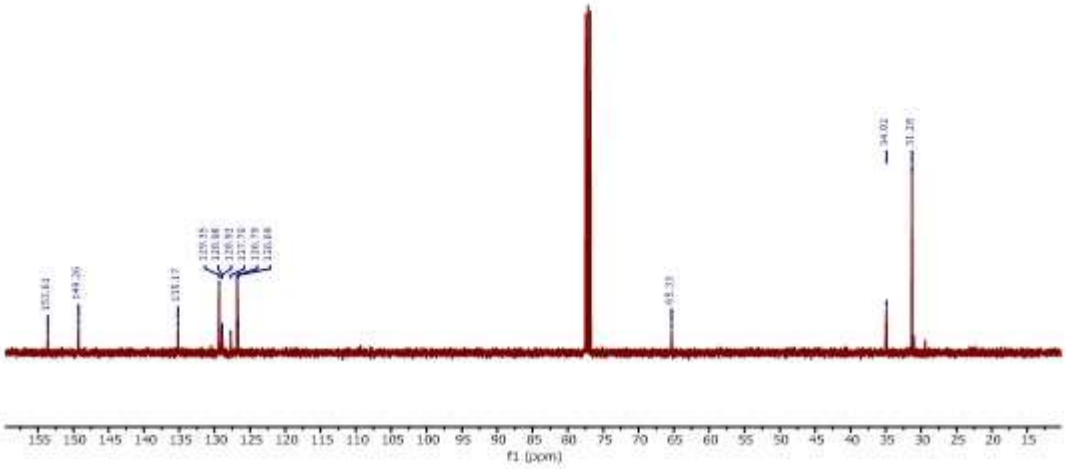

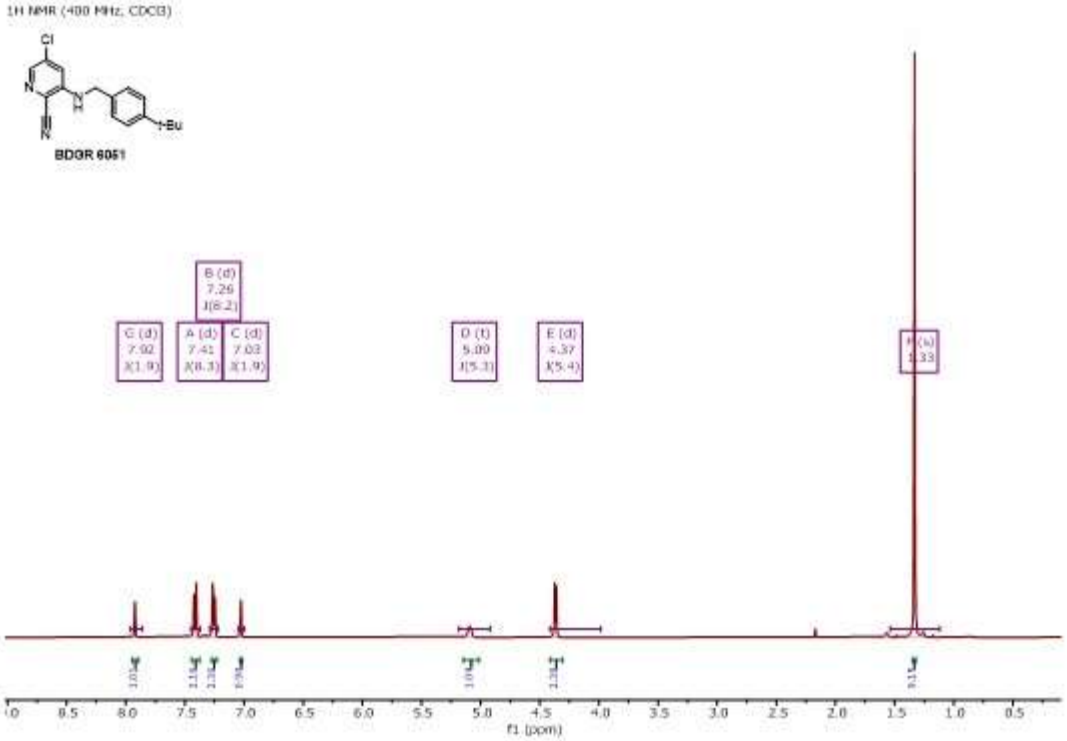
1H NMR (400 MHz, CDCl3)
BDGR 6051
B (d)
7.26
J(8.2)
G (d)
7.92
J(1.9)
A (d)
7.41
J(8.3)
C (d)
7.03
J(1.9)
D (t)
5.00
J(5.3)
E (d)
4.37
J(5.4)
F (s)
1.33
f1 (ppm)

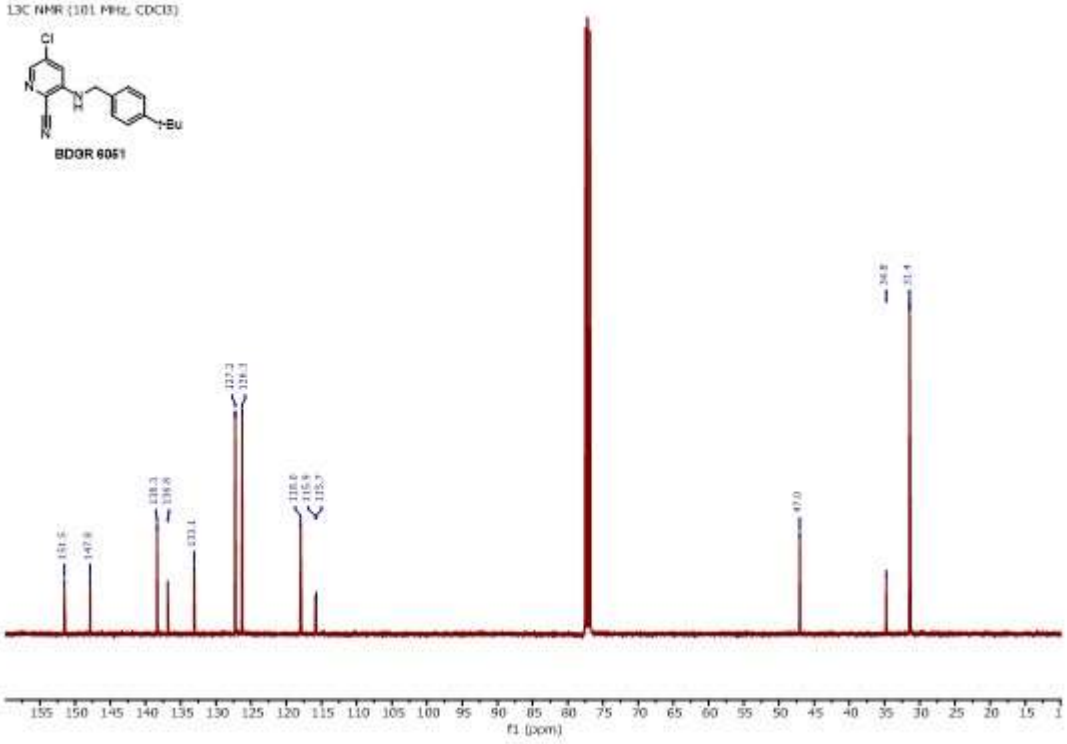
13C NMR (101 MHz, CDCl3)
BDGR 6051
f1 (ppm)

1H NMR (400 MHz, CDCl3)

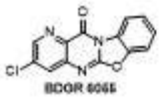

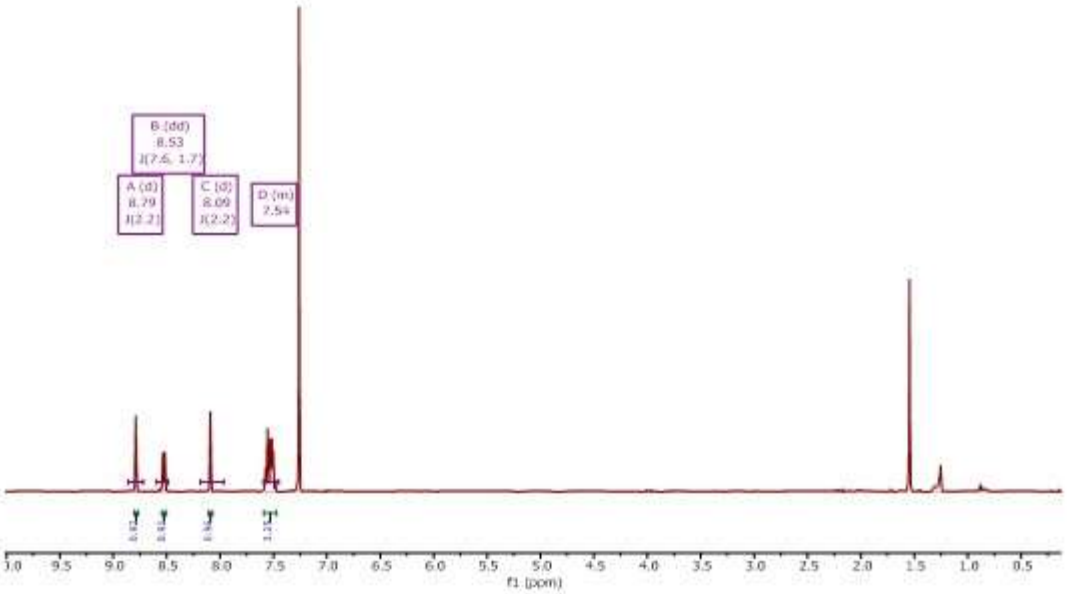

13C NMR (101 MHz, CDCl3)

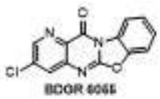

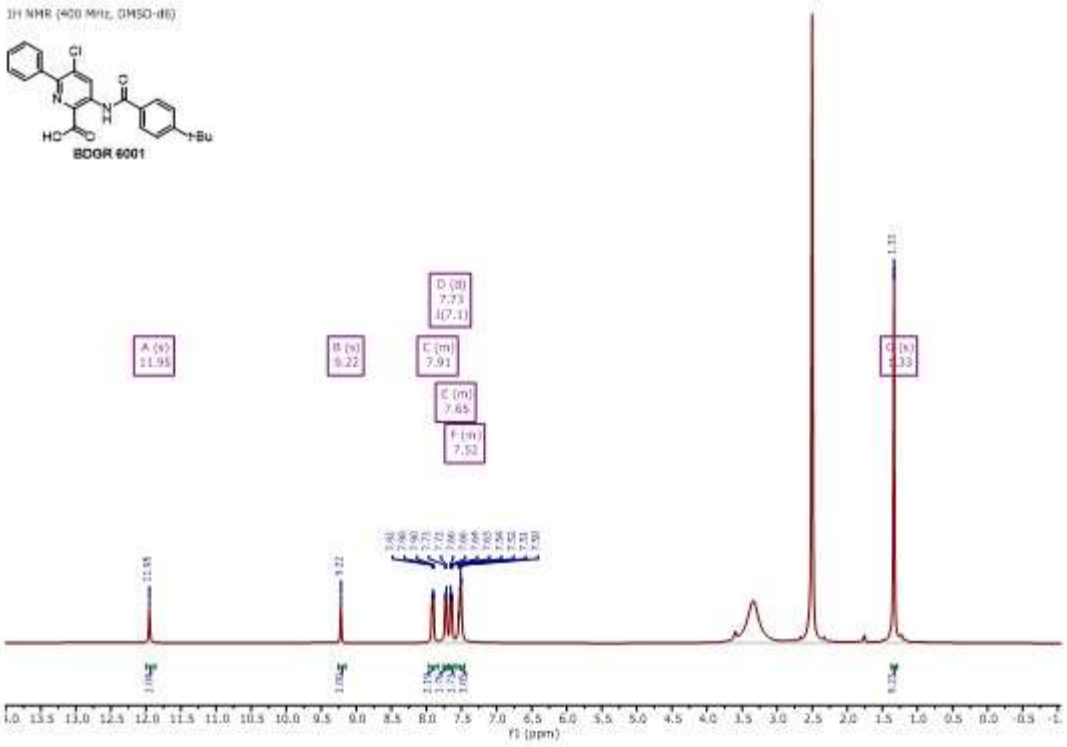
1H NMR (400 MHz, DMSO-d6)
BDGR 6001
A (s) 11.95
B (s) 9.22
D (d) 7.73 J(7.1)
E (m) 7.91
E (m) 7.65
F (m) 7.52
G (s) 1.33
11.95
9.22
1.33
f1 (ppm)

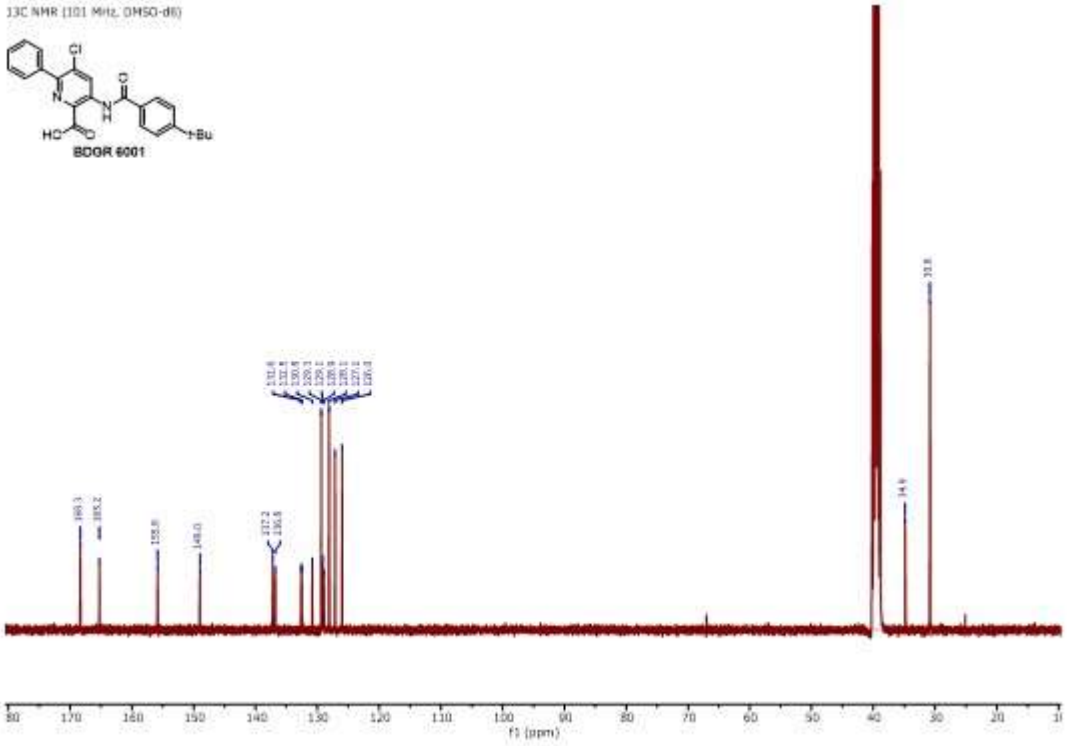
13C NMR (101 MHz, DMSO-d6)
BDGR 6001
169.3
165.2
155.8
148.0
137.2
136.6
34.9
33.8
f1 (ppm)

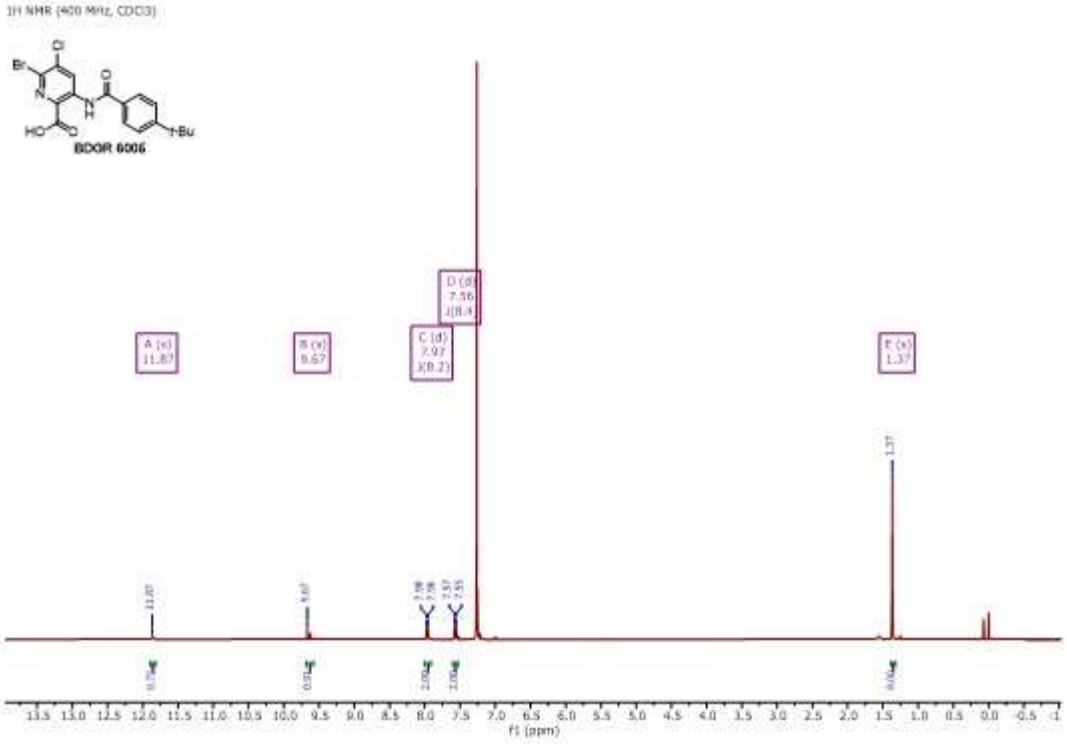
1H NMR (400 MHz, CDCl3)
BDOR 6006
A (s)
11.87
B (s)
9.67
C (d)
7.97
J(8.2)
D (d)
7.56
J(8.4
E (s)
1.37
f1 (ppm)

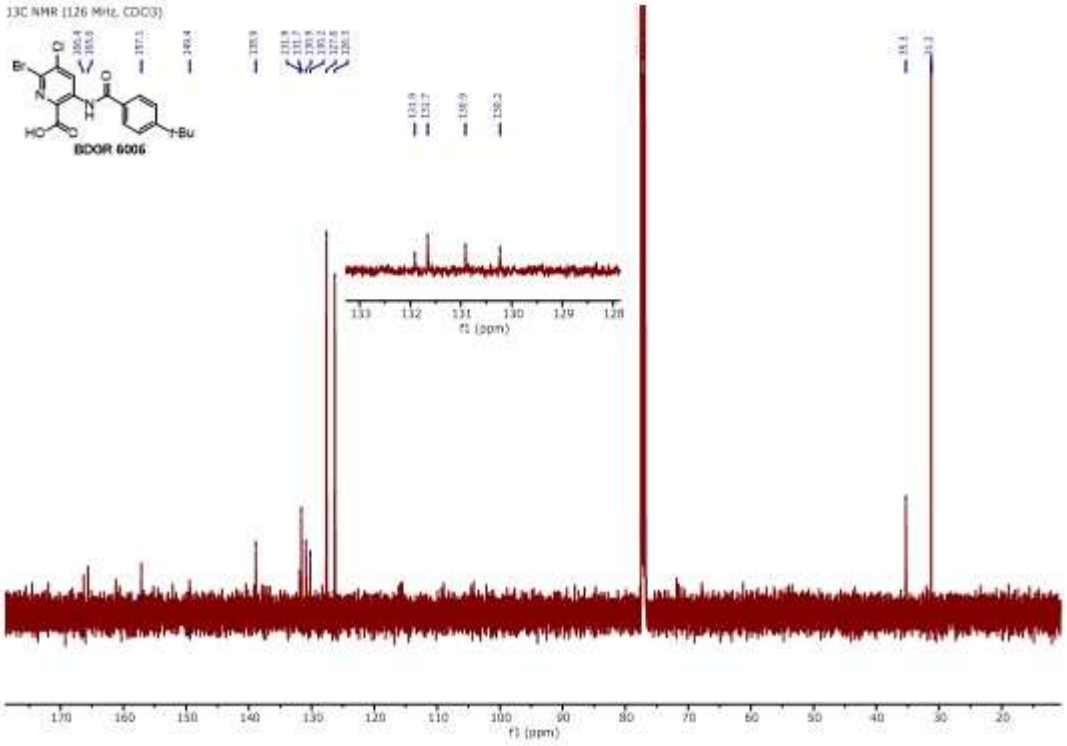
13C NMR (126 MHz, CDCl3)
BDOR 6006
f1 (ppm)

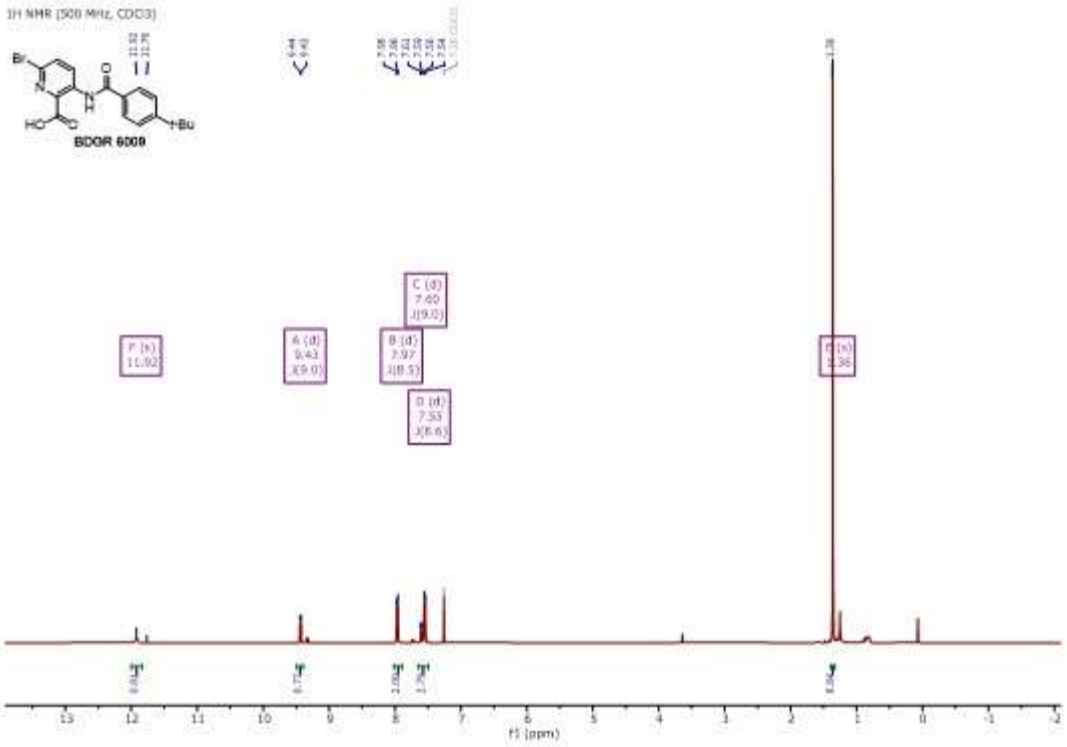
1H NMR (500 MHz, CDCl3)
BDGR 6009
F (s)
11.92
A (d)
9.43
J(9.0)
B (d)
7.97
J(8.5)
C (d)
7.60
J(9.0)
D (d)
7.55
J(8.6)
E (s)
1.36
f1 (ppm)

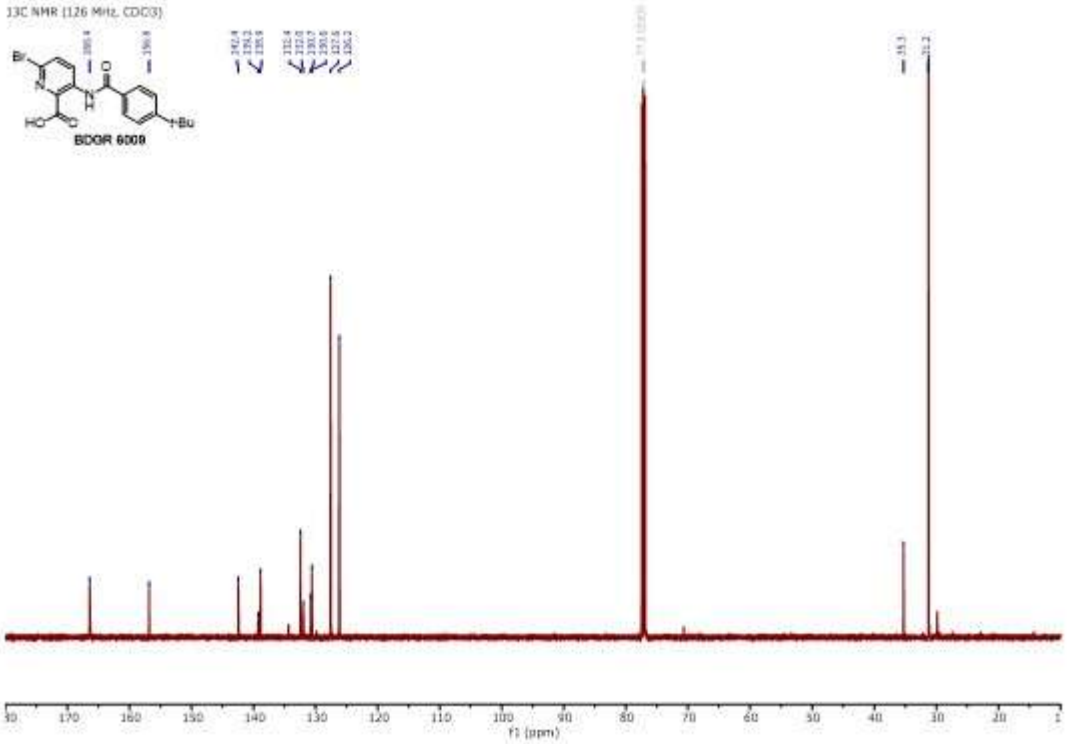
13C NMR (126 MHz, CDCl3)
BDGR 6009
f1 (ppm)

1H NMR (500 MHz, CDCl3)

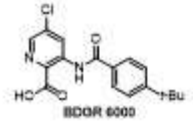

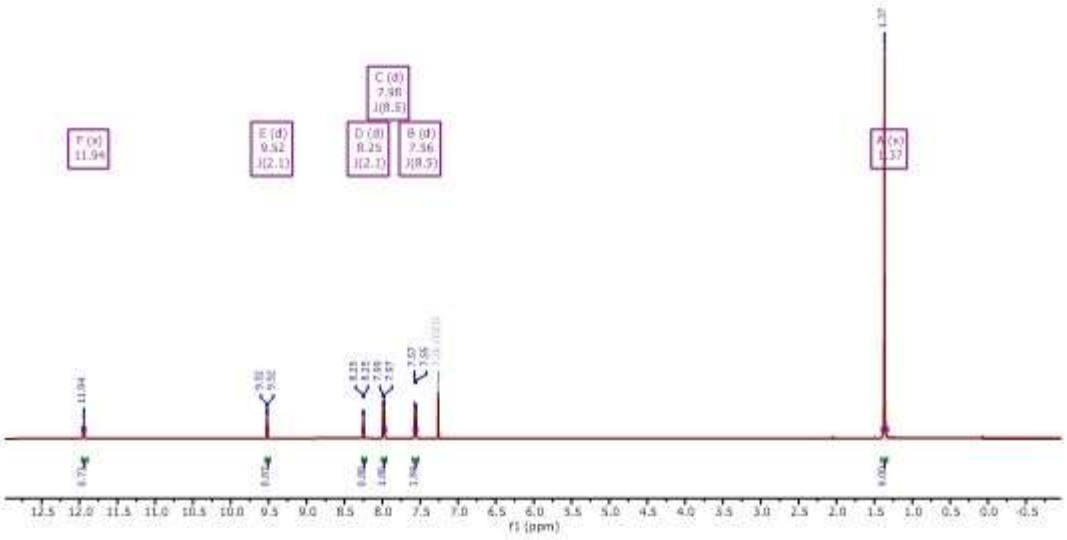

13C NMR (126 MHz, CDCl3)

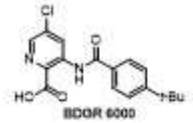

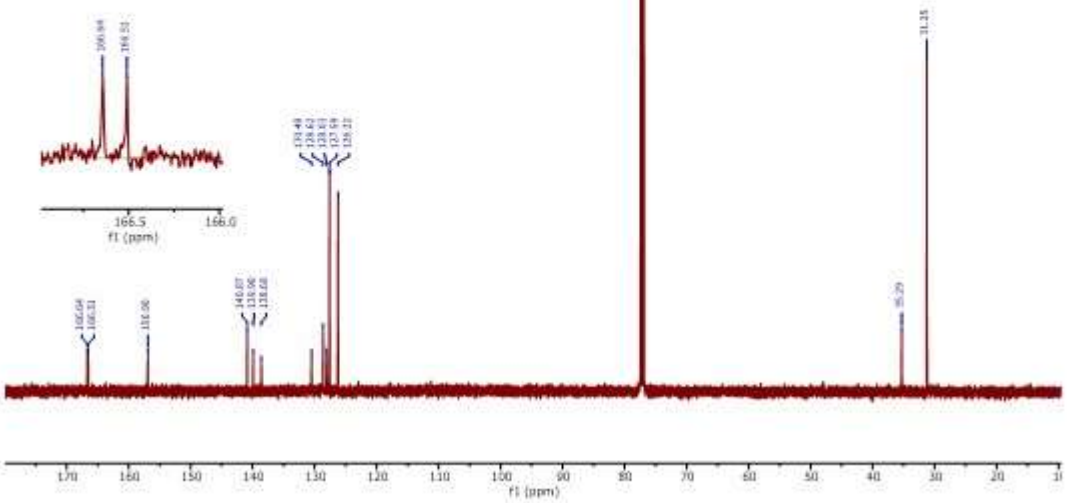

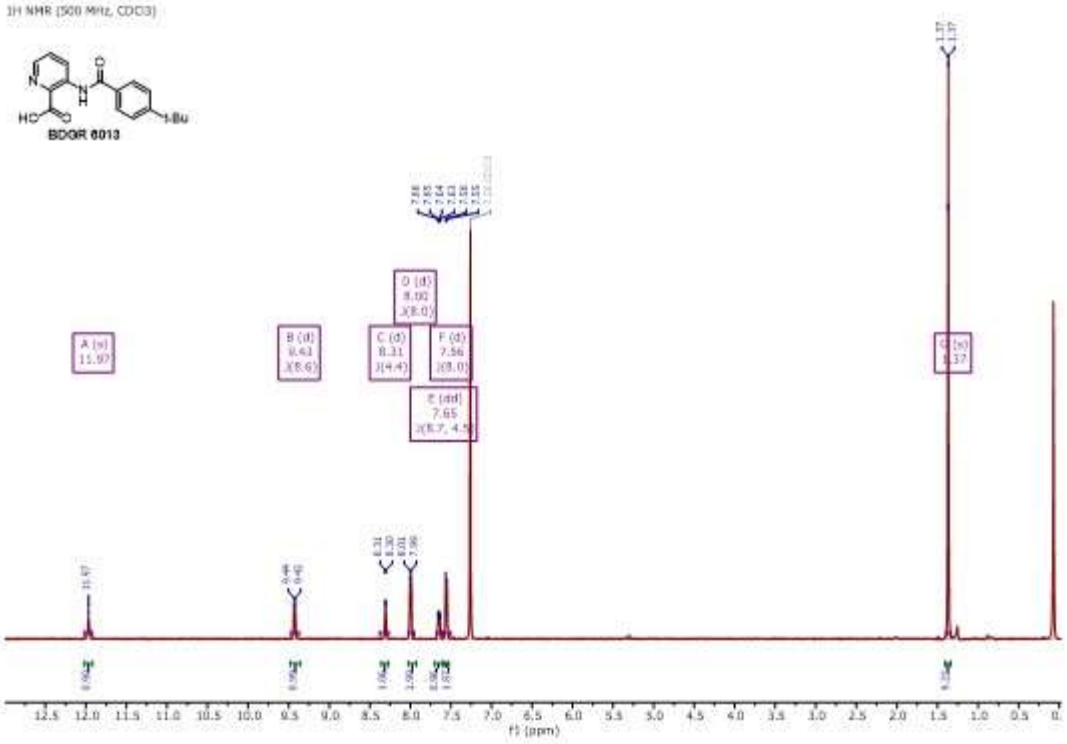
1H NMR (500 MHz, CDCl3)
BDGR 6013
t-Bu
A (s)
11.97
B (d)
9.43
J(8.6)
C (d)
8.31
J(4.4)
D (d)
8.00
J(8.0)
F (d)
7.56
J(8.0)
E (dd)
7.65
J(8.7, 4.5)
9.00
12.5 12.0 11.5 11.0 10.5 10.0 9.5 9.0 8.5 8.0 7.5 7.0 6.5 6.0 5.5 5.0 4.5 4.0 3.5 3.0 2.5 2.0 1.5 1.0 0.5 0
f1 (ppm)

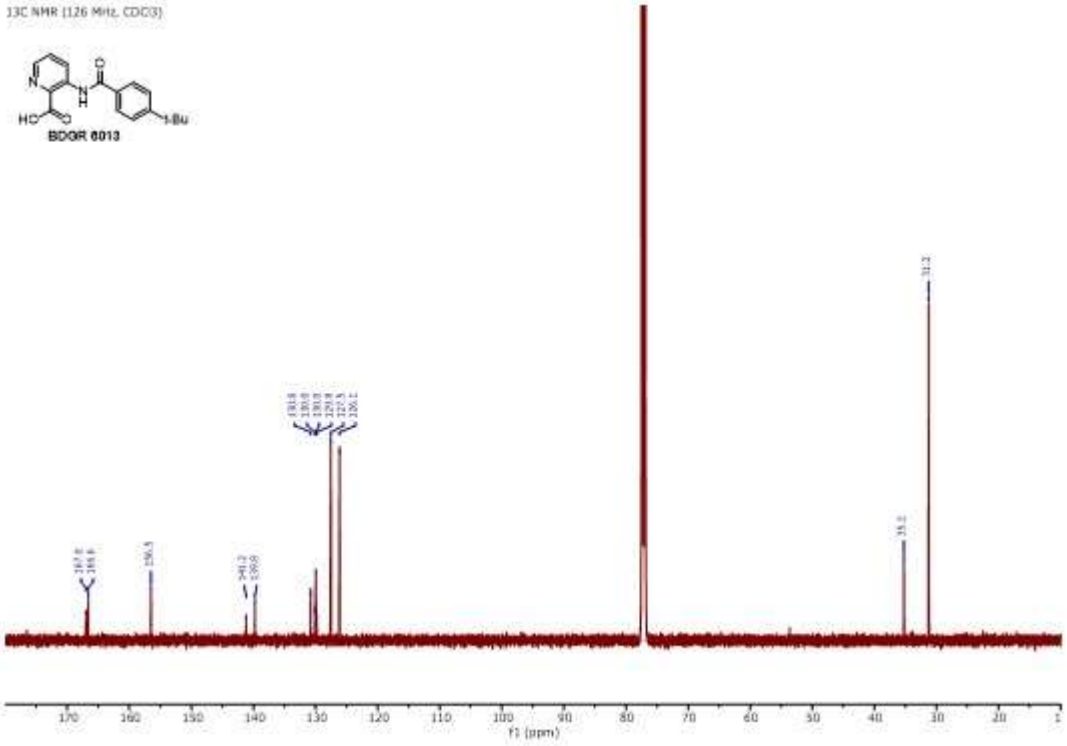
13C NMR (126 MHz, CDCl3)
BDGR 6013
t-Bu
170 160 150 140 130 120 110 100 90 80 70 60 50 40 30 20 1
f1 (ppm)

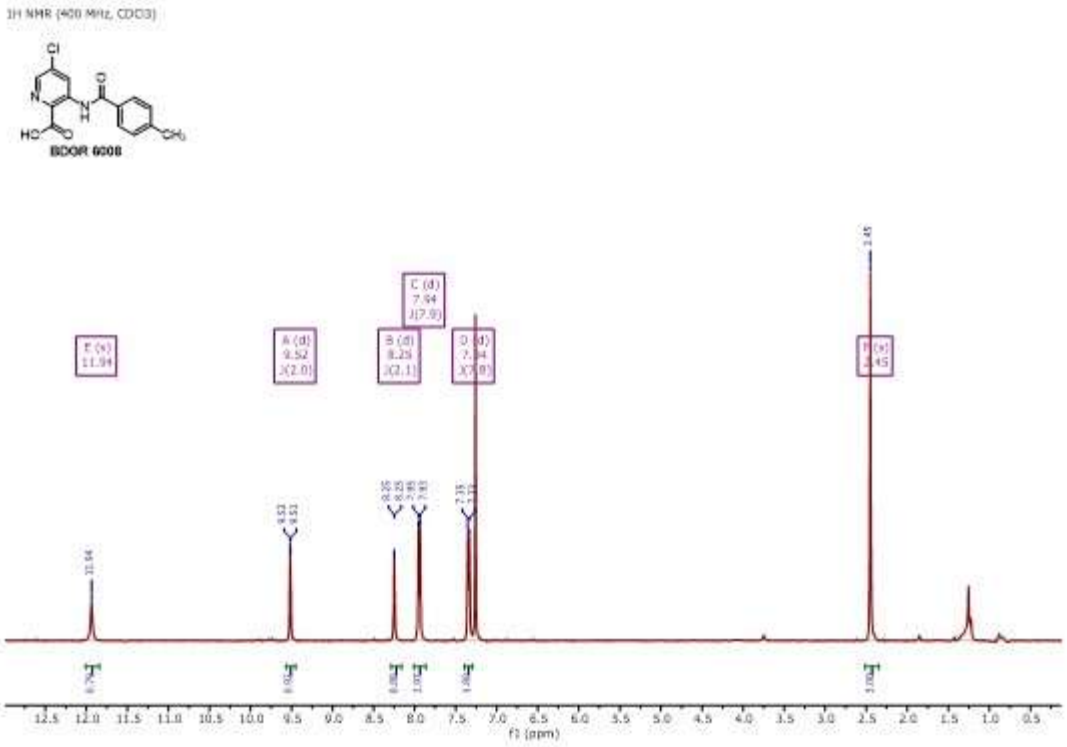
1H NMR (400 MHz, CDCl3)
BDOR 6008
F (s) 11.94
A (d) 9.52 J(2.0)
B (d) 8.29 J(2.1)
C (d) 7.94 J(7.9)
D (d) 7.84 J(7.8)
E (s) 2.45
f1 (ppm)

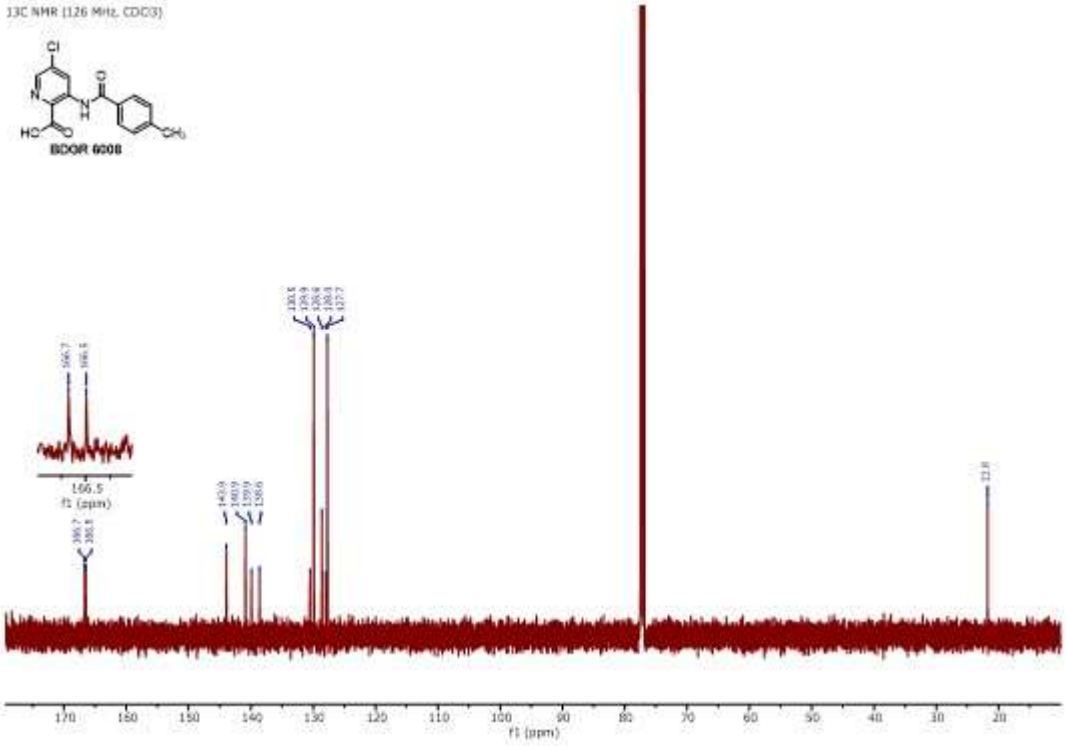
13C NMR (126 MHz, CDCl3)
BDOR 6008
166.5
f1 (ppm)

1H NMR (400 MHz, CDCl3)

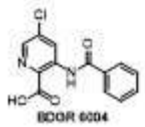

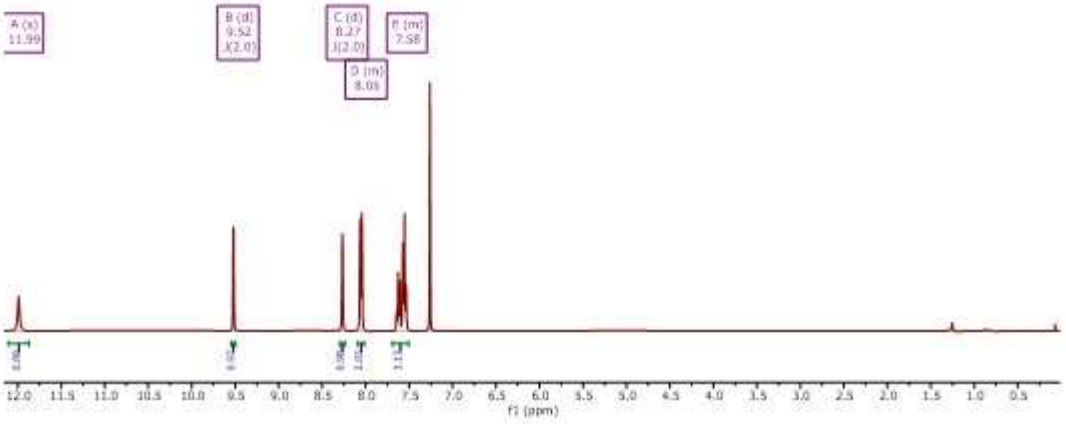

13C NMR (126 MHz, CDCl3)

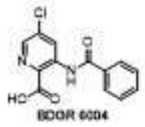

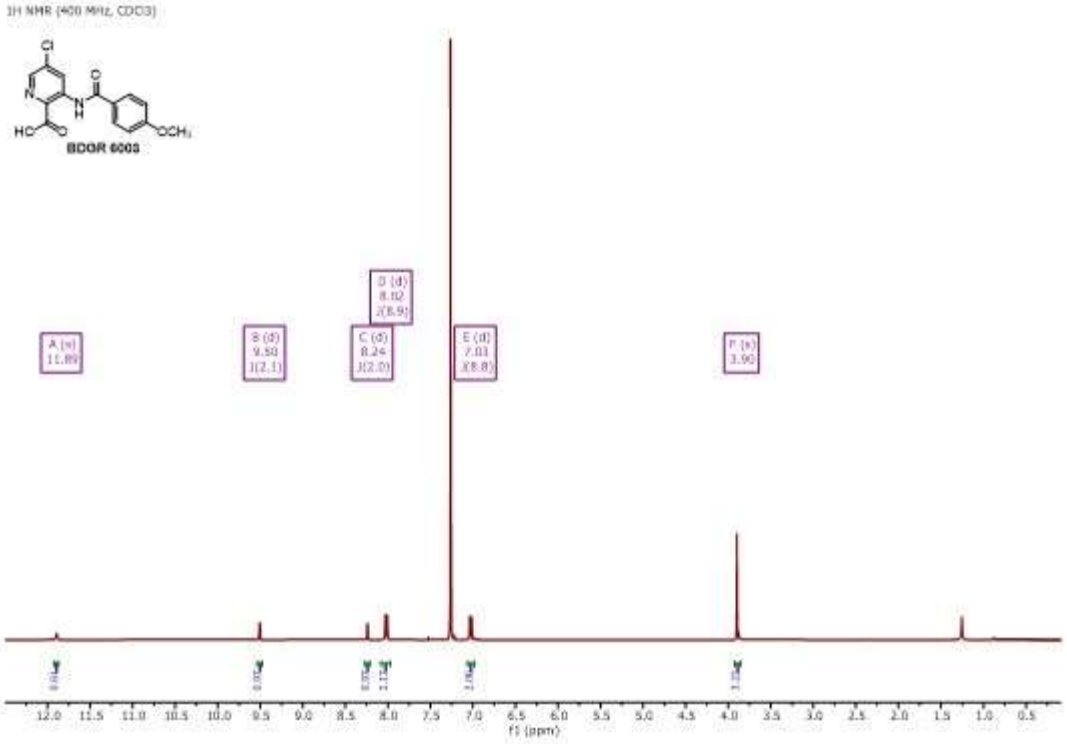
1H NMR (400 MHz, CDCl3)
BDOR 6003
A (s)
11.89
B (d)
9.50
J(2.1)
C (d)
8.24
J(2.0)
D (d)
8.02
J(8.9)
E (d)
7.03
J(8.8)
F (s)
3.90
f1 (ppm)

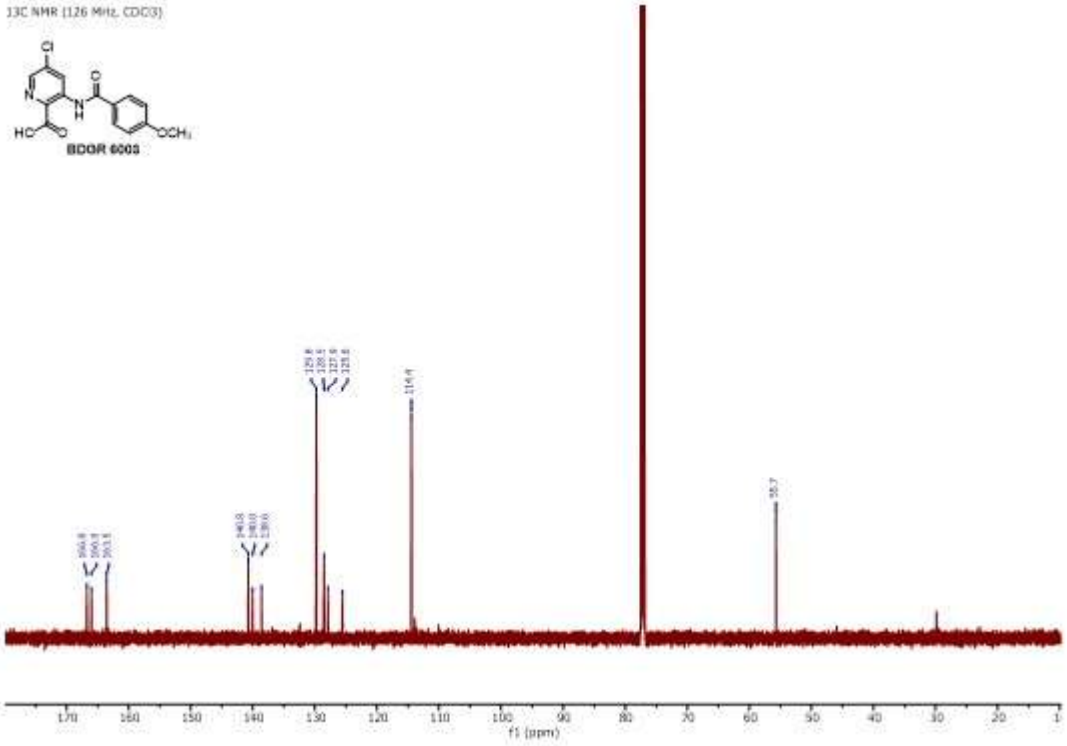
13C NMR (126 MHz, CDCl3)
BDOR 6003
f1 (ppm)

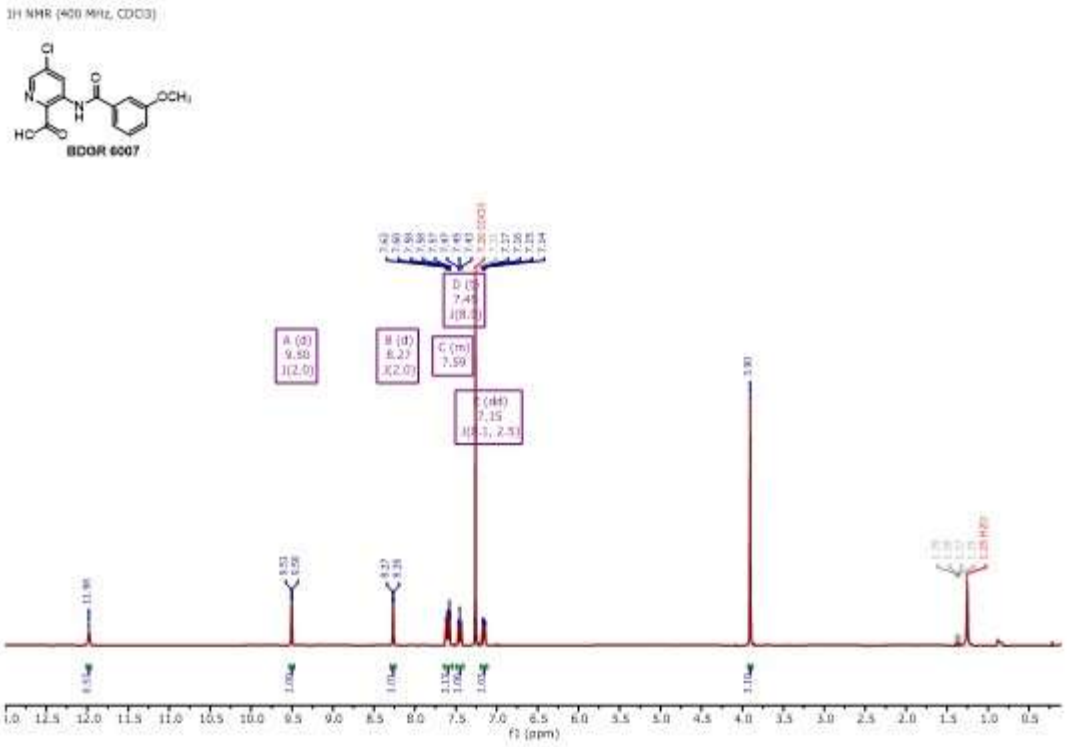
1H NMR (400 MHz, CDCl3)
BDGR 6007
A (d)
9.50
J(2.0)
B (d)
8.27
J(2.0)
C (m)
7.59
3.90
11.90
8.53
8.50
8.27
8.25
f1 (ppm)

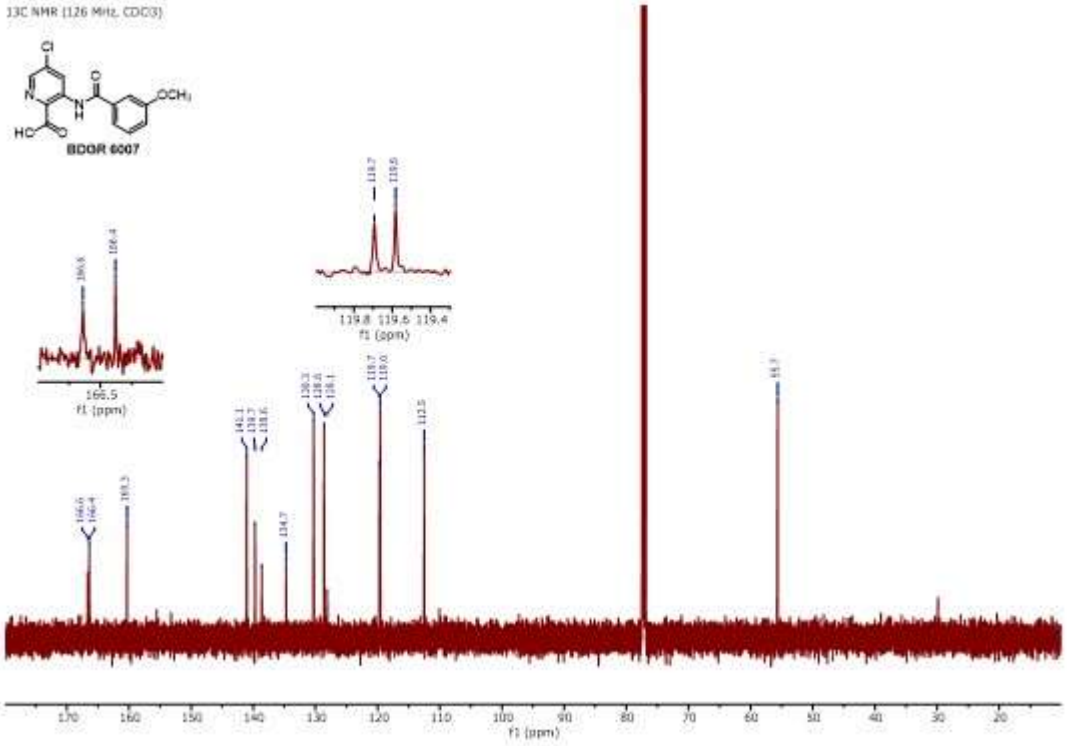
13C NMR (126 MHz, CDCl3)
BDGR 6007
166.5
f1 (ppm)
119.8 119.6 119.4
f1 (ppm)
f1 (ppm)

1H NMR (500 MHz, CDCl3)

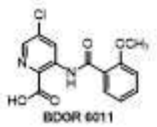

BDOR 6011

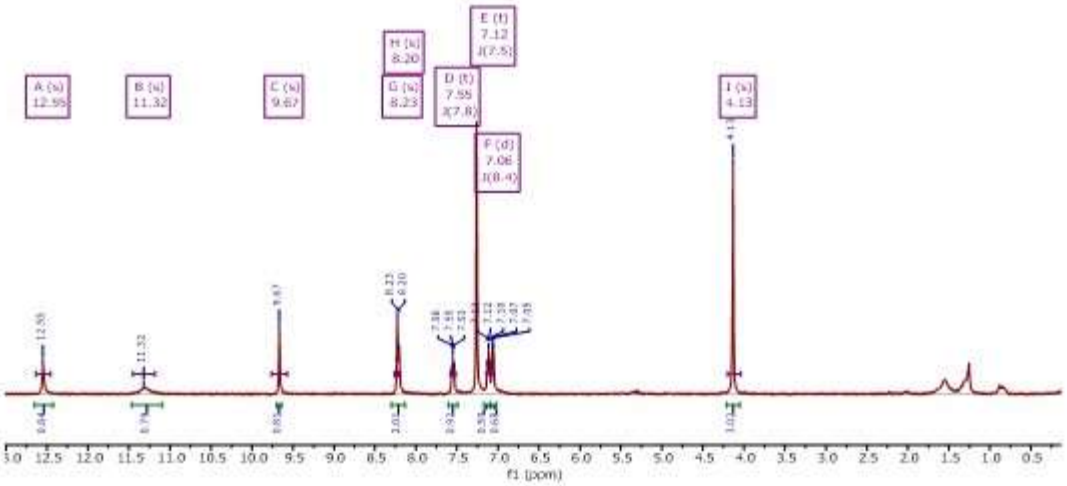

13C NMR (126 MHz, CDCl3)

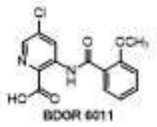

BDOR 6011

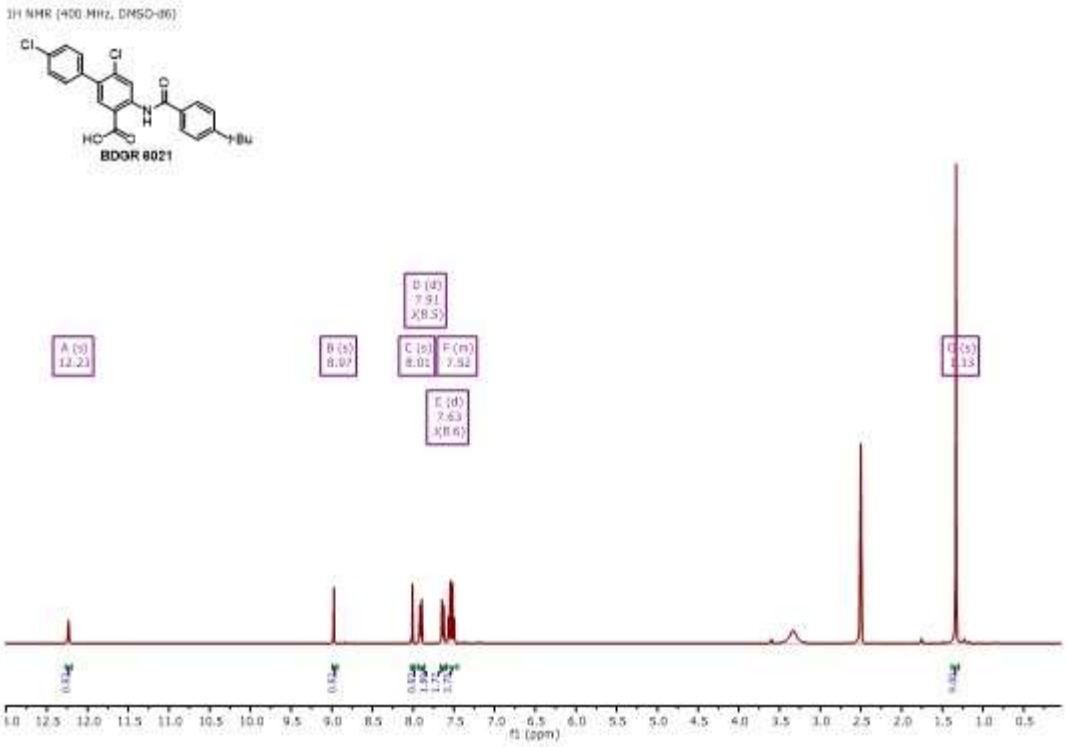
1H NMR (400 MHz, DMSO-d6)
BDGR 6021
A (s) 12.23
B (s) 8.07
C (s) 8.01
D (d) 7.91 J(8.5)
E (d) 7.63 J(8.6)
F (m) 7.52
G (s) 1.33
f1 (ppm)

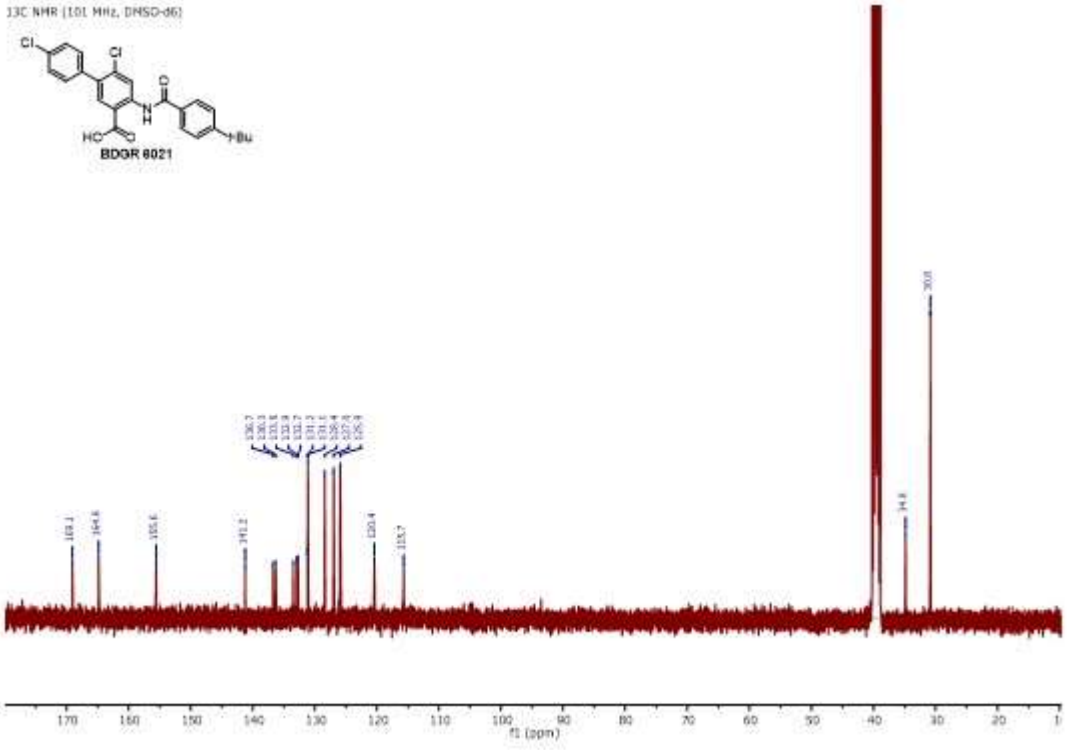
13C NMR (101 MHz, DMSO-d6)
BDGR 6021
f1 (ppm)

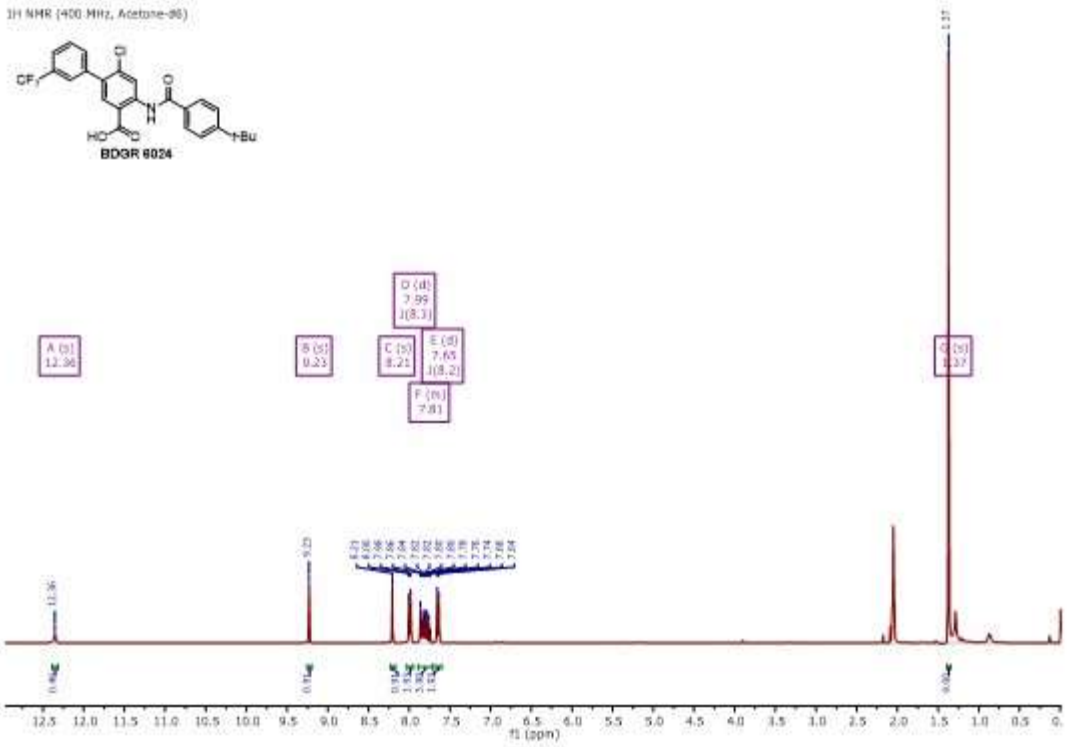
1H NMR (400 MHz, Acetone-d6)
BDGR 6024
A (s) 12.36
B (s) 9.23
C (s) 8.25
D (d) 7.99 J(8.3)
E (d) 7.65 J(8.2)
F (m) 7.81
G (s) 1.37
f1 (ppm)

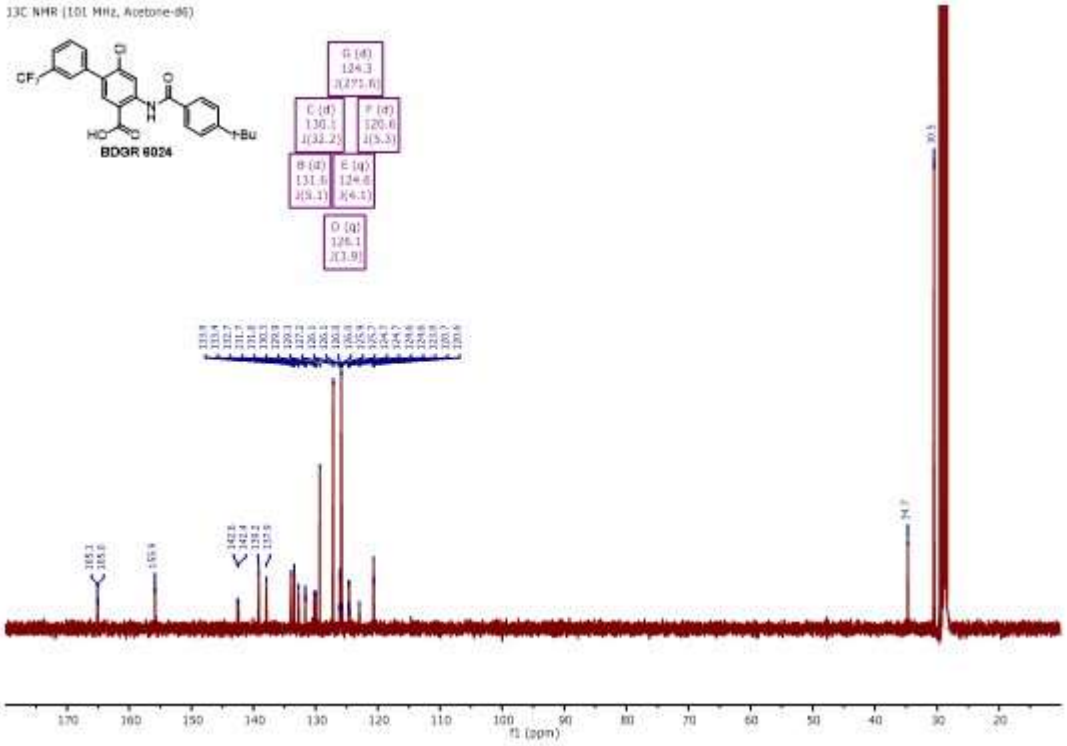
13C NMR (101 MHz, Acetone-d6)
BDGR 6024
G (d) 124.3 J(271.6)
C (d) 130.1 J(32.2)
F (d) 120.6 J(5.3)
B (d) 131.6 J(5.1)
E (q) 124.6 J(4.1)
D (q) 126.1 J(3.9)
f1 (ppm)

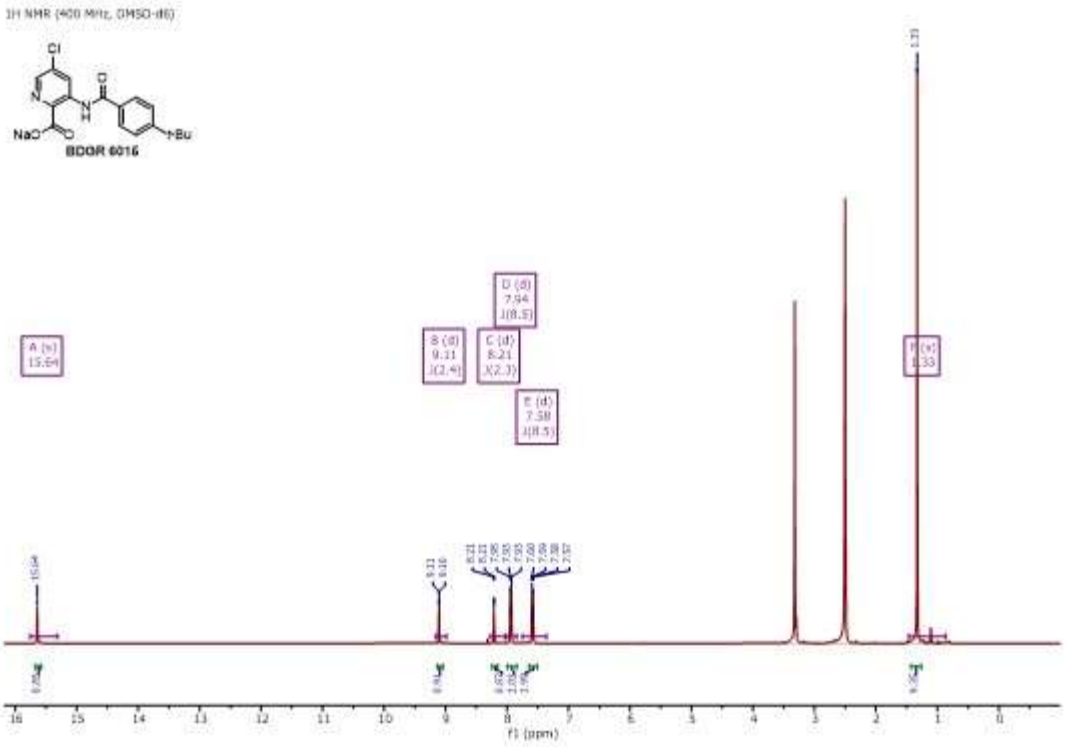
1H NMR (400 MHz, DMSO-d6)
BDGR 6016
A (s)
15.64
B (d)
9.11
J(2.4)
C (d)
8.21
J(2.3)
D (d)
7.94
J(8.5)
E (d)
7.58
J(8.5)
F (s)
1.33
f1 (ppm)

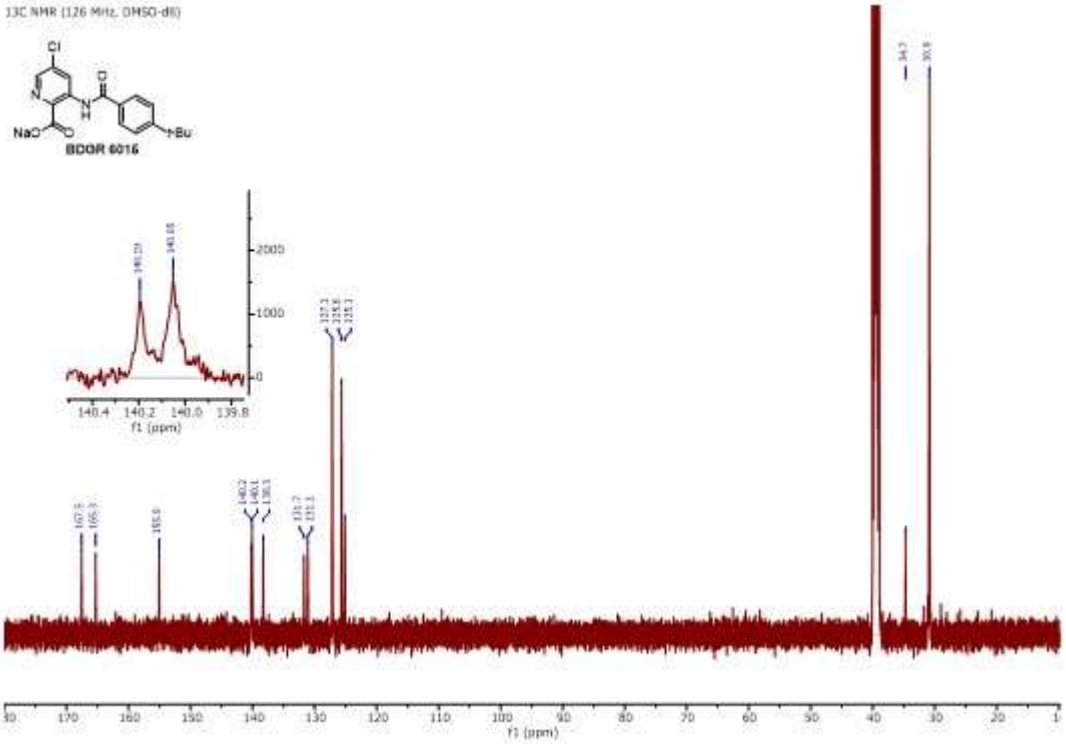
13C NMR (126 MHz, DMSO-d6)
BDGR 6016
140.19
140.05
140.4
140.2
140.0
139.8
f1 (ppm)
f1 (ppm)

1H NMR (400 MHz, CDCl3)

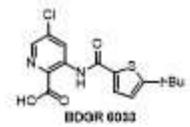

BDGR 6033

13C NMR (101 MHz, CDCl3)

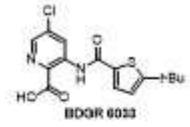

BDGR 6033

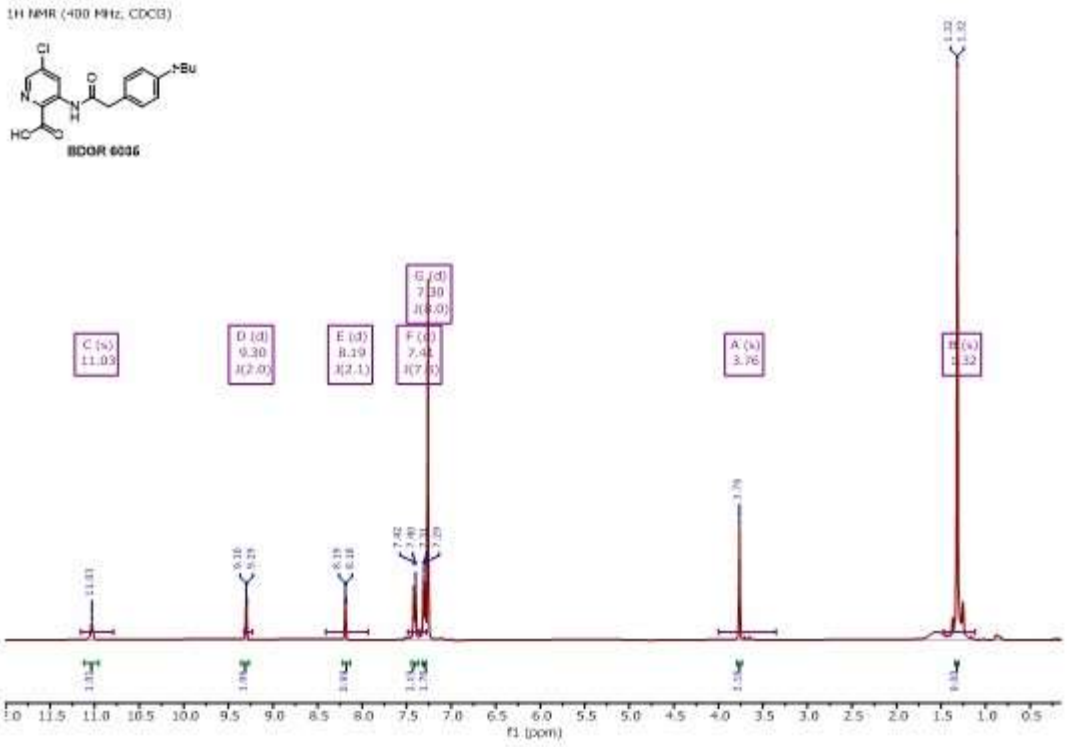
1H NMR (400 MHz, CDCl3)
BDOR 6036
f1 (ppm)

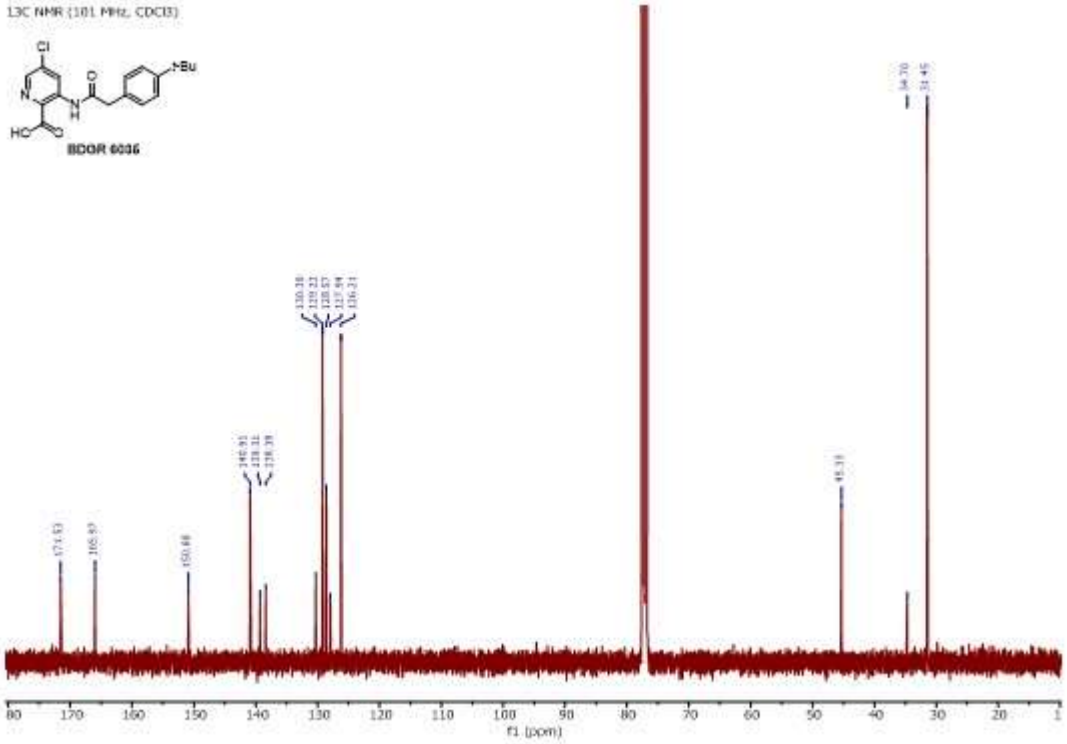
13C NMR (101 MHz, CDCl3)
BDOR 6036
f1 (ppm)

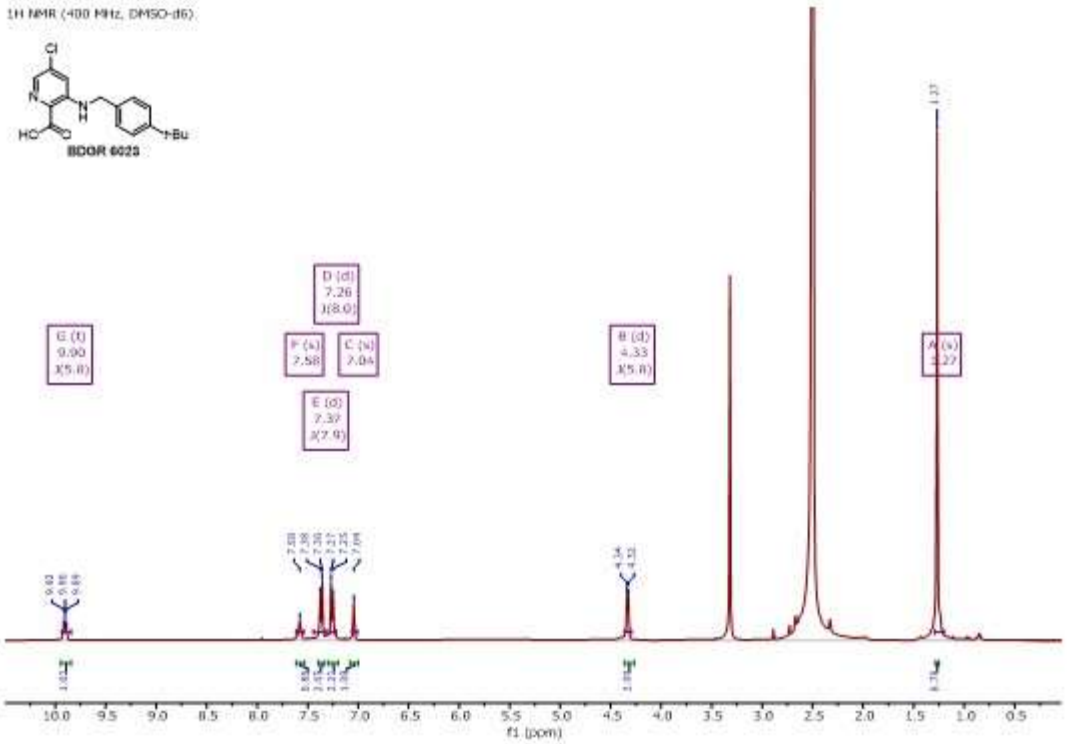
1H NMR (400 MHz, DMSO-d6)
BDGR 6023
G (t)
9.00
J(5.8)
D (d)
7.26
J(8.0)
F (s)
7.58
C (s)
7.04
E (d)
7.37
J(7.9)
B (d)
4.33
J(5.8)
A (s)
1.27
f1 (ppm)

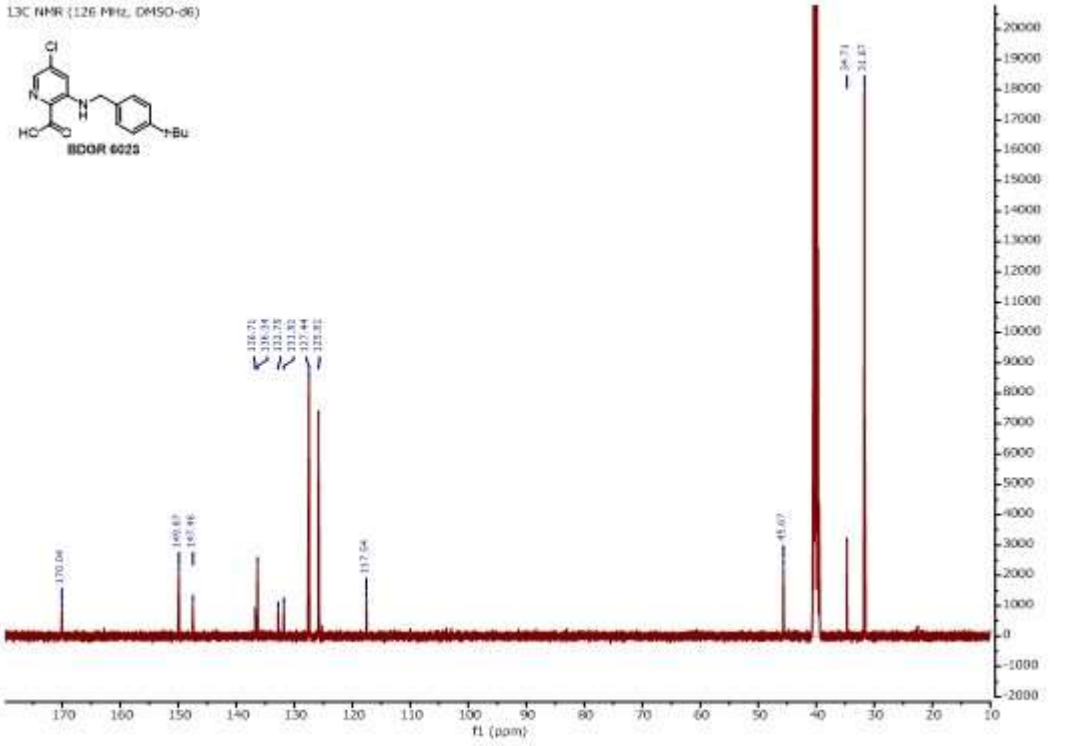
13C NMR (126 MHz, DMSO-d6)
BDGR 6023
170.04
149.67
147.46
136.71
136.34
132.75
132.35
132.44
131.81
117.54
45.67
34.71
31.47
f1 (ppm)

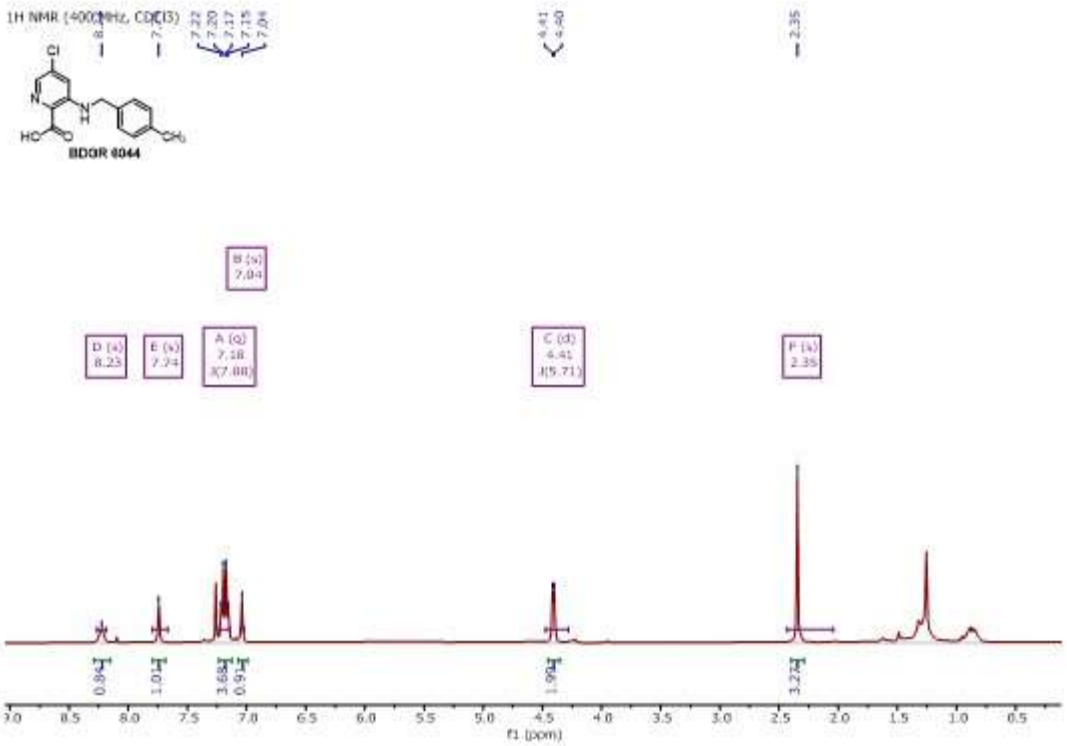
1H NMR (400 MHz, CDCl3)
BDQR 4044
f1 (ppm)

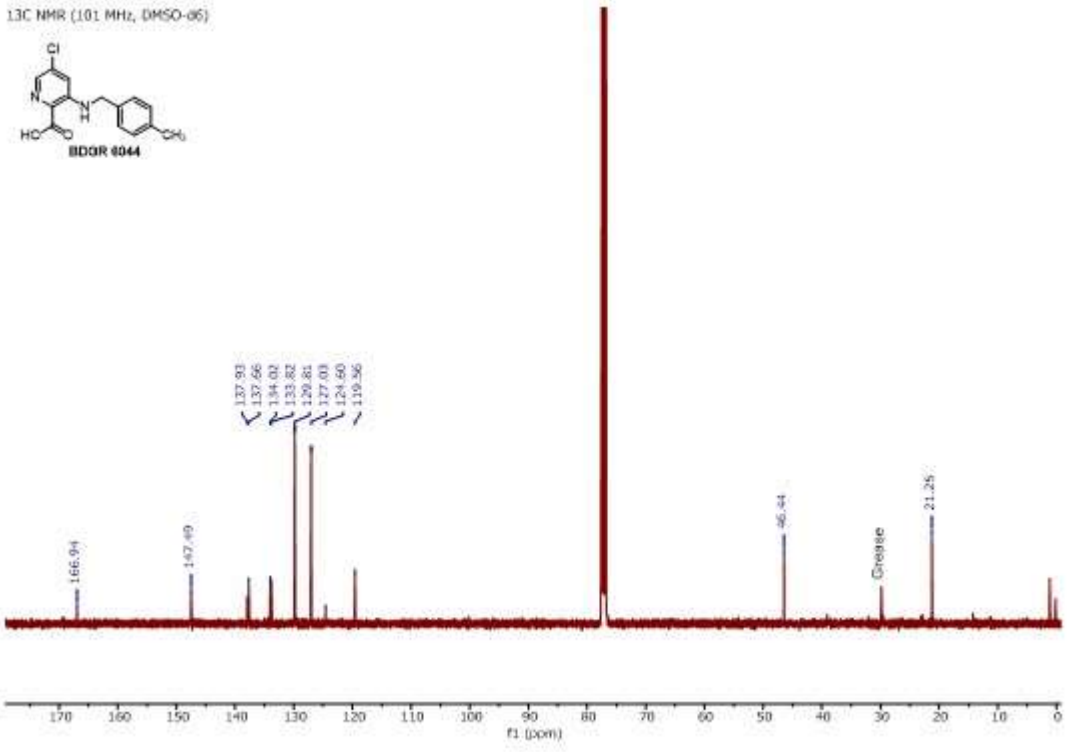
13C NMR (101 MHz, DMSO-d6)
BDQR 4044
166.94
147.49
137.93
137.66
134.02
133.82
129.81
127.03
124.60
119.96
46.44
Grease
21.25
f1 (ppm)

1H NMR (400 MHz, CDCl3)

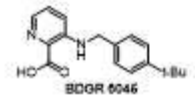

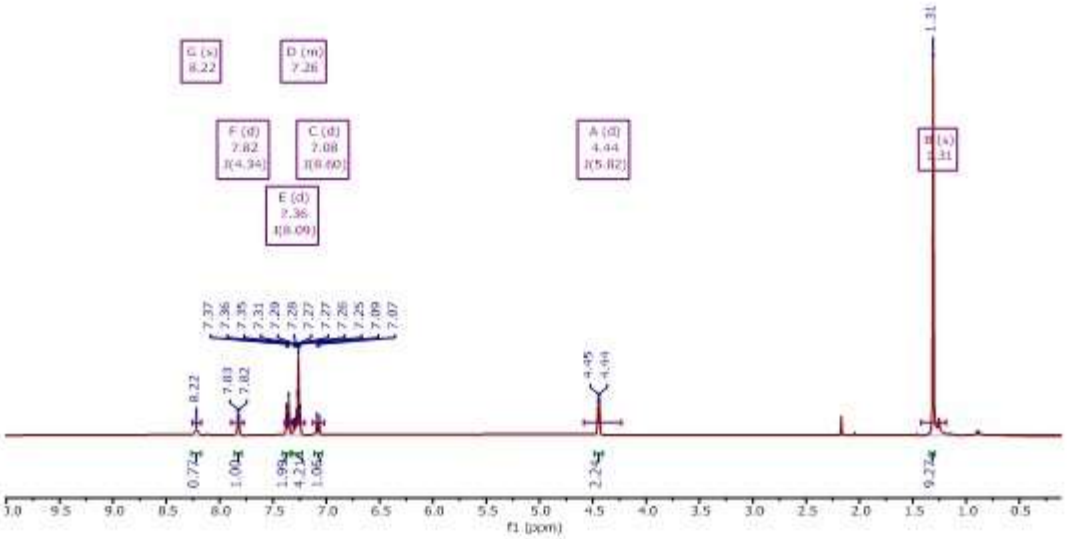

13C NMR (101 MHz, CDCl3)

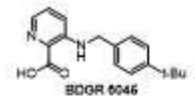

1H NMR (400 MHz, CDCl3)

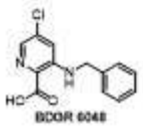

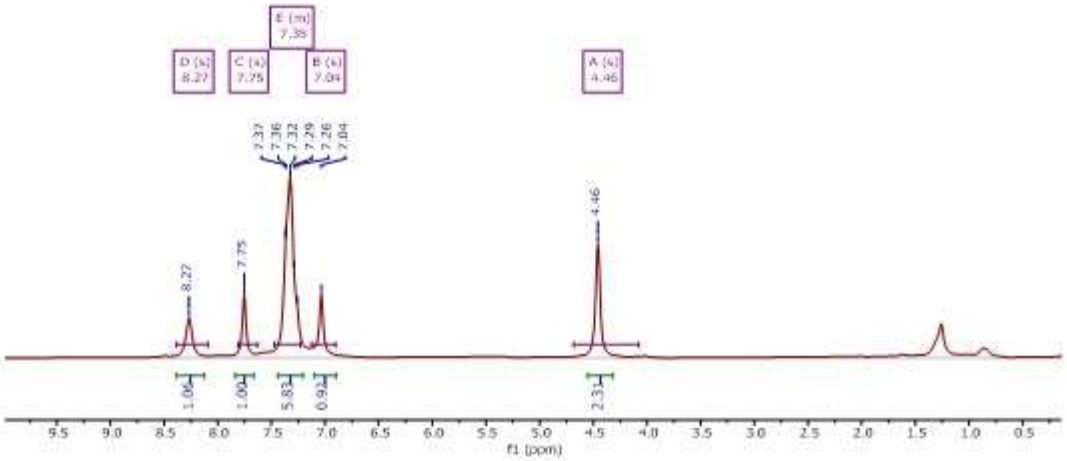

13C NMR (101 MHz, CDCl3)

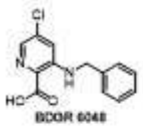

1H NMR (400 MHz, CDCl3)

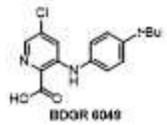

BDGR 6049

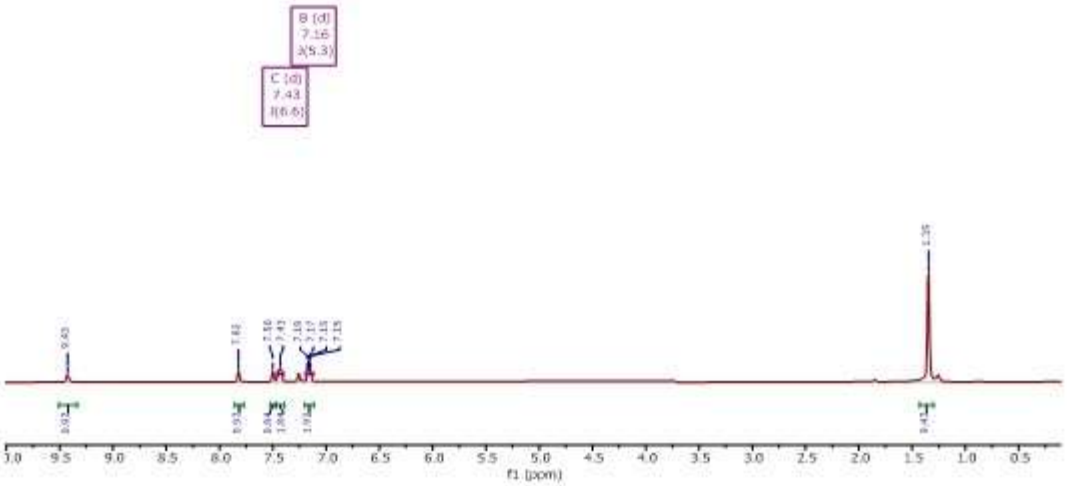

13C NMR (101 MHz, CDCl3)

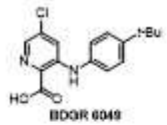

BDGR 6049

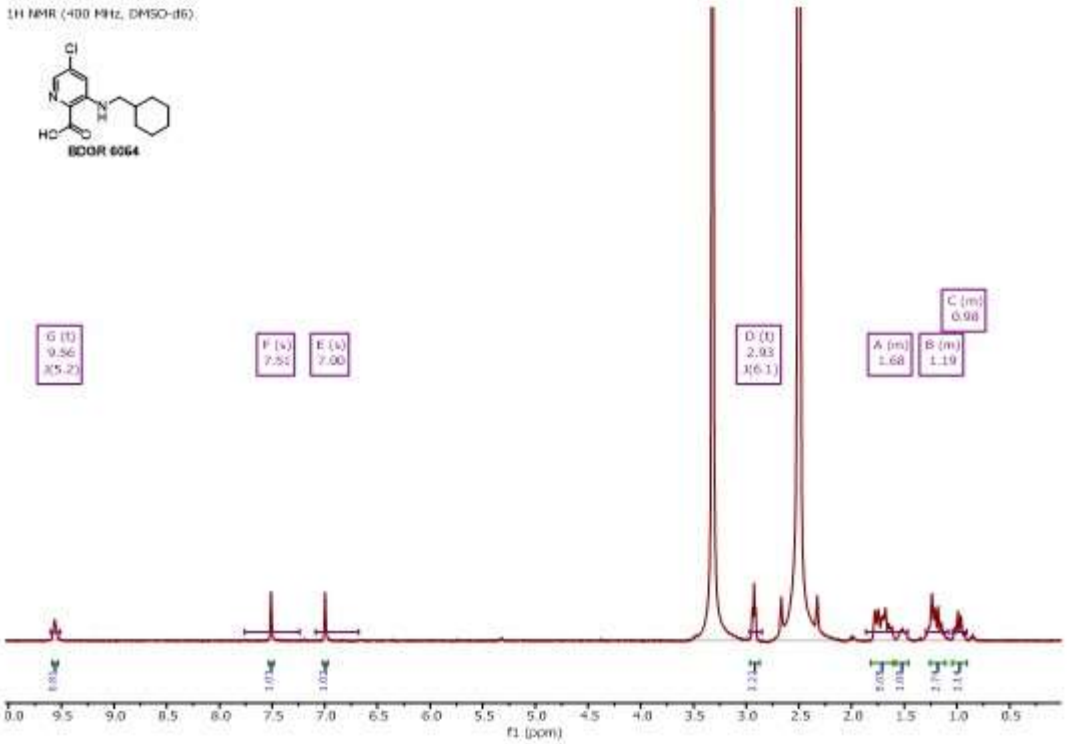
1H NMR (400 MHz, DMSO-d6)
BDOR 6064
G (t) 9.56 J(5.2)
F (s) 7.51
E (s) 7.00
D (t) 2.93 J(6.1)
A (m) 1.68
B (m) 1.19
C (m) 0.98
f1 (ppm)

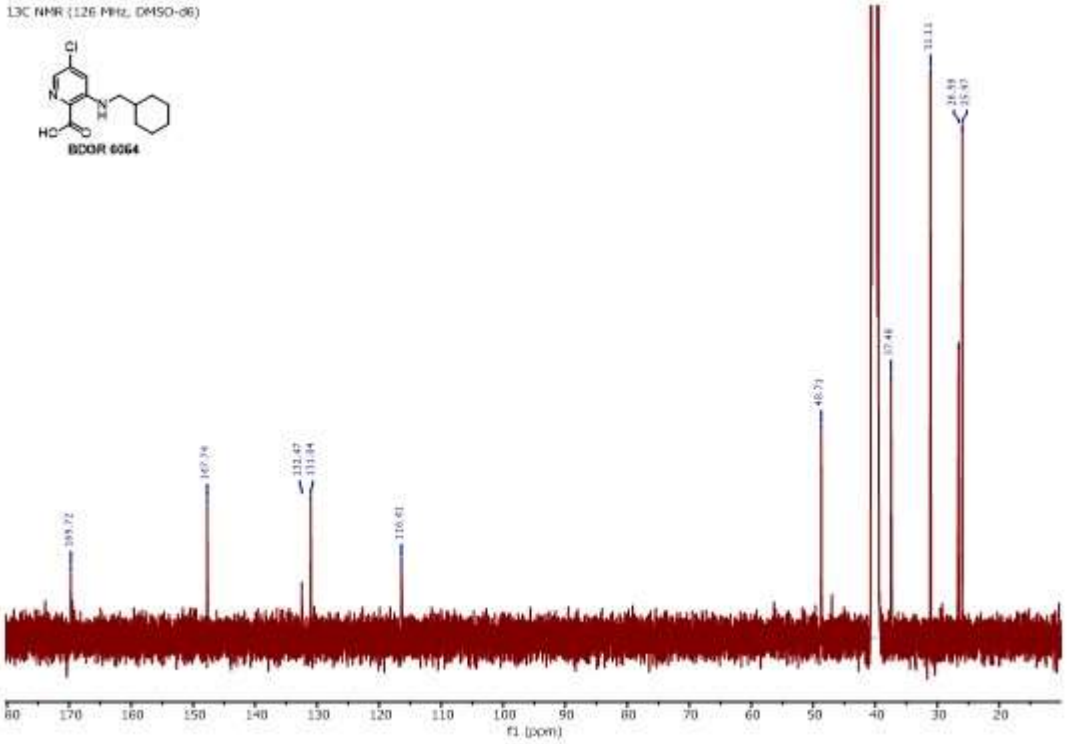
13C NMR (126 MHz, DMSO-d6)
BDOR 6064
169.72
167.79
152.47
151.84
126.61
48.73
37.48
33.11
26.59
25.47
f1 (ppm)

1H NMR (400 MHz, DMSO-d6)

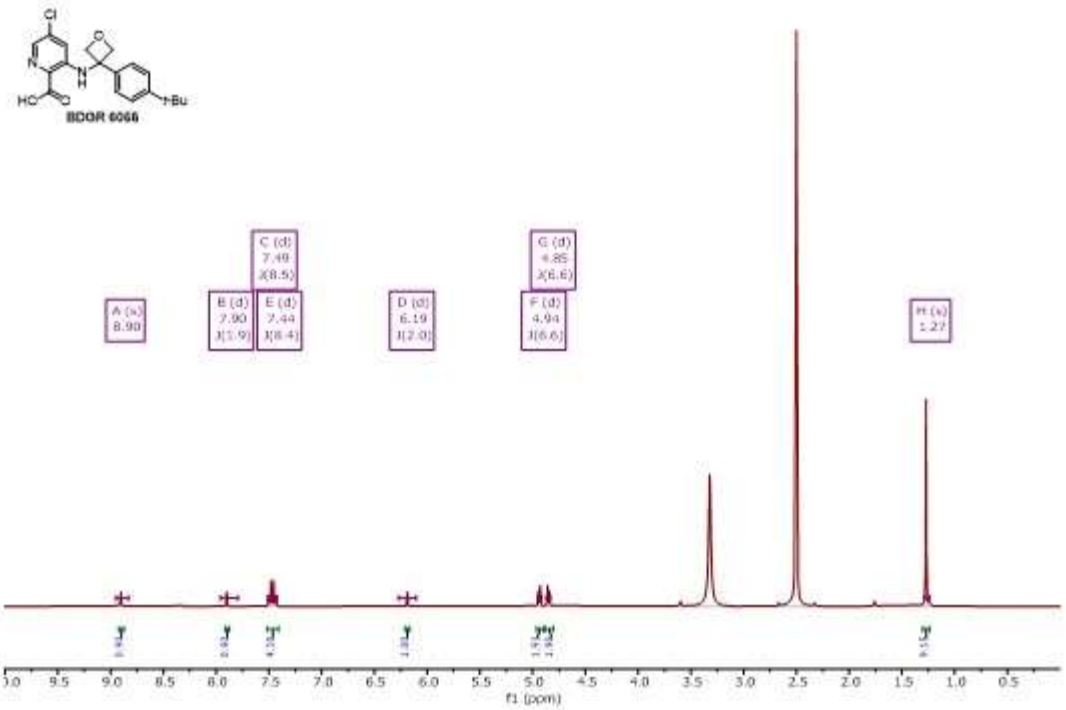

13C NMR (101 MHz, DMSO-d6)

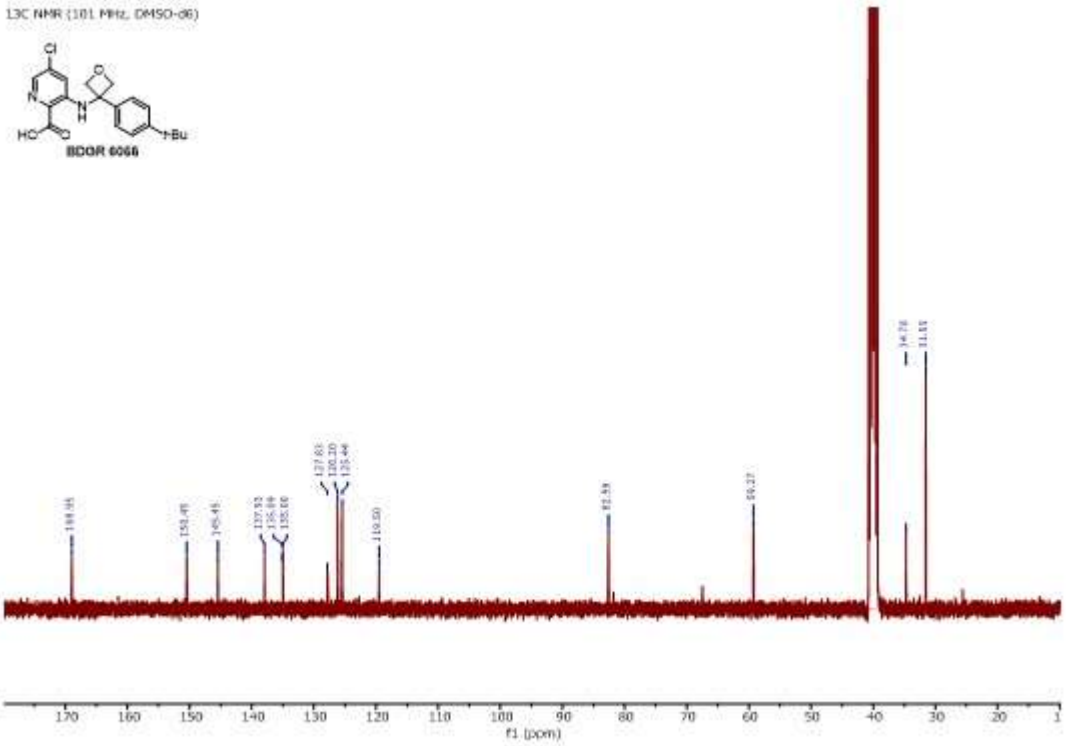

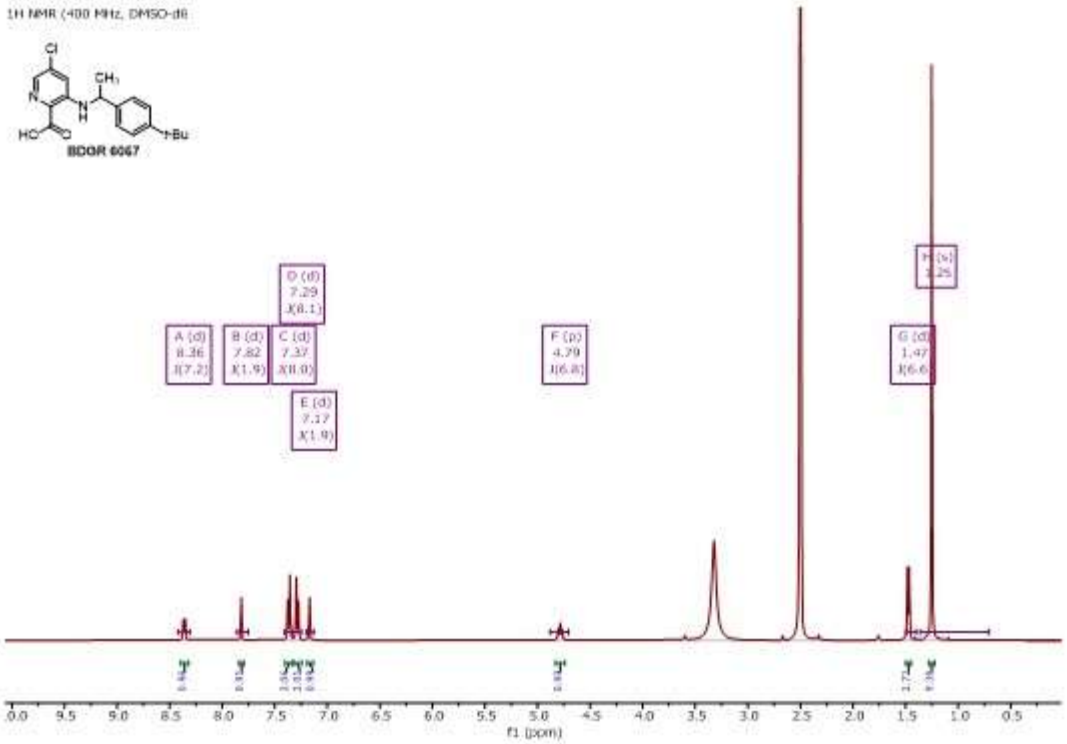
1H NMR (400 MHz, DMSO-d6)
BDGR 6067
A (d)
8.36
J(7.2)
B (d)
7.82
J(1.9)
C (d)
7.37
J(8.0)
D (d)
7.29
J(8.1)
E (d)
7.17
J(1.9)
F (p)
4.79
J(6.8)
G (d)
1.47
J(6.6)
f1 (ppm)

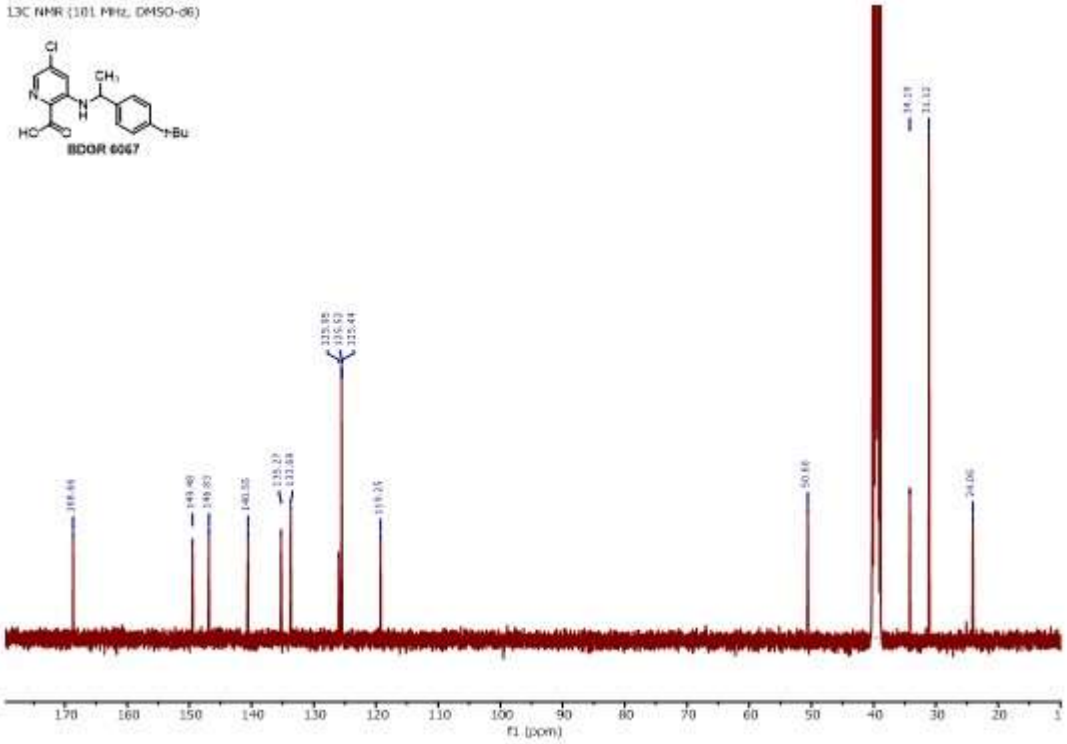
13C NMR (101 MHz, DMSO-d6)
BDGR 6067
f1 (ppm)

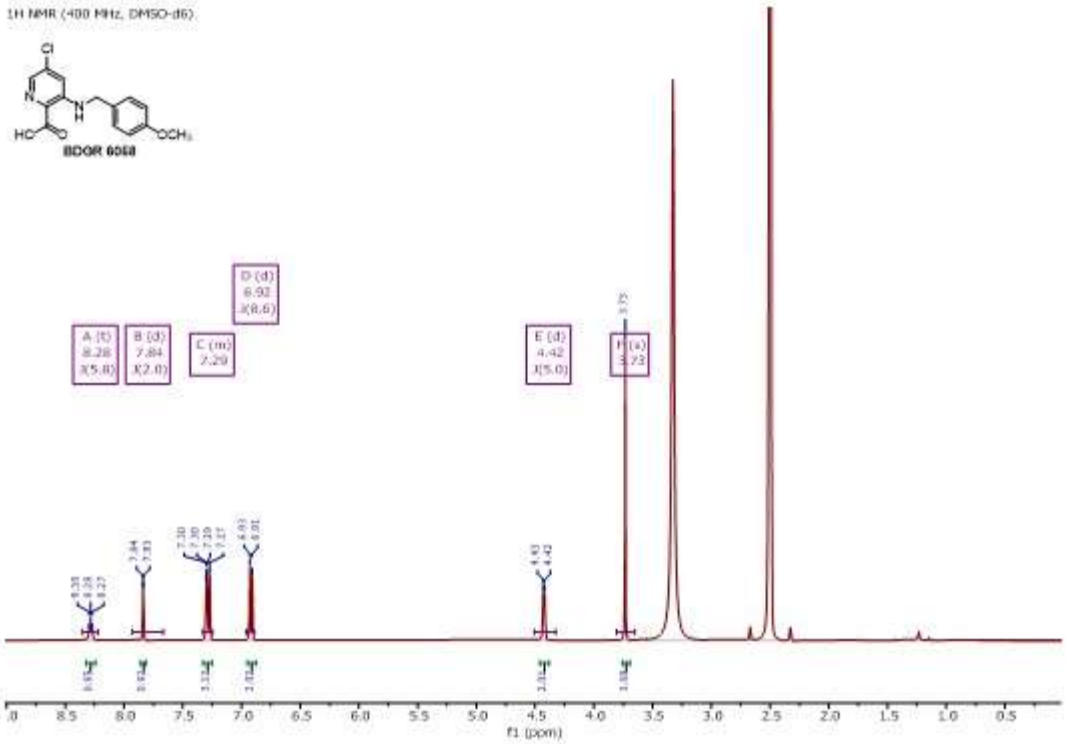
1H NMR (400 MHz, DMSO-d6)
BDOR 6068
A (t)
8.28
J(5.8)
B (d)
7.84
J(2.0)
C (m)
7.29
D (d)
6.92
J(8.6)
E (d)
4.42
J(5.0)
F (s)
3.73
f1 (ppm)

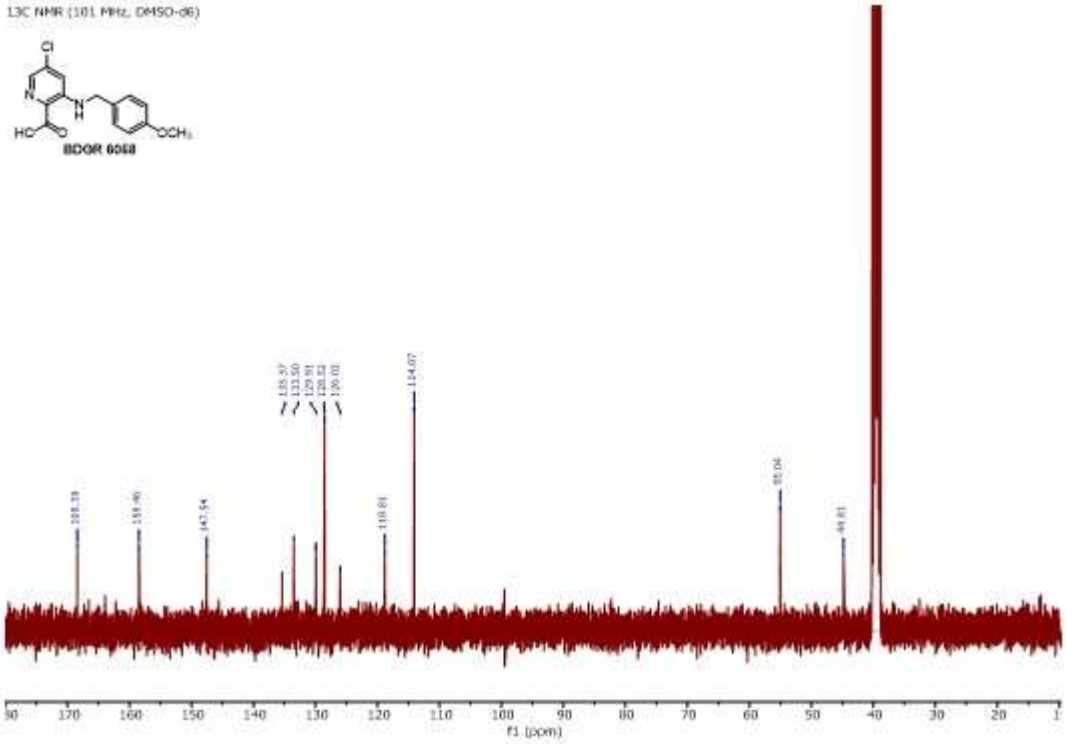
13C NMR (101 MHz, DMSO-d6)
BDOR 6068
f1 (ppm)

1H NMR (400 MHz, DMSO-d6)

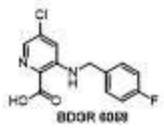

BDOR 6089

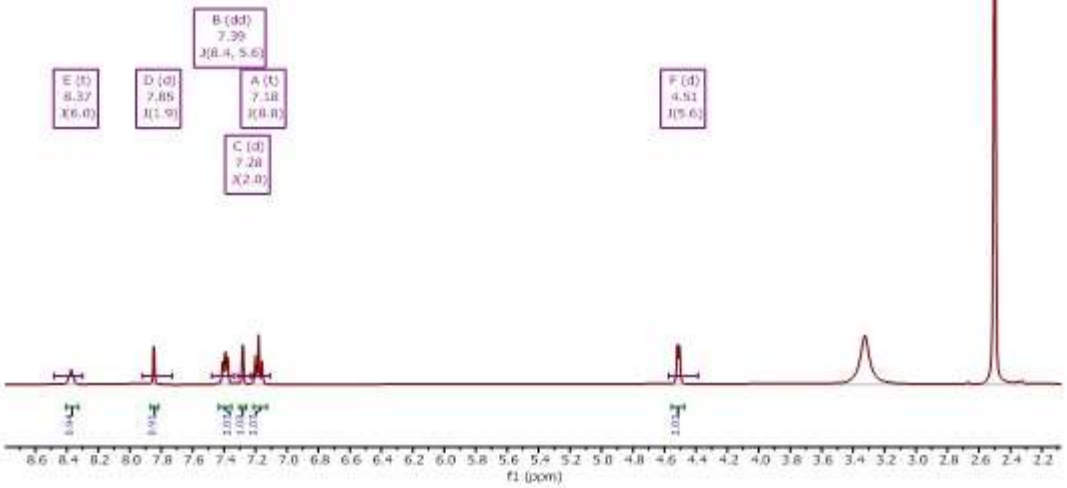

19F NMR (376 MHz, DMSO-d6)

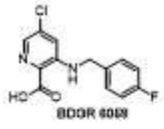

BDOR 6089

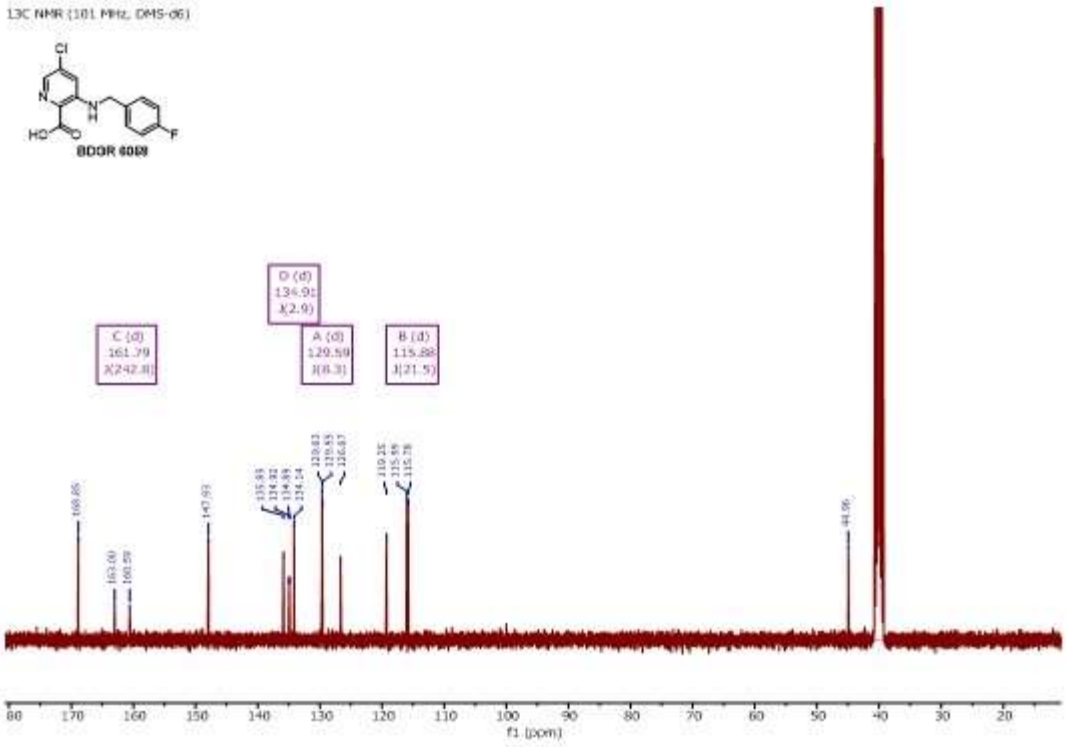
13C NMR (101 MHz, DMS-d6)
BDOR 6089
D (d)
134.91
J(2.9)
C (d)
161.79
J(242.8)
A (d)
129.59
J(8.3)
B (d)
115.88
J(21.5)
f1 (ppm)

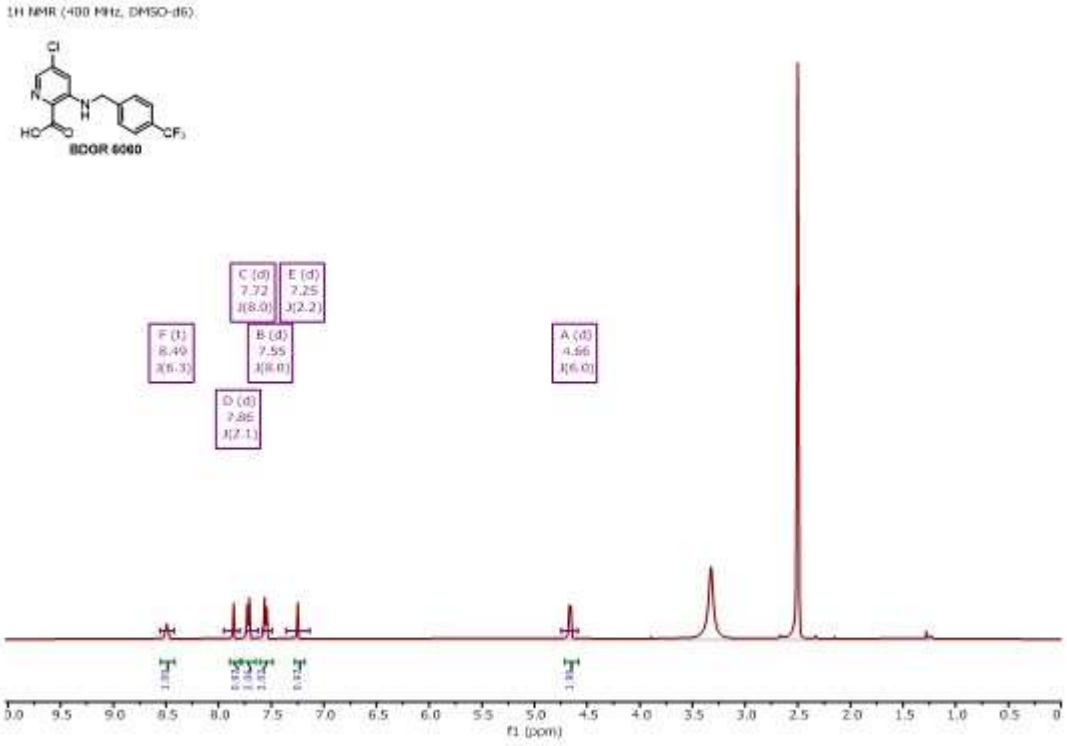
1H NMR (400 MHz, DMSO-d6)
BDOR 6060
C (d)
7.72
J(8.0)
E (d)
7.25
J(2.2)
F (t)
8.49
J(6.3)
B (d)
7.55
J(8.0)
A (d)
4.66
J(6.0)
D (d)
7.85
J(2.1)
f1 (ppm)

19F NMR (376 MHz, DMSO-d6)

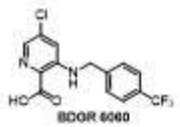

BCOR 6060

13C NMR (101 MHz, DMSO-d6)

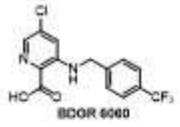

BCOR 6060

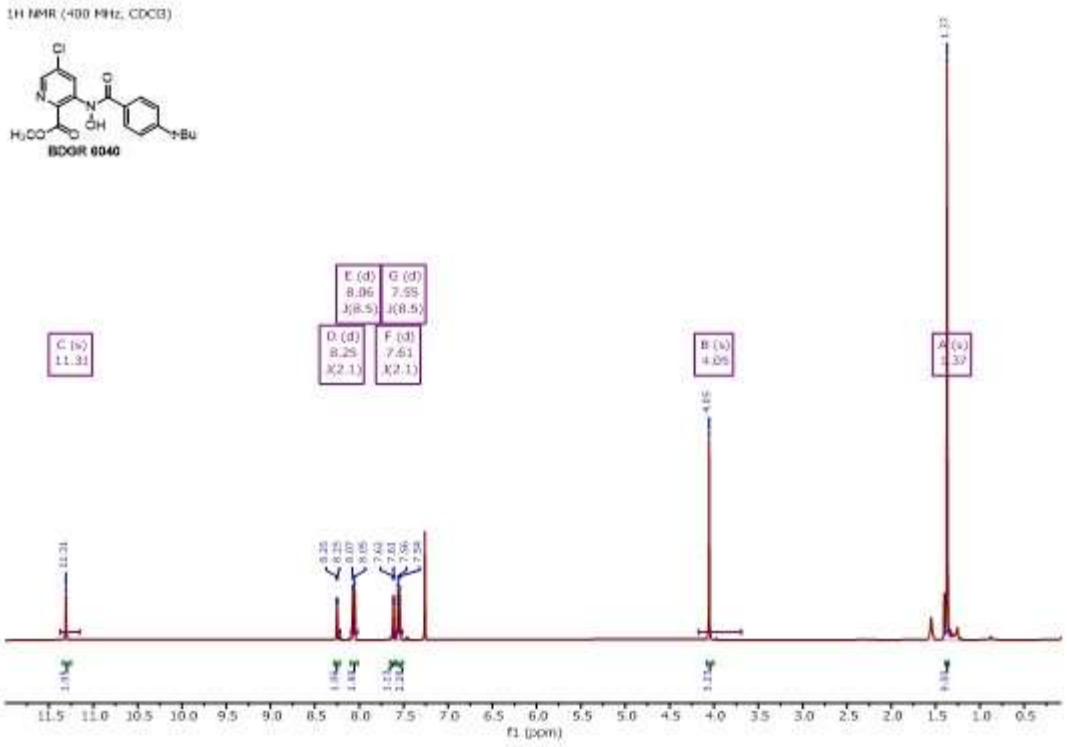
1H NMR (400 MHz, CDCl3)
BDGR 6040
C (s)
11.31
E (d)
8.06
J(8.5)
G (d)
7.55
J(8.5)
D (d)
8.25
J(2.1)
F (d)
7.61
J(2.1)
B (s)
4.05
A (s)
1.37
f1 (ppm)

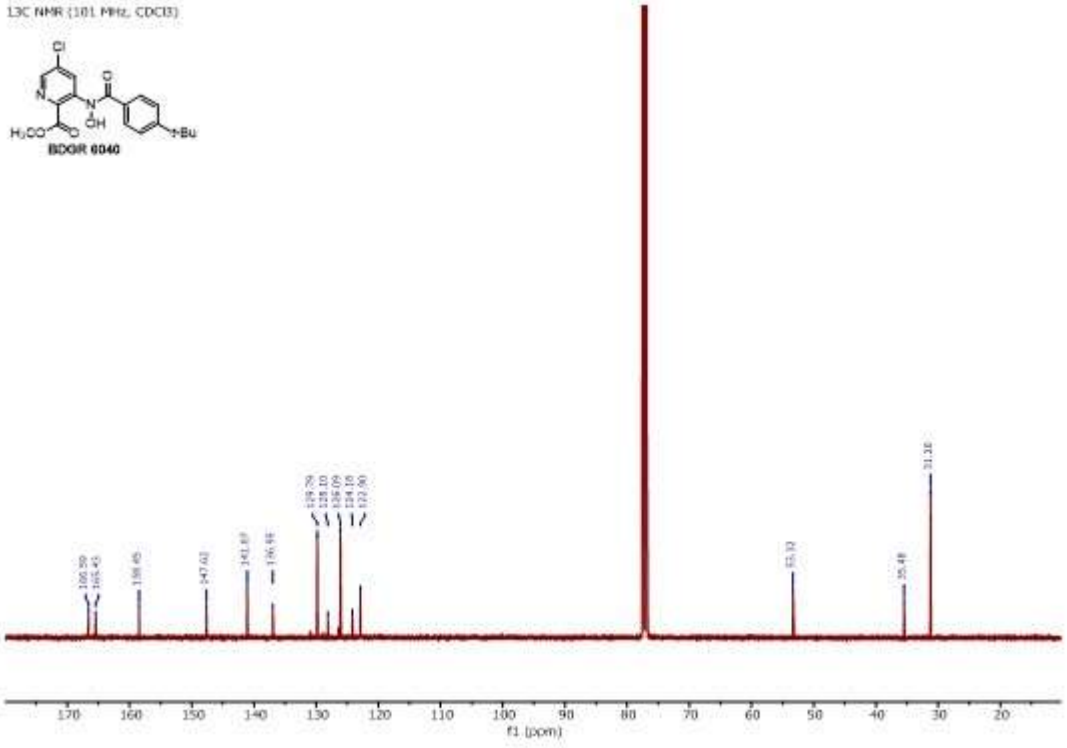
13C NMR (101 MHz, CDCl3)
BDGR 6040
f1 (ppm)

1H NMR (400 MHz, CDCl3)

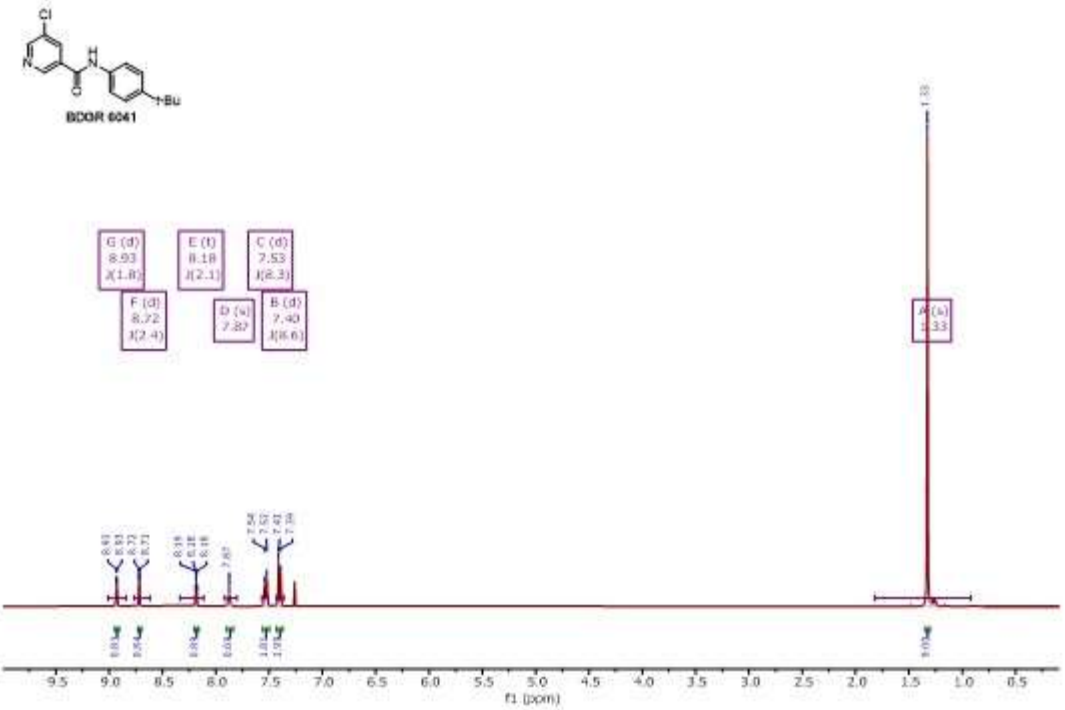

13C NMR (101 MHz, CDCl3)

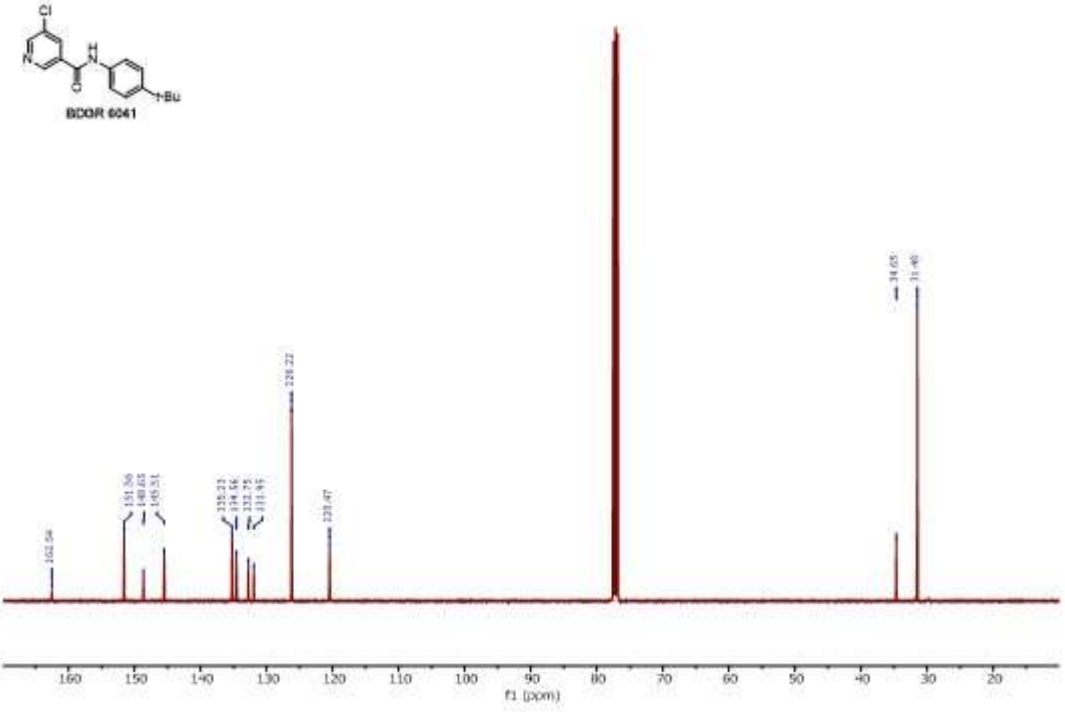

1H NMR (400 MHz, CDCl3)

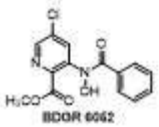

BDOR 6062

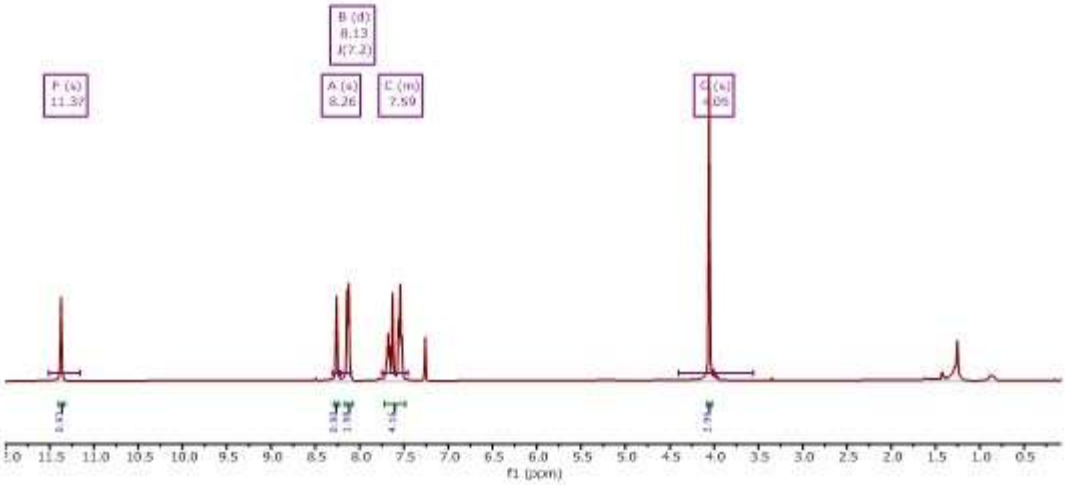

13C NMR (101 MHz, CDCl3)

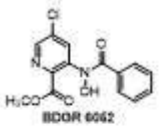

BDOR 6062

1H NMR (400 MHz, CDCl3)

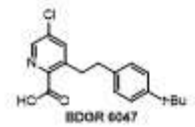

13C NMR (101 MHz, CDCl3)

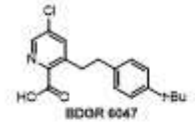

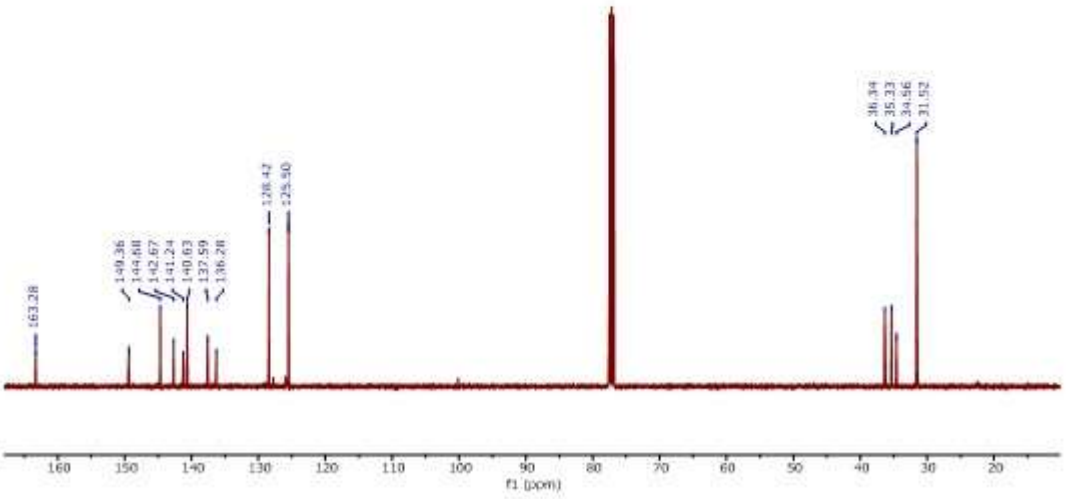

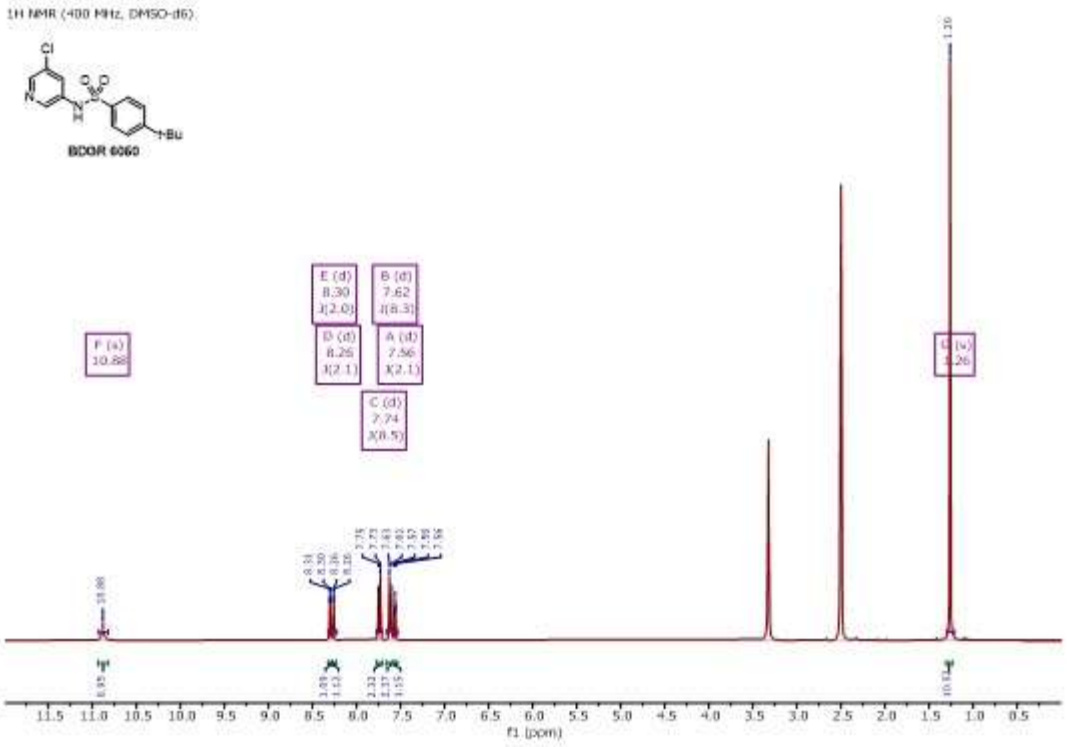
1H NMR (400 MHz, DMSO-d6)
BDOR 6060
F (s) 10.88
E (d) 8.30 J(2.0)
B (d) 7.62 J(8.3)
D (d) 8.26 J(2.1)
A (d) 7.56 J(2.1)
C (d) 7.74 J(8.5)
G (s) 1.26
f1 (ppm)

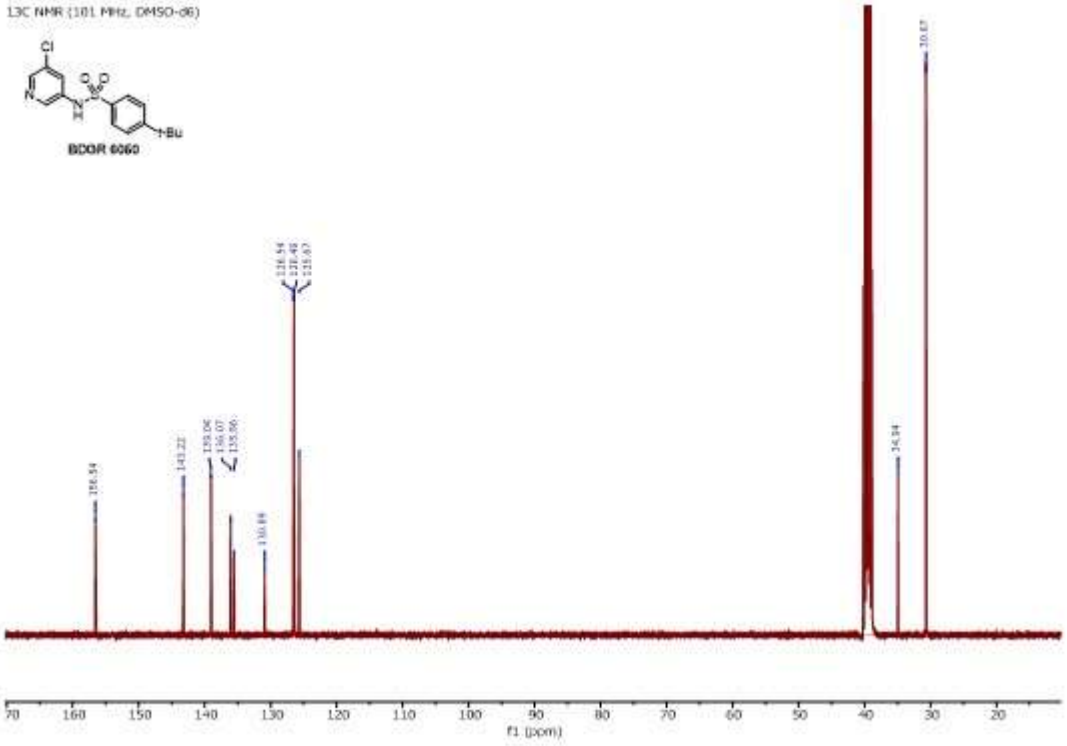
13C NMR (101 MHz, DMSO-d6)
BDOR 6060
f1 (ppm)

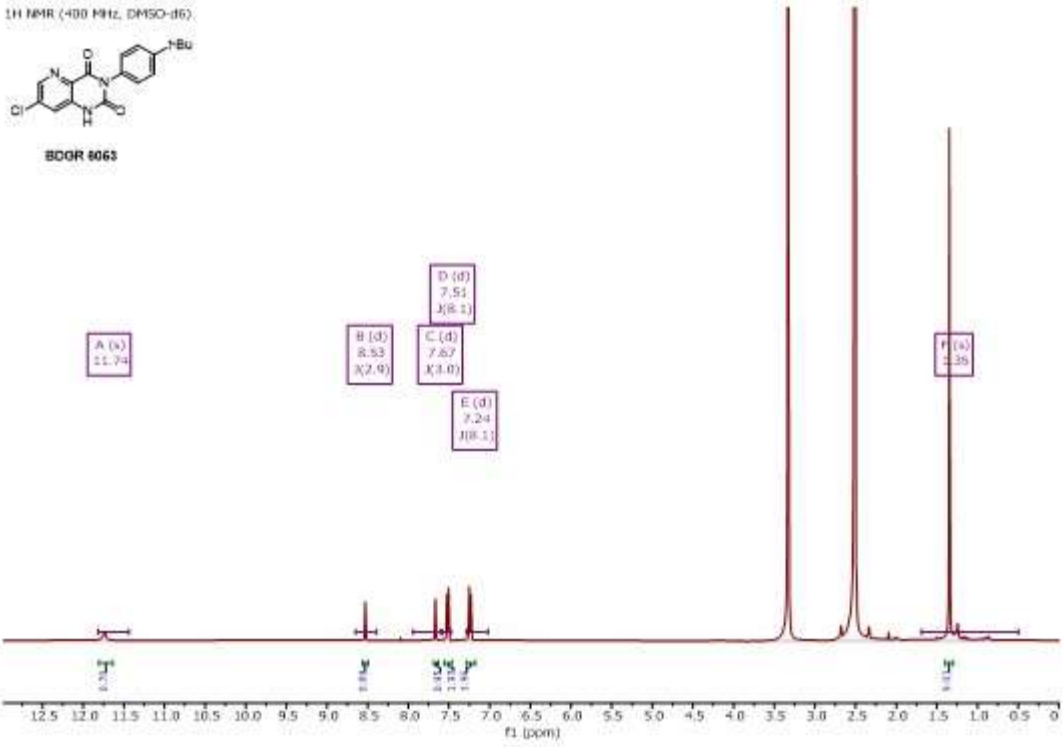
1H NMR (400 MHz, DMSO-d6)
BDGR 6063
A (s)
11.74
B (d)
8.53
J(2.9)
C (d)
7.67
J(3.0)
D (d)
7.51
J(8.1)
E (d)
7.24
J(8.1)
F (s)
1.35
f1 (ppm)

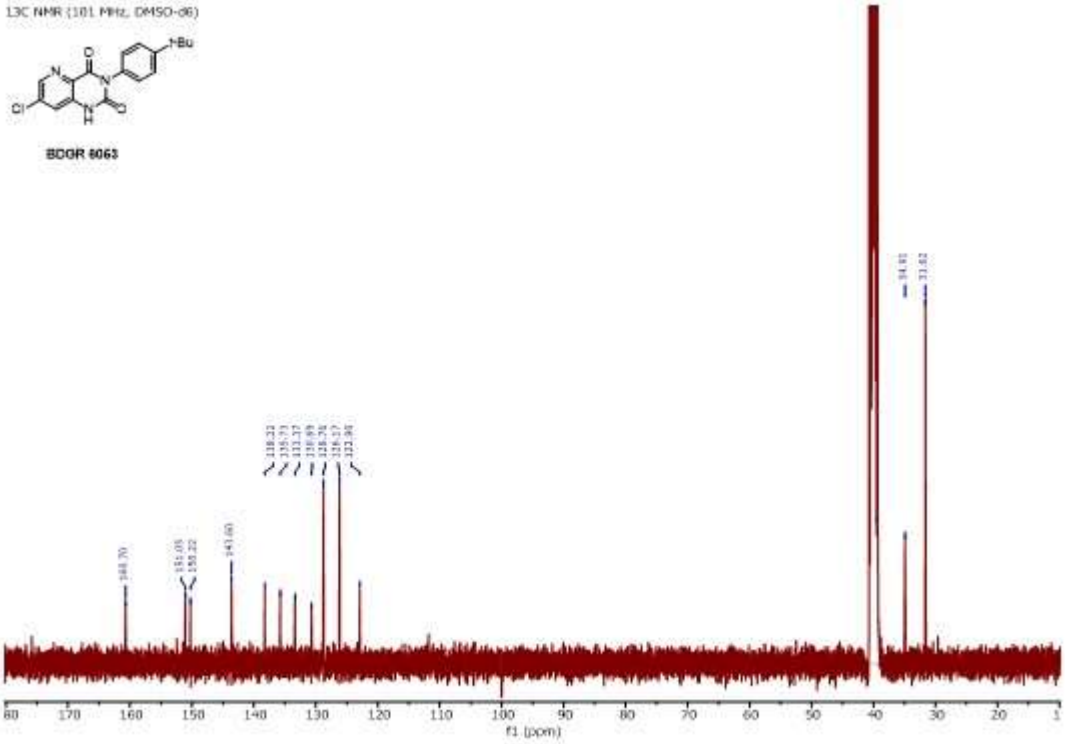
13C NMR (101 MHz, DMSO-d6)
BDGR 6063
f1 (ppm)